New Approaches for Cooling Photovoltaic/Thermal (PV/T) Systems

Thesis by

Asterios Bouzoukas, BEng, MSc, MBA

Thesis submitted to the University of Nottingham
for the degree of Doctor of Philosophy

March 2008

Contents Page

Contents Page.....I

Abstract.....X

Acknowledgement.....XII

Nomenclature.....XIII

Figure List.....XVII

Table List.....XXX

Chapter 1: Introduction

1.1 Background..... 1

1.1.1 Oil and Gas Prices..... 2

1.1.2 UK Electricity Generation Mix..... 3

1.1.3 UK Energy Consumption Sectors..... 4

1.1.4 Environmental Impact..... 6

1.1.5 Renewable Energy..... 8

1.1.6 General description of Solar Energy..... 9

1.2 PV/Thermal System Description..... 10

1.2.1 Hybrid PV/Thermal Panels..... 11

1.3 Research Aims..... 13

1.4 Novelty of the Research..... 14

1.5 Structure of the Thesis..... 14

Chapter 2: Literature Review

2.1 Introduction..... 16

2.2 Solar Sun..... 17

2.2.1 Technologies for conversion of solar energy..... 18

2.3 Solar Thermal Collectors..... 19

2.3.1 Flat-plate collectors..... 19

2.3.2 Evacuated tube collectors..... 24

2.3.3 Thermal analysis of collectors..... 26

2.3.4 Solar Collector Applications..... 32
2.3.4.1 Solar water heating systems..... 32
2.3.4.2 Solar space heating systems..... 34
2.4 Photovoltaic..... 35
2.4.1 How PV Cells Work..... 36
2.4.2 Types of PV Cell..... 37
2.4.3 Cells, Modules and Arrays..... 39
2.4.4 How a PV System Works..... 40
2.4.5 Types of PV Systems..... 41
2.4.6 PV Performance..... 43
2.4.7 Temperature influence on PV module performances..... 47
2.5 PV/Thermal Systems..... 49
2.5.1 Flat plate PV/T collectors..... 50
2.5.1.1 Water PV/T collectors..... 51
2.5.1.2 Air PV/T collectors..... 52
2.5.2 Parameters affecting PV/T performance..... 54
2.5.2.1 Manufacturing aspects of PV/T systems..... 54
2.5.2.2 Covered versus uncovered PV/T collectors..... 55
2.5.2.3 Thermal module efficiency..... 57
2.5.2.3.1 Reflection losses..... 59
2.5.2.3.2 Absorber plate parameters..... 63
2.5.2.3.3 Absorber to liquid thermal conductance..... 64
2.5.2.3.4 Absorber to air thermal conductance..... 66
2.5.2.3.5 Mass flow rate..... 67
2.5.2.4 Electrical module efficiency..... 68
2.5.2.4.1 Type of PV..... 69
2.5.2.4.2 Temperature effect..... 69
2.5.2.4.3 Temperature homogeneity..... 71
2.5.2.5 Reliability..... 72
2.5.2.5.1 Stagnation temperature..... 72
2.5.3 Analytical models of PV/T collectors..... 73

2.5.4 Modeling and simulation..... 77
2.5.5 Qualitative evaluation of thermal/electrical output..... 78
2.5.6 Discussion..... 79
2.6 Heat Pipe..... 84
2.6.1 Brief History of Heat Pipe Technology..... 84
2.6.2 Heat Pipe Structure..... 85
2.6.3 Heat Pipe Design..... 85
2.6.3.1 Limits to Heat Transport..... 86
2.6.3.2 Wicked and Wickless Heat Pipes..... 87
2.6.3.3 Length and diameter of a heat pipe..... 89
2.6.3.4 Inclination of heat pipe..... 90
2.6.3.5 Heat pipe flattening or bending..... 91
2.6.3.6 Working Fluids..... 92
2.6.3.7 Heat pipe reliability..... 93
2.6.3.8 Type of Heat Pipes..... 93
2.6.4 Gravity assisted wickless heat pipes..... 97
2.6.5 Solar Heat Pipe Collectors..... 100
2.6.5.1 Solar Collectors with gravity assisted heat pipes..... 102
2.6.5.2 Solar collectors heat exchanger types..... 104
2.6.5.3 Solar collectors heat pipes with different working fluid.... 106
2.6.6 PV/T Systems incorporating Heat Pipes..... 107
2.6.7 Discussion..... 109
2.7 Phase Change Material (PCM)..... 111
2.7.1 Latent heat of fusion..... 112
2.7.2 Classification of PCM..... 112
2.7.2.1 Organic PCM..... 113
2.7.2.2 Inorganic PCM..... 114
2.7.2.3 Eutectic PCM..... 114
2.7.3 Desired PCM Properties..... 116
2.7.3.1 Thermo physical properties determination..... 117
2.7.3.2 Stability of the PCM-container system..... 118

2.7.3.3 Corrosion of the materials..... 118
2.7.3.4 Encapsulation of the materials..... 119
2.7.3.5 Nucleation and Supercooling..... 119
2.7.3.6 Stratification and Agglomeration..... 120
2.7.3.7 Storage capacity..... 121
2.7.3.7 Charge and discharge..... 123
2.7.4 Commercially produced PCM and products..... 123
2.7.5 PCM Heat Transfer Enhancement Techniques..... 124
2.7.5.1 Heat transfer enhancement..... 125
2.7.5.2 PCM based Heat Sink..... 127
2.7.6 PCM use in Buildings..... 130
2.7.7 Solar Collectors using PCM..... 132
2.7.8 Building Integrated PV system incorporating PCM..... 136
2.7.9 Discussion..... 137
2.8 Microencapsulated Phase Change Material (MCPCM)..... 139
2.8.1 Functionally Thermal Fluids..... 139
2.8.2 Phase Change Slurries..... 141
2.8.3 Microencapsulated PCM slurry..... 142
2.8.4 Parameters affecting the Heat Transfer Enhancement of PCM Slurry 144
2.8.4.1 Laminar Flow Conditions..... 145
2.8.4.2 Turbulent Flow Conditions..... 146
2.8.4.3 Effective Specific Heat..... 146
2.8.4.4 Super cooling..... 148
2.8.5 MicroPCM Applications..... 149
2.8.6 Discussion..... 152
Chapter 3: PV Performance
3.1 Introduction..... 154
3.2 Solar cell losses..... 154
3.3 Module Temperature Effect..... 155
3.4 Cell and Module $I-V$ Systems..... 156
3.5 Standard Reporting Conditions (SRC)..... 159

3.6 Experimental Rig Apparatus..... 159
3.7 Experimental work..... 166
3.7.1 PV Performance with uninsulated model..... 166
3.7.1.1 V_{oc} Temperature Coefficient..... 169
3.7.1.2 I_{sc} Temperature Coefficient..... 170
3.7.1.3 Power Temperature Coefficient..... 171
3.7.2 PV Performance with insulated model..... 172
3.7.3 Comparison of PV uninsulated with insulated..... 174
3.8 Conclusion..... 176

Chapter 4: Photovoltaic/Thermal System - Water

4.1Introduction..... 178
4.2 Aspects of the two PV/T water systems..... 179
4.3 Theoretical model of the PV/T panel..... 181
4.3.1 The PV/T panel performance equation..... 182
4.3.2 Energy into the PV/T panel..... 184
4.3.3 Heat Losses from the Collector..... 185
4.3.4 Calculation of module temperature of PV..... 186
4.3.5 Collector Efficiency..... 187
4.3.6 Electrical Performance of the PV/T..... 187
4.4 TRNSYS simulation program..... 188
4.4.1 Simulation Program..... 189
4.5 PV/T system yield..... 191
4.5.1 Evaluation of Total Efficiency Performance..... 192
4.5.2 Energy Saving Efficiency..... 192
4.5.3 Performance evaluation for PV/T collector Exergy Efficiency..... 193
4.6 Experimental PV/T systems..... 194
4.6.1 Heat transfer between PV cells and absorber plate (Theoretical Evaluation)..... 195
4.6.2 Heat transfer coefficient between cells and absorber (Experimental Evaluation)..... 196
4.7 Experimental Results..... 196

4.7.1 First set of experiments..... 198
4.7.2 Second set of experiments..... 199
4.7.3 Third set of experiments..... 201
4.8 Conclusions..... 205
Chapter 5: Photovoltaic/Thermal Air
5.1 Introduction..... 208
5.2 Technical issues..... 208
5.2.1 Heat transfer from absorber to air..... 209
5.3 Thermal energy..... 209
5.3.1FIN system..... 210
5.3.1.1 Heat convection from fins..... 211
5.4 Experimental systems..... 212
5.5 Design procedure for cooling ducts to minimize efficiency loss due to temperature rise in PV arrays..... 214
5.6 Experimental results..... 215
5.6.1 First set of experiments..... 215
5.6.2 Second set of experiments..... 216
5.6.3 Third set of experiments..... 219
5.7 Discussion..... 223
5.8 Conclusions..... 224
Chapter 6: Photovoltaic/Thermal – Heat Pipe
6.1 Introduction..... 226
6.2 Heat Pipe Capacity Limits..... 228
6.2.1 Capillary Limit..... 228
6.2.2 Sonic Limit..... 230
6.2.3 Boiling Limit..... 230
6.2.4 Entrainment Limit..... 231
6.2.5 Viscous Limit..... 231
6.3 Simulation to calculate heat transfer limits..... 232
6.3.1 Working fluid effect on heat pipe performance..... 234
6.3.2 Diameter effect on heat pipe performance..... 236

6.3.3 Fill liquid level effect on heat pipe performance..... 236
6.3.4 Inclination angle effect on heat pipe performance..... 237
6.4 Experimental Performance of Heat Pipes..... 238
6.4.1 Heat Pipe with a Tank..... 239
6.4.2 Heat Pipe with Manifold..... 242
6.5 Design of the PV/T Heat pipe model..... 246
6.5.1 Sensitive parameters that affect the performance of a solar collector 248
6.5.1.1 Correlation of the heat removal factor and design parameters of a thermosyphonic wickless heat pipe solar collector..... 249
6.5.1.2 Evaporator and condenser thermal resistances..... 250
6.6 Experimental PV/T Heat Pipe Model..... 255
6.6.1 Description of the PV/T Heat Pipe with Tank system..... 255
6.6.2 Description of the PV/T Heat Pipe with Manifold system..... 257
6.7 Experimental Results..... 258
6.7.1 Calorimetric method of testing used in the PV/T heat pipe with tank..... 258
6.7.2 Instantaneous method used in PV/T heat pipe with the manifold..... 262
6.7.3 Comparing PV/T Heat Pipe system with Manifold and Tank..... 265
6.8 Conclusion..... 269
Chapter 7: Photovoltaic/Thermal - Phase Change Material (PCM)
7.1 Introduction..... 273
7.2 PCM Thermo physical Properties..... 274
7.2.1 Description of the method..... 274
7.3 PV/PCM Thermal Model..... 279
7.3.1 Detailed Description of PV/PCM..... 279
7.3.2 Completely Solidified or Completely Liquefied Glazed PV/PCM.... 280
7.3.3 Two Phase Region between the Liquefaction and Solidification Temperatures..... 283
7.4 TRNSYS 601 Model Simulation Results..... 285
7.4.1 Thermal conductivity influence on PV/PCM performance..... 286
7.4.2 Parametric analysis..... 288

7.4.2.1 The performance PV/ PCM system with different PCM material thickness..... 288
7.4.2.2 Thermal control achieved for different ambient temperatures and insolations..... 289
7.4.3 PV/PCM A28 system simulation for one day, under realistic ambient temperatures and insolation and 3 different PCM thicknesses..... 292
7.4.4 PV/PCM A28 system simulation for three days, under realistic ambient temperatures and insolation and 3 different PCM thicknesses..... 294
7.5 Experimental work..... 296
7.5.1 PV/PCM A28 experiment..... 298
7.5.2 PV/PCM A28 with Water Pipes Experiments..... 300
7.5.2.1 Varying the Flow Rate..... 302
7.5.2.2 Varying Inlet Temperature..... 304
7.6 Conclusion..... 308
Chapter 8: Photovoltaic/Thermal - Microencapsulated Phase Change Material Slurry (MCPCM)
8.1 Introduction..... 311
8.2 Microcapsules and slurry..... 312
8.3 Slurry Performance..... 314
8.3.1 Thermal Analysis (TA)..... 317
8.3.2.1 Methodology..... 318
8.3.2.2 TA Experimental Observations..... 318
8.4 MCPCM Slurry..... 321
8.4.1 MCPCM Slurry in a Closed Loop System..... 322
8.5 Description of the PV/MicroPCM Slurry System..... 324
8.5.1 Experimental apparatus and method..... 324
8.5.2 Calibration and verification..... 327
8.5.3 Performance of the PV/Thermal collector with the use of MCPCM slurry..... 329
8.5.4 Efficiency of the PV/MCPCM collector..... 332
8.6 Conclusion..... 336

Chapter 9: Photovoltaic/Thermal Systems - Technical, Economic and Environmental Comparison

9.1 Introduction..... 338

9.2 PV/Thermal Systems - Technical Comparison..... 338

9.2.1 Total Energy Efficiency..... 339

9.2.2 Primary Energy Saving Efficiency..... 341

9.2.3 Exergy Efficiency..... 342

9.3 PV/Thermal Systems - Economic Comparison..... 344

9.3.1 Comparison of a PV/T system with side-by-side PV and Solar Thermal Collector system..... 346

9.4 PV/Thermal Systems Environmental Comparison..... 358

9.4.1 Energy Payback Time of PV Systems..... 358

9.4.2 Factors Driving the Results of PV LCA..... 359

9.4.2.1 Technological Options..... 360

9.4.2.2 Incident Solar Radiation..... 362

9.4.2.3 Balance of the System (BOS)..... 362

9.4.2.4 Installation Type..... 363

9.4.2.5 Conversion Efficiency Trend..... 364

9.4.2.6 Lifetime of the System..... 364

9.4.3Energy Return Factor..... 365

9.5 Conclusions..... 370

Chapter 10: Conclusions and Further Work

10.1 Conclusions..... 373

10.2 Recommendations for Future Work..... 387

References..... 389

Appendix 1..... 412

Appendix 2..... 413

Abstract

Today the majority of UK's energy needs are met by fossil fuels. An energy sector that uses 30% of this energy and generates 28% of the total emissions is domestic sector. To reduce the emissions generated by fossil fuels UK government decided to increase the energy coming from renewable sources by 2020. A renewable energy that can contribute is solar energy. Solar thermal collectors and photovoltaics are two means of transforming solar energy to thermal and electrical energy.

The limited space in the roofs and the cost of the technologies will prevent families to use both systems together in their roof. A hybrid energy system combine the use of two or more alternative power sources will help to increase the system's total efficiency. The photovoltaic/thermal (PV/T) system is a hybrid structure that converts part of the sun's radiation to electricity and part to thermal energy.

This research work focuses on the production of new approaches on hybrid PV/T systems. PV/T systems using water and air have been introduced and a literature review conducted in order to identify positives and negatives of these systems. Experiments also conducted by using water and air as heat transfer medium, and the results helped to work as a benchmark performance to the new approaches.

These technologies were heat pipes, phase change materials and microencapsulated phase change materials. The technologies exist for years but their use in the specific application is new. A literature review was undertaken to provide an understanding of these technologies and identified findings that have contributed to the design of the systems. Experimental work was carried out incorporating these technologies in the rear of a PV and the results indicated comparable performance with PV/T-water and PV/T-air.

Five performance indicators were employed to help with the comparison of the systems. These were electrical and thermal efficiency, the total energy efficiency, the primary energy saving efficiency and the exergy efficiency. From these five indicators the primary energy saving efficiency that shows how much fossil fuel is saved and the exergy efficiency that could give the optimum working conditions of each system was the most valuable ratings.

For the PV/PCM model a new simulation program was developed to help validate the experimental work. Also an environmental and economic study was undertaken to compare if the new systems could help reduce the CO_2 emissions and if they were feasible to become commercial products.

Finally the conclusions gained have been presented and recommendations for future work have been made.

Acknowledgement

I would like to express my thanks and gratitude to Professor Saffa Riffat who gave me the opportunity to complete this PhD. I would extend my sincere thanks to Dr. Robin Wilson whom guided, advised and encouraged me throughout the process of writing my research work.

I also would like to appreciate the School of the Built Environment, the University of Nottingham and EPSRC for their financial support for tuition fees and living expenses.

Many thanks to all other staff in this school who gave me a lot of help during my study and without them I could not complete my research work. They are Dr Siddig Omer, Mr Bob Clarke, Mr Dave Oliver, Mr Dave Taylor, and Mr Jonathan Moss.

Special thanks to CIBASC and to Martin Butters and Ian Biggins for their assistance and for providing the necessary material and information. Also to Thermal Energy Systems Specialists (TESS) and David Bradley who helped in the creation of the TRNSYS model.

Great thanks to the whole family for their support for so many years.

Dedication

This dissertation is dedicated to my grandmother and grandfather (Αφιερώνω αυτή την εργασία στην γιαγιά και τον παππού)

Nomenclature

A_a	aperture area of PV module (m^2)
C_p	specific heat of fluid (J/(kg K))
D	diameter (m)
D_h	hydraulic diameter (m) = (4*flow area)/p
ΔP	pressure drop
$\Delta_{pc,m}$	maximum capillary force (Pa)
ΔT	temperature difference = ($T_{in} - T_a$) (^oC)
EPBT	energy payback time (years) = $E_{invested}/E_{PV}$
ERF	energy return factor (dimensionless) = Life Time/EPBT
EVA	ethyl vinyl acrelate
E_f	primary energy saving efficiency (%)
F	fin coefficient
F_R	heat removal factor
F'	collector efficiency factor
FF	fill factor
f_v	frictional resistance coefficient
G	solar radiation intensity (W/m^2)
G	minimum filled liquid mass (kg)
g	gravitational acceleration (m/s^2)
H	depth of duct (m)
H_{lg}	latent heat of vaporization (J/kg)
HP	Heat Pipe
$h_{f,i}$	convective heat transfer of fluid ($W/(m^2\ ^oC)$)
h_{fg}	latent heat (J/kg)
I	current (A)
I	incident solar radiation intensity (W/m^2)
k	thermal conductivity (W/(m K))
L	length of collector
L	latent heat of PCM (kJ/kg)

L_e	length of evaporation section of heat pipe (m)
L_a	length of adiabatic section of heat pipe (m)
L_c	length of condenser section of heat pipe (m)
M	merit number (W/m^2)
M_v	Mach number of vapor flow (N/m^2)
MCPCM	Microencapsulated Phase Change Material
m	mass flow rate (kg/s)
N	number of glass covers
N_u	Nusselt number
n_{ele}	PV electrical efficiency (%)
n_f	fin efficiency
n_{power}	efficiency of conventional power (0.38)
n_{th}	System thermal efficiency (%)
n_{tot}	Total PV/T system efficiency (%)
n_{ref}	PV efficiency at reference conditions (%)
P_{max}	power in max power point (W)
P_a	atmospheric pressure (Pa)
P_{sat}	saturation pressure (Pa)
PV/T	Photovoltaic-Thermal
PCM	Phase Change Material
p	channel wetted perimeter = $2D + 2W$ (m)
Q_u or q_u	rate of useful heat gain (W)
q	heat flux (W/m^2)
$q_{s,m}$	sonic limit for heat transport (W)
$q_{e,m}$	entrainment limit for heat transport (W)
$q_{b,m}$	boiling limit for heat transport (W)
$q_{v,m}$	viscous limit for heat transport (W)
q_{max}	maximum heat transport capacity (W)
q_c	heat input (W)
R_v	water vapour constant (J/kg K)
R	universal constant 8317 (J/kg K)

R_e	Reynolds number
r	radius (m)
Ste	Stefan number, i.e ratio of sensible heat capacity to latent heat capacity
T	temperature (^oC)
t	time (s)
U	heat loss coefficient ($W/(m^2\ ^oC)$)
u	flow velocity (m/s)
V	Voltage (V)
W	width of collector (m)
W	tube spacing for tube-and-sheet collector configuration (m)
$X_{capsule}$	percentage concentration of capsules in slurry

Greek

α	absorber plate absorptance
β_r	PV cell temperature coefficient ($1/^oC$)
γ	solar irradiance coefficient for PV module
γ	specific heat ratio
Δ	difference
ε	emissivity
λ	latent heat (J/kg)
μ	dynamic viscocity (kg/m s)
μ	PV efficiency temperature coefficient ($\%/^oC$)
ξ	exergy efficiency
ρ	density (kg/m^3)
σ	the Stefan – Boltzmann constant = 5.6697×10^{-8} ($W/m^2\ K^4$)
σ	surface tension (N/m)
τ_α	transmission absorption coefficient
$(\tau\alpha)$ collector	the transmittance-absorptance product of the photovoltaic–thermal
Φ	angle of inclination relative to horizontal (deg)

Subscript

amb	ambient temperature
b	bottom loss coefficient
ca	the heat transfer coefficient between cell and absorber
col	hybrid PV/T collector
con	condenser
c or conv	convetion
cell	solar cell
e	edge loss coefficient
el	electrical
eff	effective
ev	evaporator
g	glass
in	fluid input temperature
L	overall loss coefficient
L or l	liquid
m	PCM melt temperature (^{o}C)
mp	maximum power point
NOCT	nominal operating cell temperature
oc	open circuit
out	fluid output temperature
PV	Photovoltaic
r or rad	radiation
ref	reference
S or s	solid
sc	short circuit
t	overall heat transfer coefficient from solar cell to ambient through glass cover
th	thermal
v	vapor

Figure List

Chapter 1:

Figure 1.1 Global Key Indicators Graph.....1

Figure 1.2 World Primary Energy Consumption.....2

Figure 1.3 Oil and Gas Prices..... 3

Figure 1.4 UK Energy Generation Mix..... 4

Figure 1.5 Breakdown of Energy Consumption by Sector..... 5

Figure 1.6 Breakdown of Domestic Energy Consumption.....6

Figure 1.7 Global Temperature Changes.....6

Figure 1.8 Breakdown of CO_2 Emissions in UK..... 7

Figure 1.9 CO_2 Emissions in Residential Sector..... 7

Figure 1.10 Renewable Energy Technologies Growth Rate..... 8

Figure 1.11 Cumulative Installed PV Power in UK..... 10

Chapter 2:

Figure 2.1 Distribution of the worldwide installed capacity by collector type..... 19

Figure 2.2 Flat Plate Solar Collector..... 21

Figure 2.3 Different Absorber Plate Designs..... 23

Figure 2.4 Glass – Metal Evacuated Tube Solar Collector.....25

Figure 2.5 Glass – Glass Evacuated Tube Solar Collector..... 26

Figure 2.6 Collector efficiencies of various liquid collectors.....31

Figure 2.7 Direct and Indirect Solar Water Heating Systems.....32

Figure 2.8 Passive and Active Solar Water Heating Systems..... 33

Figure 2.9 Diagram of a photovoltaic cell..... 36

Figure 2.10 Mono - crystalline Silicon Cell..... 37

Figure 2.11 Multi – crystalline Silicon Cell..... 38

Figure 2.12 Amorphous Silicon Cell..... 38

Figure 2.13 Cadmium Telluride Cell..... 39

Figure 2.14 Photovoltaic cells, modules, panels and arrays..... 40

Figure 2.15 Major photovoltaic system components..... 41

Figure 2.16 Diagram of grid-connected photovoltaic system..... 42

Figure 2.17 Direct-coupled PV systems..... 42
Figure 2.18 Diagram of stand-alone PV system with battery storage powering DC and AC loads..... 43
Figure 2.19 Measurement circuit for a PV-cell's characteristic curve..... 43
Figure 2.20 Typical I-V curve of a PV module..... 44
Figure 2.21 Current–voltage characteristics of a 72-cell PV module at: 25 and 60 °C under the irradiance of 830 W/m^2..... 46
Figure 2.22 Temperature dependence of the maximum output power..... 46
Figure 2.23 Cross section of a PV/T collector..... 50
Figure 2.24 A typical water PV/T collector..... 51
Figure 2.26 Example of an air PV/T collector..... 53
Figure 2.27 Cross-sectional view of PVT/Air collector models..... 54
Figure 2.28 Typical thermal efficiency curves for PV/T collectors and PV/T panels56
Figure 2.29 Thermal Efficiencies of a PV/T-liquid collector..... 57
Figure 2.30 The loss mechanisms in the PV/T collector. Note the large effect of radiation losses from the PV/T absorber to the top glass, compared to convective and back loss..... 58
Figure 2.31 Starting from the efficiency curve for the liquid PV/T collector, successively removing the special features of the PV/T module finally results in the curve for a conventional solar thermal collector. h_{ca} is the heat transfer coefficient between cells and absorber..... 59
Figure 2.32 Thermal efficiency affected by the optical characteristics of an absorber60
Figure 2.33 Heat Removal Factor versus Thermal Resistance (PV/T-liquid collector; calculated from Hottel–Whillier model adapted for PV/T as described in Zondag et al. (2002). U_L = 6 W/m^{2}K corresponds to a glazed PV/T module and U_L = 16 W/m^{2}K to an unglazed module..... 63
Figure 2.34 Two absorber PV/T air model..... 66
Figure 2.35 Thermal and electrical efficiencies with respect to mass flow rate for various thermal conductances between absorber plate and tubes; 1: 10,000 W/m K (best conductance), 2: 100 W/m K, 3: 45 W/m K, 4: 25W/ m K..... 68
Figure 2.36 Electrical Efficiencies of a PV/T-liquid collector..... 69

Figure 2.37 Cell Efficiency drop per °C of increase..... 70
Figure 2.38 Effect of tube spacing on average absorber temperature (G_{py}= 800W/m^2, τα =0.8). The figure is calculated from the Hottel–Whillier model adapted for PV/T as described in Zondag et al. (2002). h_{ca} is the heat transfer coefficient between cells and absorber..... 71
Figure 2.39 Schematics of the various PV/T models..... 74
Figure 2.40 Schematic diagram of an integrated PV/T System (IPVTS)..... 74
Figure 2.41 The front view of the flat-box PV/T collectors..... 75
Figure 2.42 Experimental dual PV/T models..... 76
Figure 2.43 Comparison between the 1D, 2D and 3D thermal models..... 77
Figure 2.44 Heat pipe construction and principle of operation..... 85
Figure 2.45 Predicted Heat Pipe Limitations..... 87
Figure 2.46 Heat pipes performance with wick or no and with various angles..... 88
Figure 2.47 Common Wick Structures..... 88
Figure 2.48 The actual test results of heat pipe with different wick structure at a) horizontal and b) vertical (gravity assist) orientations..... 89
Figure 2.49 Performance of copper water groove heat pipe at vertical orientation...90
Figure 2.50 Groove wick heat pipe operated at inclination condition..... 91
Figure 2.51 Comparison of round and flat heat pipes under different orientations...91
Figure 2.52 A cross section of a Flat Heat Pipe.....94
Figure 2.53 Rectangular Micro Heat Pipe..... 95
Figure 2.54 Variable Conductance Heat Pipe, a) Condenser partially active b) Condenser fully active..... 96
Figure 2.55 Capillary pumped loop heat pipe..... 96
Figure 2.56 Schematics of a pulsating heat pipes and its design variations..... 97
Figure 2.57 Capillary and gravity induced heat pipes. (a) Conventional gravity assisted heat pipe. (b) Capillary induced heat pipes..... 98
Figure 2.58 Gravity assisted heat pipe (a) with separator only, (b) with separator and wick at the evaporator only..... 100
Figure 2.59 The experimental assembly: (a) CEOHP flat plate solar collector; (b) condenser water tank; (c) wooden frame..... 101

Figure 2.60 Schematic of a solar heating system assisted by one capillary pump... 101
Figure 2.61 Proposed configuration of the compact Solar Domestic Heating Water system..... 103
Figure 2.62 Cross-sectional views of the prototype wickless heat pipe flat plate solar collector..... 104
Figure 2.63 Experimental set-up of thermosyphon two-phase solar collector together with the temperature measurement points..... 105
Figure 2.64 The two phase thermosyphon system..... 107
Figure 2.65 PV/T Heat pipe based cooling system..... 108
Figure 2.66 Classification of energy storage materials..... 113
Figure 2.67 Supercooling of a phase change material..... 120
Figure 2.68 Stored enthalpy H (J/kg) as a function of temperature T for a material undergoing a phase transition at the melting point T_m..... 121
Figure 2.69 PCM storage allows a narrower temperature range for the system centered on the desired application temperature..... 122
Figure 2.70 The limitations on heat transfer between PCM units and heat carrier during charge and discharge results in temperature degradation and exergy loss..... 123
Figure 2.71 Schematic diagram of a rectangular enclosure with PCM..... 128
Figure 2.72 Comparison of the variation with time of the PCM's temperature at the centre of the rectangular and cylindrical containers..... 129
Figure 2.73 Comparison of the melting time for rectangular and cylindrical containers of equal volume and heat transfer area..... 129
Figure 2.74 The forms and effects of PCM building envelope..... 131
Figure 2.75 Latent heat storage system for solar thermal application..... 133
Figure 2.76 Schematic of the experimental apparatus cross section..... 133
Figure 2.77 Schematic of the hybrid thermal energy storage system..... 134
Figure 2.78 Cross-sectional view of the collector assembly..... 135
Figure 2.79 Schematic view of the solar collector and its parts..... 136
Figure 2.80 Schematic diagram of heat transfer in PV/PCM system..... 137
Figure 2.81 Thermodynamic functions of multifunctional fluids. A Phase Change Slurries can fulfill five or more functions simultaneously..... 141

Figure 2.82 Ice Vs Phase Change Material Micro-encapsulated Slurries..... 142
Figure 2.83 Schematic view of a lightweight wall. The PCM micro-capsules are integrated into the interior plaster..... 150
Figure 2.84 Schematic diagram of the chilled ceiling in the test chamber..... 151
Figure 2.85 A schematic diagram of the system simulated..... 152

Chapter 3:

Figure 3.1 Sketch of the partition of the incoming sunlight converted to electricity or to heat as a function of wavelength..... 155
Figure 3.2 PV operating performance of I-V curve with a) increase in temperature and b) increase in irradiance..... 157
Figure 3.3 Typical current versus voltage measurement system..... 158
Figure 3.4 I-V and P-V characteristics of a typical Si PV cell..... 158
Figure 3.5 Experimental Rig..... 160
Figure 3.6 Tungsten Lamp Emission Spectrum..... 160
Figure 3.7 Spectral response characteristics of cells..... 161
Figure 3.8 Tungsten Halogen Lamp 500 W..... 162
Figure 3.9 SX-20 PV Module..... 162
Figure 3.10 CM3 Pyranometer..... 164
Figure 3.11 Irradiation map of the PV module – a) I_{av} = 993 W/m^2, b) 788 W/m^2, c) 581 W/m^2..... 165
Figure 3.12 Equivalent circuit model of a photovoltaic cell..... 166
Figure 3.13 P-V Curve of the PV module..... 168
Figure 3.14 I-V Curve of the PV module..... 168
Figure 3.15 PV Temperatures for 1000, 800 and 600 W/m^2..... 169
Figure 3.16 Open Circuit Voltage V_{oc} Vs Temperature Difference of PV with 25 °C Reference Temperature..... 170
Figure 3.17 Short Circuit Current Isc Vs Temperature Difference of PV with 25 °C Reference Temperature..... 171
Figure 3.18 PV Power Vs Temperature Difference of PV with the Reference Temperature..... 171
Figure 3.19 P-V Curve of Insulated PV..... 173

Figure 3.20 I-V Curve of Insulated PV..... 173
Figure 3.21 PV Temperatures for 1000, 800 and 600 W/m^2..... 174
Figure 3.22 I-V Curve of PV Free Vs Insulated Panel..... 174
Figure 3.23 P-V Curve of PV Free Vs Insulated Panel..... 175
Figure 3.24 PV Temperature for Free and Insulated Panel at 1000 W/m^2..... 175
Figure 3.25 PV Power for Free and Insulated Panel at 1000 W/m^2..... 176
Figure 3.26 PV Efficiency for Free and Insulated Panel at 1000 W/m^2..... 176

Chapter 4:

Figure 4.1 PV/T model heat balance model..... 181
Figure 4.2 PV/T Thermal Performance with respect to temperature difference of PV with ambient..... 183
Figure 4.3 Flow diagram of the simulation program for PV/T collectors..... 189
Figure 4.4 Two heat exchanger systems used in the back of the PV/T a) the small rectangular water tank b) the copper sheet and serpentine pipe..... 194
Figure 4.5 The rear of the PV covered with the thermal paste..... 195
Figure 4.6 PV/T and Water Temperature with Tank in the back..... 198
Figure 4.7 PV/T and Water Temperature with serpentine pipes in the back..... 199
Figure 4.8 PV/T Electric Efficiency for the Tank, Copper pipe and Simulated model..... 200
Figure 4.9 PV/T Thermal Efficiency for the Tank, Copper pipe and Simulated model..... 200
Figure 4.10 PV/T Water Temperature Difference for the Tank, Copper pipe and Simulated model..... 201
Figure 4.11 PV/T Panel Temperature for the Tank, Copper pipe and Simulated model..... 201
Figure 4.12 PV/T Electric Efficiency for the Tank, Copper pipe and Simulated model..... 202
Figure 4.13 PV/T Thermal Efficiency for the Tank, Copper pipe and Simulated model..... 203
Figure 4.14 PV/T Total Energy Efficiency for the Tank, Copper pipe and Simulated model..... 203

Figure 4.15 PV/T Energy Saving Efficiency for the Tank, Copper pipe and Simulated model..... 204
Figure 4.16 PV/T Exergy Efficiency for the Tank, Copper pipe and Simulated model..... 205

Chapter 5:

Figure 5.1 PV/T using Air as a fluid carrier..... 208
Figure 5.2 PV/T Air Heat Transfer..... 210
Figure 5.3 Schematic diagram of a Fin..... 211
Figure 5.4 PV/T Air Reference Model..... 212
Figure 5.5 PV/T Air Model using fins in the back..... 212
Figure 5.6 Left: Fan used to suck air Right: PV/T Air Rig..... 213
Figure 5.7 PV/T Air Reference Temperature at 0.9 m/s..... 216
Figure 5.8 PV/T Air FIN Temperature model at 0.9 m/s..... 216
Figure 5.9 PV/T for REF and FIN models Temperature at different flow rates and compared with simulation..... 217
Figure 5.10 PV/T for REF and FIN models Air Temperature Difference at different flow rates and compared with simulation..... 217
Figure 5.11 PV/T for REF and FIN models Electrical Efficiency at different flow rates and compared with simulation..... 218
Figure 5.12 PV/T for REF and FIN models Thermal Efficiency at different flow rates and compared with simulation..... 218
Figure 5.13 PV/T for REF and FIN models Electrical Efficiency as a function of Temperature Difference of PV and a Reference Temperature (25 °C) and compared with simulation..... 219
Figure 5.14 PV/T for REF and FIN models Thermal Efficiency as a function of ΔT/G and compared with simulation..... 220
Figure 5.15 PV/T for REF and FIN models Energy Saving Efficiency as a function of ΔT/G and compared with simulation..... 222
Figure 5.16 PV/T for REF and FIN models Total Energy Efficiency as a function of ΔT/G and compared with simulation..... 222

Figure 5.17 PV/T for REF and FIN models Exergy Efficiency as a function of DT/G and compared with simulation..... 222

Chapter 6:

Figure 6.1: Schematic of a gravity assisted heat pipe..... 227

Figure 6.2 Flow chart of programming for heat transfer limitation of heat pipe.... 233

Figure 6.3 Heat transfer limit against working fluid..... 234

Figure 6.4 Liquid Transport Factor K of Water, n-Pentane and HFE-7100..... 236

Figure 6.5 Heat transfer limit against the inner diameter for 60 °C operating temperature..... 236

Figure 6.6 Heat transfer limit against liquid filling level..... 237

Figure 6.7 Heat transfer limit against inclination angle measured from horizontal..... 238

Figure 6.8 Schematic of PV/T heat pipe with tank and manifolds..... 238

Figure 6.9 Heat Pipe Experimental Rigs, a) Heat pipe with Tank, b) Heat pipe with Manifold..... 239

Figure 6.10 Heat Pipe Experiment with Tank..... 240

Figure 6.11 Temperature profile of Heat pipe experiment with Tank..... 241

Figure 6.12 Temperature Difference of Evaporator and Condenser section..... 241

Figure 6.13 Thermal Conductivity of Heat Pipe..... 242

Figure 6.14 Heat Pipe with Manifold Test Rig..... 243

Figure 6.15 Heat Pipe Temperature at Different Power Input..... 244

Figure 6.16 Input Power to Heat Pipe versus Useful Power..... 244

Figure 6.17 Heat Flux Vs Evaporator Temperature..... 245

Figure 6.18 Heat Transfer Coefficient of Heat Pipe..... 245

Figure 6.19 Back of PV with two copper plates incorporating four heat pipes..... 247

Figure 6.20 Effect on the heat removal factor of varying the ratio of the coefficient of heat loss from the collector to the coefficient of heat transfer across the evaporator..... 251

Figure 6.21 Effect on the heat removal factor of varying the ratio of the coefficient of heat loss from the collector to the coefficient of the heat transfer from condensate to manifold..... 252

Figure 6.22 Effect on the heat removal factor of varying the ratio of the heat transfer area at the condenser to the area of collector plate..... 253
Figure 6.23 Effect on the heat removal factor varying the ratio of the resistance to heat loss from collector to the resistance to heat transfer from condensate to manifold..... 254
Figure 6.24 PV/T Heat Pipe with Tank..... 256
Figure 6.25 PV/T Heat Pipe with Tank using Fins..... 256
Figure 6.26 PV/Heat Pipe with Manifolds..... 257
Figure 6.27 Comparison of electrical efficiency of PV/T Heat Pipe with and without Fins 259
Figure 6.28 Comparison of thermal efficiency of PV/T Heat Pipe with or without Fins..... 260
Figure 6.29 PV/Heat Pipe Temperature..... 261
Figure 6.30 Temperature distributions along the length of the pipe..... 262
Figure 6.31 PV/T Heat Pipe Temperature with Manifold..... 263
Figure 6.32 Water Temperature Difference for different flow rates..... 263
Figure 6.33 PV/T Temperature for different flow rates..... 264
Figure 6.34 PV/T Heat Pipe Electrical Efficiency with Manifold..... 264
Figure 6.35 PV/T Heat Pipe Thermal Efficiency with Manifold..... 265
Figure 6.36 Comparison of the PV/T Heat Pipe Electrical Efficiency with Manifold and Tank..... 265
Figure 6.37 Comparison of the PV/T Heat Pipe Thermal Efficiency with Manifold and Tank..... 266
Figure 6.38 Comparison of the PV/T Heat Pipe Total Energy Efficiency with Manifold and Tank..... 268
Figure 6.39 Comparison of the PV/T Heat Pipe Energy Saving Efficiency with Manifold and Tank..... 268
Figure 6.40 Comparison of the PV/T Heat Pipe Exergy Efficiency with Manifold and Tank..... 268

Chapter 7:

Figure 7.1 Schematic diagram of the experimental rig..... 275

Figure 7.2 Experimental results for A28 and Water Sample during cooling..... 277
Figure 7.3 Experimental results for E44 and Water Sample during cooling..... 277
Figure 7.4 A typical T-history curve during cooling process with supercooling.... 278
Figure 7.5 PV/PCM Array Configuration..... 279
Figure 7.6 Cooling Curves for the Solidification of a Pure Material..... 284
Figure 7.7 Duration Index for Phase Change Materials..... 286
Figure 7.8 Comparisons of 4 Phase Change Materials..... 286
Figure 7.9 PV/PCM A28 Temperature performance at different thermal conductivities..... 287
Figure 7.10 PV/PCM A28 Electrical Efficiency at different thermal conductivities..... 288
Figure 7.11 PV/PCM A28 Melting Period for different material thickness..... 289
Figure 7.12 PV/PCM A28 Cooling Period for different material thickness..... 289
Figure 7.13 PV/PCM A28 Performance at different Ambient Temperature..... 290
Figure 7.14 PV/PCM A28 Performance at different Incident Irradiation..... 291
Figure 7.15 Comparing a PV free system with a PV/PCM A28 temperature..... 291
Figure 7.16 Comparing a PV free system with a PV/PCM A28 Electrical Efficiency..... 292
Figure 7.17 Comparison of a PV free system with a PV/PCM A28 Temperature for a typical summer day..... 293
Figure 7.18 Comparison of a PV free system with a PV/PCM A28 Electrical Efficiency for a typical summer day..... 293
Figure 7.19 24 hr predicted electrical conversion efficiency on the front surface of the base case PV and at the front surfaces of system with a PCM depth of 30, 60 and 90 mm with $(T_{pv} - T_{amb})/I$ for a south–east orientation with insolation and ambient temperature for SE England on the 3rd of June. * T_{PV} and T_{amb} are the front surface temperature and ambient temperature, I is insolation W/m^2..... 294
Figure 7.20 Average temperature evolutions for a three day simulation using weather data for the base case PV and at the front surface of PV/PCM system with PCM depths of 30, 60 and 90 mm..... 295

Figure 7.21 Electrical Efficiency evolutions for a three day simulation using weather data for the base case PV and at the front surface of PV/PCM system with PCM depths of 30, 60 and 90 mm..... 296
Figure 7.22 PCM Copper Container..... 297
Figure 7.23 PV/PCM A28 Temperature with low and high thermal conductivity. 298
Figure 7.24 PV/PCM A28 Electrical Efficiency with low and high thermal conductivity..... 299
Figure 7.25 PV/PCM A28 for different incident irradiation conditions..... 300
Figure 7.26 PV/PCM A28 Cooling Process..... 300
Figure 7.27 PV/PCM A28 Container with incorporating Pipes..... 301
Figure 7.28 PV/PCM A28 – Water Temperature..... 302
Figure 7.29 Water Temperature Difference at different Flow Rates..... 303
Figure 7.30 PV Temperature of the PV/PCM system for different Flow Rates.... 303
Figure 7.31 PV/PCM A28 – Water Thermal Efficiency at different Flow Rates... 304
Figure 7.32 PV/PCM A28 – Water Electrical Efficiency at different Flow Rates. 304
Figure 7.33 PV/PCM – Water Thermal Efficiency..... 305
Figure 7.34 PV/PCM – Water Electrical Efficiency..... 305
Figure 7.35 PV/PCM – Water Total Energy Efficiency..... 306
Figure 7.36 PV/PCM – Water Energy Saving Efficiency..... 307
Figure 7.37 PV/PCM – Water Exergy Efficiency..... 308

Chapter 8:

Figure 8.1 Microscopic Photo of Micro-PCM particles..... 313
Figure 8.2 Enthalpy curves of PCS with different concentration of capsules and a melting range from 25 – 27 °C..... 316
Figure 8.4 Glass test tube apparatus for TA measurement..... 318
Figure 8.5 Temperature variations of MCPCM slurries (10% to 40%) in heating mode with PCM melting at 26 °C..... 320
Figure 8.6 Temperature variations of MCPCM slurries (10% to 40%) in heating mode with PCM melting at 33 °C..... 320
Figure 8.7 Temperature variations of MCPCM slurries (10% to 40%) in cooling mode with PCM melting at 26 °C..... 321

Figure 8.8 Temperature variations of MCPCM slurries (10% to 40%) in heating mode with PCM melting at 33 °C..... 321
Figure 8.9 a) One way flow rig b) Closed loop rig..... 323
Figure 8.10 Left – Primary Circuit, Right – Secondary Circuit..... 325
Figure 8.11 Left – Pump of Primary Circuit, Right – Heat Exchanger Unit connecting Primary and Secondary circuit..... 325
Figure 8.12 Operation cycle of the experiment..... 326
Figure 8.13 Calibration of the PV/Thermal system using Water..... 329
Figure 8.14 Thermal Power Calibration of the PV/Thermal system using Water... 329
Figure 8.15 PV/MCPCM Slurry Melting Temperature at 26 °C..... 330
Figure 8.16 Temperature difference at various irradiation between water and MCPCM 20% (26 °C)..... 330
Figure 8.17 Thermal Efficiency of PV/MCPCM system in comparison with water at different irradiations..... 331
Figure 8.18 Pump Power Consumption of Water & MCPCM Slurry (20% - 26 °C)..... 331
Figure 8.19 PV/MCPCM Thermal Efficiency in comparison with water and MCPCM slurry (26 oC and 33 oC PCM)..... 333
Figure 8.20 PV/MCPCM Electrical Efficiency in comparison with water and MCPCM slurry (26 °C and 33 °C PCM)..... 334
Figure 8.21 PV/MCPCM Total Energy Efficiency in comparison with water and MCPCM slurry (26 °C and 33 °C PCM)..... 334
Figure 8.22 PV/MCPCM Energy Saving Efficiency in comparison with water and MCPCM slurry (26 oC and 33 oC PCM)..... 335
Figure 8.23 PV/MCPCM Exergy Efficiency in comparison with water and MCPCM slurry (26 °C and 33 °C PCM)..... 335
Figure 8.24 PV/MCPCM Exergy Efficiency in comparison with water and MCPCM slurry (26 °C and 33 °C PCM) at a range of ΔT/G from 0.001 to 0.11..... 336

Chapter 9:

Figure 9.1 PV/Thermal Systems - Electrical Efficiency Comparison..... 339
Figure 9.2 PV/Thermal Systems - Thermal Efficiency Comparison..... 340

Figure 9.3 PV/Thermal Systems - Total Energy Efficiency..... 341
Figure 9.4 PV/Thermal Systems - Energy Saving Efficiency Comparison..... 342
Figure 9.5 PV/Thermal Systems - Exergy Efficiency..... 343
Figure 9.6 Uni-Solar-64 Thin Film PV Characteristics..... 345
Figure 9.7 Global Incident Irradiation in Collector Plane..... 346
Figure 9.8 Sustainable Research Building PV Monthly Energy Production..... 346
Figure 9.9 kg of CO2 emissions saved every month..... 347
Figure 9.10 Monthly Inverter Efficiency..... 347
Figure 9.11 Monthly Performance Ratio..... 348
Figure 9.12 Monthly PV Plant Overall Efficiency..... 348
Figure 9.13 Payback Period for PV and PV/Thermal Systems for diffent panel area..... 352
Figure 9.14 Payback period of PV and PV/Thermal Systems for different cost of electricity..... 353
Figure 9.15 Payback period of PV and PV/Thermal Systems for different percentage contribution of grant schemes..... 353
Figure 9.16 Cost of the PV and PV/Thermal systems per kWh energy produced..... 354
Figure 9.17 PV and PV/Thermal Technologies EBPT, CO_2 Payback and ERF... 369
Figure 9.18 Emissions of CO2 saved per year with different PV panel area..... 369
Figure 9.19 Greenhouse gas emissions of PV systems based on thin film technologies, compared with a number of other energy technologies. The PV systems are installed on a roof-top in UK (irradiation 888 kWh/m^2/yr) and have a 30 year life time. N.B. The emission from a coal-fired power plant (1000 gr/kWh) exceeds the Y-axis maximum (Sources: Coal, CC gas, nuclear, biomass and wind data derived from Ecoinvent database [6])..... 370

Table List

Chapter 1:

-

Chapter 2:

Table 2.1 Different Collector Types Thermal Efficiency and Thermal Loss Factor 29

Table 2.2 Photovoltaic Cell Efficiencies..... 39

Table 2.3 PV dependence of efficiency from temperature effect..... 47

Table 2.4 PV temperature coefficients for different type of cells..... 48

Table 2.5 Efficiency comparison between Single and Double pass PV/T..... 73

Table 2.6 Thermal and electrical efficiencies of various design concepts..... 75

Table 2.7: Various working fluids and their useful range..... 93

Table 2.8 Organic Substances with potential use as PCM..... 114

Table 2.9 Inorganic substances with potential use as PCM..... 114

Table 2.10 Eutectics with potential use as PCM..... 115

Table 2.11 Comparison of Organic and Inorganic Materials Advantages and Disadvantages..... 115

Table 2.12 Comparison of various thermal storage media..... 116

Table 2.13 Commercial PCM Products..... 124

Table 2.14 PCM useful for Building Applications..... 131

Table 2.15 Classifications of Solar Air Heaters..... 132

Chapter 3:

Table 3.1 Values of P_{max}, V_{mp}, I_{mp}, V_{oc} and I_{sc} for 1000, 800 and 600 W/m^2..... 167

Table 3.2 Values of P_{max}, V_{mp}, I_{mp}, V_{oc} and Isc for 1000, 800 and 600 W/m^2..... 172

Chapter 4:

Table 4.1 PV/T parameters and inputs used for evaluating the specific output..... 190

Chapter 5:

Table 5.1 PV/T Air electrical efficiencies for experimental and simulated models. 219

Table 5.2 PV/T Air thermal efficiencies for experimental and simulated models.. 221

Chapter 6:

Table 6.1 Parameters against conditions for vapour pressure drop..... 230

Table 6.2 Thermal Conductance of the heat pipe..... 246

Table 6.3 Heat pipe dimensions..... 248
Table 6.4 PV/T Heat Pipe Electrical and Thermal Linear Equations for Manifold and Tank models..... 267
Chapter 7:
Table 7.1 PCM Properties of A28 and E44 given and calculated..... 278
Table 7.2 EPS provided Thermo-Physical Properties of Phase Change Material (EPS Ltd)..... 297
Chapter 8:
Table 8.1 Physical Properties of MCPCM Slurry (26 °C) and its Components..... 314
Table 8.2 Heat input and output of the PV/MCPCM collector system using water as the primary working fluid..... 328
Chapter 9:
Table 9.1 Electrical and Thermal Efficiency Equations of PV/T Systems..... 340
Table 9.2 PV/T systems - total energy, energy saving and exergy efficiency equations..... 343
Table 9.3 PV and PV/Thermal Panel Cost Estimation for 1 m^2..... 349
Table 9.4 Monthly Electrical and Thermal Energy Produced for 1 m^2 of PV and PV/Thermal Panel..... 350
Table 9.5 Payback period, annual CO_2 emission saving and cost of a PV system per kWh of energy produced..... 351
Table 9.6 Estimates of energy payback times for various solar technologies..... 359
Table 9.7 Factors affecting the EPBT of a system..... 360
Table 9.8 Primary energy requirements for the production of PV modules (REF)..... 361
Table 9.9 Energy requirements for the production of PV components..... 363
Table 9.10 PV and PV/Thermal Components and Materials Energy Requirements..... 367

CHAPTER 1: INTRODUCTION

1.1 Background

At present, the large scale use of fossil fuels is a dominant feature of industrial societies. It is regarded as essential for the growing, distribution and preparation of foods, for construction, manufacturing, communication and organisation activities. Also fossil fuels are used for the construction and operation of buildings that host a range of different energy services including in particular: heating, cooling, appliances and lighting.

Energy fuelled the industrial revolution and has continued to drive economic development. The *Figure 1.1* shows the close link between economic prosperity and energy use – especially electricity. The graph also shows how greenhouse gas emissions have followed the curve of energy use, and are expected to continue to rise if consumption continues unabated.

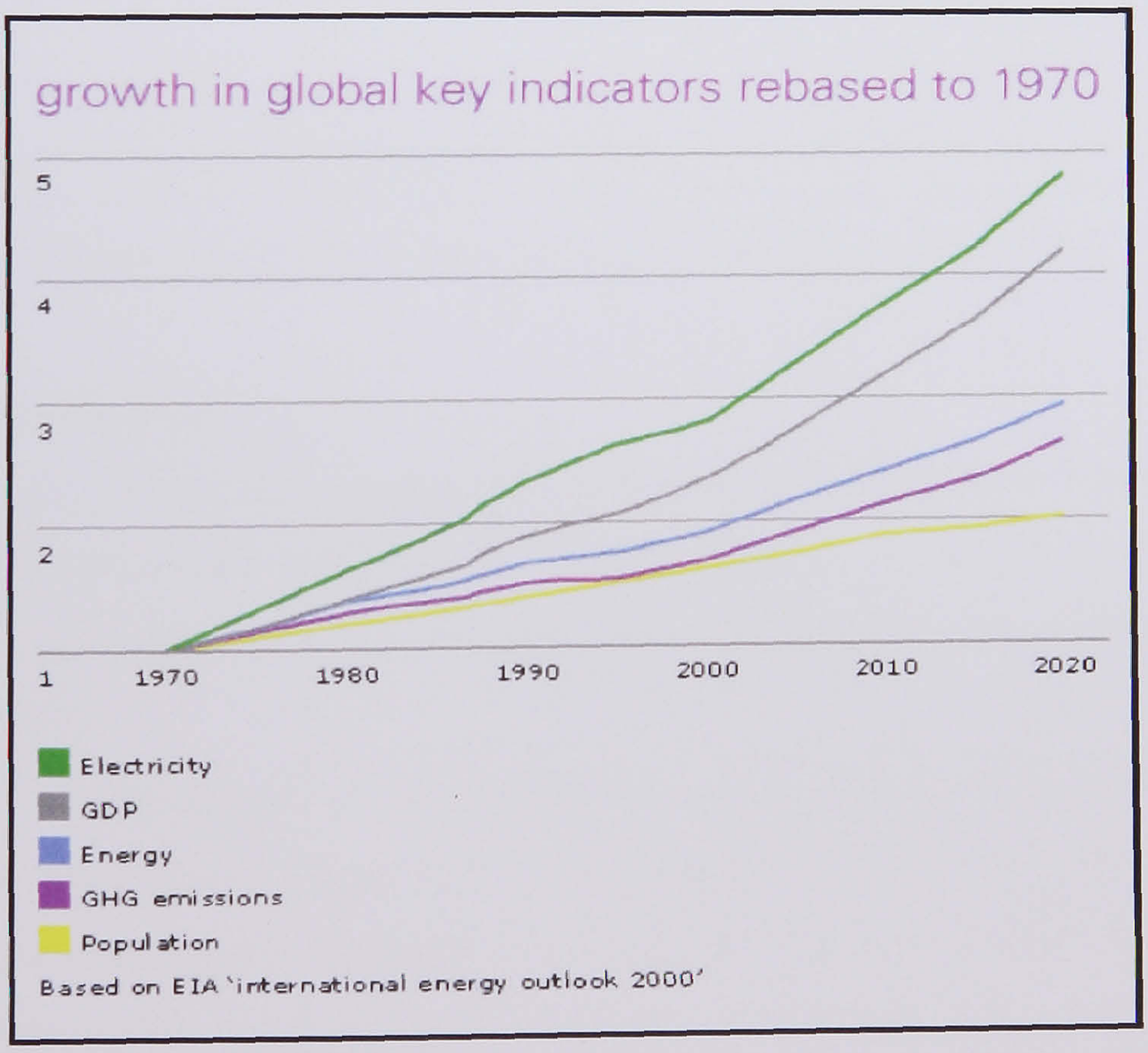

Figure 1.1 Global Key Indicators Graph (EIA 2000)

In 2000, the estimated total world consumption of primary energy, in all forms, was approximately 417 EJ per year, equivalent to some 9,958 million tonnes of oil per year (BP, 2006). Assuming a world population of about 6000 million in that year, this gives an annual average fuel use for every man, woman and child in the world equivalent to about 1.66 tonnes of oil. A breakdown of world primary energy consumption by source until 2030 in is shown in *Figure 1.2*. Figure shows that coal, oil and gas will still be the dominant energy sources but with a new rival coming from renewable energy.

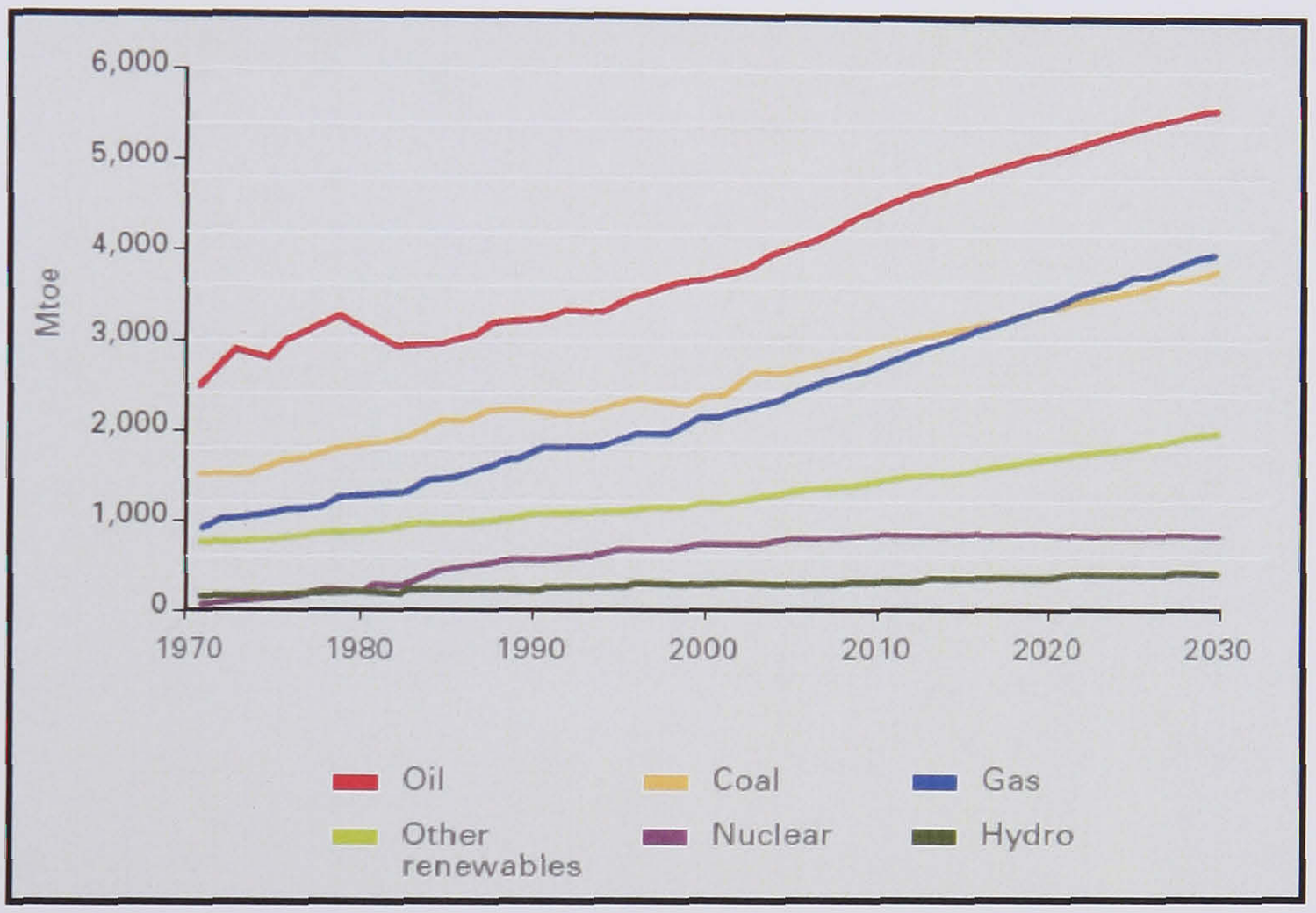

Figure 1.2 World Primary Energy Consumption (IEA 2005)

1.1.1 Oil and Gas Prices

The distribution of fossil fuels around the world is uneven. The Middle East possesses more than half of the known oil reserves. This fact leads to economical instabilities around the world which affect the whole economic and geopolitical system (Roger Kubarych, 2005).

Figure 1.3 shows the price of oil and gas during the last 6 years. Oil prices have more than doubled and coal prices have risen by nearly a third over the last three years. Gas prices have also increased by more than 50% over the same period. There are many reasons for the increase of oil and gas prices. Labor strikes, hurricane threats to oil platforms, fires and terrorist threats at refineries, and other short-lived problems are

solely responsible for the higher prices. Such problems periodically push prices higher, but they are neither fundamental nor long-lived. A possible fundamental problem that some believe causes the price to rise involves peak oil. Not only is there a limited amount of fossil fuel which has been burnt as fuel, but the remaining accessible supply will be consumed more rapidly by a growing, industrializing Third World. What remains becomes more difficult to extract as the easiest wells have been tapped. Producing many remaining known reserves is more technically difficult and therefore more expensive, so it is only economically feasible in high price environments. The remaining sources either have not been discovered yet, or at this point in time are unable to be utilized due to political or other reasons in the countries of discovery (Wikipedia, 2007).

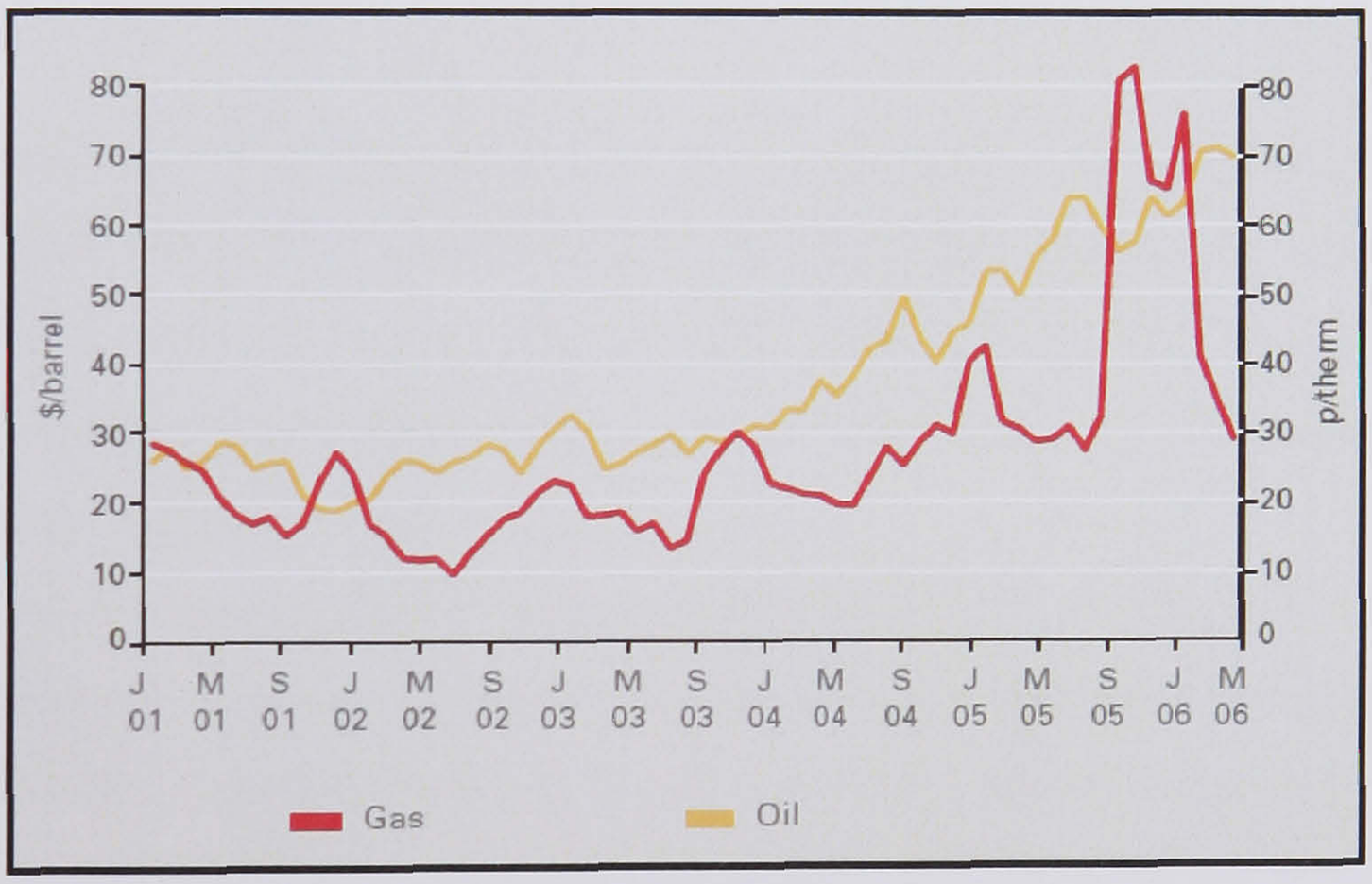

Figure 1.3 Oil and Gas Prices (IEA 2005)

1.1.2 UK Electricity Generation Mix

Today around 90% of the UK's energy needs are met by fossil fuels, and they will continue to be the predominant source of energy for decades to come as may be seen from *Figure 1.4*. UK currently benefits from a diverse electricity generation mix; 37% is generated by gas-fired power stations, 34% from coal, 20% from nuclear, 5% from renewable and the remainder from other sources (DTI, 2006). This diverse generation

mix reduces the UK's dependency on a single fuel type and helps maintain a secure supply of electricity.

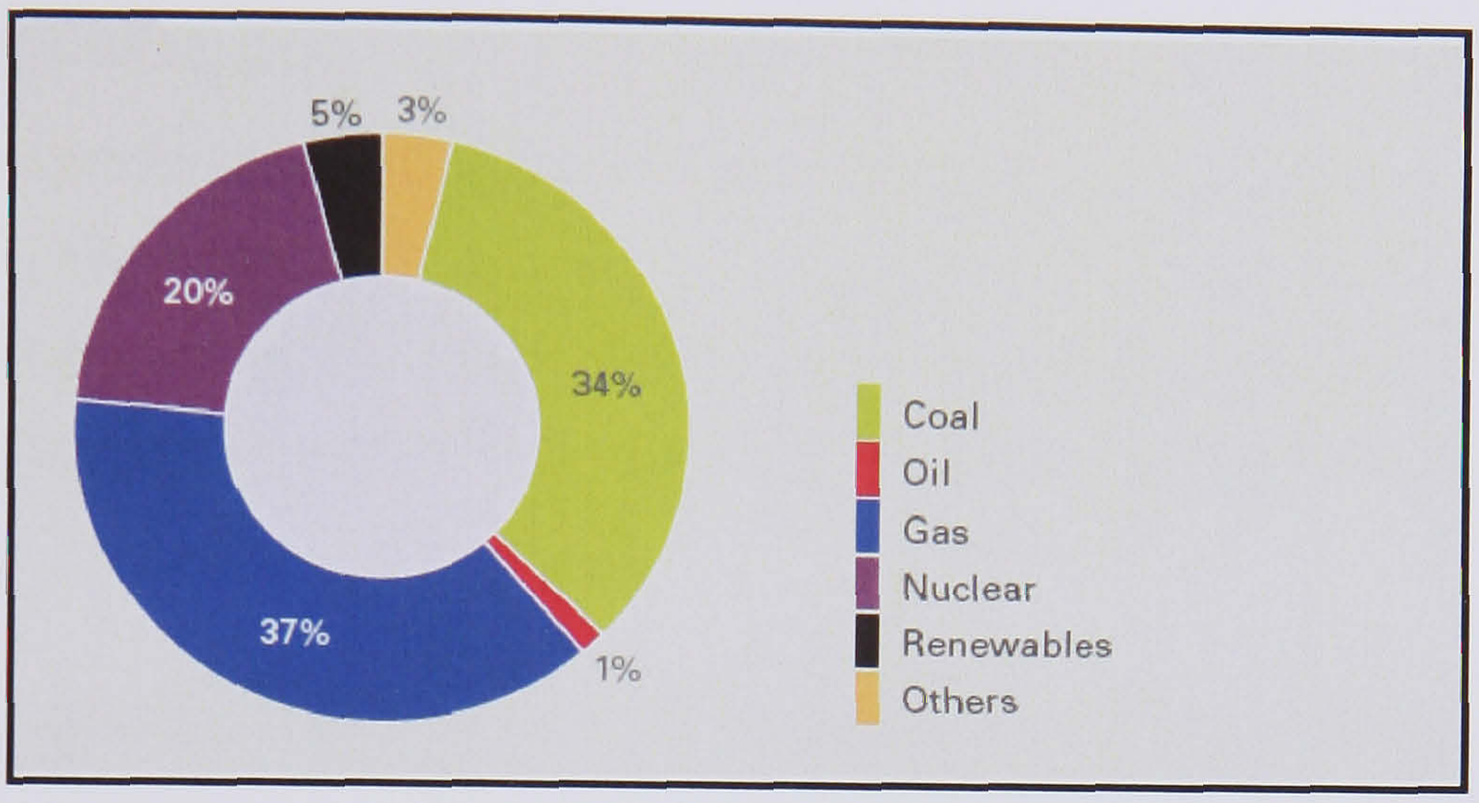

Figure 1.4 UK Energy Generation Mix (DTI, 2006)

But as production from its own oil and gas fields and coal reserves declines the UK's shortage of fuel will be covered by imports. By 2010, imports could be meeting up to 40% of the UK's total gas demand, rising to 80 – 90% by 2020. The UK is also expected to become a net importer of oil (on a sustained basis) by 2010, and is already a net importer of coal (DTI, 2006).

Over the next two decades the UK will need substantial new investment in electricity generation capacity to replace absolute coal, oil and nuclear power stations and to meet expected growth in electricity demand. In total, the UK is likely to need around 25GW of new electricity generation capacity by 2025, equivalent to more than 30% of today's existing capacity (DTI, 2006). Developments in low carbon technologies and improvements in energy efficiency offer the potential to reduce demand and thus decrease the reliance on imported fossil fuels.

1.1.3 UK Energy Consumption Sectors

To understand how best to make use of renewable sources, and also to understand fully the problems caused by the present use of fuels, it is helpful to take a closer look at the way energy is currently used in industrial societies.

To make some sense of the great variety of energy use, it is necessary to categorise it. In most official statistics human activity is divided into four main sectors:

- The *transport* sector
- The *domestic* sector
- The *commercial* and *institutional* sector
- The *industrial* sector

The first question to consider is how much energy is used by each sector. The domestic sector comprises the second most important energy consumer as may be seen from *Figure 1.5*.

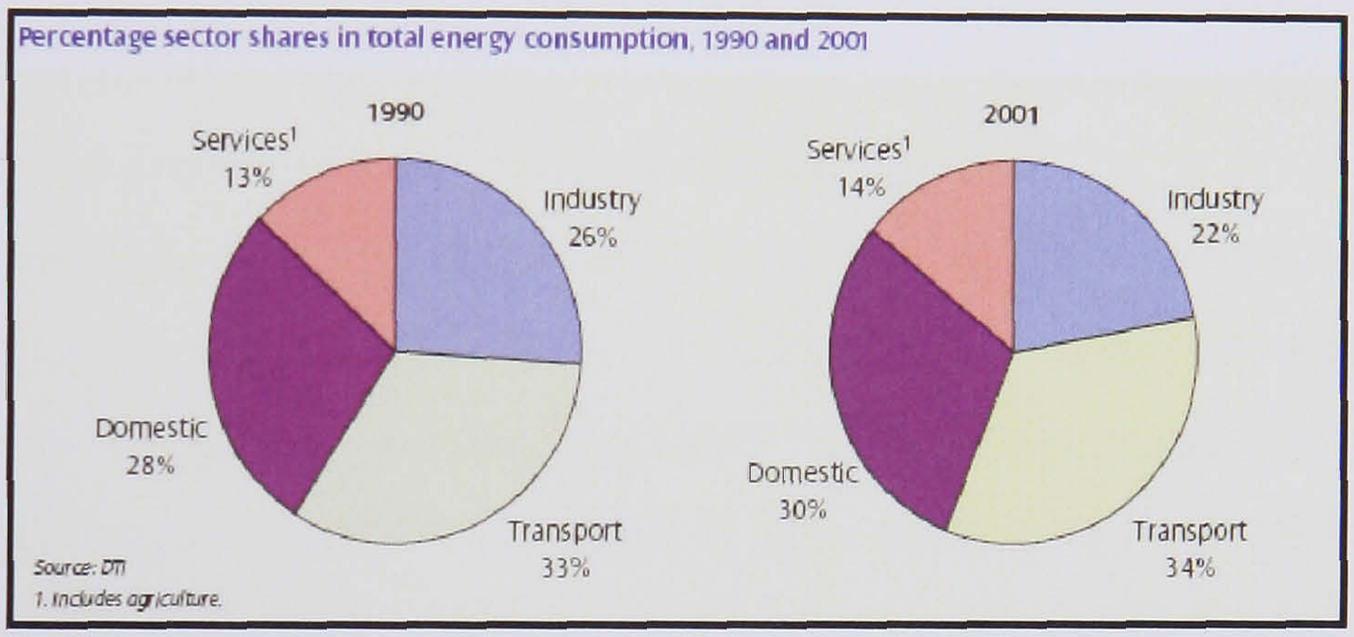

Figure 1.5 Breakdown of Energy Consumption by Sector (DTI 2006)

The total demand in the UK domestic sector has increased because of the socio-demographic changes that have occurred during the last three decades. These changes include:

- Increased rate of population in the UK
- Increase in the number of people that live alone
- Increase in the household numbers

The principal uses of energy in the domestic sector, which is the main area of concern in this thesis, are for space heating, water heating, cooking, lighting and electrical appliances. *Figure 1.6* gives an overall picture of energy use in the domestic sector.

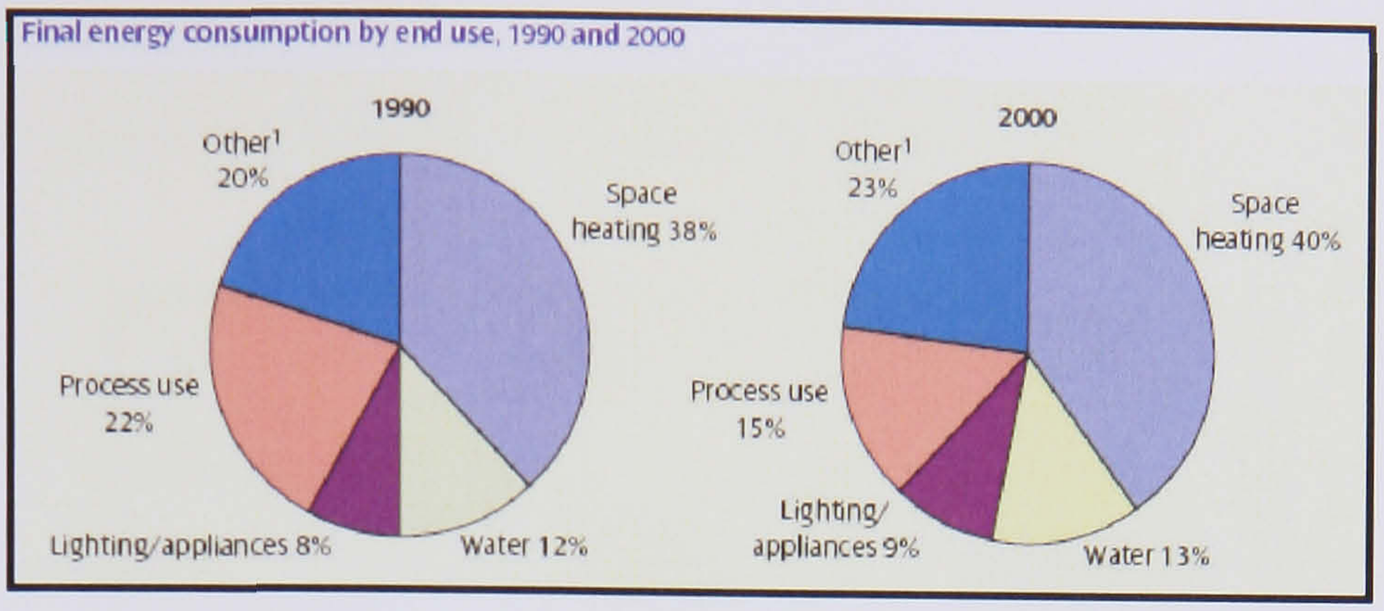

Figure 1.6 Breakdown of Domestic Energy Consumption (DTI 2006)

1.1.4 Environmental Impact

Today the energy related problems that hit the headlines most often are environmental ones. Various environmental problems look large in the public consciousness at present. Many of these are largely a result of large scale fuel use.

One of the most significant problems appears to be that of global warming, a gradual increase in the global average air temperature at the earth's surface. The majority of scientists believe that global warming is probably taking place, at a rate of around 0.3 ^{o}C per decade, and that it is caused by increases in the concentration of so called 'greenhouse gases' in the atmosphere. *Figure 1.7* shows the global temperature changes from 1880 until 2000.

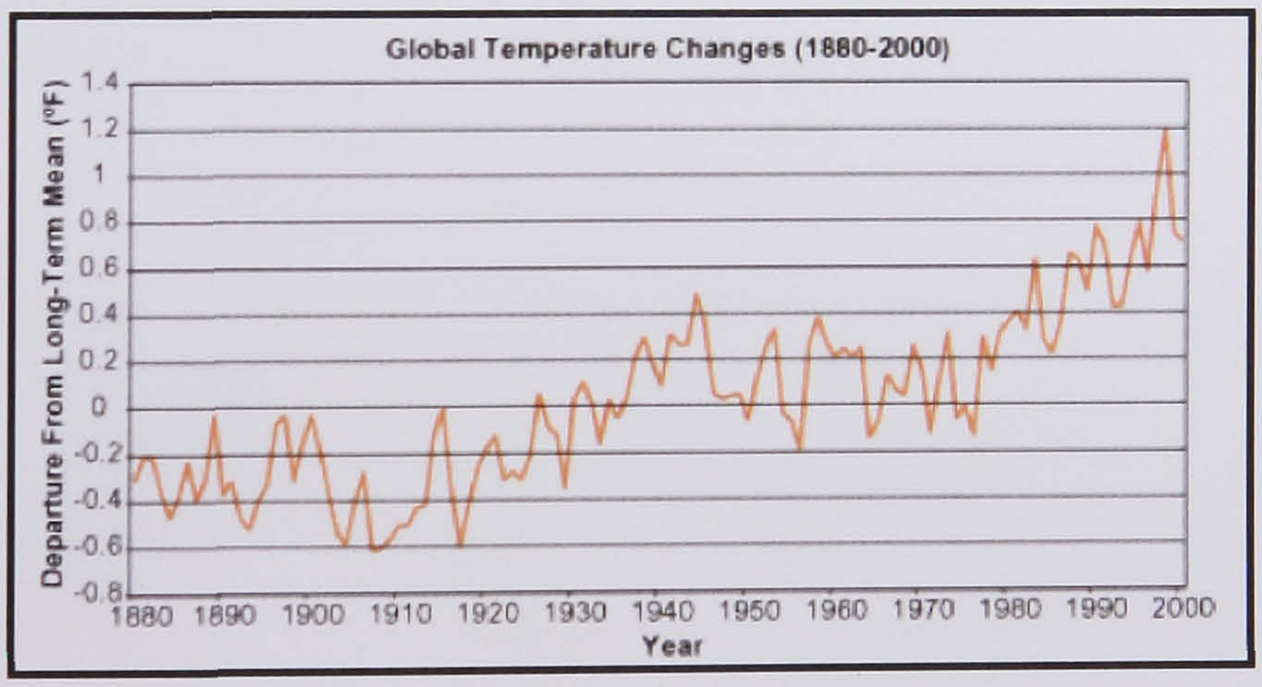

Figure 1.7 Global Temperature Changes (Matter and energy laws, 2007)

The most significant single component of these greenhouse gas emissions is carbon dioxide (CO_2) released by the burning of fossil fuels. The UK contributes around 2% of

the global CO_2 emissions. The emissions from residential sector account to 28% of the total emissions generated from UK as indicated in *Figure 1.8*.

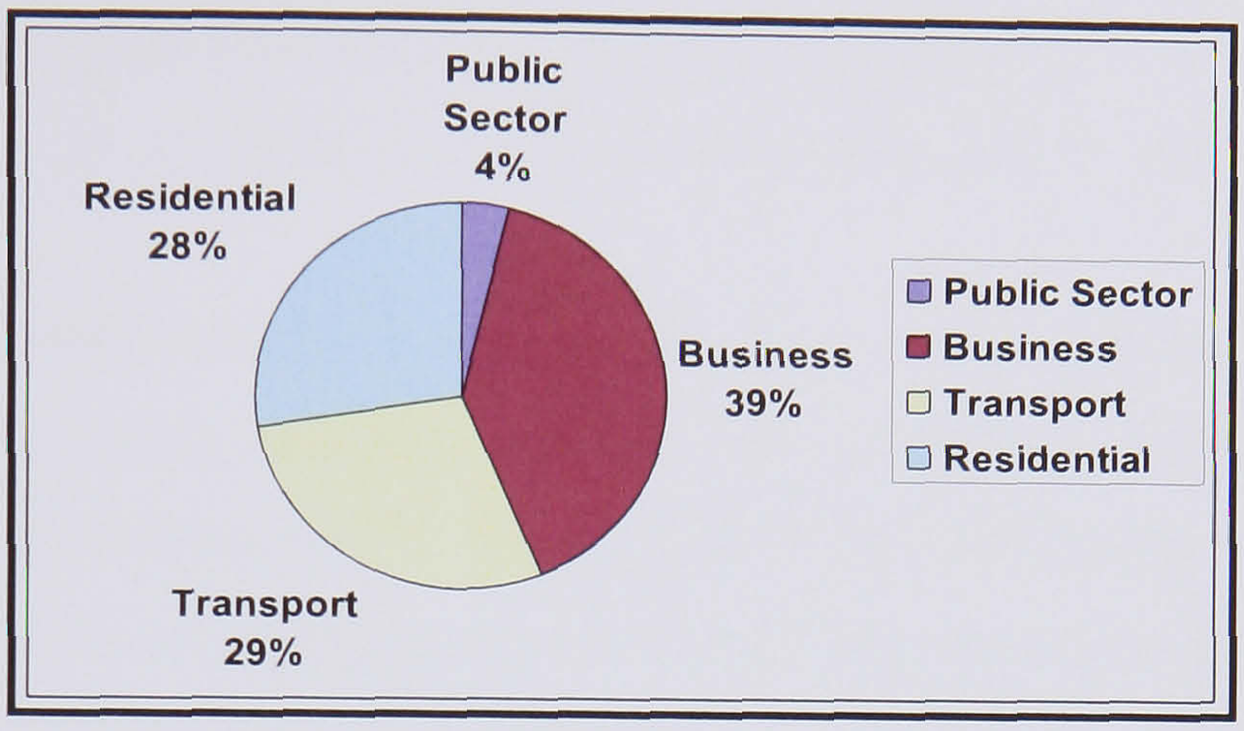

Figure 1.8 Breakdown of CO_2 Emissions in UK (DTI, 2006)

Of these emissions the majority, around 73%, stem from the need for space and water heating (*Figure 1.9*). Space heating and hot water represent the largest demand, and the required energy is "low quality" heat characterized by obtaining temperature differences in the range of 10 – 70 °C (SHIA, 2006). In the industrialized world this demand for low temperature heat is usually covered by consuming "high quality" resources such as fossil fuels, which are both limited in abundance and have a negative effect on the global environment. So in order to reduce the negative effects we could use renewable energy such as solar energy to provide the necessary low quality heat for building operation.

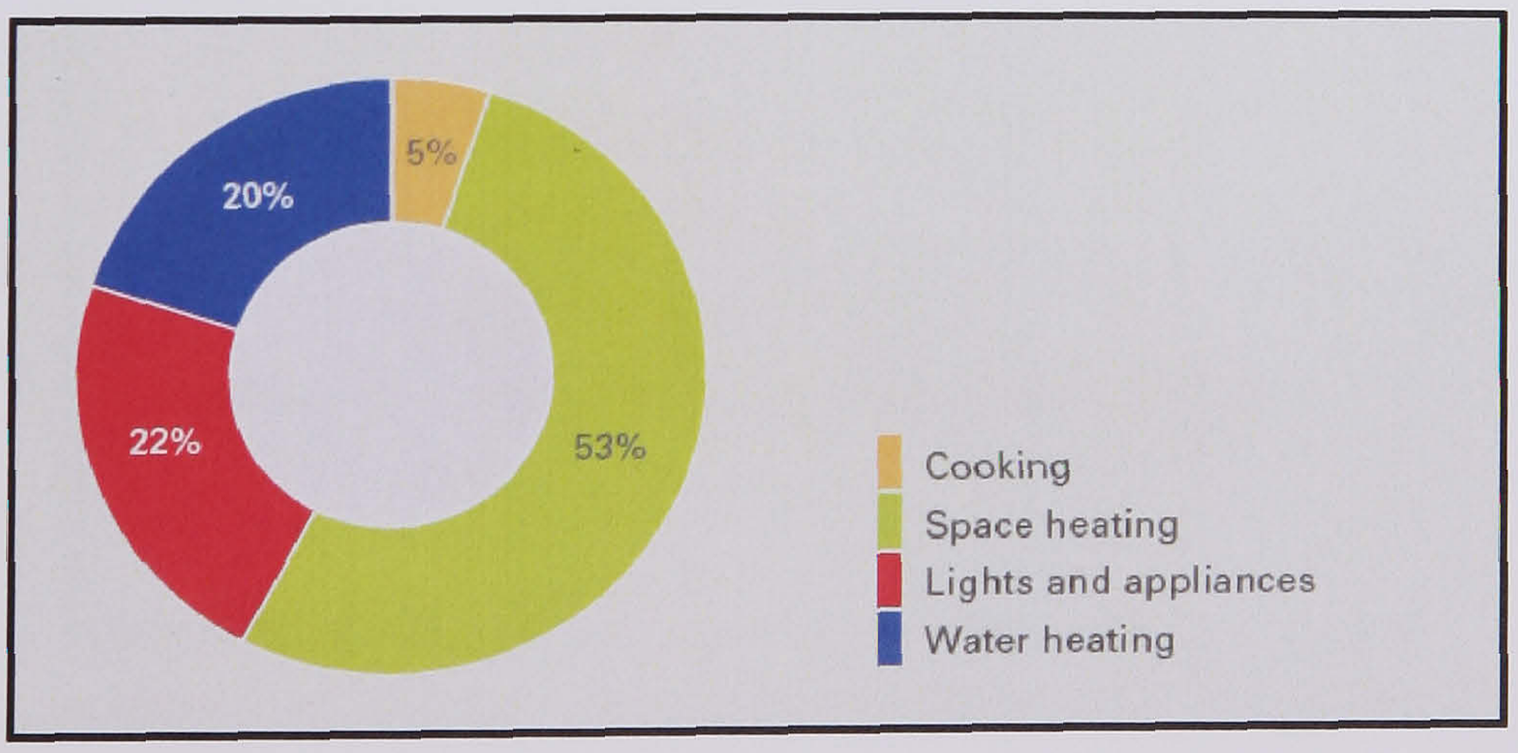

Figure 1.9 CO_2 Emissions in Residential Sector (DTI, 2006)

1.1.5 Renewable Energy

After considering the ways in which energy is used and the scale of its use and after looking at the various problems associated with the current use of fossil and nuclear fuels such as the environmental impact we are now in a position to look more closely at renewable sources, to see whether and to what extent they offer solutions to these problems.

Most renewable energy sources are derived from solar radiation, including the direct use of solar energy for heating or electricity generation, and indirect forms such as energy from the wind, waves and running water, and from plants and animals. Tidal sources of energy result from the gravitational pull of the moon and sun, and geothermal energy comes from the heat generated within the earth.

The use of renewable on a more significant scale than at present would at the very least replace a further significant proportion of fossil and nuclear fuel use, thereby reducing the associated environmental impacts. As may be seen *Figure 1.10* renewable energy technologies underwent significant growth in the period of 2000-2004.

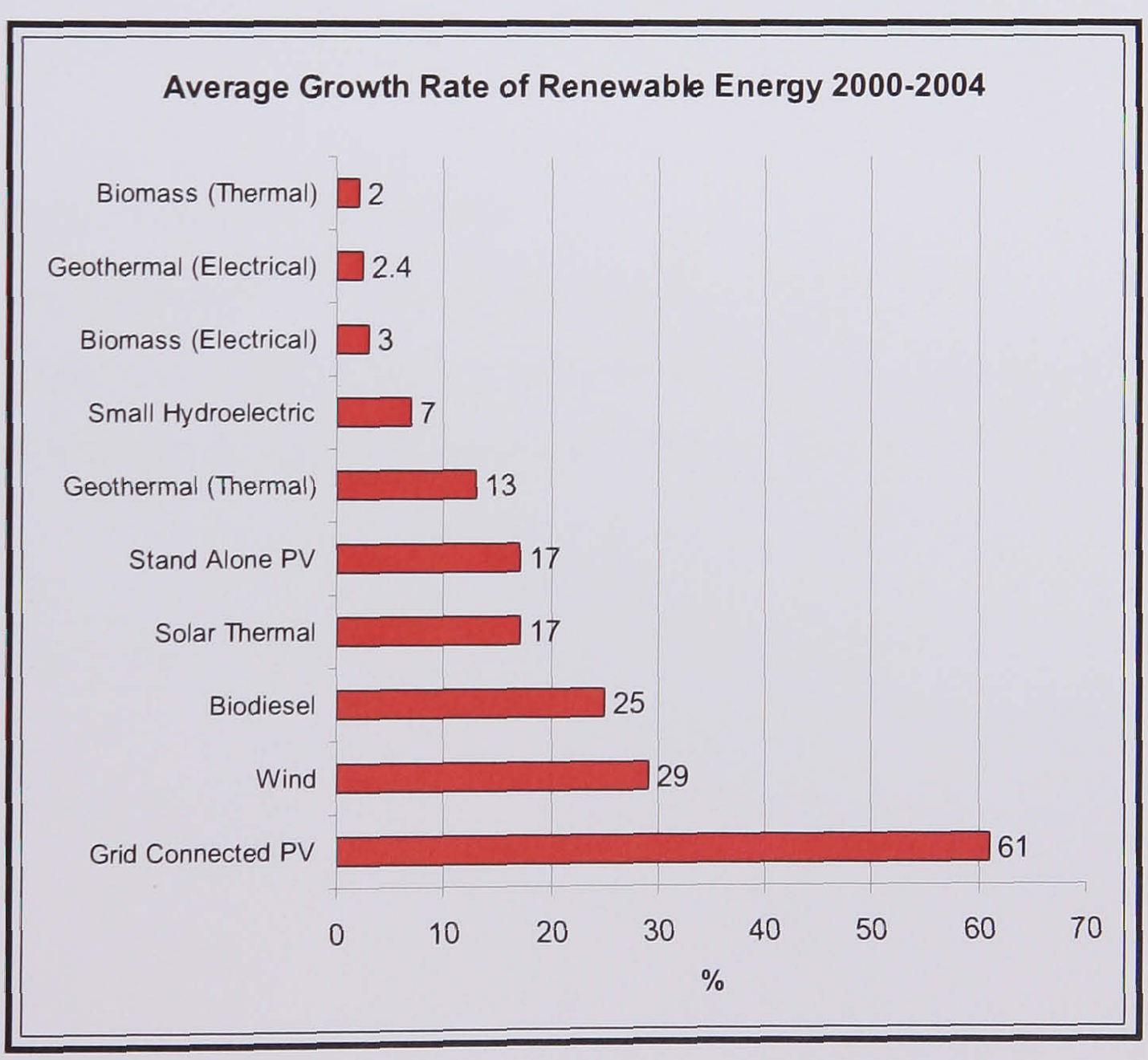

Figure 1.10 Renewable Energy Technologies Growth Rate (World Watch Institute 2006)

1.1.6 General description of Solar Energy

The conversion of solar energy to electrical and thermal energy has been practiced for many years. In order to convert the solar energy to electrical, photovoltaics are used. The widely used heat collection systems are flat-plate collectors for thermal applications.

PV

Photovoltaic panels in particular can provide a good source of *clean* electricity. The photovoltaic effect was first discovered by the physicist Edmund Becquerel in 1839. Present photovoltaic technology has been well developed since 1941. PV panels are used as the primary electricity source in space missions and satellites. The cost of producing electricity for house applications has dropped dramatically and increasingly PV panels are becoming economicaly viable. New materials have been developed and new technology has created PV panels at efficiencies of 20% in many cases.
Photovoltaic panels convert solar radiation to electricity with efficiencies in the range of 5% to 20%, depending on the type of the solar cell, radiation level and cell temperature. Polycrystalline silicon solar cells offer the highest range of possibilities for applications.

The PV Industry - Installed PV power

The rate of annual installed PV capacity was similar to that in 2004. A total of 2,713 kW was installed in the UK in 2005. The cumulative installed PV generation capacity increased by over 33 % during 2002 reaching a total of 10.9 MW (*Figure 1.11*).

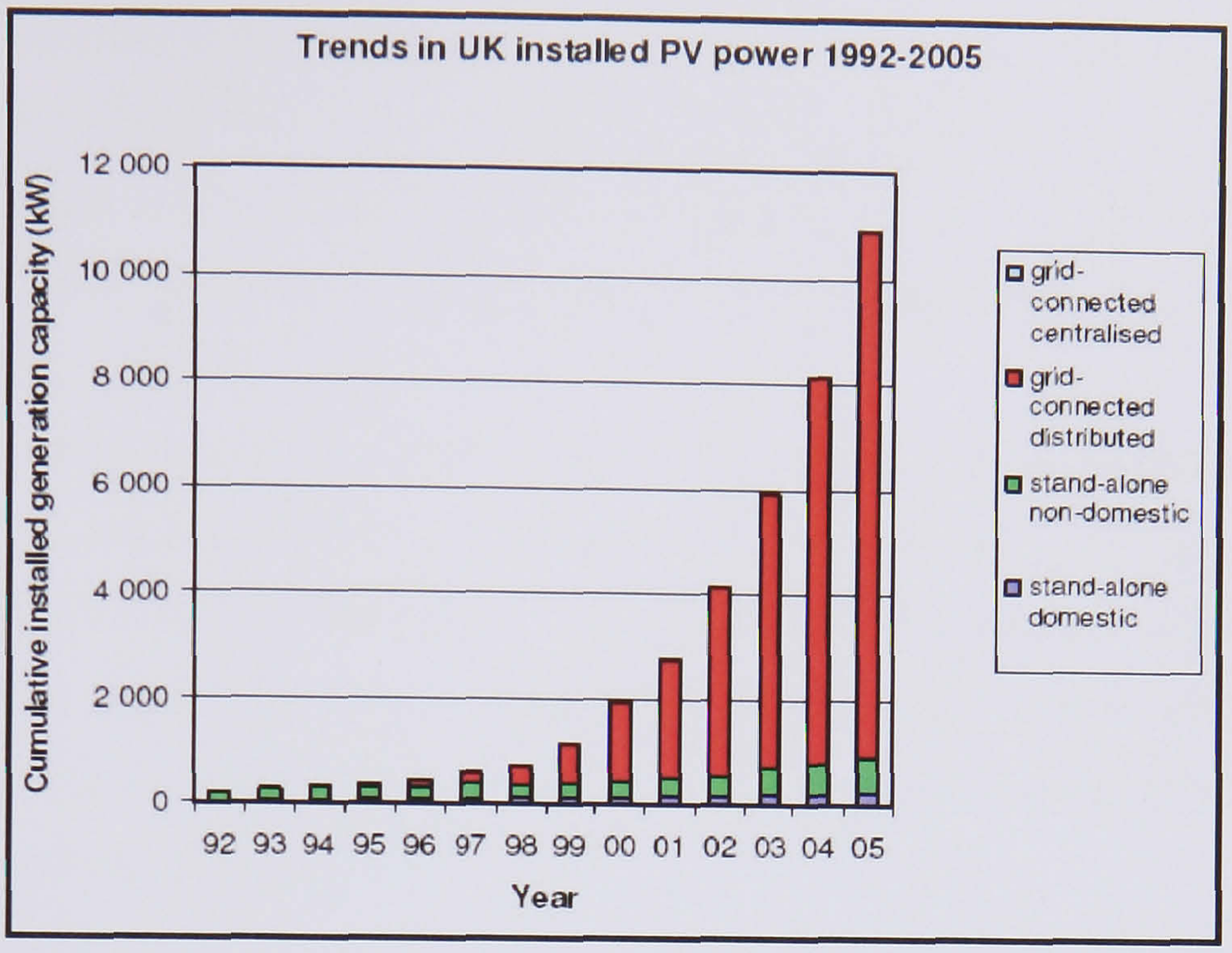

Figure 1.11 Cumulative Installed PV Power in UK (IEA 2005)

Solar Thermal

Solar thermal systems are based on a simple principle known for centuries: the sun heats up water contained in a dark vessel. Solar thermal technologies on the market are now efficient and highly reliable, providing solar energy solutions for a wide range of areas of use and potential users. Most of the systems sold today are intended to supply domestic hot water, and an increasing number of combined-systems additionally provide thermal energy for space heating, thus lowering the conventional energy demand for space heating.

In UK the last decade has witnessed an increase in domestic solar collectors of 24.3% (Chris Laughton, 2007). It is estimated that 4.2 million new homes in the UK are due for construction by the year 2016. Therefore it is important that these new technologies can be integrated in buildings in order to reduce the CO_2 emissions by providing environmentally friendly electrical and heat energy in buildings.

1.2 PV/Thermal System Description

The EU has set targets for 2010 of 100 million m^2 for solar thermal collectors (corresponding to 70 GWp thermal) and 3 GWp for PV, SHIA (2006). The markets for both solar thermal and PV are growing rapidly globally, but often the two technologies

find themselves competing for sales in the residential sector. This competition arises because some families will choose to buy solar thermal collectors in order to heat their houses and others to supply them with green electricity. The limited space in the roofs and the cost of the technologies will prevent families to integrate both systems in their roof (Report IEA, 2002).

To overcome this competition a new market can be exploited by incorporating both technologies in one panel and thus provide a hybrid PV/T panel recovering part of heat from PV back surface that would result in lowered PV cell temperature thus an improvement in electrical efficiency. If the complete power of 3 GWp would be realized by installing 30 million m^2 of PV/T, 30 million m^2 (= 21 GWp thermal) of solar thermal would be installed simultaneously.

1.2.1 Hybrid PV/Thermal Panels

Hybrid energy systems combine the use of two or more alternative power sources and aim to increase the system's total efficiency. One relatively new type of PV panel is the hybrid PV panel. This type of panel converts part of the sun's radiation to electricity whilst harnessing the remaining thermal components which for conventional PV systems are regarded as an important to system performance, as a source of useful heat. The photovoltaic/thermal (PV/T) system is a hybrid structure that has been examined quite thoroughly over the past years and makes use of the 70-95% of collected solar energy that is not converted into electricity by conventional solar cells. This heat extraction can be achieved by either air or a fluid coolant. The cooling medium apart from conducting heat serves to cool the panel making it more efficient.

When the temperature of a photovoltaic module is increased, the efficiency drops. For every 1˚C rise in PV panel temperature, there is 0.4 to 0.5% drops in the electrical output PV efficiency. The operating temperature is increased because a large part of the solar radiation is not converted to electricity but is absorbed by the panel as heat. Natural circulation of air is the easiest and cheapest way to remove this heat from the panel and consequently increase the efficiency. Another, more efficient way is to use a liquid as the coolant of the panel. This is the general philosophy of hybrid photovoltaic-thermal collectors. In these systems the natural or forced circulation of a heat removing

fluid can be used not only for PV cooling, but also for heat generation. These Low temperature solar thermal systems collect solar radiation to heat air and water for industrial applications including:

• preheat for space heating for homes, offices and greenhouses

• preheat of domestic and industrial hot water

• pool heating

By using this PV/Thermal technology the UK government could achieve their target of 20% of energy coming from renewable by 2020 and reduce the carbon emissions by 60% until 2050 (DTI, 2006). This potential increase in renewable energy will force to reduce the primary energy consumption from fossil fuels and specifically provide buildings with clean electricity and thermal energy.

The obvious advantages of such a system are:

- The total area used to extract a given amount of electricity and heat may be smaller than for two separate systems depending upon heating fluid temperature
- The materials used for a PV/T plant, and thus the total energy and economy balance, may be better than for separate units.
- Any roof or facade into which they may be integrated will have a more uniform look.
- The system generates clean and renewable electricity and hot water all year round
- The system contributes increased savings on carbon emissions and energy bills compared with a PV system
- Systems are currently eligible for PV grant from Energy Savings Trust and solar DHW grant from Clear Skies

The drawbacks and barriers of PV/Thermal systems are:

- Special integrated absorbers are required, for which the thermal resistance between PV and collector fluid should be sufficiently small
- Leakage or freezing may occur in case of faulty design

- Low heat capacity, low heat conductivity and air leakage result in low heat transfer for PV/T systems using air as cooling medium
- In general PV/T systems should be able to withstand direct insolation without active cooling
- Climatic conditions and location can affect the performance and type of PV/T that is more appropriate to be used
- Lack of proper standard and certification procedures for the performance and reliability of the systems
- Electrical and thermal performance have to be evaluated into a combine PV/T energy rating
- Cost of a PV/T system will be higher than a separate PV and Solar Thermal collector

1.3 Research Aims

This PhD research focuses entirely on the production of a hybrid PV/T and aims to:

- identify the temperature effect on PV performance
- experimentally evaluate the PV/T system with water and air as a heat transfer medium and use the results as a benchmark
- investigate the heat pipe performance and develop a PV/T system that incorporates heat pipes
- evaluate the developed phase change material technology used as an absorber in back of the PV
- investigate and evaluate micro-encapsulated phase change materials for PV/T integration
- from the PV/T systems produce higher energy yield per surface area than a PV
- use of an appropriate energy rating for electrical and thermal performance
- cost analysis of the systems and comparison with PV
- achieve improvements in greenhouse gas emissions savings in comparison with PVs

1.4 New Application of Technologies

The research is novel in the following ways:

1. A PV/T model using phase change material as an absorber was simulated and tested
2. An improved PV/Water system was tested with the integration of pipes inside a PCM beam placed in the back of the PV.
3. Heat pipes that are widely used already were used as energy carriers and integrated in the back of the PV for cooling them
4. A Microencapsulated PCM slurry was used as a heat transfer cooling fluid
5. A cost analysis of the models was carried out and a payback period estimated based on monitored performance of the Sustainable Research Building PV plant
6. A Life Cycle Energy Analysis (LCEA) was used in order to identify the energy needed and the emissions produced to build the systems as also the CO_2 emissions saved per m^2 during the life cycle of the models.

1.5 Structure of the Thesis

This thesis describes the design of 4 PV/Thermal panels from the design concept drawn up from a list of desirable behaviours, modelling of these concepts, experimental verification and finally, economic and environmental evaluation in order to find the most promising design.

The program involved the following sections:

- Chapter 2 reviewed the technologies applied to the research work and provided an in-depth understanding in PV cooling, PV/Thermal systems, phase change material, microencapsulated phase change slurry and heat pipes. Each review included theoretical and experimental investigation of system performance and their application in low-grade energy systems.
- Chapter 3 presented experimentally the electrical performance of a PV with and without insulation in order to identify the effect of temperature in PVs electrical output efficiency.

- Chapter 4 covers the theoretical modelling using TRNSYS and experimental work of the PV/Thermal system based on water as the medium to extract heat from the back of the PV.
- Chapter 5 describes the analysis of the PV/Thermal system using natural and forced air circulation and introduced 2 different approaches for heat removal with and without fins in the back of the PV.
- Chapter 6 involves a study of a PV/Heat Pipe panel. Based on the heat transfer limits of a gravitational heat pipe an experimental rig was developed. Experimental work was carried out for 2 different concepts. In the first the condenser part of the pipes was extracting their heat inside a water tank and in the second manifolds were constructed that incorporated the condenser side of the heat pipe for the heat transfer.
- Chapter 7 analysed the performance of a system by incorporating a phase change material beam in the back of the PV. A model was produced in TRNSYS that simulated the behaviour of a glazed or unglazed photovoltaic array that includes a layer of phase change material and the results were compared with the experiments.
- Chapter 8 involves the use of microencapsulated phase change material slurry as a fluid energy carrier from the back of a PV. The experimental results were compared with a reference case using water.
- Chapter 9 compares the systems studied in the previous sections with respect to their thermal and electrical performance. A cost analysis was carried out in order to identify the most economic PV/T system in terms of payback time. Also a Life Cycle Analysis helped identify the amount of CO_2 emissions produced and saved from each PV/T system.
- Chapter 10 presents the conclusions from this study above and the merits of the proposed systems are highlighted. The limitations of the research were pointed out and potential for further research was illustrated.

CHAPTER 2: LITERATURE REVIEW

2.1 Introduction

This chapter reviews existing relevant research work and provides an in-depth understanding of the different technologies used. The purpose of the review is to identify key points in each technology that affect their performance in order to achieve the best possible integration between them.

In section 2.3 a survey of the various types of solar thermal collectors and applications is presented. An introduction into the uses of solar energy is attempted followed by a description of the various types of collectors including flat-plate, and evacuated tube. This is followed by thermal and thermodynamic analysis of the collectors and a description of the methods used to evaluate their performance. Typical applications of the various types of collectors are presented in order to show to the reader the extent of their applicability. These include solar water heating, which comprise thermosyphon, integrated collector storage, direct and indirect systems and air systems, space heating and cooling.

Section 2.4 starts with the basic principles underline the PV technology; the different cell technologies that exist and on typical system applications including both stand alone and grid connected options. The construction and performance of photovoltaic modules will be discussed and the temperature effect on the performance of PVs is presented.

Work in section 2.5 presents a review of the available literature on PV/T collectors. The review is presented in a thematic way, in order to enable an easier comparison of the findings obtained by various researchers, especially on parameters affecting PV/T performance (electrical and thermal). The review covers the description of flat plate and concentrating, water and air PV/T collector types, analytical and numerical models, simulation and experimental work and qualitative evaluation of thermal/electrical output. The parameters affecting PV/T performance, such as covered versus uncovered PV/T collectors, optimum mass flow rate, absorber plate parameters (i.e. tube spacing, tube diameter, fin thickness), absorber to fluid thermal conductance and configuration design types are extensively discussed.

Section 2.6 introduces the basic principles of heat pipes. An overview of heat pipe structure, operation and limitations is analysed. Different types of heat pipes are investigated in accordance with their structure, shape and working fluid used. Finally this part describes the performance of solar thermal collectors incorporating heat pipes with different working fluids.

Purpose of section 2.7 is to look at the current state of research in phase change materials, with the main focus being on the assessment of the thermal properties of various PCMs, methods of heat transfer enhancement and design configurations of heat storage facilities to be used as a part of solar passive and active space heating systems and greenhouses. Experimental and theoretical studies have been presented to determine the performance of phase-change energy storage materials for solar collector systems.

Finally section 2.8 presents a study that has been performed to understand the heat transfer enhancement characteristics of the microencapsulated solid-liquid phase change materials (PCM) slurry. The flow and convective heat transfer behaviors of microencapsulated phase change material (MPCM) slurries have been investigated experimentally for use as a heat-transfer fluid.

2.2 Solar Sun

The sun is a sphere of intensely hot gaseous matter with a diameter of 1.39×10^9 m and 1.5×10^{11} m away from Earth. The solar energy strikes our planet a mere 8 min and 20 s after leaving the giant furnace. The sun has an effective blackbody temperature of 5762 K (Kreith, 1978). The temperature in the central region is much higher and it is estimated at 8×10^6 to 40×10^6 K. In effect the sun is a continuous fusion reactor in which hydrogen is turned into helium. The sun's total energy output is 3.8×10^{20} MW which is equal to 63 MW/m^2 of the sun's surface. This energy radiates outwards in all directions. Only a tiny fraction, 1.7×10^{14} kW, of the total radiation emitted is intercepted by the earth (Kreith, 1978). However, even with this small fraction it is estimated that 30 min of solar radiation falling on earth is equal to the world energy demand for one year.

Basically, all the forms of energy in the world as we know it are solar in origin. Oil, coal, natural gas and woods were originally produced by photosynthetic processes,

followed by complex chemical reactions in which decaying vegetation was subjected to very high temperatures and pressures over a long period of time (Kreith, 1978). Even the wind and tide energy have a solar origin since they are caused by differences in temperature in various regions of the earth. The greatest advantage of solar energy as compared with other forms of energy is that it is clean and can be supplied without any environmental pollution.

2.2.1 Technologies for conversion of solar energy

The energy contained in sunlight is critical to life on Earth and fundamental to human survival. The use of solar energy is usually identified in two contexts: passive solar energy systems, which uses natural processes without mechanical equipment or additional energy to operate and active solar energy systems, which utilise solar energy with the assistance of mechanical equipment or electronic hardware. Solar thermal collectors, photovoltaic and photovoltaic-thermal cogeneration systems count as active systems. The most significant difference between solar thermal and photovoltaic systems is that solar thermal systems produce heat and photovoltaic produce electricity.

2.3 Solar Thermal Collectors

Solar thermal energy collectors are special kind of heat exchangers that transform solar radiation energy to thermal energy. The major component of any solar system is the solar collector. This is a device that absorbs the incident solar radiation, converts it into heat, and transfers this heat to a fluid (usually air, water, or oil) flowing through the collector. The solar energy collected is carried by the circulating fluid either directly to the hot water or space conditioning equipment or to a thermal energy storage tank from which can be drawn for use at night and/or cloudy days.

Three of the most important types of collectors are:

1. Flat plate collectors (FPC);
2. Evacuated tube collectors (ETC);
3. Stationary compound parabolic collectors (CPC);

Figure 2.1 shows the worldwide installed capacity by collector type.

This review will cover the first two types.

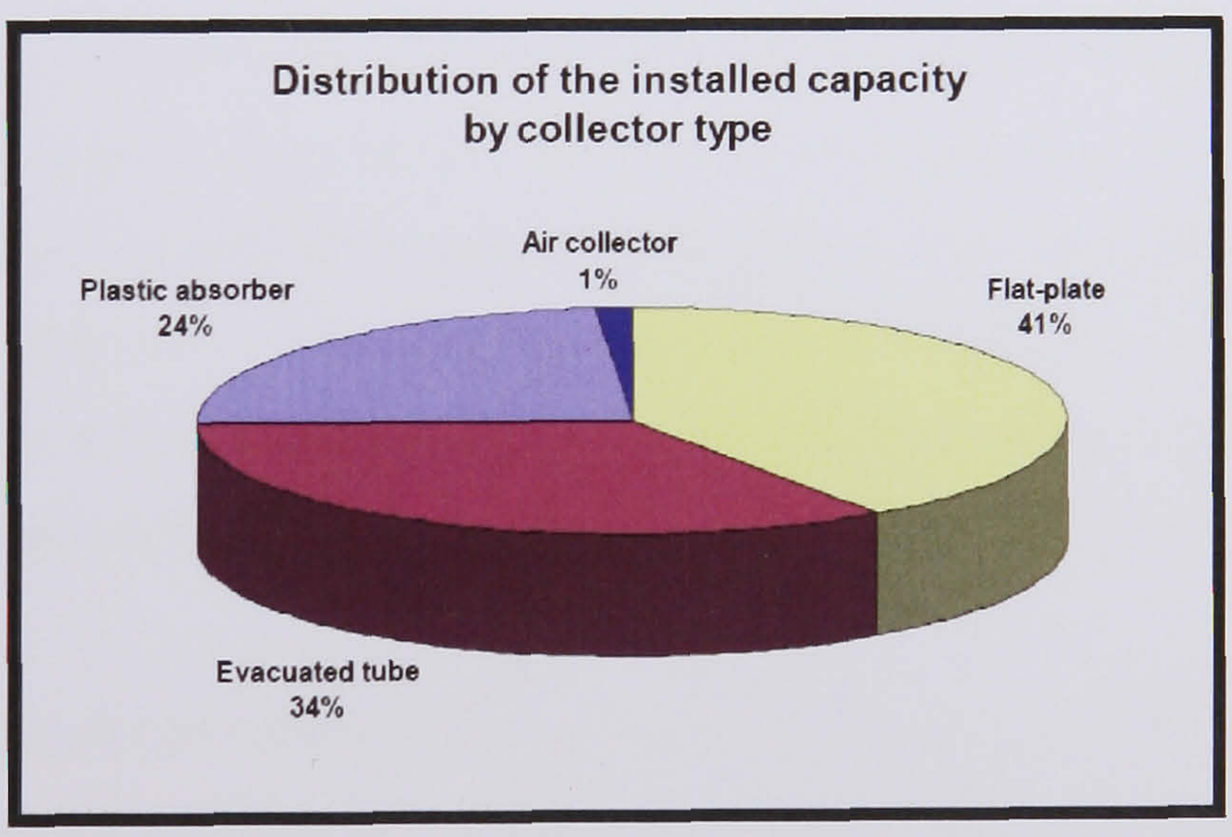

Figure 2.1 Distribution of the worldwide installed capacity by collector type (Werner, 2003)

2.3.1 Flat-plate collectors

Glazed flat-plate collectors are insulated and weatherproof boxes containing a dark absorber plate under one or more glass or plastic covers. Unglazed collectors, typically

used for solar pool heating, have a dark absorber plate made of metal or polymer, without a cover or enclosure. With both types, small tubes run through the box and carry a fluid (either water or an antifreeze solution). As the sunlight hits the dark absorber plate, it heats up and transfers heat to the fluid passing through the tubes.

A FPC generally consists of the following components as shown in *Figure 2.2*.

Their major purpose is to collect as much solar energy as possible at the lower possible total cost. The collector should also have a long effective life, despite the adverse effects of the sun's ultraviolet radiation, corrosion and clogging because of acidity, alkalinity or hardness of the heat transfer fluid, freezing of water, or deposition of dust or moisture on the glazing, and breakage of the glazing because of thermal expansion, hail, vandalism or other causes. These causes can be minimized by the use of tempered glass.

Glazing and the absorbing plate are important components of the system.

Glazing: The glazing should admit as much solar irradiation as possible and reduce the upward loss of heat as much as possible. Although glass is virtually opaque to the longwave radiation emitted by collector plates, absorption of that radiation causes an increase in the glass temperature and a loss of heat to the surrounding atmosphere by radiation and convection. Glass has been widely used to glaze solar collectors because it can transmit as much as 90% of the incoming shortwave solar irradiation while transmitting virtually none of the long wave radiation emitted outward by the absorber plate. Glass with low iron content has a relatively high transmittance for solar radiation (approximately 0.85–0.90 at normal incidence), but its transmittance is essentially zero for the longwave.

Various prototypes of transparently insulated (TI) FPC have been built and tested in the last decade (Spate 1999, Schweiger 1997). A prototype FPC covered by TI was developed by Benz et al. (1998) and it was experimentally proved that the efficiency of the collector was comparable with that of ETC.

Absorber plates: The collector plate absorbs as much of the irradiation as possible through the glazing, while loosing as little heat as possible upward to the atmosphere and downward through the back of the casing. The collector plates transfer the retained

heat to the transport fluid. The absorptance of the collector surface for short wave solar radiation depends on the nature and colour of the coating and on the collector angle. By suitable electrolytic or chemical treatments, surfaces can be produced with high values of solar radiation absorptance (α) and low values of longwave emittance (ε). Usually black colour is used, however various colour coatings have been proposed in Tripanagnostopoulos (2000) and Orel (2002) mainly for aesthetic reasons. These typical selective surfaces consist of a thin upper layer, which is highly absorbent to shortwave solar radiation but relatively transparent to longwave thermal radiation, deposited on a surface that has a high reflectance and a low emittance for longwave radiation. Selective surfaces are particularly important when the collector surface temperature is much higher than the ambient air temperature.

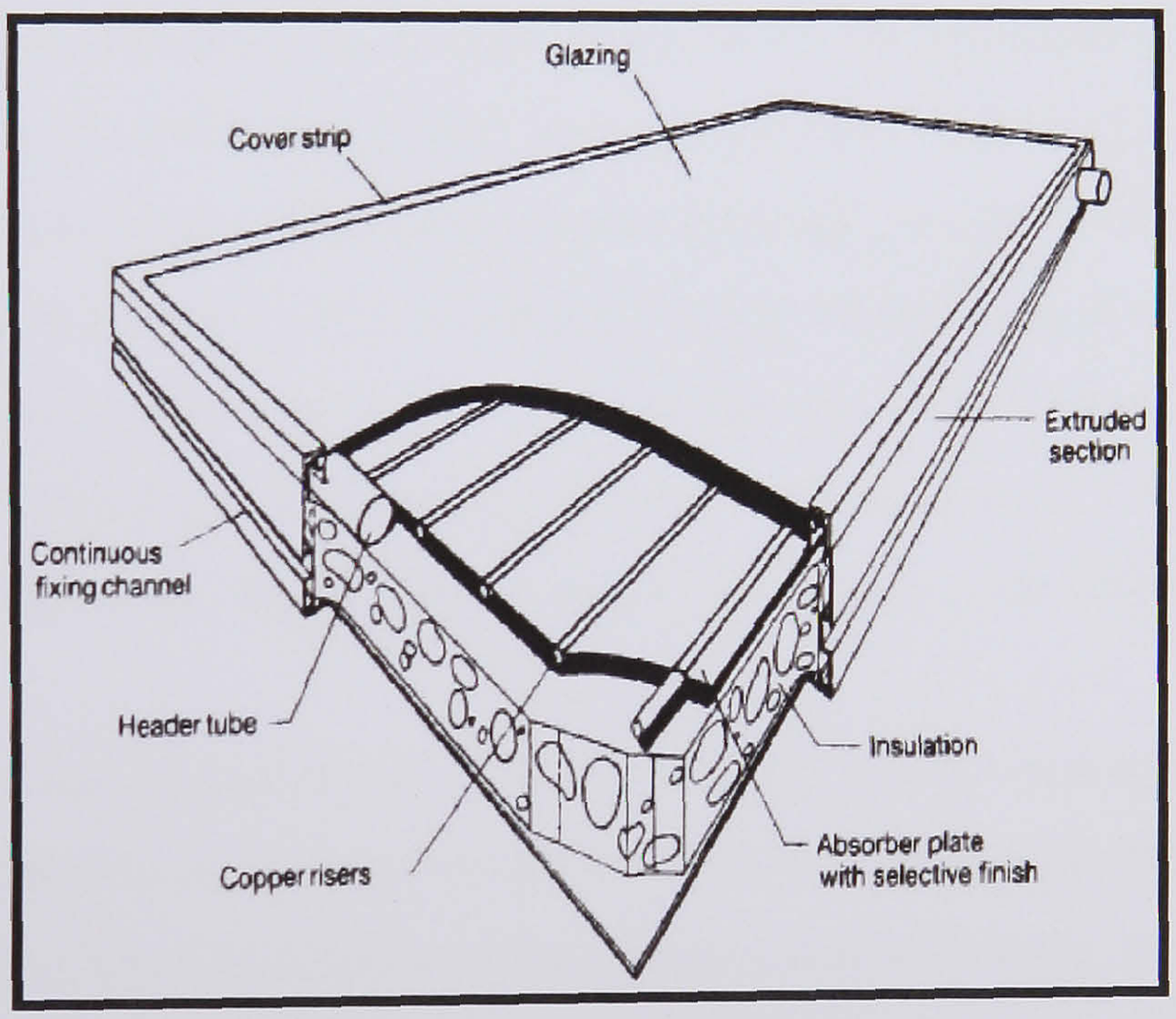

Figure 2.2 Flat Plate Solar Collector (Kalogirou, 2004)

Fluid-heating collectors, passages must be integral with or firmly bonded to the absorber plate. A major problem is obtaining a good thermal bond between tubes and absorber plates without incurring excessive costs for labor or materials. Material most frequently used for collector plates are copper, aluminum, and stainless steel.

Flat plate solar collectors can be further distinguished according to the heat transfer fluid as liquid and air. Liquid flat-plate collector's heat liquid as it flows through tubes in or adjacent to the absorber plate. The simplest liquid systems use potable household water, which is heated as it passes directly through the collector and then flows to the house. Air flat-plate collectors are used primarily for solar space heating. The absorber plates in air collectors can be metal sheets, layers of screen, or non-metallic materials. The air flows past the absorber by using natural convection or a fan. Because air conducts heat much less readily than liquid does, less heat is transferred from an air collector's absorber than from a liquid collector's absorber, and air collectors are typically less efficient than liquid collectors.

Figure 2.3 shows a number of absorber plate designs for solar water and air heaters that have been used with varying degrees of success (Kreider, 1982).

Figure 2.3A shows a bonded sheet design, in which the fluid passages are integral with the plate to ensure good thermal conduct between the metal and the fluid. *Figure 2.3B* and *2.3C* shows fluid heaters with tubes soldered, brazed, or otherwise fastened to upper or lower surfaces of sheets or strips of copper. Copper tubes are used most often because of their superior resistance to corrosion. Thermal cement, clips, clamps, or twisted wires have been tried in the search for low-cost bonding methods. *Figure 2.3D* shows the use of extruded rectangular tubing to obtain a larger heat transfer area between tube and plate.

Air or other gases can be heated with FPC, particularly if some type of extended surface (*Figure 2.3E*) is used to counteract the low heat transfer coefficients between metal and air (Kreider, 1982). Metal or fabric matrices (*Figure 2.3F*) (Kreider, 1982), or thin corrugated metal sheets (*Figure 2.3G*) may be used, with selective surfaces applied to the latter when a high level of performance is required. The principal requirement is a large contact area between the absorbing surface and the air.

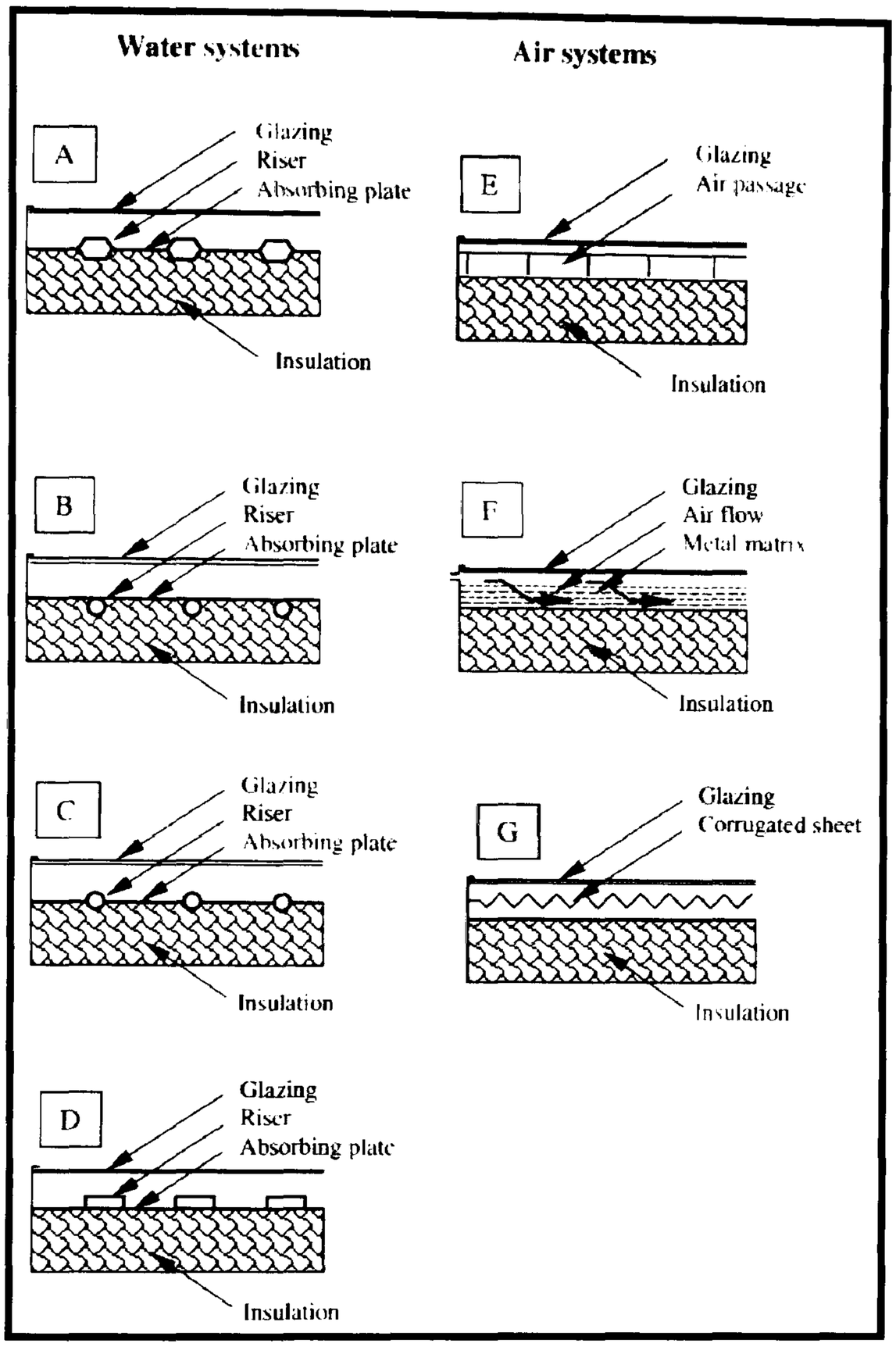

Figure 2.3 Different Absorber Plate Designs (Kalogirou, 2004)

As we mentioned transparent cover is used to reduce convection losses from the absorber plate through the restraint of the stagnant air layer between the absorber plate and the glass. It also reduces radiation losses from the collector as the glass is transparent to the short wave radiation received by the sun but it is nearly opaque to long-wave thermal radiation emitted by the absorber plate (greenhouse effect). Another category of collectors which is not shown in *Figure 2.3* is the uncovered or unglazed solar collector that Soltau (1992) reports. These are usually low-cost units that can offer

cost effective solar thermal energy in applications such as water preheating for domestic or industrial use.

2.3.2 Evacuated tube collectors

Conventional simple flat-plate solar collectors were developed for use in sunny and warm climates. Their benefits however are greatly reduced when conditions become unfavourable during cold, cloudy and windy days. Evacuated heat pipe solar collectors (tubes) operate differently from other collectors available on the market.

Evacuated-tube collectors can achieve extremely high temperatures (70°C to 170°C), making them more appropriate for cooling applications and commercial and industrial application. However, evacuated-tube collectors are more expensive than flat-plate collectors, with unit area costs about twice that of flat-plate collectors.

The collectors are usually made of parallel rows of transparent glass tubes. Each tube contains a glass outer tube and metal absorber tube attached to a fin. The fin is covered with a coating that absorbs solar energy well, but which inhibits radiative heat loss. Air is removed, or evacuated, from the space between the two glass tubes to form a vacuum, which eliminates conductive and convective heat loss. These solar collectors consist of a heat pipe inside a vacuum-sealed glass tube, as shown in *Figure 2.4*. The heat pipe contains a small amount of fluid (e.g. methanol) that undergoes an evaporating-condensing cycle. In this cycle, solar heat evaporates the liquid, and the vapour travels to the condenser side of the pipe. There water, or glycol, flows through the manifold and picks up the heat from the condensed side of the tube. The condensed fluid returns back to the evaporative side of the tube and the process is repeated. The vacuum envelope reduces convection and conduction losses, so the collectors can operate at higher temperatures than FPC. Like FPC, they collect both direct and diffuse radiation. However, ETC efficiency is higher at low incidence angles. This effect tends to give ETC an advantage over FPC in day-long performance. Because no evaporation or condensation above the phase-change temperature is possible, the heat pipe offers inherent protection from freezing and overheating. This self limiting temperature control is a unique feature of the evacuated heat pipe collector.

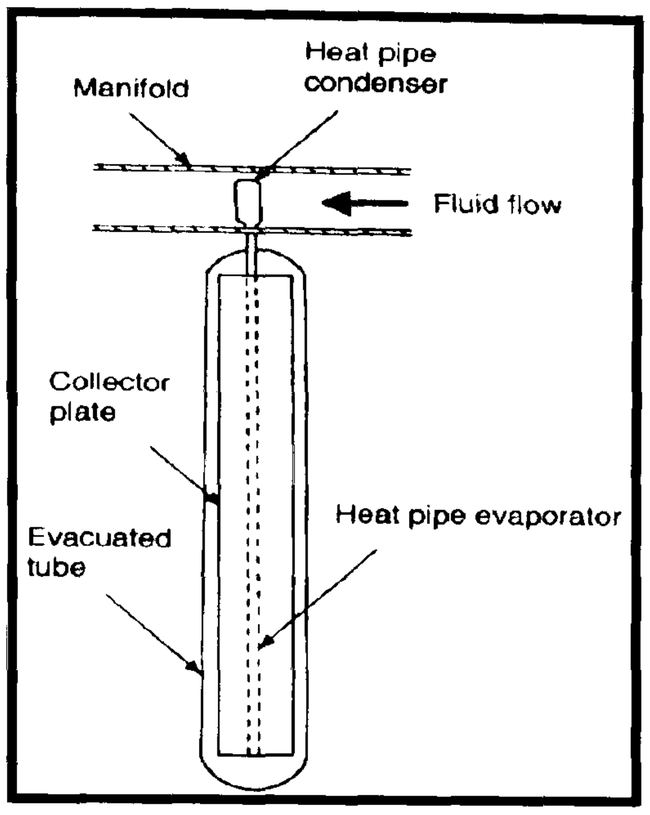

Figure 2.4 Glass – Metal Evacuated Tube Solar Collector (Kalogirou, 2004)

A large number of variations of the absorber shape of ETC are on the market (Lin, 1998). One manufacturer recently presented an all-glass ETC, which may be an important step to cost reduction and increase of lifetime. Another variation of this type of collector is what is called Dewar tubes as seen in *Figure 2.5*. In this two concentric glass tubes are used and the space in between the tubes is evacuated (vacuum jacket). The advantage of this design is that it is made entirely of glass and it is not necessary to penetrate the glass envelope in order to extract heat from the tube thus leakage losses are not present and it is also less expensive than the single envelope system.

Another type of collector developed recently is the integrated compound parabolic collector (ICPC). This is an ETC in which at the bottom part of the glass tube a reflective material is fixed (Winston et al., 1999). The collector combines the vacuum insulation and non-imaging stationary concentration into a single unit.

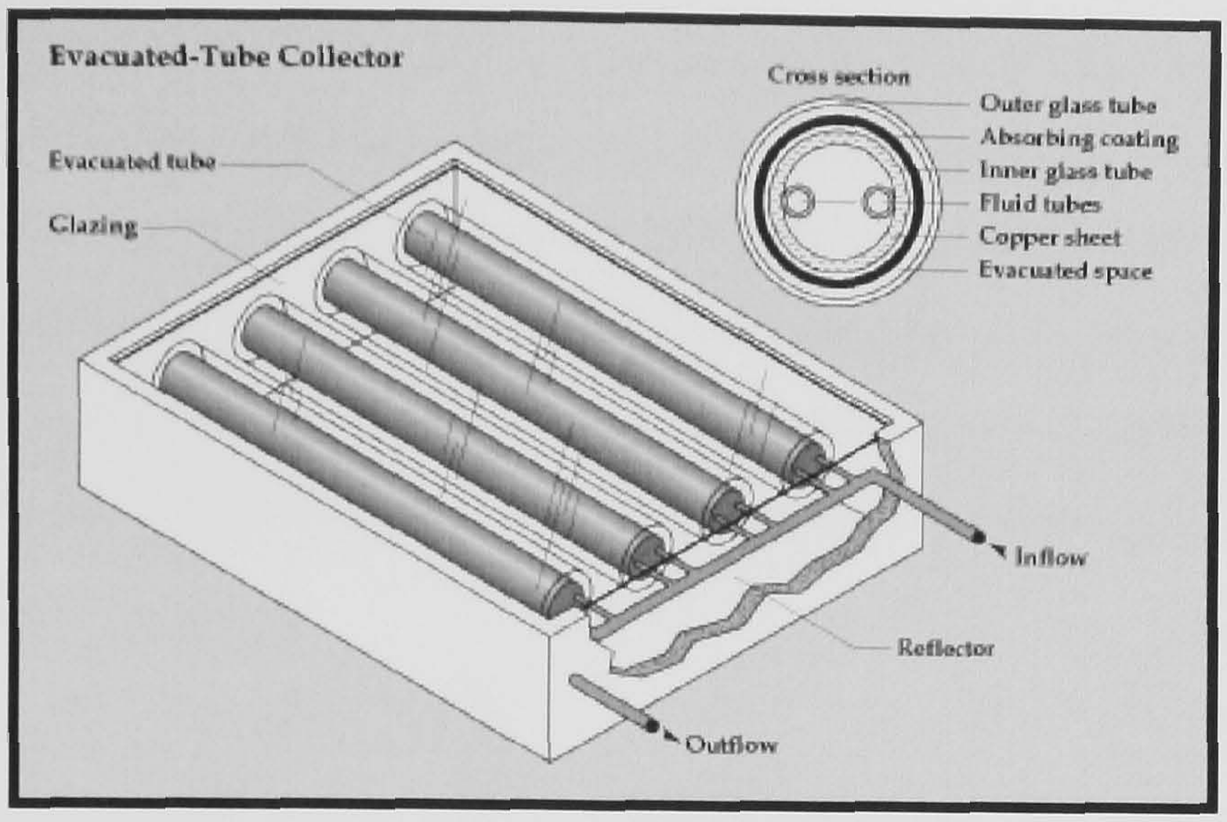

Figure 2.5 Glass – Glass Evacuated Tube Solar Collector (US Department Energy Efficiency and Renwable Energy, 2007)

2.3.3 Thermal analysis of collectors

The basic parameter to consider for a collector is thermal efficiency. This is defined as the ratio of the useful energy extracted from the fluid passing the collector to the energy incident on the collector aperture. The incident solar flux consists of direct and diffuse solar radiation.

Under steady-state conditions, the useful heat delivered by a solar collector is equal to the energy absorbed by the heat transfer fluid minus the direct or indirect heat losses from the collector to the surroundings. Duffie (1991) and Klein (1975) give detailed information about the formulae that are used to calculate the thermal gains and losses in order to estimate the collector efficiency.

The useful energy collected from a collector can be obtained from the following formula:

$$q_u = A_c[G_t\tau\alpha - U_L(T_p - T_a)] = mc_p[T_o - T_i] \quad \text{Eq. (2.3.1)}$$

Eq. (2.3.1) can be modified by substituting inlet fluid temperature T_i for the average plate temperature T_p; if a suitable correction factor is included. The resulting equation is

$$q_u = A_c F_R[G_t(\tau\alpha) - U_L(T_i - T_a)] \quad \text{Eq. (2.3.2)}$$

where F_R is the correction factor, or collector heat removal factor.

Heat removal factor can be considered as the ratio of the heat actually delivered to that delivered if the collector plate were at uniform temperature equal to that of the entering fluid. In Eq. (2.3.2) the temperature T_i of the inlet fluid depends on the characteristics of the complete solar heating system and the hot water demand or heat demand of the building. However, F_R is affected only by the solar collector characteristics, the fluid type, and the fluid flow rate through the collector. F_R may be obtained from Duffie and Beckman (1991).

$$F_R = \frac{mc_p}{A_c U_L}\left(1 - \exp\left[\frac{U_L F' A_c}{mc_p}\right]\right) \qquad \text{Eq. (2.3.3)}$$

where F' is the collector efficiency factor.

Where the collector efficiency factor F' is given by:

$$F' = \frac{\frac{1}{U_L}}{W\left[\frac{1}{U_L[D + (W - D)F]} + \frac{1}{C_b} + \frac{1}{\pi D_i h_{fi}}\right]} \qquad \text{Eq. (2.3.4)}$$

A physical interpretation of F' is that it represents the ratio of the actual useful energy gain to the useful energy gain that would result if the collector absorbing surface had been at the local fluid temperature. It should be noted that the denominator of Eq. (2.3.4) is the heat transfer resistance from the fluid to the ambient air.

Factor F in Eq. (2.3.4) is the standard fin efficiency for straight fins with rectangular profile, obtained from:

$$F = \frac{\tanh[m(W - D)/2]}{m(W - D)/2} \qquad (2.3.5)$$

The collector efficiency factor is essentially a constant factor for any collector design and fluid flow rate. The ratio of U_L to C_b; the ratio of U_L to h_{fi}; and the fin efficiency F are the only variables appearing in Eq. (2.3.4) that may be functions of temperature. For most collector designs F is the most important of these variables in determining F': The factor F' is a function of U_L and h_{fi}; each of which has some temperature dependence. Additionally, the collector efficiency factor decreases with increased tube center-to-center distances and increases with increases in both material thicknesses and thermal

conductivity. Increasing the overall loss coefficient decreases F' while increasing the fluid-tube heat transfer coefficient increases F'.

The overall heat loss coefficient is a complicated function of the collector construction and its operating conditions and it is given by the following expression

$$U_L = U_t + U_b + U_e \qquad \text{Eq. (2.3.6)}$$

i.e. it is the heat transfer resistance from the absorber plate to the ambient air.

In addition to serving as a heat trap by admitting shortwave solar radiation and retaining longwave thermal radiation, the glazing also reduces heat loss by convection. The insulating effect of the glazing is enhanced by the use of several sheets of glass, or glass plus plastic. The top loss coefficient in Eq. (2.3.6) is given by (Klein, 1975):

$$U_t = \frac{1}{\dfrac{N_g}{\dfrac{C}{T_p}\left[\dfrac{T_{av} - T_a}{N_g + f}\right]^{0.33} + \dfrac{1}{h_w}}} + \frac{(\sigma T_{av}^2 + T_a^2)(T_{av} + T_a)}{\dfrac{1}{\varepsilon_p + 0.05N_g(1-\varepsilon_p)} + \dfrac{2N_g + f - 1}{\varepsilon_g} - N_g} \qquad \text{Eq. (2.3.7)}$$

$$h_w = 5.7 + 3.8W$$

$$f = (1 - 0.04h_w + 0.0005h_w^2)(1 + 0.091N_g)$$

$$C = 365.9(1 - 0.00883\beta + 0.0001298\beta^2)$$

and T_p is the collector stagnation temperature, i.e. the temperature of the absorbing plate when the flow rate is equal to zero, and is obtained from

$$T_p = \frac{G_t(\tau\alpha)}{U_L} + T_a \qquad \text{Eq. (2.3.11)}$$

Finally, the collector efficiency can be obtained by dividing q_u by $(G_t A_c)$. Therefore

$$n = F_R\left[\tau\alpha - \frac{U_L(T_i - T_a)}{G_t}\right] \qquad \text{Eq. (2.3.12)}$$

The efficiency of solar collectors depends on the design of the collector and on the system of which the collector is a part. *Table 2.1* summarises different thermal collectors' efficiencies and heat loss coefficients.

Table 2.1 Different Collector Types Thermal Efficiency and Thermal Loss Factor (www.solarserver.de)

Type of Collector	Thermal Efficiency	Heat loss coefficient ($W/m^{2o}C$)	Temperature range (^oC)
Uncovered absorber	0.82 – 0.90	10 – 30	Up to 40
Flat – plate	0.66 – 0.83	2.9 – 5.3	20 – 80
Evacuated tube	0.62 – 0.84	0.7 – 2	50 – 120
Air collector	0.75 – 0.90	8 - 30	20 - 50

ASHRAE Standard 93 (1986) for testing the thermal performance of collectors is the one most frequently used to evaluate the performance of flat-plate, evacuated tube and concentrating solar collectors. The thermal performance of the solar collector is determined by the variables of incident radiation, ambient temperature, and inlet fluid temperature. This requires experimental measurement of the rate of incident solar radiation falling onto the solar collector as well as the rate of energy taken from the transfer fluid as it passes through the collector, all under steady state or quasi-steady-state conditions.

In reality the heat loss coefficient U_L in Eqs (2.3.2) is not constant but is a function of collector inlet and ambient temperatures. Therefore:

$$F_R U_L = c_1 + c_2(T_i - T_a) \qquad \text{Eq. (2.3.13)}$$

Applying Eq. (2.3.13) in Eqs. (2.3.2) we have For FPC:

$$q_u = A_c F_R[\tau\alpha G_t - c_1(T_i - T_a) - c_2(T_i - T_a)^2] \qquad \text{Eq. (2.3.14)}$$

Therefore for FPC, the efficiency can be written as:

$$\eta = F_R \tau\alpha - c_1 \frac{(T_i - T_a)}{G_t} - c_2 \frac{(T_i - T_a)^2}{G_t} \qquad \text{Eq. (2.3.15)}$$

Usually, the second-order terms are neglected in which case c_2=0 and k_2=0. Therefore, Eq. (2.3.15) plot as a straight line on a graph of efficiency versus the heat loss parameter $(T_i - T_a)/G_t$ for the case of FPC.

The intercept (intersection of the line with the vertical efficiency axis) equals to $F_R \tau\alpha$ for the FPCs. The slope of the line, i.e. the efficiency difference divided by the corresponding horizontal scale difference, equals to $-F_R U_L$. If experimental data on collector heat delivery at various temperatures and solar conditions are plotted, with efficiency as the vertical axis and $\Delta T/G$ as the horizontal axis, the best straight line through the data points correlates collector performance with solar and temperature conditions. The intersection of the line with the vertical axis is where the temperature of the fluid entering the collector equals the ambient temperature, and collector efficiency is at its maximum. At the intersection of the line with the horizontal axis, collector efficiency is zero. This condition corresponds to such a low radiation level, or to such a high temperature of the fluid into the collector, that heat losses equal solar absorption, and the collector delivers no useful heat. This condition, normally called stagnation, usually occurs when no fluid flows in the collector.

Collector testing is required in order to evaluate the performance of solar collectors and compare different collectors to select the most appropriate one for a specific application. The best way to accomplish this is to identify the expected range of the parameter $\Delta T/G$ for the load and climate on a plot of efficiency n_{th} as a function of the heat loss parameteras indicated in *Figure 2.6*.

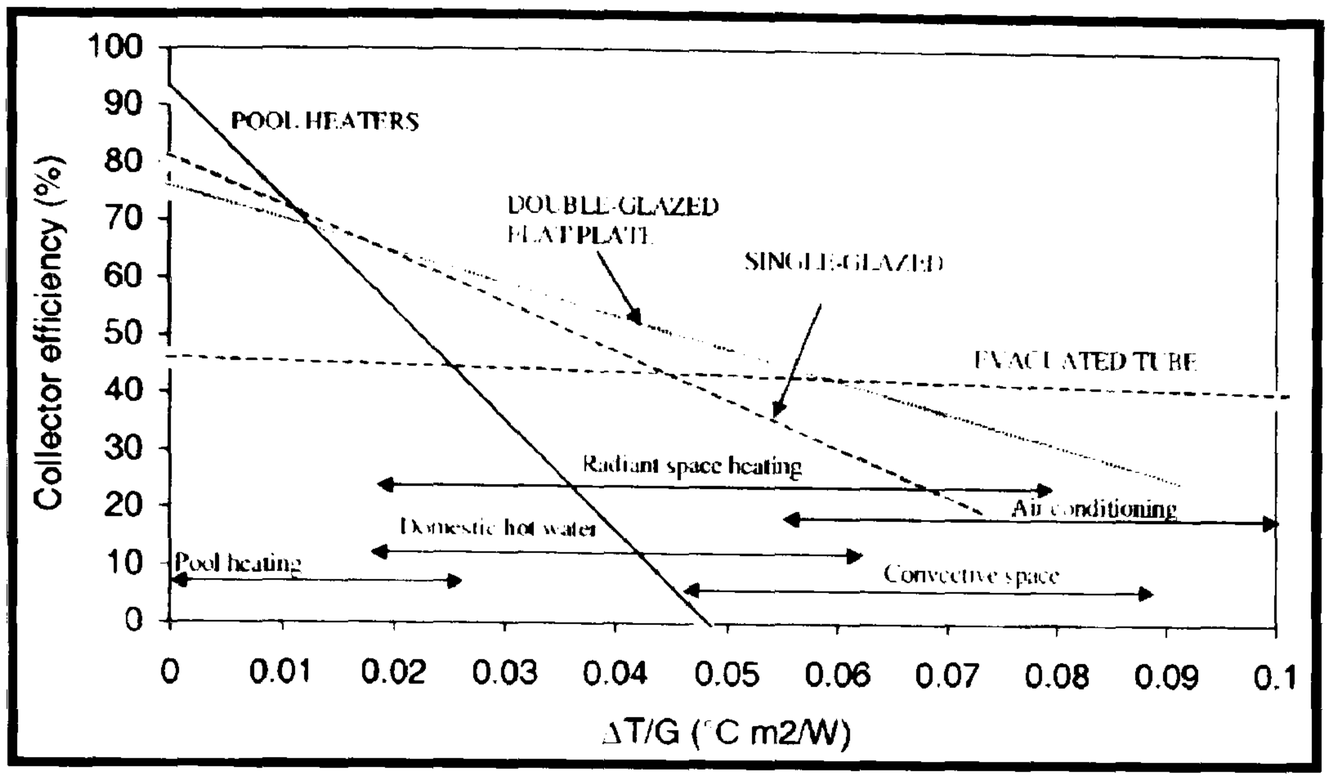

Figure 2.6 Collector efficiencies of various liquid collectors (Kalogirou, 2004)

Collector efficiency curves may be used for preliminary collector selection. However, efficiency curves illustrate only the instantaneous performance of a collector. They do not include incidence angle effects, which vary throughout the year, heat exchanger effects, probabilities of occurrence of T_i; T_a; solar irradiation, system heat loss, or control strategies. Final selection requires determining the long term energy output of a collector as well as performance cost-effectiveness studies.

The desired temperature range of the material to be heated is the most important factor in choosing the correct type of collector. An uncovered absorber is certainly not suitable for producing process heat. The amount of radiation on that spot, exposure to storms, and the amount of space must all be carefully considered when planning a solar array. The specific costs of collectors are also important. Evacuated-tube collectors are substantially more expensive than flat-plate collectors or even plastic absorbers. However, a good collector does not guarantee a good solar system. Rather, all components should be of high quality and similar capacity and strength.

Estimating the annual performance of a particular collector and system requires the aid of appropriate analysis tools such as F-Chart, Watsun, or TRNSYS.

2.3.4 Solar Collector Applications

Solar collectors have been used in a variety of applications. These are described in this section.

2.3.4.1 Solar water heating systems

Solar water heaters use the sun to heat either water or a heat-transfer fluid in the collector. Heated water is then held in the storage tank ready for use, with a conventional system providing additional heating as necessary. The tank can be a modified standard water heater, but it is usually larger and very well insulated. Solar water heating systems can be either active or passive, but the most common are active systems. Active solar water heaters rely on electric pumps, and controllers to circulate water, or other heat-transfer fluids through the collectors. These are the two types of active solar water-heating systems (*Figure 2.7*):

1. Direct-circulation systems use pumps to circulate pressurized potable water directly through the collectors. These systems are appropriate in areas that do not freeze for long periods and do not have hard or acidic water.
2. Indirect-circulation systems pump heat-transfer fluids through collectors. Heat exchangers transfer the heat from the fluid to the potable water.

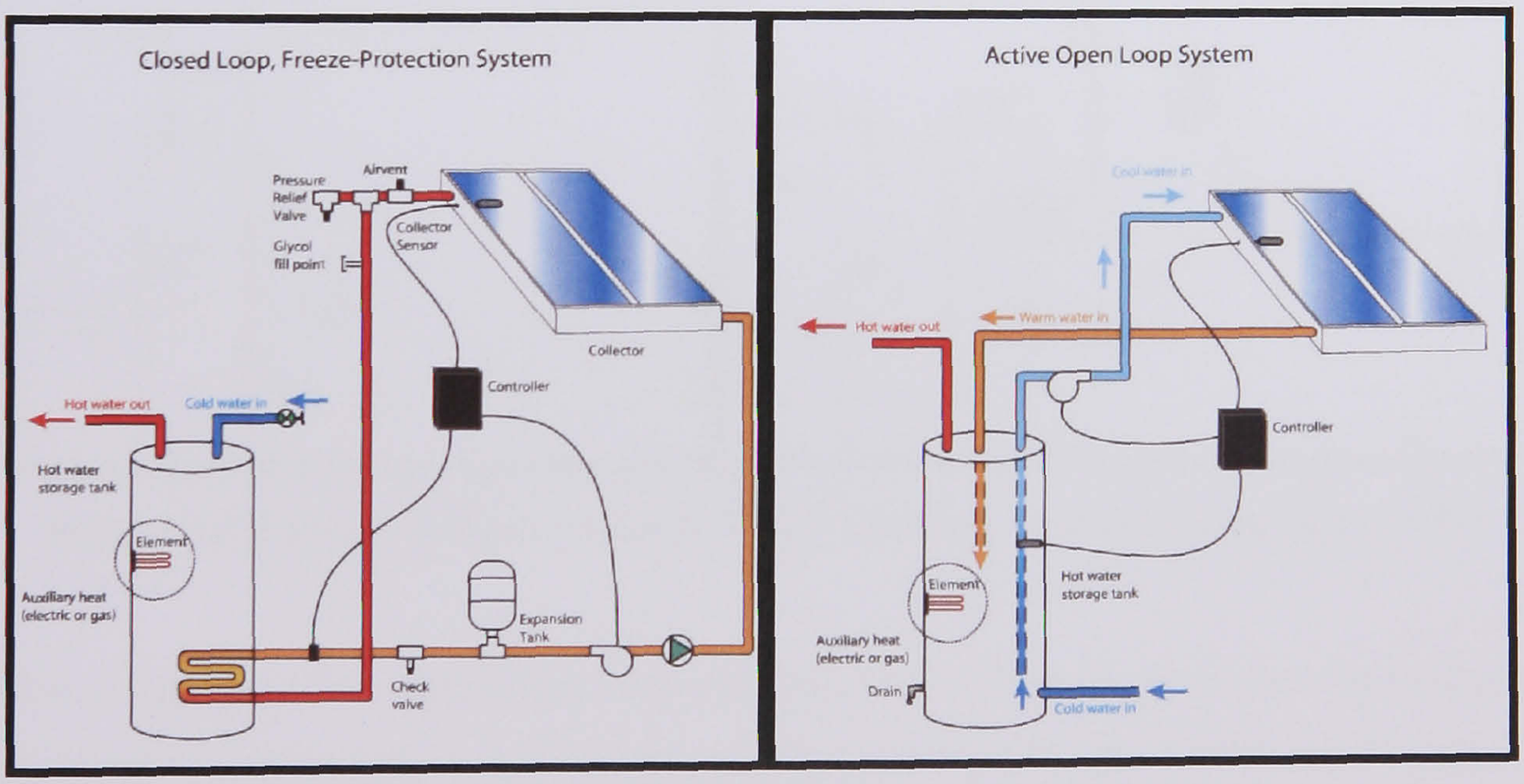

Figure 2.7 Direct and Indirect Solar Water Heating Systems (Southface, 2007)

Passive solar water heaters rely on gravity and the tendency for water to naturally circulate as it is heated. Because they contain no electrical components, passive systems are generally more reliable, easier to maintain, and possibly have a longer work life than active systems. The two most popular types of passive systems are (*Figure 2.8*):

1. Integral-collector storage systems consist of one or more storage tanks placed in an insulated box with a glazed side facing the sun. These solar collectors are suited for areas where temperatures rarely go below freezing.
2. Thermosyphon systems are an economical and reliable choice, especially in new homes. These systems rely on the natural convection of warm water rising to circulate water through the collectors and to the tank (located above the collector). As water in the solar collector heats, it becomes lighter and rises naturally into the tank above. Meanwhile, the cooler water flows down the pipes to the bottom of the collector, enhancing the circulation.

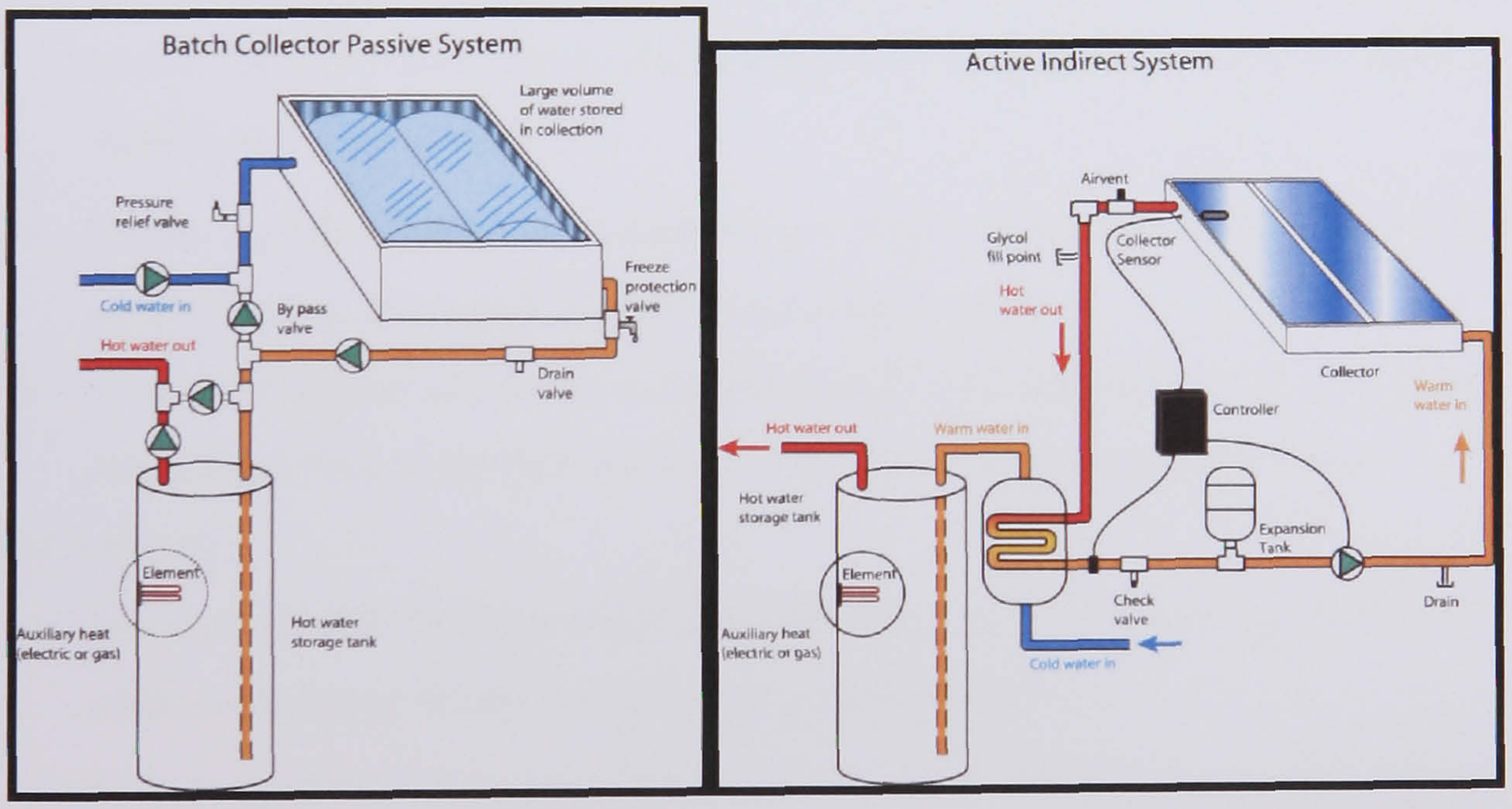

Figure 2.8 Passive and Active Solar Water Heating Systems (Southface, 2007)

All these systems offer significant economic benefits with payback times, depending on the type of fuel they replace and fuel prices, between 4 years (electricity) and 7 years (diesel oil).

2.3.4.2 Solar space heating

Air based systems circulate air through the solar collector with fans. Air collectors can be installed on a roof or an exterior (south facing) wall for heating one or more rooms. The collector has an airtight and insulated metal frame and a black metal plate for absorbing heat with glazing in front of it. Solar radiation heats the plate that, in turn, heats the air in the collector. An electrically powered fan or blower pulls air from the room through the collector, and blows it back into the room. Roof mounted collectors require ducts to carry air between the room and the collector. Wall mounted collectors are placed directly on a south-facing wall, and holes are cut through the wall for the collector air inlet and outlets. The air either enters the house directly or is channelled through some kind of storage system, often masonry, so that the heat will be available at night.

Advantages of air systems over liquid systems:

- Solar air collectors produce heat earlier and later in the day than liquid systems, so they may produce more usable energy over a heating season than a liquid system of the same size.
- Unlike liquid systems, air systems do not freeze, and minor leaks in the collector or distribution ducts will not cause significant problems.
- Can be integrated into walls and roofs to hide their appearance e.g. a tile roof could have built in air flow paths to make use of heat absorbed by tiles.

Disadvantages:

- Air is a less efficient heat transfer medium than liquid, so solar air collectors operates at lower efficiencies than solar liquid collectors.
- The air handling equipment (ducts and fans) need more space than piping and pumps, air leaks are difficult to detect, and power consumption is generally higher than that of liquid systems.

2.4 Photovoltaic

The history of photovoltaics dates back to 1839, when the French physicist Edmond Becquerel first observed the photovoltaic effect. In 1886, the American Charles Fitts constructed a selenium photovoltaic cell that converted visible light into electricity with an efficiency of 1% (Adams, 1887). In the 1930s photoelectric effect theory was developed for the electrical properties of silicon and other crystalline semi-conductors. In the early 1950s the Czochralski method for production of high purity crystalline silicon was developed, and in 1954 scientists at Bell laboratories in search of a practical way to generate electricity for telephone systems in rural areas far from the power lines, produced a silicon photovoltaic cell with 6% efficiency (Chapin, 1954). Soon the efficiency was raised to 11% and it was realized that solar cells could have numerous practical applications.

The 1950s were an unfavourable time to develop an energy technology based on the photovoltaic effect. The price of oil was less than $2 per barrel and large fossil fuelled power plants were built. Moreover, in 1954 construction began on the world's first commercial nuclear reactor. Also photovoltaic researchers faced an unsettling economic reality. Silicon cells developed in the 1950s were extremely expensive, with costs as high as $600 per watt compared with $5 today.

The space programmes rescued photovoltaics and in 1957 Russians and 1958 the Americans launched their first solar powered satellites (Sayigh, 1991).

Achievements in solar cell research during the peak years of the space programmes included a major increase in efficiency and reduction in cost. During the first oil crisis in 1973-74 the need for alternative energy sources promoted great interest in the photovoltaic industry. Although the oil crisis proved short-lived and the financial incentive to develop solar cells abated, solar cells had entered the arena as a power generating technology. Their application and advantage to the "remote" power supply area was quickly recognized and prompted the development of terrestrial photovoltaics industry. Small scale transportable applications (such as calculators and watches) were utilised and remote power applications began to benefit from photovoltaics.

In 1980s there was a relative disinterest in solar power, while the Gulf war of 1990 again sparked an interest in non-fossil fuel energy alternatives. Since the beginning of the 1990s the annual growth of the global solar cell market has been 20 – 40%. In 2005 the cumulative worldwide installed solar cell capacity reached 10,877 MW. Since 1999 the twenty IEA-PVPS countries have accounted for more than 90% of global solar cell production and around 80% of this production has been installed in these countries (IEA, 2002).

2.4.1 How PV Cells Work

A typical silicon PV cell comprises a thin wafer consisting of an ultra-thin layer of phosphorus-doped (N-type) silicon on top of a thicker layer of boron-doped (P-type) silicon. An electrical field is created near the top surface of the cell where these two materials are in contact, called the P-N junction (*Figure 2.9*).

When light energy is applied to a PV cell, i.e. when the sun shines on it, it gives the electrons enough energy to move across the p-n junction. At this point there is an energy variation across the p-n junction which is called a potential difference or voltage. The existence of this voltage when a PV cell is exposed to light is called the photovoltaic effect. The word photovoltaic comes from the Greek word 'photos' meaning light and from the name of the Italian scientist, Volta, who studied electricity. If a circuit is made, via a cable to the electrical loads, the potential difference drives a current and the electrons can flow through the circuit.

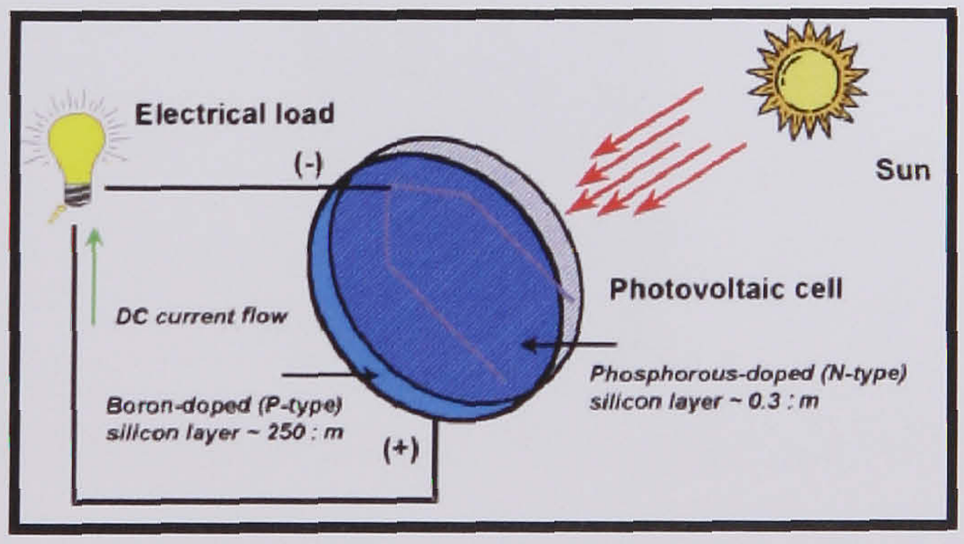

Figure 2.9 Diagram of a photovoltaic cell (Florida solar energy centre, 2007)

Regardless of size, a typical silicon PV cell produces about 0.5 – 0.6 volt DC under open-circuit, no-load conditions. The current (and power) output of a PV cell depends on its efficiency and size (surface area), and is proportional to the intensity of sunlight striking the surface of the cell.

2.4.2 Types of PV Cell

Photovoltaic cells are made from a semiconducting material, generally silicon crystal. When sunlight hits the photovoltaic panel, the light is absorbed by the silicon crystal. This absorption loosens the electrons from their atoms, causing the electrons to flow through the silicon crystal and generate electricity.

There are three basic types of photovoltaic cells: monocrystalline cells, polycrystalline cells, and amorphous cells

Mono-crystalline Silicon Cells:

These are made using cells saw-cut from a single cylindrical crystal of silicon (*Figure 2.10*). The principle advantage of mono-crystalline cells is their high efficiencies, typically around 15%, although the manufacturing process required to produce mono-crystalline silicon is complicated, resulting in slightly higher costs than other technologies. Solar cells made from single crystal silicon are currently limited to about 15% efficiency because they are most sensitive to infrared light, and radiation in this region of the electromagnetic spectrum is relatively low in energy

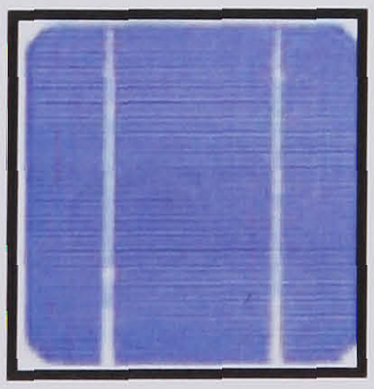

Figure 2.10 Mono - crystalline Silicon Cell (Florida solar energy centre, 2007)

Multi-crystalline Silicon Cells:

These are made from cells cut from an ingot of melted and re-crystallised silicon. In the manufacturing process, molten silicon is cast into ingots of polycrystalline silicon; these

ingots are then saw-cut into very thin wafers and assembled into complete cells (*Figure 2.11*). This process results in cells that are significantly cheaper to produce than single crystal cells, but whose efficiency is limited to around 12% due to internal resistance at the boundaries of the silicon crystals.

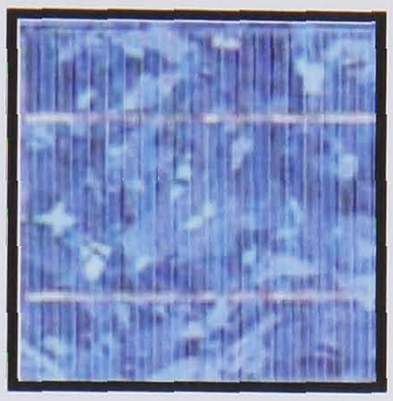

Figure 2.11 Multi – crystalline Silicon Cells (Florida solar energy centre, 2007)

Amorphous Silicon:

Amorphous silicon cells comprise of silicon atoms in a thin homogenous layer rather than a crystal structure. Amorphous silicon absorbs light more effectively than crystalline silicon, so the cells can be thinner. For this reason, amorphous silicon is also known as a "thin film" PV technology (*Figure 2.12*). Amorphous silicon can be deposited on a wide range of substrates, both rigid and flexible, which makes it ideal for curved surfaces and "fold-away" modules. Since amorphous silicon cells have no crystal structure at all, their efficiencies are presently only about 6% due to significant internal energy losses.

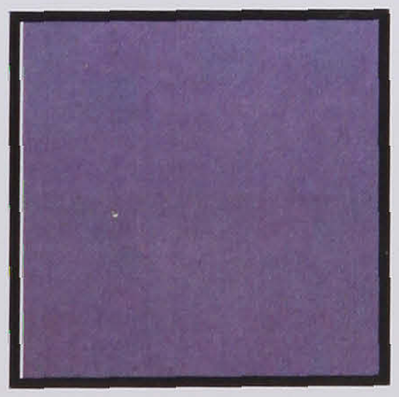

Figure 2.12 Amorphous Silicon Cell (Florida solar energy centre, 2007)

Other Thin Films:

A number of other promising materials such as cadmium telluride (CdTe) and copper indium diselenide (CIS) are now being used for PV modules (*Figure 2.13*). The

attraction of these technologies is that they can be manufactured by relatively inexpensive industrial processes, certainly in comparison to crystalline silicon technologies, yet they typically offer higher module efficiencies than amorphous silicon.

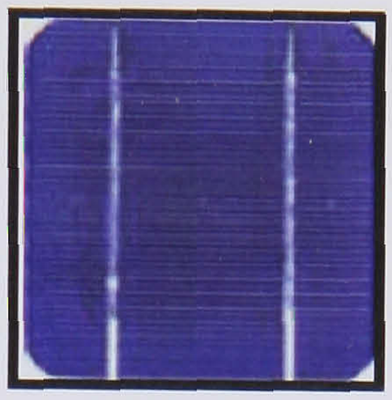

Figure 2.13 Cadmium Telluride Cell (Florida solar energy centre, 2007)

Table 2.2 show the electrical efficiency for different PV cells taken from different manufacturers.

Table 2.2 Photovoltaic Cell Efficiencies (Zondag, 2004)

type of cell	range commercial module efficiencies	producer highest performance modules	corresponding cell manufacturer
multicrystalline Si	11-15%	Sharp	Sharp
monocrystalline Si	10-17%	Suntechnics	SunPower
HIT cells	16-17%	Sanyo Electric	Sanyo Electric
ribbon & EFG cells	12-13%	Titan Energy	RWE Schott
a-Si (single junction)	4-6%	Mitsubishi	Mitsubishi Heavy
a-Si (triple junction)	5-7%	Sunset	United Solar
CIS	9-11%	Würth Solar	Würth Solar
CdTe	6-9%	First Solar	First Solar

2.4.3 Cells, Modules and Arrays

Photovoltaic cells are connected electrically in series and/or parallel circuits to produce higher voltages, currents and power levels. Photovoltaic modules consist of PV cell circuits sealed in an environmentally protective laminate of glass, ethylene-vinyl acetate (EVA) copolymers and Tedlar, and are the fundamental building blocks of PV systems. Photovoltaic panels include one or more PV modules assembled as a pre-wired, field-installable unit (*Figure 2.14*). A photovoltaic array is the complete power-generating unit, consisting of any number of PV modules and panels.

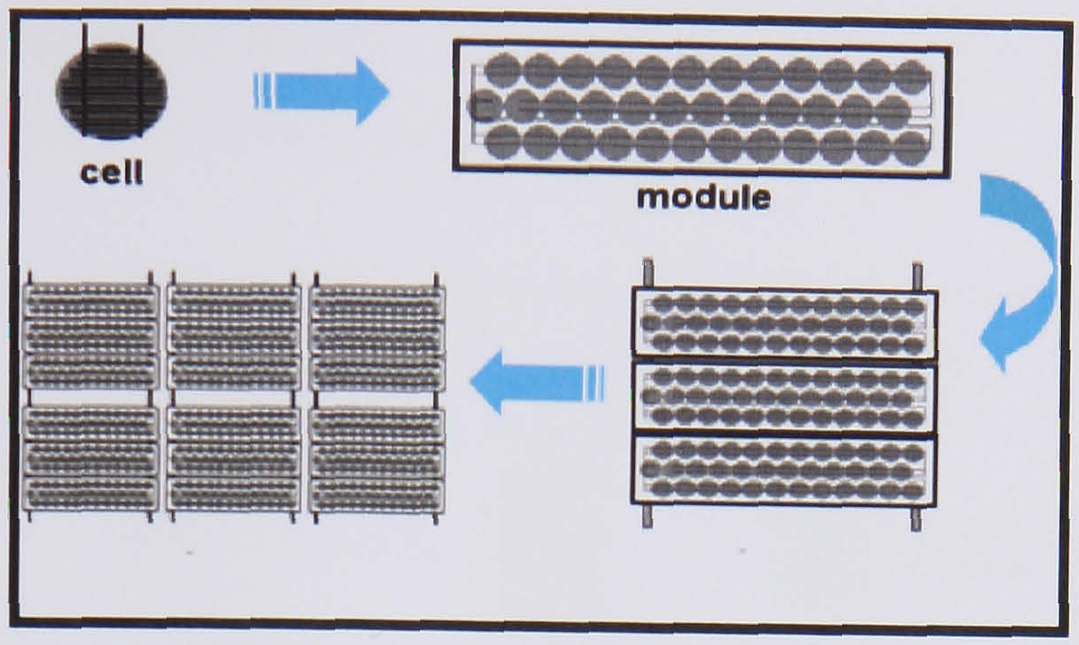

Figure 2.14 Photovoltaic cells, modules, panels and arrays (Florida solar energy centre, 2007)

The performance of PV modules and arrays are generally rated according to their maximum DC power output (watts) under Standard Test Conditions (STC). Standard Test Conditions are defined by a module (cell) operating temperature of 25 ^{o}C, and incident solar irradiance level of 1000 W/m^2 under Air Mass 1.5 spectral distribution. Since these conditions are not always typical of how PV modules and arrays operate in the field, actual peak is usually 85 to 90 percent of the STC rating.

Today's photovoltaic modules are extremely safe and reliable products, with minimal failure rates and projected service lifetimes of 20 to 30 years (Colexon Webpage, 2007). Most major manufacturers offer warranties of 20 or more years for maintaining a high percentage of initial rated power output.

2.4.4 How a PV System Works

Although a PV array produces power when exposed to sunlight, a number of other components are required to properly conduct, control, convert, distribute, and store the energy produced by the array.

Depending on the functional and operational requirements of the system, the specific components required may include major components such as a DC-AC power inverter, battery bank, system and battery controller, auxiliary energy sources and sometimes the specified electrical load (appliances). In addition, an assortment of balance of system (BOS) hardware, including wiring, surge protection and disconnect devices, and other

power processing equipment. *Figure 2.15* shows a basic diagram of a photovoltaic system and the relationship of individual components.

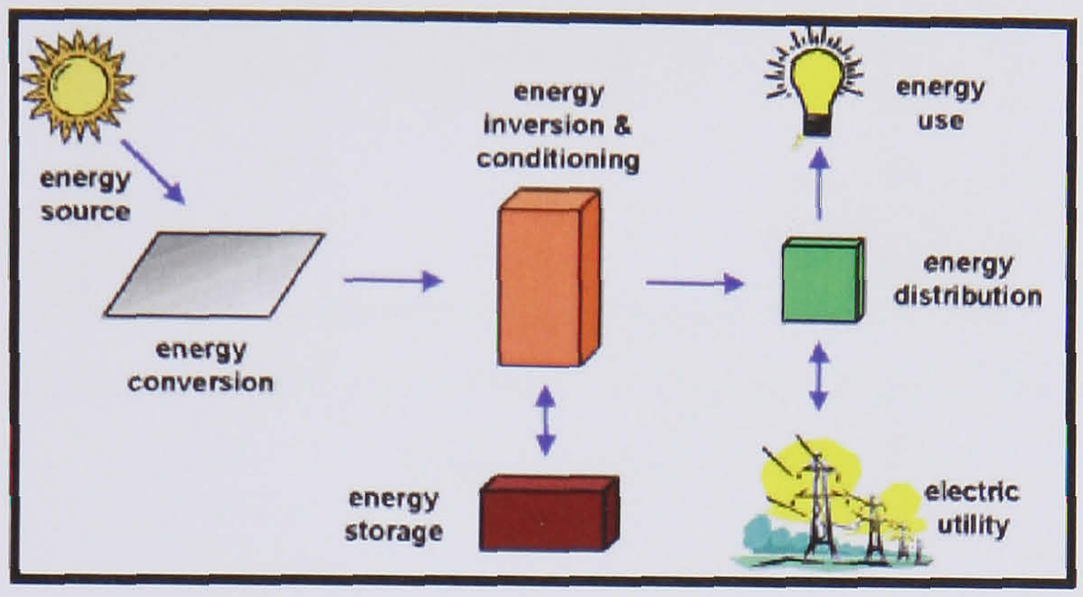

Figure 2.15 Major photovoltaic system components (Florida solar energy centre, 2007)

2.4.5 Types of PV Systems

Photovoltaic power systems are generally classified according to their functional and operational requirements, their component configurations, and how the equipment is connected to other power sources and electrical loads. The two principal classifications are grid-connected or utility-interactive systems and stand-alone systems.

Grid Connected System

Grid-connected or utility-interactive PV systems are designed to operate in parallel with and interconnected with the electric utility grid (*Figure 2.16*). The primary component in grid-connected PV systems is the inverter, or power conditioning unit (PCU). The PCU converts the DC power produced by the PV array into AC power consistent with the voltage and power quality requirements of the utility grid, and automatically stops supplying power to the grid when the utility grid is not energized. This allows the AC power produced by the PV system to either supply on-site electrical loads or to back-feed the grid when the PV system output is greater than the on-site load demand.

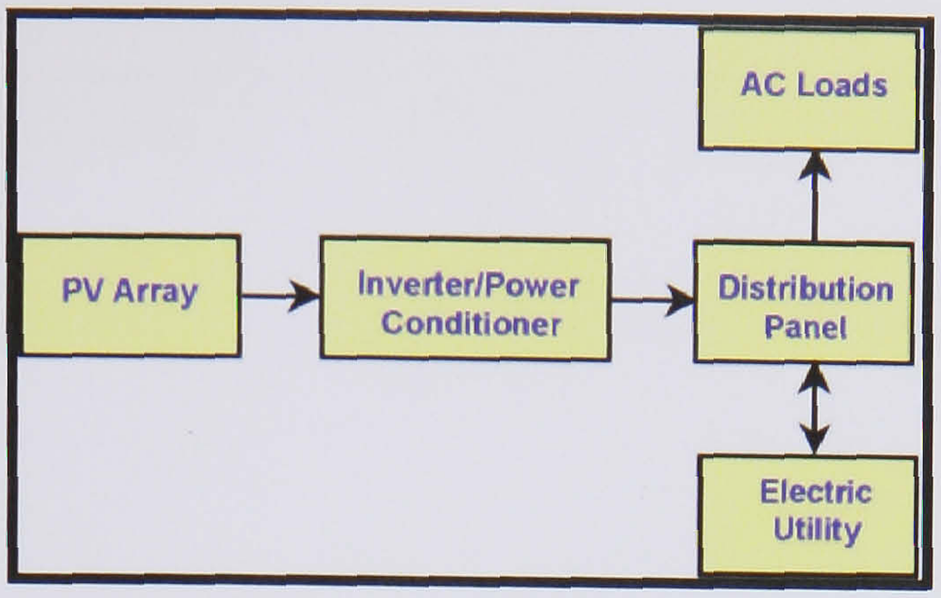

Figure 2.16 Diagram of grid-connected photovoltaic system (Florida solar energy centre, 2007)

Stand-Alone Photovoltaic Systems

Stand-alone PV systems are designed to operate independently of the electric utility grid, and are generally designed and sized to supply certain DC and/or AC electrical loads. The simplest type of stand-alone PV system is a direct-coupled system, where the DC output of a PV module or array is directly connected to a DC load (*Figure 2.17*). Since there is no electrical energy storage (batteries) in direct-coupled systems, the load only operates during sunlight hours, making these designs suitable for common applications such as ventilation fans, water pumps, and small circulation pumps for solar thermal water heating systems.

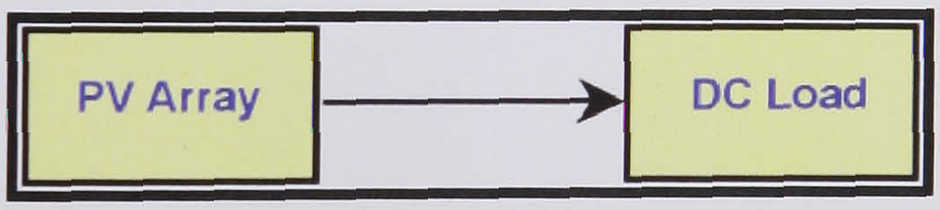

Figure 2.17 Direct-coupled PV systems (Florida solar energy centre, 2007)

In many stand-alone PV systems, batteries are used for energy storage. *Figure 2.18* shows a diagram of a typical stand-alone PV system powering DC and AC loads.

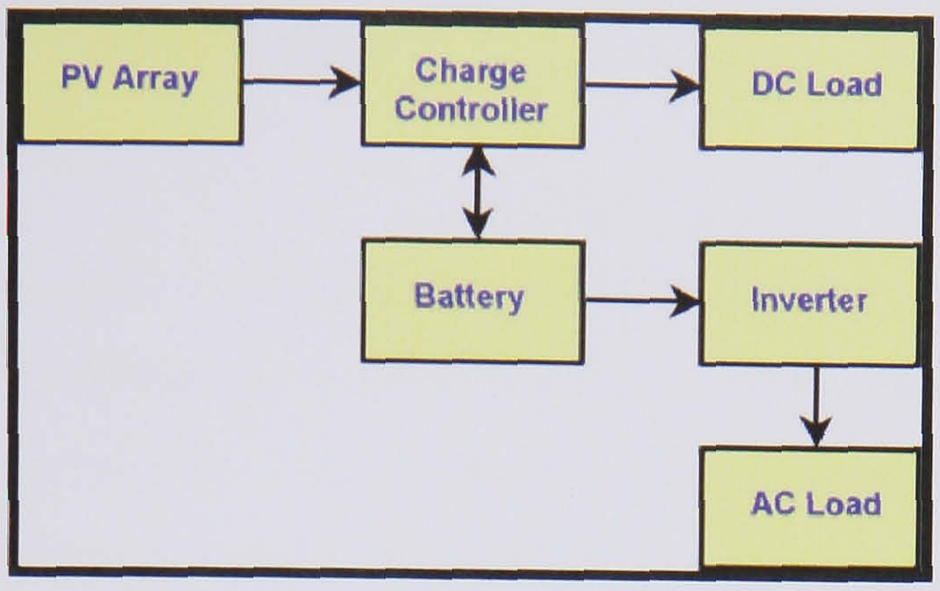

Figure 2.18 Diagram of stand-alone PV system with battery storage powering DC and AC loads (Florida solar energy centre, 2007)

2.4.6 PV Performance

Researchers measure the performance of a PV device to predict the power the cell will produce. Current-voltage (I-V) relationships measure the electrical characteristic of PV device and are depicted by what called "I-V curves." These I-V curves are obtained by exposing the cell to a constant level of light, while maintaining a constant cell temperature, varying the resistance of the load, and measuring the current that is produced. The characteristic curve of a PV-cell can be obtained through measurement of the PV cell according to the circuit shown in Figure *2.19*.

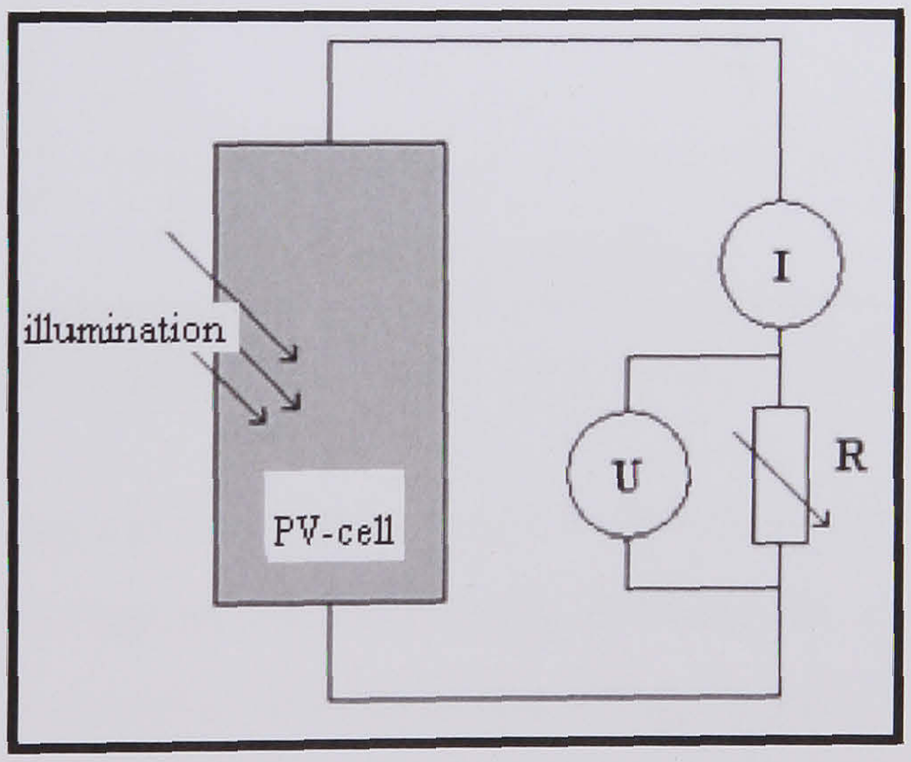

Figure 2.19 Measurement circuit for a PV-cell's characteristic curve

The resistance in the circuit can be changed by using an adjustable resistor *R*. The current (*I*) in the circuit is measured by connecting an ammeter in series with the

resistor. The voltage (U) across the resistor is measured by connecting a voltmeter in parallel with the resistor.

A current-voltage (I-V) curve shows the possible combinations of current and voltage output of a photovoltaic device. A PV device, such as a solar module, produces its maximum current when there is no resistance in the circuit, i.e. when there is a short circuit between its positive and negative terminals. This maximum current is known as the short circuit current and is abbreviated I_{sc}. When the module is shorted, the voltage in the circuit is zero. Conversely, the maximum voltage occurs when there is a break in the circuit. This is called the open circuit voltage (V_{oc}). Under this condition the resistance is infinitely high and there is no current, since the circuit is incomplete. These two extremes in load resistance, and the whole range of conditions in between them, are depicted on the I-V curve as shown in *Figure 2.20.* Current, expressed in amps, is on the vertical y-axis. Voltage, in volts, is on the horizontal x-axis.

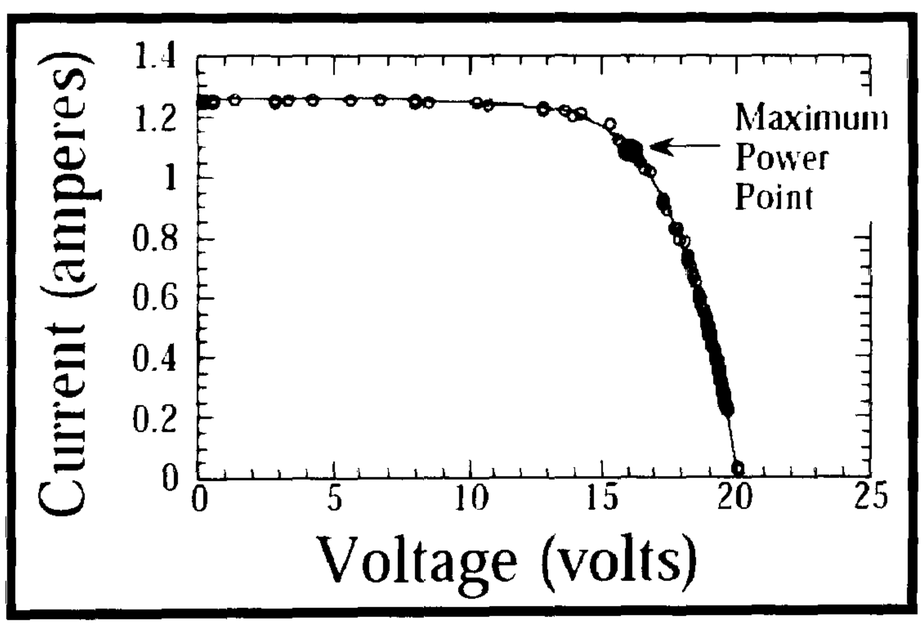

Figure 2.20 Typical I-V curve of a PV module (Kammen, 2007)

The power available from a photovoltaic device at any point along the curve is just the product of current and voltage at that point and is expressed in watts. At the short circuit current point, the power output is zero, since the voltage is zero. At the open circuit voltage point, the power output is also zero, but this time it is because the current is zero. There is a point on the knee of the curve where the maximum power output is located.

Energy conversion efficiency

A solar cell's *energy conversion efficiency* (η_{ele}) is the percentage of power converted (from absorbed light to electrical energy) and collected, when a solar cell is connected to an electrical circuit. This term is calculated using the ratio of P_m, divided by the input light irradiance under "standard" test conditions (E, in W/m²) and the *surface area* of the solar cell (A_c in m²).

$$\eta = \frac{P_m}{E \times A_c} \qquad \text{Eq. (2.4.1)}$$

The quality of a cell can be described by the *fill factor* (*FF*), which is the ratio of the cell's maximum power to the product of the short-circuit current and open-current voltage

$$FF = I_{mp} U_{mp} / I_{sc} U_{oc} \qquad \text{Eq. (2.4.2)}$$

The closer the value of the fill factor is to unity, the better the operation of the PV-cell. The fill factor is lowered by the ohmic resistance of the cell. When the temperature of a cell increases, both the short-circuit voltage and fill factor decrease.

Factors Affecting Conversion Efficiency

Much of the energy from sunlight reaching a PV cell is lost before it can be converted into electricity. But certain characteristics of solar cell materials limit a cell's efficiency. Some characteristics are fixed, but others can be improved by selecting appropriate materials and carefully designing the cell. Some of these factors that affect the performance of the PV are:

- Wavelength of light
- Electrical resistance
- Reflection
- Shading
- Temperature of PV

The influence of temperature on the current–voltage characteristic of a PV module is shown in *Figure 2.21* for a module consisting of 72 single-crystalline silicon solar cells at 25 and 60 °C under the irradiance of 830 W/m2, Radziemska (1999). Therefore, it is necessary to cool the modules in order to eliminate the negative effect of elevated temperature of PV module power output as seen from *Figure 2.22* using the modules of silicon solar cells.

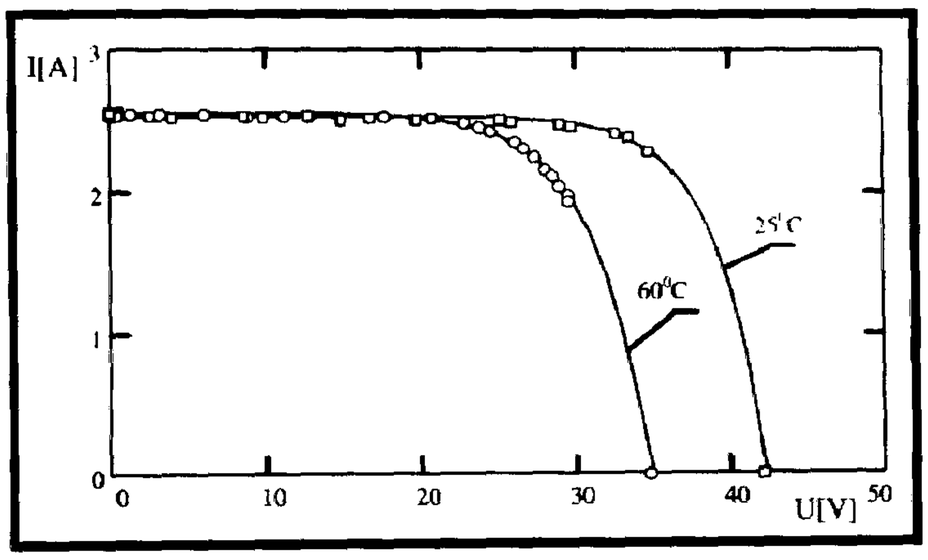

Figure 2.21 Current–voltage characteristics of a 72-cell PV module at: 25 and 60 °C under the irradiance of 830 W/m^2 (Radziemska, 2002)

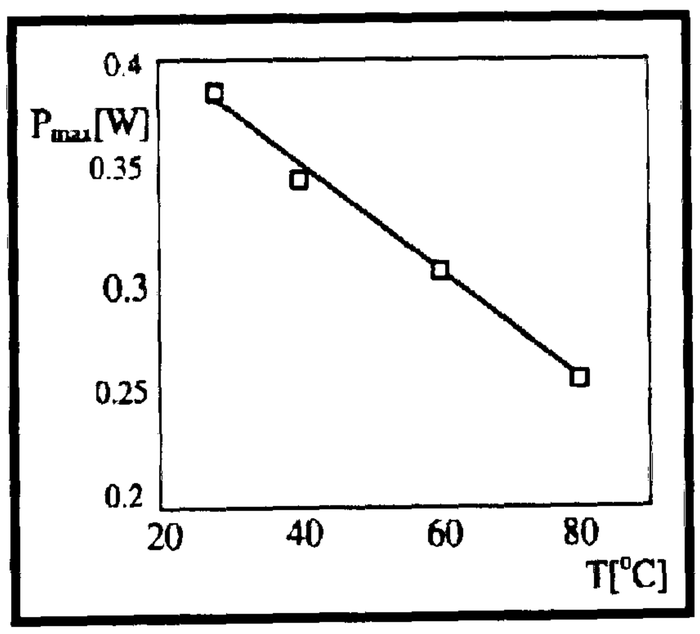

Figure 2.22 Temperature dependence of the maximum output power (Radziemska, 2002)

2.4.7 Temperature influence on PV module performances

The most common manner to determine the cell temperature T_c consists of using the Normal Operating Cell Temperature (NOCT) (Nolay, 1987). The value of this parameter is given by the PV module manufacturers. T_c is then dependent on the ambient temperature T_a and on the solar irradiance according to Eq. (2.4.3)

$$T_c = T_a + (\mathrm{NOCT} - 20\ ^\circ\mathrm{C})\frac{\phi}{800} \qquad \text{Eq. (2.4.3)}$$

This simple method yields satisfactory results if the PV modules are not roof-integrated. A complete definition of NOCT and the conditions of determination of this parameter are presented by Mayers (2002) and ASTM (1998). NOCT is calculated for a wind speed of υ = 1 m/s, an ambient temperature T_a=20 °C and a hemispherical irradiance G= 800 W/m^2. NOCT depends strongly of the type of encapsulation of the PV module. The relative temperature coefficient of crystalline silicon solar modules is in the range 0.4–0.6%/°C according to Moshfegh and Sandberg (1998). Del Cueto (2002) studied the performance of several photovoltaic modules using various technologies: crystalline silicon (c-Si), Polycrystalline silicon (pc-Si), Cadmium Telluride (CdTe), and Copper Indium Diselenide (CIS). He noted that for all c-Si, poly c-Si and CIS modules, the changes in efficiency due to temperature dependence appear to be in the range of 10–15% over a temperature change span of 30 °C. The dependences in %/°C of the module efficiency are given in *Table 2.3* for these technologies.

Table 2.3 PV dependence of efficiency from temperature effect (Radziemska, 2002)

Effect of the temperature on the module efficiency according to Del Cueto [13]							
Module type	c-Si	c-Si	c-Si	pc-Si	pc-Si	CIS	CdTe
% °C^{-1}	−0.496	0.388	−0.427	−0.401	−0.431	−0.484	−0.035

All these effects must be considered in any model for photovoltaic module efficiency. The best known model is given by the following equation:

$$\eta = \eta_r[1 - \beta(T_c - T_r) + \gamma \,\mathrm{Log}\,\phi] \qquad \text{Eg (2.4.4)}$$

where n_r is the reference module efficiency at a PV cell temperature T_r of 25 °C and at a solar irradiance on the module equal to 1000 W/m^2. γ and β are respectively the solar

irradiance and temperature coefficients for the PV module. T_c is the PV cell temperature, which depends on the environmental conditions. Generally, these parameters (T_r, n_r, γ, β) are given by the photovoltaic manufacturer, but γ and β depend on the material used for the PV module. Evans (1981) suggested values for silicon of β= 0.0048 1/°C and γ=0.12.

Another formulation has been used by Sandnes and Rekstad (2002), which implies that the efficiency depends linearly on cell temperature:

$$\eta = \eta_r - \mu(T_c - T_r) \quad \text{Eq. (2.4.5)}$$

It may be noticed that for γ=0 Eq. (2.4.4) is identical to Eq. (2.4.5) with $\mu=\beta x n_r$. In the two models the cell temperature appears, thus to be an important parameter to study. *Table 2.4* shows various temperature coefficients for different type of modules taken from manufacturers.

Table 2.4 PV temperature coefficients for different type of cells (Zondag, 2004)

producer	type of cell	temperature coefficient (based on power)
(reference)	crystalline Si	-0.4%/K to -0.5%/K
Mitsubishi Heavy	a-Si	-0.2%/K
RWE Schott Solar	a-Si	-0.2%/K
Uni-Solar	a-Si	-0.21%/K
Kaneka	a-Si/μc-Si hybrid	-0.23%/K
Würth	CIS	-0.36%/K
First Solar	CdTe	-0.25%/K

2.5 PV/Thermal Systems

Hybrid photovoltaic/thermal (or simply PV/T) collectors are devices that simultaneously converts solar energy into electricity and heat. A significant amount of research on PV/T collectors has been carried out over the last 25 years. The review covers analytical and numerical models, simulation and experimental work, and qualitative evaluation of thermal/electrical output. The main developments were as follows:

- **PV/T Liquid collectors**: The liquid PV/T collectors are similar to conventional flat plate liquid collectors; an absorber with a serpentine tube or a series of parallel risers is applied, onto which PV has been laminated or glued.
- **PV/T Air collectors**: The PV/T air collectors are similar to a conventional underflow air collector with a PV laminate functioning as the top cover of the air channel.
- **Ventilated PV with heat recovery**: In conventional PV facades or PV roofs, an air gap is often present at the rear in order to allow the air to cool the PV by means of natural convection (ventilated PV). If this heat can be recovered from the PV and be used in the building, the PV functions as a PV/T collector.
- **PV/T Concentrators**: Research on concentrating PV was based on the idea of replacing expensive PV by cheap reflectors. A point of attention was the high temperature that could be reached by the cells. Therefore, cooling of the cells was necessary. By using active cooling the heat could be used as well.

In the present paper the emphasis will be on PV/T liquid and air systems. This choice was made because our research lies in these two systems. In addition, the results are presented in the form of a thematic overview in order to present the mass of results in a clear and comprehensive way.

PV/T collectors can be flat plate or concentrating and are classified according to the type of the working fluid used (water or air).

2.5.1 Flat plate PV/T collectors

Flat plate PV/T collectors look very similar to the well known flat plate thermal collectors. The only significant difference is the PV panel which is attached on the top of the metallic absorber plate.

A PV/T collector, shown schematically in *Figure 2.23*, typically consists of a PV module on the back of which an absorber plate (a heat extraction device) is attached. PV modules convert solar radiation into electricity with peak efficiencies in the range of 5–17% as we've seen from the previous section. The purpose of the absorber plate is twofold. Firstly, to cool the PV module and thus improve its electrical performance and secondly to collect the thermal energy produced, which would have otherwise been lost as heat to the environment. This collected heat could be used, for low temperature applications such as domestic hot water.

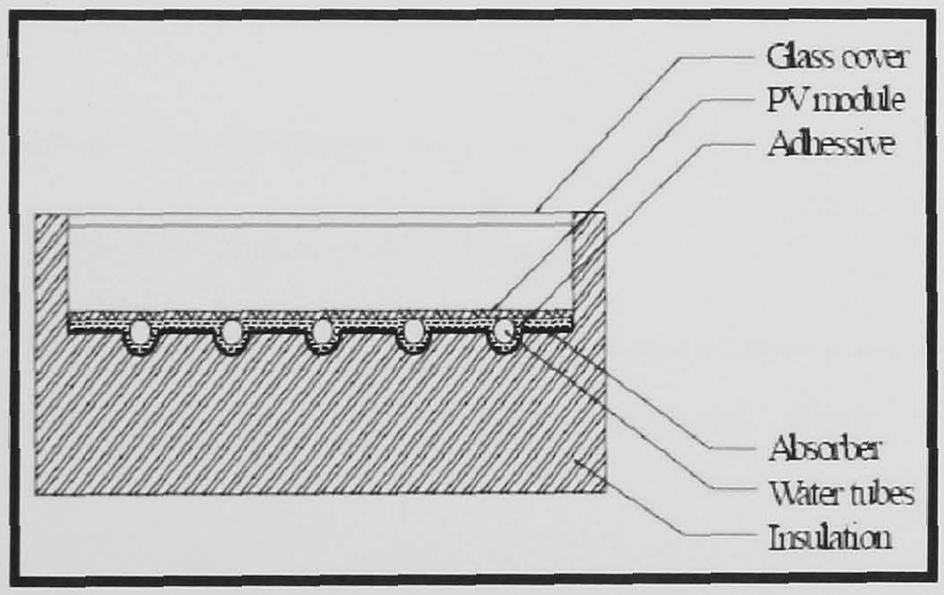

Figure 2.23 Cross section of a PV/T collector (Charalambous, 2007)

As reported by Zondag et al. (1999) the electrical and the thermal performance of PV/T collectors depending upon the absorber temperature is lower than that of separate PV panels and conventional thermal collectors. However, they emphasized that the two collectors in a PV/T module produce more energy per unit surface area than one PV panel and one thermal collector next to each other. This is particularly important in applications where surface area availability is limited. Flat plate PV/T collectors can work with water or air as a heat transfer medium.

2.5.1.1 Water PV/T collectors

For these systems, water is used as the heat transfer fluid. The PV cells are adhered either directly to the absorber or to the interior on a cover plate with a dielectric material. This means that the contact between the PV cells and the absorber or the cover plate is of high thermal conductivity. The heat transfer fluid runs inside the pipes on the absorber and collects heat from the absorber. If the PV cells are mounted on the absorber as shown in *Figure 2.24*, heat is also extracted from the PV cells resulting in a higher electrical efficiency of the PV cells. Useful thermal energy is extracted to one end of the pipes where it can be utilised. The pipes can be coupled either in series as serpentine tubes or in parallel riser tubes. The heat transfer fluid can be circulated by either a pump (a pumped system) or by the difference in specific gravity of the heat transfer fluid (a gravity system) as we discussed also for the solar thermal collectors.

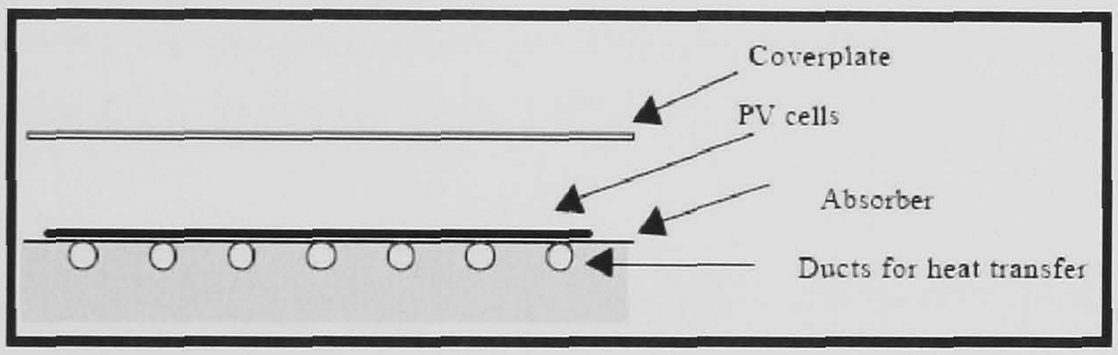

Figure 2.24 A typical water PV/T collector (Sorensen, 2003)

Furthermore, water PV/T collectors can be divided into groups according to temperature levels of the heat transfer fluid. These range from low-temperature applications for e.g. swimming pool and heat pump applications to medium-temperature applications around 55°C for e.g. domestic hot water applications. In the study of F. Leenders et al. (2000, 2001) it was noticed that PV/T systems are suitable for low temperature applications. For medium temperature applications, the thermal and electrical yield of the hybrid system is lower than that of the two separate systems. This is due to the very basic reason that for water heating the solar collector works in higher temperatures, whereas the PV panel reaches its' maximum yield at low temperatures. The combination of the two will always be a compromise.

Water type PV/T collectors can be distinguished also according to the water flow pattern. As shown in *Figure 2.25*, these are differentiated as sheet and tube, channel, free flow and two absorber type.

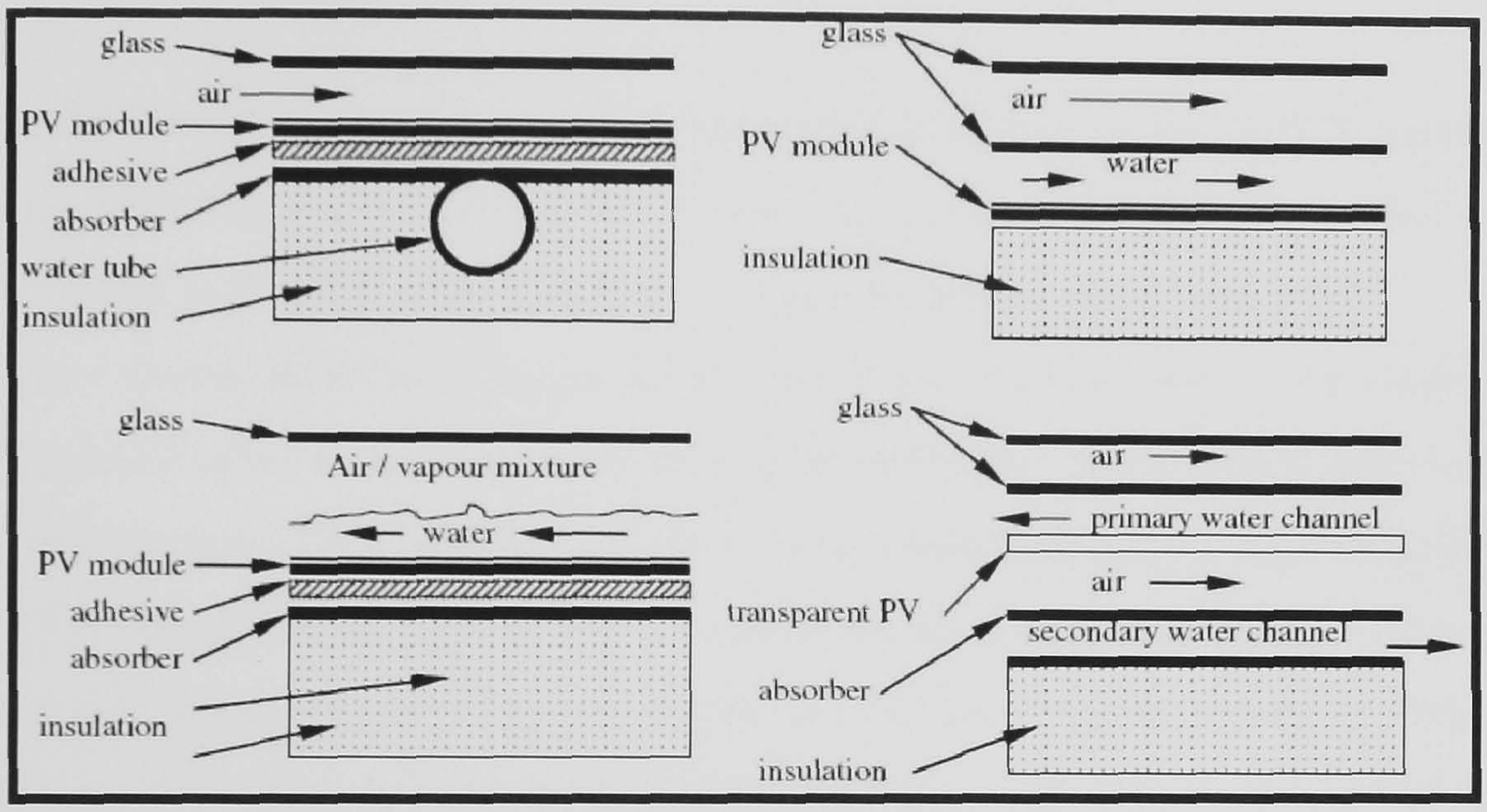

Figure 2.25 Types of water PV/T collectors. (Zondag, 2005)

A number of PVT prototypes have been constructed, such as sheet-and-tube PV/T collectors (De Vries, 1998), channel type PV/T collectors (Zondag et al. 2003), PV/T collectors with plastic absorbers (Sandnes, 2002), thermosyphon PV/T collectors (Agarwal & Garg, 1994; Chow et al. 2006) and ICS PV/T collectors (Krauter, 2004). Purpose of all these types of PV//T systems is to keep the PVs as cool as possible and at the same time extract the heat and use it.

2.5.1.2 Air PV/T collectors

The other type of PV/T collector is an air-based system as shown in *Figure 2.26*. Instead of water, air is used as heat transfer fluid. The PV cells are either adhered to the interior of the cover plate or to an absorber or the PV cells can serve as either the absorber or cover plate itself. The air can be circulated by either natural ventilation or forced ventilation.

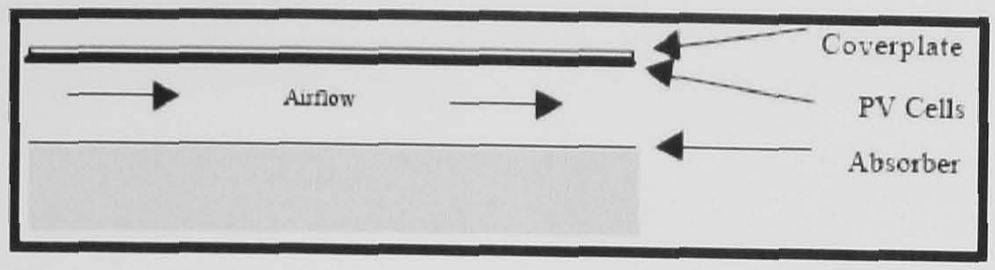

Figure 2.26 Example of an air PV/T collector (Sorensen, 2003)

Air type PV/T collectors may also be distinguished according to the air flow pattern. These are differentiated with respect to the flow of air above the absorber, below the absorber or on both sides of the absorber in single or double pass *Figure 2.27*.

Only a few studies have been carried out into PVT air collectors, which is probably due to the limited market share of solar air heating. Performance studies for single channel glazed and unglazed PVT air collectors have been undertaken (Tripanagnostopoulos et al., 2002). The additional glazing helped to increase the thermal efficiency of the system by about 30% but in the same time the electrical efficiency was decreased by 16%. Comparisons of single channel and dual channel PVT air collectors were carried out by Sopian (1997) and Hegazy (2000). The finding was the increase in the thermal efficiency and a decrease in electrical efficiency of the system. Tonui (2006) investigated the performance of two low cost heat extraction improvement modifications in the channel of a PV/T air system to achieve higher thermal output and PV cooling so as to keep the electrical efficiency at acceptable level. These involved the use of thin flat metal sheet suspended at the middle of the duct or a finned back wall to the air channel in the PV/T air configuration. Both modifications showed thermal and electrical efficiency increase but a factor that influenced the performance were the channel length of the system. As channel length increased after a point both electrical and thermal efficiencies decreased. The length that this effect took place was at 3 and 6 meters for electrical and thermal efficiency.

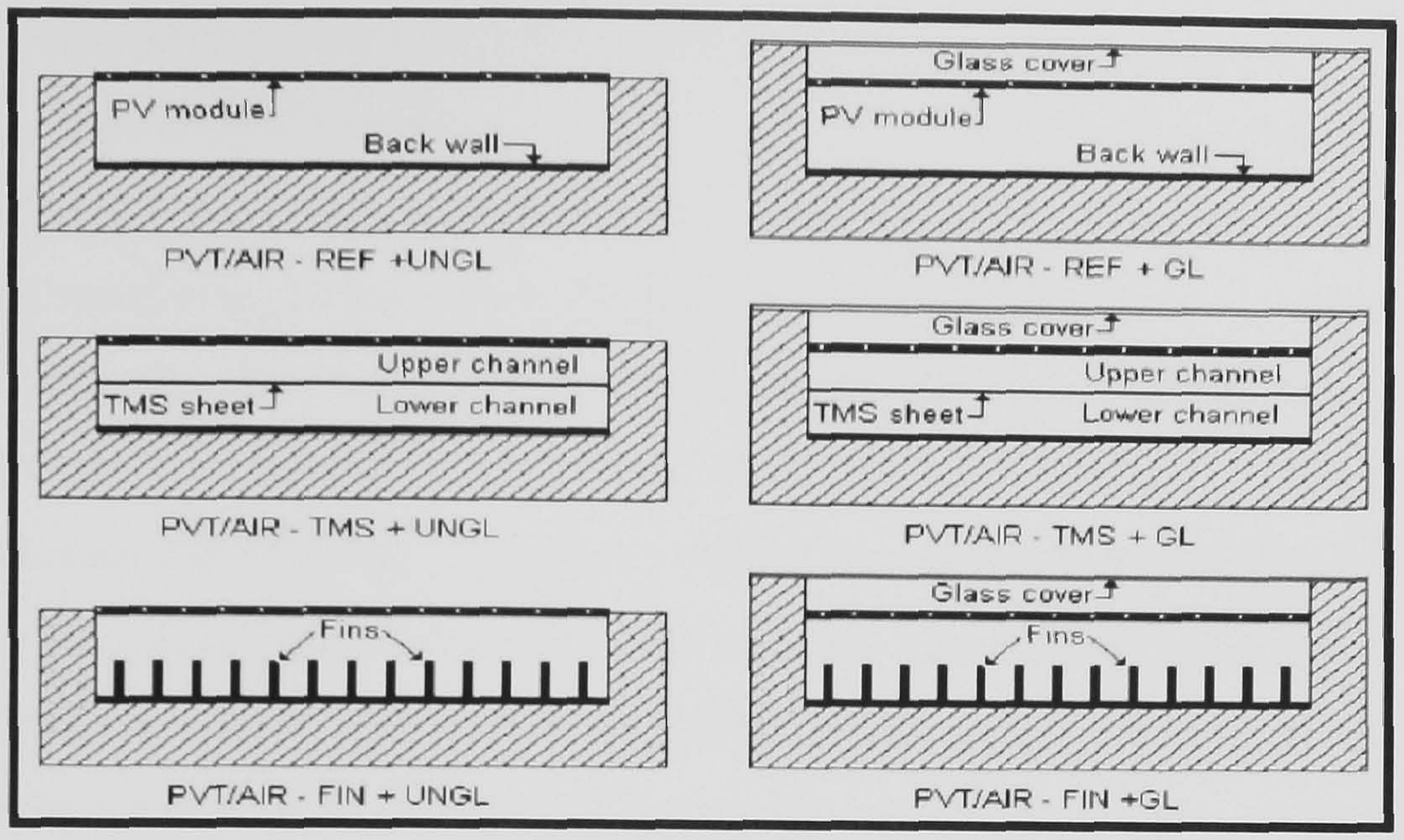

Figure 2.27 Cross-sectional view of PVT/Air collector models (Tonui, 2006)

2.5.2 Parameters affecting PV/T performance

A number of parameters have been identified that affect PV/T performance. These include the manufacture and the design characteristics of such a system such as mass flow rate, inlet temperature of working fluid, number of covers, absorber to fluid thermal conductance and, in the case of water type PV/T collectors, absorber plate design parameters such as tube spacing, tube diameter and fin thickness.

All these parameters affect the thermal and electrical efficiency of the system. An analysis of these parameters follows.

2.5.2.1 Manufacturing aspects of PV/T systems

The most basic technique for manufacturing a PV/T collector is to glue either PV cells or an entire commercial PV laminate to the absorber of a commercial thermal collector. This technique has been applied in many research projects (see De Vries 1998, Sandnes 2002). The drawback of gluing PV cells is the insufficient protection from the environment and the electrical insulation. The drawback of gluing an entire PV laminate to a thermal collector is the large thermal resistance that occurs between the laminate and the absorber. Also the white Tedlar in the back of a PV that is generally used for c-Si modules has relatively large reflection losses.

A more advanced technique is to laminate the whole package of top cover, PV cells, electrical insulation and absorber together in one step. Normally an additional electrically insulating foil is laminated between the cells and the absorber, but also an electrically insulating coating may be applied directly to the absorber. A number of sheet-and-tube absorber configuration designs are compared by Affolter et al. (1997). For a sheet-and-tube absorber soldering the tubes after lamination is normally not feasible because the soldering temperature would damage the encapsulation whereas gluing the tubes may compromise reliability and heat transfer. Instead of a sheet-and-tube absorber, also an extruded aluminium plate may be applied, as used by Chow et al. (2006). Whichever technique is chosen, it is necessary to take care that encapsulate is able to withstand the high temperatures that occur in stagnating glazed PV/T modules, which can be as high as 130 ^{o}C (Zondag 2002).

Instead of lamination, a low-temperature encapsulation technique may be used, such as the application of silicones (see e.g. Komp 2002). Komp first applies a layer of silicone over the absorber onto which he presses a layer of cloth, followed by a second layer of silicone for the fastening of the cells.

Research has been carried out in finding high-temperature-resistant plastics suitable for glazed applications but Sandnes and Rekstad (2002) warn that the difference in thermal expansion between the cells and the absorber is substantial, which they overcame by applying a layer of elastic silicone adhesive.

2.5.2.2 Covered versus uncovered PV/T collectors

PV/T systems can be subdivided as PV/T panels and PV/T collectors. PV/T panels have no extra transparent cover and therefore will loose heat to the ambient relatively easily and PV/T collectors like most solar thermal collectors have an additional transparent cover preventing heat losses to the environment. When low temperature heat is needed then PV/T panels give good thermal efficiencies. And when higher thermal efficiencies are needed then a PV/T collector is chosen. *Figure 2.28* illustrates the difference in thermal efficiency between the two systems.

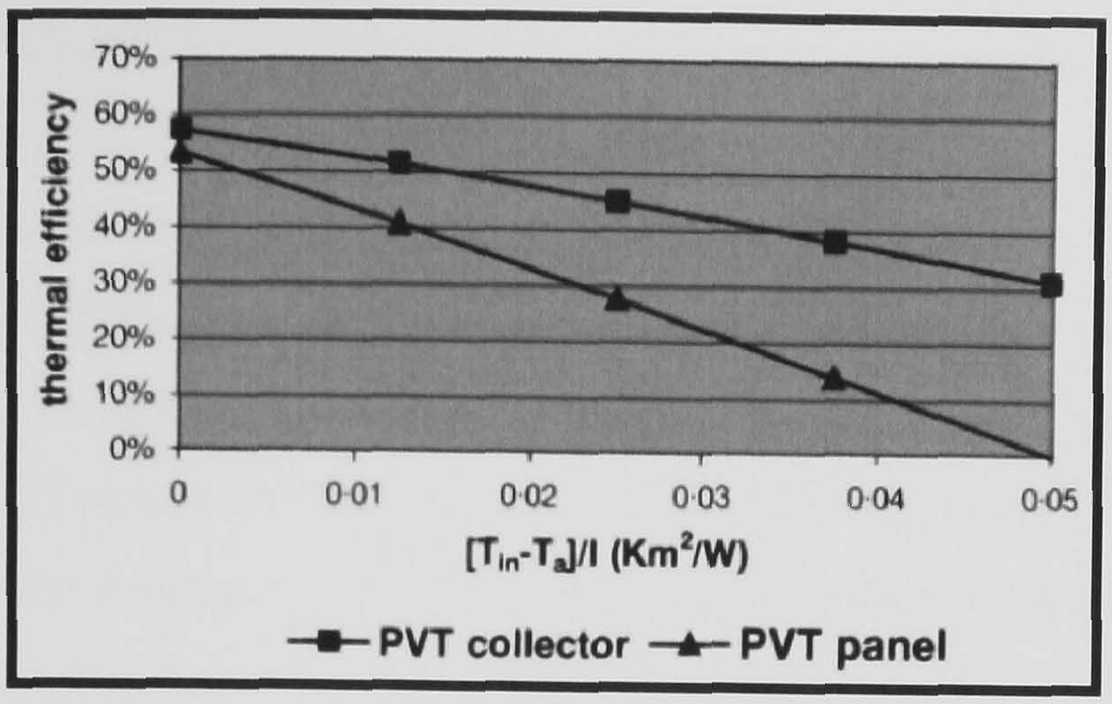

Figure 2.28 Typical thermal efficiency curves for PV/T collectors and PV/T panels (Wim, 2004)

Sandnes and Rekstad (2002) explained that the effect of adding a glass cover to the PV/T collector is to reduce the heat losses to the surroundings. However, the energy absorptance is also reduced by reflection (around 10%) from the glass. From the results it was clear that the PV/T without glass cover produced the highest total electrical energy. Although not stated it is likely that this performance of the uncovered PV/T collector is attributed firstly to the entire transmittance of radiation to the PV cells and secondly to the cooling of the PV cells. On the other hand, the worst electrical performance of the glazed PV/T case is due to the reduced transmittance of radiation due to the presence of the glass cover.

Unglazed PV/T panels have a lower output temperature and are therefore often combined with a heat pump in system studies (Ito et al., 2004; Bakker et al., 2005; Nishikawa et al., 1993).

On the other hand glazed PV/T collectors can produce high temperature heat directly, and are therefore suitable for direct heating of water. Various systems studies on glazed PV/T systems were carried out (Zondag, 2001). A similar study was of Fujisawa and Tani (1997) who designed and constructed a PV/T collector. They used exergy analysis in order to evaluate its experimental performance, since exergy enables qualitative evaluation by comparing electrical and thermal energy on the same basis. They found that the coverless PV/T collector produced the highest electrical exergy. On the other hand, the thermal performance of the PV/T collector was comparable to that of the flat

plate collector (FPC) and that of the coverless PV/T panel was inferior due to the heat losses from the top.

Zondag et al. (2003) in their numerical study of various PV/T concepts also emphasized that the PV/T panel offer a poor thermal performance due to the large top heat losses to the environment. As a summary the choice of a PV/T panel or collector depends on the application needed. For low temperature applications and when electrical energy is more important an uncovered panel works better. When the system is needed for higher temperature applications then a PV/T collector is the best choice.

2.5.2.3 Thermal module efficiency

Thermally, a PV/T module is similar to a solar thermal collector. As in the case of a solar thermal collector, a good efficiency requires good solar absorption and a good heat transfer. Typical thermal curves for a PV/T collector are indicated in *Figure 2.29*. The figure clearly shows that the glazed PV/T-liquid module has a higher thermal performance than the unglazed module. Also for PV/T air collectors, the literature indicates the strong increase in thermal performance if top glazing is used (Tiwari 2007, Nagano 2001). On the other hand, the glazing reduces the electrical performance due to additional reflection at the cover.

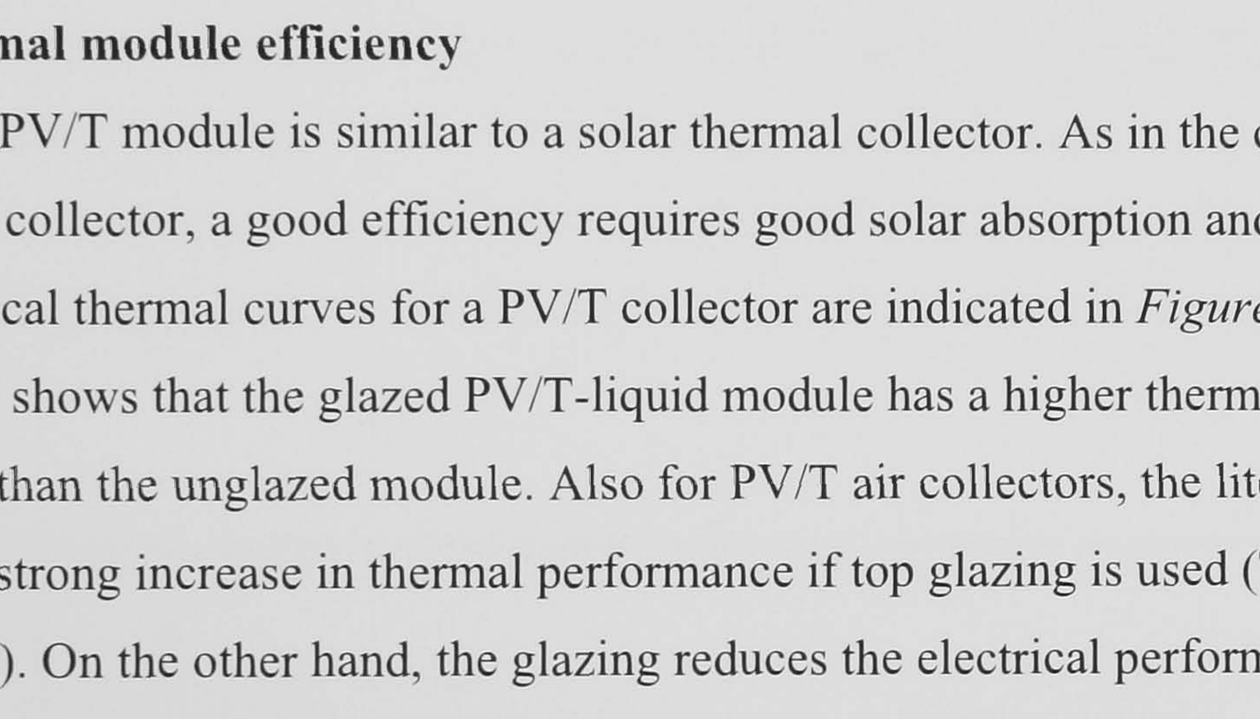

Figure 2.29 Thermal Efficiencies of a PV/T-liquid collector (Zondag, 2005)

The reduction in thermal efficiency is due to 4 effects:

1. The absorption factor of the PV-surface is lower than the absorption factor of a conventional collector surface due to reflections at the various layers in the PV laminate;
2. The PV-surface is not spectrally selective, resulting in large thermal radiation losses;
3. The heat resistance between the absorbing surface and the heat transfer medium is increased due to additional layers of material. This implies a relatively hot surface on the PV/T module, leading to additional heat losses and a decrease in electrical performance
4. The energy that is converted to electrical output is lost from the thermal output.

These effects will be explained below and can be illustrated in *Figure 2.30*. This figure shows the relative magnitude of the different loss terms, for the case of a typical glazed PV/T module consisting of a conventional PV c-Si module glued to a solar thermal collector. In addition, *Figure 2.31* indicates the effect of the successive removal of these loss terms.

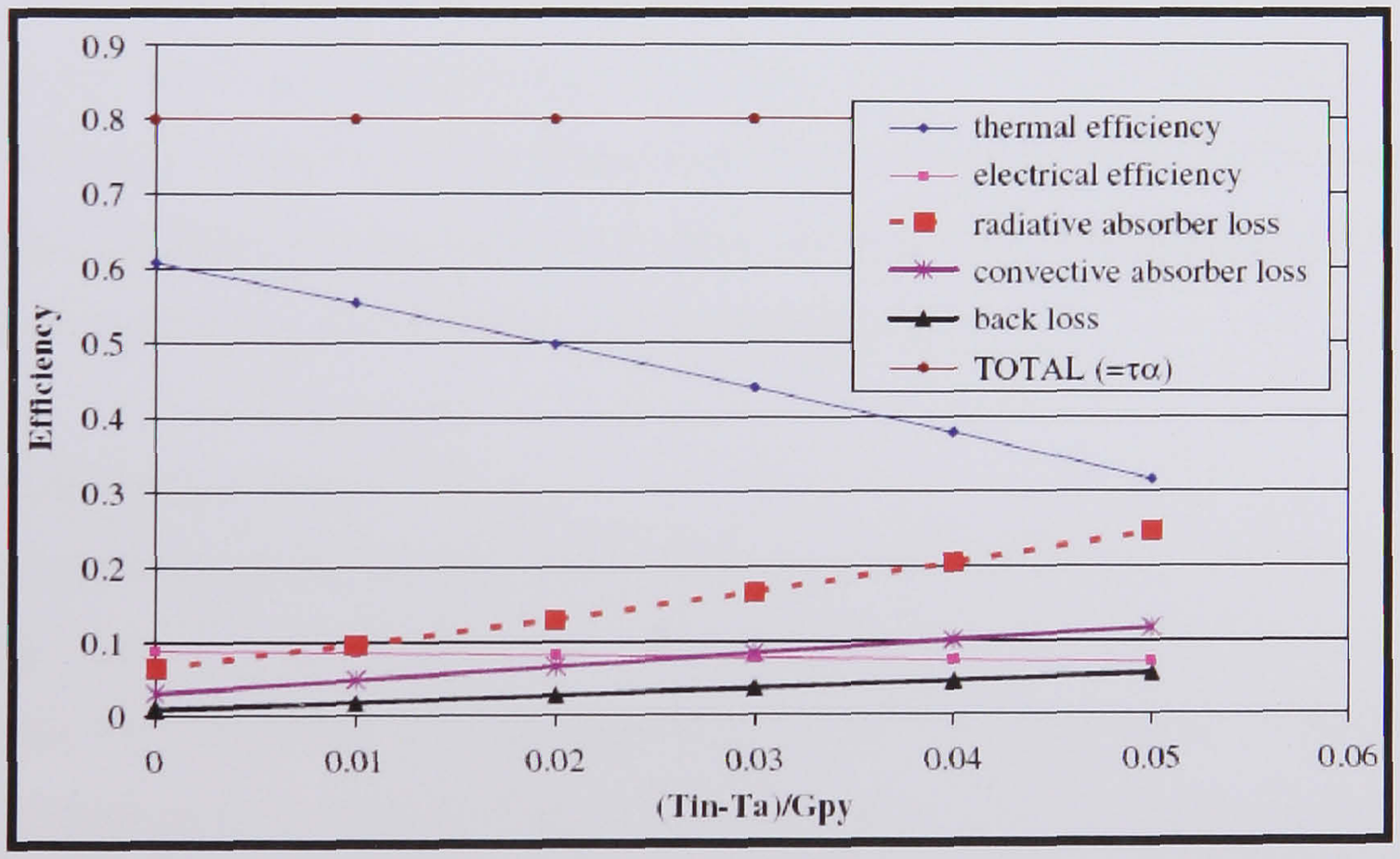

Figure 2.30 The loss mechanisms in the PV/T collector. Note the large effect of radiation losses from the PV/T absorber to the top glass, compared to convective and back loss. (Zondag, 2005)

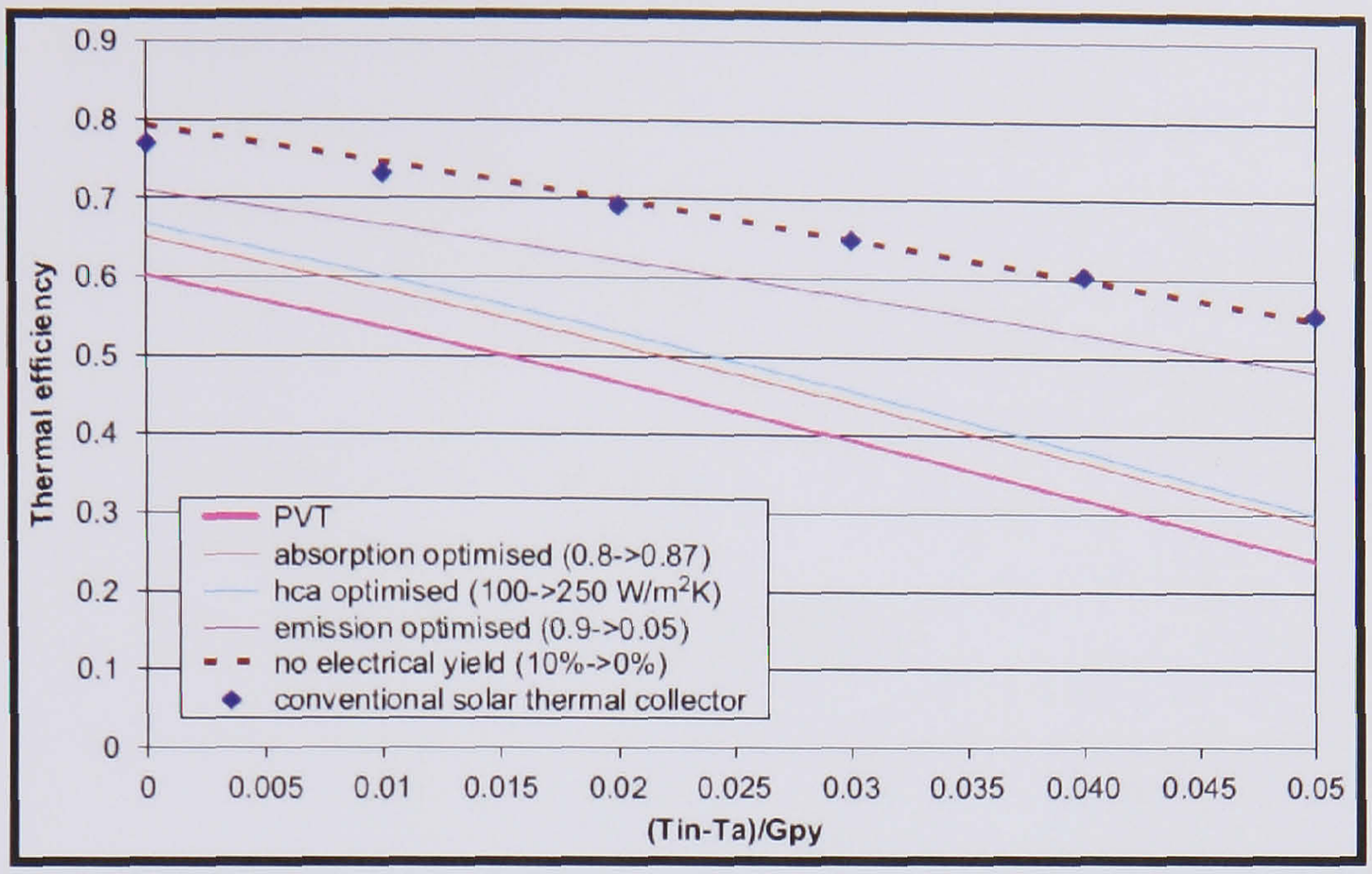

Figure 2.31 Starting from the efficiency curve for the liquid PV/T collector, successively removing the special features of the PV/T module finally results in the curve for a conventional solar thermal collector. h_{ca} is the heat transfer coefficient between cells and absorber (Zondag, 2005)

It is clear that the effect of low absorption and the radiative loss are responsible for the largest reduction in PV/T performance, while also the effect of the thermal resistance is substantial. The three loss mechanisms (reflection loss, spectral selectivity and thermal resistance), will be the subject of the following paragraphs

2.5.2.3.1 Reflection losses

The low transmission-absorption factor is an important loss mechanism in PV/T collectors. Typically, the absorbers of solar thermal collectors have absorption of up to 95%, while PV/T absorbers are typically limited to 75–85%, depending on the PV type and the absorbing surface underneath.

The effect of the transmission-absorption on the efficiency curve is indicated in *Figure 2.32*.

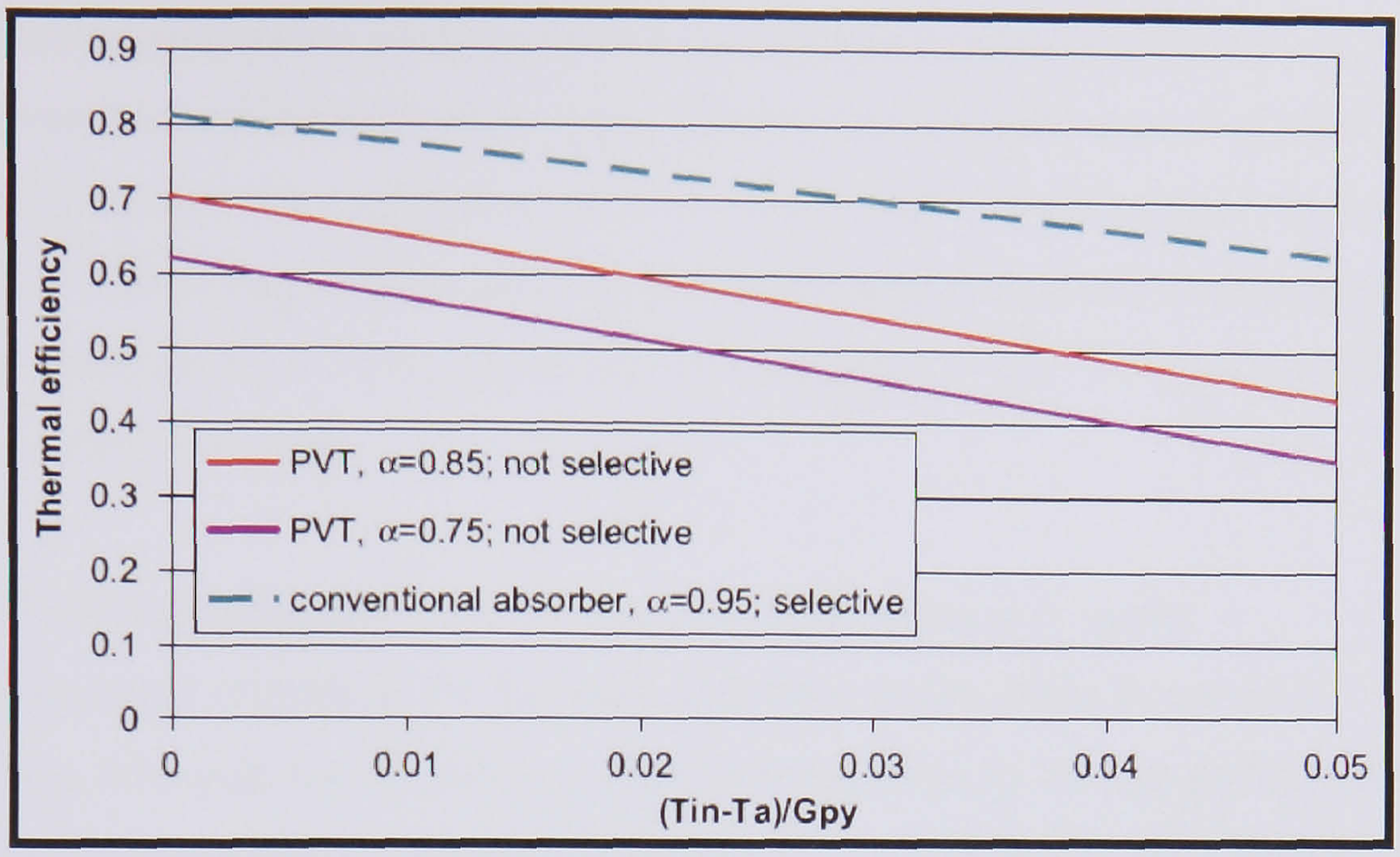

Figure 2.32 Thermal efficiency affected by the optical characteristics of an absorber (Zondag, 2005)

Four aspects have been found in the literature relating to the absorbance of PV/T collectors:

1. Reducing reflection at the top cover;

For glazed PV/T collectors, the reflection at the top cover affects both the electrical and the thermal performance. Typically for glazed conventional and PV/T collectors, low-iron glass is used for the top cover, with a transmission of about 91–92%. In recent years, glass with 96% transparency is becoming available from the companies. This glass is suitable for both collector glazing (Furbo 2003) and PV coverage (Furbo 2004), and seems very interesting for PV/T application.

Plastic cover materials offer potential for cost savings (both materials and handling), but lower optical performance and lower reliability make such materials less suitable for PV/T applications. Hendrie (1982) reported the first generation PV/T air collector with a Teflon film over the PV-cells. It was found that the Teflon film was not stable at the operating temperatures encountered during testing. For the module with different cover materials (Urethane, Tefzel, and fibreglass), values of 67–75% of thermal efficiency were found.

Reflection of the sun's irradiance typically reduces the electrical yield of PV modules by 8–15%. Numerous ideas to reduce reflection have been proposed, but most have

drawbacks: antireflective- coatings are not durable and surfaces are expensive, gather accumulate dust and are difficult to clean. Krauter (2004) used water, flowing in the front of the cover, with a refractive index of 1.3 as a viable intermediary between glass (n_{glass}=1.5) and air (n_{air}=1.0). In addition to help keeping the surface clean, water reduced reflection by 2–3.6%, decreased cell temperatures up to 22 °C and achieved an 8% of net electrical gain.

2. Reducing reflection at the PV electrical wire connectors (grid);

In a conventional crystalline PV laminate, reflection occurs at the silver wire connectors. Although the reflection is large, the area taken by the top grid is small, which makes this effect of secondary importance. Younger et al. (1981) tried to blacken the top grid using tellurium-oxide a black chrome plating and a sodium cyanide-based black electroplate was applied but the results was unsuccessful. Loferski et al. (1982) blackened the top-grid of a cell with anti-reflection coating and measured the absorptance between 92% and 94%.

3. Increasing absorption in PV and rear contact;

Due to the fact that a large difference exists between the indices of refraction of the silicon and the EVA in the PV laminate, the silicon is coated with an anti-reflection coating in order to reduce the reflection at the top of the cell. Crystalline silicon is a good absorber in the spectral range between 0.5–1.1 μm but is almost transparent for light with wavelength longer than 1.1 μm. In a PV-system, this long-wavelength energy is not useful as it cannot contribute to the generation of electrical energy, but for a PV/T system this energy should be retained for heat production. In the case of crystalline silicon cells, only about 70% of the solar spectrum is absorbed by the silicon. Absorption measurements have been carried out by Affolter et al. (2000) and Platz et al. (1997). For different encapsulated a-Si cells, Affolter found that the absorption over the solar spectrum varied between 71% and 91%. Platz found this absorption to be within the range 78–85% for various encapsulated a-Si cells, while 88% was found for an encapsulated multi-crystalline Si cell.

4. Increasing absorption in the opaque surface below the PV

A different strategy is not to absorb all energy in the cell, but to let part of the long-wave irradiance proceed to a secondary absorber underneath. This requires the use of a back contact grid instead of a solid-back contact. However the reflection at the back contact grid (covering usually 20–30% of the area) as well as reflection at the silicon–EVA interface can be substantial. The simulations by Cox and Raghuraman (1985) showed an increase from 34% to 39% in thermal efficiency due to back contact gridding in combination with a separate absorber underneath. A back contact grid was also reported by Hayakashi et al. (1989), who put underneath his PV-cells a thermal collector consisting of glass tubes filled with a strongly absorbing black collector fluid. In this way, long-wavelength radiation is directly absorbed by the collector fluid. The PV-cells were connected to the thermal absorber by means of an aluminum strip which was located midway between the silicon cells in order to collect heat from the PV as well. He reported a thermal efficiency of approximately 64% and simultaneously an electrical efficiency of 8%.

Another strategy is to use a transparent surface below the PV. This effect implies that only a small part of the irradiance will make it through the cells to the secondary absorber. However, the secondary absorber will still function to catch light that was transmitted through the spacing between the cells. The secondary absorber may be the rear surface of the PV/T absorber. If a commercial PV laminate is used, this is the PV rear foil, which may be of various colors, affecting the magnitude and the spectral variation of the absorption factor. If the cells are laminated to a solar thermal absorber, the solar absorption will be high and largely independent of the wavelength. However, in the case in which the collector medium flows through a channel, it is also possible to have a transparent PV laminate and to have the secondary absorbing surface at the other side of the channel (below the collector medium). In this way, the collector medium is enclosed between the primary absorber (with the PV cells) and the secondary absorber, which makes the heat transfer from the collector to the medium more efficient. Zondag et al. (2003) calculated the thermal efficiency of a PV/T liquid channel collector, with either the channel underneath opaque PV, or the channel underneath transparent PV

with a secondary absorber at the rear. It was found that for the case with the additional rear absorber, the thermal efficiency was 63% instead of 60% for the opaque PV case.

2.5.2.3.2 Absorber plate parameters

The thermal resistance between the PV-cells and the collector fluid should be minimised. A low heat transfer results in a large temperature gradient and therefore in a high PV temperature. The first consideration should be to keep all layers of material between the silicon and the absorber as thin as possible and preferably have them made of materials with a high thermal conduction.

The effect of thermal resistance on the heat removal factor F_R is shown in *Figure 2.33*. The heat removal factor is directly related to the efficiency by:

$\eta = \mathrm{FR} \times [\tau\alpha - U \times (T_{\mathrm{in}} - T_{\mathrm{a}})/\mathrm{Gpy}]$, where τ is the transmission-absorption coefficient, U is the collector loss coefficient and G_{py} is the irradiation. T_{in} represents the collector inflow temperature and T_a the ambient temperature. It can be seen that a good heat transfer is particularly important for unglazed PV/T.

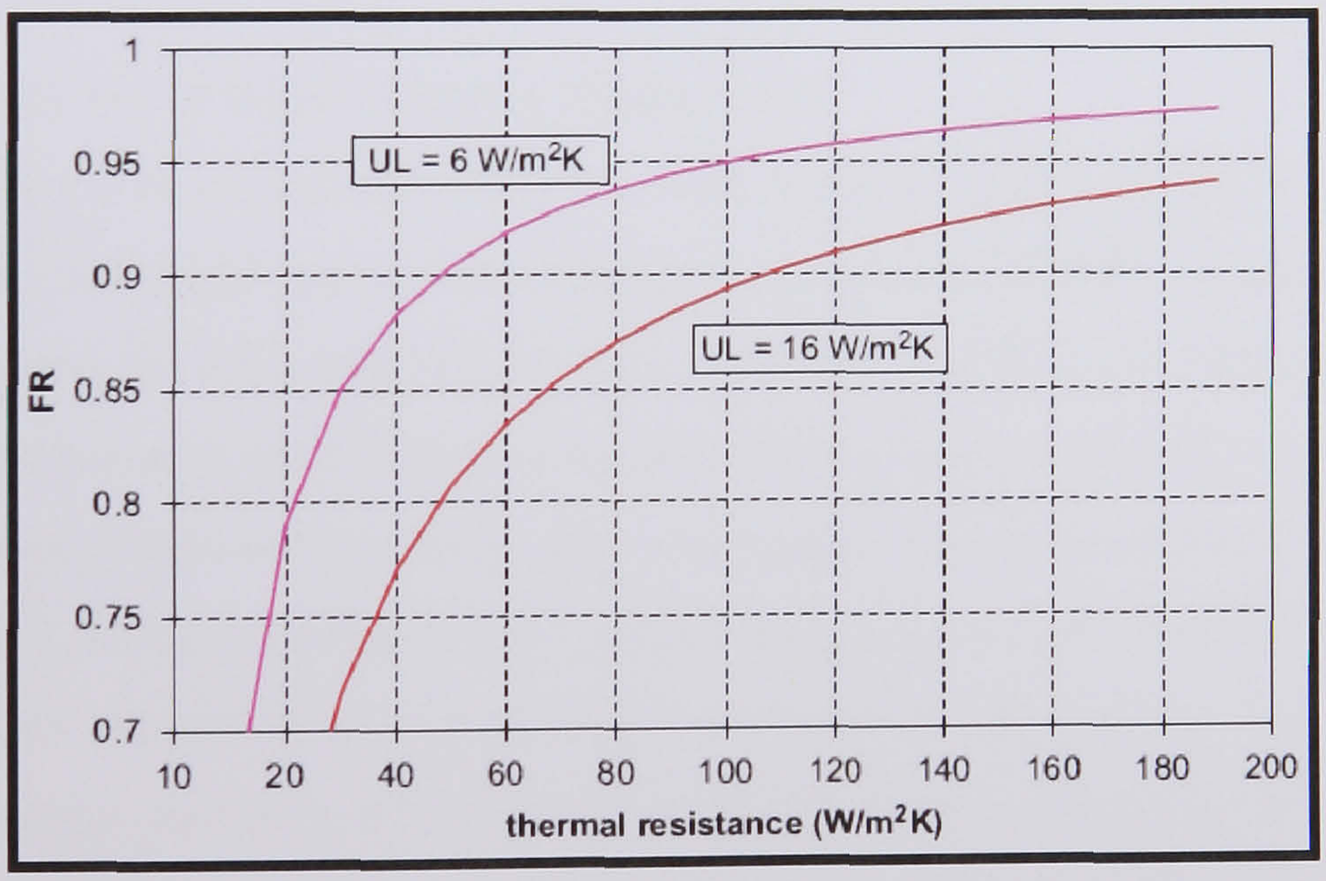

Figure 2.33 Heat Removal Factor versus Thermal Resistance (PV/T-liquid collector; calculated from Hottel–Whillier model adapted for PV/T as described in Zondag et al. (2002). U_L = 6 W/m^{2}K corresponds to a glazed PV/T module and U_L = 16 W/m^{2}K to an unglazed module.

Van der Ree (1996) studied a PV-laminate that was clamped to a plastic thermal absorber. A copper foil was set between the PV and the absorber in order to cover the gaps and improve the thermal contact between the PV cells and the plastic absorber. Poor thermal contact was also reported to be a problem by Sudhakar and Sharon (1994) who found a temperature difference of about 15 ^{o}C between PV-laminate and water output temperature for their unglazed PV/T.

In order to increase the heat transfer, De Vries (1998) applied an aluminium-oxide-filled two-component epoxy glue to connect a conventional PV-laminate to a sheet-and-tube absorber. The glue was reported to have a heat conductance of 0.85W/mK but in practice a lower value was found. This led to a heat transfer coefficient of 45W/m^{2}K between the cells and the absorber and a decrease in thermal efficiency from 37% to 33%. Raghuraman (1981) reported on a PV/T-liquid system consisting of solar cells that are glued directly (no tedlar or EVA in between) to the thermal absorber plate. The thermal conductivity of the silicone were 0.2W/mK and the thickness of the layer 5 mm, which resulted in a heat transfer of 40W/m^{2}K and in a thermal efficiency decrease of about 10%.

2.5.2.3.3 Absorber to liquid thermal conductance

Conventionally, a sheet-and-tube design is used for solar collectors. The thermal efficiency of a sheet-and-tube collector depends on its ratio of W/D, in which W is the distance between the tubes and D is the tube diameter. The W/D ratio used in practise is a compromise between optimised heat transfer and economic aspects (more copper tube increases material cost and handling). The best heat transfer is obtained by leading the heat-collecting medium through a thin channel over the full width of the absorber. Although a thin channel is very interesting from the point of good heat transfer and small temperature gradients, the difficulty of the use of such channels is often in the design of the header, to obtain a sufficiently reliable construction with low-pressure loss and an even flow distribution. In addition, one should realise that a reduction of the W/D ratio has two effects; one is the increase of the fin efficiency due to the shorter fin length, while the other is a decrease of the flow velocity in the case of parallel risers

(due to the increased flow area, assuming the flow rate is kept constant) or an increase in pressure drop in the case of a spiral tube.

Bergene and Lovvik (2003), elaborated on the effect of tube spacing to tube diameter ratio (W/D). They reported that:

• The thermal efficiency was approximately halved when the fin width to tube diameter, W/D increases from 1 to 10, by keeping W constant.

• Increasing W/D from 1 to 10, decreases outlet fluid temperature.

• Even though the electrical efficiency was not heavily affected by fin size, total efficiency is largely dependent on fin size. They explain that there was not much point to increase the cost of a system by decreasing W/D if the main point is cells cooling. On the contrary, if the thermal efficiency is important, the fin's dependence on the relative tube diameter should be weighed against the cost of the tubes.

• When dealing with thermal efficiency improvement studies, its dependence on material cost (such as that of the tube) should always be taken into consideration.

Huang et al. (1999, 2001) built 2 unglazed PV/T prototypes based on a sheet and tube construction. They used W/D ratios of 10 (copper tube to aluminium plate) and 6.2 (extruded tube-and-sheet aluminium) and the result was a low thermal efficiency. Then a polycarbonate multi-channel structure was built (W/D=1) and the temperature difference between the PV and the water in the tank was found to be 4 ^{o}C. A similar rig was constructed by Chow et al. (2006) that built a thermosyphon PV/T system with a PV/T module based on an extruded aluminium channel absorber with a W/D ratio of 1 and compared the thermal efficiency with a conventional thermal collector. The result was about the 76% of the value for a conventional solar collector. De Vries (1998) proposed a dual-flow PV/T-collector like that of Hendrie (1982), but with a reversed water flow (water inlet above the PV, water exit below the PV). In addition, he proposed an additional insulating air layer between the PV and the lower channel. Cause of robustness in the design the thermal and electrical efficiencies were decreased from 69% to 66% for thermal and 10% to 8.5% for electrical respectively. The design is shown in *Figure 2.34*. However the thermal efficiency was 10% higher than for a corresponding

sheet-and-tube collector, due to the good insulation of the high-temperature part of the collector and the larger contact area.

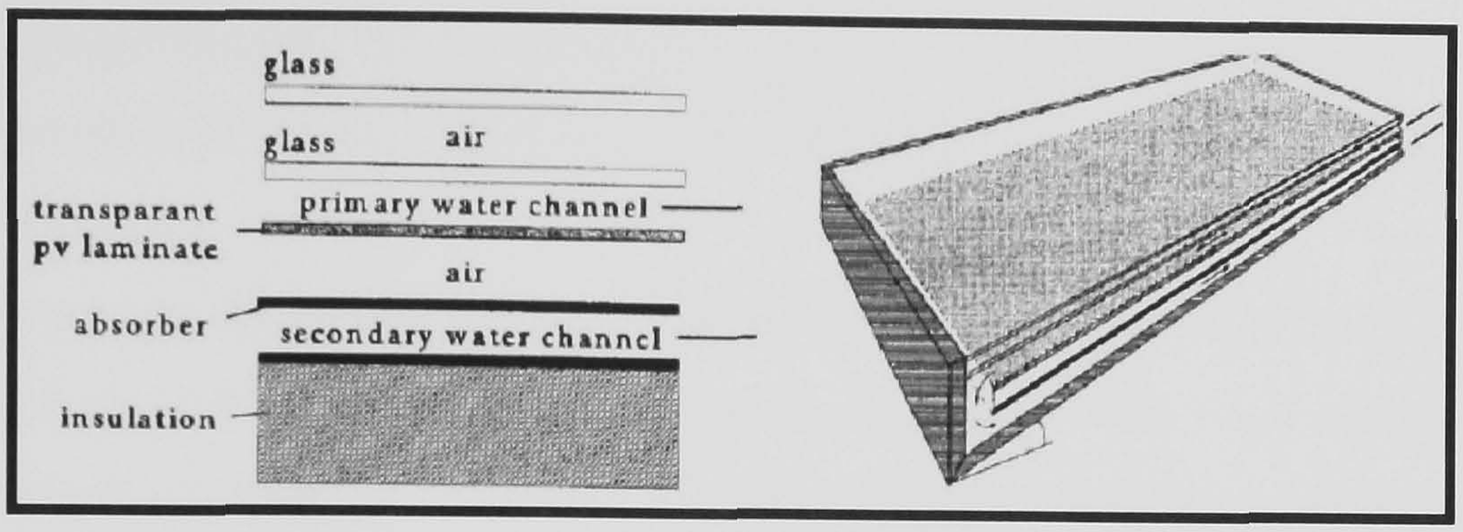

Figure 2.34 Two absorber model of De Vries (1998).

Chow (2003) concentrated on the two manufacturing defects found in PV/T collectors, imperfect adhesion between PV plate and absorber plate, imperfect bonding between absorber plate and tubes and for a range of thermal conductivity of 25-10,000 W/m K (*Figure 2.35*). Using his dynamic model, he found that the maximum combined efficiency (thermal + electrical) of a good collector can be 70% and for a low quality collector, may decrease to 60%.

2.5.2.3.4 Absorber to air thermal conductance

In air collectors, the air is always transported through a channel. However, the thermal performance of air collectors is not as high as the performance of liquid collectors. Air has a thermal conductivity that is 24 times lower than for water and a much lower heat capacity, therefore the flow rate in an air collector is necessarily much larger than in a liquid collector.

Prakash (1994) modelled a channel-type PV/T collector for the cases of both air (100–300 kg/h) and water (40–120 kg/h). For the case of 1 cm duct depth, increasing the flow rate from 100 to 300 kg/h increased the thermal performance of the air heater from 34% to 51%, while for the water heater an increase of 40–120 kg/h increased the efficiency from 64% to 67%.

Loferski et al. (1982) reported on a PV/T-air system in which a fin is connected to the back of each PV-cell. The fins increase the surface area available for heat-exchange by a

factor of 4 and the thermal yield of the cells by a factor of 2 over non-finned cells. Tripanagnostopoulos et al. (2000, 2001, 2002, and 2006) has improved the heat transfer in his PVT air collector by inserting a blackened metal sheet at half height along the full length of the air channel. The metal sheet gets heated due to thermal radiance from the PV, and thereby adds to the effective heat transfer area, increasing his thermal efficiency from 35% to 40%.

Another important factor that influences the air collector's performance is the channel height. Prakash (1994) found that decreasing the duct depth from 3 to 1 cm increases the thermal performance from 17% to 34% for an air heater (100 kg/h) and from 50% to 64% for a water heater (40 kg/h).

2.5.2.3.5 Mass flow rate

PV/T collectors can work with natural circulation (Chow, 2006) or with forced circulation using pump or fan to move the fluid (Tonui, 2007). A number of authors have investigated the influence of mass flow rate on PV/T performance. The generic conclusion they reached was that PV/T efficiency is dependent on flow rate (mass flux). This is because as the water velocity in the tube increases, the tube side heat transfer coefficient also increases which in turn maximizes both the cooling of the PV and the heat transfer to the water.

Bergene and Lovvik (1995) carried out a parametric study of flow rate as a function of the geometric parameter W/D. They found that, the thermal efficiency increases only by a factor of 0.10 when the flow rate increases from 0.001 to 0.075 kg/s. The same is being reported by Chow (2003) as can be seen from *Figure 2.35.* The increase of flow rate after a point doesn't improve the thermal and electrical performance too much and in the contrary it affects the net electrical gain when more power is needed to run the pump or fan of the system.

Kalogirou (2001) in his simulations using TRNSYS found that the optimum flow rate of the PV/T system was 25 l/h (0.007 kg/s), for a 5.1 m2 PV/T collector area (i.e. 0.0014 kg/s m2). Moreover, the annual electrical efficiency of the standard PV system was reported to increase from 2.8% to 7.7% for the PV/T system operating at the obtained optimum flow rate (25 l/h). Garg and Adhikari (1997) as Sopian et al. (2000), tested the

performance of PV/T air heating collectors and noticed that by increasing the air mass flow rate reduces the PV cell and outlet temperatures and consequently increases the thermal and electrical efficiencies.

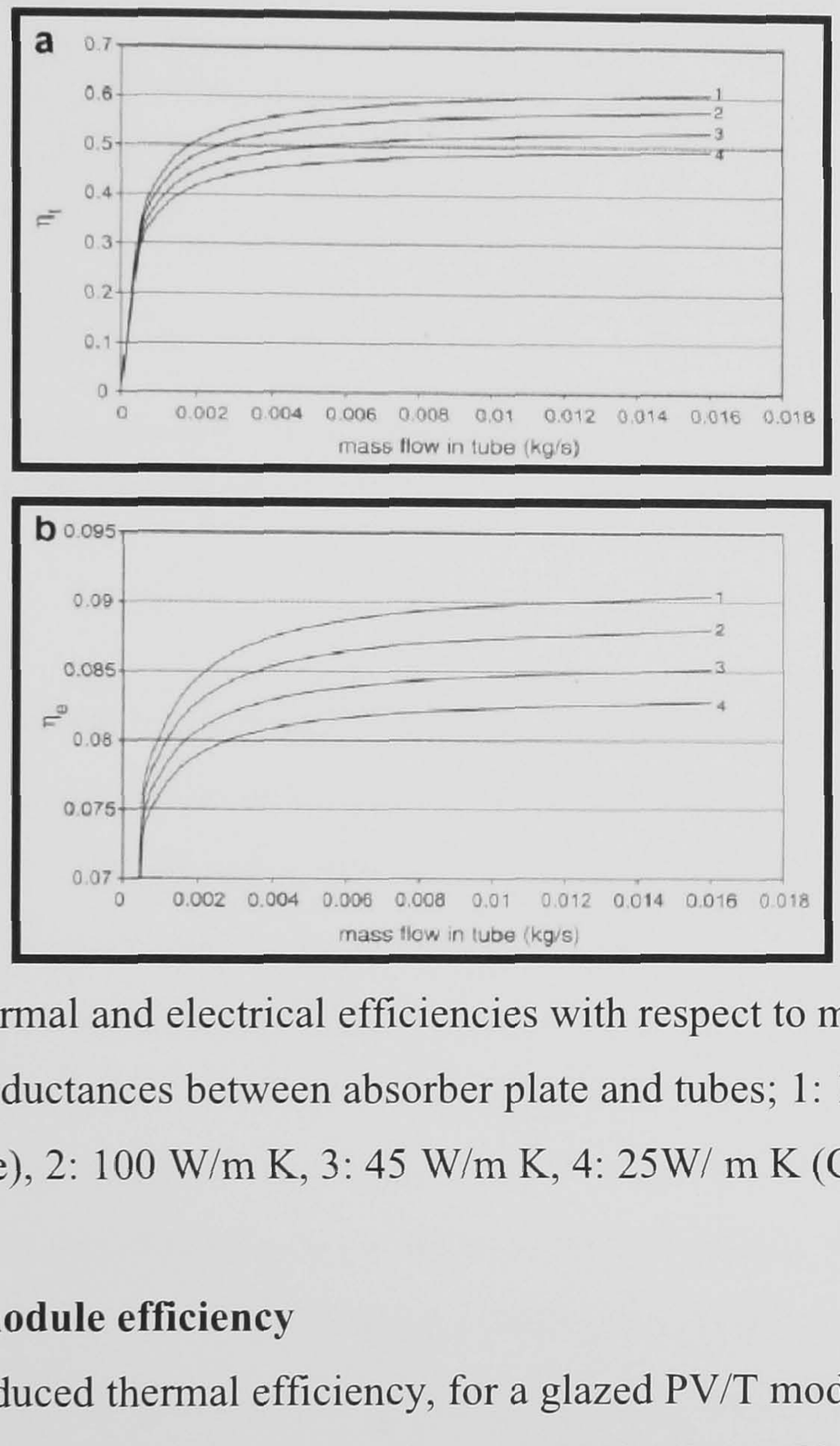

Figure 2.35 Thermal and electrical efficiencies with respect to mass flow rate for various thermal conductances between absorber plate and tubes; 1: 10,000 W/m K (best conductance), 2: 100 W/m K, 3: 45 W/m K, 4: 25W/ m K (Chow 2003).

2.5.2.4 Electrical module efficiency

In addition to the reduced thermal efficiency, for a glazed PV/T module, the electrical efficiency of the PV/T is somewhat lower than of a PV laminate. The reduction in electrical efficiency is largely due to the additional reflection of solar radiation caused by the additional glass cover as we discussed earlier, which for good low-iron glass would result in 8% decrease in efficiency, while the use of high transmission glass would reduce this to 4%. The PV/T with or without a cover affects the electrical efficiency as shown in *Figure 2.36*.

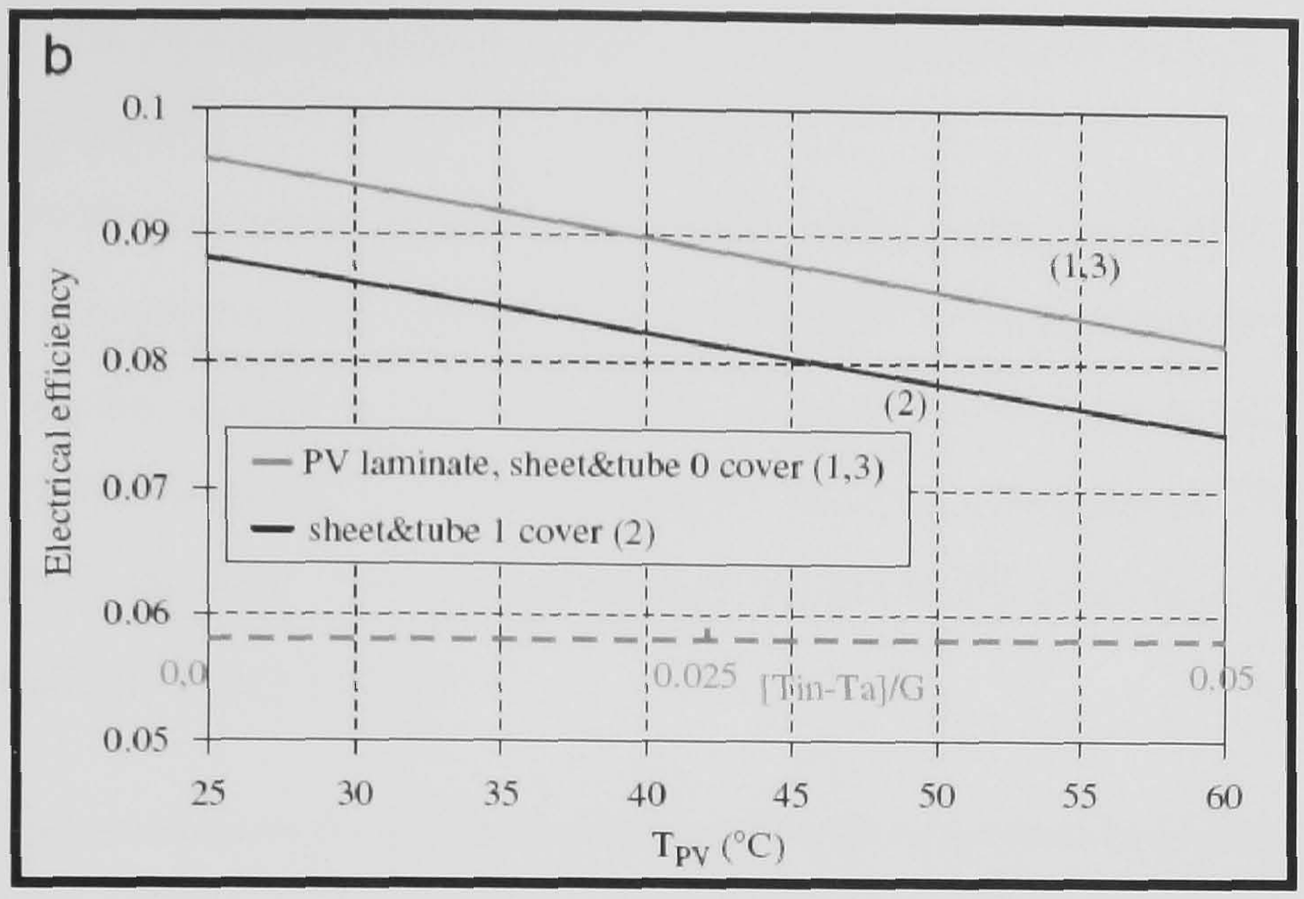

Figure 2.36 Electrical Efficiencies of a PV/T-liquid collector (Zondag, 2005)

2.5.2.4.1 Type of PV

The electrical performance is primarily influenced by the type of PV used. In practice, only a-Si and crystalline Si have been found in the literature on PV/T. The higher efficiency of crystalline Si will result in a higher electrical efficiency and a higher electrical-to-thermal ratio of the PV/T than in the case of a-Si.

Tripanagnostopoulos et al. (2002) presented experimental measurements on PV/T-liquid and PV/T-air collectors for both a-Si and c-Si. He found that for his PV/T liquid collector, the efficiency of his c-Si prototype was 55% and his a-Si prototype 60%, while for his PVT air collector the c-Si prototype was 38% and the a-Si prototype 45%. However, the electrical performance for the c-Si modules was 12% and for the a-Si 6%. A higher thermal yield was also found for a-Si by Ji et al. (2003). However, in other experiments Versluis (1997) a lower thermal efficiency was found for a-Si than for c-Si. Possibly, this can be explained by the range of absorptivities found for a-Si by Affolter et al. (2000) and Platz et al. (1997) as indicated before.

2.5.2.4.2 Temperature effect

The efficiency of crystalline silicon cells decreases with increasing temperature. *Figure 2.37* shows the efficiency drop of mono crystalline and amorphous silicon with temperature increase. The temperature coefficient depends on the PV material used:

about 0.45%/K for crystalline silicon, 0.35%/K for CIS, 0.25%/K for CdTe and 0.2%/K for a-Si Zondag (2005).

For unglazed PV/T, this effect is purely beneficial, since it implies that the PV is cooled compared to a conventional PV laminate. For a glazed PV/T, the temperature effect will be positive when the storage is still cold, while being negative when it has heated up. Zondag et al. (2003) compared a conventional PV module, an unglazed PV/T module and a glazed PV/T module. The average annual electrical efficiency was found to be 7.2%, 7.6% and 6.6% respectively.

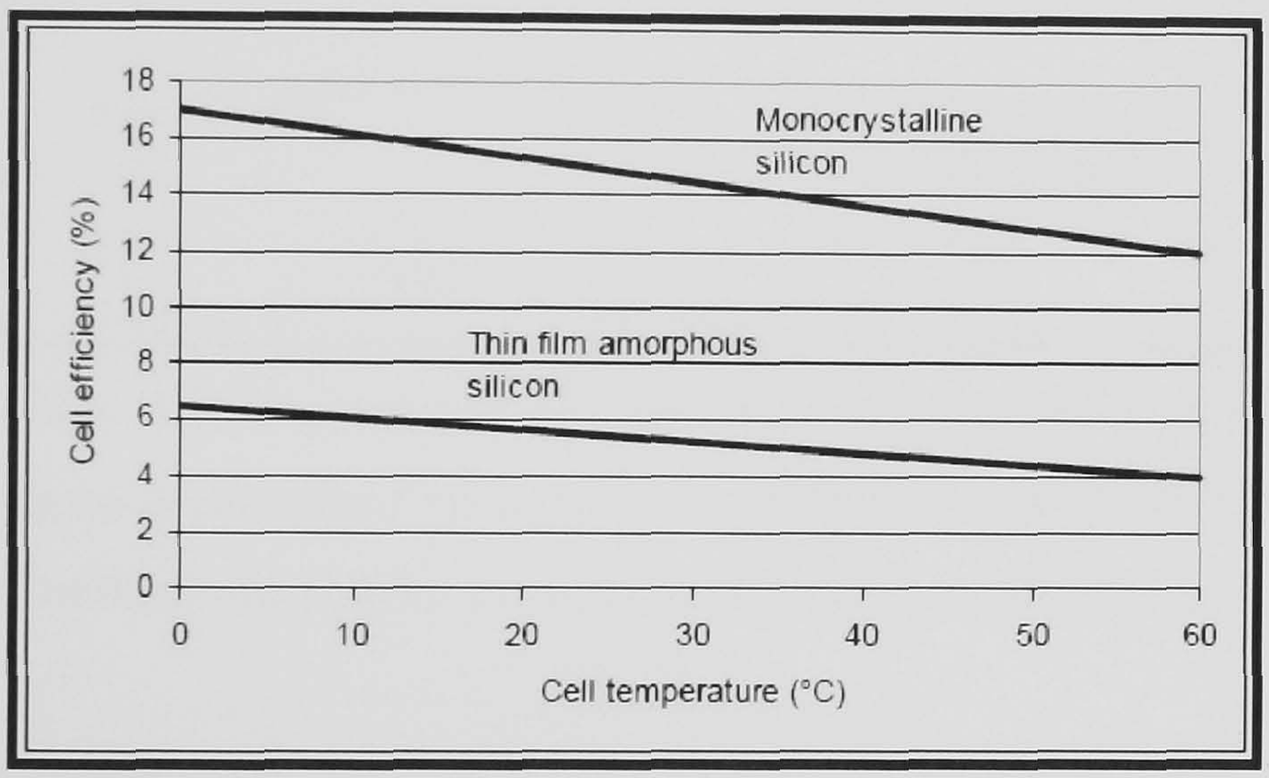

Figure 2.37 Cell Efficiency drop per ^{o}C of increase

Krauter (2004) has been developing an unglazed integrated solar home system, in which a PV laminate is connected to a triangular water tank. The tank serves to cool the PV by means of an 'extended heat capacity'. Typically, at high irradiance a PV temperature reduction of about 20 ^{o}C is reported relative to a conventional solar home system, which leads to a 9–12% increase in electrical yield, depending on the stratification. Naveed et al. (2006) examined a PV/T air system in which PV was connected to an unglazed transpired collector. It was found that a temperature reduction of 3–9 ^{o}C resulted in an improved electrical performance.

Thermal resistance between the PV and the collector fluid will increase the PV temperature, with negatively affecting both the electrical and the thermal performance. *Figure 2.38* indicates the effect of the tube spacing on the average absorber temperature,

clearly showing that wide tube spacing will lead to lower electrical performance. The figure also indicates the effect of the thermal resistance between PV cells and absorber, which can be substantial.

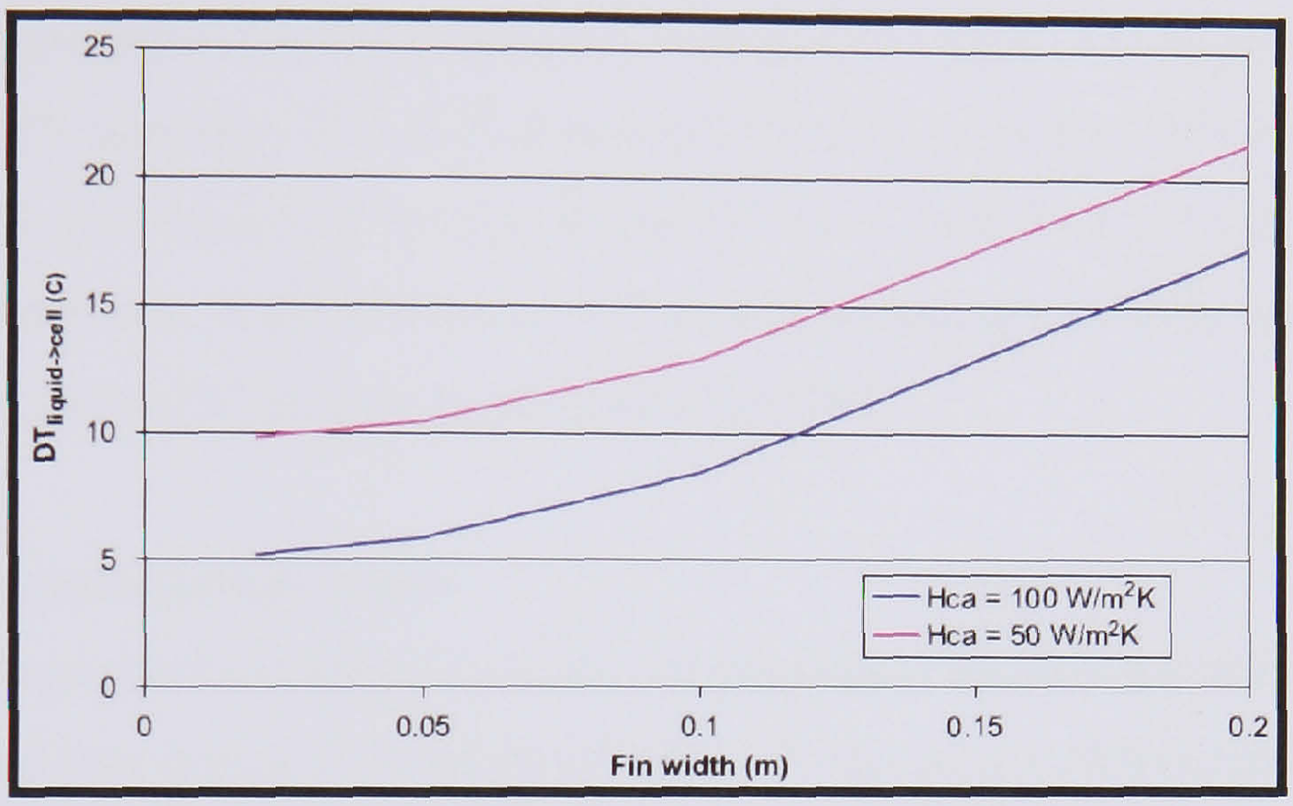

Figure 2.38 Effect of tube spacing on average absorber temperature (G_{py}= 800W/m^2, $\tau\alpha$ =0.8). The figure is calculated from the Hottel–Whillier model adapted for PV/T as described in Zondag et al. (2002). h_{ca} is the heat transfer coefficient between cells and absorber

2.5.2.4.3 Temperature homogeneity

PV-cells that are connected in series have to operate at the same current, while PV-cells that are connected in parallel have to operate at the same voltage. The IV-characteristics depend on the temperature, however. Since a temperature gradient exists over the PV/T, not all cells may be able to operate in their maximum power point at the same time. This effect was examined experimentally by Smith et al. (1978), who measured the electrical performance of series connected cells and found no effect of the temperature gradient, which he varied between 3.9 and 38 °C. Numerically, the effect was examined by Lambarski (1984), who found only a very small effect of the temperature in the case of series connection (<1%), but a large effect in the case of parallel connection of about 17% loss. He concluded that series strings may be represented by their average temperature and that cells at different temperatures should be connected in series and

not parallel. The case of series connection was also examined numerically by De Vries (1998), who found no effect of the temperature gradient.

2.5.2.5 Reliability

No dedicated guidelines for PV/T reliability testing exist today. Although the testing standards for PV laminate (IEC 61215) and solar thermal collectors (EN-12975) handle most of the relevant aspects, a number of specific issues exist for PV/T that is not covered by these tests. A guideline for PV/T testing including reliability issues has been drafted as part of the PVCatapult project (Zondag 2005).

2.5.2.5.1 Stagnation temperature

In a conventional thermal collector system, the stagnation temperature is likely to occur several times a year during some hours when the storage is completely loaded. Since the heat is not drawn off from the collector in these cases, high module temperatures will result. Typical stagnation temperatures in a conventional thermal collector are around 180–200 °C. For unglazed PV/T-systems these stagnation conditions are not a problem, as the temperature is the same as that for a badly ventilated PV module. For example, Sudhakar and Sharon (1994) reported a stagnation temperature of 75 °C for their unglazed PV/T module.

However, for glazed PV/T systems the situation is different. Fortunately, the stagnation temperature for a covered PV/T system is lower than that of a convectional collector system, due to the lower absorption and the fact that the absorber surface is not spectrally selective. Nevertheless, stagnation temperatures of around 130 °C can be expected (Zondag, 2002). Under these high-temperature conditions, deterioration of the encapsulation material or the top film might occur.

Affolter et al. (1997) indicates that EVA becomes doughy at 70 °C but that a stable elastomer up to 130 °C can be created by adding a curing additive. For temperatures over 130 °C he indicates that the EVA looses its mechanical properties and could become brown under UV exposure, reducing the absorption in the PV. Komp (1983) warns that, for PV/T applications, silicone encapsulation should be preferred over EVA.

2.5.3 Analytical models of PV/T collectors

Florschuetz (1979) modified the Hottel–Willier (1958) analytical model for flat plate collectors so that it applies to PV/T collectors. It was concluded that for practical purposes F' and F_R of the PV/T collector may be considered identical to F' and F_R of the thermal collector. This means that the values of these quantities (F' and F_R) apply to PV/T collectors as well.

Bergene and Lovvik (1995), proposed a detailed model predicting the performance of PV/T collectors that was based on energy transfer analysis and to some extent on the models for flat plate solar collectors presented by Duffie and Beckman (1991). The model predicted PV/T efficiency (thermal + electrical) to be about 60–80%.

Sandnes and Rekstad (2002) have also developed an analytical model for the PV/T collector by modifying the well known Hottel and Willier model for flat plate collectors, in order to include the effects of the additional solar cells.

Sopian et al. (1996) analyzed with steady state models the performance of single and double-pass PV/T air collectors. The results showed (*Table 2.5*) that double-pass PV/T air collectors have superior efficiencies compared with the single-pass ones.

Table 2.5 Efficiency comparison between Single and Double pass PV/T (Sopian 1996)

Table 1
Thermal, PV and combined efficiencies

Efficiency	Single-pass	Double-pass
Thermal	24–28%	32–34%
PV	6–7%	8–9%
Combined	30–35%	40–45%

Hegazy (2000) (*Figure 2.39*) considered four popular designs with the air flowing either over the absorber or under it and on both sides of the absorber, in a single pass or in a double pass fashion. Heat balance equations were written for each model and numerically solved, incorporating measured climate data.

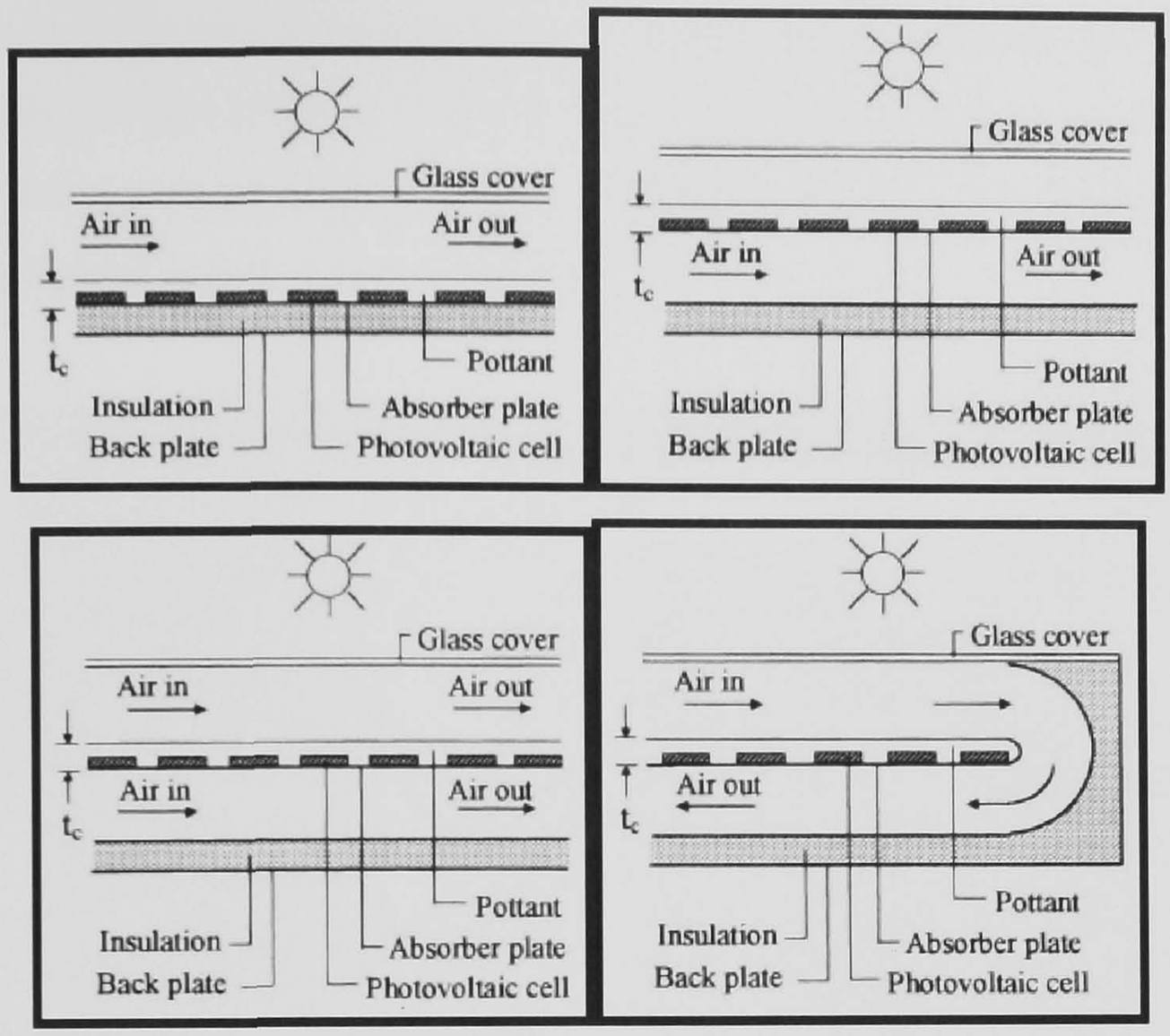

Figure 2.39 Schematics of the various PV/T models (Hegazy, 2000)

Tiwari (2006, 2007) (*Figure 2.40*) also developed a thermal model of an integrated photovoltaic and thermal solar (IPVTS) water/air heating system considering four configurations, namely (a) unglazed with tedlar (UGT), (b) glazed with tedlar (GT), (c) unglazed without tedlar (UGWT) and (d) glazed without tedlar (GWT).

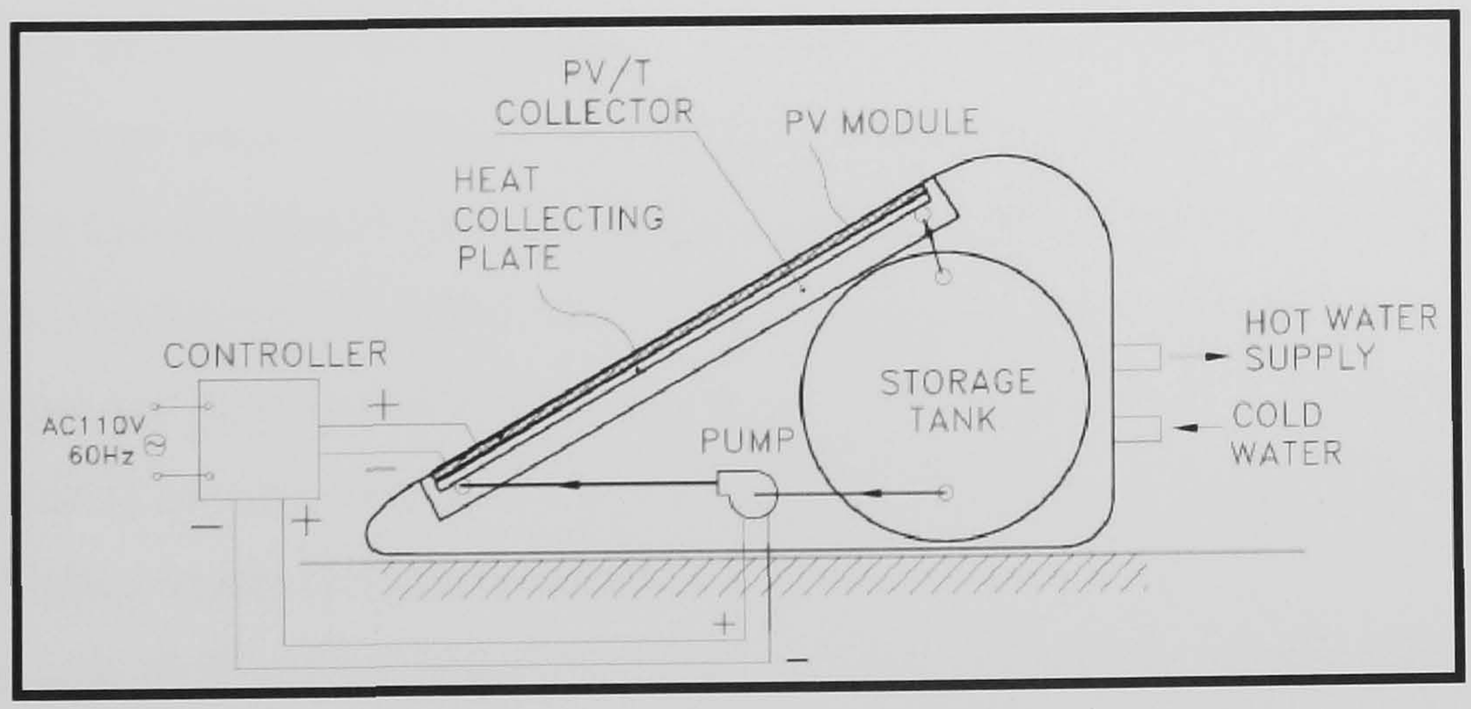

Figure 2.40 Schematic diagram of an integrated PV/T System (IPVTS) (Huang 2000)

Chow (2006) used the thermosyphon principle that eliminates the expense of pumping power and built two rigs (*Figure 2.41*) that were simulated and validated by the experimental measurements, together with two other similar models developed for PV module and solar hot-water collector.

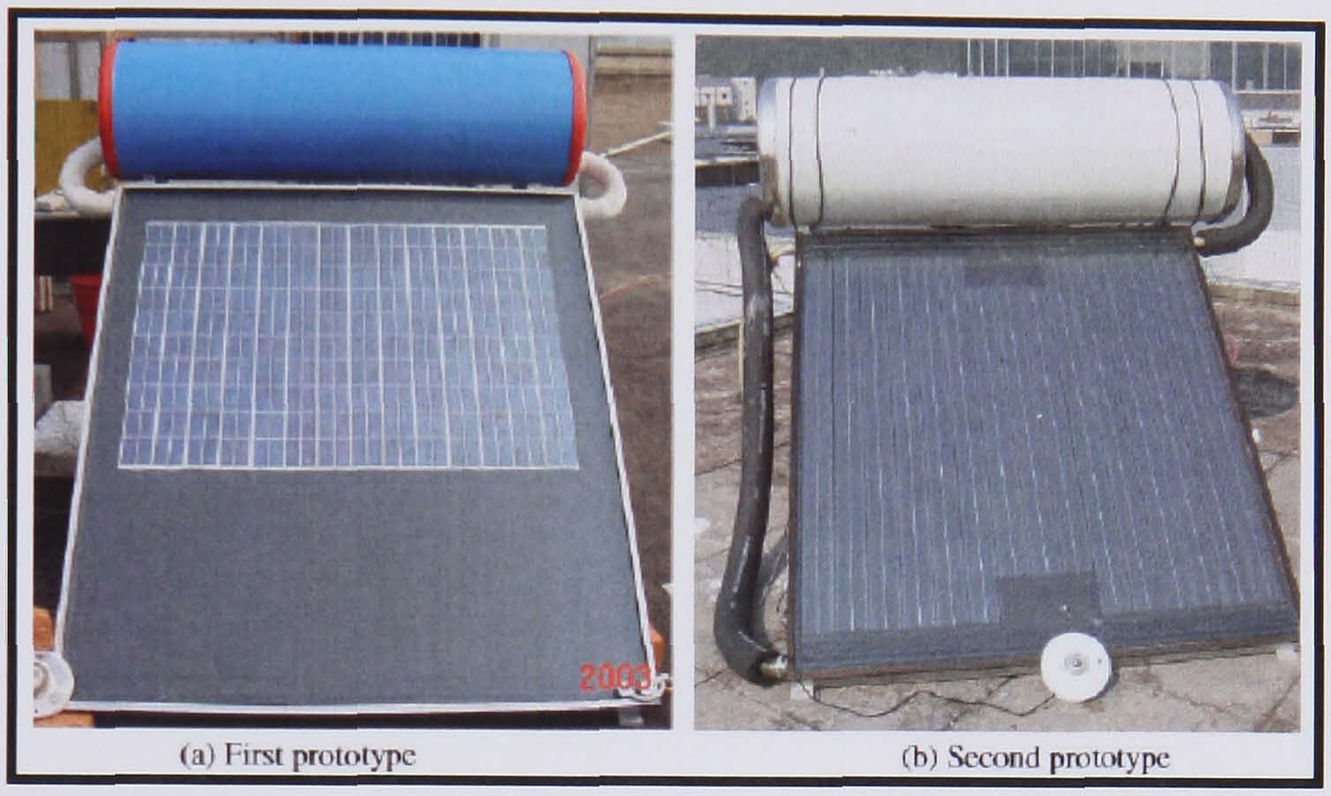

Figure 2.41 The front view of the flat-box PVT collectors. (Chow 2006)

Tripanagnostopoulos (2000) presented a PV/T system with dual heat extraction operation, either with water or with air circulation. The experimental model consisted of a pc-Si PV module with an air channel at rear PV surface. Three design modes (*Figure 2.42*) were tested and the results showed that the placement of it on PV rear surface presents the most effective combination of water and air heat extraction. Focusing on the performance improvement of air heat extraction, the heat exchanging surface was increased in the air channel and test results confirmed a rise in thermal efficiency for air circulation. Zondag (2003) tested various PV/T collector design concepts and the results from thermal and electrical efficiencies can be seen from *Table 2.6*. He observed that:

a) All channel concepts have a substantially higher efficiency than sheet and tube due to the better heat transfer characteristics of channels.

b) In the case of free flow panel, evaporation strongly reduced the thermal efficiency and condensate on top of the glass causes additional reflection.

c) Since the sheet and tube design is the easiest to manufacture (and is only 2% less in efficiency), it is the most promising of the different design concepts examined.

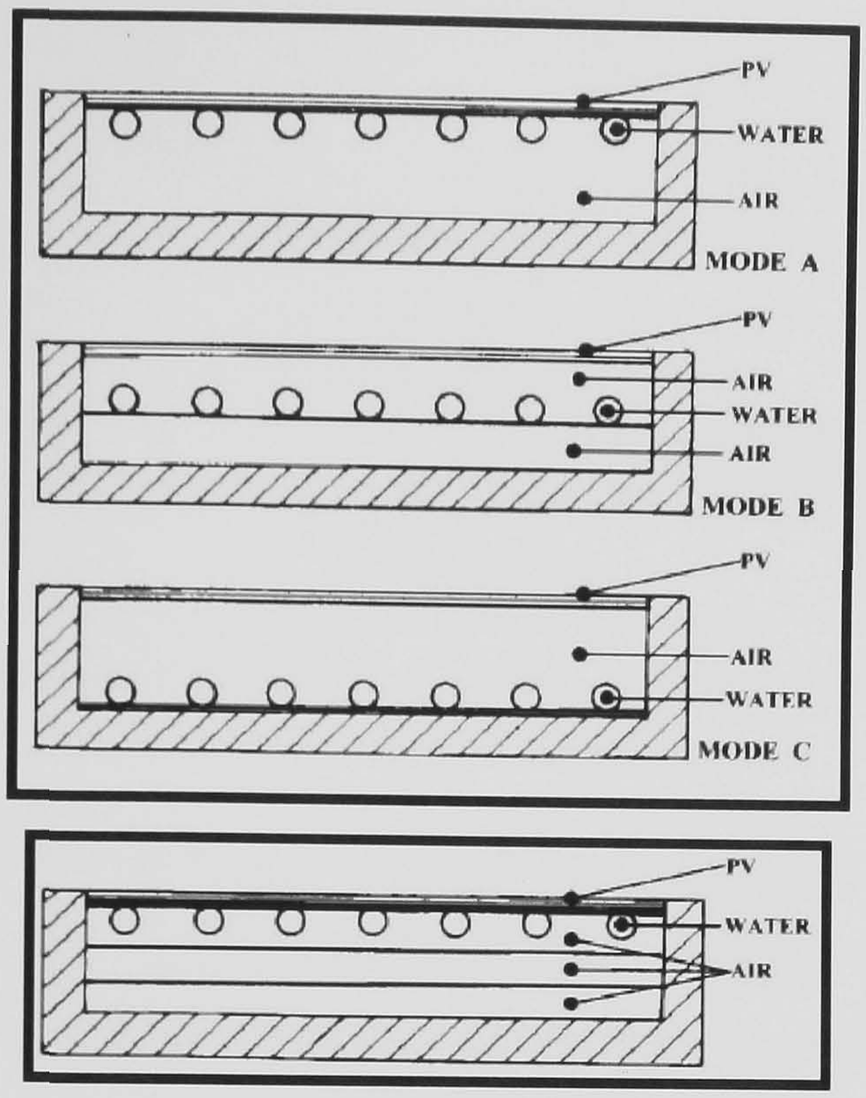

Figure 2.42 Experimental dual PV/T models (Tripanagnostopoulos 2000)

Table 2.6 Thermal and electrical efficiencies of various design concepts (Zondag 2003)

Table 2
Thermal efficiency of various PV/T collector design concepts [6]

Panel type	Thermal efficiency	Electrical efficiency
PV panel	–	0.097
Sheet and tube PV/T, no cover	0.52	0.097
Sheet and tube PV/T, 1 cover	0.58	0.089
Sheet and tube PV/T, 2 covers	0.58	0.081
PV/T collector with cannel above PV	0.65	0.084
PV/T collector with cannel below opaque PV	0.60	0.090
PV/T collector with cannel below transparent PV	0.63	0.090
Free flow PV/T collector	0.64	0.086
Two-absorber PV/T collector (insulated type)	0.66	0.085
Two-absorber PV/T collector (noninsulated type)	0.65	0.084
Thermal collector	0.83	–

Zondag et al. (2002) developed and run four numerical models for predicting the performance of PV/T collectors. The models included one 3D (three dimensional) dynamic and three steady state (3D, 2D and 1D) models (*Figure 2.43*).

The simple 1D steady state model performed almost as well as the much more time consuming 3D dynamic model. However, as they reported, the 2D and 3D models could be used to provide more detailed information required for collector optimization. All models followed the experiments to within 5% of accuracy.

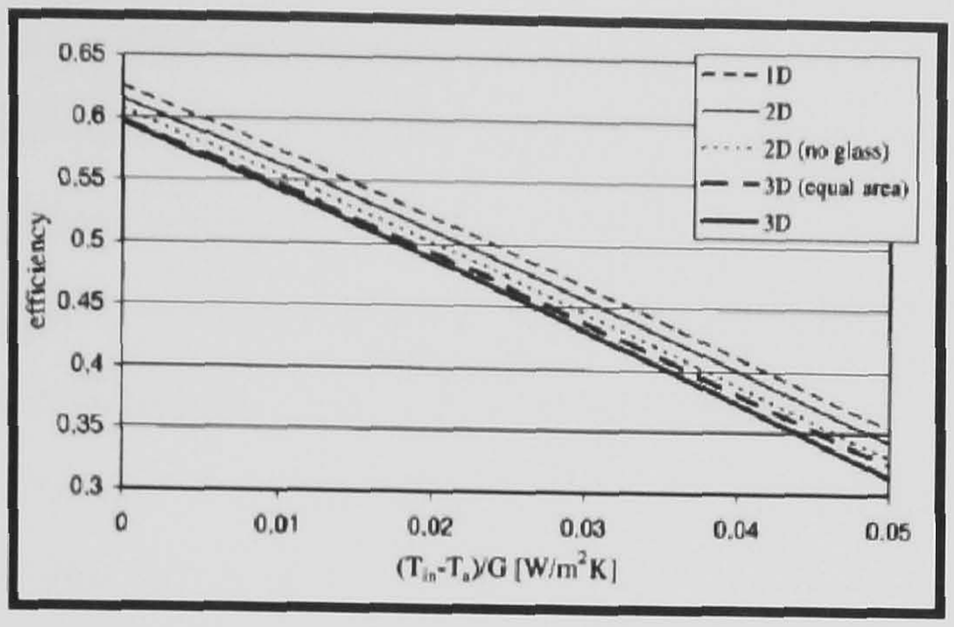

Figure 2.43 Comparison between the 1D, 2D and 3D thermal models (Zondag 2002)

It was explained that by attaching solar cells onto an absorbing surface, reduces the solar energy absorbed by about 10% due to mainly the reduced optical absorption properties of the solar cells, compared to the black absorber. In addition, the available solar energy was reduced by the fraction of the incident energy converted to electricity by the PV cells. Moreover, an increased heat transfer resistance between the absorber and the heat transfer fluid was reported to exist.

2.5.4 Modelling and simulation

Kalogirou (2001) modelled and simulated a PV/T system using the well known TRNSYS simulation program and a typical meteorological year for Nicosia, Cyprus and optimized the water flow rate for the system. The PV/T system consisted of a series of PV panels, a battery bank, an inverter, a hot water storage cylinder a pump and a differential controller.

Garg and Adhikari (1997) simulated the performance of single and double glass configurations PV/T air heating collectors based on the analytical solution of a differential equation that yields the working fluid temperature along the direction of fluid flow. They found that by increasing the cell density (i.e. increasing the area covered by cells) results in higher values of electrical efficiency, although the thermal efficiency drops. Overall system efficiency increased with increase in collector length, mass flow rate and cell density and decreased with increase in duct depth.

Cox and Raghuraman (1985) performed numerous computer simulations towards improving the solar absorptance and reducing the IR (infrared) emittance of flat plate air

PV/T collectors. In their study, they found that air PV/T collectors are generally less efficient than the liquid ones due to low PV cell packing factor, low solar absorptance, high IR emittance and poor absorber to air heat transfer coefficient. It was also found that a 13% increase in the packing factor results in a corresponding increase in both thermal and electrical efficiencies. The optimum combination of an air PV/T collector was found to consist of a non selective absorber and a high transmissivity/low emissivity glass above the photovoltaic cells.

A theoretical study of a photovoltaic–thermal system for domestic heating and cooling from Vokas (2006) has led to the result that the system can cover a remarkable percentage of the domestic heating and cooling demands. Furthermore, the performance of the PV/T collector with respect to the variation of geographical region as well as to different total surface areas of the system was also investigated.

2.5.5 Qualitative evaluation of thermal/electrical output

Electrical and thermal energies are not qualitatively the same as explained by Fujisawa and Tani (1997); thermal energy cannot produce work until a temperature difference exists between a high temperature source and a low temperature source, but electrical energy can completely transform into work irrespective of the ambient conditions. The use of exergy, defined as the maximum theoretical useful work obtainable from a system as it returns to equilibrium with the environment, enables qualitative evaluation by comparing electrical and thermal energy based on the same basis. Morita et al. (2000) performed a numerical analysis and determined the optimum operating conditions by using exergetic evaluation for single and no cover PV/T collectors. The maximum exergetic efficiencies for the single cover were 13.36% and for the coverless 11.92%. The corresponding optimum flow rates were 0.0014 and 0.0049 kg/s, respectively and the corresponding optimum fluid temperatures were 83.6 ^{o}C and 38.3 ^{o}C, respectively. It is clear that the glass cover function is to raise both the maximum exergetic efficiency and the optimum outlet temperature. It is also clear that in order to obtain the most thermal exergy, the electrical exergy has to be sacrificed.

However, the significance of an exergy comparison is not clear if electrical or mechanical work is not the only desired output from the system, such as when the

thermal output is hot water used directly for showers and washing. Coventry and Lovegrove (2003), used three different methodologies (thermodynamic, market based and environmental) for determining an electrical to thermal energy ratio. For the thermodynamic methodology, an electrical/thermal ratio of 2.5 was used (due to the fact that a power plant is usually 40% efficient). However, they reported that low temperature hot water from a PV/T is not as thermodynamically useful as high temperature steam from a coal-fired boiler. For the renewable energy market methodology, the grid connected photovoltaic energy cost was reported to be US $0.367/kW h and the solar hot water energy cost was reported to be US $0.087/kW h. Thus, the ratio of electrical to thermal value was found to be 4.24. This means that electricity is 4.24 times more precious than hot water. In the environmental evaluation approach, based on avoided emissions from the use of PV/T, the ratio of electrical to thermal avoided CO_2 emissions was reported to be 7.58 (including life cycle emissions).

Joshi (2006) attempted to evaluate exergy analysis of a hybrid photovoltaic–thermal (PV/T) parallel plate air collector for cold climatic condition of India (Srinagar). It was observed that an instantaneous energy and exergy efficiency of PV/T air heater varies between 55–65 and 12–15%, respectively.

Huang (2001) used a commercial polycrystalline PV module in the solar PV/T collector made from a corrugated polycarbonate panel and introduced the concept of primary-energy saving efficiency for the evaluation of a PV/T system. The primary-energy saving efficiency of the present PV/T exceeded 0.60. This was higher than for a pure solar hot water heater or a pure PV system.

2.5.6 Discussion

The literature review introduced the concept of PV/T systems. From this it was possible to understand the key issues underlying this technology. The most important findings that will help us to design our models in this thesis were:

- Covered versus uncovered PV/T

The different system options lead to different collector design options. For uncovered systems, the focus is on low-cost which may lead to plastic PV/T collectors. Uncovered PV/T collectors have several advantages such as a better electrical performance and a

lower stagnation temperature. However their thermal efficiency is strongly reduced at higher operating temperatures.

Covered PV/T can be applied in solar DHW systems replacing conventional thermal absorbers. The electrical yield is somewhat less than a similar area of PV laminates mainly due to additional reflection losses at the cover. For covered systems the focus is on high yield which puts emphasis on increasing the thermal efficiency by increasing the solar absorption over the entire solar spectrum and the possibilities of spectral selectivity. Due to the additional insulating cover, problems are cause since the PV is subject to short but high stagnation temperatures.

- Manufacturing Techniques

The most basic technique to fabricate a covered PV/T collector is to glue a commercial PV laminate to the absorber of a commercial thermal collector. Care should be taken to reduce the thermal resistance between the PV and the absorber.

For uncovered PV/T panels the best choice is to mount the PV laminate with a metallic absorber. The mounting of the collector tubes to the absorber should be done before mounting the absorber to the PV and care should be taken to retain the surface of the absorber flat in order to avoid air layers between absorber and PV.

- Stagnation temperatures

For covered PV/T temperatures can reach as high as 130 ^{o}C and specific attention should be paid to prevent delaminating of the encapsulant. Uncovered PV/T systems work with maximum temperatures reaching 75 ^{o}C.

- Absorption

For a PV/T collector is important to absorb as much as possible of the incoming solar radiation, including the fraction that is not useful for photovoltaic conversion. A first step to optimise the absorption of the PV is the use of black rear material instead of the standard white to maximise the absorption in the spacing between the cells.

- Electrical Efficiency

For an uncovered PV/T module the electrical efficiency will generally be larger than for a PV laminate. For a covered PV/T the electrical efficiency is reduced due to the

reflection losses at the top cover and the relatively high temperatures that the PV is being exposed.

- Heat Transfer

A problem in the PV/T literature is the thermal resistance between the PV and the thermal absorber. If this resistance is too high, this implies a relatively large temperature difference between the PV and the collector medium, leading to increased thermal losses and a reduced PV performance. The thermal resistance is increased substantially by air enclosure which should therefore be avoided.

- Electrical Wiring

In a PV/T collector a temperature gradient will occur over the thermal collector due to the fluid heating up. This implies that not all PV cells will be operating at the same temperature. Since the PV current is much less temperature dependent than the PV voltage, good electrical performance is obtained by a series connection of PC cells operating at different temperatures, while a parallel connection of cells at different temperature will cause significant power losses.

- Type of PV

It was noticed that there is a difference in thermal efficiency in respect with the type of PV cell used. When polycrystalline is used then higher electrical efficiency is achieved and lower thermal in comparison with an amorphous cell. Depending from the application needed the choice of PV cell can determine the thermal and electrical efficiency of the system.

- Spectral Selectivity

A widely applied technique to raise the performance of a thermal collector is to use spectrally selective absorber. This absorber has a high absorptivity for solar light, but a low emissivity for longwave thermal radiation. In PV/T collector the surface of the PV will often consist of glass which has a very high emissivity of 90%. This leads to much higher radiative losses than those from a conventional thermal absorber. This can be remedied by applying a coating on top of the glass that reflects in the IR part of the spectrum, while being transparent in the solar part of the spectrum.

- Flow Channels

For PV/T liquid collectors, the sheet-and-tube design is very reliable and has a good heat transfer, but channel plate constructions may provide interesting ways of further increasing the heat transport, provided that the channels are made sufficiently thin.
For PV/T air collectors, attention should be paid to improved heat transfer devices.
A direct consequence of the improved absorption in combination with reduced heat loss will be higher stagnation temperatures. This demands continued efforts to find stagnation resistant encapsulation materials.

- Mass flow rate

By increasing the mass flow rate the thermal and electrical performance of a system increases but there is a point that further increase does not give higher performance and instead causes more power used for pump or fan circulation.

- Energy Rating

In the literature review many researchers used different performance indicators to evaluate the PV/T system performance. Three of the most important were the total energy efficiency, the primary energy efficiency and the exergy efficiency. This can cause confusion in deciding which method is best to choose so all of them should to be taking under consideration.

PV/T applications

For PV/T-liquid application, glazed PV/T systems for domestic water heating are a promising application, but also utility buildings with a high tap water demand should be considered. In addition, the combination of unglazed PV/T with a heat pump is considered as very interesting, but the electrical consumption of the heat pump is substantial and should be taken into account in the system evaluation. It is clearly shown that the required area for a PV/T system is less than for a corresponding side-by-side system, which it especially interesting for applications where available area is small, such as multi-family buildings, but also utility buildings with a large tap water demand such as hotels and hospitals should be considered.

For PV/T air applications, preheating of ventilation air seems a very logical application, especially for buildings with a large ventilation demand. However, since this is required only during the heating season, it is worthwhile to look for summer application of the heat as well. For domestic application, as well as for utility applications with a large tap water demand, the heat may be used for the heating of water through a heat exchanger. For utility buildings, the heat may be used for solar cooling, or the buoyancy effect may be used to assist the ventilation.

2.6 Heat Pipe

The heat pipe is a passive heat transfer device with an extremely high effective thermal conductivity. Its heat transfer capability ranges from one hundred to several thousand times that of an equivalent piece of copper because of its two-phase heat transfer mechanism (Dunn, 1994).

2.6.1 Brief History of Heat Pipe Technology

The rudiments of the modern day heat pipe can be traced to the Perkins Tube patented in the mid-1800s. The Perkins Tube, classified now as a thermosyphon heat pipe, provided the initial building blocks for the heat pipe. General Motors patented the idea of heat pipes in 1935, but it was George M. Grover from Los Alomos National laboratory who got credited with inventing and building the first working heat pipe in 1963.

Initially, heat pipes saw very little potential, but until the mid 1960's, when several national and commercial labs were seeking new ways to improve heat transfer, the heat pipe gradually went from a laboratory curiosity to a device that gained the attention of electronics designers. However, the introduction of heat pipes into the commercial world was really slow due to its extremely high cost and lack of demand. They were not widely accepted by commercial industries, and mostly applied in aerospace and military forefront appliances. The first commercial use of heat pipes would be that installed in a satellite system (Ali 1999).

In the 1980's, the heat pipe was progressively accepted as a thermal management tool for advanced electronic devices in several market places. Consequent to this general acceptance, the demand growth dramatically reduced its cost, which allowed thermal designers to implement the heat pipe into more products. By early 1990's, the heat pipes were already being implemented in high volume consumer electronics; and in today's market, thousands of electronics applications have already accepted the heat pipe as their thermal management tool. One of the most common uses would be that integrated in the notebook's heat dissipation system. Ali (1999) estimated that approximately 60% of current notebooks today utilize heat pipes in their thermal management solution. Presently, Thermacore manufactures several thousand heat pipes per day at a price suitable for use.

2.6.2 Heat Pipe Structure

The structure of a heat pipe is simple. It consists of three main regions, including an evaporator section, an adiabatic section, and a condenser section as shown in *Figure 2.44*. Heat pipes are sealed vacuum vessels that are partially filled with working fluid, which serves as the heat transfer media. The heat pipe envelope is normally made of copper in different shapes including cylindrical, rectangular, or any other enclosed geometry. The wall of the envelope is lined with a wick structure, which provides surface area for the evaporation/condensation cycle and capillary capability. The main distinction of heat pipes from other thermal management modules, besides working fluid, is the wick structure. There are several types of wick structures used in copper/water heat pipes: wire mesh, groove, fiber/spring and powder metal.

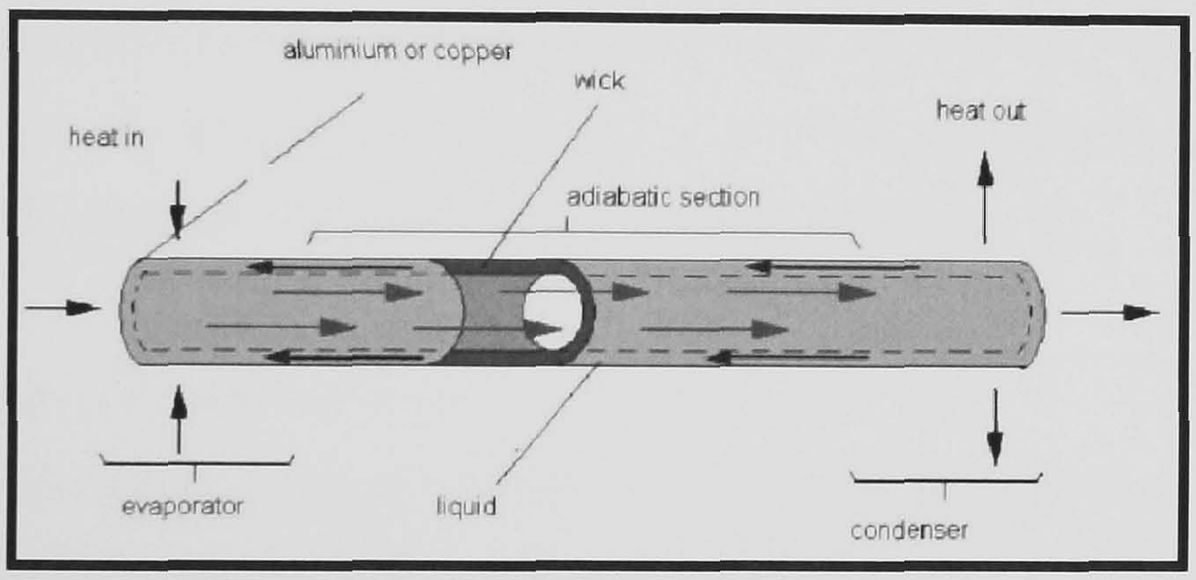

Figure 2.44 Heat pipe construction and principle of operation. (Legierski, 2005)

2.6.3 Heat Pipe Design

As an effective heat conductor, heat pipe can be used in situations when a heat source and a heat sink need to be placed apart, to aid heat conduction of a solid, or to aid heat spreading of a plane. However, not every heat pipe is suitable for all applications. For that reason, the following need to be considered when designing heat pipes:

1) Heat transport limitation of the heat pipe
2) Wick structure of the heat pipe
3) Length and diameter of the heat pipe
4) Heat pipe orientation
5) Effect of bending and flattening of the heat pipe
6) Working fluid

7) Heat pipe reliability

2.6.3.1 Limits to Heat Transport

The most important heat pipe design consideration is the amount of power the heat pipe is capable of transferring. Heat pipes can be designed to carry a few watts or several kilowatts, depending on the application. Heat pipes can transfer much higher powers for a given temperature gradient that even the best metallic conductors can't. If driven beyond its capacity, however, the effective thermal conductivity of the heat pipe will be significantly reduced. Therefore, it is important to assure that the heat pipe is designed to safely transport the required heat load.

The maximum heat transport capability of the heat pipe is governed by several limiting factors which must be addressed when designing a heat pipe. There are five primary heat pipe heat transport limitations. These heat transport limits, which are a function of the heat pipe operating temperature, include: viscous, sonic, capillary pumping, entrainment or flooding, and boiling and can be seen in *Figure 2.45*.

The five heat transport limitations can be simplified as follows;

1) *Sonic limit* – the rate that vapours travels from evaporator to condenser.

2) *Entrainment limit* – Friction between working fluid and vapour that travel in opposite directions.

3) *Capillary limit* – the rate at which the working fluid travels from condenser to evaporator through the wick.

4) *Boiling limit* – the rate at which the working fluid vaporizes from the added heat

5) *Viscous limit* - at low temperatures the vapour pressure difference between the condenser and the evaporator may not be enough to overcome viscous forces.

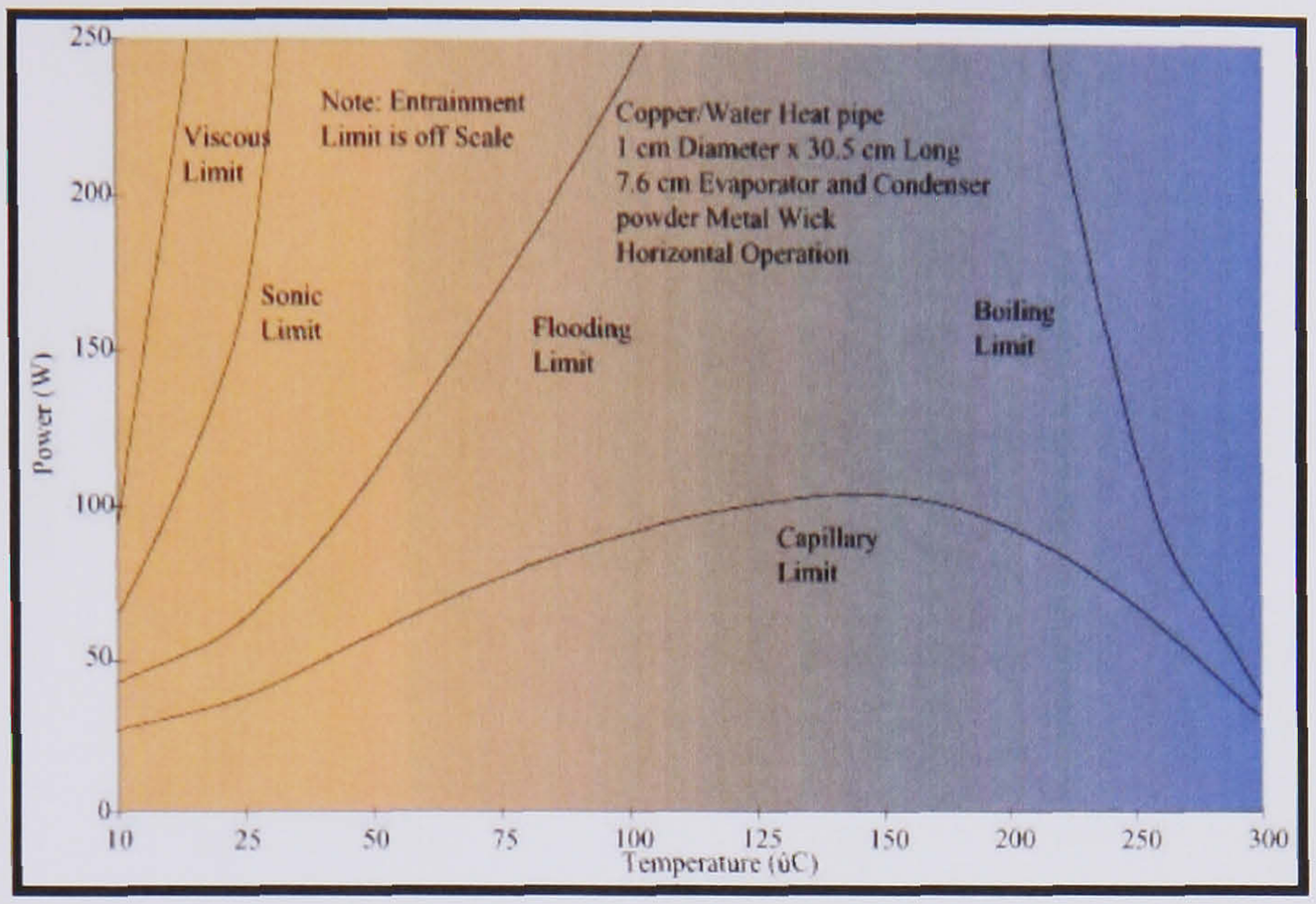

Figure 2.45 Predicted Heat Pipe Limitations (Thermacore Inc.)

2.6.3.2 Wicked and Wickless Heat Pipes

Heat pipes can be classified into wick and wickless heat pipes. Said and Akash (1999) studied experimentally two types of heat pipes using water as a working fluid, one with a wick and another with no wick. The wick was made of cotton, which is normally used in oil lamps. The heat pipe was positioned at different angles and the results showed that the performance of the heat pipe that contained a wick was more significant in terms of overall heat transfer coefficient than that with no wick, for the temperature range studied (*Figure 2.46*). *Figure 2.46* shows the temperature at the evaporator section.

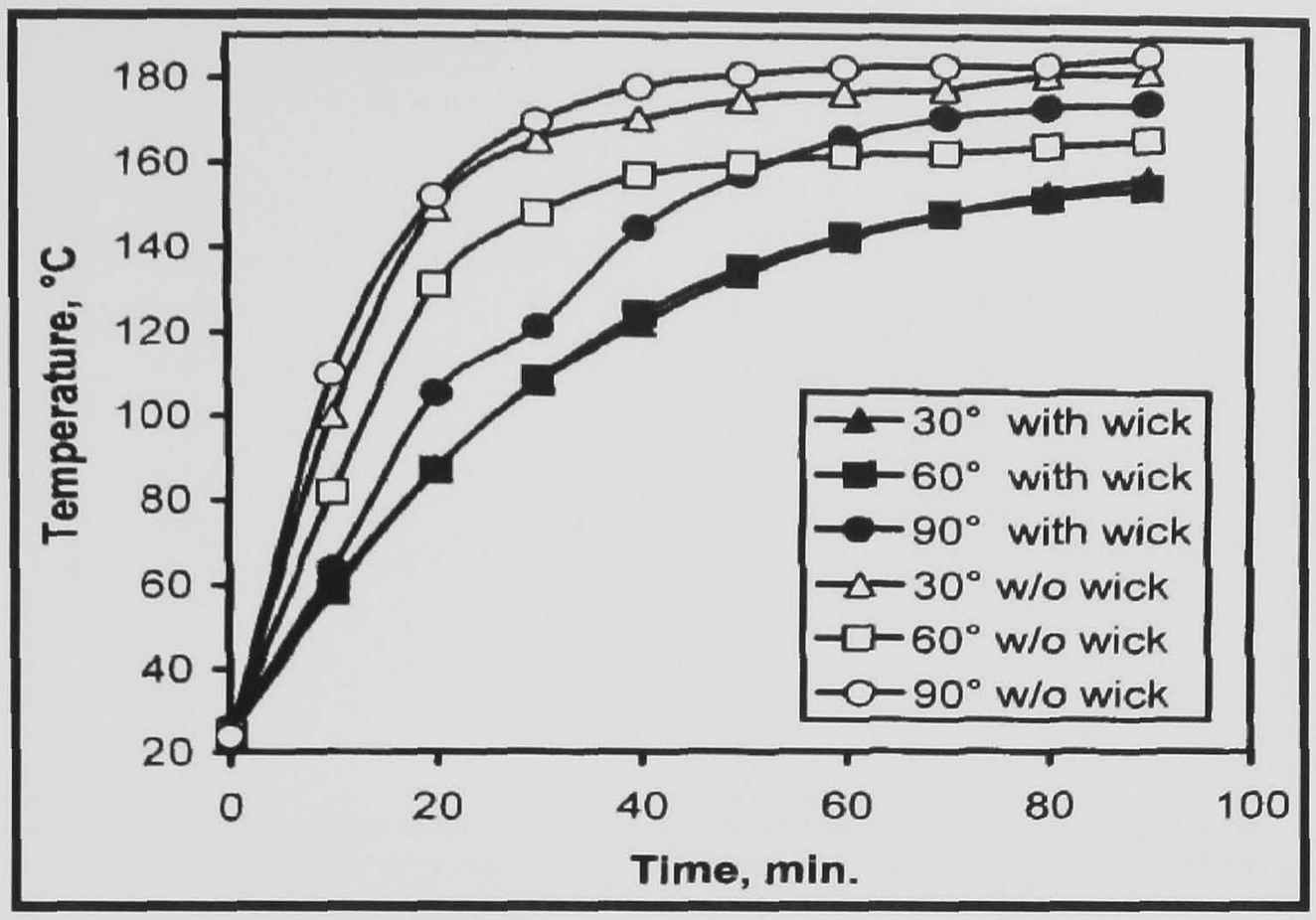

Figure 2.46 Variation of evaporator's temperature with time for different heat pipes at different tilt angles (Said 1999)

There are four common wick structures used in commercially produced heat pipes; groove, wire mesh, powder metal and fiber/spring (*Figure 2.47*).

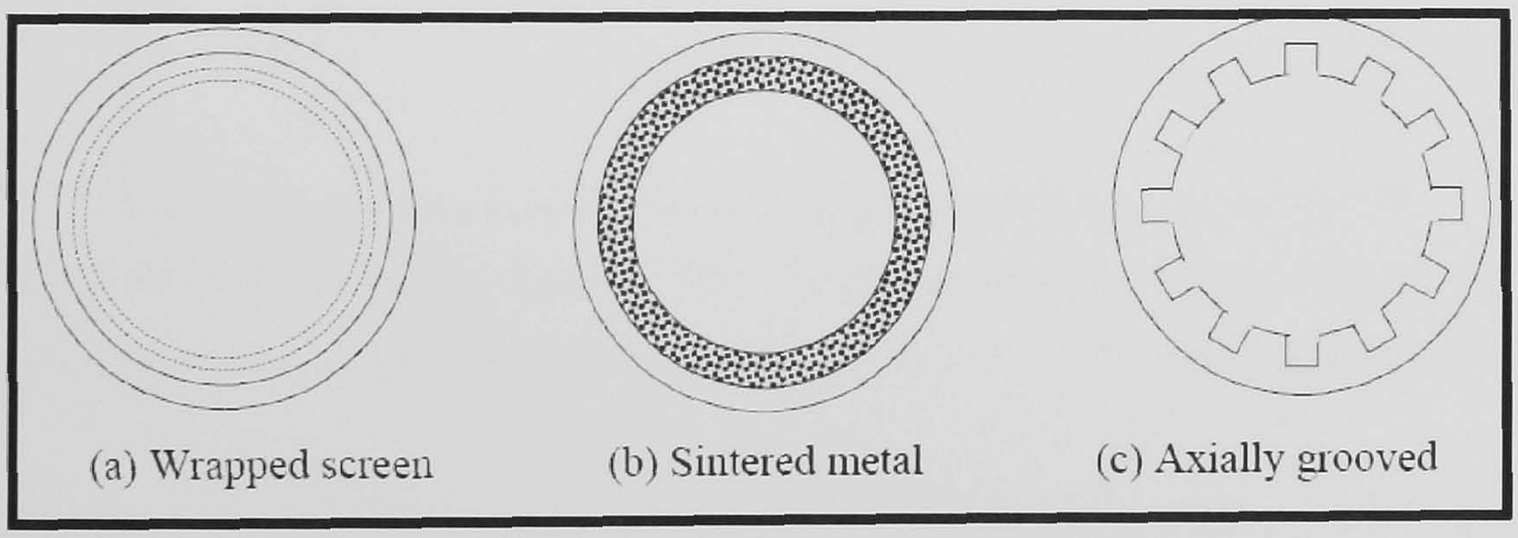

Figure 2.47 Common Wick Structures (Dunn, 1994)

Each wick structure has its advantages and disadvantages. Every wick structure has its own capillary limit. The groove heat pipe has the lowest capillary limit among the four, but works best under gravity assisted conditions where the condenser is located above the evaporator. *Figure 2.48* show the thermal resistance of the different wick types in horizontal and in vertical position along different heat pipe lengths.

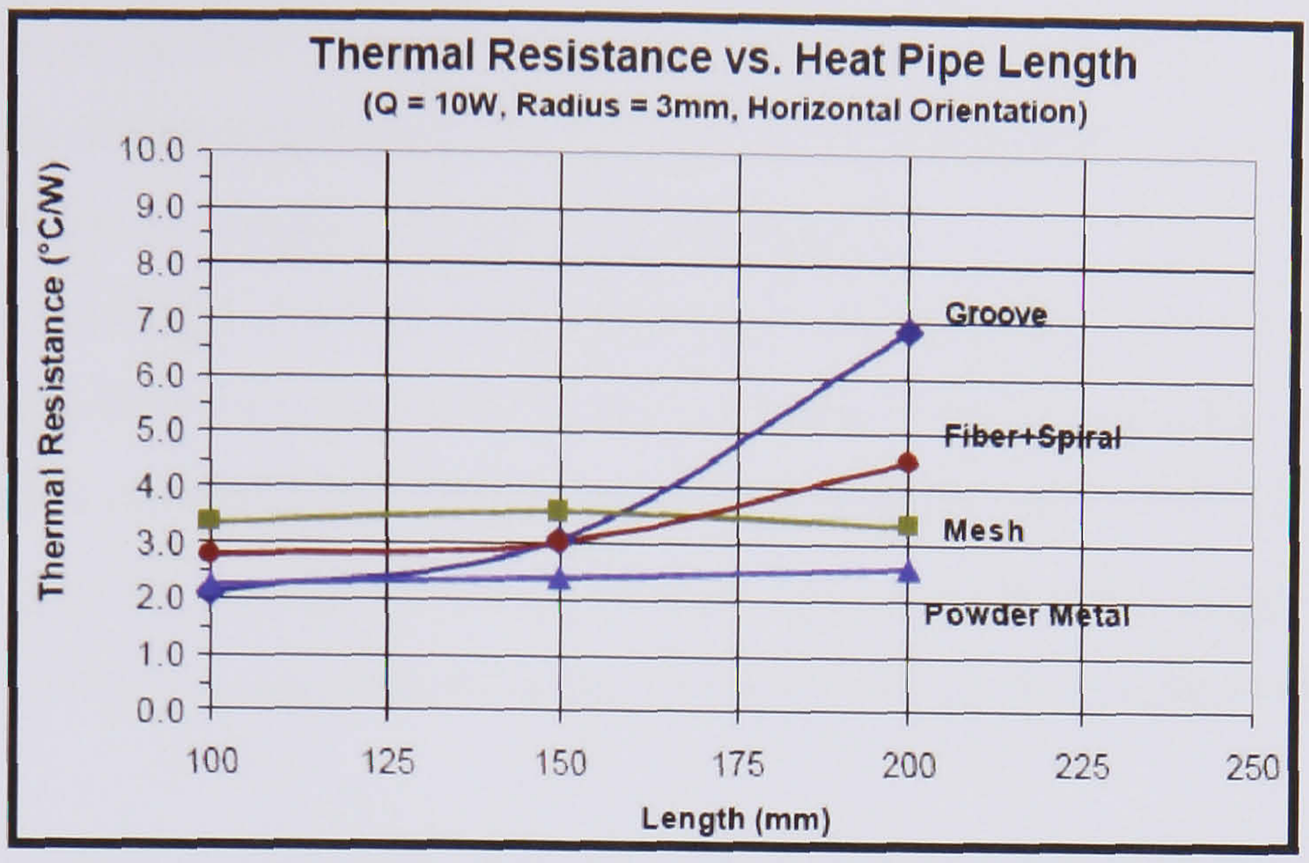

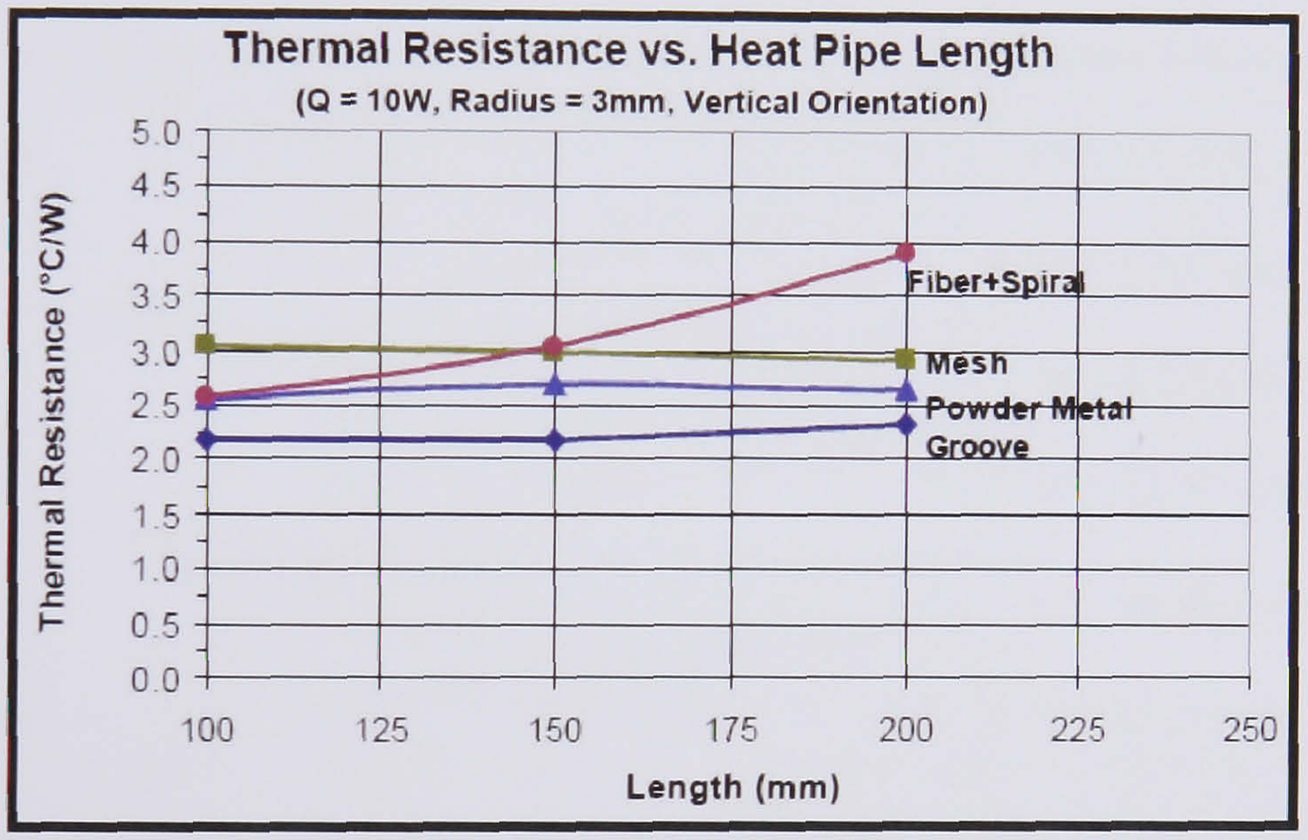

Figure 2.48 The actual test results of heat pipe with different wick structure at a) horizontal and b) vertical (gravity assist) orientations. (www.enertron-inc.com)

2.6.3.3 Length and diameter of a heat pipe

The difference in vapor pressure between the condenser and the evaporator governs the rate at which the vapor travels between them. Also, the diameter and the length of the heat pipe affect the rate at which the vapor travels, and therefore need to be considered when designing heat pipes.

Larger cross sectional areas of the heat pipe (i.e. larger diameter of the heat pipe) will allow higher vapor volume to be transported from the evaporator to the condenser. The cross sectional area of a heat pipe is the direct function of both the sonic and entrainment limit of the heat pipe. However, the operational temperature of the heat pipe

also affects the sonic limit of the heat pipe. *Figure 2.49* compares the heat transport for heat pipes with different diameters. One can see that the heat pipes transport more heat at larger diameters and higher operational temperatures.

The rate of at which the working fluid returns from the condenser to the evaporator is governed by capillary limit and is the reciprocal function of the heat pipe's length. Longer heat pipe transports less heat than shorter heat pipes. In *Figure 2.50*, $Q_{max}L_{eff}$ (W-m) represents the amount of heat a heat pipe will carry per meter length. Therefore, if the pipe is a meter, it can carry twice the wattage a two meter long heat pipe would carry.

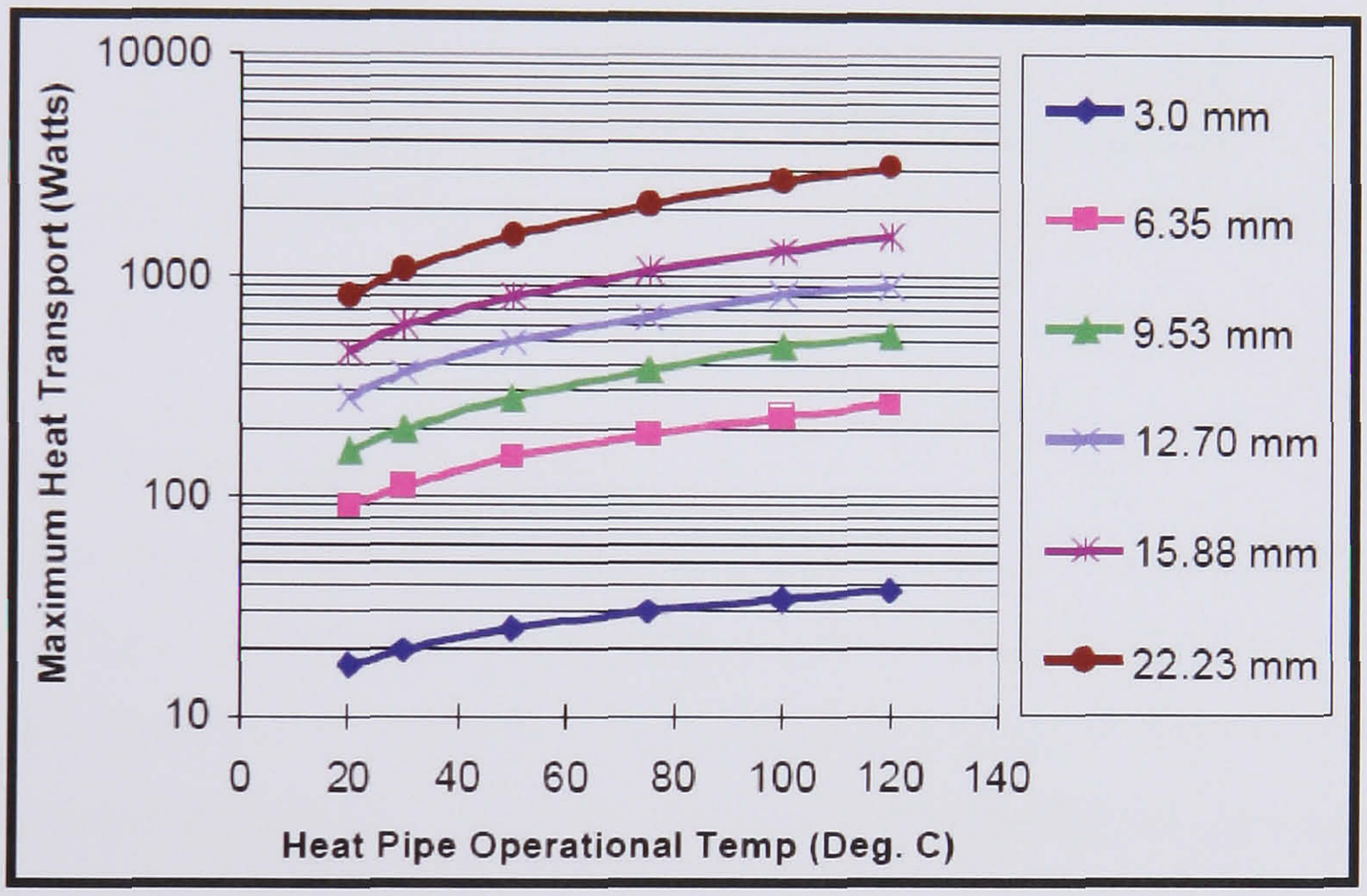

Figure 2.49 Performance of copper water groove heat pipe at vertical orientation (gravity assist) (www.enertron-inc.com)

2.6.3.4 Inclination of heat pipe

A wick structure with a higher capillary limit can transport more working fluid from the condenser to the evaporator against gravity. But as previously mentioned, the groove heat pipe, with the lowest capillary limit, works best under gravity-assisted conditions where the evaporator is located below the condenser. *Figure 2.50* shows the effect of inclination on groove wick heat pipes. As mentioned also from Terdtoon et. al. (1990, 1999) and Negishi (1982) the maximum heat transport is achieved between the 50 and

80 angle degrees. This happens because at that inclination range the heat transfer rate is higher and the thermal resistance is lower.

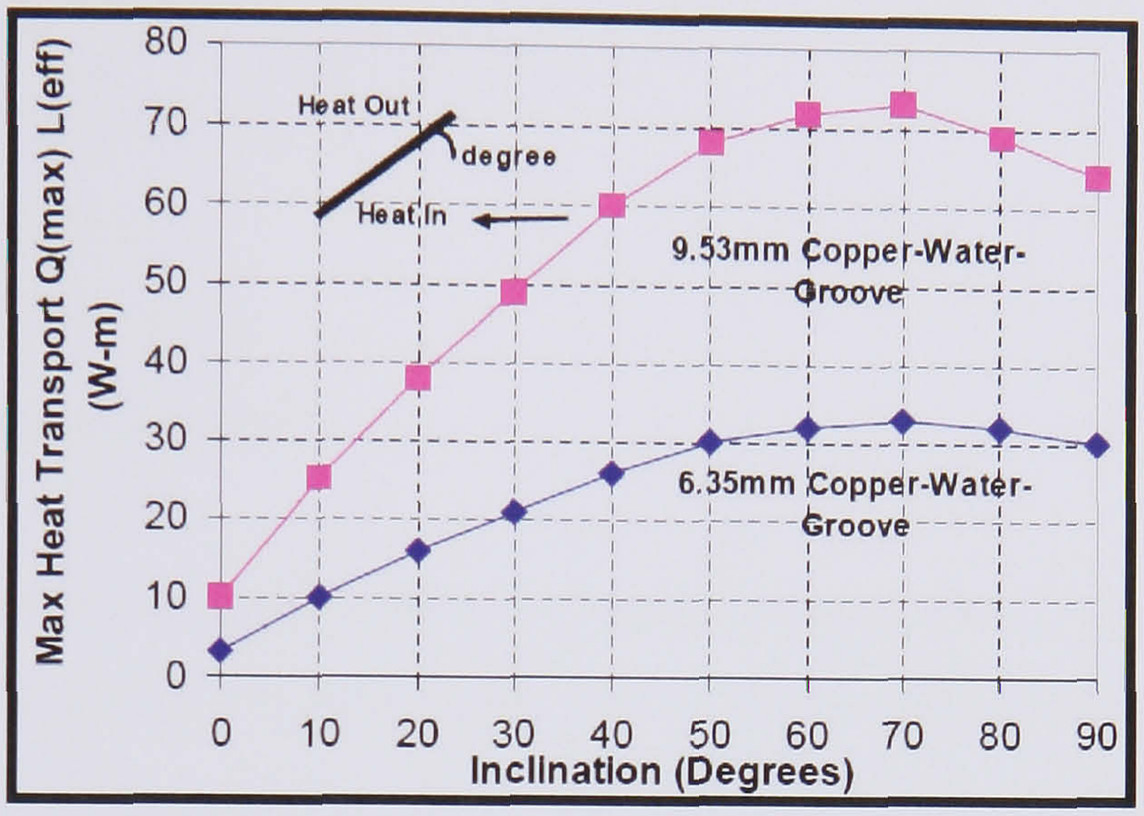

Figure 2.50 Groove wick heat pipe operated at inclination condition (www.enertron-inc.com)

2.6.3.5 Heat pipe flattening or bending

If a heat pipe is flattened or bent, the sonic limit and entrainment limit will be reduced in relation to the flattened thickness, the number of bends and the angle of each bend. Therefore, any flattening or bending to a heat pipe will reduce the amount of heat that can be transported. *Figure 2.51* shows the effect of the flattening on a heat pipe.

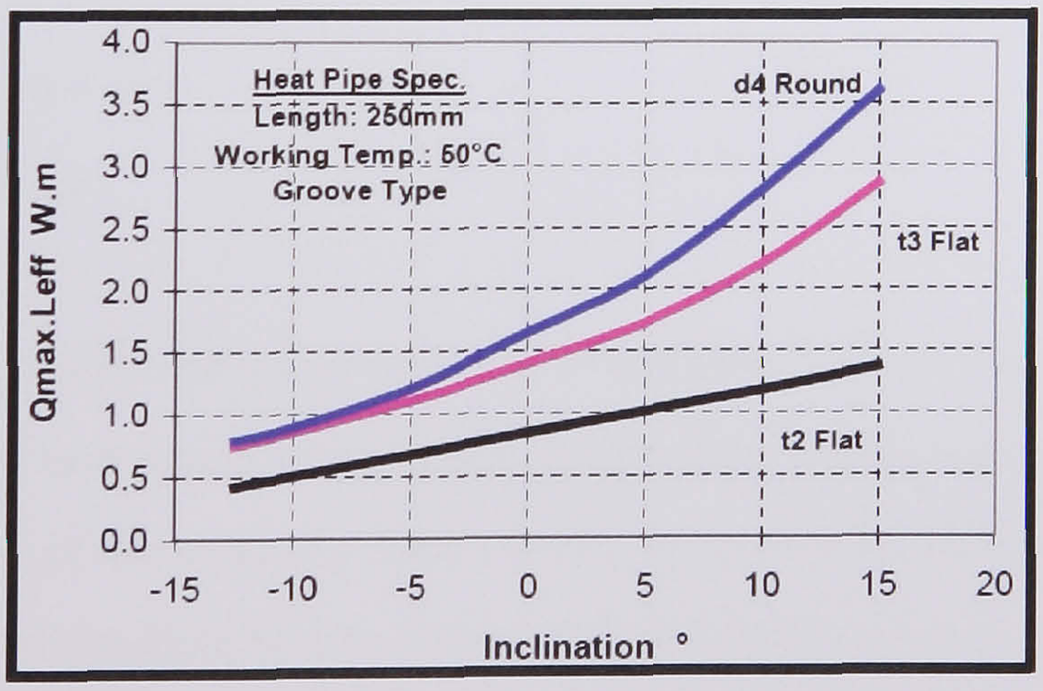

Figure 2.51 Comparison of round and flat heat pipes under different orientations (www.enertron-inc.com)

2.6.3.6 Working Fluids

Different working fluids can be used in heat pipes to suit different temperature requirements. The operating temperature can be set into one of the following ranges *Table 2.7*:

- Cryogenic (4-200 K)
- Low (200-550 K)
- Medium (550-750 K)
- High (750 and above K)

The first consideration in the selection of a suitable working fluid is the operating vapour temperature range. Different applications dissipate different heat loads. Within the approximate temperature range, several possible working fluids may exist, and a variety of characteristics must be examined in order to determine the most accepted of these fluids for the application considered. The prime requirements are:

- Vapour pressure not too high or low over the operating temperature range
- Compatibility with wick and wall materials
- Wet ability of wick and wall materials
- Low liquid and vapour viscosities
- Acceptable freezing or pour point
- High thermal conductivity
- Good thermal stability
- High surface tension
- High latent heat

A high latent heat or vaporization is essential to transfer large amounts of heat with minimum fluid flow, and hence to maintain low pressure drops within the heat pipe. The thermal conductivity of the working fluid should preferably be high in order to minimize the radial temperature gradient and to reduce the possibility of nucleate boiling at the wick or wall surface. Choosing fluids with low values of vapour and liquid viscosities will minimize the resistance to fluid flow.

Table 2.7: Various working fluids and their useful range

Source: (www.cheresources.com/htpipes)

Medium	Melting Point (˚C)	Boiling Point at Atm. Pressure (˚C)	Useful Range (˚C)
Helium	-271	-261	-271 to –269
Nitrogen	-210	-196	-203 to –160
Ammonia	-78	-33	-60 to 100
Acetone	-95	57	0 to 120
Methanol	-98	64	10 to 130
Flutec PP2	-50	76	10 to 160
Ethanol	-112	78	0 to 130
Water	0	100	30 to 200
Toluene	-95	110	50 to 200
Mercury	-39	361	250 to 650
Sodium	98	892	600 to 1200
Lithium	179	1340	1000 to 1800
Silver	960	2212	1800 to 2300

2.6.3.7 Heat pipe reliability

Heat pipes have no moving parts and can be in operation for 20 years. However, care must be given when designing and manufacturing the heat pipe. Two manufacturing factors can reduce the reliability of the heat pipe: the seal of the pipe and the cleanness of pipe internal chamber. Any leakage in the heat pipe will eventually fail the pipe. If the internal chamber is not thoroughly clean, when the heat pipe subjected to heat, the residual may generate non-condensable gas and degrade the pipe performance. Improper bending and flattening of the pipe may also cause the leakage on the pipe seal. There are some external factors that may also shorten the life of a heat pipe such as shock, vibration, force impact, thermal shock and corrosive environment.

2.6.3.8 Type of Heat Pipes

There are many types of heat pipe configurations built for different applications. It can be classified in the following category in terms of structure:

Heat Pipe:

- Annual heat pipe

- Flat plate heat pipe
- Conical heat pipe
- Leading edge heat pipe
- Gas loaded heat pipe
- Capillary pumped loop heat pipe
- Monogroove heat pipe

Flat Plate- much like traditional cylindrical heat pipes but rectangular. Used to cool and flatten temperatures of semiconductor or transistor packages assembled in arrays on the top of the heat pipe (*Figure 2.52*).

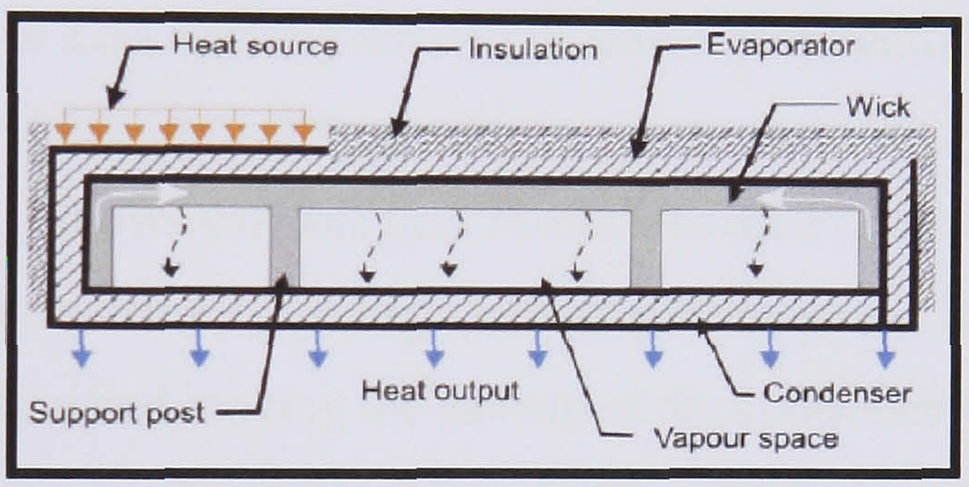

Figure 2.52 A cross section of a Flat Heat Pipe (Boukhanouf, 2006)

Micro heat pipes- small heat pipes that are noncircular and use angled corners. Employed in cooling semiconductors (improve thermal control), laser diodes, photovoltaic cells, medical devices (*Figure 2.53*).

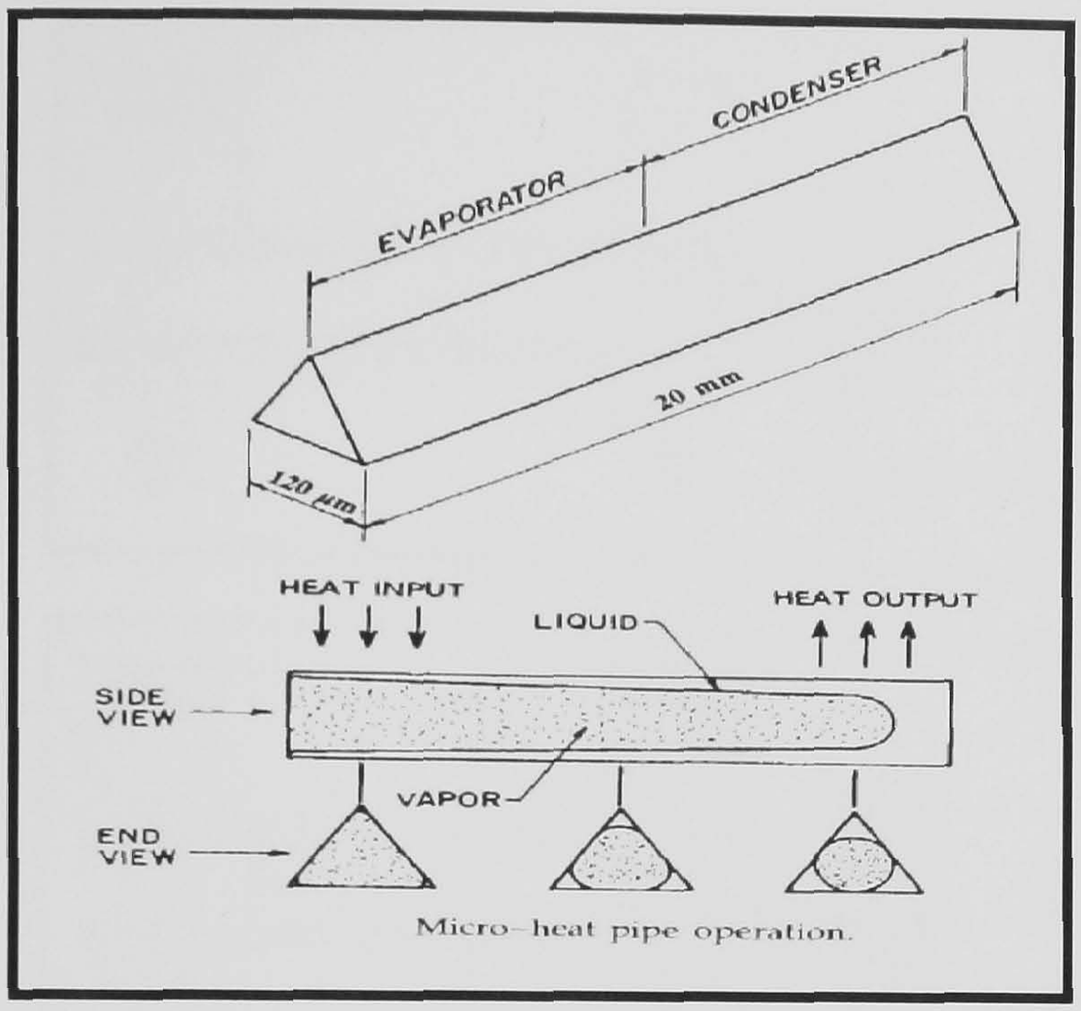

Figure 2.53 Rectangular Micro Heat Pipe (Dunn, 1994)

Variable conductance- allows variable heat fluxes into the evaporator while evaporator temperature remains constant by pushing a non- condensable gas into the condenser when heat fluxes are low and moving the gas out of the condenser when heat fluxes are high, thereby, increasing condenser surface area. They come in various forms like excess-liquid or gas-loaded form (*Figure 2.54*).

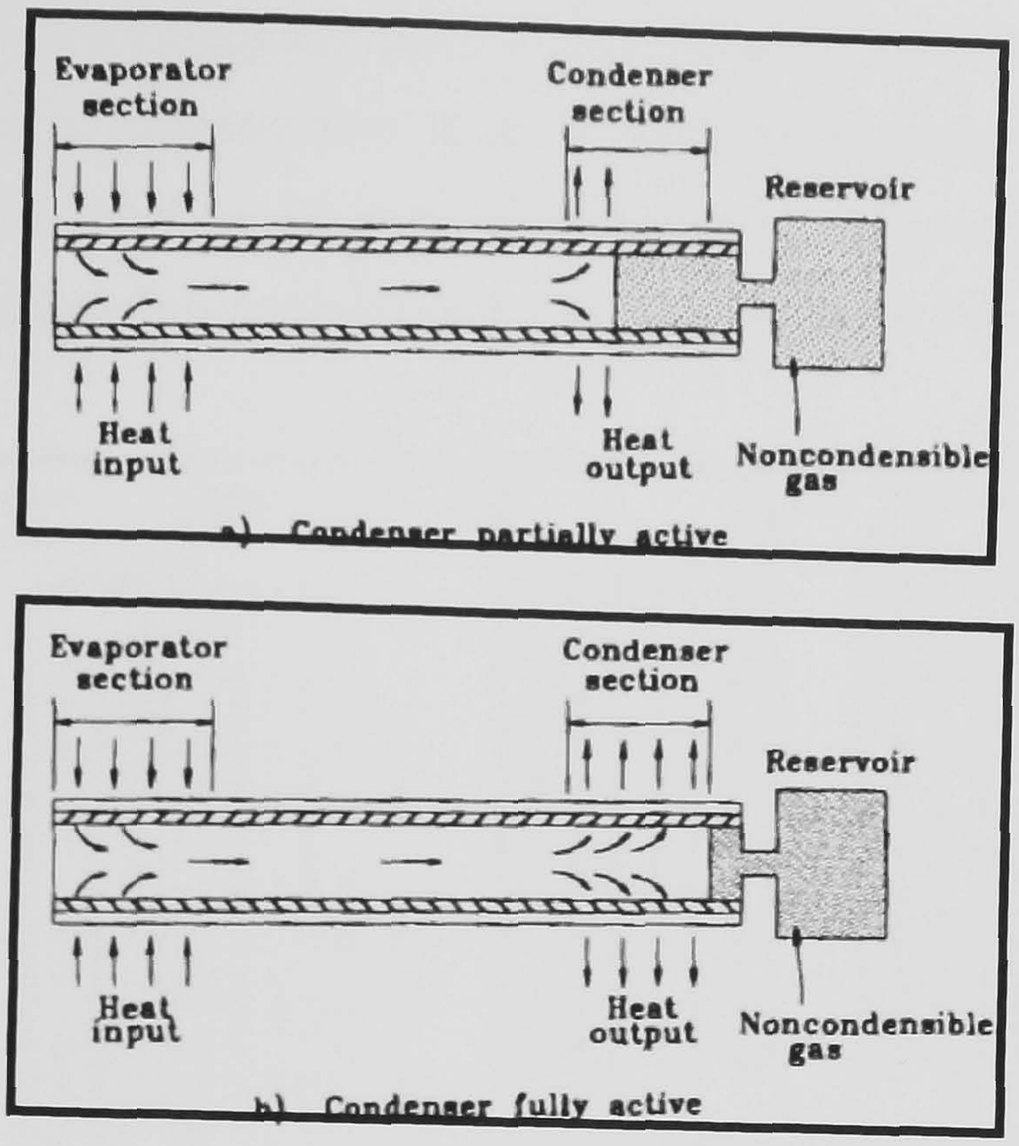

Figure 2.54 Variable Conductance Heat Pipe, a) Condenser partially active b) Condenser fully active (Dunn, 1994)

Capillary pumped loop heat pipe- for systems where the heat fluxes are very high or where the heat from the heat source needs to be moved far away. In the loop heat pipe, the vapor travels around in a loop where it condenses and returns to the evaporator (*Figure 2.55*).

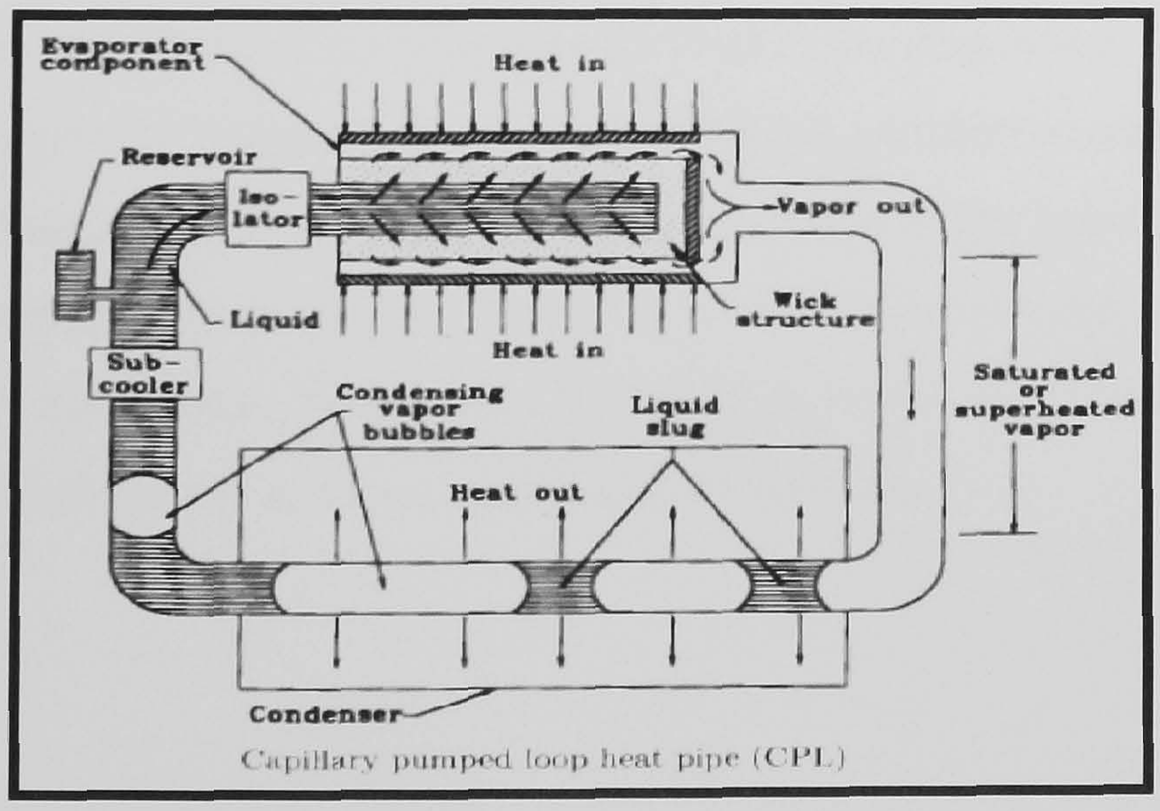

Figure 2.55 Capillary pumped loop heat pipe (Dunn, 1994)

The basic structure of a typical pulsating heat pipe consists of meandering capillary tubes having no internal wick structure. It can be designed in at least three ways: (i) open loop system, (ii) closed loop system and (iii) closed loop pulsating heat pipe (CLPHP) with additional flow control check valves, as shown in *Figure 2.56*.

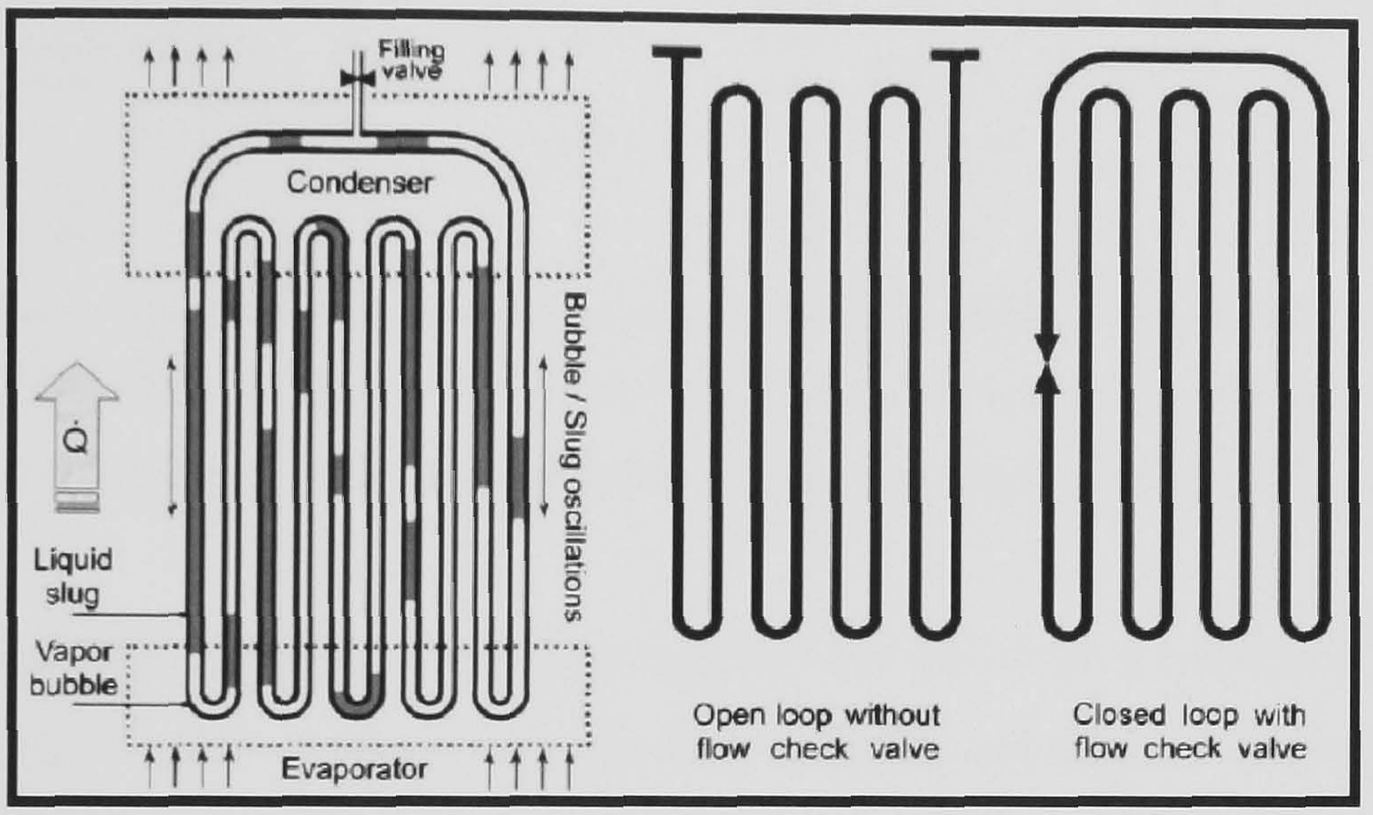

Figure 2.56 Schematics of a pulsating heat pipes and its design variations. (Piyanun, 2003)

2.6.4 Gravity assisted wickless heat pipes

As we mentioned the heat pipe is a thermal device which affords efficient transport of thermal energy by use of an intermediate heat transfer fluid. Heat pipes working under gravity with the condenser above the evaporator do not need any external power or capillary structure for return of the heat transfer fluid to the evaporator. This type of heat pipe is known as gravity assisted heat pipe, two phase closed thermosyphon (TPCT) or wickless gravity assisted heat pipe. However, the operation of the gravity assisted heat pipe may be enhanced by introducing an internal wick structure to distribute circumferentially the working fluid inside the heat pipe evaporator (Dunn, 1994). *Figure 2.57* shows a typical gravity and capillary induced heat pipes.

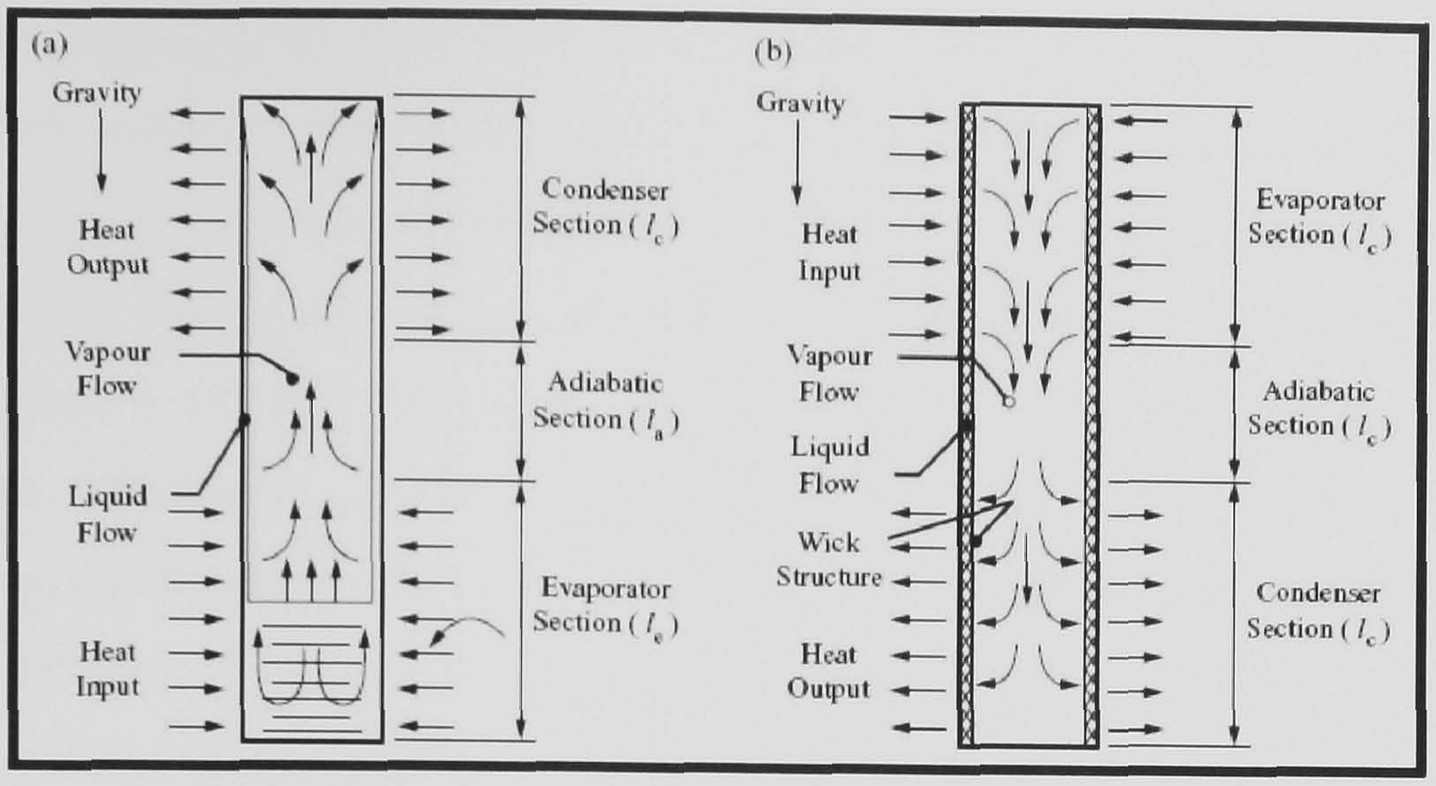

Figure 2.57 Capillary and gravity induced heat pipes. (a) Conventional gravity assisted heat pipe. (b) Capillary induced heat pipes. (Joudi, 1991, 2000)

Gravity assisted heat pipes have received considerable attention in terrestrial applications due to their efficient heat transfer capability, simple construction and durability. Therefore, numerous applications exist for heat recovery systems (Littwin 1985, Chaudourene 1987), solar energy (Bloem 1982) and, recently, in light water nuclear reactors (Kaminaga 1997).

The thermosyphon has been proved as a promising heat transfer device with very high thermal conductance. The two-phase closed thermosyphon is widely used because of their simple structure when compared with other types of heat pipes. Therefore, thermosyphons are being used in many applications such as: heat exchangers (air pre-heaters or systems that use economizers for waste heat recovery), cooling of electronic components, solar energy conversion systems, spacecraft thermal control, cooling of gas turbine rotor blades, etc. (Dunn 1994).

A considerable experimental and theoretical work has been done on the application and design modification for improving thermosyphon performance. Nguyen-Chi et al. (1979) investigated experimentally the performance of vertical two-phase close thermosyphon and used water as a working fluid. They investigated the influence of operating parameters on the maximum performance. One of the parameters was the working fluid as Li et al. (1991) investigated experimentally with a vertical two-phase

closed thermosyphon with R11, R22, and water as working fluids. The same work was done by Park and Lee (1991) who made an experimental study on the performance of stationary two-phase closed thermosyphon with three working fluid mixtures (water–glycerin, water ethanol, and water–ethylene glycol). Shiraishi et al. (1996) investigated experimentally a critical heat transfer rate in thermosyphons by taking into account the aspect ratio, filling ratio and working fluid property. Terdtoon et al. (1996, 1999) also studied experimentally the effect of aspect ratio on heat transfer characteristics of two-phase closed thermosyphon at normal operating condition. They used R-22, ethanol, and water as working fluids. Shalaby et al. (2000) studied experimentally the heat transfer performance of a two-phase closed thermosyphon with R22 as working fluid.
From all studies authors concentrate their research on working fluid, inclination angle, filling ratio and aspect ratio (Length of pipe/Pipe Diameter). The outcome of the studies was that the temperature distribution along the thermosyphon wall in the evaporator section was almost isothermal. The measured temperature along the condenser showed lower values. This drop of temperature is expected because of the internal resistances due to boiling and condensation. Also filling ratio doesn't have any effect on the heat transfer coefficient at different angles. But the working fluid has an effect when the inclination angle is between 20 and 70 degrees. A lower heat vaporisation exhibits a larger heat transfer. At different aspect ratios the outside temperature of the evaporator and the maximum heat transfer rates comes with different filling ratios.

Joudi and Witwit (2000) studied the performance of conventional gravity assisted heat pipe and a modified heat pipe with a separator in the adiabatic section (*Figure 2.58*). Heat pipes with a three layered wick in the evaporator section, in addition to the separator, were also investigated. Water was employed as the working fluid in all heat pipes. The presence of the adiabatic separator caused a marked improvement in all heat pipes tested for all lengths and inclination angles. A pronounced reduction in heat pipe evaporator temperature was obtained, which is accompanied by an improvement in the heat transfer coefficient. Increasing the gravity assisted heat pipe length the heat pipe operating temperature decreased, which is always a desirable feature.

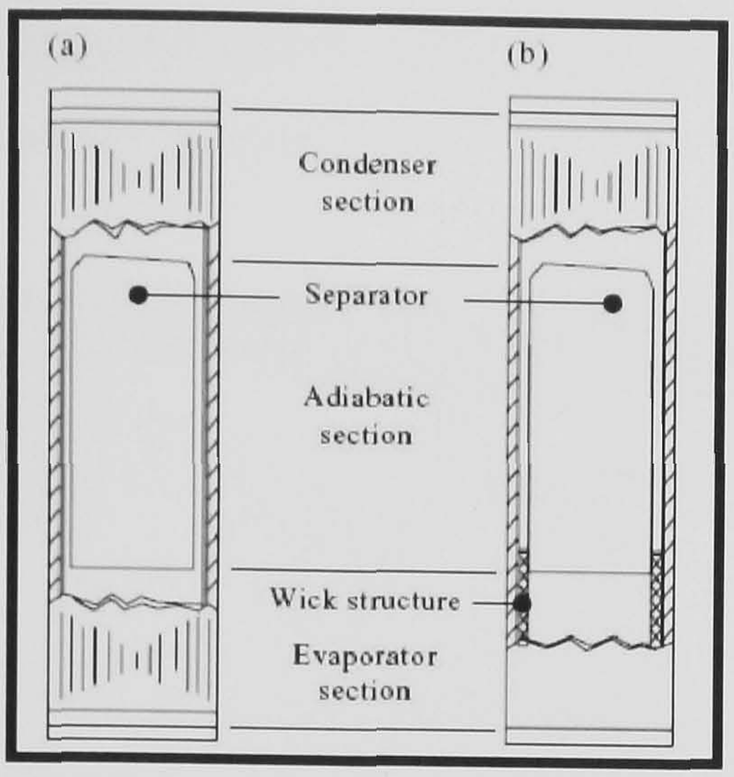

Figure 2.58 Gravity assisted heat pipe (a) with separator only, (b) with separator and wick at the evaporator only (Joudi, 2000)

2.6.5 Solar Heat Pipe Collectors

Solar thermal utilization is of great importance for environmental protection and conventional energy saving. A variety of flat plate solar collectors and evacuated tubular solar collectors have been produced and applied around the world.

Usually, conventional solar collectors use pipes attached to the collecting plate and a heat transfer fluid, such as water, to transfer by natural or forced circulation the heat captured by the solar collector to a storage tank. Some of the shortcomings associated with conventional solar collectors include extra expense of the forced circulation system due to the pump and its extracted power, extra space required for the natural circulation system due to the position limitations required, the night cooling due to the reverse flow of cooled water, freezing of the water on cold nights, pipe corrosion due to the use of water and the limited quantity of heat transferred by the heat transfer fluid.

Heat pipes offer a promising solution to these problems. An experimental flat plate solar collector operating in conjunction with a closed-end oscillating heat pipe (CEOHP) offers a reasonably efficient and cost effective alternative to conventional solar collector system that use heat pipes. The CEOHP system (*Figure 2.59*) described by Rittidech and Wannapakne (2007) relies on the natural forces of gravity and capillary action and does not require an external power source. An efficiency of approximately 62% was achieved, which correlates with the efficiency of the more expensive heat pipe system.

The CEOHP system offers the additional benefits of corrosion free operation and absence of freezing during winter months.

Figure 2.59 The experimental assembly: (a) CEOHP flat plate solar collector; (b) condenser water tank; (c) wooden frame. (Rittidech 2007)

Bazzo and Nogoseke (2003) proposed a capillary pumping system attached to a flat solar collector, using fine circumferential grooves as capillary structure and acetone as the working fluid (*Figure 2.60*). The working fluid was pumped from a condenser designed to delivery heat to the water storage. The system presented reliable start-ups and good performance in continuous operation. According to the results, heat loads up to 507 W/m^2 were expected for transporting.

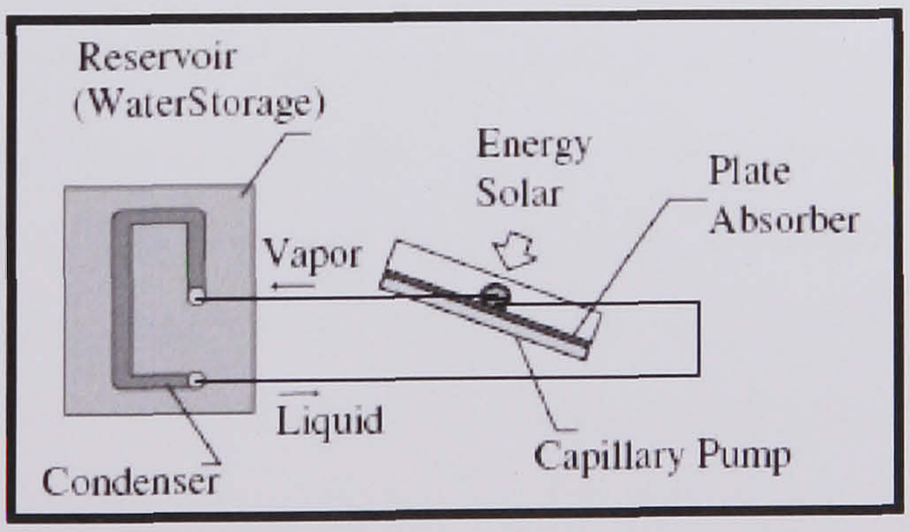

Figure 2.60 Schematic of a solar heating system assisted by one capillary pump. (Bazzo 2003)

2.6.5.1 Solar Collectors with gravity assisted heat pipes

Heat pipes working under gravity with the condenser above the evaporator do not require external power or capillary action in order to return the heat transfer fluid to the evaporator. This type of heat pipe is known as the gravity assisted heat pipe, or wickless gravity assisted heat pipe.

The thermosyphon flat- plate solar collector has many advantages over the conventional flat-plate solar collector such as:

1. A thermal diode benefit when the collector temperature is less than storage water temperature;
2. A small heat capacity;
3. A reasonable resistance against corrosion by selecting a suitable working fluid to be compatible with the pipe wall material;
4. Easy freeze protection;
5. Lower pumping requirements.

De Vries et al. (1980) investigated theoretically the influence of the pump control unit of a conventional flat plate solar collector and the diode resistance of a planar wickless heat pipe solar collector on their efficiencies during periods of transient insolation. They concluded that the performance of the wickless heat pipe collector was as good as that of a conventional solar collector with fluid circulation control. Akyurt (1984) designed, manufactured and tested numerous prototypes wickless heat pipe flat plate solar collectors made of different materials and filled with different working fluids. An extensive testing program revealed that the wickless heat pipe performs satisfactorily as a heat transfer element in solar collectors without start up difficulties. Henyue (1987) concluded that increasing the heat transfer surface of the condenser section of the wickless heat pipe was an effective way to improve the instantaneous efficiency of wickless heat pipe flat plate solar water heaters. Hussein et al. (1999a, 1999b) investigated theoretically and experimentally that the effect of the pitch distance ratio W/D on the instantaneous efficiency of the wickless heat pipe flat-plate solar collector decreases as the wickless heat pipe diameter decreases and the inlet cooling water temperature increases.

Abreu and Colle (2004) investigated experimentally the transient thermal behaviour of a wickless heat pipe flat plate solar water heater characterized by a semi-circular condenser and a straight evaporator (*Figure 2.61*). From the results they observed that:

- By increasing the cooling temperature the overall thermal resistance decreased.
- The thermal resistance decreased for the lowest fill ratio.
- As the evaporator temperatures and area increase with the evaporator length, the heat losses are also increased thus the lowest thermal resistances were achieved for the shortest evaporator.

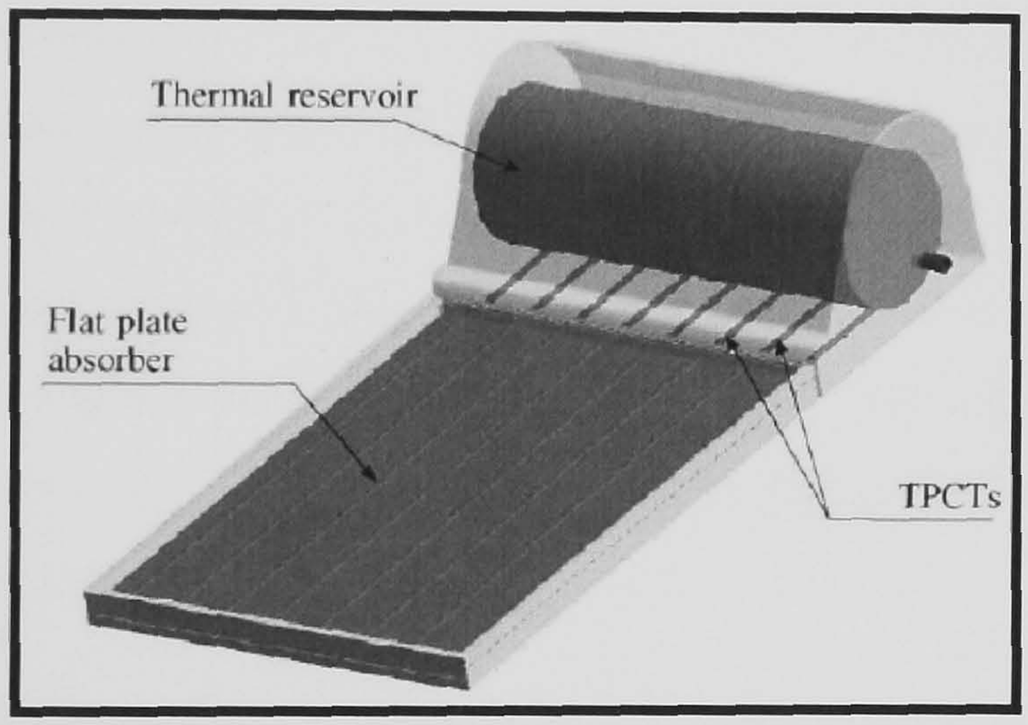

Figure 2.61 Proposed configuration of the compact Solar Domestic Heating Water system (Abreu 2004)

Hussein (2006) studied the effect of wickless heat pipe cross section geometry and its working fluid filling ratio on the performance of flat plate solar collectors. Three groups of wickless heat pipes having three different cross section geometries (namely, circular, elliptical and semi-circular cross sections) were designed and manufactured. It was concluded that the elliptical cross section improved the performance in comparison with the circular and that the optimum filling ratio dropped from 20% to 10%. In the contrary the semi-circular section had a bad performance compared with the other two heat pipe cross section.

In contrast of the advantages a wickless heat pipe absorber in flat-plate solar heater also has several disadvantages compared to conventional flat-plate solar heaters. One of

these disadvantages is the need for a heat exchanger between the condenser section of the heat pipe and the storage tank.

2.6.5.2 Solar collectors heat exchanger types

The existing applications of the heat-pipe in solar thermal collectors can be divided into two categories, depending on the region in which condensation takes place. In the first category are the systems in which heat is transferred with a heat-pipe from the evaporator, which is actually the collector absorbing surface, towards the header in which the condenser is placed (Ortabasi and Fehlner, 1979; Ismail and Abogderah, 1998; Hussein *et al*., 1999). Heat transfer from header–condenser to the tank is done in the usual way, i.e. using a pump which moves the heating fluid (*Figure 2.62*). The second category concerns transfer of thermal energy to the tank, that is systems in which the evaporator inside the collector while the condenser is inside the tank (*Figure 2.63*). These systems usually employ heat-pipes assisted by gravity, where the tank is placed in the upper part of the collector with the liquid phase being transported naturally to the lower part of the collector through the same heat-pipe.

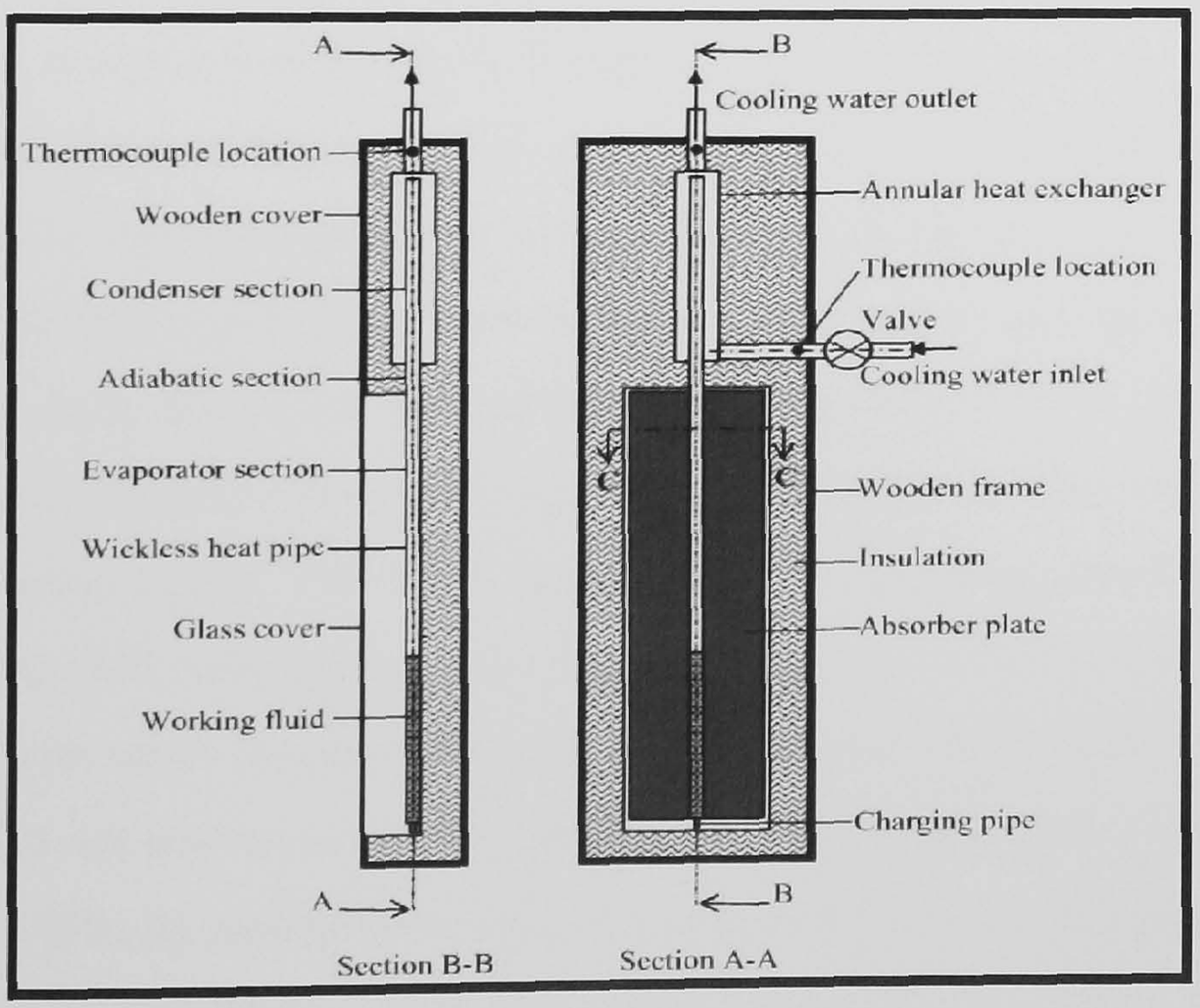

Figure 2.62 Cross-sectional views of the prototype wickless heat pipe flat plate solar collector. (Hussein 2005)

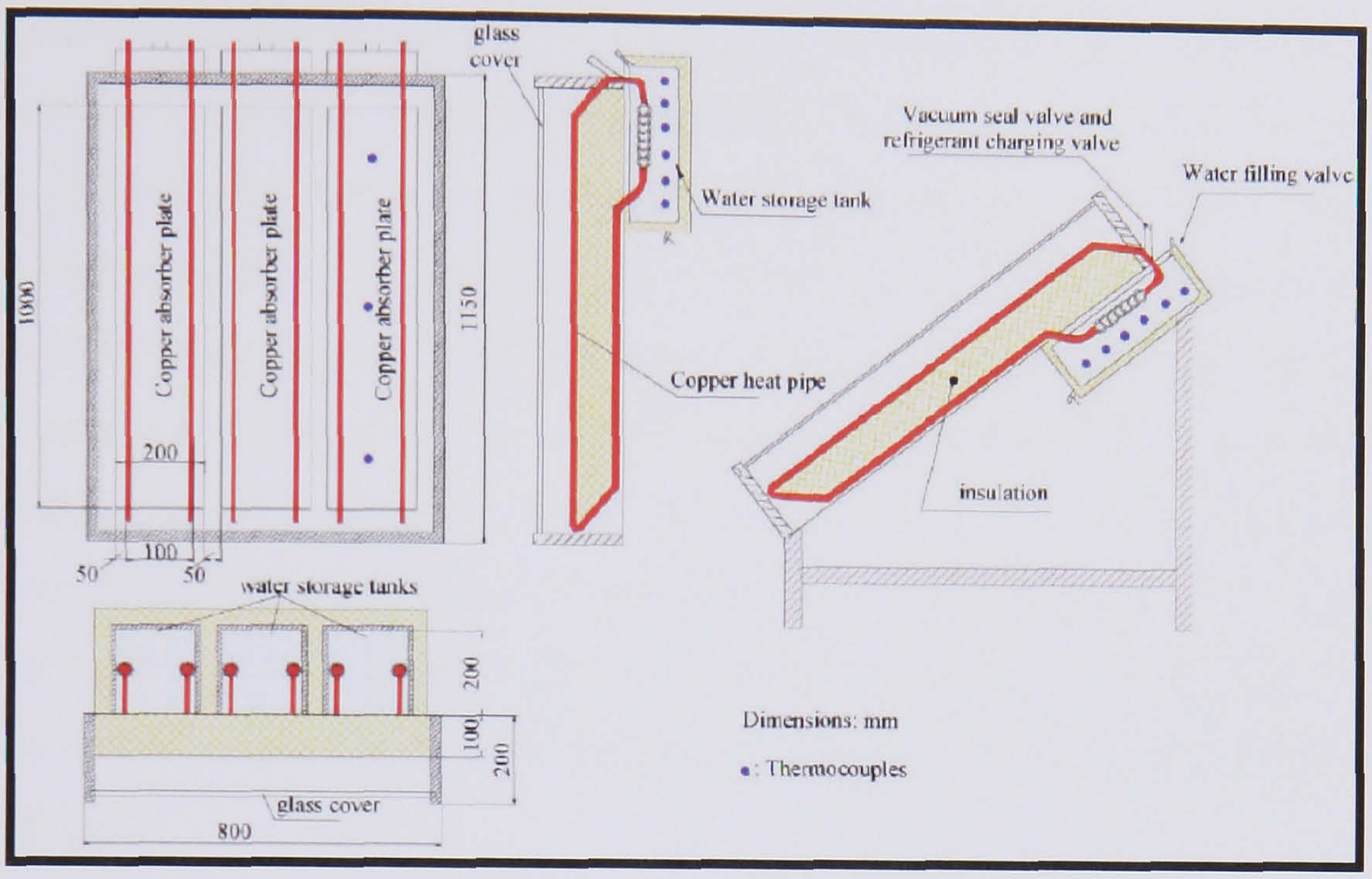

Figure 2.63 Experimental set-up of thermosyphon two-phase solar collector together with the temperature measurement points. (Esen 2005)

The common way used by most of the previous studies [Hussein 1999, Ismail 1998, Ortabasi 1979] was circulating the water from the heaters tank to a header through which the water was distributed to flow through a separate annulus around the condenser section of each thermosyphon tube of the collector. Then the water outlet from each annulus was collected in an outlet header to flow again to the tank. Mathioulakis and Belessiotis (2001) conducted an experimental and theoretical investigation to study the performance of a new ethanol thermosyphon solar water heater. In this system the condenser section of the thermosyphon tube was placed inside the tank of the water heater. The results showed that the system can reach satisfactory efficiencies up to 60% working in a wide range of operating temperatures and be effective even with small temperature difference between collector and tank.

The works of Oliveti and Arcuri (1996), Ismail and Abogderah (1992, 1998) and Hussein et al. (1999a,b) present the results obtained with heat pipe flat plate solar collectors where the condensers of the pipes were immersed in a cooling manifold. Oliveti and Arcuri and Hussein et al. made use of TPCTs with water as the working fluid, while Ismail and Abogderah made use of heat pipes with internal capillary

structure in the evaporator section and methanol as the working fluid. Another work, from Chun et al. (1999), presented a similar configuration where five individual modules of only one pipe coupled with a thermal reservoir were tested. Different working fluids (water, methanol, acetone and ethanol) were compared and it was revealed that the system performance is insensitive to the working fluids. Recently Hussein (2006) studied a wickless heat pipes flat plate solar collector with a cross flow heat exchanger and the results showed that the optimal mass flow rate is very close to the ASHRAE standard mass flow rate (0.02 kg/s) for testing conventional flat plate solar collectors. Also the experimental and theoretical results indicated that there is an optimum number of wickless heat pipes to be used in designing the wickless heat pipes flat plate solar collectors with cross flow heat exchanger. This optimum number was about 12 pipes.

2.6.5.3 Solar collectors heat pipes with different working fluid

A number of studies have been previously conducted in which various phase change fluids or refrigerants have been evaluated for use in a thermosyphon solar water heater. Pluta and Pomierny (1995) studied a two-phase solar thermosyphon for domestic hot water, with Freon R22 and filled at 1/3 of total heat pipe length and indicated that proper construction and choosing suitable phase change medium play very important role in assuring proper operating conditions of a phase-change thermosyphon. Ghaddar and Nasr (1998) fabricated and tested an R-11 charged solar collector with an integrated condenser for secondary-cooling water flow. Forced circulation flow demonstrated instantaneous system efficiency values varying from 60% to 20%, which is in range of conventional water solar collectors. Joudi and Al-Tabbakh (1999) (*Figure 2.64*) conducted a theoretical analysis by computer simulation of a two phase thermosyphon solar domestic hot water system using R-11. The results showed that, in the two-phase system, the collector efficiency did not reveal a serious change with the loading condition. The collector efficiency of the two-phase system was approximately 20% higher than a single phase collector. Also, the response of the two-phase system was faster than a single phase system. Esen and Yu¨ ksel (2000) manufactured a two-phase thermosyphon solar collector with heat pipes, and studied experimentally various phase-

change fluids (acetone, methanol, ethanol) to evaluate the effect of insolation and mass of fluid on the collector performance. It was found out that such a collector can be successfully used, especially during cold, cloudy and windy days. Payakaruk et al. (2000) studied the inclined thermosyphon that employed with R-22, R-123, R- 134a, ethanol, and water as working fluid. The selected filling ratios were 50%, 80%, and 100%. It was found from the experiments that the filling ratio had no effect on the ratio of heat transfer characteristics at any angle to that of the vertical position, but the properties of the working fluid affected the mentioned ratio of heat transfer rate.
Esen et al. (2005) presented the results of an experimental investigation of a two-phase closed thermosyphon solar water heater. The results were analyzed with regard to various working fluids (R134a, R407C, and R410a). It was concluded that the working fluid had an effect on thermal performance of a two-phase thermosyphon solar collector. Best performance was obtained using R410A probably due to its higher latent heat, higher liquid thermal conductivity, and lower viscosity.

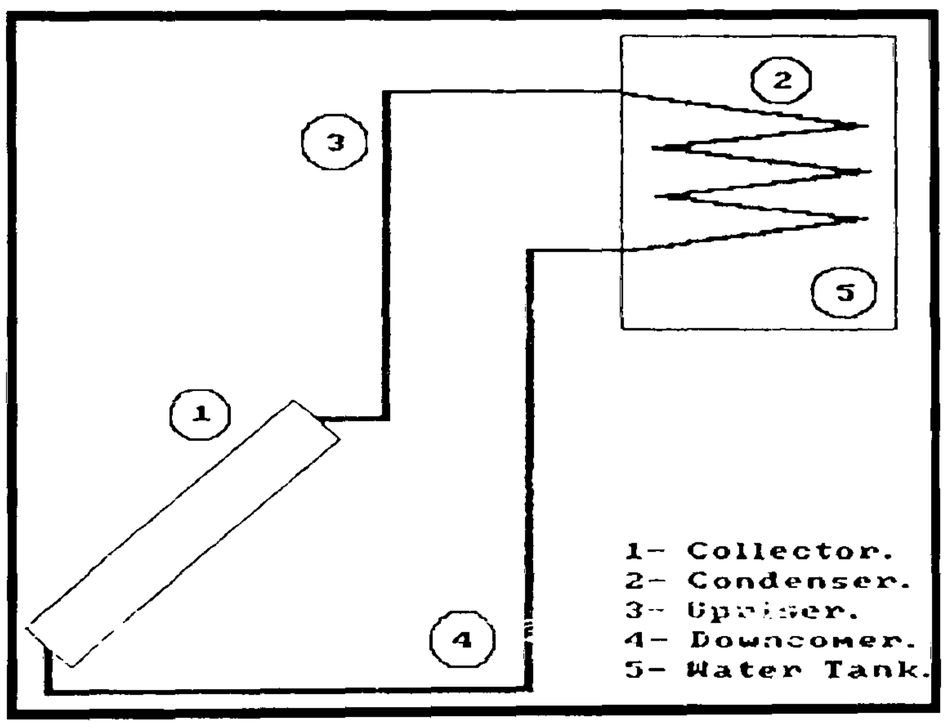

Figure 2.64 The two phase thermosyphon system (Joudi, 1997)

2.6.6 PV/T Systems incorporating Heat Pipes

Cooling of photovoltaic cells is one of the main concerns when designing concentrating photovoltaic systems. Cells may experience both short-term (efficiency loss) and long-term (irreversible damage) degradation due to excess temperatures. Design considerations for cooling systems include low and uniform cell temperatures, system

reliability, sufficient capacity for dealing with 'worst case scenarios', and minimal power consumption by the system.

The heat pipe approach was explored by Feldman et al. (1981) on a concentration ratio of about 24 suns. The evaporative working fluid was benzene with a maximum evaporator surface temperature of about 140 °C. The model showed that the heat transfer in this system is highly dependent on the condenser surface area. The prototype had an evaporator area of $0.61m^2$ and a condenser area of $2.14m^2$.

Akbarzadeh and Wadowski (1996) reported on a linear, trough-like system which also used heat pipes for cooling. In this case, the reflector is not a parabola, but an 'ideal reflector' which is said to give a uniform illumination across the cells. Each cell is mounted vertically on the end of a thermosyphon, which is made of a flattened copper pipe with a finned condenser area. The system was designed for 20 suns concentration, and the cell temperature reported not to rise above 46 °C on a sunny day, as opposed to 84 °C in the same conditions but without fluid in the cooling system.

Russell (1982) has patented a heat pipe cooling system. His design uses linear Fresnel lenses, each focusing the light onto a string of cells mounted along the length of a heat pipe of circular cross-section (*Figure 2.65*). Several pipes were mounted next to each other to form a panel. The heat pipe had an internal wick that pulled the liquid up to the heated surface. Thermal energy was extracted from the heat pipe by an internal coolant circuit, where inlet and outlet is on the same pipe end, ensuring a uniform temperature along the pipe. The coolant water was fed and extracted by common distribution pipes.

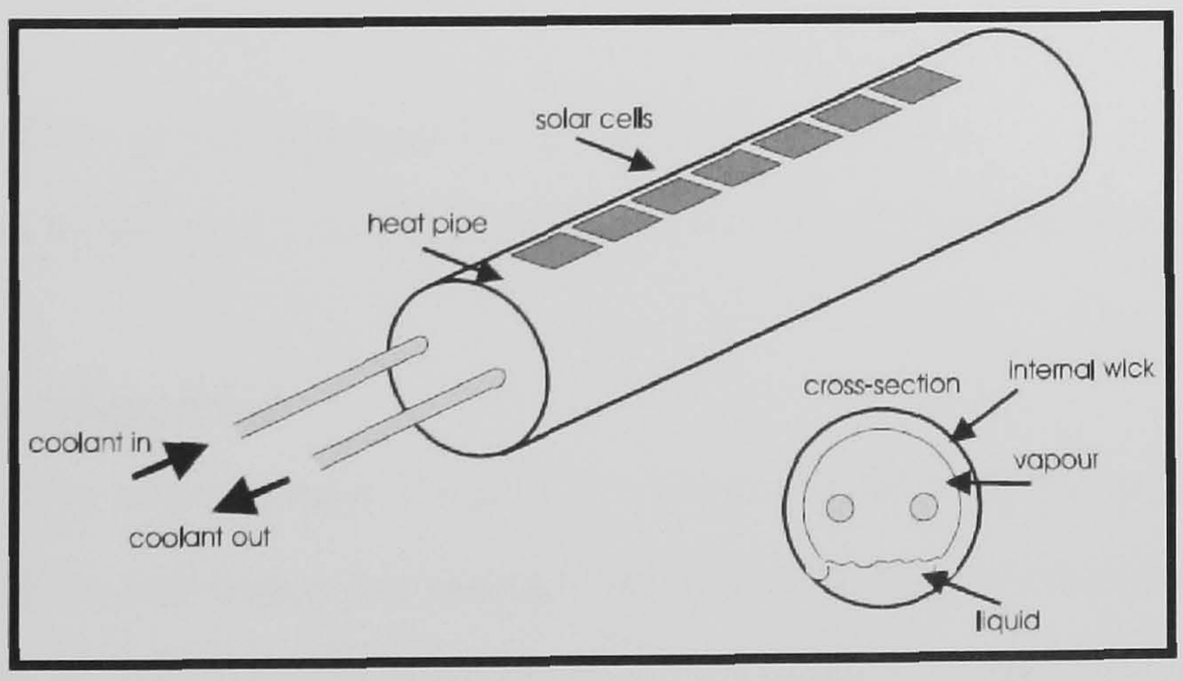

Figure 2.65 PV/T Heat pipe based cooling system as suggested by Russell (1982).

2.6.7 Discussion

Heat pipes are high heat transfer devices that have been used in various applications so far as in solar collectors. The review identified some important parameters that should be taken into consideration when designing an application.

The following need to be considered when designing heat pipes:

1) Heat transport limitation of the heat pipe

The most important heat pipe design consideration is the amount of power the heat pipe is capable of transferring. Heat pipes can be designed to carry a few watts or several kilowatts, depending on the application. However if driven beyond its capacity the effective thermal conductivity of the heat pipe can be significantly reduced. Therefore, it is important to assure that the heat pipe is designed to safely transport the required heat load.

2) Wick structure of the heat pipe

The performance of the heat pipe that containes a wick was more significant in terms of overall heat transfer coefficient than that with no wick.

3) Length and diameter of the heat pipe

Larger cross sectional areas of the heat pipe (i.e. larger diameter of the heat pipe) allow higher vapor volume to be transported from the evaporator to the condenser. Longer heat pipe transports less heat than shorter heat pipes.

4) Heat pipe orientation

The inclination angle of the heat pipe affects the performance of the system. The review informed that the maximum heat transport is achieved between the 50 and 80 angle degrees.

5) Effect of bending and flattening of the heat pipe

Any flattening or bending to a heat pipe reduces the amount of heat that can be transported.

6) Working fluid

A high latent heat or vaporization is essential to transfer large amounts of heat with minimum fluid flow, and hence to maintain low pressure drops within the heat pipe. The thermal conductivity of the working fluid should preferably be high in order to minimize the radial temperature gradient and to reduce the possibility of nucleate boiling at the

wick or wall surface. Choosing fluids with low values of vapour and liquid viscosities will minimize the resistance to fluid flow.

7) Heat pipe reliability

Two manufacturing factors reduce the reliability of the heat pipe: the seal of the pipe and the cleanness of pipe internal chamber. Any leakage in the heat pipe will eventually fail the pipe and if the internal chamber is not thoroughly clean then will face poor performance.

Another important aspect of heat pipes working under gravity with the condenser above the evaporator do not need any external power or capillary structure for return of the heat transfer fluid to the evaporator. Also a thermal diode benefit exists when the collector temperature is less than storage water temperature.

When designing a system careful consideration should be given to the heat transfer surface of the condenser section of the wickless heat pipe. An effective way to improve the instantaneous efficiency of wickless heat pipe flat plate solar water heaters is achieved when the surface of the condenser increases. Also as the evaporator temperatures and area increase with the evaporator length, the heat losses are also increased thus the lowest thermal resistances were achieved for the shortest evaporators. So far heat pipes have been used for cooling of photovoltaic cells when desining concentrating systems. To incorporate heat pipes in the rear of a flat plate PV can achieve cooling and transfer the extracted heat quickly without having many losses.

2.7 Phase Change Material (PCM)

Energy storage plays an important role in conserving available energy and improving its utilization, since many energy sources are intermittent in nature. Short term storage of only a few hours is essential in most applications; however, long term storage of a few months may be required in some applications.

Solar energy is available only during the day, and hence, its application requires efficient thermal energy storage so that the excess heat collected during sunshine hours may be stored for later use during the night. Similar problems arise in heat recovery systems where the waste heat availability and utilization periods are different, requiring some thermal energy storage. Hence, the successful application of load shifting solar energy depends to a large extent on the method of energy storage used.

The most commonly used method of thermal energy storage is the sensible heat method. The most common method of storing solar thermal energy as sensible heat is water. As well as being abundant, cheap, non-toxic etc., water has a high heat capacity, and can be used both as energy storage and transport medium in the system. The amount of stored energy Q is given by the temperature difference between final and initial states, the specific heat capacity C_p, and mass, m:

$$Q = m*Cp*(Tout - Tin) \qquad \text{Eq. (2.7.1)}$$

Water has a specific heat capacity of about 4.2 kJ/kg K, thus a 10 °C temperature difference in 1 m^3 water represents 42 MJ, or 11.7 kWh stored energy.

The latent heat method of storage has attracted a large number of applications. This method of heat energy storage provides much higher energy storage density with a smaller temperature range when compared with the sensible heat storage method. However, practical difficulties usually arise in applying the latent heat method due to the low thermal conductivity, density change, and stability of properties under extended cycling and sometimes phase segregation and sub cooling of the phase change materials. The following section provides an overview of PCMs, indicating the most suitable class of PCM for use with PVs and solar collectors, and providing the thermodynamics of phase change. This section also presents some of the physical characteristics of PCM

that had to be understood and some of the problems that would be faced when developing and choosing the PCM for use with the system.

2.7.1 Latent heat of fusion

As has been known for more than 200 years, heat must be added to a crystalline solid at its melting point to transform it into a liquid (Chalmers, 1964). The added energy breaks up the bonds between the atoms or molecules in the ordered crystal structure, thereby raising their potential energy while the temperature remains constant during the process. The energy that must be added in the phase transition from solid to liquid is called the *latent heat of fusion* and when the substance recrystallizes upon subsequent cooling, this heat is recovered, again at the temperature of equilibrium between the solid and liquid phase. The amount of latent heat associated with a phase transition can be substantial. For example, the latent heat of fusion in the ice/water transition at 0 ºC (334 kJ/kg) corresponds to a temperature increase of about 80 ºC in liquid water.

The relatively large amount of latent heat associated with the phase transition gives a higher energy storage density compared to the traditional sensible heat storage systems, and therefore allows a reduction of volume and mass. Another advantage is the isothermal behaviour during melting/freezing which reduces the temperature range of operation. Typically the PCM is encapsulated in suitable containers, and used in storage tanks in combination with water as heat transfer fluid.

2.7.2 Classification of PCM

In 1983 Abhat (1983) gave a useful classification of the substances used for TES (thermal energy storage), as shown in *Figure 2.66*. Among the most thorough references related with phase change materials, one can cite Abhat (1983), Lane (1983, 1986) and Dincer and Rosen (2002). These contain a complete review of the types of material which have been used, their classification, characteristics, advantages and disadvantages and the various experimental techniques used to determine the behaviour of these materials in melting and solidification.

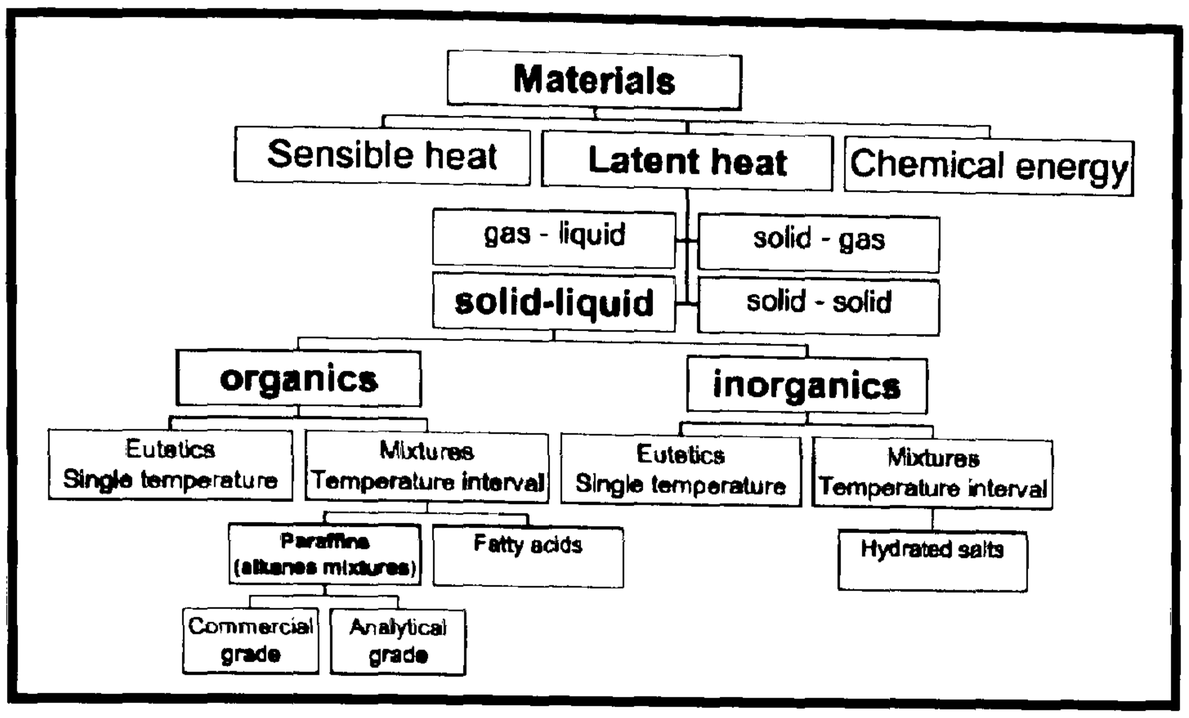

Figure 2.66 Classification of energy storage materials (Abhat, 1983).

PCMs are categorized as Organic, Inorganic and Eutectic materials.

2.7.2.1 Organic PCM

Organic compounds comprise of paraffin and non-paraffin. Paraffin is a substance that has a waxy consistency at room temperature. They contain a major component called alkanes characterised by C_nH_{2n+2}; the n-alkane content in paraffin waxes usually exceeds 75% and may reach 100%. Another primary component of paraffin waxes is straight-chain hydrocarbons with only a small amount of branching, such as 2-methyl groups near the end of the chain. Pure paraffin consists of only alkanes, for instance, paraffin octadecane, $C_{18}H_{38}$. The melting point of alkanes increases as the number of carbon increases. Paraffin waxes are chemically stable and non-corrosive, exhibit little or no super cooling properties (that is, they do not need to be cooled below their freezing point to initiate crystallisation), are compatible with most building materials (*Table 2.8*), have a high latent heat per unit weight and are recyclable. Their disadvantages are low thermal conductivity, high changes in volume during phase change and flammability.

Non paraffin involves a wide variety of organic materials for instance fatty acids, esters, alcohols and glycols. A study by Hasnain (1998) shows that fatty acids have melting points suitable for heating applications and they exhibit excellent melting and freezing

cycles without any supercooling. Their major drawback however is their cost which is about three times greater than that of paraffin.

Table 2.8 Organic Substances with potential use as PCM (Veer Tyagi, 2005)

Organic substances with potential use as PCM		
Compound	Melting point (°C)	Heat of fusion (kJ kg)
Butyl stearate	19	140
Paraffin C_{16} C_{18}	20–22	152
Capric–Lauric acid	21	143
Dimethyl sabacate	21	120
Polyglycol E 600	22	127.2
Paraffin C_{13} C_{24}	22–24	189
(34% Mistiric acid + 66% Capric acid)	24	147.7
1-Dodecanol	26	200
Paraffin C_{18} (45–55%)	28	244
Vinyl stearate	27–29	122
Capric acid	32	152.7

2.7.2.2 Inorganic PCM

Inorganic compounds such as salt hydrates (salts, metals and alloys) have much higher latent heat per unit volume, higher thermal conductivity, are non-flammable and lower in cost in comparison to organic compounds (*Table 2.9*). Potentially, they can be recycled after their useful life. However, they are corrosive to most metals and suffer from decomposition and super cooling, which can affect their phase change properties. Nucleating and thickening agents can be added to inorganic PCMs to minimise super cooling and decomposition.

Table 2.9 Inorganic substances with potential use as PCM (Veer Tyagi 2005)

Inorganic substances with potential use as PCM		
Compound	Melting point (°C)	Heat of fusion (kJ/kg)
$KF \cdot 4H_2O$	18.5	231
$Mn(No_3)_2 \cdot 6H_2O$	25.8	125.9
$CaCl_2 \cdot 6H_2O$	29	190.8
$LiNO_3 \cdot 3H_2O$	30	296
$Na_2SO_4 \cdot 10H_2O$	32	251

2.7.2.3 Eutectic PCM

An eutectic is a minimum-melting composition of two or more components, each of which melts and freeze congruently forming a mixture of the component crystals during

crystallization (*Table 2.10*). Some candidate materials having acceptable values of fusion are pentaerythiol, pentaglycerine, neopentyl glycol. These eutectics can be used for cool and passive solar storage with low or medium temperature flat plate collectors, according to their melting point.

Table 2.10 Eutectics with potential use as PCM (Veer Tyagi, 2005)

Inorganic eutectics with potential use as PCM		
Compound	Melting temperature (°C)	Heat of fusion (kJ/kg)
66.6% $CaCl_2 \cdot 6H_2O$ + 33.3% $Mgcl_2 \cdot 6H_2O$	25	127
48% $CaCl_2$ + 4.3% NaCl + 0.4% KCl + 47.3% H_2O	26.8	188
47% $Ca(NO_3)_2 \cdot 4H_2O$ + 53% $Mg(NO_3)_2 \cdot 6H_2O$	30	136
60% $Na(CH_3COO) \cdot 3H_2O$ + 40% $CO(NH_2)_2$	30	200.5

A comparison of the advantages and disadvantages of organic and inorganic materials is shown in *Table 2.11*.

Table 2.11 Comparison of Organic and Inorganic Materials Advantages and Disadvantages

Comparison of organic and inorganic materials for heat storage	
Organics	Inorganics
Advantages	Advantages
No corrosives	Greater phase change enthalpy
Low or none undercooling	
Chemical and thermal stability	
Disadvantages	Disadvantages
Lower phase change enthalpy	Undercooling
Low thermal conductivity	Corrosion
Inflammability	Phase separation
	Phase segregation, lack of thermal stability

Typical data of some relevant properties of thermal storage materials are given in *Table 2.12* for comparison (Hasnain, 1998). The masses and volumes in the table correspond to a heat storage capacity of 1000 MJ and a temperature rise of 15°C during heat storage.

The relative mass and volume occupied by each storage media is based on ice. The table shows that in comparison to other thermal storage materials such as rock or water, PCMs have a higher energy storage density, so that less material is needed. PCMs also

have the advantage that thermal energy is stored and released at an almost constant temperature.

Table 2.12 Comparison of various thermal storage media. Stored energy = 1,000 MJ or 278 kWh, change in temperature = 15°C. Relative mass and volume are based on ice. (Bruno, 2004)

Material	Mass (Kg)	Relative Mass	Volume (m^3)	Relative Volume
Rock	67,000	22	30	10
Water (liquid)	16,000	5.3	16	5.3
PCM (organic)	5,300	1.8	6.6	2.2
PCM (inorganic)	4,350	1.5	2.7	0.9
Ice	3,000	1.0	3	1.0

2.7.3 Desirable Properties of PCM

The PCM to be used in the design of thermal storage system should have desirable thermo physical, kinetic and chemical properties, which are recommended as follows: (Sharma 1999).

Thermo physical properties

(i) Melting temperature in the desired operating temperature range.

(ii) High latent heat of fusion per unit volume so that the required volume of the container to store a given amount of energy is less.

(iii) High specific heat to provide additional significant sensible heat storage.

(iv) High thermal conductivity of both solid and liquid phases to assist the charging and discharging energy of the storage system.

(v) Small volume change on phase transformation and small vapour pressure at operating temperature to reduce the containment problem.

(vi) Congruent melting of the phase change material for a constant storage capacity of the material with each freezing/melting cycle.

Kinetic properties

(i) High nucleation rate to avoid super cooling of the liquid phase.

(ii) High rate of crystal growth, so that the system can meet demand of heat recovery from the storage system.

Chemical properties

(i) Complete reversible freeze/melt cycle.

(ii) No degradation after a large number of freeze/melt cycles.

(iii) No corrosiveness to the construction materials.

(iv) Non-toxic, non-flammable and non-explosive material for safety.

2.7.3.1 Thermo physical properties determination

Analysis techniques used to study phase change are mainly conventional calorimetry, differential scanning calorimetry (DSC) and differential thermal analysis (DTA). Speyer (1994) gave a good overview of the thermal analysis methods in general, but also Eckert et al. (1994) should be mentioned. Naumann and Emons (1989) and Inaba (1997) focussed their studies on thermal analysis methods for PCMs. Among studies relating to DSC, it is worth citing Flaherty (1971) for characterisation of hydrocarbons and natural waxes, Giavarini (1973) for characterisation of petroleum products and Salyer (1986) for characterisation of paraffins. As is mentioned in Gibbs (1995), there is considerable uncertainty about the property values provided by manufacturers and it is therefore advisable to use DSC to obtain more accurate values.

Yinping (1999) reviewed the above-mentioned conventional methods of PCM property analysis and points out their limitations, of which the following stand out:

(a) Small quantities of sample are analysed (1–10 mg), although some behaviour of the PCM depends on their quantity.

(b) The analysis instrumentation is complex and expensive.

(c) Phase change cannot be visually observed.

Yinping proposes a simple method for determining phase change temperature, under cooling, enthalpy, specific heat, and thermal conductivity in solid and liquid phases. Temperature–time graphs are drawn and properties evaluated for comparison with the graphs of the other known materials are used (usually pure water) as reference.

Marn et al developed a further evaluation procedure to determine specific heat and enthalpy as temperature dependent values. The results obtained are presented in the form of enthalpy–temperature curves, and an experimental improvement is proposed.

2.7.3.2 Stability of the PCM-container system

A relevant aspect is the useful life of these systems, and the number of cycles they can withstand without any degrading of their properties. Insufficient long term stability of the storage materials is mainly due to poor stability of the materials' properties and corrosion between the PCM and container (Zalba, 2003). Abhat (1982) observed that laboratory measurements comprising at least 1,000 – 2,000 cycles are recommended to establish the long term stability of the PCM. Other authors, such as Gibbs (1995), also confirm that neither the cycles nor contact with metals degrade the thermal behaviour of paraffin and that they therefore have excellent thermal stability.

2.7.3.3 Corrosion of the materials

A compatibility of PCMs with conventional materials for construction is particularly important for an assurance of a life of a latent heat storage system. Studies of PCMs including organics, inorganics salt hydrates and inorganics eutectic compounds for corrosion tests with storage containment have been carried out by Heine (1981) and Schroder (1980). Results show that the most compatible materials with metal containers (i.e., stainless steel, mild steel, copper, tin plated mild steel etc.) are organic materials. Porisini (1988) tested the corrosion of four commercially available salt hydrates used as PCM with stainless steel, carbon steel and the results showed that the most corrosion-resistant alloy to all the hydrated salts is stainless steel. Recently, Cabeza et al. (2001) studied corrosion resistance of five common metals (aluminium, brass, copper, steel and stainless steel) in contact with molten salt hydrates in an immersion corrosion test. From the above investigations it can be concluded that stainless steel is the only metal that is compatible with all phase change materials. Copper is compatible with all heat storage materials, except sodium thiosulphate 5-hydrate. Aluminium is incompatible with the salt hydrates. Furthermore common plastics are stated to be generally corrosion resistant to most inorganic salt hydrates and their eutectic compounds.

2.7.3.4 Encapsulation of the materials

The encapsulation of the PCM has developed interest in several researchers. Advantages and disadvantages of different geometries of PCM encapsulation with different materials and their compatibility was discussed by Lane (1986). The freezing and melting processes of water contained in spherical elements were studied experimentally by Eames et al. (2002). He proposed semi empirical equations that allow the mass of ice within a sphere to be predicted at any time during the freezing or melting processes.
For the use of PCM in buildings applications, an encapsulation of PCM (50–80%) with unsaturated polyester matrix (45–10%), and water (5–10%) was studied by Morikama et al. (1985). Polymerisation of PCMs has been also studied for other applications, like insulation materials for use in clothing or bedding articles (Salyer, 1999). In the same area, Inaba (1997) and Lee and Choi (1998) proposed using the storage substance integrated with the building materials without encapsulation (''Shape-stabilised paraffin'': 74% paraffinþ26% high-density polyethylene (HDPE)). Structural stability is achieved using HDPE which retains the paraffin when in liquid phase.
For many applications, PCMs are microencapsulated, and this has been studied by several researchers (Brown, 1998) and developed by companies like BASF (Jahns, 1999). Nevertheless, the potential use of microencapsulated PCMs in various thermal control applications is limited to some extent by their cost.

2.7.3.5 Nucleation and Supercooling

Nucleating and crystal growth are characteristic terms that refer to conduction heat transfer and the formation of solid mass as it liberates heat. During heat gain, where melting occurs, nucleation does not exist because convective heat transfer enhances the process.
During the solidification process of a PCM, nuclei must from and grow for the crystallization to continue. There are many PCMs which have the disadvantage of the tendency to supercool upon liberation of heat. This characteristic is quite apparent in PCMs such as salt-hydrates compounds, where the temperature drops below their transition temperatures, as it leads subsequently to the delayed development of the crystallisation process (see *Figure 2.67*) (Burns, 1981).

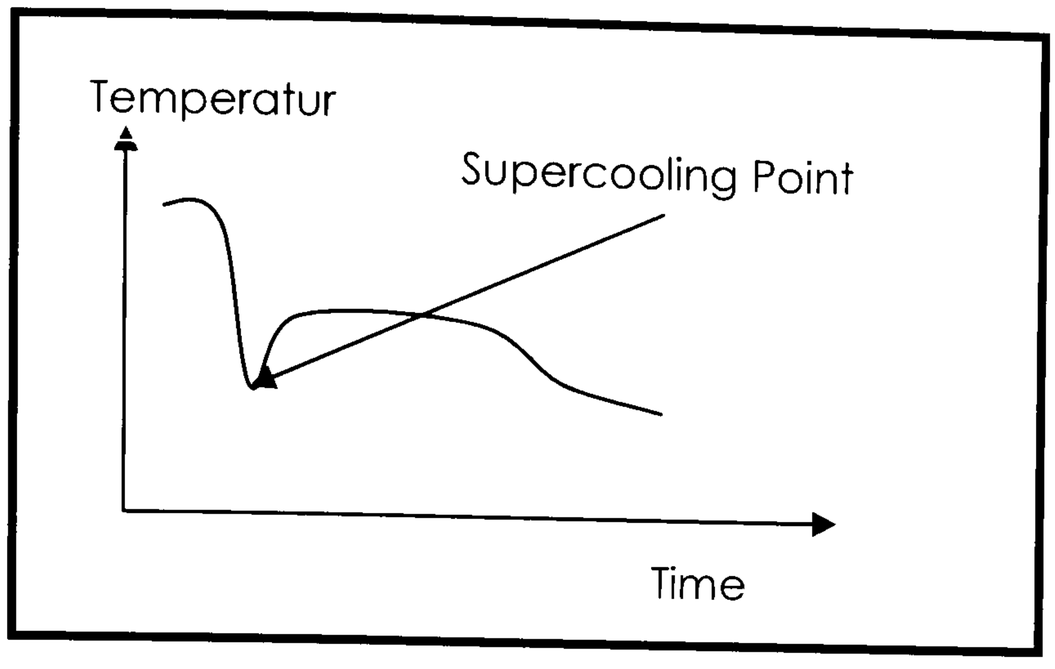

Figure 2.67 Supercooling of a phase change material (Burns, 1981)

Since solidification involves nucleation, numerous nucleating additives have been investigated in order to reduce supercooling. A nucleating agent is a material having a crystal structure similar in lattice spacing to that of the phase change substance. They serve as nuclei for the PCM crystals to grow on them during freezing of the PCM and are also termed as seed-crystals (Abhat, 1982). Ryu (1992) studied various inorganic salt-hydrates as a latent heat storage medium. He found that for thickened Glauber's salt, Borax could reduce supercooling of the salt from 15 °C to 3-4 °C. Biswas (1977) has suggested the use of the extra water principle to prevent formation of the heavy anhydrous salt. Although this makes the system stable with cycling, it reduces the storage density and requires the system to be operated with a large temperature swing.

2.7.3.6 Stratification and Agglomeration

Stratification is usually associated with phase separation after it cycles through the phase change process a number of times. This phenomenon limits the usefulness of the PCM. For example Glauber's salt has an incongruent melting point, and as its temperature increases beyond the melting point it separates into a liquid phase and a solid. Since the density of the solid is higher than the density of the solution, phase separation occurs. As a consequence, the salt settles to the bottom of the tank. With complete stratification, the storage capacity of the PCM decreases about 40% (Hariri, 1988). To overcome the problem, the addition of suspension media or thickening agents to the PCM could be used to prevent separation. Thickening agents however displace a

part of the PCM in the heat store, thus reducing the volumetric heat capacity of the store (Abhat, 1982).

2.7.3.7 Storage capacity

To understand the storage capacity of a PCM we can see *Figure 2.68* showing the enthalpy (energy stored per unit mass) as a function of temperature for a pure substance (solid line). During a charging process, the state of the system moves from left to right along the curve, with increasing enthalpy and temperature. Initially the temperature of the PCM increases with added energy which is stored as sensible heat in the solid phase material. The heat of fusion is absorbed as the substance undergoes a phase transition from solid (s) to liquid (l) at the constant melting point temperature (T_m), and when the melting process is complete, further energy input again results in a temperature increase (sensible heat in liquid phase). The solid and liquid phase heat capacities are given by the slope of the s and l lines respectively. For impure or incongruently melting substances, the temperature during the phase transition is not well defined as indicated by the dashed line.

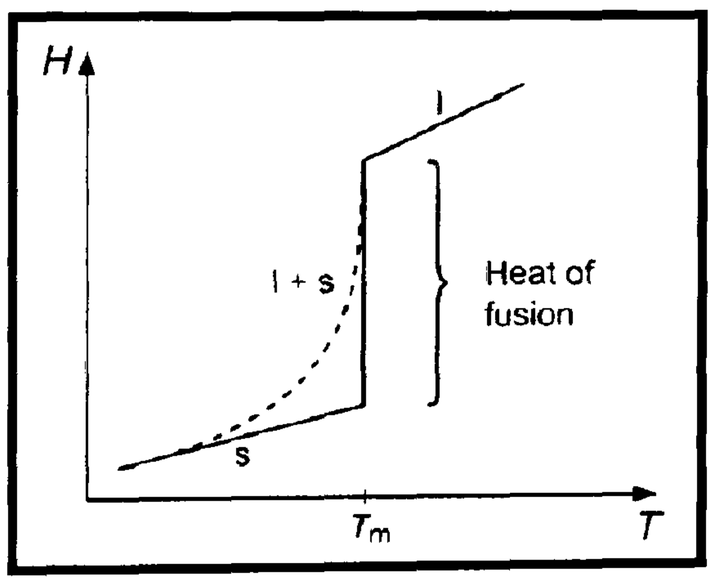

Figure 2.68 Stored enthalpy H (J/kg) as a function of temperature T for a material undergoing a phase transition at the melting point T_m. (Sandnes, 2003)

The charge/discharge cycle must necessarily span a range of temperatures to facilitate heat transfer to/from the PCM units. The stored energy will therefore usually be a combination of latent heat and solid and liquid sensible heat as the store is charged from an initial temperature T_i, to a final temperature T_f:

$$Q = mc_{p,s}(T_m - T_i) + mL + mc_{p,l}(T_f - T_m).$$ Eq. (2.7.2)

where L is the heat of fusion for the material. The heat of fusion for different salt hydrates that are potential PCMs ranges from 100 – 280 kJ/kg (Zalba et al., 2003). The obtainable enthalpy density in a real application will be somewhat lower than suggested by the measured thermo physical properties since bulk materials are less pure, the encapsulation adds mass and volume, as does air pockets in the containers that buffers volume expansion upon melting. Additives to reduce super cooling (nucleating agents) and thickening agents to limit phase segregation also reduces the enthalpy density of the PCM product. The increased energy storage density of a PCM/water store compared to sensible heat storage allows a size reduction of the store which may be beneficial in cases where cost related to space area is high or a large store unit is impractical.

As an alternative to size reduction, one can consider the possibility of reducing the temperature range of operation for the system. *Figure 2.69* shows a schematic drawing of enthalpy as a function of temperature comparing a store including PCM to a sensible heat water store. The graph illustrates that the same amount of energy can be stored over a narrower temperature range when PCM is included. Another important advantage of using PCM in a solar heating system is that the store/system temperature does not increase at the same rate as in a water store. The solar collectors can therefore operate at lower temperatures for an extended period of time, thus increasing the total amount of solar energy collected by the system.

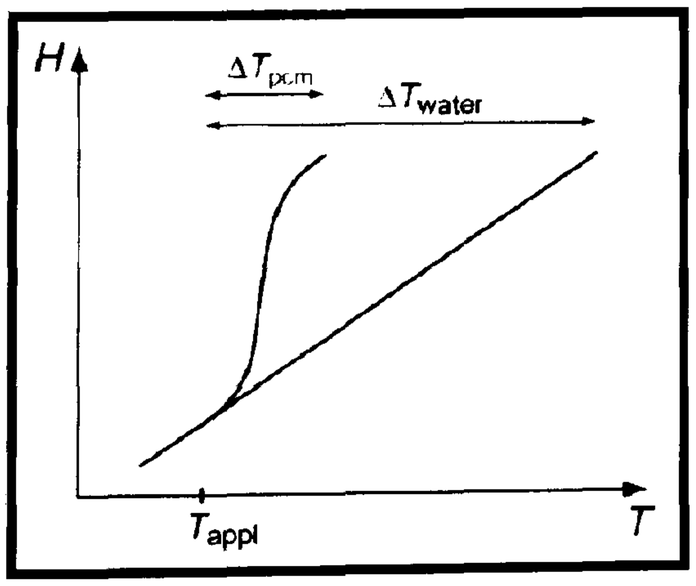

Figure 2.69 PCM storage allows a narrower temperature range for the system centred on the desired application temperature. (Sandnes, 2003)

2.7.3.7 Charge and discharge

The rates of energy absorption and release by the PCM units must be sufficiently high to meet the power requirements during charge and discharge respectively. The rate of heat transfer depends on both the temperature difference between PCM and heat carrier, and the sum of the heat transfer resistances at the encapsulation/water interface (convective), through the encapsulation material (conductive) and internally within the PCM (conductive and convective).

A certain degree of exergy loss is inherent in the PCM system since the containers act as heat exchangers (*Figure 2.70*). The PCM heat absorption/release is driven by the temperature difference between the PCM and the heat transfer medium during the charge/discharge process. This results in a temperature degradation since the stored energy is retrieved at a lower temperature than at which it was delivered.

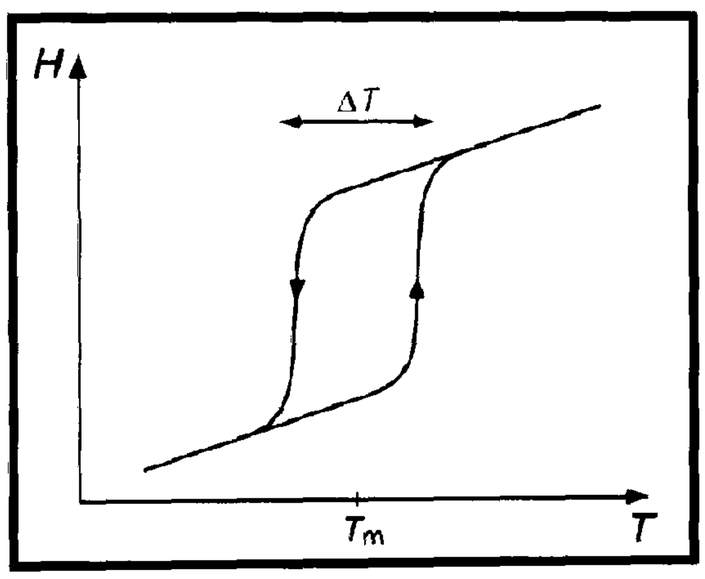

Figure 2.70 The limitations on heat transfer between PCM units and heat carrier during charge and discharge results in temperature degradation and exergy loss. (Sandnes, 2003)

2.7.4 Commercially produced PCM and products

By 1990, only about 12 companies, mainly in the USA, were engaged in the manufacture of heat storage products. Manufactured heat storage modules in the form of polyethylene tubes and polyolefin balls used calcium chloride hexahydrate, sodium sulphate decahydrate, paraffin etc., as PCM.

At present, the main supply companies in the market of phase change heat and cold storage materials include Cristopia (France), TEAP Energy (Australia), Rubitherm

GmbH (Germany), EPS Ltd. (UK), PCM Thermal Solutions (USA), Climator (Sweden) and Mitsubishi Chemical (Japan).

Due to a phase change in the process of exploitation, PCMs are usually encapsulated in various containers. The investigations of chemical compatibility of low-temperature PCMs and design structure materials have shown that stainless steel, polypropylene, and polyolefin can be used in most cases as suitable container materials. In *Table 2.13* we can see PCMs at melting temperature from 22 – 31 °C.

Table 2.13 Commercial PCM Products (Veer Tyagi, 2005)

Commercial PCMs available in the International market				
PCM name	Type of product	Melting point (°C)	Heat of fusion (kJ/kg)	Source
RT 20	Paraffin	22	172	Rubitherm GmBH
Climsel C23	Salt hydrate	23	148	Climator
ClimselC24	Salt hydrate	24	216	Climator
RT 26	Paraffin	25	131	Rubitherm GmBH
RT 25	Paraffin	26	232	Rubitherm GmBH
STL 27	Salt hydrate	27	213	Mitsubishi chemical
S27	Salt hydrate	27	207	Cristopia
RT 30	Paraffin	28	206	Rubitherm GmBH
RT 27	Paraffin	28	179	Rubitherm GmBH
TH 29	Salt hydrate	29	188	TEAP
Climsel C32	Salt hydrate	32	212	Climator
RT32	Paraffin	31	130	Rubitherm GmBH

2.7.5 PCM Heat Transfer Enhancement Techniques

A common problem in latent heat thermal storages is the poor conductivity of the phase change materials. The crystallising and thickening agents which prevent super cooling and phase separation in the PCM lower the thermal conductivity of the PCM and the inhibiting convection motion in the liquid PCM (Padmanabhan 1986, Velraj 1999). During the phase change the solid–liquid interface moves away from the heat transfer surface. Thus, the surface heat flux decreases due to the increasing thermal resistance of the growing layer of molten or solidified PCM. The problem arises especially in solidification processes where the sole heat transfer mode is conduction. PCM melts more quickly than it solidifies because natural convection speeds up the melting of PCM. PCM solidifies on the heat transfer surface and acts as a self-insulator because of low heat conductivity. In practice some kind of heat transfer enhancement technique has

to be used in LHTS because of the low heat conductivity of the PCM. Heat transfer in LTHS can be enhanced by the following techniques:

(a) Active methods such as agitators/vibrators, scrapers and slurries (Lane, 1983).

(b) Using microencapsulated PCM (www.frisby.com, 2007).

(c) Using PCM containing dispersed high conductivity particles or lessing rings (Siegel 1977).

(d) Using PCM graphite composite material (Mehling, 2000).

(e) Using extended surfaces such as fins and honeycombs (Stritih 2000, Humphries 1977).

2.7.5.1 Heat transfer enhancement

The use of finned tubes with different configurations has been proposed by various researchers such as Abhat et al. (1981), Morcos et al. (1990), Sadasuke (1991), Costa et al. (1998), Padmanabhan (1986), Velraj (1999) and Ismail et al. (2001) use finned tubes in thermal storage systems.

Several other heat transfer enhancement techniques have been reported. Siegel (1977) studied the improvement in solidification rate in molten salt dispersed with high conductivity particles. Another method used is to embed the PCM in a metal matrix structure (Kamimoto 1985, Hoogendoorn 1992, Khan 1994, Tong 1996). The use of thin aluminium plates filled with PCM was developed by Bauer and Wirtz (2000).

Mehling et al. (1999, 2000) and Py et al. (2001) proposed a graphite-compound-material, where the PCM is embedded inside a graphite matrix. The main advantage of such a material is the increase in heat conductivity in the PCM without much reduction in energy storage, but other advantages are the decrease in sub cooling of salt hydrates and the decrease of volume change in paraffins. The use of graphite as heat transfer enhancement material has also been studied by other researchers, such as Fukai et al. (2000, 2002). They developed brushes made of carbon fibres. The feature of this method is that the volume fraction of the fibres is accurately and easily controlled and that the fibres with low volume fraction are entirely dispersed in the PCM. Xiao et al. (2001) developed composite based on paraffin, styrene–butadiene–styrene triblock copolymer and exfoliated graphite. They claimed that in the composite paraffin undergoes solid–

liquid phase change, and there is no leakage of it even in the state of melting. The composite exhibits high thermal conductivity and nearly 80% of the latent heat of fusion per unit mass of the paraffin.

Velraj at al. (1997) have numerically and experimentally investigated solidification in a finned pipe. They determined the solidification time for pipes with different parameters and different fins. Stritih (2000) made parametrical identification of fins to heat enhancement in the rectangular heat storage and Yamaha (2002) made experiments to evaluate the effect of fins to heat transfer.

Al-Jandal (1992) studied experimentally what affects the fin; metal honeycomb and copper matrix structure have on the total melting and solidification time. The results showed that the average thermal conductivity enhancement factors for melting were in the order of 3.3 and for solidification in the order of 1.7 and natural convection had a significant effect on the acceleration of melting. Bugaje (1997) made experiments on the use of methods for enhancing the thermal response of paraffin wax heat storage tubes with the incorporation of aluminium fins and star structures. The conclusion was that internal fins performed much better than the star matrices reducing the loading time in the order of 2.2 and the cooling time in the order of 4.2.

Eftekhar et al. (1984) presented experimental data on the rate of the production of liquid as a function of time in a thermal storage system consisting of vertically arranged fins between heated and cooled surfaces. Natural convection was observed to play an important role in melting the phase change material.

It is evident that fins and different kind of matrix structures enhance the internal heat transfer of a phase change material. In practice some kinds of heat transfer enhancement techniques have to be used in LHTS. To achieve the best economical and technical benefit of the storage, the loading and unloading time should be optimised. The geometry of the latent heat storage plays a very important role.

In engineering there is often no opportunity for complicated numerical computations when a pre-design of a storage is made. A fast analytical model saves time and effort.

2.7.5.2 PCM based Heat Sink

Numerous engineering applications have made the topic of melting of phase-change material in enclosures one of the most active fields in heat transfer research today. Due to complexity of the problem, the majority of the existing work avoided analytical solutions and dealt with numerical and experimental ones. As a result, the analytical results have not been reported except for limited approximated solutions with simple boundary conditions.

Design of PCM-based heat sinks for electronics has been analyzed by Pal and Joshi (1997), who provide special recommendations concerning organic materials.

Hale and Viskanta (1980) performed an experimental and analytical study of melting and solidification of several PCMs, including n-octadecane, cooled or heated from above or below. It was found that when melting from below, the natural convection influences the heat transfer and the motion of the phase-change boundary during the process.

Ho and Viskanta (1984) studied melting of n-octadecane from an isothermal vertical wall of a rectangular cavity 130 mm high, 50 mm wide, and 50 mm deep. In order to accommodate the volume expansion associated with the phase-change process from solid to liquid, a small air gap was maintained between the top of the material and the insulated top surface of the cavity. It has been shown that the time-wise variation of the molten volume fraction, could be expressed as a function of the Stefan number, Ste, the Fourier number, Fo, and the Rayleigh number, Ra.

Gadgil and Gobin (1984) simulated numerically two dimensional melting of a solid phase-change material in a rectangular enclosure heated from one side. Of special interest was the influence of the enclosure aspect ratio, A, on the melting curve, since this can be relevant to optimizing the dimensions of latent heat storage elements. The results of Gadgil and Gobin (1984) show that A has a strong influence on the melting curve, e.g. an increase in A from 1.13 to 5.25 causing more than 16- fold decrease in the time required to melt 80% of the PCM. Zhang and Bejan (1989) have reported results of their study of the time-dependent melting within a relatively large enclosure 74 cm high (height/width ratio equals 5) filled with n-octadecane, subjected to a constant heat flux boundary condition. They show that for the heated plate itself, first its temperature raises

from the ambient level to the melting point of the phase-change material. Then, there is a period when the temperature of the plate is uniform and rises linearly in time. Finally, the wall temperature reaches a plateau in the convection melting regime. Pal and Joshi (2001) studied computationally and experimentally melting of ntriacontane in a side heated tall enclosure of aspect ratio 10, by a uniformly dissipating heat source. They show how buoyancy driven convection in the molten PCM starts to develop. An implicit enthalpy-porosity approach was utilized for computational modelling of the melting process, and showed good agreement with the experiments.

In the problems of phase change in an enclosure with one heated surface, like those discussed above, longitudinal heat conduction in the enclosure boundaries is commonly neglected. The longitudinal conduction is, however, important when conducting partitions are used, as shown by Eftekhar et al. (1984) and most recently by Casano and Piva (2003).

Hamdan and El-Werr (1996) predicted the evolution of the liquid–solid interface and the melted fraction using analytical solution, they assumed that the interface remains straight during the melting process and it was limited to isothermal heating of a rectangular enclosure (*see Figure 2.71*).

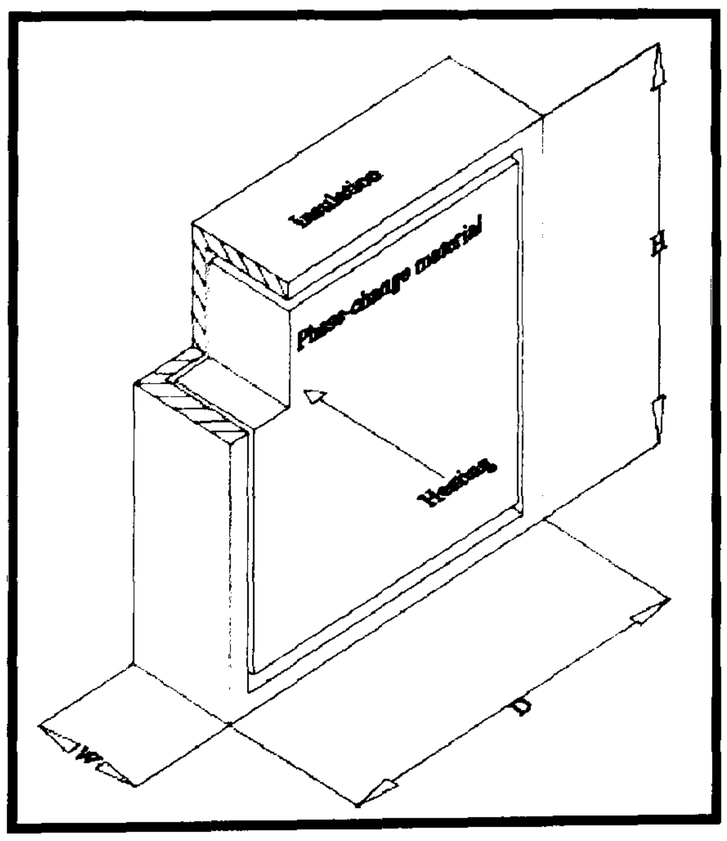

Figure 2.71 Schematic diagram of a rectangular enclosure with PCM (Hamdan, 2004)

Zivkovic (2001) presented a simple computational model for isothermal phase change of phase change material (PCM) encapsulated in a single container. The numerical analysis of the melting time for rectangular and cylindrical containers was then performed and the results showed that the rectangular container requires nearly half of the melting time as for the cylindrical container of the same volume and heat transfer area (see *Figure 2.72 and 2.73*).

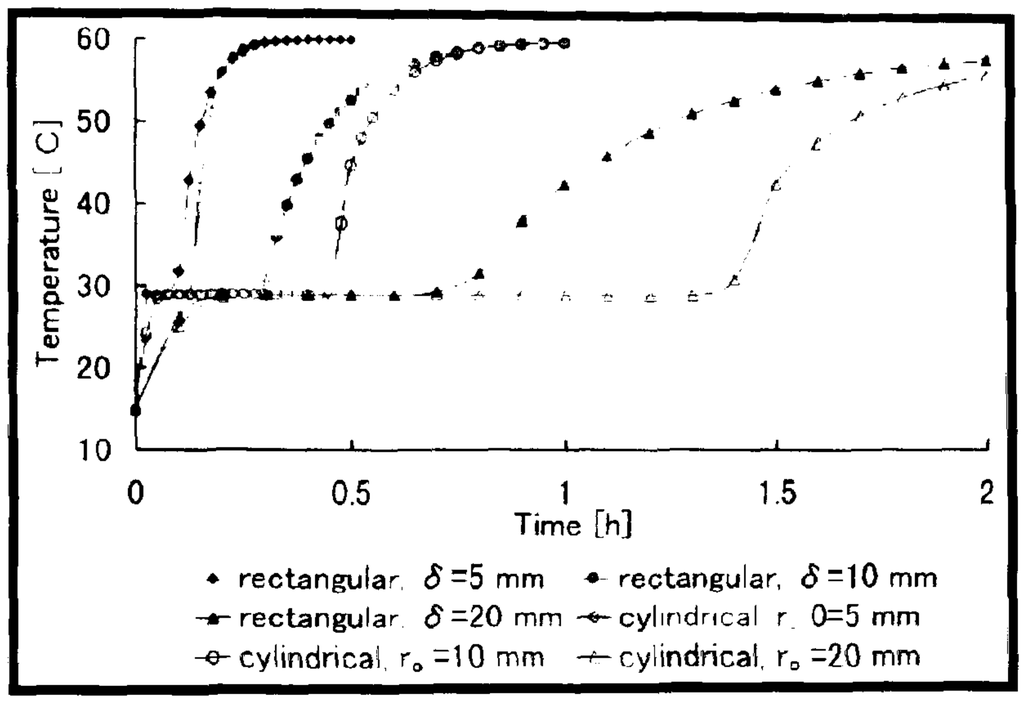

Figure 2.72 Comparison of the variation with time of the PCM's temperature at the centre of the rectangular and cylindrical containers. (Zivkovic, 2001)

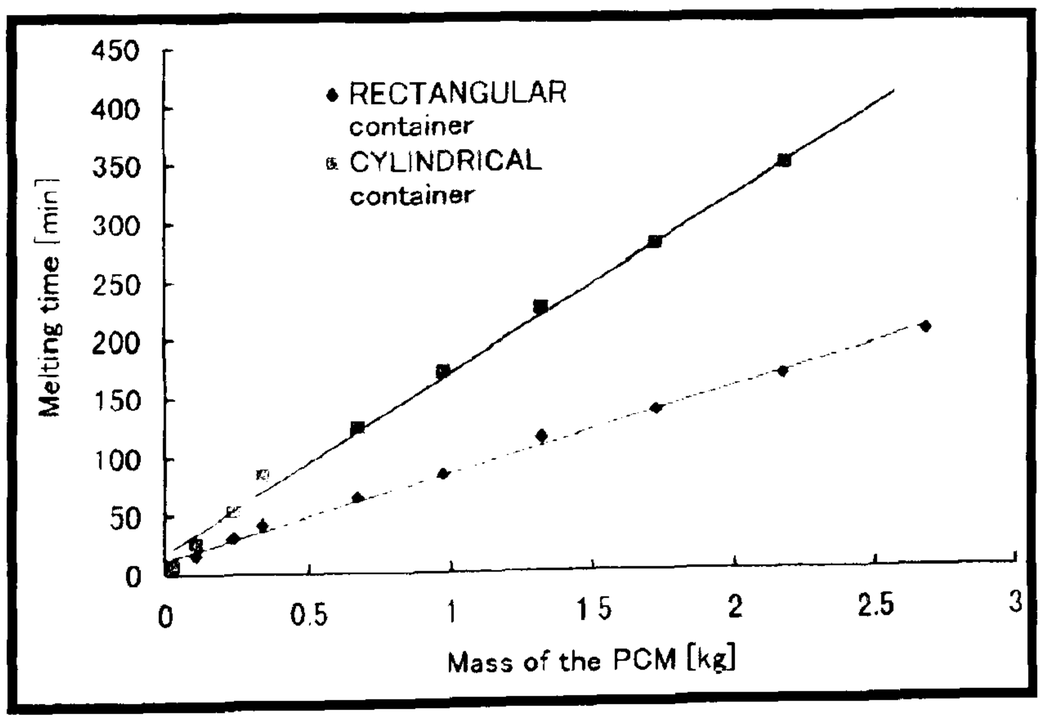

Figure 2.73 Comparison of the melting time for rectangular and cylindrical containers of equal volume and heat transfer area. (Zivkovic, 2001)

2.7.6 PCM use in Buildings

The application of PCMs in buildings can have two different goals. First by using natural heat that is solar energy for heating or night cold for cooling. Second by using man made heat or cold sources. In any case, storage of heat or cold is necessary to match availability and demand with respect to time and also with respect to power. Basically three different ways to use PCMs for heating and cooling of buildings are (see *Figure 2.74*):

(i) PCMs in building walls;

(ii) PCMs in other building components other than walls; and

(iii) PCMs in heat and cold storage units.

The first two are passive systems, where the heat or cold stored is automatically released when indoor or outdoor temperature rises or falls beyond the melting point. The third one is active system, where the stored heat or cold is in containment thermally separated from the building by insulation. Therefore, the heat or cold is used only on demand not automatically. Depending on where and how the PCM is integrated, PCMs with different melting points are applied. Currently, there is a lack of commercial PCMs in the lower temperature range that is between 5 and 25 °C. Especially between 15 and 20 °C available products show too low enthalpies. Most important PCMs are in the range of 22–25 °C, as almost everybody agrees that this is the range for building passive heating and cooling. Various possible latent heat thermal energy storage (LHTES) devices studied for space heating and cooling are as follows.

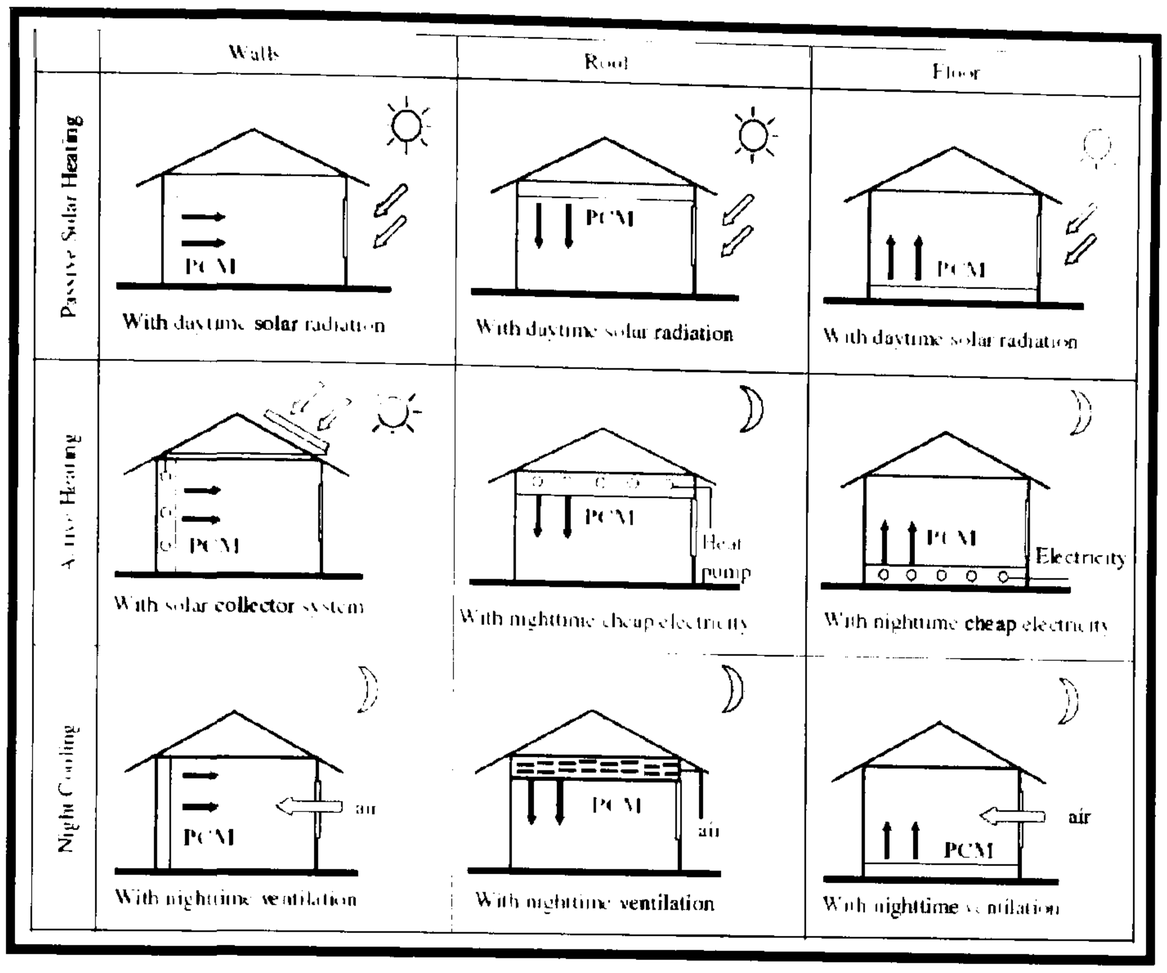

Figure 2.74 The forms and effects of PCM building envelope (revised from Macro's presentation, 2005).

In building applications, only PCMs that have a phase transition close to human comfort temperature (20 °C) can be used. From the many hydrated salts and organic PCMs investigated, those shown in *Table 2.14*, are possible candidates for applications in buildings.

Table 2.14 PCM useful for Building Applications. (Khudhair, 2004)

Hydrated salts and organic PCMs		
PCM	Melting point (°C)	Heat of fusion (kJ/kg)
$KF \cdot 4H_2O$ Potassium fluoride tetrahydrate	18.5–19	231
$CaCl_2 \cdot 6H_2O$ Calcium chloride hexahydrate	29.7	171
$CH_3(CH_2)_{16}COO(CH_2)_3CH_3$ Butyl stearate	18–23	140
$CH_3(CH_2)_{11}OH$ Dodecanol	17.5–23.3	188.8
$CH_3(CH_2)_{16}CH_3$ Tech. grade octadecane	22.5–26.2	205.1
$CH_3(CH_2)_{12}COOC_3H_7$ Propyl palmitate	16–19	186
45% $CH_3(CH_2)_8COOH$ 55% $CH_3(CH_2)_{10}COOH$ 45/55 Capric–lauric acid	17–21	143

2.7.7 Solar Collectors using PCM

Solar energy, an abundant, clean and safe source, is an attractive substitute for conventional fuels for passive and active heating applications. During the day, excess solar heat is collected for short or long term storage, and it is recovered at night in order to satisfy the heating needs of houses. Efficient and economical heat storage is the main factor in utilization of solar energy.

Solar thermal energy can be stored as sensible heat, latent heat, heat of reaction or a combination of these. In most storage systems, it is stored as sensible heat in materials such as water and rocks. In air collection systems, rock beds are normally used to store heat, while water tanks store the heat in liquid systems. In latent heat storage (LHS) systems, the latent heat arising from the phase change of a material is used for thermal energy storage. The phase change materials (PCMs) can store large amounts of heat (latent heat of fusion) in changing phase from solid to liquid. LHS systems using PCM, in general, provide much higher energy storage density than systems using sensible heat storage. The efficiency of seasonal storage as well as that of daily storage depends on system configurations, climate conditions and various set points for environmental control.

Solar air or water heaters can be used for many purposes, including crop drying, space heating and regenerating dehumidifying agents (*Figure 2.75*). Solar air heaters are classified according to their application and use (*Table 2.15*).

Table 2.15 Classifications of Solar Air Heaters (Tiwari, 1998)

Table 1. Classifications of solar air heaters

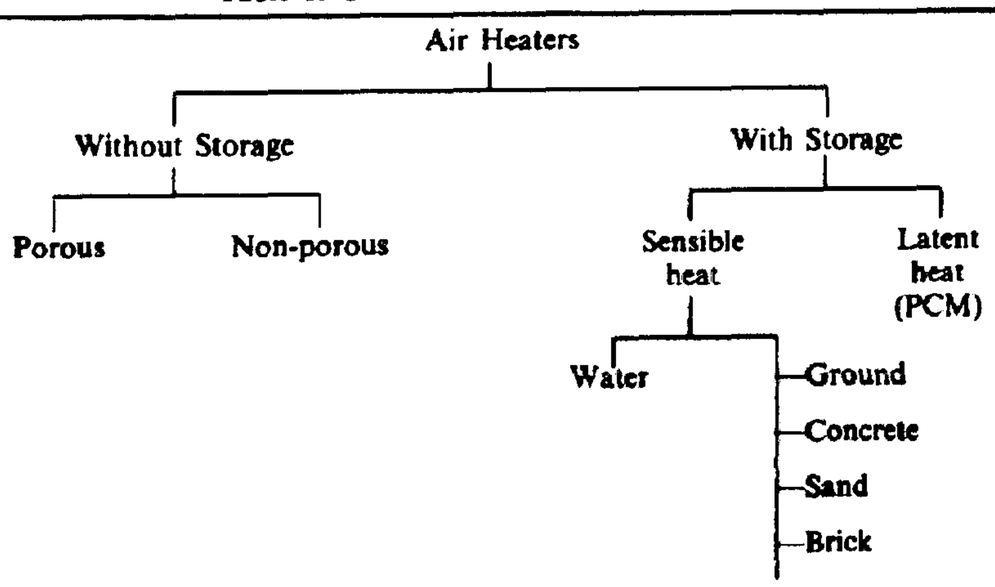

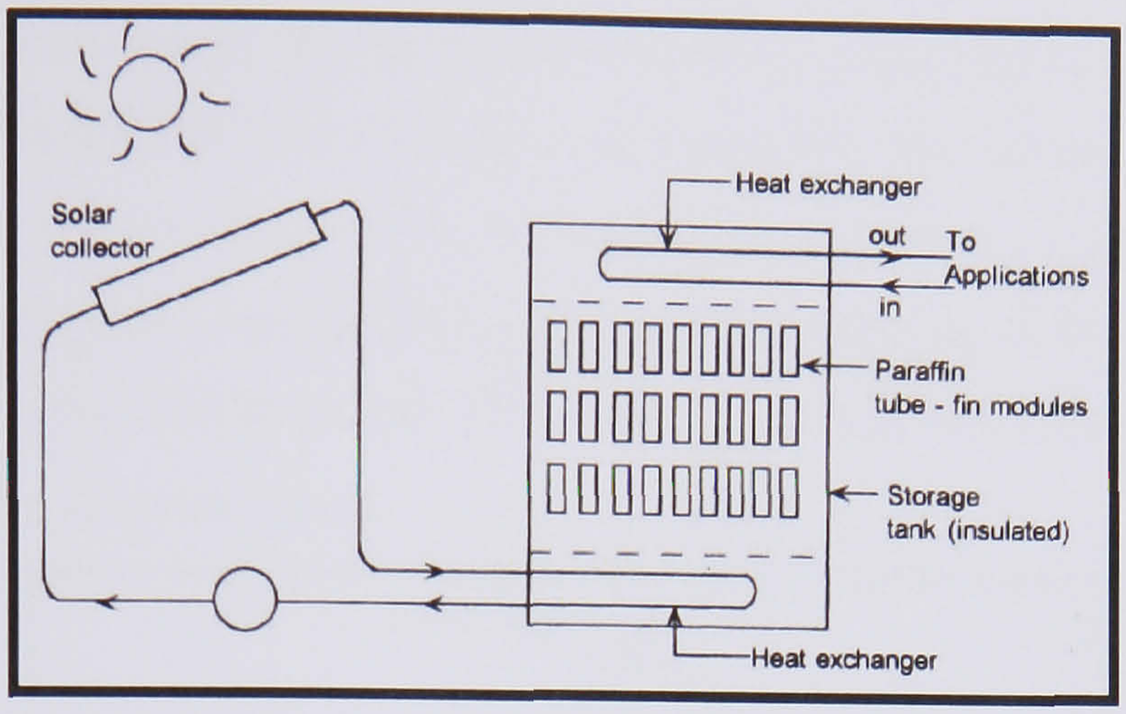

Figure 2.75 Latent heat storage system for solar thermal application (Velraj, 1999)

The performance of a compact phase change material (PCM) solar collector based on latent heat storage was investigated by Mettawee (2004). In this collector, the absorber plate–container unit performs the function of both absorbing the solar energy and storing PCM (*Figure 2.76*). The solar energy was stored in paraffin wax, which was used as a PCM, and was discharged to cold water flowing in pipes located inside the wax. Experiments were conducted for different water flow rates of 8.3–21.7 kg/h. The experimental results showed that in the charging process, the average heat transfer coefficient increases sharply with increasing the molten layer thickness, as the natural convection grows strong. In the discharge process, the useful heat gain was found to increase as the water mass flow rate increases.

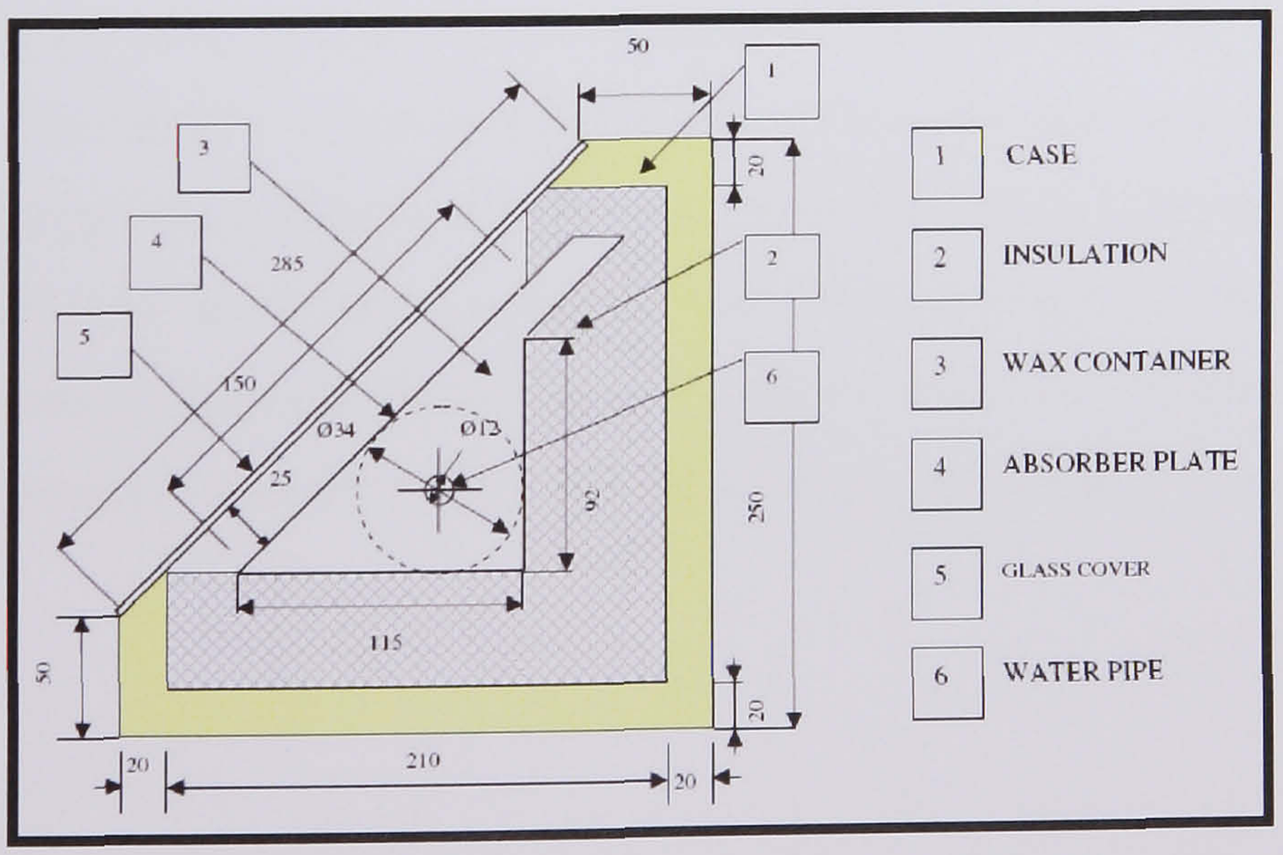

Figure 2.76 Schematic of the experimental apparatus cross section. (Mettawee, 2004)

A new hybrid thermal energy storage system (HTESS), using phase change materials, is proposed by Hammou (2006) for managing simultaneously the storage of heat from solar and electric energy (*Figure 2.77*). Simulations carried out for a period of 4 consecutive winter months indicate that, with such a system, the electricity consumption for space heating is reduced by nearly 32%. Also, more than 90% of the electric energy is consumed during off-peak hours.

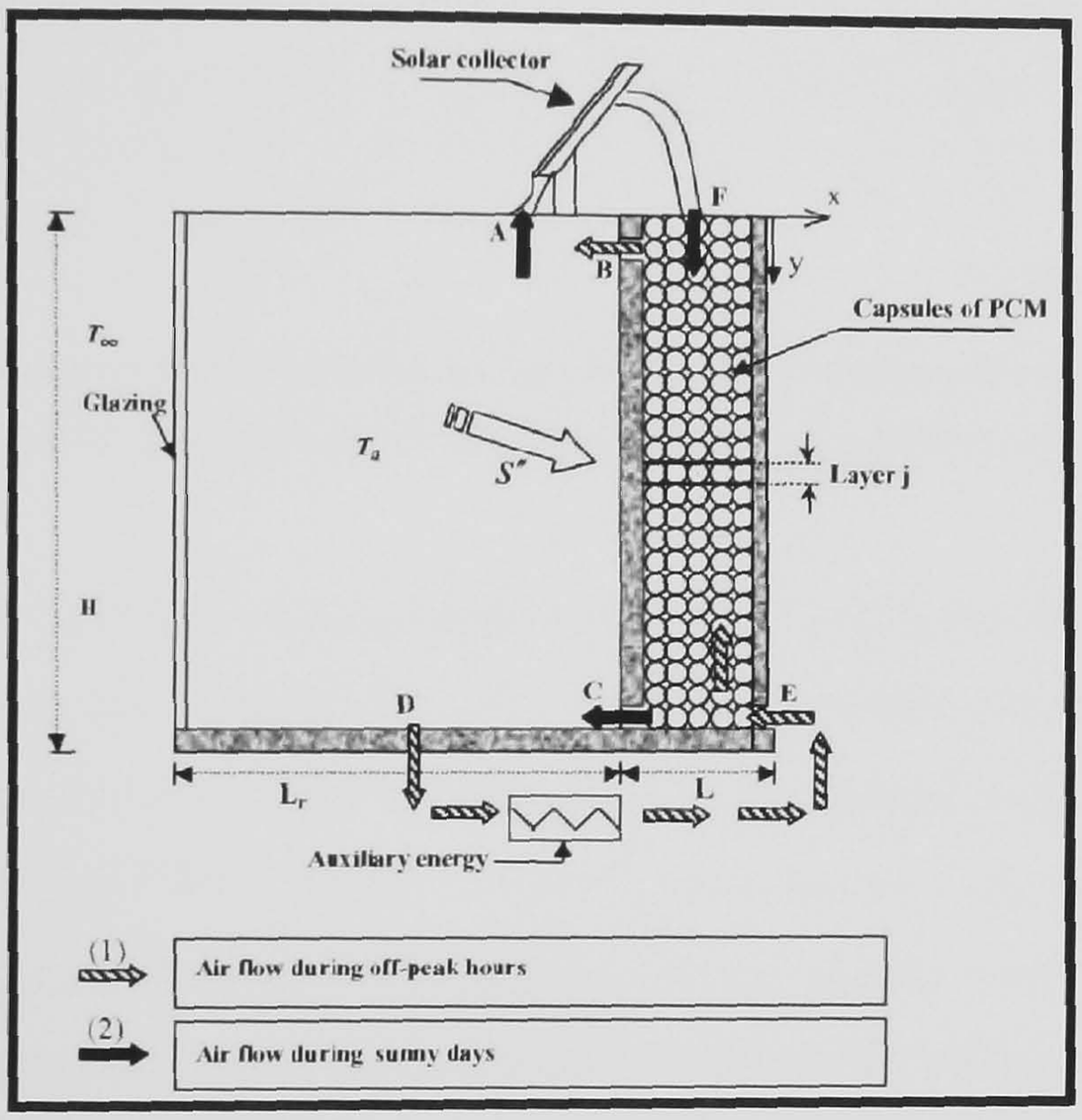

Figure 2.77 Schematic of the hybrid thermal energy storage system. (Hammou, 2006)

A transient thermal analysis of a natural convection solar air heater is presented by Enibe (2003). The heater consists of a single-glazed flat plate solar collector integrated with a paraffin type phase change material (PCM) energy storage subsystem and a rectangular enclosure which serves as the working chamber (*Figure 2.78*). Air flow through the system is by natural convection. Maximum predicted cumulative useful and overall efficiencies of the system were within the ranges 2.5–13 and 7.5–18%, respectively.

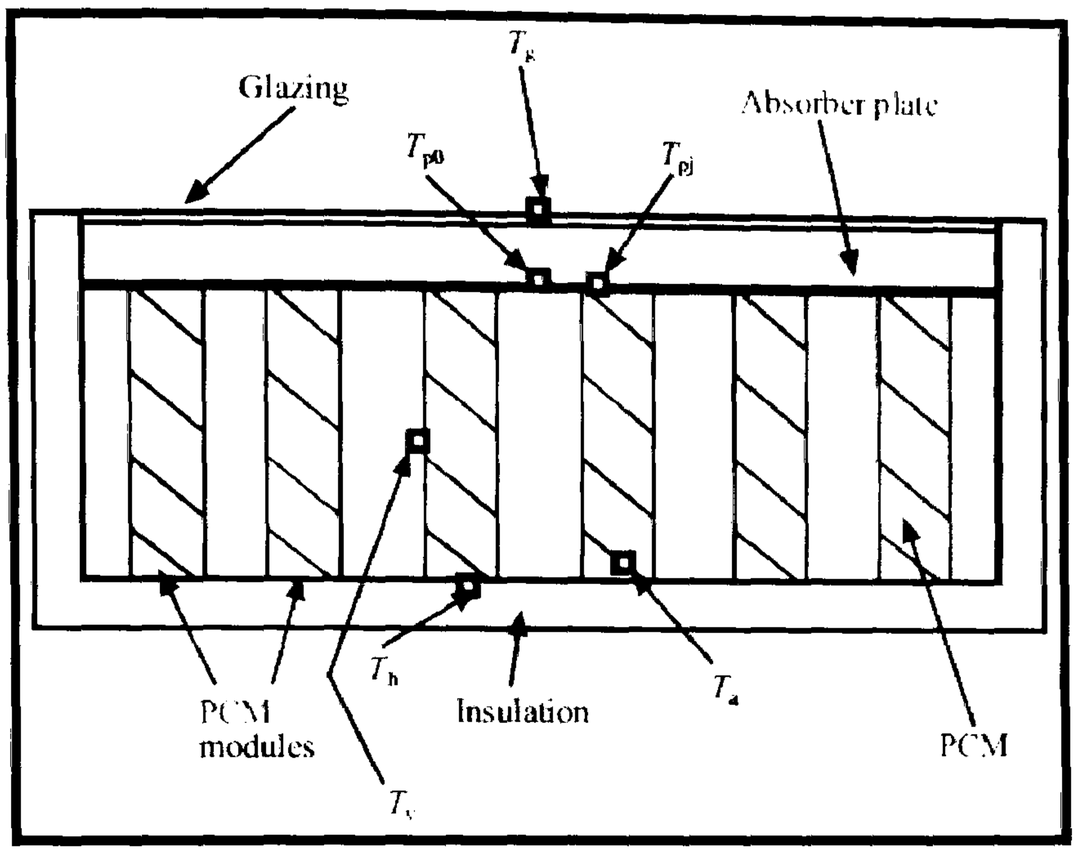

Figure 2.78 Cross-sectional view of the collector assembly. (Enibe, 2003)

A new type of solar collector was developed by Kurklu (2002) and its short term thermal performance was investigated. The solar collector consisted of two adjoining sections one filled with water and the other with a phase change material with a melting and freezing range of about 45–50 °C, i.e. paraffin wax in this study (see *Figure 2.79*). The phase change material functioned both as an energy storage material for the stabilisation, theoretically, of the water temperature and as an insulation material due to its low thermal conductivity value. The results of the study indicated that the water temperature exceeded 55 °C during a typical day of high solar radiation and it was kept over 30 °C during the whole night. The instantaneous thermal efficiency values were between about 22% and 80%.

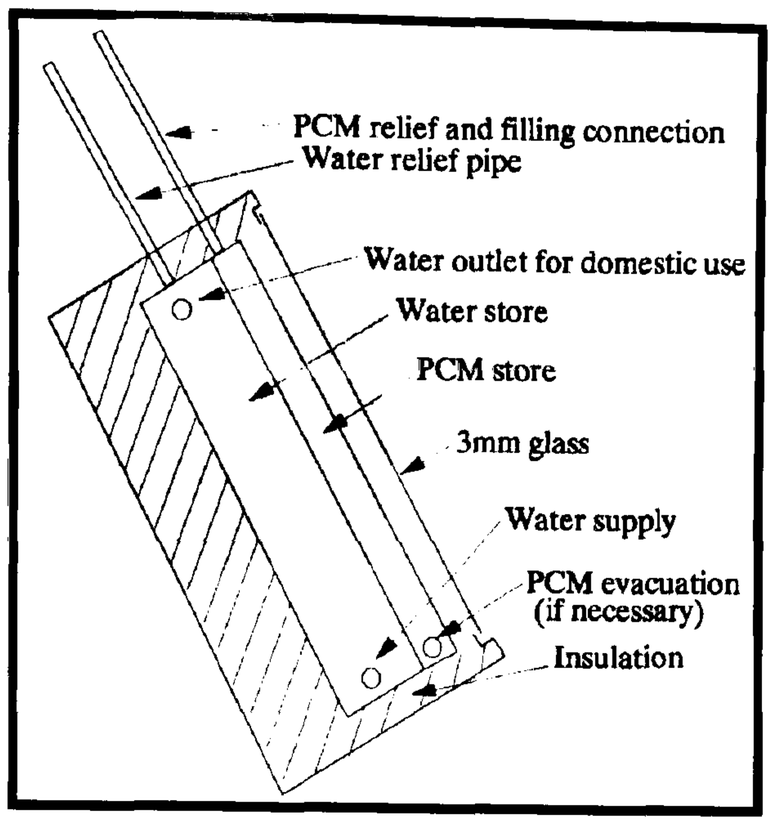

Figure 2.79 The schematic view of the solar collector and its parts (Kurklu, 2002)

2.7.8 Building Integrated PV system incorporating PCM

As we mentioned in section 2.3 only about 16% of the solar energy incident on a photovoltaic (PV) device is converted to electricity and the remaining insolation absorbed is transformed into heat. Active heat dissipation in building integrated PV (BIPV) using air or water cooling can require high levels of maintenance. Incorporating a solid–liquid PCM with a phase change similar to the PV characterising temperature of 25 °C for the thermal regulation of building integrated

PV under cyclic time-dependent solar energy input is a novel approach to BIPV temperature control (*Figure 2.80*). Depending on ambient conditions, a PV/PCM system may enable the PV to operate near its characterising temperature and thus with good solar to electrical conversion efficiency. An additional potential benefit is that the energy stored in the PCM may be released to provide building heating at night. An extensive experimental test campaign has been undertaken by Huang (2004, 2005, and 2006) on the thermal behaviour of a phase change material, when used to moderate the temperature rise of PV in a PV/PCM system.

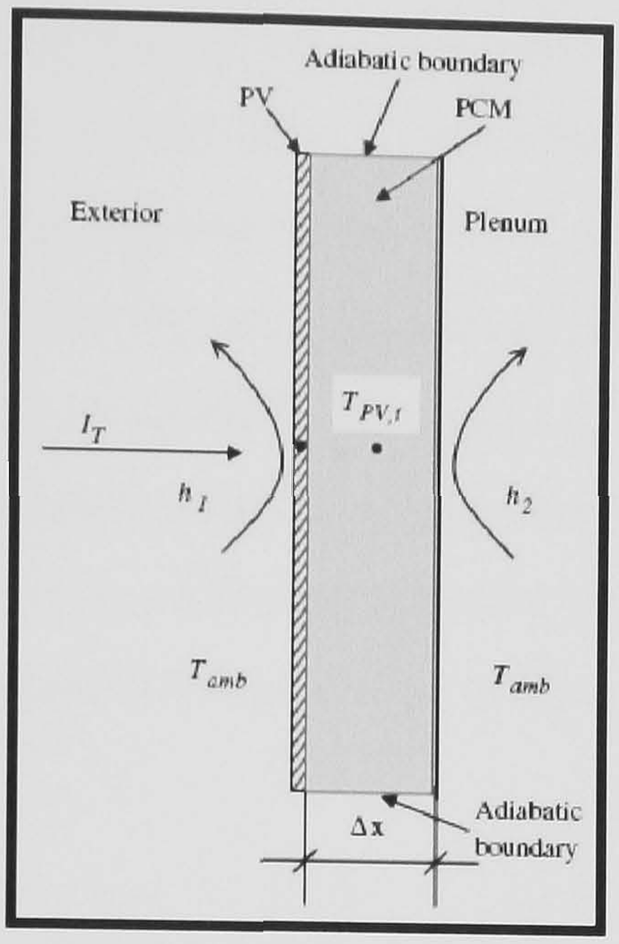

Figure 2.80 Schematic diagram of heat transfer in PV/PCM system. (Huang, 2004)

2.7.9 Discussion

PCM provides much higher energy storage density with a smaller temperature range when compared with the sensible heat storage method. However, practical difficulties usually arise in applying the latent heat method due to the low thermal conductivity, density change, and stability of properties under extended cycling and sometimes phase segregation and sub cooling of the phase change materials.

Therefore in order to design a system using PCM as an absorber some criteria should be fulfilled. Some of these criteria is the melting temperature, the need for high latent heat, high thermal conductivity, no corrosiveness to container material and supercooling phenomenon. From the literature review some of these issues could be resolved like using stainless steel or copper that is compatible to PCM. Also can use additives or thickening agents in order to reduce the supercooling and prevent separation.

Special attention should be given when design systems with PCM to take into consideration factors like impure or incongruently melting substances causing the obtainable enthalpy density in real application to be somewhat lower than suggested by the measured thermo physical properties. Also incorporating fins and different kind of matrix structures can enhance the internal heat transfer of a phase change material.

Solar energy is available only during the day, and hence, its application requires efficient thermal energy storage so that the excess heat collected during sunshine hours may be stored for later use during the night. The solar collectors when using PCM can therefore operate at lower temperatures for an extended period of time, thus increasing the total amount of solar energy collected by the system. Thus a PV/PCM system may enable the PV to operate near its characterising temperature and thus with good solar to electrical conversion efficiency. An additional potential benefit is that the energy stored in the PCM may be released to provide building heating at night.

2.8 Microencapsulated Phase Change Material (MCPCM)

Multifunctional (thermal) fluids and suspensions, also named "intelligent fluids", yield new classes of fluids with improved (thermal) properties. These fluids can be designed to optimally fulfil particular objectives. These fluids can be seen in refrigeration and air conditioning and can enhance the thermal conductivity of a fluid, improve the heat transfer characteristic and increase the thermal energy storage capacity, achieve temperature stabilization and reduce pressure drop. Increasing the convective heat transfer coefficient of a working fluid would permit the use of a smaller volumetric flow rate which would reduce pumping power.

Functionally thermal fluids offer an attractive opportunity for solar collectors to enhance thermal energy transportation and heat transfer of heat exchangers to reduce system size, volume and pumping loads. Hence, reduce system cost, improve thermal stability and increase the overall thermal efficiency.

This section reviews the current status of research on thermal energy transportation using functionally thermal fluids. These fluids are a mixture of a heat transfer medium such as water and another material with or without phase change as a latent heat storage material.

2.8.1 Functionally Thermal Fluids

The most impressive multifunctional suspension is a biological fluid, namely the blood in living creatures. Blood transports oxygen from the lung and nutrients from the intestines to the cells, and removes carbon dioxide and other products to the secrete organs (lung, kidney) (Egolf, 2001).

A review paper on multifunctional thermal fluids was published by Inaba (2000). These fluids are produced by mixing an ideal thermal fluid, which is named the continuous phase, and some additives, mostly solid particles with different properties, as a dispersed phase. Inaba (2000) distinguishes the following fluids:

- Ice slurries
- Micro-capsule slurries
- Micro-emulsion slurries
- Clathrate slurries

- Shape-stabilized paraffins
- Carbon dioxyde slurries.

All these fluids show enhanced thermal energy densities due to a change of phase, e.g. a solid-liquid transition or a similar physical and/or chemical bonding of molecules, which stabilizes the temperature in the working domain around a mean (melting) temperature with a total (melting) range width.
Regardless of the differences in existing compositions, these fluids all have in common the notion of combining multiple functionalities in a fluid with the intention of customising it for the relevant temperature range of a thermal process and fulfilling the transport and the storage of thermal energy with a single suspension. In this sense, with regard to the relevant temperature range, ice slurry, for example, is appropriate for freezing processes, whereas for air-conditioning, micro-capsule phase change slurry (PCS), designed for the use at air-conditioning temperatures, may be most efficient.
In the *Figure 2.81* below we can see the thermodynamic functions that are desirable for a multifunctional fluid to have. It can be seen that five or more of the functions can be met by phase change slurries alone.

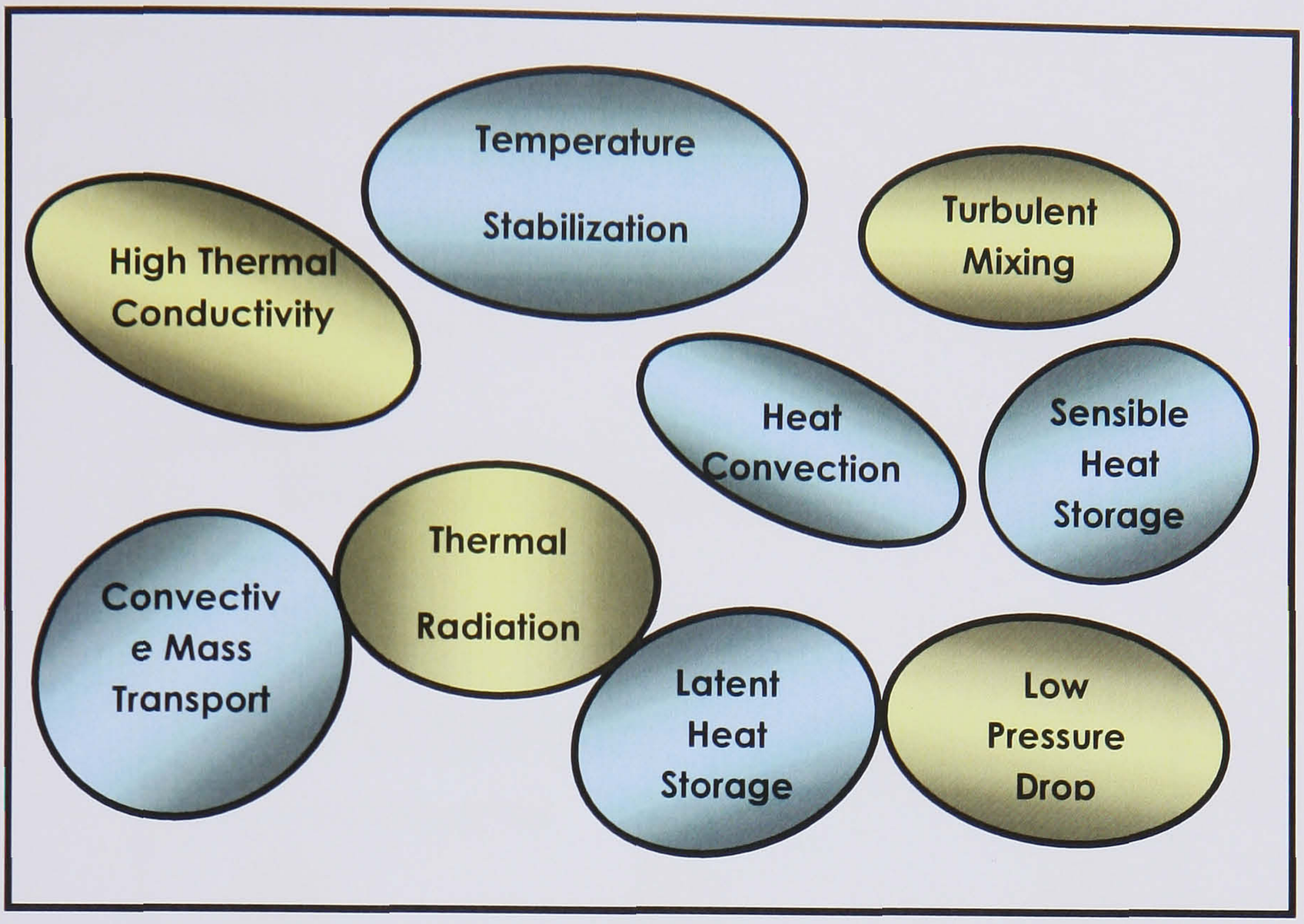

Figure 2.81 Thermodynamic functions of multifunctional fluids. A Phase Change Slurries can fulfil five or more functions simultaneously (e.g. see blue circles). (Abhat 2000)

The key element to the success of a multifunctional fluid is the match between the fluid and the application. If the operating conditions are outside of the fluid boundaries then a reduced performance of the system will be observed.

2.8.2 Phase Change Slurries

Phase change slurries are fluids with dispersed particles, which show a phase change at the melting temperature of the dispersed phase. In a water/ice transition the stored energy is high, namely 332 kJ/kg. Because the concentration of ice particles in technical applications usually is less than fifty percent, the enthalpy density can reach 170 kJ/kg. Other substances have slightly smaller enthalpy densities, but they are still of high technical interest.

Ice storage has been widely used in district space cooling applications as ice making is undertaken using cheaper night-time electrical power. However, Augood et al. (2001) demonstrated that the rate of discharge for such stores is limited by the thermal

resistance of ice and thermal capacity of secondary coolants (such as glycol solutions). Ice is limited to applications where the temperature storage takes place at 0 °C and iced based slurries also need constant stirring to maintain the slurry in a pumping form. If the temperature of ice slurry is increased, the particles melt. In micro-capsule slurry the PCM in the capsule becomes mushy, but the particle size remains (*Figure 2.82*).

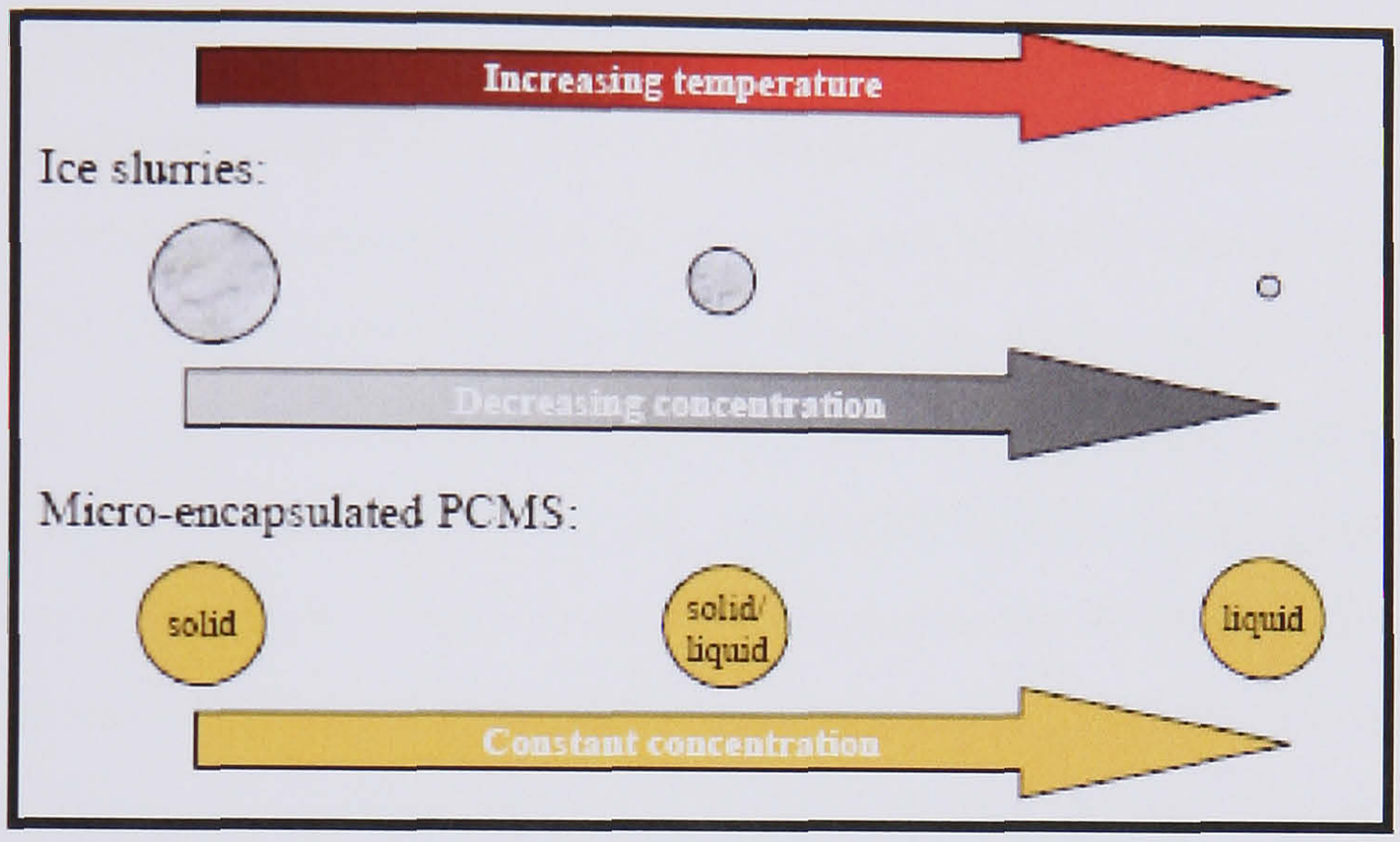

Figure 2.82 Ice Vs Phase Change Material Micro-encapsulated Slurries (Egolf, 2001)

PCMs can be encapsulated in small micro-spheres and suspended in a working fluid to form slurry. This is intended to improve the thermal characteristics of a heat transfer fluid through use of the latent heat of fusion.

2.8.3 Microencapsulated PCM slurry

The use of solar energy for low-temperature applications, such as water heating, is gaining momentum. In fact, for water heating, solar energy is considered an economic alternative. The supply of solar energy is intermittent and, to match the demand with the supply, a storage system is required. Usually, water is used as a storage material for such application. When thermal energy is added to water as sensible heat then a temperature rise is being observed and, the efficiency of the solar collector decreases. This led to the development of a storage system making use of latent heat of phase change material (PCM). Latent heat storage material has the advantage of performing

the storage function at nearly constant temperature, which enables solar collectors to operate at higher efficiencies, and has a large specific storage capacity.

However, there are some inherent drawbacks when PCM are used in thermal storage system (Abhat, 1983). For example, (1) during the freezing (heat release) process in typical latent heat storage devices, the PCM freezes on the heat transfer surface, thereby, increasing the thermal resistance. In addition, the super cooling and thermal conductivity properties also affect the effective application of PCM in a system; (2) some PCMs are highly corrosive to certain container materials, hence, the material of the container should be so selected that it is compatible with the corrosive nature of PCM; (3) the PCMs, generally, exhibit a large change in volume during phase transition and limit the use of simple containment and heat exchanger geometry; (4) some PCMs are highly toxic and poisonous, and require completely sealed storage system resulting in expensive systems (Lane, 1986). In order to overcome the inherent difficulties, various active heat transfer enhancement concepts have been identified such as agitators and scrapers. However, all these additional features greatly increase the complexity and cost of solar storage devices (Fouda *et al.*, 1984; Garg *et al.*, 1985; Yanadori and Masuda, 1989).

One of the promising ways to solve problems mentioned previously is to choose the encapsulated PCM as a storage material. Therefore, encapsulated PCM will be greatly different from the traditional PCM, making the heat storage system more effective and simpler.

Micro encapsulation is the packaging of micronized materials (both liquids and solids) in the form of capsules, which range in size from less than 1 μm to more than 300μm. The encapsulation process was discovered and developed by Barrett K Green (1953) of the National Cash Register Corporation (NRC) in the 1940's and 1950's. The capsule wall material can be formulated by using a wide variety of materials including natural and synthetic polymers. The advantages of microencapsulated paraffin wax are (1) reduction of the paraffin wax reactivity towards the outside environment (2) increase in heat transfer area and (3) shielding the core material by coating to withstand frequent changes in the storage material volume as phase change occurs.

The micro encapsulation techniques were well developed, mainly by the pharmaceutical industries, because they were used to produce pills, copy papers, composites, powders, coatings, foams, fibers. Furthermore, they were applied in apparels for a heat capacity enhancement. A newer application is plastic microcapsules, containing a PCM, floating in a carrier fluid for thermal energy transportation. Micro-PCMs are very attractive since the rate of heat transfer per unit volume to or from the material in the particles is high, and the ratio of surface area to volume of the small particles is large (Charunyakorn, 1991). The slurry may also serve as both energy storage and heat transfer media, so the requirement of separate heat transfer media is eliminated.

2.8.4 Parameters affecting the Heat Transfer Enhancement of PCM Slurry

The dominant parameters affecting the heat transfer enhancement of the phase change slurry were the bulk Stefan number, the volumetric concentration of the microcapsules, and the dimensionless initial degree of sub cooling, the dimensionless phase change temperature range and the microcapsule diameter. (Charunaykorn, 1991, Goel, 1994, Zhang, 1995, Yasushi, 1999, Alisetti, 2000).

The Stefan number is defined as:

$St = C_p *(q_w*R/k)/c_m*L$

Where Cp is the specific heat of suspension, qw the wall heat flux, R the radius of pipe, k the thermal conductivity of suspension, cm is the mass fraction of PCM in suspension and L the latent heat of fusion. According to Goel et al. (1994) St should be less than 1 for optimal effectiveness. From the heat capacity point of view, higher mass fraction and latent heat of fusion values are preferred because increase the heat capacity of the slurry (Choi, 1993). Alternatively higher mass fractions increase apparent viscosity which increases the pumping power (Bellas et al., 2002, Choi, 1993). As pointed out by Alvarado (2006) the impact of higher viscosity and higher mass fraction should also be taken into consideration when selecting operating conditions or sizing equipment, because higher viscosity represents higher pumping power, lower turbulence, and lower overall thermal conductivity, which could reduce local heat transfer rates in the absence of a phase change process. Yamagishi (1999) also showed that the flow structure of

MCPCM slurry changed from turbulent to laminar as the particle volume fractions in the slurry were increased under a constant flow-rate condition.

Moreover, for internal flow of a phase change slurry, the current analysis shows that, the conventional Nusselt number is not suitable for accurately describing the heat transfer enhancement because the heat transfer rates depend not only on the convective heat transfer coefficient but also on the temperature difference in a very non-linear way, since the apparent specific heat of the slurry is closely related to the bulk temperature during the phase change.

In fact, for fluids with variable thermal physical properties, the variable specific heat induced by phase change could strongly affect the convective heat transfer rate.

Hu with Zhang (2002) analysed the forced convective heat transfer enhancement with micro capsulated phase change slurries for laminar flow in a tube with constant heat flux. The conventional Nusselt number definition for internal flow was modified so that it can describe such degree of heat transfer enhancement more concisely.

2.8.4.1 Laminar Flow Conditions

In previous studies, the flow and melting heat transfer characteristics of microencapsulated phase change material (MPCM) slurry at laminar flow condition have been investigated by a number of researchers. Sohn and Chen (1981) observed enhanced thermal conductivity of solid– liquid slurry at a low flow velocity due to the effects of micro convection around the small solid particles. In an analytical study, Kasza and Chen (1985) presented that up to a 10-fold enhancement increase of heat transfer coefficient might be obtained in some specific flow conditions, however the result has not been confirmed by the experiments. Charaunyakorn et al. (1991) developed a model to predict laminar MPCS flow in a heated circular duct and showed that about 2–4 times increase in mean Nusselt number is possible in comparison with single phase fluid flow. Goel et al. (1994) reported that the reduction of the rise of in-wall temperature is by up to 50% compared to a single phase flow in the same dimensionless conditions. The experimental results were compared with those predicted by the numerical simulation of Charaunyakorn et al. (1991), and they found the similar trends, although the difference between them was about 45% because of super cooling

of the phase change material. Other related numerical investigations of melting heat transfer of laminar flow of MPCM slurries in the circular duct include the works of Zhang and Faghri (1995), Alisetti and Roy (1999), Hu and Zhang (2002), and Ho et al. (2004).

2.8.4.2 Turbulent Flow Conditions

Several past studies also attempted to deal with the flow and melting behaviours of phase change slurry in turbulent conditions. Choi et al. (1993) measured the local pressure drop and heat transfer coefficient of turbulent phase change emulsion flow (mixture of water and PCM with additive of emulsion) in a horizontal tube with constant heat rates, however only the results for 10% mass particle fraction were presented. They observed a significant enhancement in heat transfer performance due to the latent heat effect when PCM was melting. They also found that both local heat transfer coefficients and pressure drop along the flow direction varied significantly when PCM was melting, which makes it difficult to apply log-mean-temperature-difference (LMTD) method to determine the heat transfer coefficient.

2.8.4.3 Effective Specific Heat

Many thermal-energy systems have long sections of piping to convey heat-transfer fluids between the heat exchangers for source and sink. In such conventional systems, thermal energy is transferred by the sensible heat of a single-phase working fluid. Because the systems are often operated with small temperature differences, the single-phase fluid must be pumped at a high-volume flow rate. As a result, the system consumes a large amount of pumping power.

The increase in the thermal capacity of heat-transfer fluid is an important problem and is of growing concern to engineers. The use of phase-change material particles suspended in a single-phase working fluid would provide additional thermal capacity from the latent heat associated with the solid-liquid phase change. Several methods for generating PCM particles have been investigated for various thermal-energy applications. For district cooling systems, ice-water slurry has been developed and is implemented in practice. Cleary et al. (1990) found that ice slurry of 25% in particle volume

concentration had a thermal capacity that was 2 to 4 times higher than that of chilled water. Choi et al. (1994) developed a system that generated solid hexadecane _C16H34.particles of 0.1 μm in size, using an emulsifier, and they studied the heat-transfer characteristics of the hexadecane-water slurry. However, because such particles of no encapsulated PCM are slightly sticky and can stick together to form large lumps, clogging often occurs in a piping system, resulting in failure to circulate the slurry through the system (Winters, 1991).

In previous works, efforts have been made to manufacture MCPCMs with sufficient strength by Hart and Thornton (1982) and Roy and Sengupta (1991). Several promising applications using MCPCM slurries as a heat-transfer and storage medium have been proposed by McMahon et al. (1982) and Colvin and Mulligan (1986).

Kasza and Chen (1984) claimed that the convective heat-transfer coefficient for laminar and turbulent slurry flows would increase because of the increase in the effective specific heat, C_{peff}, and the effective thermal conductivity, k_{eff}. One of the heat-transfer correlations for a fully developed turbulent flow of a single-phase fluid shows that the relationship between the Nusselt number, *Nu*, and the Prandtl number, *Pr*, is $Nu = Pr^{0.4}$ (Holman, 1981). Therefore, the convective heat-transfer coefficient, *h*, for a single-phase fluid can be described in terms of thermal conductivity, *k*, and specific heat, *Cp*, as

$$h \sim k^{0.6} Cp^{0.4}. \qquad \text{Eq. (2.8.1)}$$

If the latent heat is viewed as a form of specific heat, the increase in effective specific heat C_{peff}, which includes the effect of latent heat, can lead to an increase in the heat transfer coefficient, since *Cp* in Eq. (2.8.1) is replaced by C_{peff} (Kasza and Chen, 1984). Chen and Chen (1987), Mulligan et al. (1994), Goel et al. (1994). The effective specific heat was defined by Colvin et al. (1992) as

$$Cp_{eff} = Cp + \epsilon c_{pcm} \lambda / \Delta T. \qquad \text{Eq. (2.8.2)}$$

where c_{pcm} is the weight fraction of the PCM in the slurry; λ is the latent heat of PCM; ΔT is the difference between the slurry temperatures at the inlet and the outlet of a heat exchanger; and ε is the fraction of MCPCM particles that undergo phase change within the heat exchanger. They claimed that the average heat-transfer coefficients in the overall heat exchanger, which were calculated from the measured effective specific heat,

were 50-100% higher than those for slurry with no phase change. As for the effective thermal conductivity, k_{eff} , Sohn and Chen (1984) showed that the thermal conductivity of solid-liquid suspensions increased effectively in a laminar flow because of the effects of micro convection around solid particles and particle-to-particle interaction. The degree of the enhancement of thermal conductivity increases as particle diameter increases. For particle diameters smaller than 100 microns, however, this enhancement can be negligible. An associated heat-transfer enhancement is therefore believed to be marginal compared to those related to latent heat (Charunyakorn et al. (1991), Mulligan et al. (1994), Goel et al. (1994), Choi et al. (1994)), although the effects on turbulent heat transfer have not yet been clarified.

2.8.4.4 Super cooling

Although MicroPCMs are widely used in many fields, the super-cooling is still an important obstacle to the industrial application of MicroPCMs. Yamagishi et al. (1996) demonstrated that the crystallization temperature of MicroPCMs with 5–100 μm in diameters lowered as their sizes decreased. Yamagishi selected 1-tetradecanol (2 wt.% by weight of the core material) as a nucleating agent for super-cooling prevention of *n*-tetradecane in MicroPCMs (microcapsule diameters 110–300 μm). Lee (2002) considered that the derivatives of *n*-paraffin, such as 1-octadecylamine, 1- octadecanol, were suitable for preventing PCM from super cooling and were used appropriately within a range of about 1–6 wt.% with respect to the weight of PCM.

Kishimoto et al. (1995) found that 1-pentadecanol was able to prevent the super-cooling of *n*-pentadecane in MicroPCMs and Zhang (2002) reported that the decrease of super-cooling improved the heat transfer enhancement.

However, the influence of nucleating agents on the enthalpies of MicroPCMs except super-cooling have not been studied. In addition, the morphology and dispersibility of microcapsules with PCM and nucleating agents have been investigated.

Fan et al. (2004) analysed the effects of the nucleating agents, including sodium chloride, 1-octadecanol and paraffin, on the melting and crystallization behaviour and morphology. The super-cooling was prevented by adding about 6 wt.% sodium chloride to the emulsion, however, the microcapsules were worse dispersed and their surfaces

were rough. Adding approximately 9 wt.% 1-octadecanol in core material was found to prevent microcapsules from super-cooling, but the microcapsules were easily conglomerated and their surfaces were extraordinarily rough. Microcapsules with approximately 20 wt.% paraffin in core material were free from super-cooling, and paraffin had no influence on the morphology and dispersibility of microcapsules.

2.8.5 MicroPCM Applications

The micro encapsulation of PCMs involves enclosing them in thin and resilient polymer shells so that the PCMs can be changed from solid to liquid and back again within the shells. Microencapsulated PCMs have been applied in many fields, including textiles (Sarier and Onder, 2007, Shin, 2004), heat storage systems for buildings, and microclimate environmental control for vegetation and seeds in agriculture.

In applications of PCM technology to garments and home furnishing products, PCM microcapsules are incorporated into acrylic fibers or polyurethane foams or are embedded into coating compounds and topically applied to fabrics or foams. A variety of outdoor apparel products with PCM microcapsules, such as ski wear, hunting clothing, boots, gloves, and ear warmers, are on the market under the trade names Outlast and ComforTemp.

The idea of improving the thermal comfort of lightweight buildings by integrating phase change materials (PCMs) into the building structure has been investigated in various research projects over several decades (Cabeza et al., 2007). Most of these attempts applied macro-capsules or direct immersion processes, which both turned out to present several drawbacks. Due to these problems, none of these PCM products was successful in the wider market. The new option to micro-encapsulate PCMs, a key technology which overcomes many of these problems, may make PCM products accessible for the building industry (*Figure 2.83*). Schossig (2005) described the work done at Fraunhofer ISE extending from building simulations to first measurements of full-size rooms equipped with PCM. The measured data showed the potential for PCM products to reduce the cooling demand and increase the comfort in lightweight buildings. The technology of microencapsulation works without problems in the range of 0 – 90 ^{o}C (www.fskab.com/annex17/).

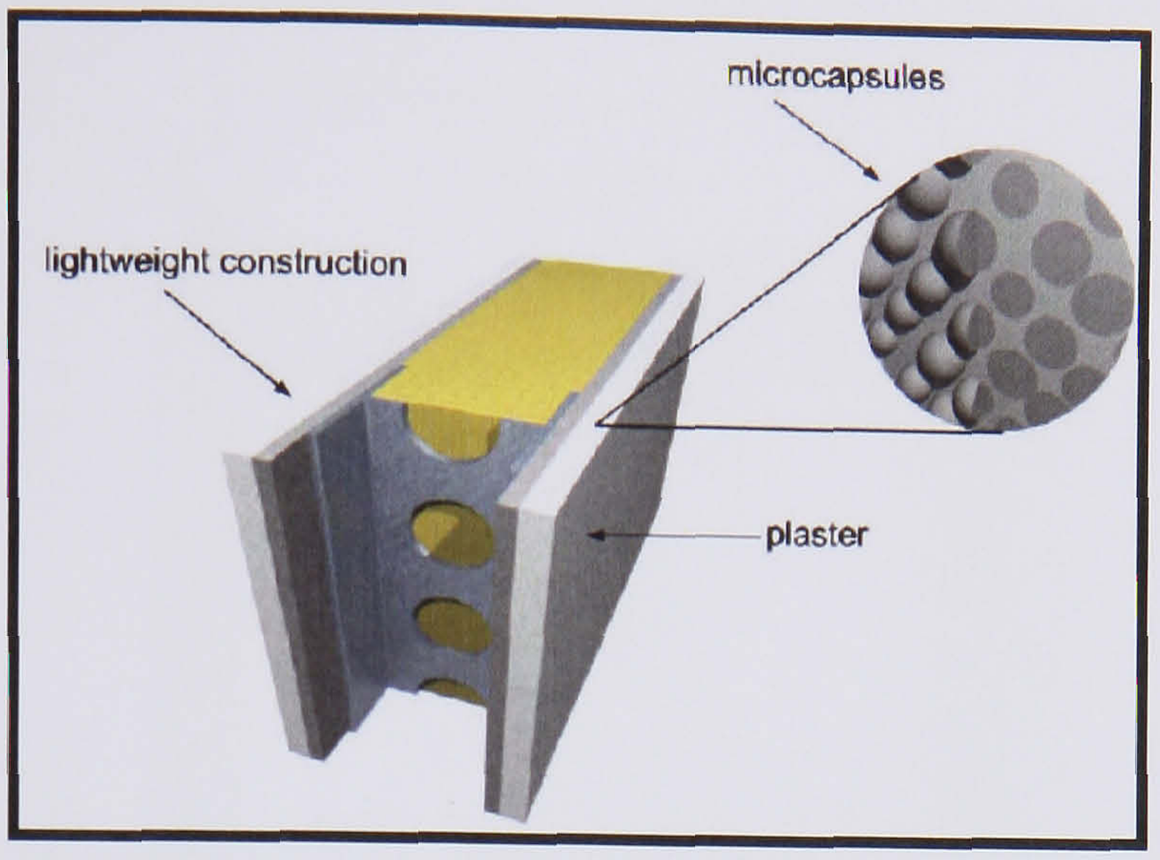

Figure 2.83 Schematic view of a lightweight wall. The PCM micro-capsules are integrated into the interior plaster. (Schossig, 2005)

New microencapsulated slurry produced by BASF (2003) with a melt temperature of 18 °C has been analysed for use in a chilled ceiling system by Griffiths (2006) as shown in *Figure 2.84*. 18 °C slurry was chosen as it matched closely with the working temperature of chilled ceiling panels (16–18 °C). The microcapsules were very small in diameter (approximately 2–8 μm) which, when suspended in water with a 40% concentration could be pumped around heating and cooling circuits using commercially available pumps and achieved reduced power consumption.

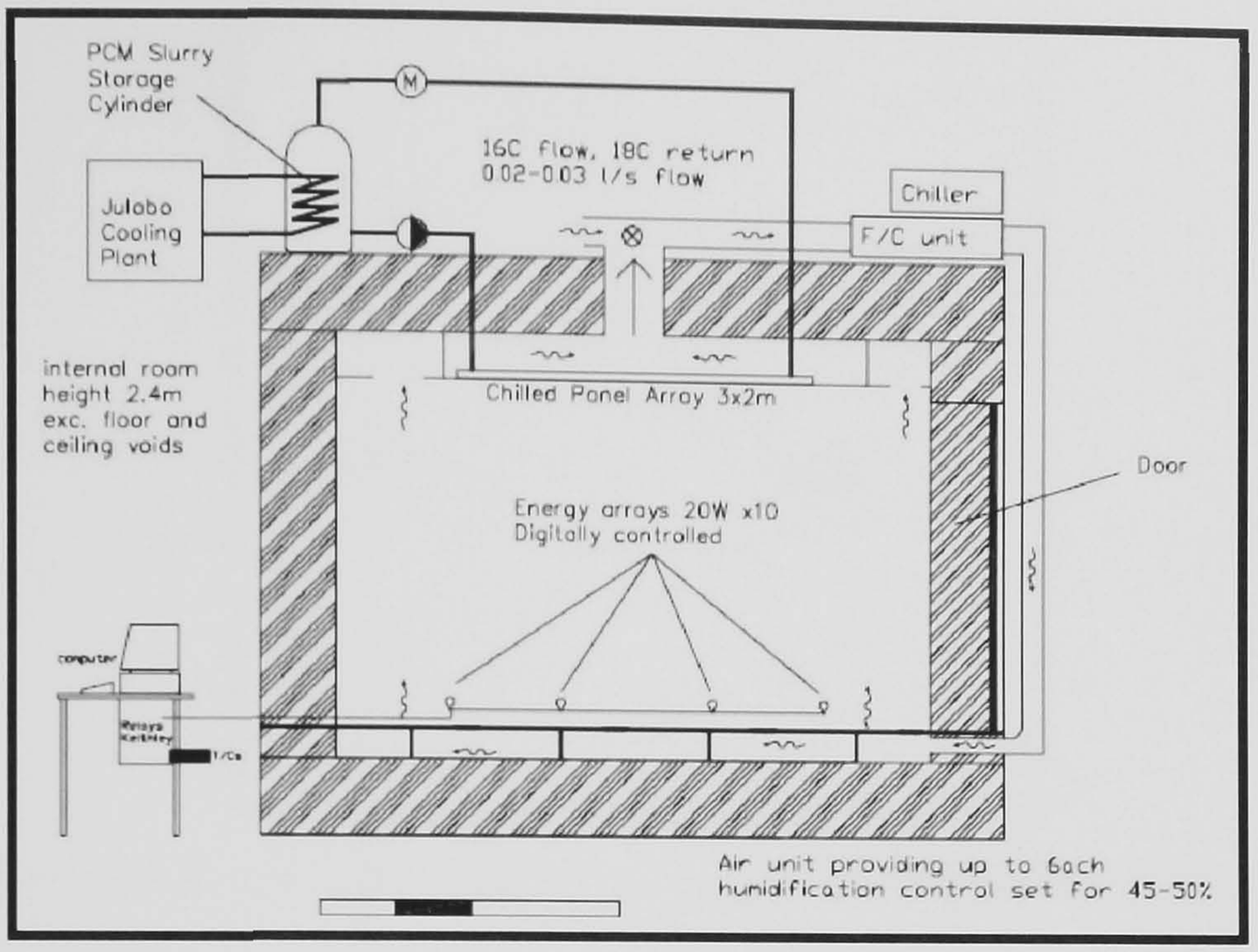

Figure 2.84 Schematic diagram of the chilled ceiling in the test chamber. (Griffiths 2006)

A transient finite volume model was used by Eames (2006) to predict collection and retention of heat for rectangular cross section solar collector/storage system when filled with water and various concentrations of phase change material (PCM) slurries with a 65 °C phase change temperature (*Figure 2.85*). It was found that the PCM slurry system collected heat marginally less effectively than water filled stores due to the lower specific heat capacity than water of the PCM slurries. However cause of the high energy of phase transition in the 58–60 °C temperature range more energy is stored for a longer period above 58 °C. Retention of heat at higher temperatures in the PCM slurry system may allow higher solar savings fractions to be realised depending on heat demand patterns.

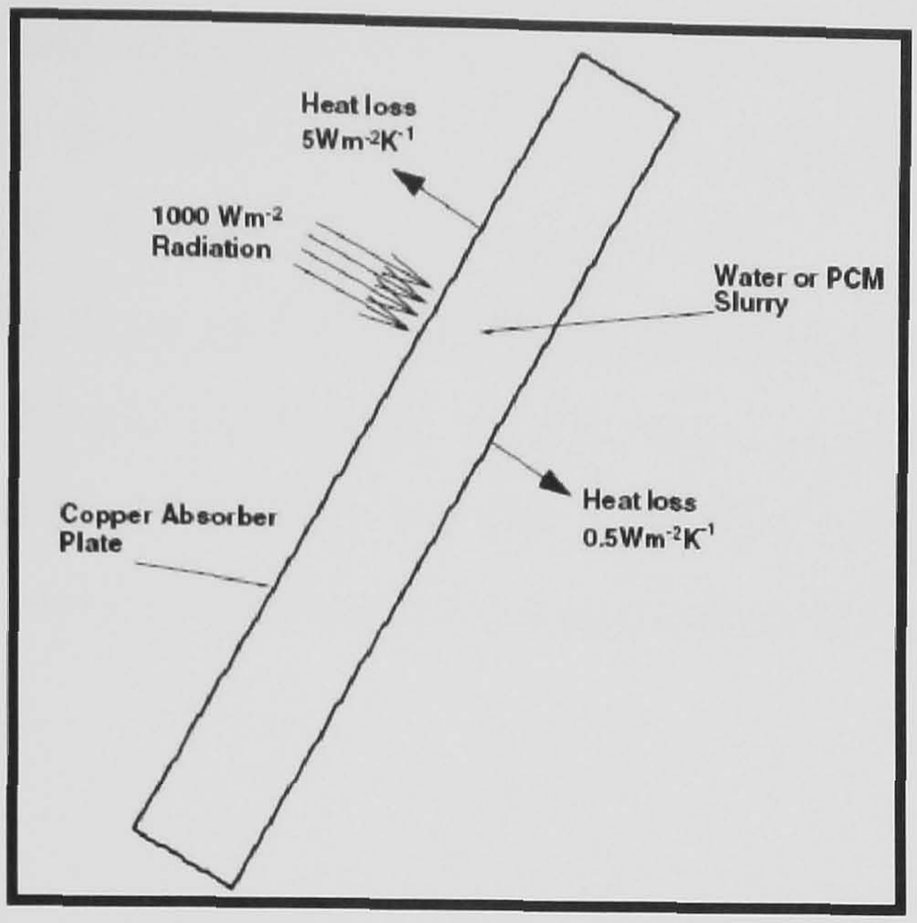

Figure 2.85 A schematic diagram of the system simulated (Eames, 2006)

2.8.6 Discussion

Functionally thermal fluids offer an attractive opportunity for solar collectors to enhance thermal energy transportation and heat transfer of heat exchangers to reduce system size, volume and pumping loads. As mentioned in section 2.7 cause of the low thermal conductivity of PCM heat transfer enhancement methods required to improve the performance of a system. Thus PCMs can be encapsulated in small micro-spheres and suspended in a working fluid to form slurry. This is intended to improve the thermal characteristics of a heat transfer fluid through use of the latent heat of fusion. Another advantage is that the slurry may also serve as both energy storage and heat transfer media, so the requirement of separate heat transfer media is eliminated. Parameters that should be taken into consideration are the impact of higher viscosity and higher mass fraction when selecting operating conditions or sizing equipment, because higher viscosity represents higher pumping power, lower turbulence, and lower overall thermal conductivity, which could reduce local heat transfer rates.

From the literature review it was noticed that the conventional Nusselt number is not suitable for accurately describing the heat transfer enhancement because the heat transfer rates depend not only on the convective heat transfer coefficient but also on the temperature difference in a very non-linear way, since the apparent specific heat of the slurry is closely related to the bulk temperature during the phase change. This makes it

difficult to apply log-mean-temperature-difference (LMTD) method to determine the heat transfer coefficient. So a new method is required in order to assess the performance of a system having MCPCM slurry as a heat transfer fluid.

From applications it was found that the PCM slurry system collectes heat marginally less effectively than water due to the lower specific heat capacity than water of the PCM slurries. However retention of heat at higher temperatures in the PCM slurry system may allow higher solar savings fractions to be realised depending on heat demand patterns.

CHAPTER 3: PV PERFORMANCE

3.1 Introduction

As we mentioned in the literature review at section 2.4 PV panels absorb up to 80% of the incident solar radiation. However, only 5-20% of the incident energy is converted to electricity, depending on the PV cell technology used. The remaining energy is converted into heat and the PV panels can reach temperatures as high as 40 °C above ambient temperature.

In this chapter an experimental evaluation of the PV performance will help to understand how the increase in temperature affects the electrical efficiency. From the experiments the I-V curve and P-V curve characteristics of a PV panel is going to be illustrated with the rear of the PV being free and insulated. The results will give an indication of the relation between PV performance and temperature. Also the performance from the two PV rigs (PV rear insulated and uninsulated) will work as a comparison indicator of the PV/T models that are going to be described in the next chapters.

3.2 Solar cell losses

In a solar cell only part of the incoming irradiation is converted into electricity as indicated in *Figure 3.1*, due to fundamental losses that occur in a single-junction cell. One of the most fundamental limitations on solar cell efficiency is the band gap of the semiconductor from which the cell is made.

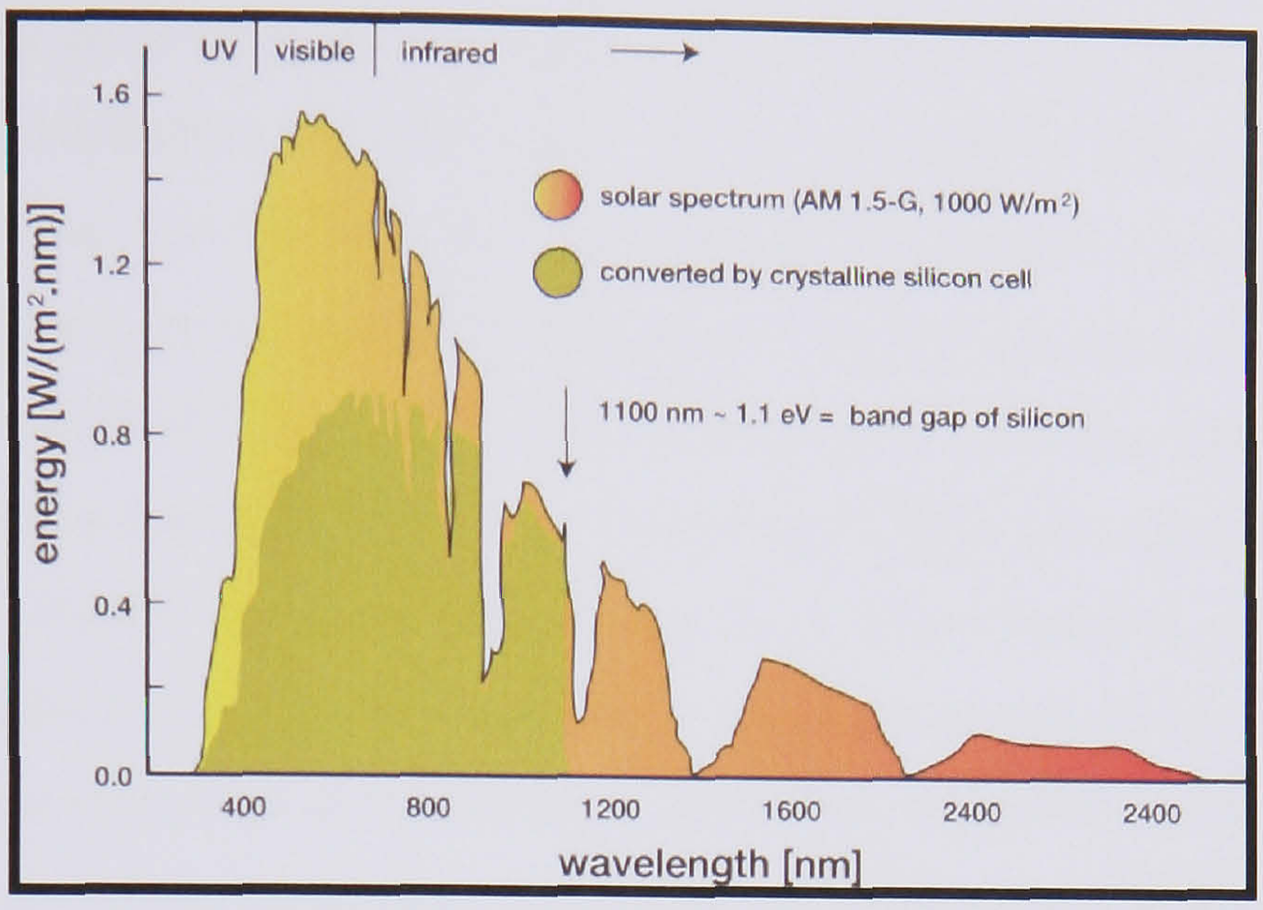

Figure 3.1 Sketch of the partition of the incoming sunlight converted to electricity or to heat as a function of wavelength (Solar spectrum vs silicon cell, 2007)

Crystalline silicon continues to be the dominant material for photovoltaic (PV) production world-wide. Taking into account the PV conversion losses of power that affect the annual performance most important are:

- Light reflection losses (3.1%),
- Low radiation and shadowing losses (3.2%),
- DC losses (1.2%),
- DC/AC conversion losses (4%),
- Auxiliary services losses (2%),
- Mismatching losses (5.7%),
- Temperature losses (7.6%),

We see that the major fraction of losses is related to the temperature increase of the silicon solar cells.

3.3 Module Temperature Effect

Module temperature is a parameter that has great influence in the behaviour of a PV system, as it modifies system efficiency and output energy. It depends on the module encapsulating material, its thermal dissipation and absorption properties, the

maximum power point of the module, the atmospheric parameters such as irradiance level, ambient temperature and wind speed and the particular installing conditions.

It is common to use NOCT (Nominal Operating Cell Temperature) as an indicative of module temperature; in fact, manufacturers usually include this parameter in module data sheets. It is defined as the mean solar cell junction temperature within an open-rack mounted module in Standard Reference Environment (SRE): tilt angle at normal incidence to the direct solar beam at local solar noon; total irradiance of 800 W/m^2; ambient temperature of 20 ^oC; wind speed of 1m/s and nil electrical load.

It is an important parameter in module characterisation, since it is a reference of how the module will work when operating in real conditions. Furthermore, in PV system design and simulation programs, many of the calculations are based on the determination of module temperature from ambient temperature and NOCT.

There are several international standards that include the means to calculate NOCT in crystalline PV modules (EN-61215), thin-film PV modules (EN-61646) or both (non-concentrator terrestrial PV modules and arrays, ASTM E1036M. All of them are based on the fact that difference between module temperatures minus ambient temperature is largely independent of air temperature and is essentially linearly proportional to irradiance level.

The module temperature can be calculated from the NOCT or installed NOCT and air temperature using (Ross, 1980) equation (2.4.3)

$$T = T_{\text{air}} + (\text{NOCT} - 20^{\circ}\text{C})E_{\text{tot}}/800\ \text{Wm}^{-2}$$

3.4 Cell and Module *I –V* Systems

The performance of a PV is determined by some important main parameters. These main parameters are short circuit current, open circuit voltage, maximum output power, fill factor, and instantaneous efficiency.

Two important parameters of the I–V curve for a PV module are the short circuit current I_{sc} and the open-circuit voltage V_{oc}. I_{sc} and V_{oc} change with the incident solar irradiance and with the ambient air temperature. The short-circuit current is about proportional to the incident solar irradiance and the open-circuit voltage increases just a little when the solar irradiance increases (see *Figure 3.2* left). On the other hand, it is important to note

that V_{oc} decreases with increasing module temperature which leads to a noticeable decrease in the available maximum electrical power, in spite of a small increasing of the short-circuit current I_{sc} (see *Figure 3.2* right).

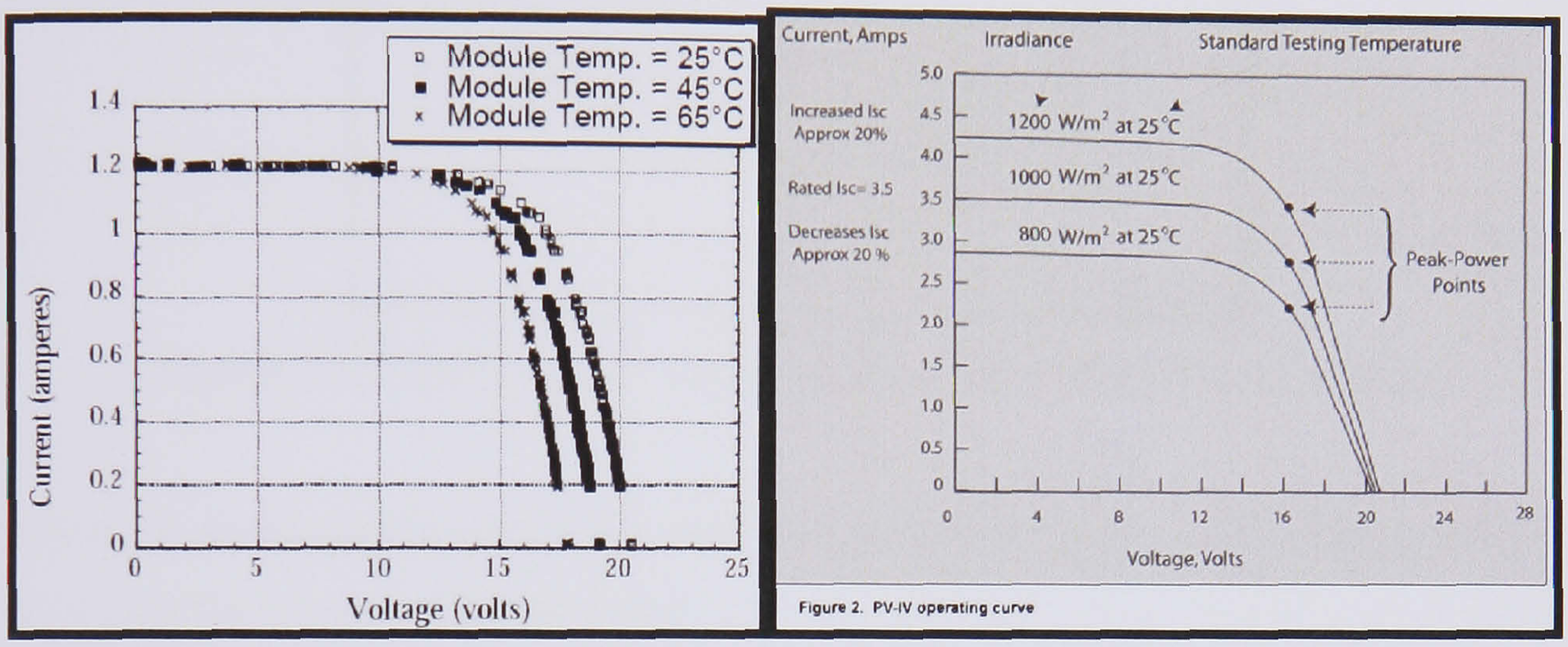

Figure 3.2 PV operating performance of I-V curve with a) increase in temperature and b) increase in irradiance (International Association of Electrical Inspectors, 2007)

A wide variety of $I-V$ measurement systems have been developed to measure the performance of PV devices, from 0.01-cm^2 area cells to multi-kilowatt arrays. A generic $I-V$ system is shown in *Figure 3.3*. The voltage across the PV device (from a cell to an array) is biased with a variable load, with the current being sensed by a precision four-terminal shunt resistor or magnetic transducer. Domestic and international standards have been developed for the minimum characteristics of typical $I-V$ measurement systems. The critical parameters on the $I-V$ curve are the open-circuit voltage (V_{oc}), the short-circuit current (I_{sc}), and the maximum-power point (P_{max}).

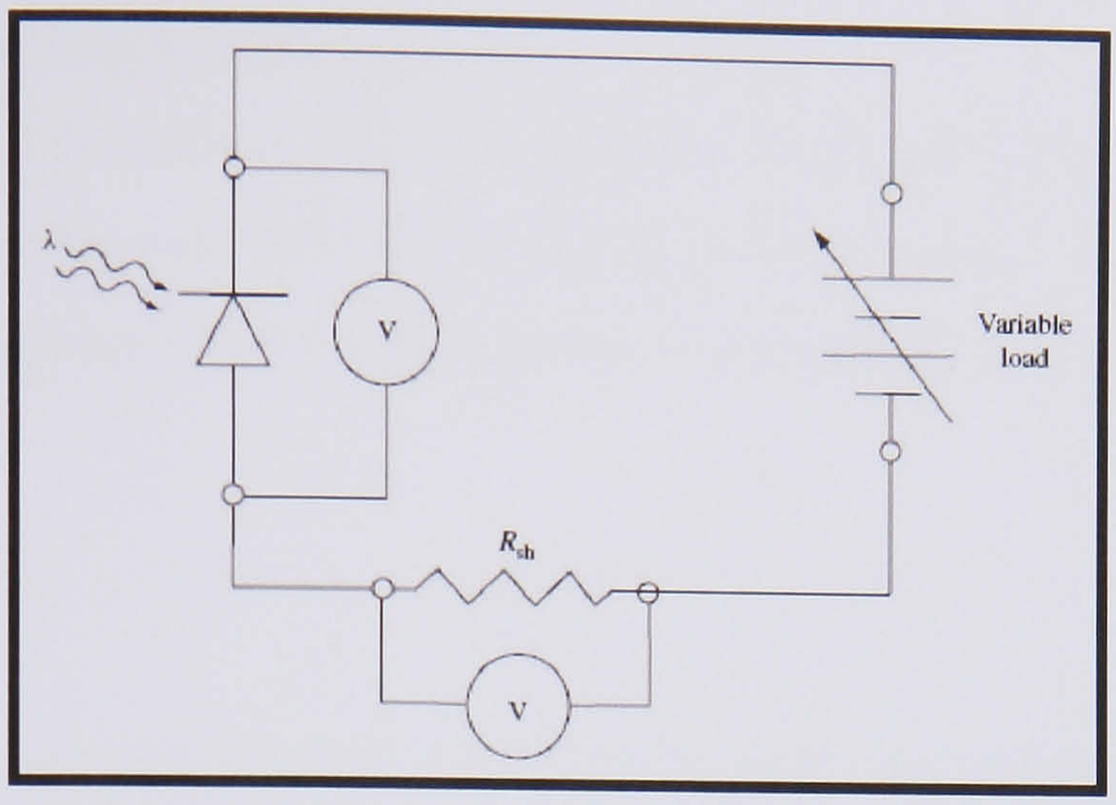

Figure 3.3 Typical current versus voltage measurement circuit system

Figure 3.4 illustrates the typical I-V and P-V characteristics of a Si PV cell, showing I_{mp} and V_{mp} at the maximum power point.

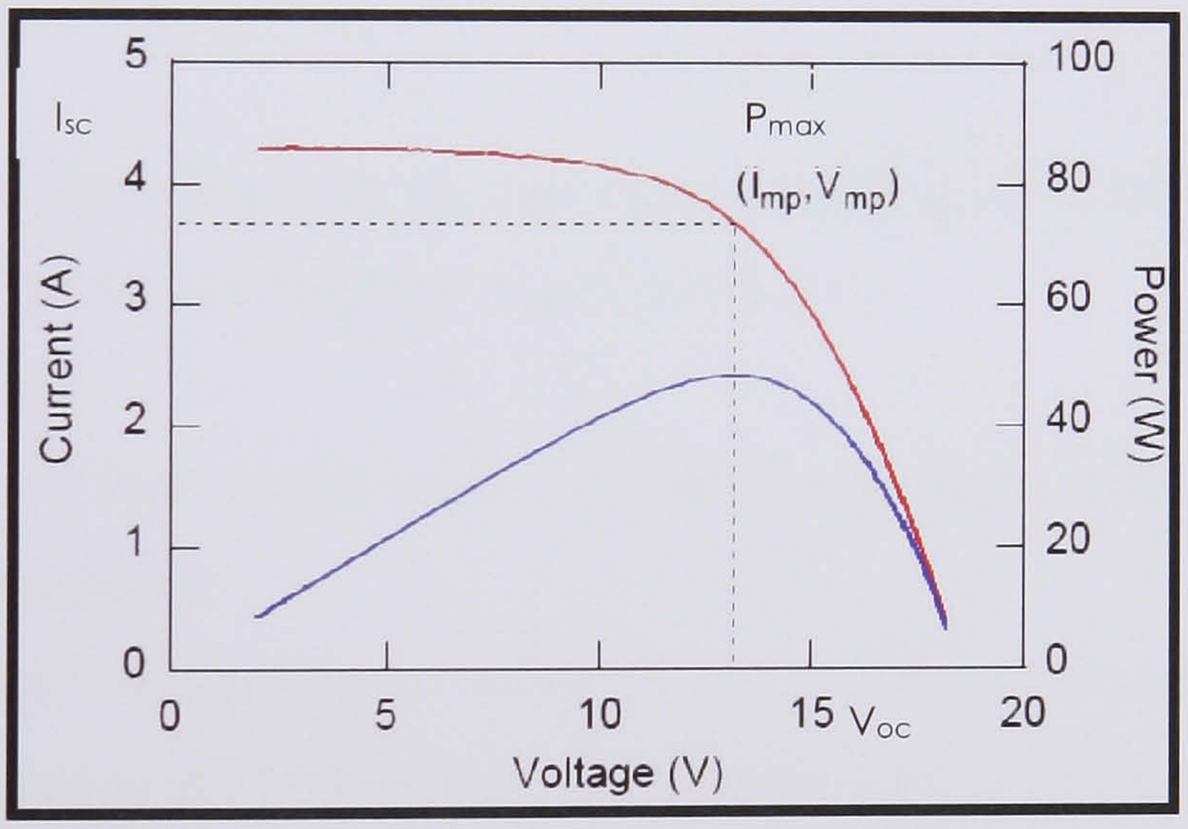

Figure 3.4 I-V and P-V characteristics of a typical Si PV cell

The fill factor (*FF*) is a normalized parameter indicating how ideal the diode properties are, and it is calculated by the following expression (2.4.2):

$$FF = \frac{P_{\max}}{V_{OC} I_{SC}}$$

3.5 Standard Reporting Conditions (SRC)

The PV performance in terms of SRC is commonly expressed in terms of efficiency. The PV conversion efficiency (η) is calculated from the measured maximum or peak PV power (P_{max}), device area (A), and total incident irradiance (E_{tot}) as shown from equation (2.4.1):

$$\eta = \frac{P_{max}}{E_{tot} A} 100$$

As mentioned in the literature review for PV and as described in this chapter the temperature affects the performance of the PV power and accordingly the efficiency of the module. The equation (2.4.5) can be used to see how the temperature affects the PV efficiency.

$$\eta = \eta_r - \mu(T_c - T_r)$$

Where n_r is $T_r = 25\ ^oC$

The aim is to study experimentally the temperature response of the thermal parameters of a polycrystalline silicon solar panel made by Solarex.

The study includes:

- Evaluation of short circuit current increase by absorption of additional photons at higher temperature,
- Evaluation of the open circuit voltage decrease change with temperature.
- Determination of the voltage and current temperature coefficients of the investigated photovoltaic panel.
- Determination of the power and electrical efficiency of the PV in relation to the temperature of the cells
- Evaluation of the PV panel in temperature when the rear of the panel insulated and uninsulated.

3.6 Experimental Rig Apparatus

This section presents and discusses laboratory experiments and the rig constructed can be seen in *Figure 3.5*. A detailed apparatus description follows.

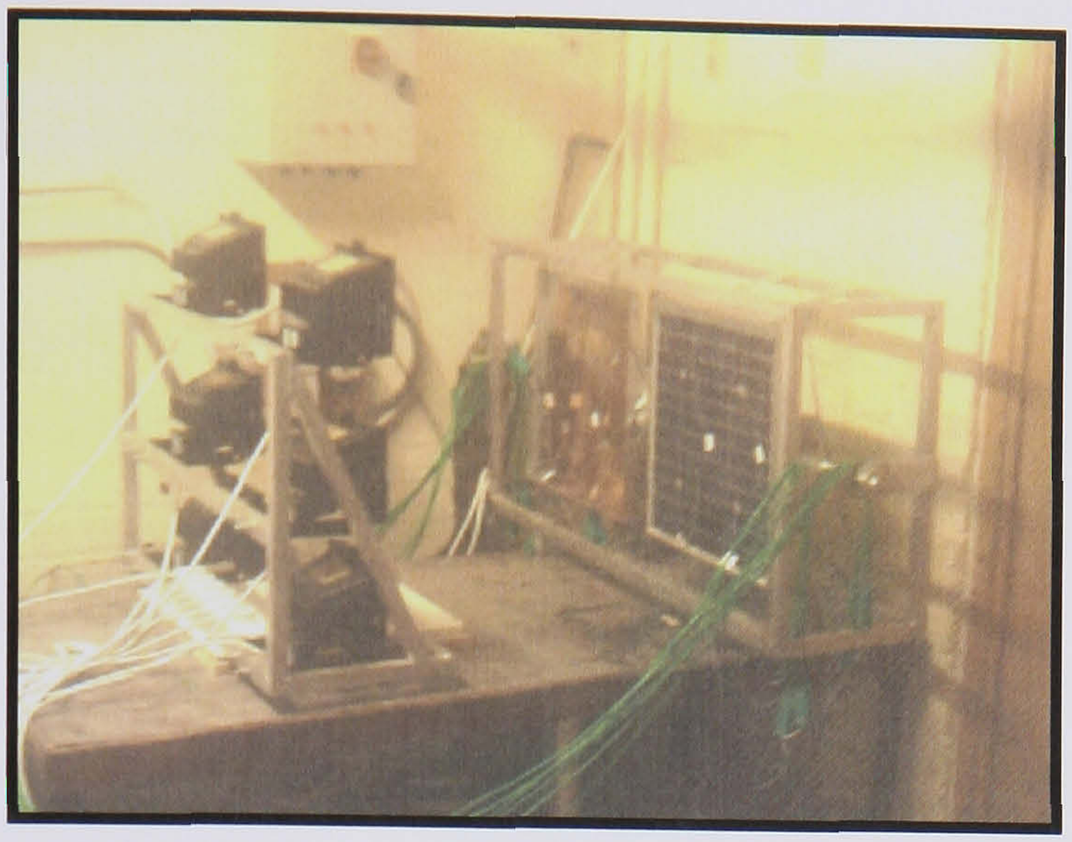

Figure 3.5 Experimental Rig

The system consisted of:

- **Irradiance source (6 Tungsten Halogen (500 W) Lamps)**

These lamps are thermal radiators that emit a continuous spectrum of light extending from about 300 nanometers to upward of 1200-1400 nanometres, with a majority of wavelength intensity centred in the 600-1200 nanometre region as illustrated in *Figure 3.6*. Because the spectral range and intensity of the daylight as seen in *Figure 3.1* is in the range of 350 – 800 nanometers instead of 600 – 1200 (see *Figure 3.6*) that is for tungsten lamp it will face a reduction in power and efficiency of the PV module in comparison with the values given from the manufacturer.

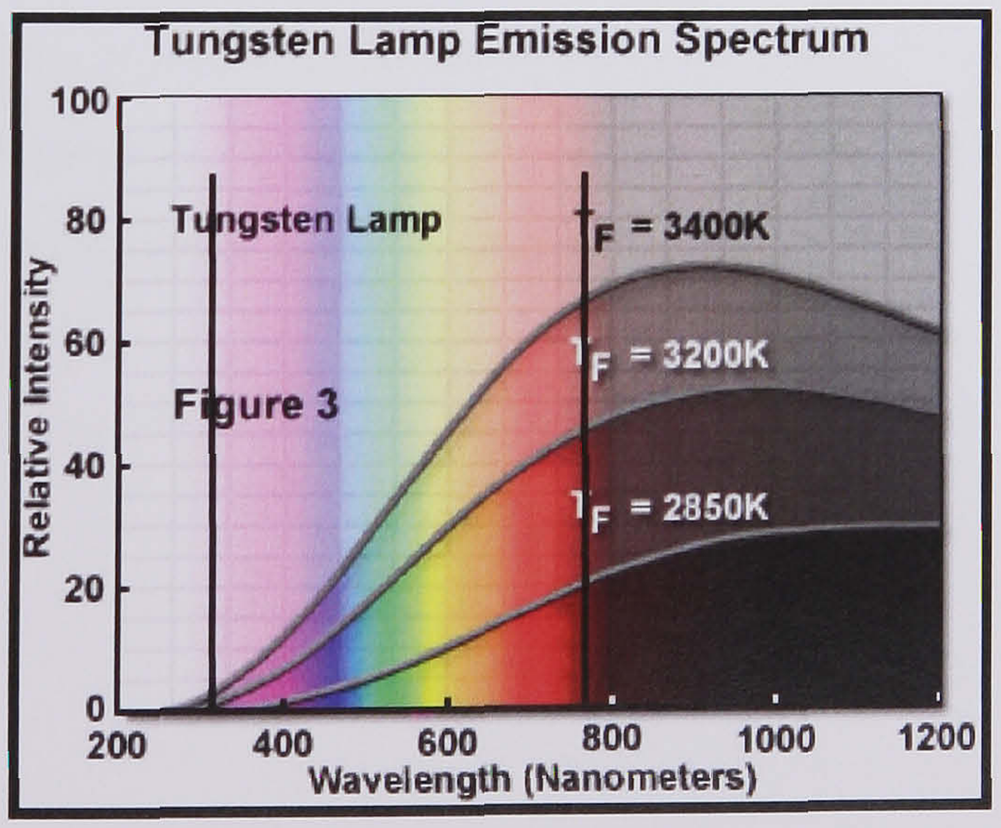

Figure 3.6 Tungsten Lamp Emission Spectrum (www.microscopyu.com)

Crystalline silicon can use the entire visible spectrum, plus some part of the infrared spectrum (see Figure 3.1, between two black lines in 3.6 and 3.7)). But energy in part of the infrared spectrum, as well as longer-wavelength radiation, is too low to produce current flow. Higher-energy radiation can produce current flow, but much of this energy is likewise not usable. In summary, light that is too high or low in energy is not usable by a cell to produce electricity and it is transformed into heat.

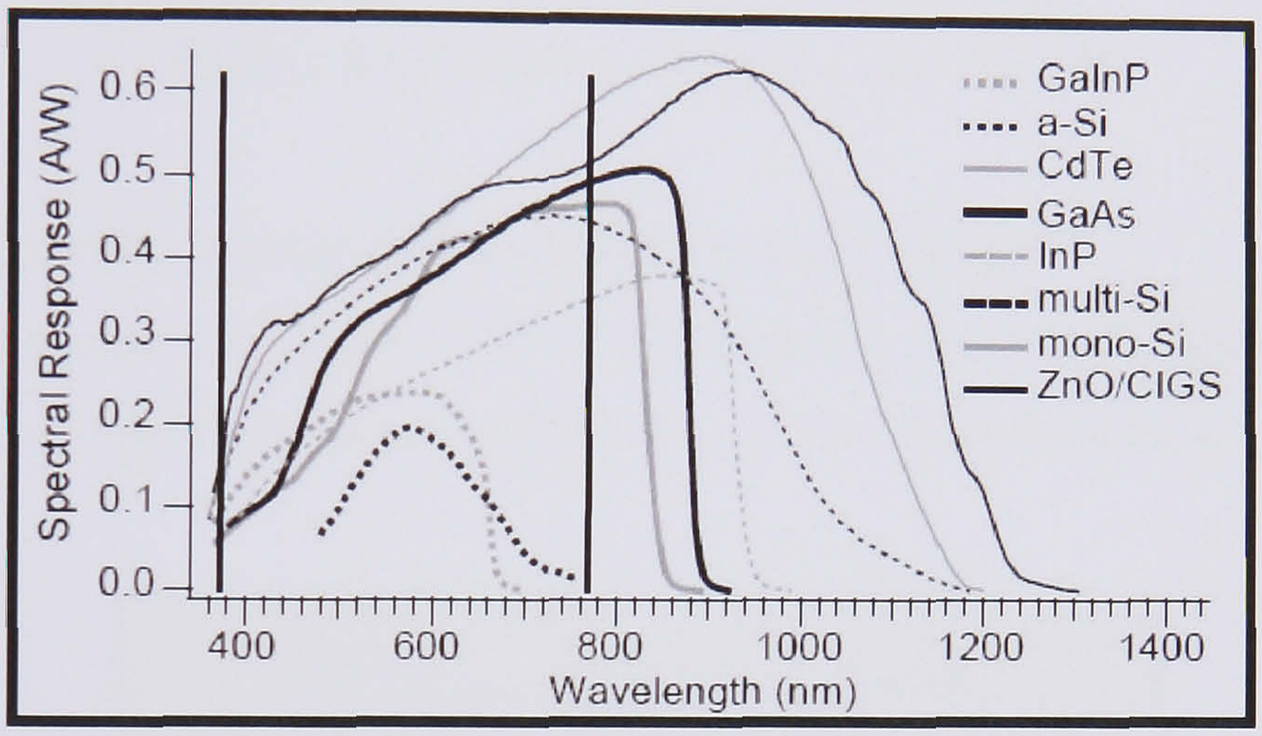

Figure 3.7 Spectral response characteristics of cells (Field H., 1997)

The design, construction, and operation of a tungsten lamp is simple consisting of an enclosed glass bulb filled with an inert gas and containing a tungsten wire filament that is energized by a DC electric current (*Figure 3.8*). The bulbs produce a tremendous amount of heat and light, but the light accounts for only 5 to 10 percent of their energy output. The colour temperature and luminance of these lamps varies with the applied voltage, but average values range from about 2200 K to 3400 K.

Figure 3.8 Tungsten Halogen Lamp 500 W

- **Polycrystalline photovoltaic module (Solarex SX-20)**

SX-20 modules are part of Solarex's new SX™ module series, with 36 polycrystalline cells in series. In *Figure 3.9* we can see the PV used for the experiments.

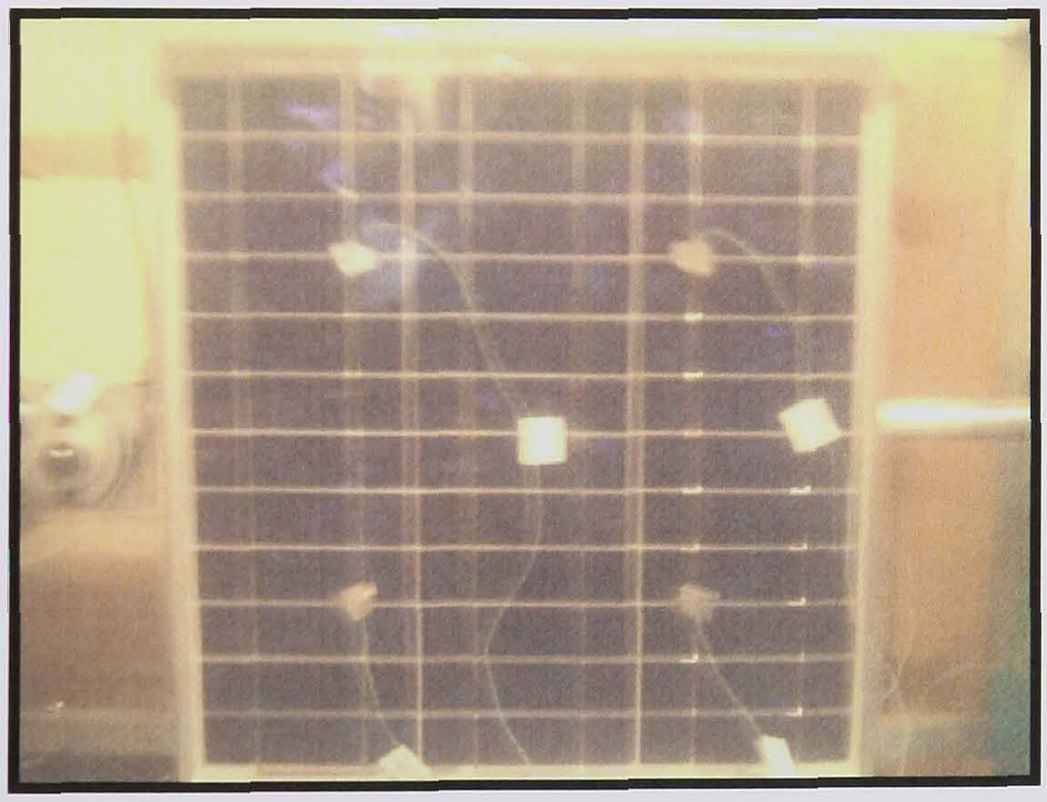

Figure 3.9 SX-20 PV Module

With square corners, Solarex's polycrystalline solar cells fill the module surface with active photovoltaic area.

Solarex's materials are:

• Cell strings laminated between sheets of ethylene vinyl acetate (EVA) and tempered glass;

• Tempered glass superstrate is highly transmissive (low iron content);

• Clear anodized frames are strong, corrosion resistant;

Module type: SX-20

Normal peak power (P_{max})	20 W
Peak power voltage (V_{mp})	16.8 V
Peak power current (I_{mp})	1.19 A
Short circuit current (I_{sc})	1.29 A
Open circuit voltage (V_{oc})	21 V
Minimum power (P_{min})	18 W
Nominal Cell Operating Temperature (NOCT)	48 °C
Temperature Coefficient (I_{sc})	(0.065+-0.015) %/°C
Temperature Coefficient (V_{oc})	- (80+-10) mV/°C
Temperature Coefficient for Power	- (0.5+-0.05) %/°C

Power specifications measured at standard test conditions, insolation of 1000 W/m^2, AM 1.5, 25 °C cell temperature. Module certified to CEC Specification 503.

From this information we can found the fill factor (F) from equation (2.4.2):

F = 0.73798

- **Instruments to measure the temperature (Data-logger DT500 and Thermocouple K Type)**

To measure the voltage, current and temperature of the PV a DataTaker (DT500) was used. The thermocouples were K type with accuracy of +- 1.5 °C or 0.004xT, where T was the real temperature. The thermocouples were calibrated inside a water bath with controlled water temperature and the relative errors were within +-1% of °C. In the experiments 12 thermocouples were placed on the front and 4 on the back of the PV in equal spaced distances in order to take measurements.

- **Measurement of light intensities**

The CM3 pyranometer (*Figure 3.10*) is an instrument for measuring solar irradiance with sensitivity of 15.36*10^{-6} V/Wm^{-2}. The sensor construction is such that it measures

the solar energy that is received from the whole hemisphere (2π degrees field of view). The output is expressed in Watts per metre square.

Because of the fact that it has a flat spectral sensitivity from 305 to 2800 nm, its calibration is valid for natural sunlight and for most types of artificial light (Xenon lamps, Halogen lamps).

Figure 3.10 CM3 Pyranometer (www.campbellsci.com)

In order to achieve a uniform level of radiation on the PV module, the calibration of the solar simulator was required. The distance between the lamps and the test area can be varied by adjusting the distance between the lights and the PV frame.

The distance between the solar simulator and the PV module was varied for the experiments in order to obtain the values of 1000, 800 and 600 W/m^2. In *Figure 3.11* a, b and c can be seen the three irradiance level that was chosen for the experiments. These values were chosen because are being used from many other researchers and are average irradiance of many areas in the world.

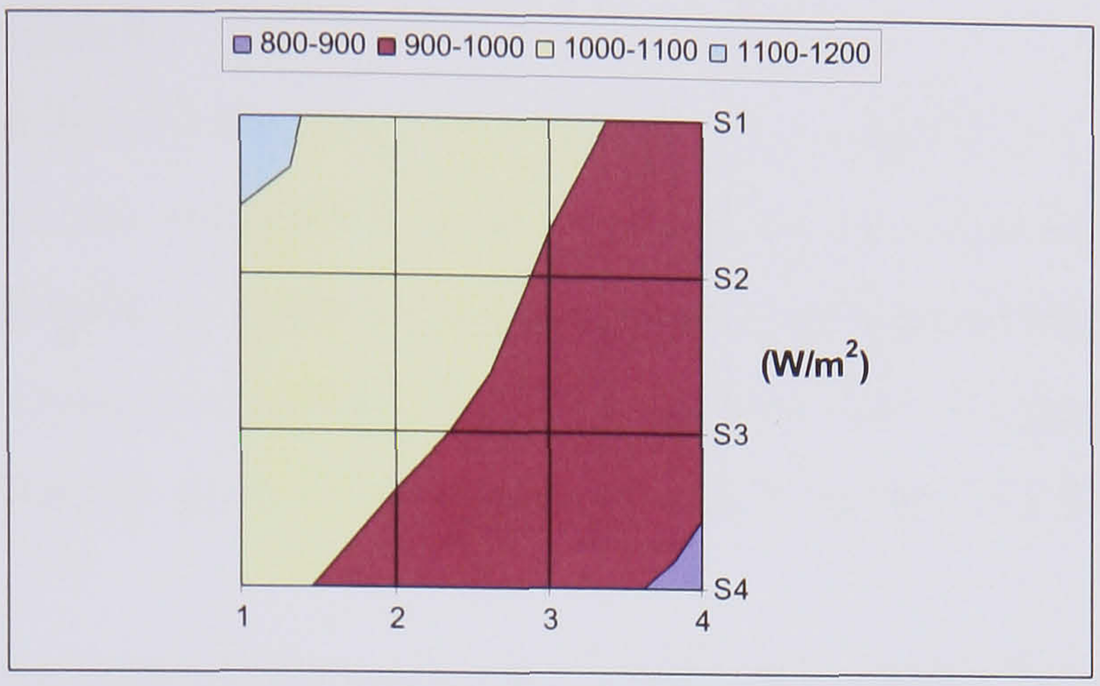

Figure 3.11a Irradiation map of the PV module – I_{av} = 993 W/m^2

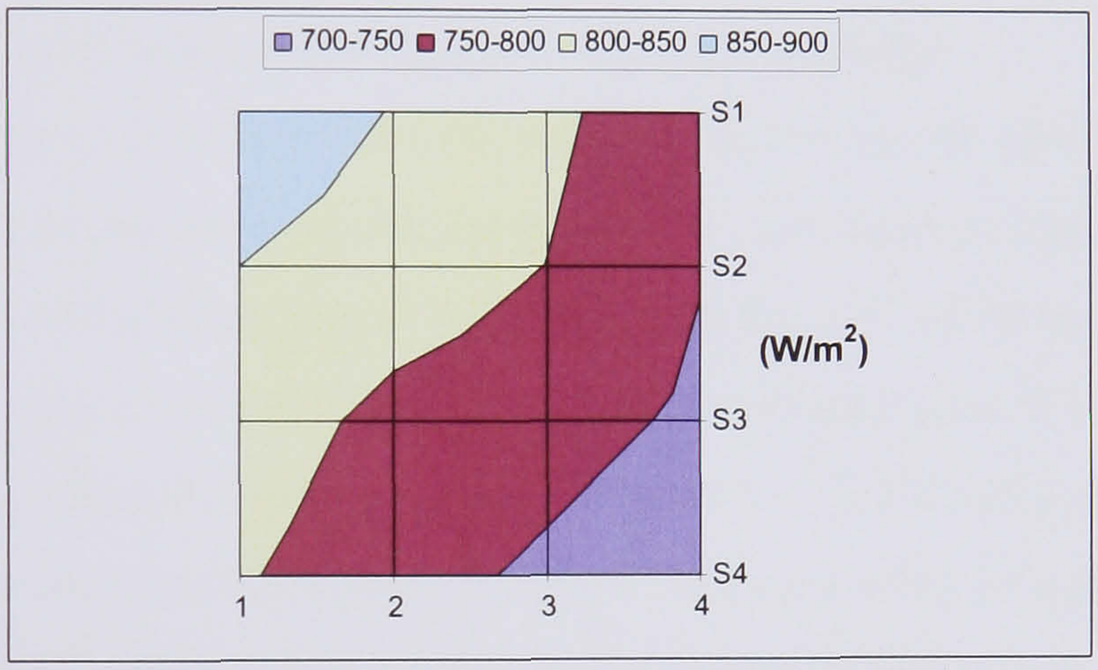

Figure 3.11b Irradiation map of the PV module – I_{av} = 788 W/m^2

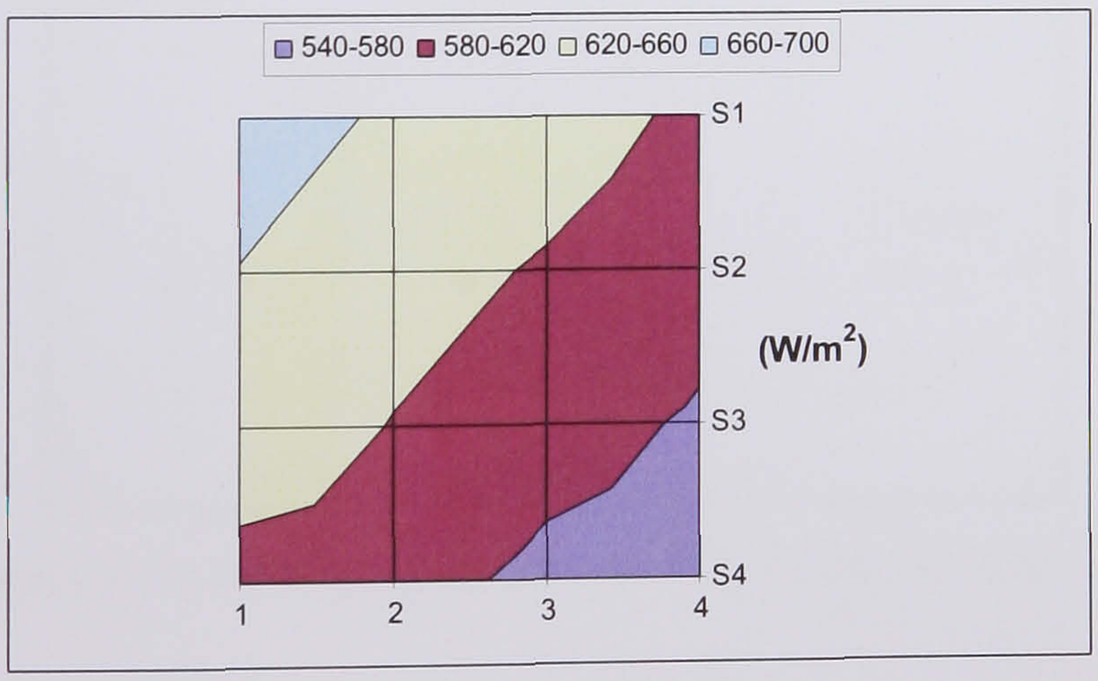

Figure 3.11c Irradiation map of the PV module – I_{av} = 581 W/m^2

3.7 Experimental work

As discussed in section 3.4 the most important characteristics of a PV system are the short circuit current, the open circuit voltage, the maximum current and voltage. From these values it is possible to find the maximum power and the efficiency of the PV.
An important performance characteristic of PV systems is the relationship between power output, efficiency, open circuit voltage and short circuit current with the cell temperature.
The objective of the experiments was to quantify this relationship by plotting all these outputs against the temperature of the photovoltaic module. This was done by irradiating the test panel and measuring its temperature over a series of time steps as the temperature of the cell increased towards the equilibrium value.
The electrical parameters were evaluated using an electric circuit shown in *Figure 3.12*. For measurements of the short circuit current I_{sc}, we have used an ammeter with a small internal resistance and a measuring error of 0.2%. In the case of the open circuit voltage V_{oc} measurements the error was 0.06%. A decade resistance class 0.1 was used as a load resistance R_L, changing from 0.1 Ohm to 10 kOhm. A PV cell may be represented by the equivalent circuit model shown in *Figure 3.11* consisting of a photon current source (I_L), a diode, a series resistance (r_s), and a shunt resistance (r_{sh}).

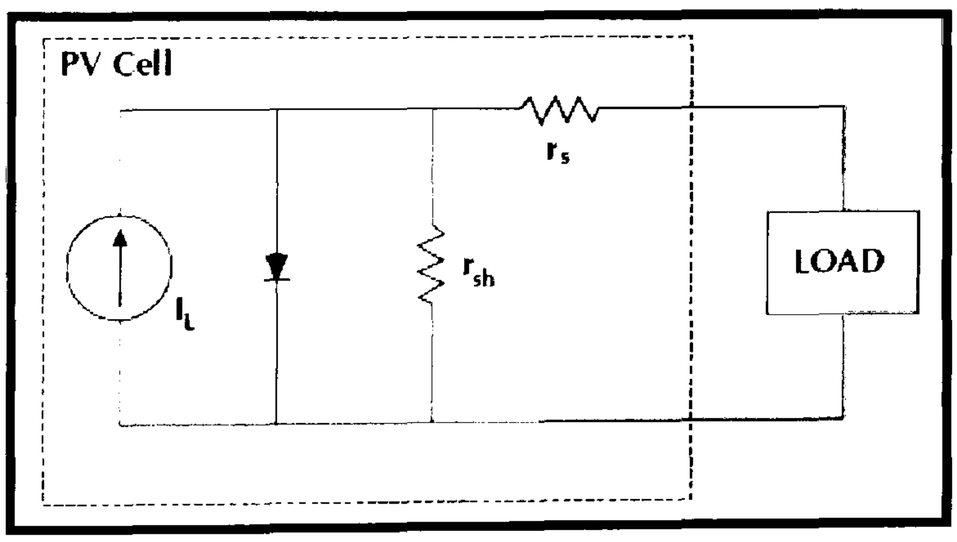

Figure 3.12 Equivalent circuit model of a photovoltaic cell

3.7.1 PV Performance with uninsulated model

The first set of experiments was to find the maximum current, voltage and power of the PV. The experiment took 3 hours to bring the PV temperature in equilibrium and then to

adjust the load in order to take the required measurements. *Figure 3.13* and *3.14* shows the P-V and I-V curve for 3 different levels of irradiance and from this found out the P_{max}, V_{mp}, I_{mp}, V_{oc} and I_{sc}. The values can be seen in *Table 3.1.* The solar cells performance by means of solars simulators like tunghsten lumps always face a problem causing errors due to source spectral irradiance mismatch and cell spectral response mismatch. Seaman (1982) derived an expression to enable the calculation of mismatch error.

Table 3.1 Values of P_{max}, V_{mp}, I_{mp}, V_{oc} and I_{sc} for 1000, 800 and 600 W/m^2

Irradiance	993 W/m^2	788 W/m^2	591 W/m^2
Pmax (W)	6.39	5.16	4.00
Imp (A)	0.467	0.365	0.280
Vmp (V)	13.685	14.136	14.282
Voc (V)	17.547	17.839	18.054
Isc (A)	0.510	0.405	0.311
Fill Factor	0.7140	0.7142	0.7124
Electrical Efficiency (%)	4.02%	4.09%	4.23%

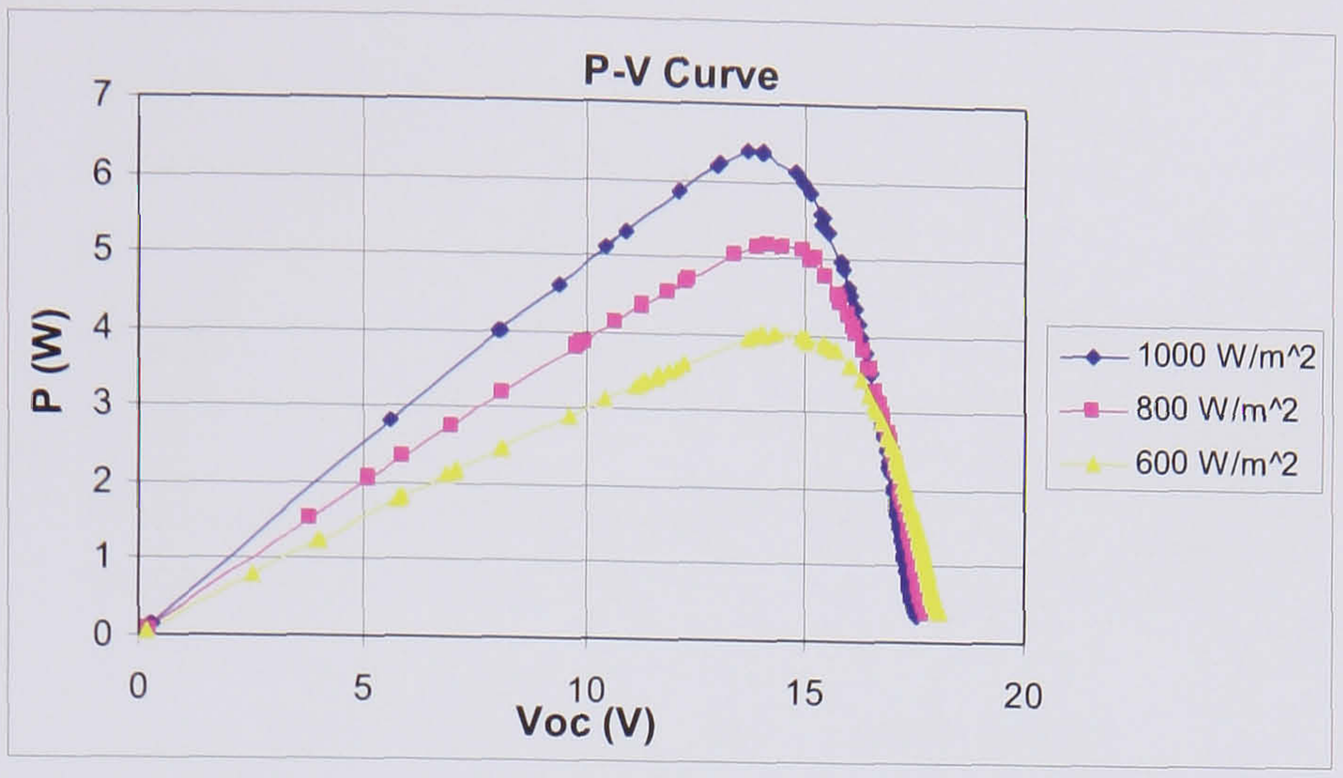

Figure 3.13 P-V Curve of the PV module

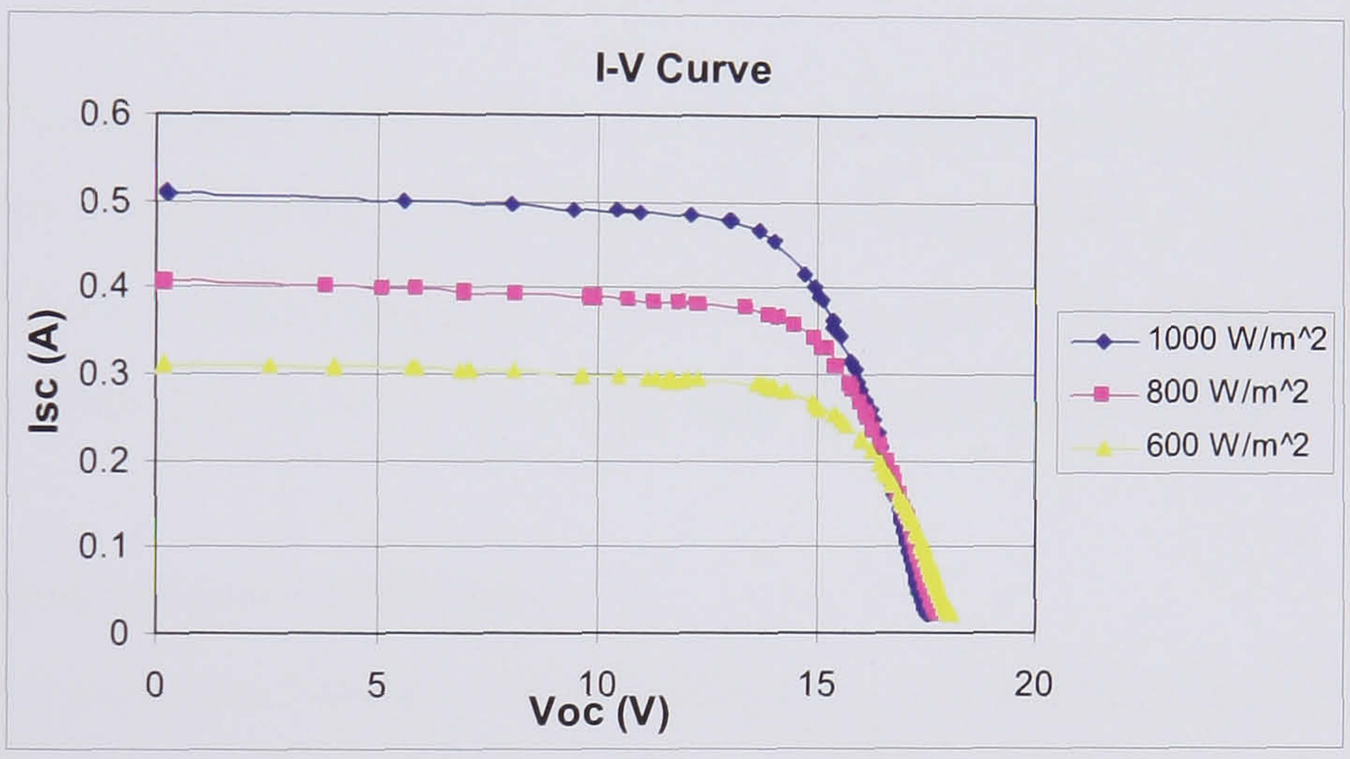

Figure 3.14 I-V Curve of the PV module

The PV temperature of the three set of experiments as shown in *Figure 3.15* were found to be 66 °C, 58 °C and 50 °C for 1000, 800 and 600 W/m^2 after the system reached equilibrium. The ambient temperature was about 19 °C for the three experiments. The variation in the PV temperature in the 800 irradiation was caused of a variation in the irradiance.

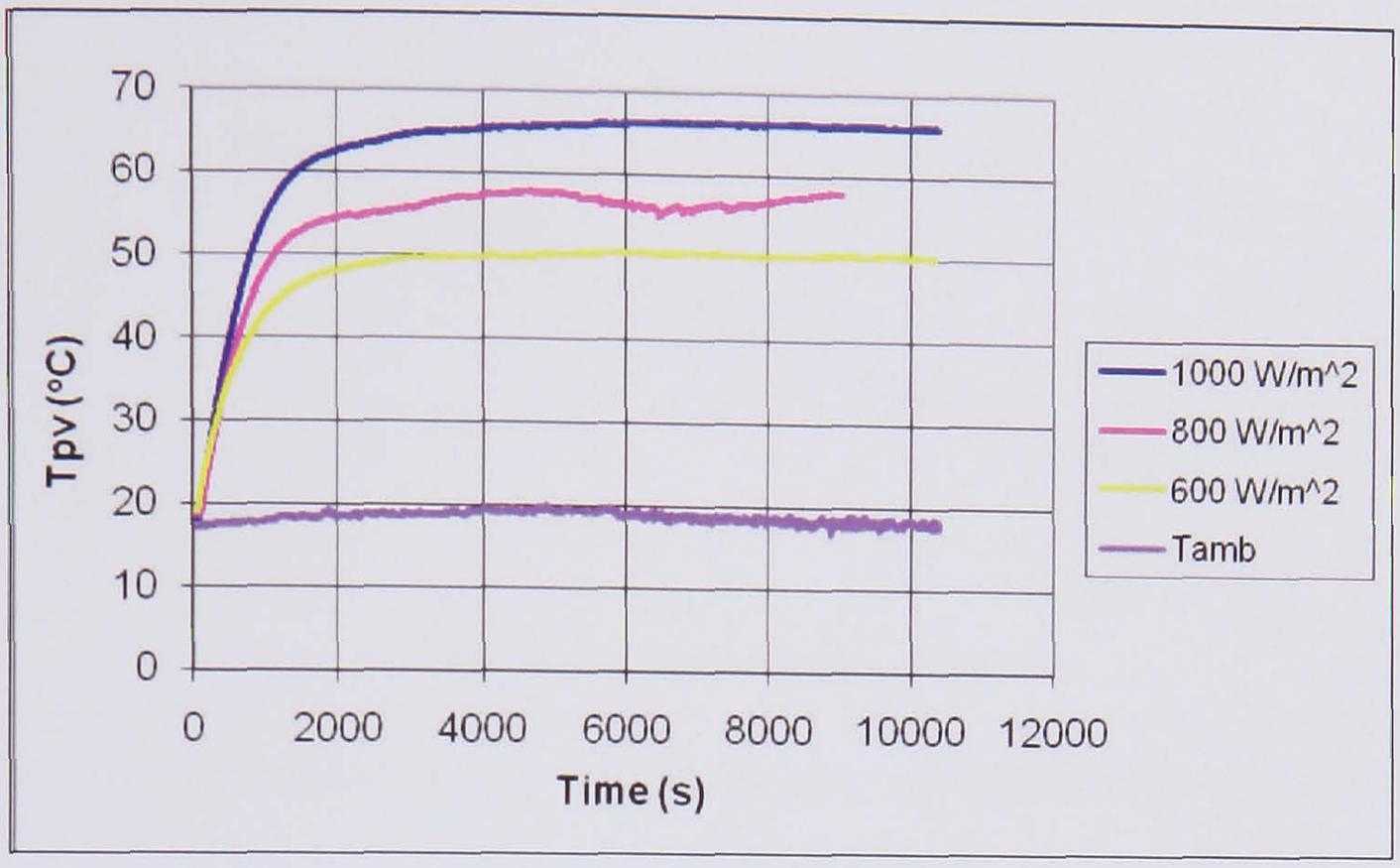

Figure 3.15 PV Temperatures for 1000, 800 and 600 W/m^2

As mentioned in section 3.6 because the spectral distribution of the artificial light is not the same as that of the natural light we have to find out the new I_{sc}, V_{oc}, power, efficiency, fill factor and temperature coefficients for the PV. So the next set of experiments was to find these values with a light intensity of 1000 W/m^2.

3.7.1.1 V_{oc} Temperature Coefficient

As temperature increases the open circuit voltage (V_{oc}) decreases. PV cells therefore have a negative temperature coefficient of V_{oc} (β). *Figure 3.16* shows a graph of open circuit voltage V_{oc} against the temperature difference taken between the PV and the reference temperature of 25 °C satisfying the following equation:

$V_{oc} = V_a*(1+\beta*(T_{PV}-T_{ref}))$ Eq. (3.1)

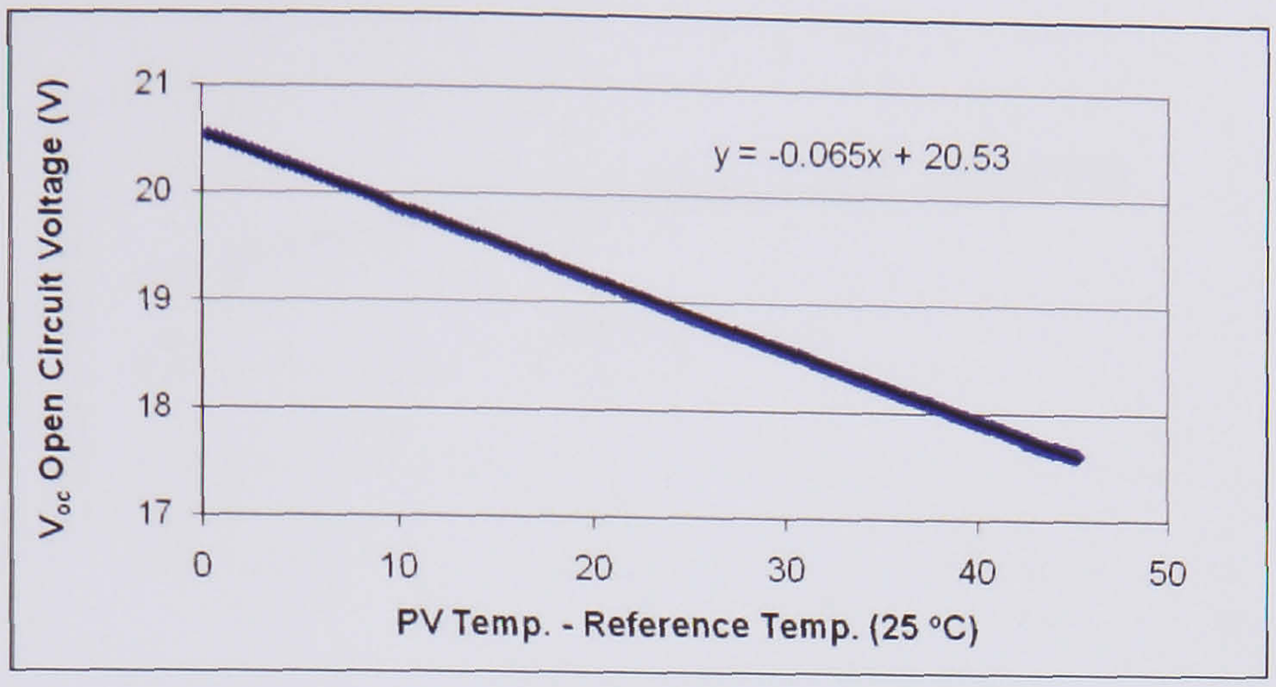

Figure 3.16 Open Circuit Voltage V_{oc} Vs Temperature Difference of PV with 25 °C Reference Temperature

From *Figure 3.15* it may be seen that the voltage temperature coefficient is - 0.065 V/°C and the V_{oc} voltage is 20.53.

3.7.1.2 I_{sc} Temperature Coefficient

A larger photocurrent results in I_{sc} increase for a given insolation, and PV cells have a positive temperature coefficient of Isc (α). The Isc vary with temperature as shown from the following equation:

$$I_{sc} = I_a*(1+\alpha*(T_{PV}-T_{ref})) \qquad \text{Eq. (3.2)}$$

In the *Figure 3.17* it may be seen that the short circuit current is 0.0009 A/°C and the I_{sc} is 0.4727 A. The I_{sc} is different from manufacturers' specifications because of the tungsten halogen spectral irradiation is not the same as natural light.

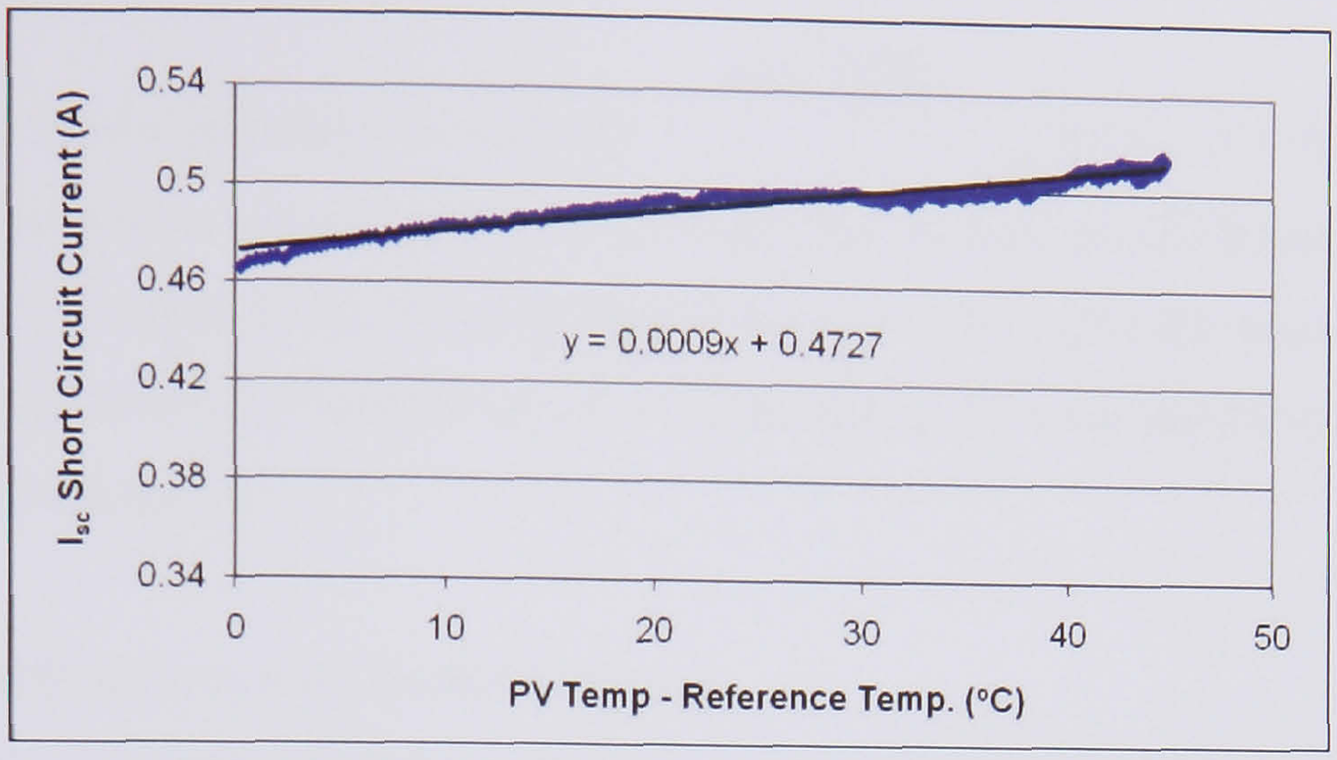

Figure 3.17 Short Circuit Current Isc Vs Temperature Difference of PV with 25 °C Reference Temperature

3.7.1.3 Power Temperature Coefficient

Using a similar equation as in sections 3.7.3 and 3.7.4 the power is being affected by the PV temperature:

$P_{max} = P_a*(1+ (\alpha+\beta)*(T_{PV}-T_{ref}))$ Eq. (3.3)

From *Figure 3.18* the given values are – 0.0145 W/°C and 6.977 W so we have a reduction of 0.208 %/°C.

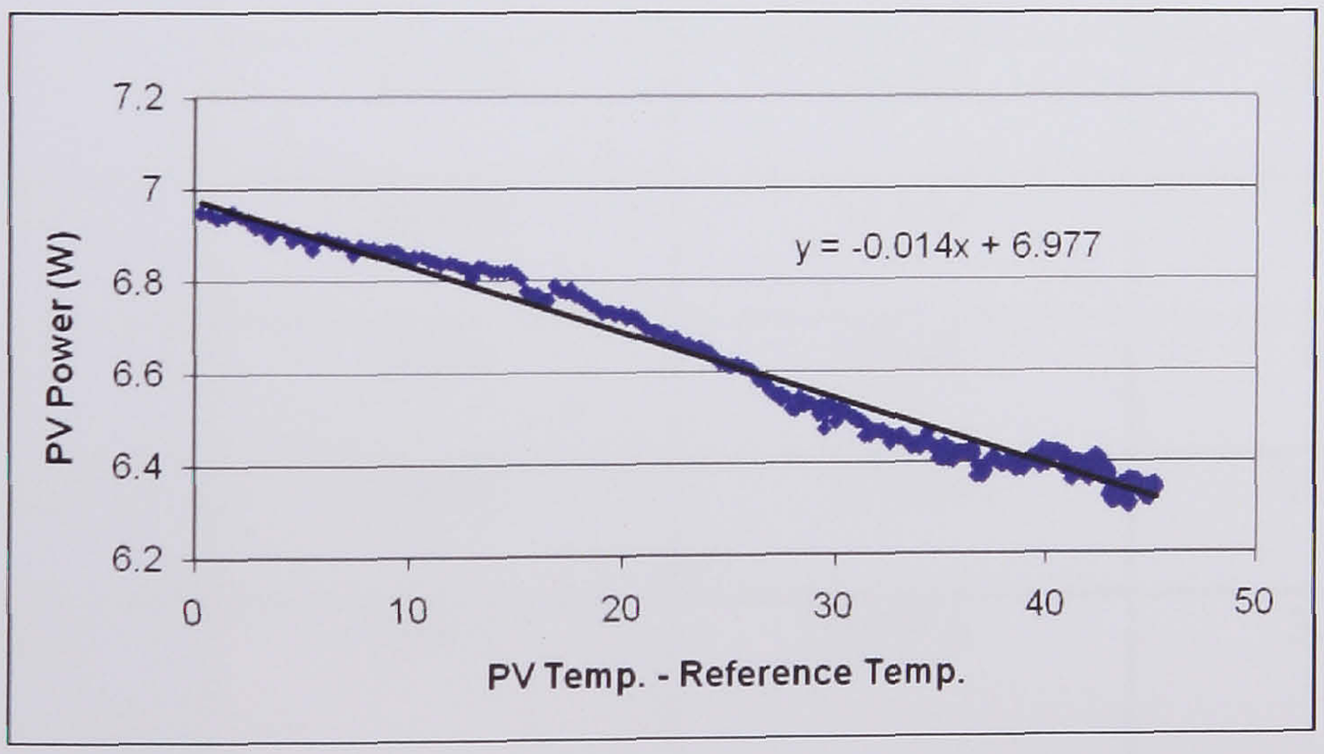

Figure 3.18 PV Power Vs Temperature Difference of PV with the Reference Temperature

The new Fill Factor according to equation $FF = \frac{P_{max}}{V_{OC} I_{SC}}$, is FF = 0.7135 that is less than the manufacturer value of 0.7379. The closer the value of the fill factor is to unity, the better the operation of the PV-cell. The fill factor is lowered by the ohmic resistance of the cell. Also when the temperature of a cell increases, both the short-circuit voltage and fill factor decrease.

3.7.2 PV Performance with insulated model

The same set of experiments was undertaken as in section 3.7.1 but this time insulation with thermal resistance of 0.35 (m^2K/W) was placed in the PV rear surface. *Figures 3.19* and *3.20* show the P-V and I-V curve and in *Table 3.2* present the values for the P_{max}, V_{mp}, I_{mp}, I_{sc}, V_{oc} and FF at different insolation levels.

Table 3.2 Values of P_{max}, V_{mp}, I_{mp}, V_{oc} and Isc for 1000, 800 and 600 W/m^2

	1006 W/m^2	**799 W/m^2**	**597 W/m^2**
Pmax (W)	**6.25**	**5.03**	**3.82**
Imp (A)	**0.4772**	**0.3769**	**0.2792**
Vmp (V)	**13.100**	**13.361**	**13.691**
Voc (V)	**16.821**	**17.234**	**17.468**
Isc (A)	**0.531**	**0.414**	**0.311**
Fill Factor	**0.6997**	**0.7049**	**0.7031**
Electrical Efficiency (%)	**3.88%**	**3.93%**	**3.99%**

As discussed in section 3.4 the insolation level affects the power, current and voltage as see from the *Figures 3.18* and *3.19* for the P-V and I-V curves.

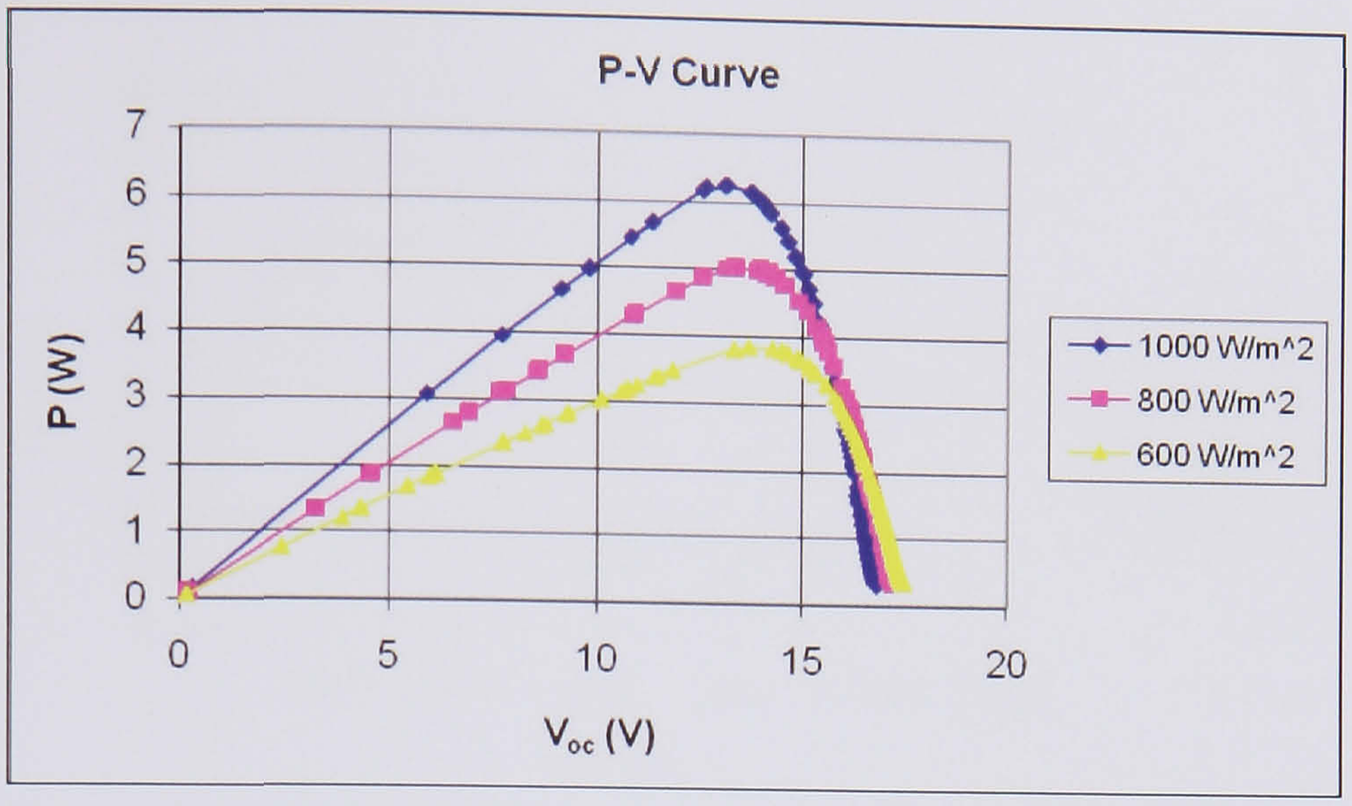

Figure 3.19 P-V Curve of Insulated PV

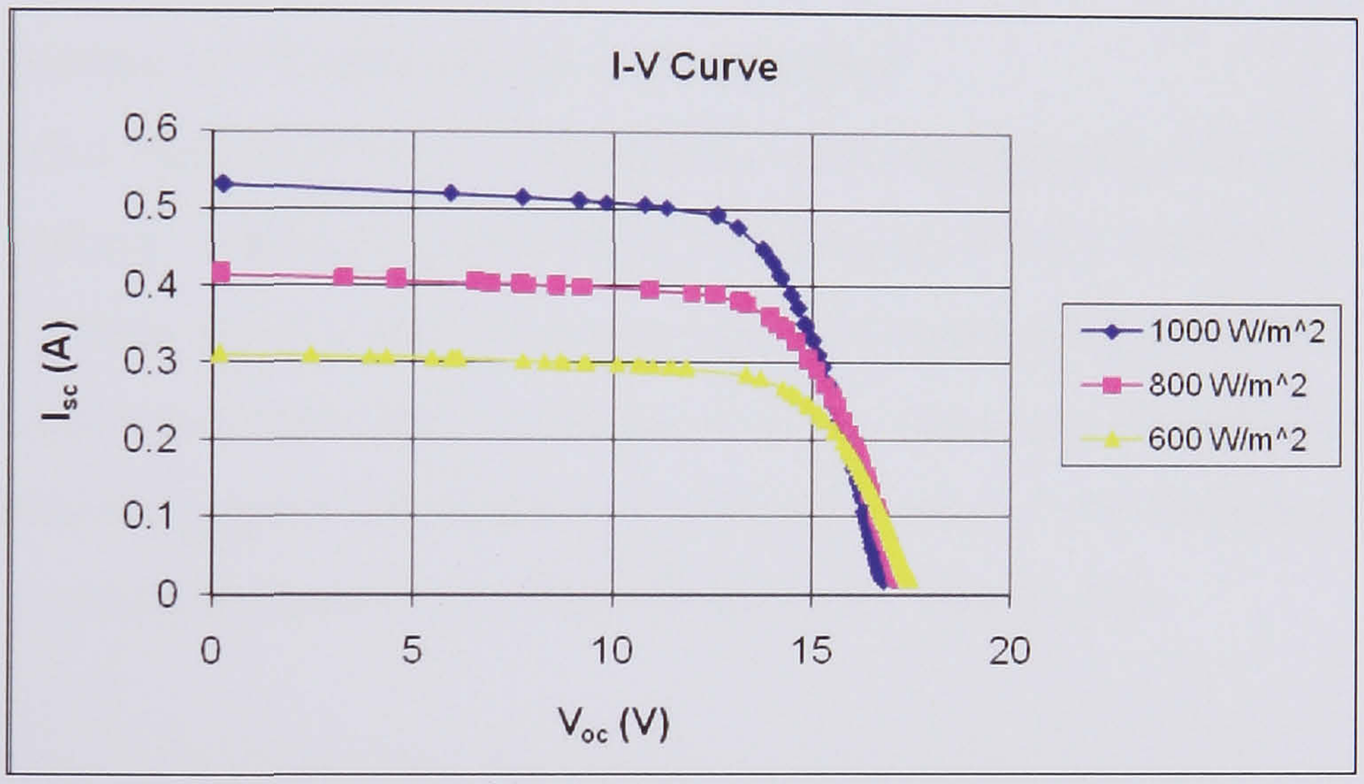

Figure 3.20 I-V Curve of Insulated PV

The maximum temperature achieved can be seen in *Figure 3.21* and was 78 °C, 68 °C and 60 °C for the 1000, 800 and 600 W/m^2 irradiance. The ambient temperature was around 19 °C and so a comparison between insulated and uninsulated panel will follow.

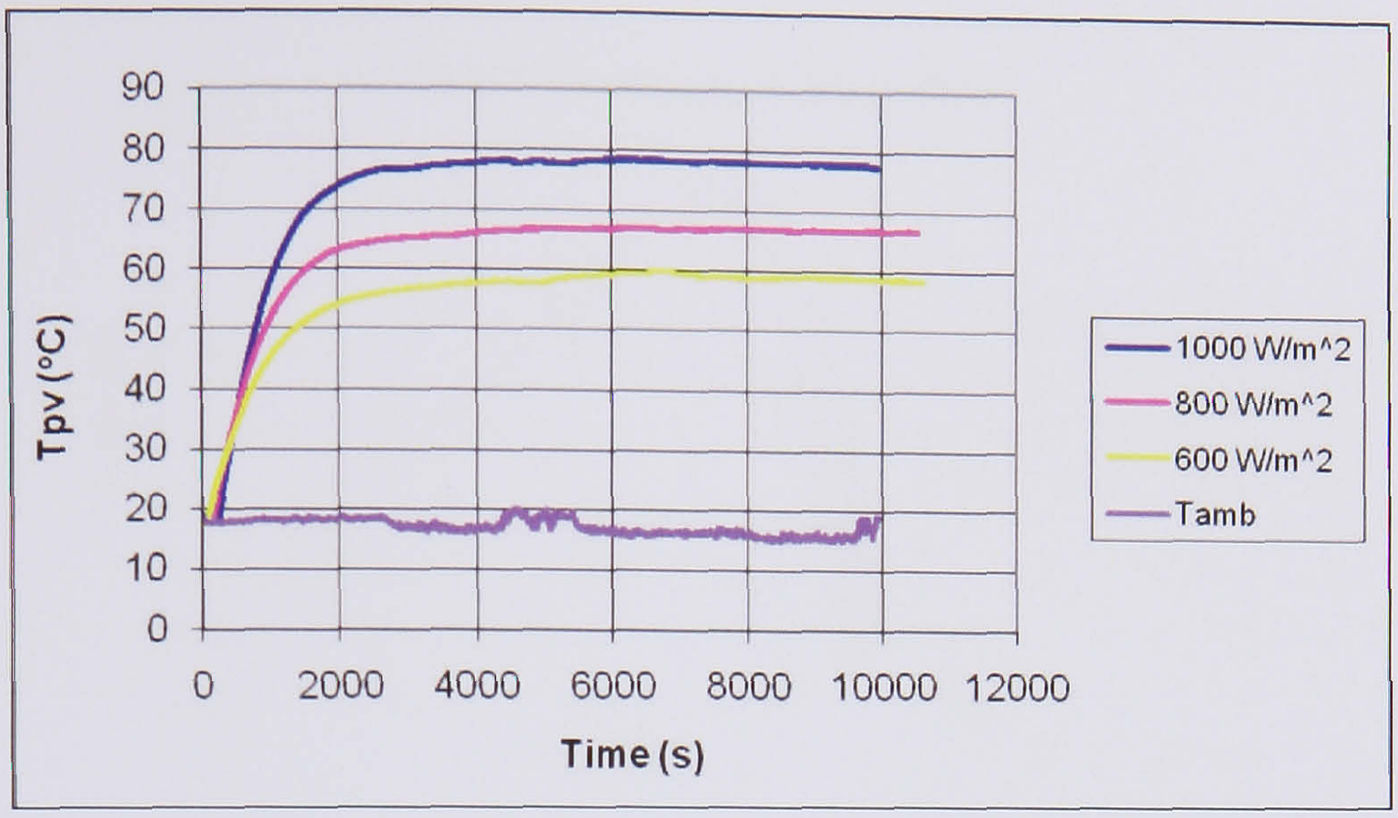

Figure 3.21 PV Temperatures for 1000, 800 and 600 W/m^2

3.7.3 Comparison of PV uninsulated with insulated

A more detailed analysis of the PV uninsulated or insulated can be seen in the next figures, by putting together in graphs the results from the PV for 1000 W/m^2. *Figures 3.22* and *3.23* show the P-V and I-V curve. In the I-V curve the increase in PV temperature decreases the voltage of the panel and increases the current, something that is being mentioned section 3.4. In the P-V curve the power of the panel decreases because the voltage decreases more than the increase of the current.

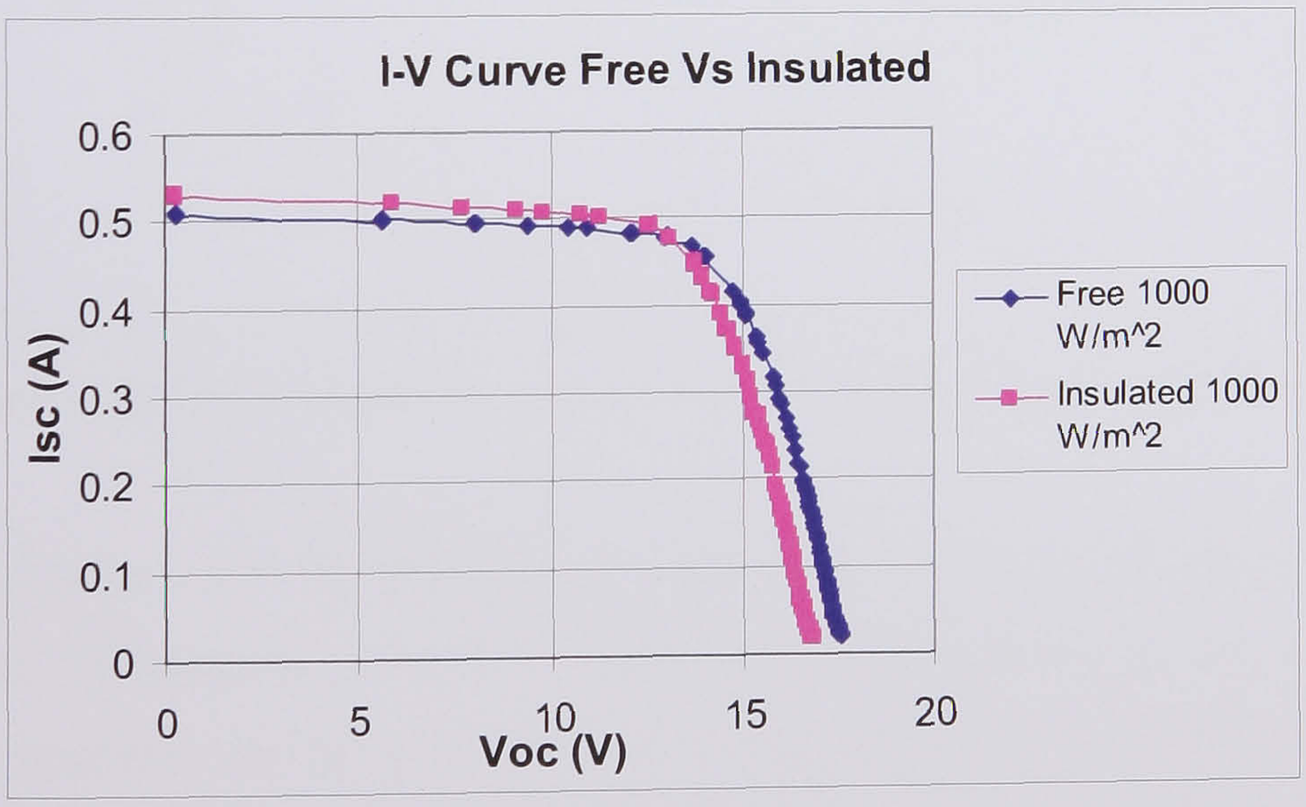

Figure 3.22 I-V Curve of PV Free Vs Insulated Panel

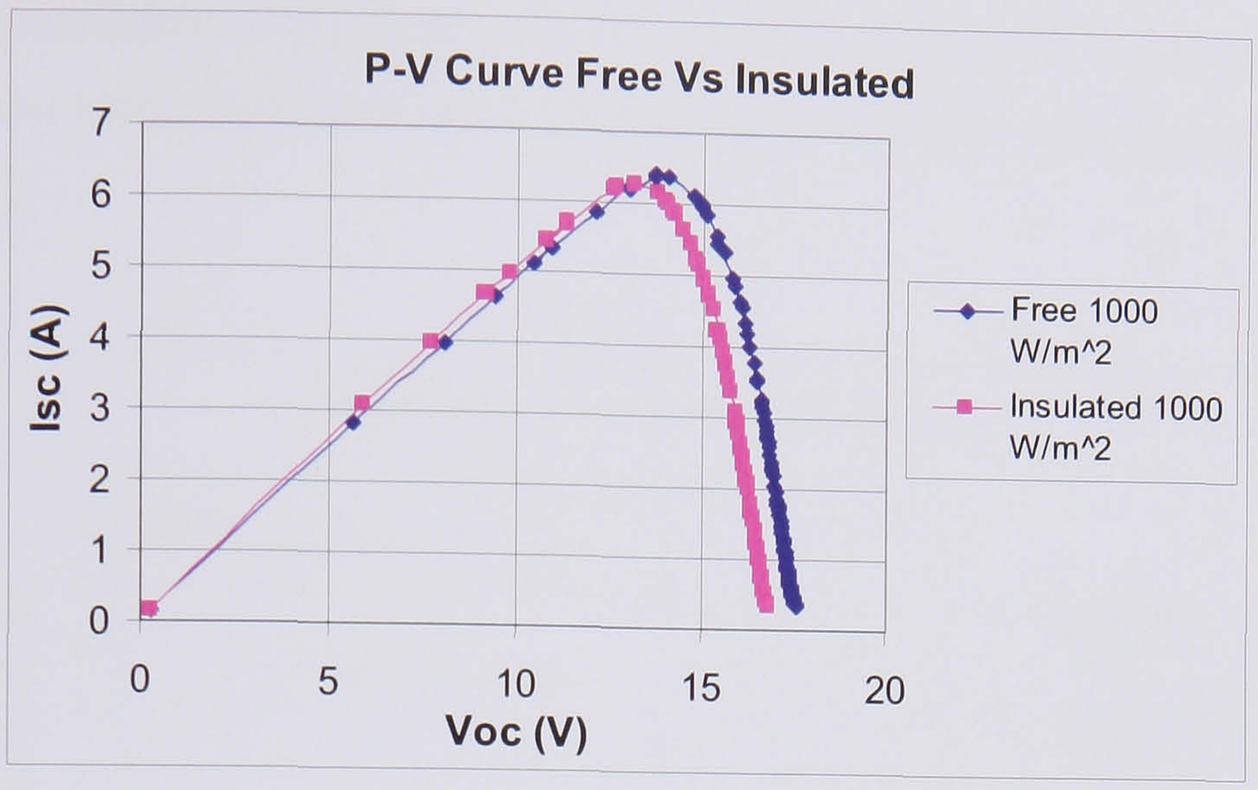

Figure 3.23 P-V Curve of PV Free Vs Insulated Panel

This temperature increase of the insulated PV panel compared to the free is in the range of 12 °C as seen from *Figure 3.24*.

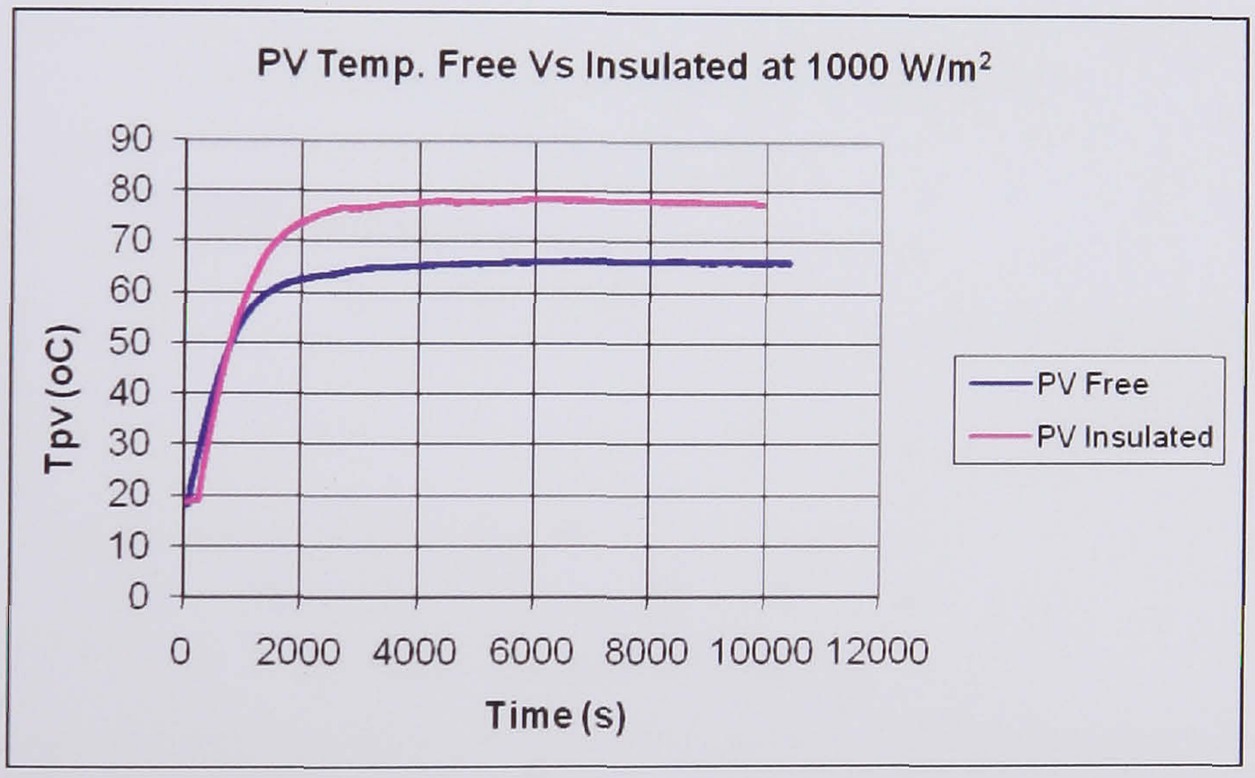

Figure 3.24 PV Temperature for Free and Insulated Panel at 1000 W/m^2

The new Fill Factor is FF = 0.7025 from 0.7135 in the uninsulated PV panel. The increase of the PV temperature by 12 °C caused this reduce in the fill factor.

From the experiments also the power and efficiency of the PV was plot in *Figures 3.25* and *3.26* by comparing uninsulated with insulated panel. From the two figures can be seen that the temperature effect the performance of the PV. The power and efficiency for the uninsulated are higher by 2.73% and 3.78% respectively. In the same time the

temperature coefficient of power from 0.0196 W/°C to 0.0315 W/°C and for electrical efficiency from 0.461 %/°C to 0.488 %/°C that agree with the manufacturers specifications.

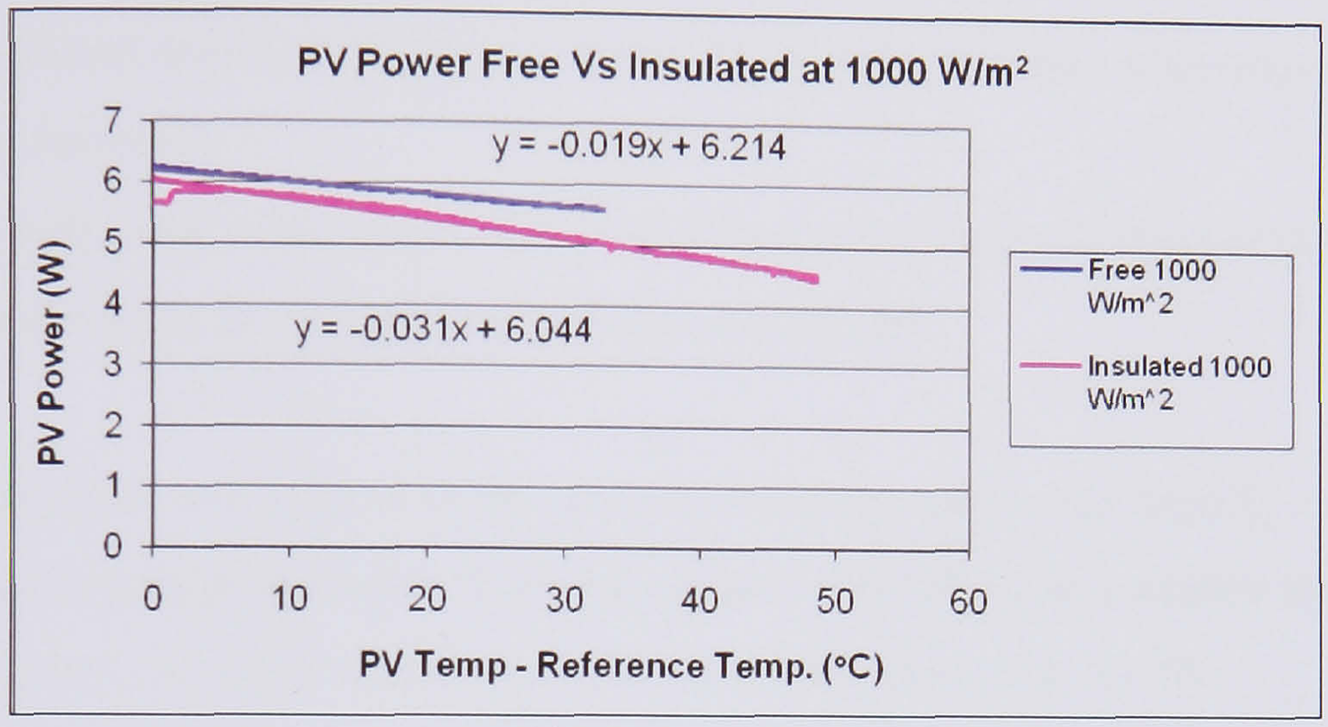

Figure 3.25 PV Power for Free and Insulated Panel at 1000 W/m^2

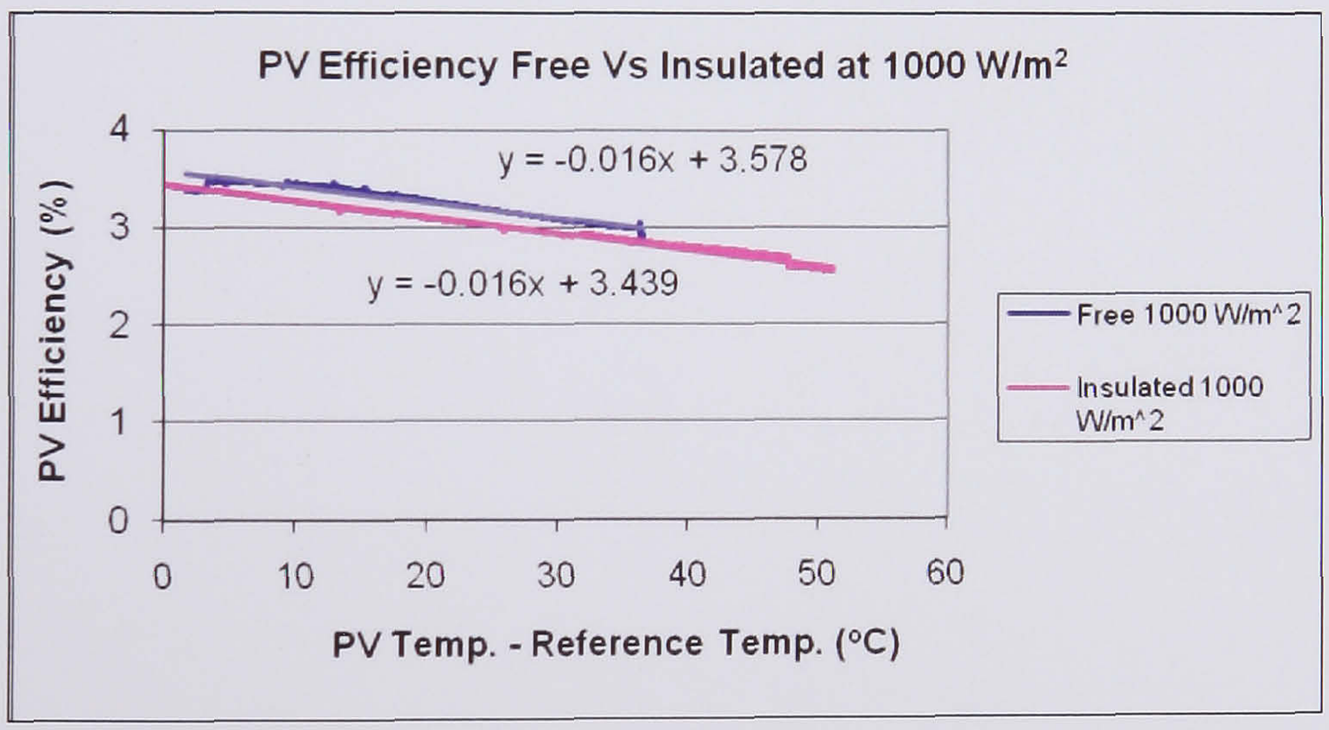

Figure 3.26 PV Efficiency for Free and Insulated Panel at 1000 W/m^2

3.8 Conclusion

In this chapter a series of experiments were undertaken with PVs panel rear being insulated and uninsulated. The aim was to observe the performance of the two PV models in relation with the temperature effect.

The findings from this study were:

- The short circuit current increases as temperature and insolation increases.

- Open circuit voltage decreases when insolation and temperature increase.
- Voltage temperature coefficient was in the range of the value given from manufacturer. Current temperature coefficient is less than the one given cause of the different spectral distribution of artificial light used for the experiments.
- Power and electrical efficiency of the PV decreases as the temperature of the cells increases
- When the rear of the panel is insulated then power and electrical efficiency underperform in comparison with the uninsulated.

These observations will help as in the next chapters to evaluate the ways to cool down the PV. The experimental results from this chapter will help us to compare the performance (i.e. electrical efficiency) of the PV/T systems with the PV.

CHAPTER 4: PHOTOVOLTAIC/THERMAL SYSTEM WATER

4.1Introduction

It is well known from theory and the experiments in chapter 3 that in the course of the conversion of solar energy into electrical energy in a photovoltaic cell, part of the photons' energy is converted into heat. In addition, the electrical efficiency of the photovoltaic panel depends on its temperature and this is reduced when the temperature increases. This is evident from equation (2.4.5), which demonstrates how the efficiency of photovoltaic cells depends on temperature (Duffie and Beckman, 1991, p. 777).

According to equation (2.4.5) the term μ is the temperature coefficient with unit %/°C indicating that each photovoltaic panel can produce not only electrical energy but thermal energy as well, when solar radiation falls on its panel.

The idea of improving the electrical efficiency, by reducing the photovoltaic collector temperature, as well as taking advantage of the thermal energy produced, constitutes the basic idea in the development of hybrid PV/T collectors.

This chapter has to do with the first try to cool down the PV by incorporating a heat extraction device in the rear of the PV. Two heat extraction devices were evaluated, the first being a serpentine tube adhered in a copper sheet and the second a rectangular tank creating a flow channel in the back of the PV. Both models used water as a heat transfer medium.

The models were experimentally tested in order to evaluate their electrical and thermal efficiency. For correctly evaluating the energy of performance of PV/T system three indicators were used i) the total energy efficiency, ii) the energy saving efficiency and iii) the exergy efficiency. Also a simulation was carried out using TRNSYS before the two experiments in order to evaluate how useful can be as a design tool.

The results from this chapter will help to compare the performance of this system, and work as a benchmark, to the new cooling approaches that are going to be introduced in the next chapters.

4.2 Aspects of the two PV/T water systems

As discussed in section 2.5 most of the water type PV/T models investigated consist of silicon PV modules with a heat extraction unit comprising a metallic sheet with pipes for water circulation, thus avoiding the direct contact of water with the PV rear surface. The heat exchanger is in thermal contact with the PV module rear surface and the back of the panel is thermally insulated. The useful heat that is provided from the PV/T systems makes them cost effective compared to separate PV and thermal units of the same total aperture surface area. *Figure 4.1* show a view of the PV/T water model that is going to be used for the simulation and experiments.

This section discusses some general requirements that a PV/T system should meet if both the thermal and photovoltaic components are to work efficiently in a combi-panel. The main requirements are:

- PV/T models may have a glass cover over the absorber to reduce the thermal losses. If such a cover is present, the collector is referred to as "glazed", otherwise as "unglazed". The terms "glazed" or "unglazed" therefore do not refer to the glass substrate that may be part of the PV/T absorber. In this case of using PV modules without additional glazing, satisfactory electrical output is expected. Between the choice of making a PV/T panel and a PV/T collector chose to construct a PV/T panel. This means that a common PV laminate used in the market will be used in order to create the PV/T model.

- In PV/T panel applications the production of electricity is the main priority, therefore it is more effective to operate the PV modules at low temperature in order to keep PV cell electrical efficiency at a sufficient level (PV/T Roadmap,).

- The heat transport medium that in this case is water does:
    - Have good heat transporting ability
    - Have good storage capacities
    - Be safe and cheap

- Whereas a PV module can reach about 90 °C under direct insolation in hot climates, the absorber of a thermal collector can reach temperatures of up to 220 °C, with a state of the art spectrally selective coating. A PV/T absorber using standard PV cells will reach temperatures of up to about 150 °C. The solar cells can withstand temperatures around 220 °C without any problem. But most encapsulation materials used for PV-modules cannot withstand these high thermal collector temperatures. Ethylene vinyl-acetate for example oxidises faster at high temperatures and solar irradiation (UV-radiation) than at lower temperatures. The maximum temperature for most polymeric encapsulation materials is around 100 °C and so this will be the maximum allowable temperature for PV/T panel.

- Absorptance of absorber (front surface of the PV cells). The absorber (PV cells) coefficient of absorptance influences the optical efficiency of the collector. By having a higher coefficient of absorptance, the PV/T panel will be more efficient. Coefficients of absorptance for crystalline Si solar cells are satisfactory, at approximately 0.9.

- Emittance of the absorber (front surface of the PV cells). The absorber (PV) coefficient of emittance affects the heat loss coefficient of the collector. In this sense, by having lower coefficient of emittance, the collector is more efficient. The coefficient of emittance for crystalline Si solar cells is approximately equal to 0.9 (as for black paint).

- Quality of the thermal contact between the PV cells and the absorber. The thermal contact between the PV cells and the absorber is essential for PV/T collectors to improve the thermal yield. A high conductance thermal paste of 3 W/m*K thermal conductivity was placed between the PV laminate and the copper plate absorber in order to increase the heat transfer.

- Rear insulation thickness. The thickness of the insulation to the rear of the panel influences heat losses at operating temperatures higher than ambient temperature. An insulated material of thermal resistance 0.35 m^2K/W was used in the back of the PV in order to reduce heat losses.

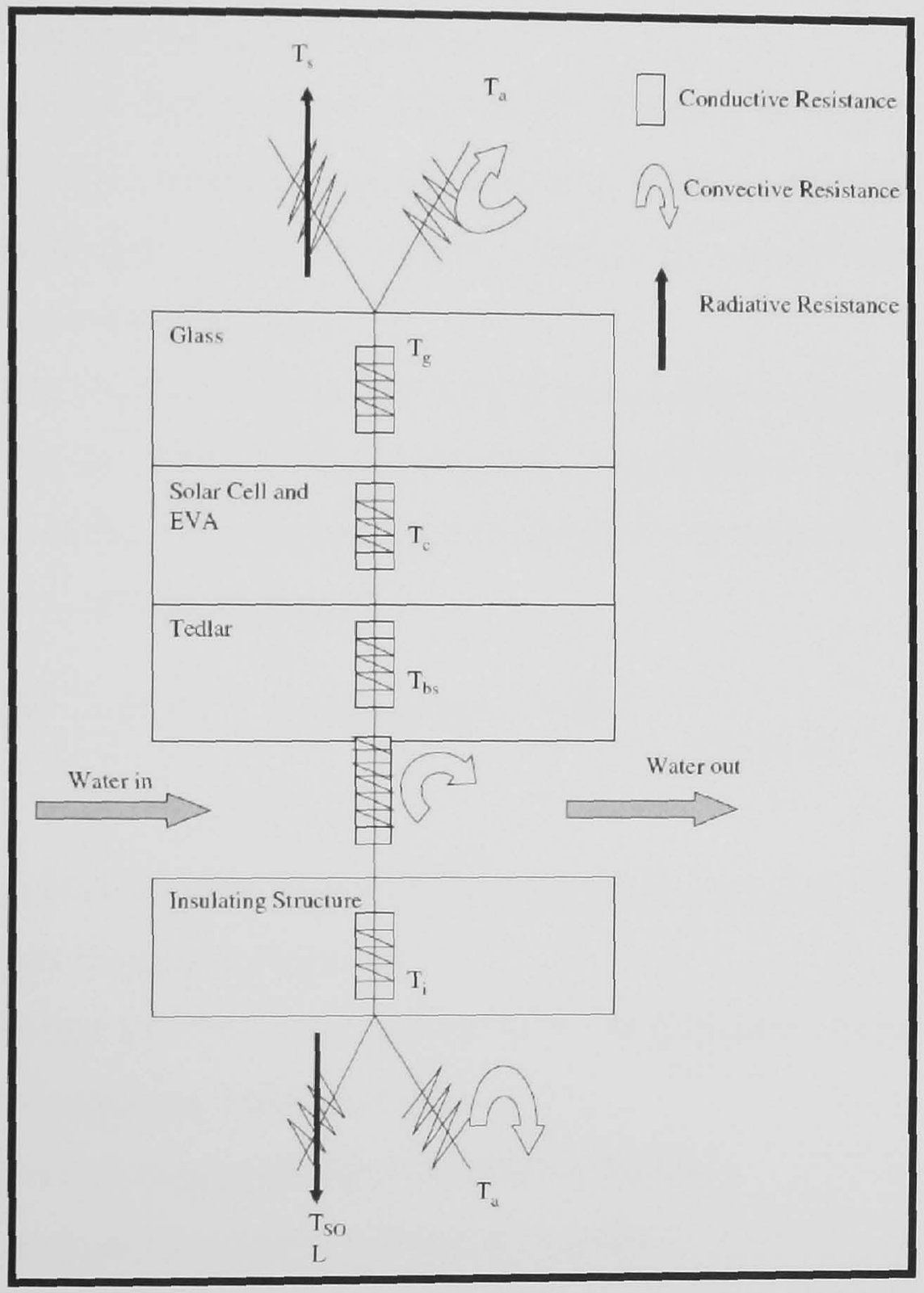

Figure 4.1 PV/T model heat balance model (Tiwari, 2006)

4.3 Theoretical model of the PV/T panel

Collector thermal performance is usually described by the useful heat output as a function of input radiation and collector operating temperature relative to its surroundings. When the equation of the performance curve is known for a specific solar collector, the system designer has the information needed to employ any of several recognized computational techniques to predict the daily, seasonal, or annual energy

output of the collector under the anticipated use conditions of the system being analyzed. The analytical derivation of this efficiency is briefly reviewed in section 2.3.3 expressed by Hotel-Whillier-Bliss (HWB). Figure 4.1 illustrates in detail the different conductive, convective and radiative resistances that exist in an unglazed PV/T model.

4.3.1 The PV/T panel performance equation

The analysis of the PV/T collector starts with the calculation of its characteristic parameters. This is achieved using the equations that refer to flat plate thermal collectors. The equations are modified in order to include the energy conversion process resulting from the addition of the PV.

In order to characterize the performance of a PV/T solar collector properly, an energy balance must be performed which considers all the energy flows to and from the collector (Bosanac, 2003). For a typical glazed flat-plate solar collector with PV cells as absorber, this balance may be expressed as

$$q_{useful} = q_{solar} - q_{loss} + q_{heatcapacity} - q_{el} \qquad \text{Eq. (4.1)}$$

where

q_{useful} = the rate at which useful energy is delivered to the heat transfer fluid

q_{solar} = the rate of solar radiation absorbed

q_{loss} = the rate of energy loss from the collector to the environment caused by convection, infrared radiation, and conduction

q_{el} = the rate of electrical energy extracted from the collector

$q_{heatcapacity}$ = the rate of energy storage within the collector

The q_{solar} term is a function of the optical properties of the collector cover plate and absorber surface (PV-cells). The q_{loss} term depends upon how well the collector is thermally isolated from its surroundings. $q_{heatcapacity}$ is a function of mass and type of materials used in the collector.

As the temperature of the collector's thermal mass increases or decreases during the day, energy is stored or released. In the most cases, collector heat capacity effects can be

neglected, yielding in quasi-steady-state conditions and simplified form of equation (Bosanac, 2003):

$$q_{useful} = q_{solar} - q_{loss} - q_{el}$$ Eq. (4.2)

The collector thermal output, q_{useful}, may be represented graphically by a second order curve as shown in *Figure 4.2*. The ordinate intercept of the curve equals the maximum output, which is achieved when the collector is delivering energy at the ambient temperature. The unavailable portion of the energy falling on the collector is that which is reflected from the cover plate or absorber, or absorbed by the cover plate.

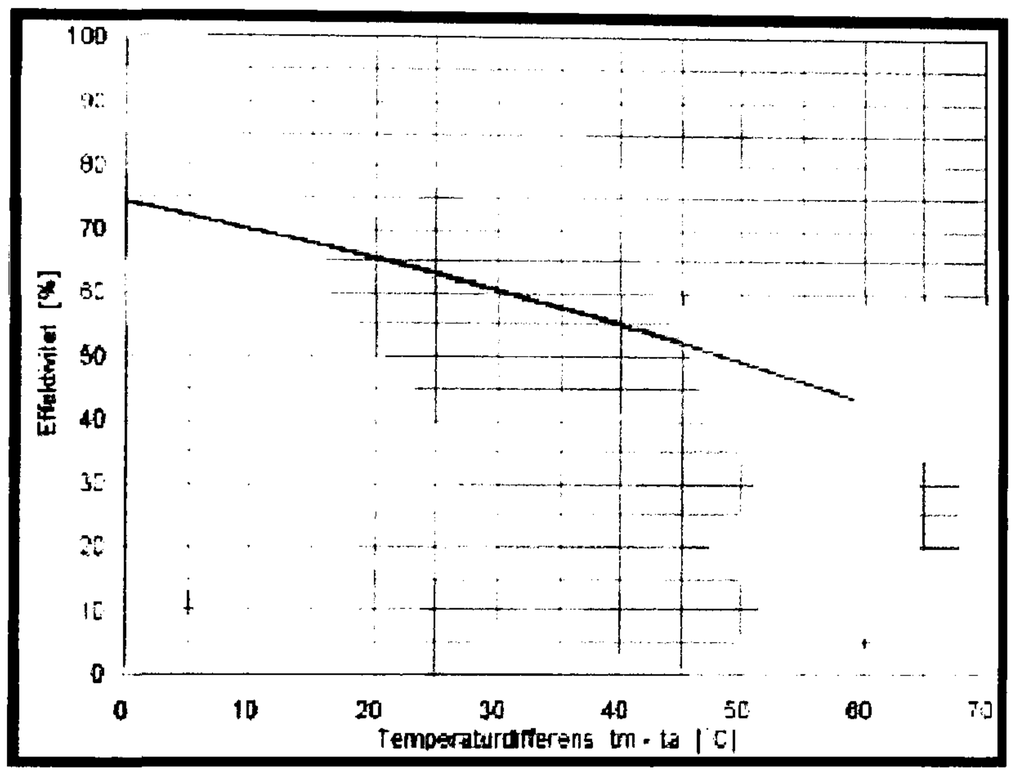

Figure 4.2 PV/T Thermal Performance with respect to temperature difference of PV with ambient (Bosanac, 2003)

As useful heat is removed from the collector at higher temperatures the efficiency decreases, since losses from the absorber increase in proportion to its temperature above its surroundings. Radiation accounts for a significantly greater proportion of the losses at elevated operating temperature from some collectors than the others. A second or higher order efficiency equation is often used to describe the performance of collectors in which radiation causes significant heat loss at higher operating temperatures.

4.3.2 Energy into the PV/T panel

The net rate of solar radiation absorbed by a collector, q_{solar}, is a function of the radiation on the cover plate and the optical and radiative properties of the materials constituting the cover plate and absorber. Since no real glazing material is perfectly transparent, part of the radiation incident on the cover is absorbed part is reflected by the glazing material and part is transmitted through the cover. The transmitted fraction is partly absorbed by the absorber and partly reflected back toward the cover; this reflected radiation is again partly transmitted through the cover, partly absorbed by it, and partly reflected back to the absorber. The result of this multiple absorption, reflection, and transmission fraction of that radiation is ultimately absorbed by the collector.

The parameter that quantifies the capability of the collector to absorb solar radiation is called the effective transmittance-absorptance product, $(\tau\alpha)_e$. The description "effective" is important while the energy absorbed is primarily a function of τ, the transmittance of the glazing, and α, the absorptance of the absorber plate surface, the complex interactions discussed above modify the product $(\tau\alpha)_e$, in complex ways, particularly in collectors that have two or more glazing layers. Using $(\tau\alpha)_e$, the net rate at which incoming solar energy absorbed by a collector may be expressed as (Bosanac, 2003)

$$q_{solar} = G A_a (\tau\alpha)_e \qquad \text{Eq. (4.3)}$$

where G is the total incident radiation per unit area, measured in the aperture plane of the collector, and A_a is the collector absorber area.

With respect to the effect of the electrical energy production, the electrical efficiency is subtracted from the transmission-absorption factor to find the amount of thermal energy that was absorbed in the system. Thus the equation of $\tau_{\alpha,eff}$ becomes (Radziemska, 2003)

$$\tau_{\alpha,eff} = \tau_{\alpha} - \tau\eta_{el} \qquad \text{Eq. (4.4)}$$

Where $\tau_{\alpha,eff}$ is the effective transmittance-absorptance product with PV power output

τ_{α} is the transmittance-absorptance product without PV power output

τ is the transmittance product of PV

n_{el} is the photovoltaic conversion efficiency

4.3.3 Heat Losses from the Collector

Thermal losses from solar collectors occur in three ways: conduction, convection and radiation. Heat losses due to conduction are usually negligible, unless poor collector design or construction results in the collector case or mounting structure coming into direct thermal contact with the absorber or inlet and outlet piping. Convective losses are a linear function of the temperature difference between the collector glazing and ambient air. These losses can be substantial due to the effects of wind on the outer glazing. Within the collector, convection also transfers heat to the glazing from the absorber. Radiative losses are relatively small at conventional domestic water or space heating temperatures. However, since these losses are a function of the difference between the fourth power of the absorber absolute temperature and the sky absolute temperature, which is usually several degrees lower than the ambient air temperature, radiative losses may become significant at higher operating temperatures. Although convective and radiative losses occur from all of the exposed surfaces of collectors, it is a common practice to express the overall heat loss from the collector as a function of the absorber area, A_a. This is because the major radiative and convective losses from a well-insulated collector occur primarily through the glazing.

For both experimental and analytical purposes, it is common to combine the convection and radiation heat transfer terms to yield a single heat loss coefficient based upon the temperature difference between the average collector absorber plate temperature and the ambient temperature. When this is done, the radiation heat transfer term must be linearized. Thus;

$$U_L = F'(U_{convection} + U_{radiation}) \qquad \text{Eq. (4.5)}$$

and

$$Q_{loss} = U_L A_a (T_p - T_a) \qquad \text{Eq. (4.6)}$$

where $U_{convection}$ and $U_{radiation}$ are the overall convection heat transfer coefficient and the linearized overall radiation heat transfer coefficient, respectively. T_p is the average absorber temperature.

These equations are the basic equation used in developing analytical models to describe collector performance. The useful energy delivered to storage or load by a collector can also be determined experimentally by measuring the inlet and outlet collector temperatures, the properties of the heat transfer fluid, and the mass flow rate of that fluid through the collector; thus

$$Q_{useful} = \dot{m}\, C_p (T_o - T_i) \qquad \text{Eq. (4.7)}$$

where

m = fluid mass flow-rate through the absorber

C_p = specific heat capacity of the fluid

T_o = outlet fluid temperature

T_i = inlet fluid temperature

In section 2.3.3 there is all the appropriate equations used for evaluating the thermal performance of the systems.

4.3.4 Calculation of module temperature of PV

The electrical performance of a PV system depends on module operating temperature. The module temperature is affected by insolation, ambient temperature, wind speed and also the type of PV installation (Davis et al., 2001). In the standard TRNSYS (simulation program) component model, NOCT is used to predict module temperature (Klein et al., 2000). The module temperature at any time step is a function of irradiance and ambient temperature given by

$$T_c = T_a + \frac{G}{G_{NOCT}}(T_{c,NOCT} - T_{a,NOCT})\left(1 - \frac{\eta_c}{\tau\alpha}\right) \qquad \text{Eq. (4.8)}$$

where T_c and T_a are the module temperature and ambient temperature, respectively at any time step, G is the incident insolation on the PV plane, G_{NOCT} is the insolation at NOCT, $T_{c,NOCT}$ and $T_{a,NOCT}$ are the module and ambient temperature at NOCT, respectively. n_c is the conversion efficiency of the module and $\tau\alpha$ is the transmittance–absorptance product of the module. Equation (4.8) is the same as equation (2.4.3). In this study, $T_{c,NOCT}$, $T_{a,NOCT}$ and G_{NOCT} were considered as 40 °C, 20 °C and 800 W/m^2, respectively.

4.3.5 Collector Efficiency

Thermal and electrical efficiency of the PV/T collector should be measured separately. The thermal efficiency of a flat-plate solar collector is defined as the ratio of the useful heat delivered by the collector to the total solar radiation intercepted by the collector:

$$\eta = \frac{actualusefulenergycollected}{solarenergyintercepted\ by\ the\ collector}$$

The instant thermal efficiency of the PV/T collector is expressed in the following equation (2.3.12):

$$n_T = F_R(\tau\alpha)_n \quad F_R U_L \cdot \frac{T_i \quad T_\alpha}{G_T}$$

The coefficient F_RU_L is an indication of the energy loss and depends on the collector insulation. Therefore, the value of F_RU_L of the PV/T collector is greatly affected by the collector insulation rather than from the interpolation of the photovoltaic laminate. The coefficient $F_R(\tau\alpha)$n of the PV/T collector is an indication of the absorbed energy and depends on the optical characteristics of the collector.

4.3.6 Electrical Performance of the PV/T

The PV electrical efficiency n_{pv} is known to decrease with the operating temperature of the module, T_{pv} and the linear correlation by Florschuetz describes this behaviour: equation (2.4.5)

$$\eta_{pv} = \eta_{ref}(1 - \beta(T_{pv} - T_{ref})).$$

where n_{ref} is the reference efficiency at the reference temperature, T_{ref} (25 °C) and β is cell efficiency temperature coefficient that can be determined experimentally.
The electrical efficiency was determined at regular time intervals in the course of experiments by disconnecting the load resistor temporarily and inserting a simple I–V circuit. The PV module electrical efficiency is calculated from the equation (2.4.1)

$$\eta_{pv} = \frac{P_{max}}{A_a G} = \frac{I_{max} V_{max}}{A_a G},$$

where P_{max} is the maximum power, A_a is the aperture area of the PV module and G is the incident solar radiation.

4.4 TRNSYS simulation program

The equations presented are being used by TRNSYS program to evaluate the performance of the PV/T model. TRNSYS is an acronym for a 'transient simulation' which is a quasi-steady simulation model. This program was developed by the University of Wisconsin by the members of the Solar Energy Laboratory. The program consists of many subroutines that model subsystem components (*Figure 4.3*). The mathematical models for the subsystem components are given in terms of their ordinary differential or algebraic equations.

Model validation studies have been conducted in order to determine the degree to which the TRNSYS program serves as a valid simulation program for a physical system. It has been shown by analysing the results of these validation studies that the TRNSYS program provides results with a mean error between the simulation results and the measured results on actual operating systems under 10% (www.trnsys.com).

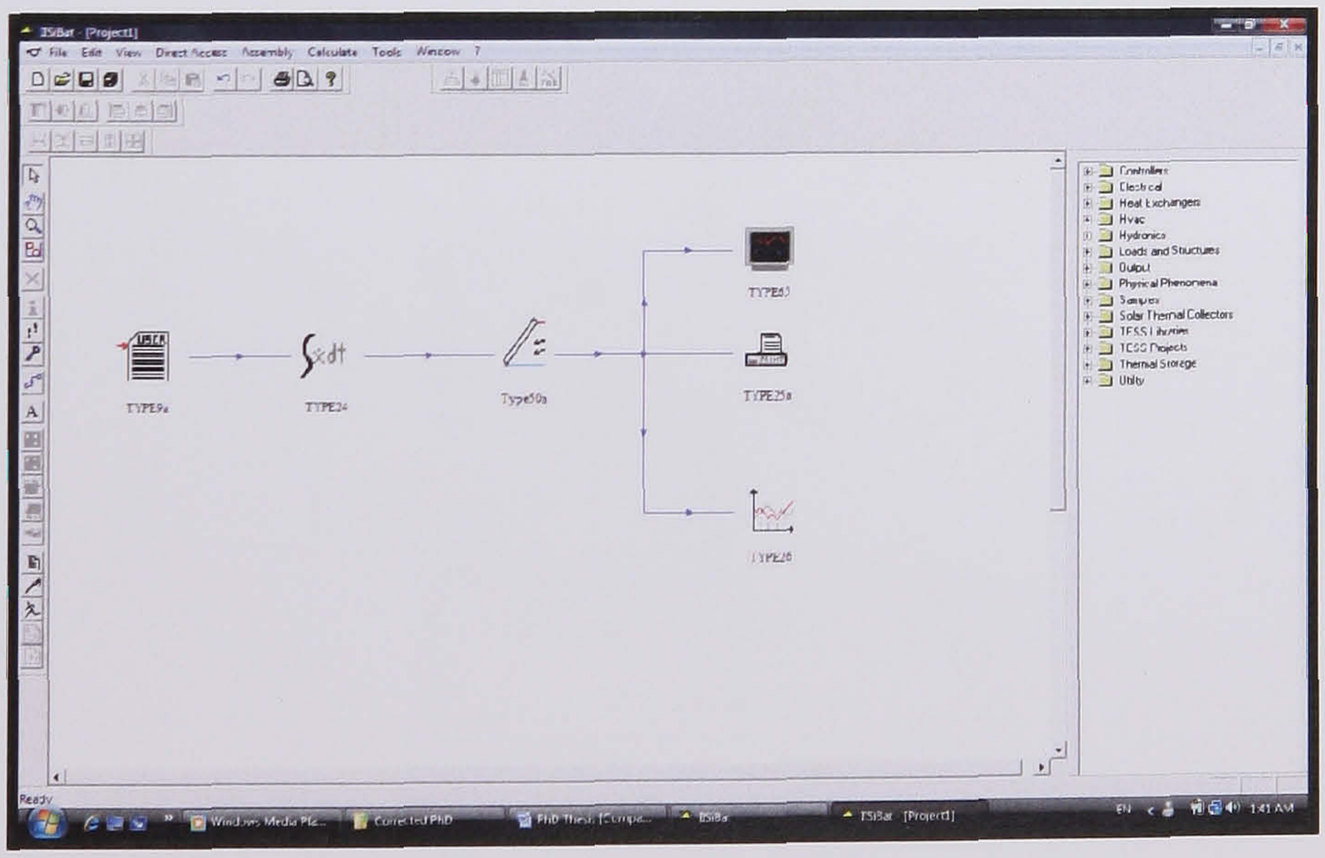

Figure 4.3 TRNSYS Software Components

4.4.1 Simulation Program

The performance of a PV/T collector depends on design parameters and on various weather and operating conditions, e.g. irradiance, ambient temperature, wind velocity, inlet fluid temperature, etc. Therefore it is necessary to develop simplified theoretical model in order to carry out multi-parameter analysis.

A module from the TRNSYS simulation program was used in order to describe the behaviour of this collector and compute the electrical and thermal yields of the system. The developed program is accompanied with user friendly interface to help those without any experience to perform the required computations. The user can simply vary the design parameters to see the response of the system under study, accordingly.

The basic principle of the simulation program built as a subroutine in the TRNSYS program is shown in *Figure 4.3*. The iterative procedure for computation of plate and cover temperature is repeated for case with electrical load. In the *Table 4.1* we see the parameters, inputs and the desired output from the PV/T model.

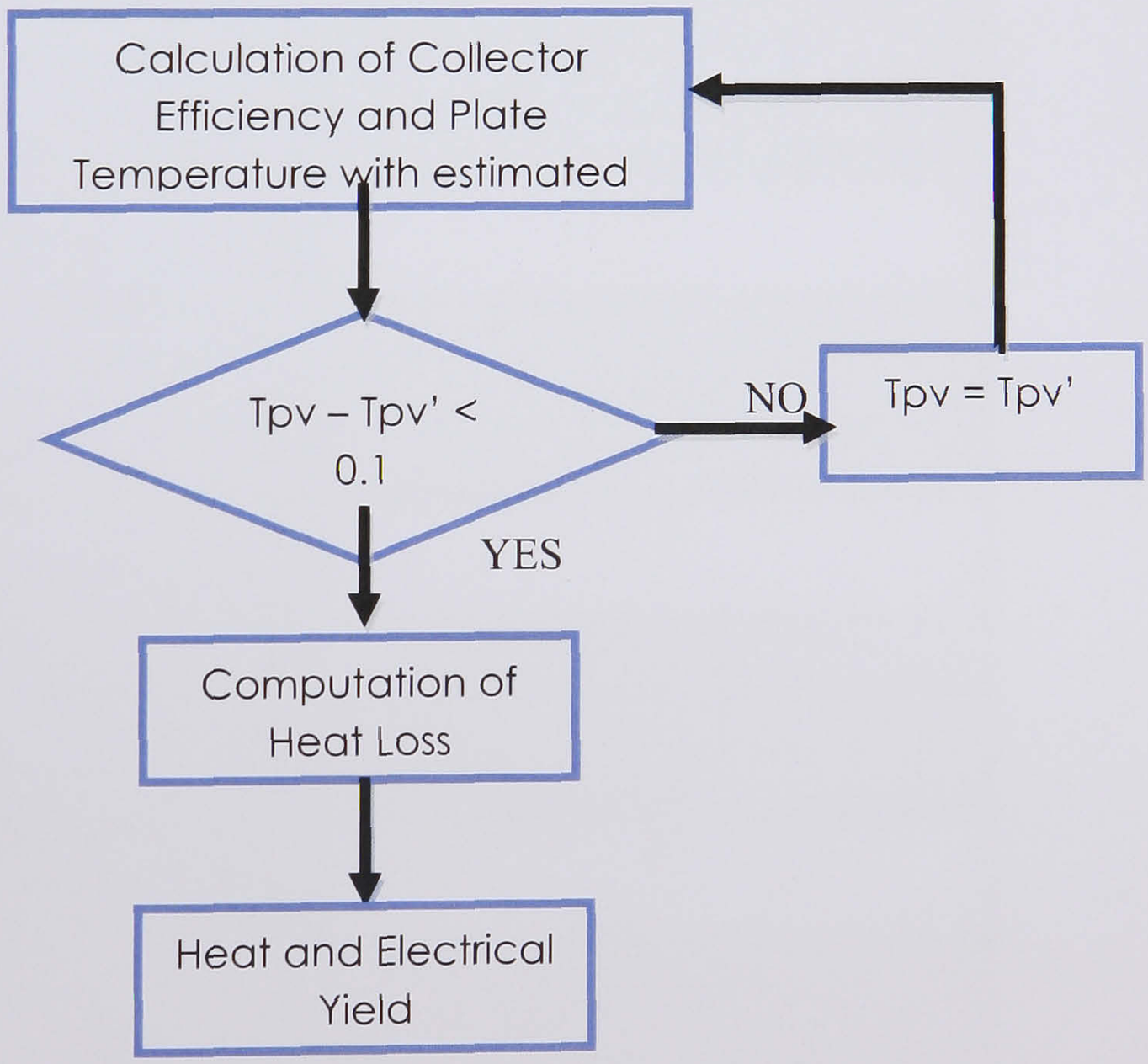

Figure 4.3 Flow diagram of the simulation program for PV/T collectors

In *Table 4.1* are illustrated all the parameters needed and used to simulate the performance of a PV/T model. The equations from section 2.3.3 were used to evaluate the possible heat loss coefficient. To mention again that the simulation was done before the experiments undertaken and did not take into account the different heat exchanger design of serpentine tube and tank. The purpose was to evaluate how this design tool can help estimating performances and not just using the experimental values to get the desired result.

Table 4.1 PV/T parameters and inputs used for evaluating the specific output

Parameters	
Collector Area (m^2)	0.16
Collector Efficiency Factor	0.8
Fluid Thermal Capacitance (kJ/kg*K)	4.2
Collector Plate Absorptance	0.9
Collector Loss Coefficient (W/m^2*K)	13
Cover Transmittance	0.9
Tempemperature Coefficient Of Solar Cell Efficiency	-0.0045
Reference Temp. Of PV (^oC)	25
Packing Factor	0.8

Input	

Inlet Fluid Temperature (^{o}C)	20 – 60
Fluid Mass Flow Rate (kg/hr)	18 – 180
Ambient Temperature (^{o}C)	20
Incident Radiation (W/m^2)	1000
Cell Efficiency (%)	4

Output
Inlet Fluid Temperature (^{o}C)
Rate of Useful Energy Gain (W)
Electrical Power Output (W)
Average Cell Temperature (^{o}C)

4.5 PV/T system yield

To indicate the yield of a PV/T system is not straightforward. Basic problem is that a collector produces both electrical and thermal output. Therefore, one either has to talk about these two yields separately, or one should choose a way to combine both yields into one quantity. There are various methods to combine the value of electricity and heat (Coventry and Lovegrove, 2003):

• Calculate the total energy by simple addition

• Calculate the primary energy (Fossil fuel energy required to produce the amount of useful thermal and electrical energy. This differs from the above due to plant and heater efficiencies)

• Calculate the exergy

In this thesis the total yield of the PV/T is calculated using all of the 3 methods mentioned above. It was decided to use them because it will help the readers to compare the results with various other authors that you one of these methods.

4.5.1 Evaluation of Total Efficiency Performance

The term total efficiency n_o has been widely used in the performance evaluation of hybrid PV/T system, i.e.

$$\eta_o = \eta_t + \eta_e \qquad \text{Eq. (4.10)}$$

where n_t and n_e are respectively the thermal efficiency and electrical-power generation efficiency of the PV/T system.

4.5.2 Energy Saving Efficiency

Considering electrical energy as higher in grade than thermal energy, Huang (1999) used the primary-energy saving E_f to evaluate the overall performance of PV/T systems, in that

$$E_f = \eta_t + \eta_e / \eta_{power} \qquad \text{Eq. (4.11)}$$

where n_{power}, often assigned a value of 38%, is the electrical-power generation efficiency of a conventional thermal power plant.

The primary energy equivalent of PV electricity has been calculated according to the partial substitution method which can be summarised by the equation below.

Replaced thermal fuel in terms of primary energy (kWh) =
= PV generation (1 kWh) / Average generation efficiency (%)

In this method, the primary energy equivalent of the renewable sources of electricity generation represents the amount of energy that would be necessary to generate a similar amount of electricity in conventional thermal power plants. The primary energy

equivalent is calculated using an average generation efficiency of these plants. For example, assuming an average thermal efficiency of 38% one unit of PV electricity would be equal to three units in terms of primary energy.

The above equations are applicable when the surface areas of the PV cells (Aa) and the absorber plate (Ac) are the same.

4.5.3 Performance evaluation for PV/T collector Exergy Efficiency

Electrical and thermal efficiency are major factors in the present performance evaluation method for a solar cell and a solar collector. However the electrical and thermal energy produced by the hybrid system were not the same in nature. Thermal energy could not produce work until a temperature difference existed between a high temperature source and a low temperature sink. But electrical energy could be completely transformed into work irrespective of the ambient condition. Use of exergy enabled quantitative evaluation by comparing electrical and thermal energy based on the same standard (Fujisawa and Tani, 1997).

Formulation of exergy

Exergy is formulated as the product of an intensive variable and an extensive variable.

(a) *Electrical exergy.* Electrical energy is not affected by ambient conditions and therefore is equivalent in work. If irradiance is E, energetic efficiency of the solar cell is ne, then the electrical of exergy is:

$e_{ele} = n_{ele} * E = \xi_{ele} * E$ Eq. (4.12)

where ξ_{ele} is exergetic efficiency of PV cell and:

$\xi_{ele} = n_{ele}$

(b) *Thermal exergy.* In order to transform thermal energy into work, there must be a temperature difference between a heat source and a heat sink. The magnitude of transformable thermal energy to work is restricted by the Carnot efficiency:

$$\eta_C = \frac{T_1 - T_0}{T_1} = 1 - \frac{T_0}{T_1}, \qquad \text{Eq. (4.13)}$$

where T_o and T_1 are the absolute temperature of the heat sink and source. Then thermal exergy is:

$$e_{thermal} = n_c * Q_{thermal} = n_c * n_{thermal} * E = \xi_{thermal} * E \qquad \text{Eq. (4.14)}$$

where $n_{thermal}$ and $\xi_{thermal}$ are the energetic and exergetic efficiency of the solar collector, respectively.

(c) *Synthetic exergy of the PV/T collector.* The synthetic exergy of the PV/T collector is the total value of the electrical and thermal exergies

$$e_{PV/T} = e_{thermal} + e_{ele} = (\xi_{thermal} + \xi_{ele}) * E = \xi_{PV/T} * E \qquad \text{Eq. (4.15)}$$

$$\xi_{PV/T} = n_{ele} + n_c * n_{thermal}$$

where $\xi_{PV/T}$ is the exergetic efficiency of the PV/T hybrid collector. All the quantities are used for steady state conditions.

4.6 Experimental PV/T systems

Two types of PV/T experimental models were studied, one with pc-Si PV using a serpentine pipe and copper sheet as a heat exchanger and with the same pc-Si PV module (the same commercial panel that was used in chapter 3) a second model with a small rectangular tank in the rear of the PV for water heating (*Figure 4.4*). The PV had a low-iron glass cover of 3 mm thickness and was thermally protected with 13 mm thermal insulation.

Figure 4.4a Two heat exchanger systems used in the back of the PV/T a) the small rectangular water tank b) the copper sheet and serpentine pipe

To increase the heat transfer between the rear of the PV and the attached copper plate, and generally the thermal and electrical performance for both systems, a thermal paste with high thermal conductivity 3 W/m*K was used as an interface (see *Figure 4.5*).

Figure 4.5 The rear of the PV covered with the thermal paste

4.6.1 Heat transfer between PV cells and absorber plate (Theoretical Estimation)

The heat transfer coefficient between the laminate and the absorber determines the PV laminate temperature. The heat resistance between cells and absorber R_{ca} consists of the heat resistances of an EVA layer (d = 0.5 mm l = 0.35 W/m*K) a Tedlar layer (d = 0.1mm l = 0.2 W/m*K) and of the adhesive layer. The thickness of the adhesive layer is estimated to be 50 μm and its coefficient of conduction is 0.85 W/m*K.

$$R_{ca} = R_{EVA} + R_{Tedlar-Al-PE} + R_{adhesive} \qquad \text{Eq. (4.16)}$$

Rca = Reva + Rpe-al-tedlar + Radhesive = 5*10^-4 / 0.35 + 1*10^-4 / 0.2 + 5*10^-5 / 0.85

Rca = 1.99*10^-3 K*m^2/W

Therefore hca = 1/Rca = 500 W/m^2*K

However the real heat transfer coefficient is different from the theoretical value and can be found using experimental measurements that will be explained later. One of the causes of the different heat transfer coefficient is the air bubbles present in the adhesive layer.

4.6.2 Heat transfer coefficient between cells and absorber (Experimental Evaluation)

The heat transfer coefficient of the layers between the PV cell and the absorber is an important parameter in the thermal model. It is determined by measuring the temperatures on the surface of the laminate and at the back of the absorber plate. The irradiance during the measurements was around 1000 W/m^2. During the experiments the inflow and outflow temperatures and the flow rate of the water were recorded. The measurements at the laminate and at the absorber were recorded in four different equal spaced points in order to get an average value.

The value of hca can be determined from the temperature difference of the glass surface of the PV and the absorber and inserting the results into the formula below (Zondag, 2002).

$$h_{ca} = \frac{cm(T_{out} - T_{in})}{A_{PV}(T_{cell} - T_{abs})} \qquad \text{Eq. (4.17)}$$

In this formula it is assumed that the heat loss to the ambient through the back of the absorber is negligible cause of the insulation used in the back as well as the temperature difference between the glass and the cell of the PV.

4.7 Experimental Results

This section includes the results taken under three different set of experiments. The first series of experiments were to evaluate the heat transfer coefficient between the PV front and rear copper plate. In the second set of experiments the two rigs were tested with different flow rates. The purpose was to evaluate how the flow rate affects the performance of the systems. Finally the third series had to do with varying the temperature entering (inlet water, T_i) the PV/T panel in order to evaluate the thermal and electrical efficiency under different operating temperatures. The experimental models were constructed and tested indoors for the determination of the steady state thermal efficiency n_{th} and the electrical efficiency n_{ele}. The thermal efficiency is determined as a function of the solar incident (G), the input fluid temperature (T_i) and the ambient temperature (T_a), while the electrical efficiency is determined as a function of the operating temperature $T_{PV/T}$.

The steady state efficiency is calculated by

$$\eta_{th} = \dot{m} C_p (T_o - T_i) / G A_a$$

where m is the fluid mass flow rate (in the tests it was 18 kg/hr), C_p is the fluid specific heat (4180 J/kg K), T_i and T_o are the input and output fluid temperatures and A_a is the aperture area of the PV/T model (0.16 m^2 for pc-Si). The thermal efficiency n_{th} of PV/T systems is calculated as a function of the ratio $\Delta T/G$ where $\Delta T = T_i - T_a$, with T_a being the ambient temperature.

During the tests for the determination of system thermal efficiency, the PV modules were connected with load to simulate real system operation and to avoid PV module overheating by the incident radiation that is converted into heat instead of electricity. Thus the maximum power point of the system was recorded in order to find the electrical efficiency. The electrical efficiency n_{ele} depends mainly on the incoming solar radiation and the PV module temperature (T_{PV}) and is calculated by:

$$\eta_{el} = I_m V_m / G A_a$$

where I_{mp} and V_{mp} are the current and the voltage of PV module operating at maximum power. The electrical efficiency of the PV cells depends on the incident radiation and their operating temperature.

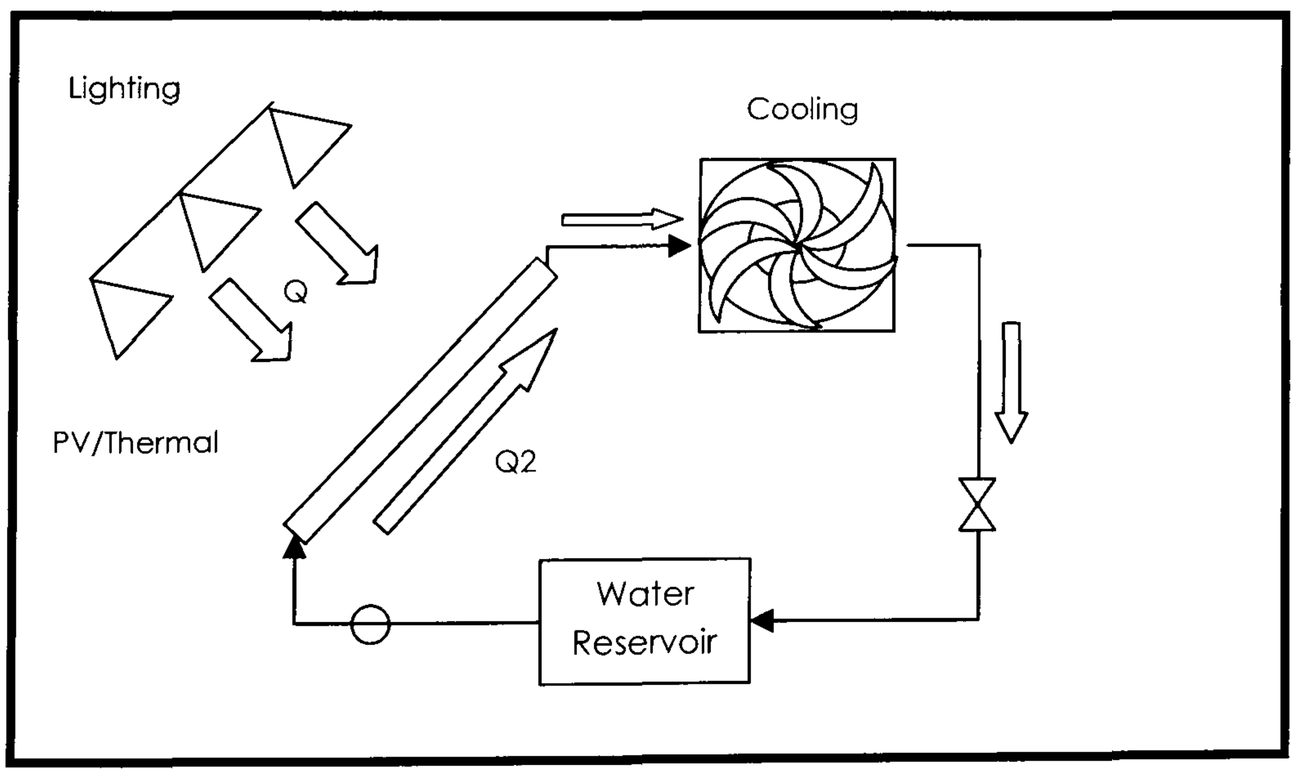

Figure 4.4b PV/T Water Rig using serpentine pipes and a free channel in the back of the PV

4.7.1 First set of experiments

Figure 4.6 and *4.7* illustrates the temperature of the PV/T models in front and at the rear as well as the inlet and outlet water temperature. The experiment was run until reach equilibrium conditions. From the results shown in the graph and using the equation (4.17) it was found that the PV/T model with the water tank in the rear had an h_{ca} = 73.87 W/m^2*K and the temperature difference of the front and back of the model was 7.32 °C. For the PV/T panel with the serpentine pipes in the back we had an h_{ca} = 129.21 W/m^2*K and the temperature difference was 4.08 °C. This is the reason that the PV/T model with the tank in the rear has a temperature of 44 °C and 36 °C in the front and rear of the PV and the serpentine pipe model had 32 °C and 28 °C respectively. The average difference between the two models was 10 °C. The main cause of this difference is that the PV/T rig with the tank in the back had a bad contact between the two surfaces of Tedlar and copper sheet.

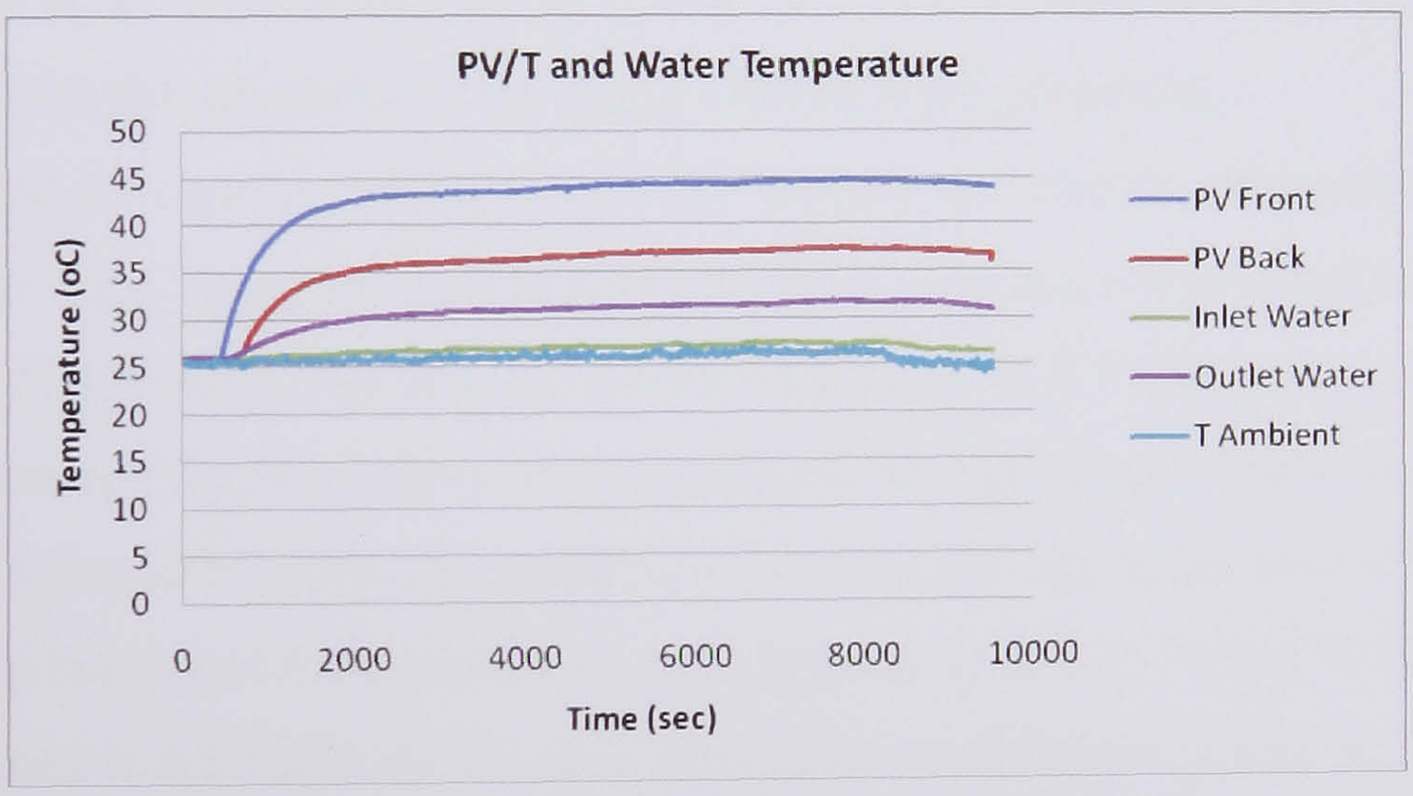

Figure 4.6 PV/T and Water Temperature with tank in the back

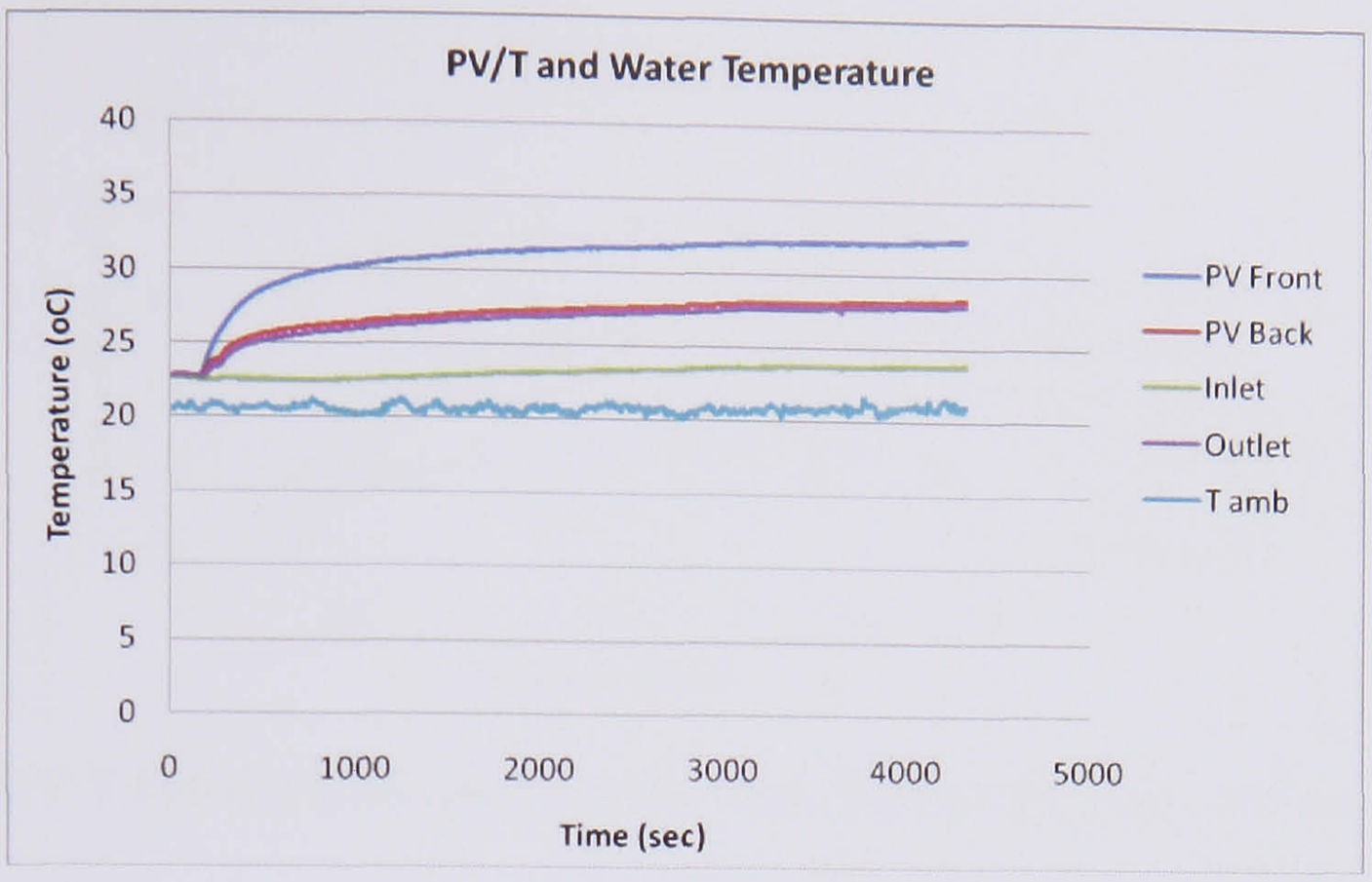

Figure 4.7 PV/T and Water Temperature with serpentine pipes in the back

4.7.2 Second set of experiments

In the second set of experiments two models in different flow rates and at an irradiation level of 1000 W/m^2 were evaluated. In *Figures 4.8, 4.9, 4.10* and *4.11* the results of the two models with the simulation done using TRNSYS are presented.

Figure 4.8 and *4.9* represent the results of the thermal and electric efficiency for different flow rates. As mentioned in section 4.4 the simulation was based to the equations of HWB and is based to the values seen in *Table 4.1*. One cause of the difference between the two experimental models is the light source variation. Another cause is the different heat transfer coefficient of water passing in the back of the PV for the serpentine tubes and for the tank. As mentioned in section 2.5.6 the W/D for serpentine tubes is 4.5 and 1 for the tank. This means that the water flowing in the tank covers all the rear area of the PV and thus works more effectively. The common fact is that as the flow rate increases an increase in electrical and thermal efficiency is being observed.

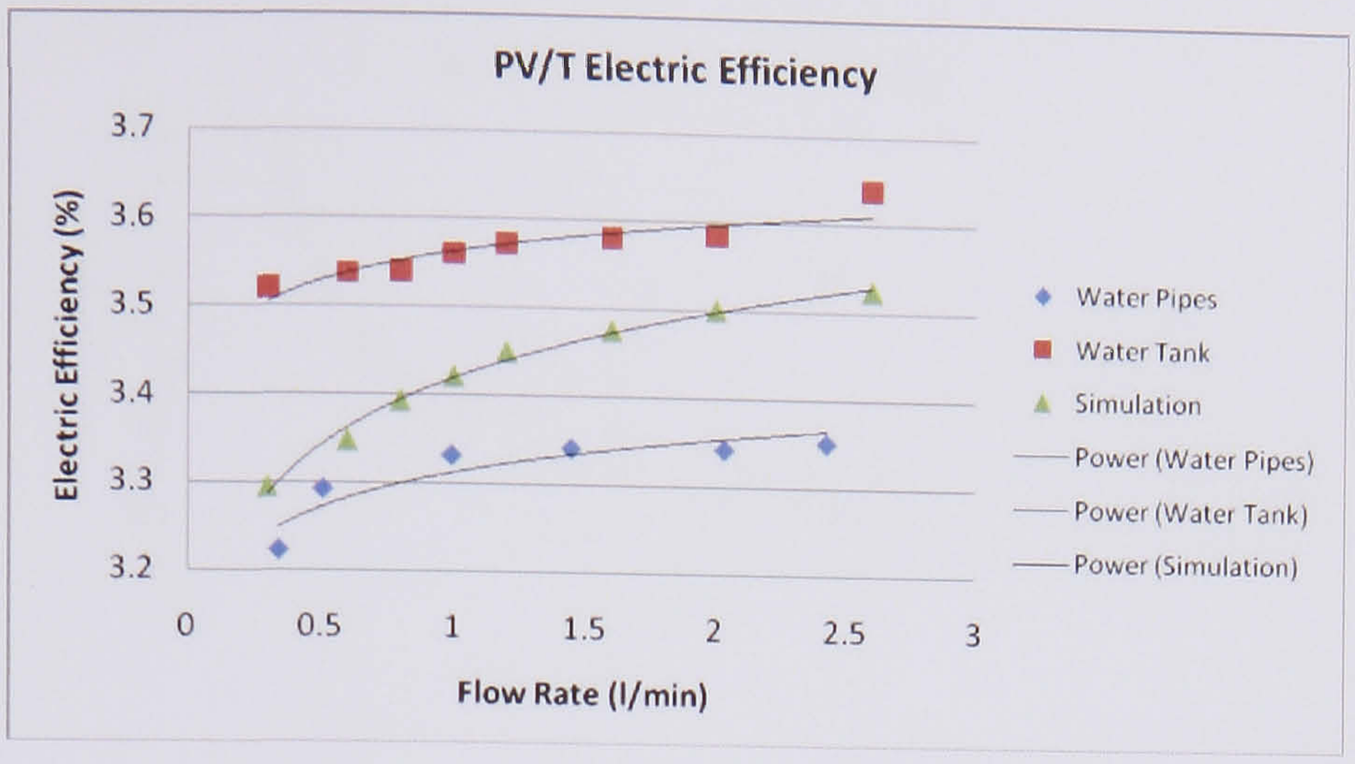

Figure 4.8 PV/T Electric Efficiency for the Tank, Serpentine pipe and Simulated model

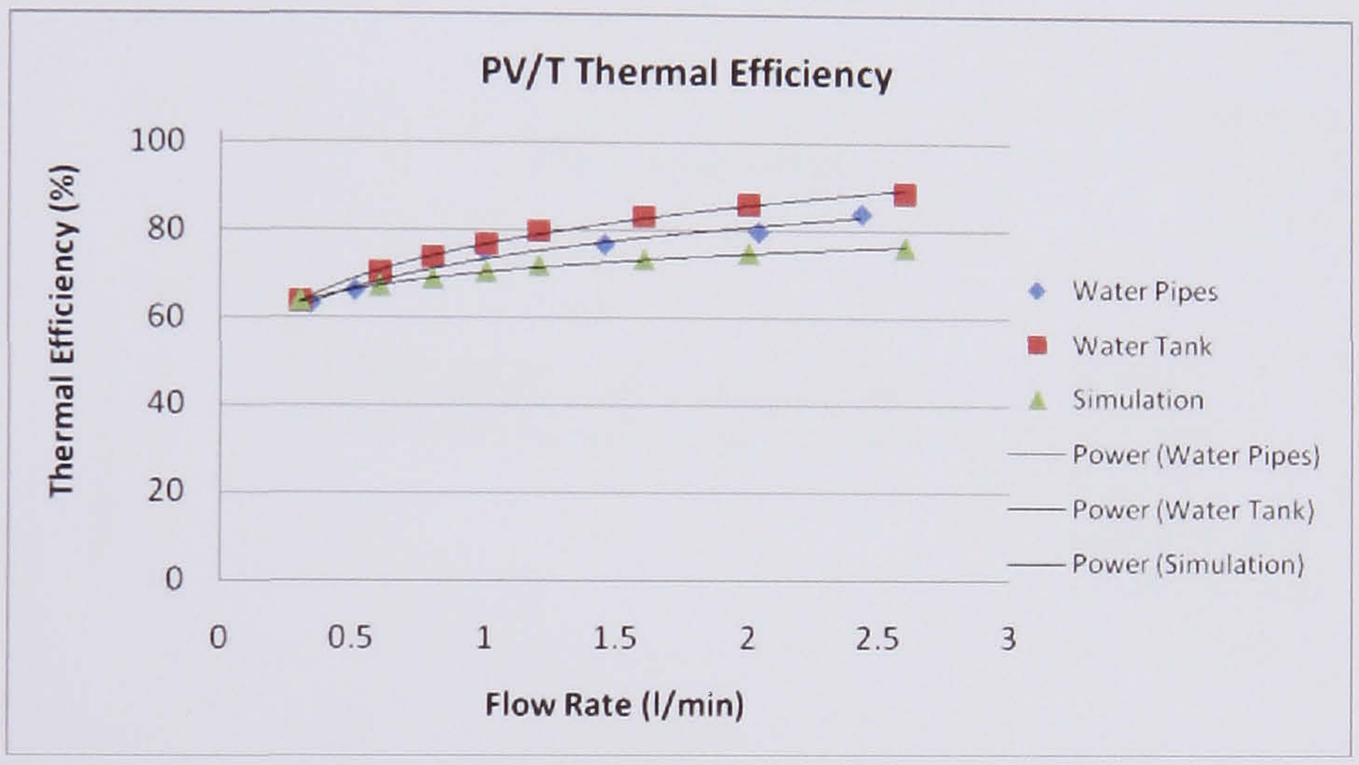

Figure 4.9 PV/T Thermal Efficiency for the Tank, Serpentine pipe and Simulated model

As the flow rate increases the inlet and outlet temperature decreases and this affects the temperature of the PV/T models. As seen from *Figure 4.10* the simulated values with the PV/T panel with the serpentine tube absorber match. For the PV/T model with the tank the difference is significant and this as mentioned is cause of the heat transfer coefficient and of the area difference in the heat exchanger systems.

Figures 4.11 and *4.12* illustrate the temperature difference between inlet and outlet water temperature and the temperature of the PV/T models at the various used flow rates. As the electrical and thermal efficiency improves with the increase of the flow rate, the temperature difference of water inlet and outlet and the PV/T temperature reduces.

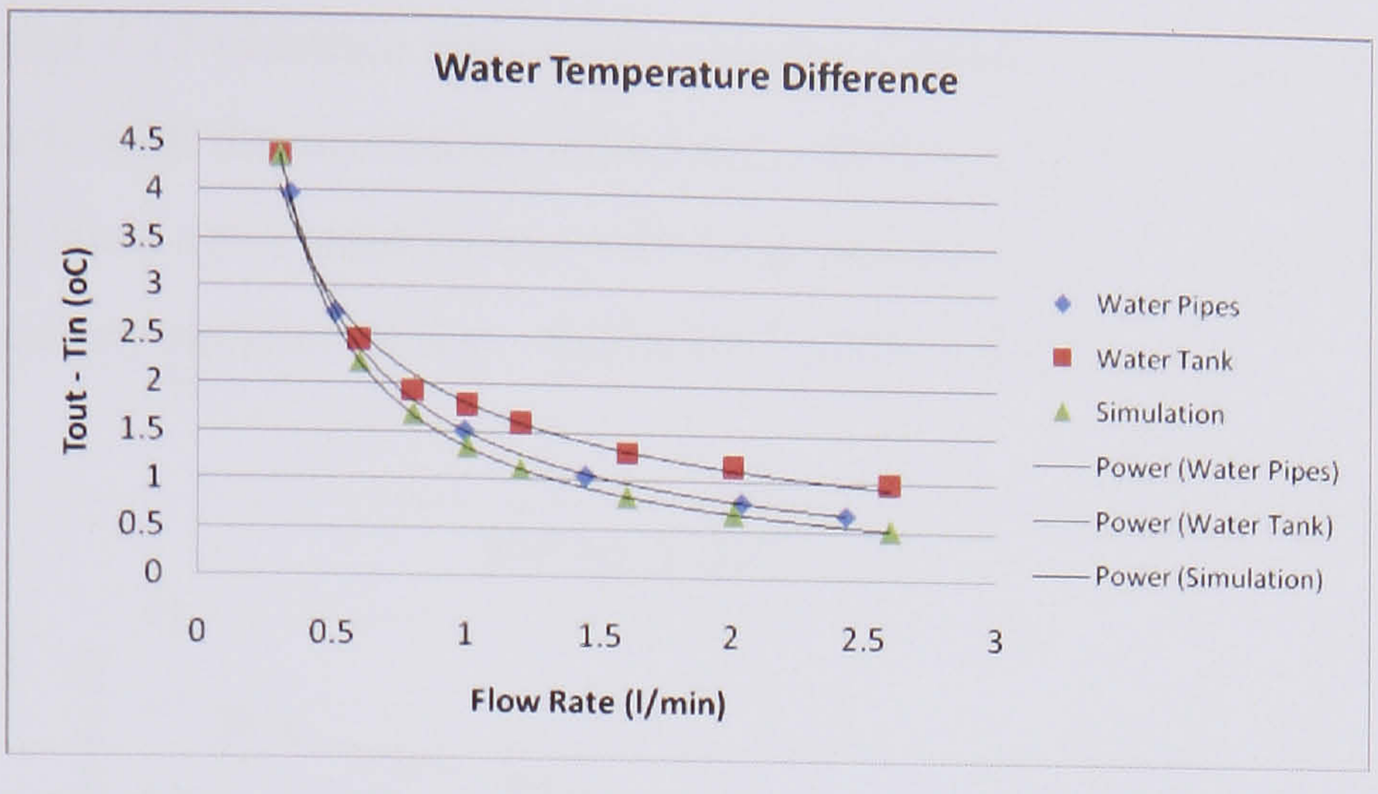

Figure 4.10 PV/T Water Temperature Difference for the Tank, Serpentine pipe and Simulated model

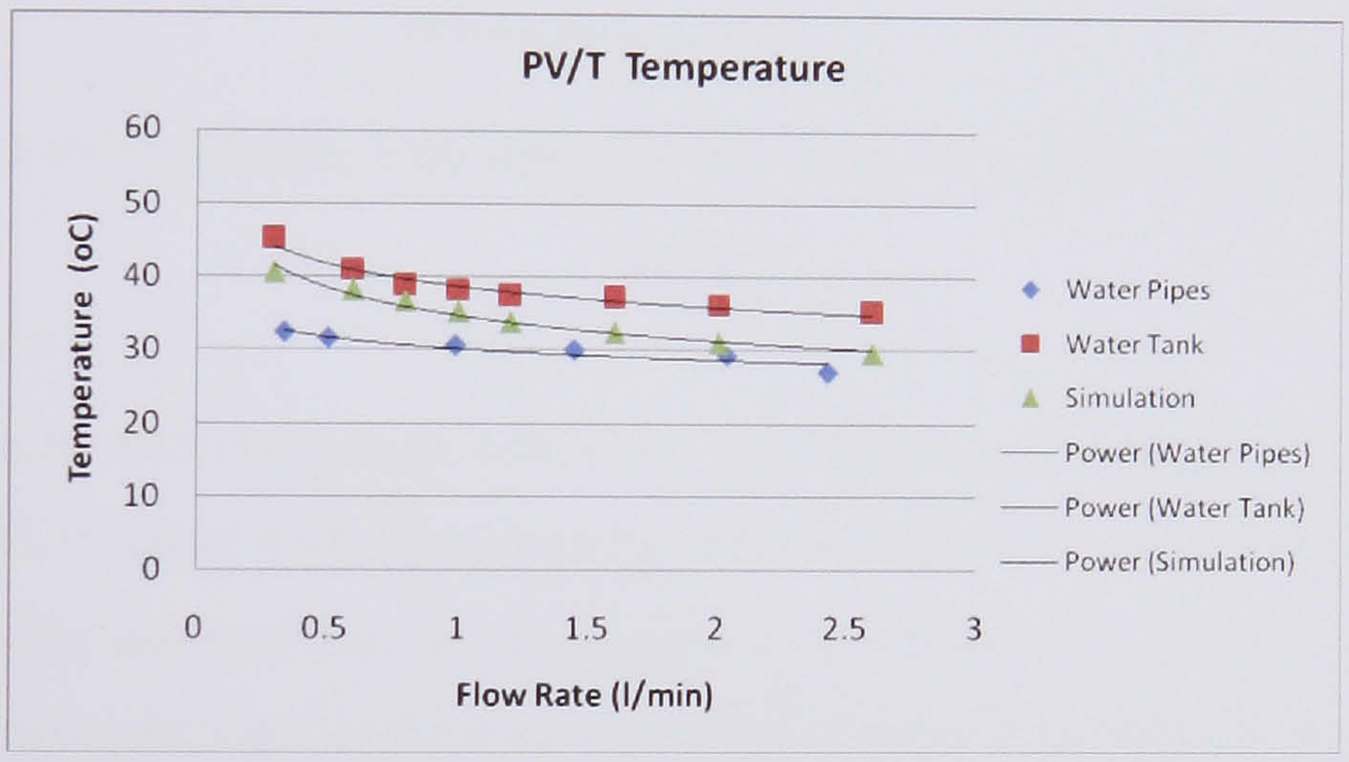

Figure 4.11 PV/T Panel Temperature for the Tank, Serpentine pipe and Simulated model

4.7.3 Third set of experiments

In the third set of experiments a steady flow rate (in this case was 0.3 l/min) was used together with the same irradiation level and only adjusted the temperature of the water flow into the system in order to be able to evaluate the performance of the system. The specific flow rate was preferred because the PV/T panel area was only 0.16 m^2 and a higher flow rate gave very small values of temperature difference between water inlet and outlet. The water temperature was adjusted with the help of a thermostat controller and a cooling fan was taking the heat from the water outlet. Again the maximum power point was used for the electrical performance after the systems had come to equilibrium.

Figures 4.12 and *4.13* illustrate the variation of the thermal and electric efficiencies. The two PV/T panels with the simulation values are represented together for better comparison. A good agreement between the two panels and the simulation with the electrical efficiency coefficient was - 0.014 %/°C or 0.384 %/°C.

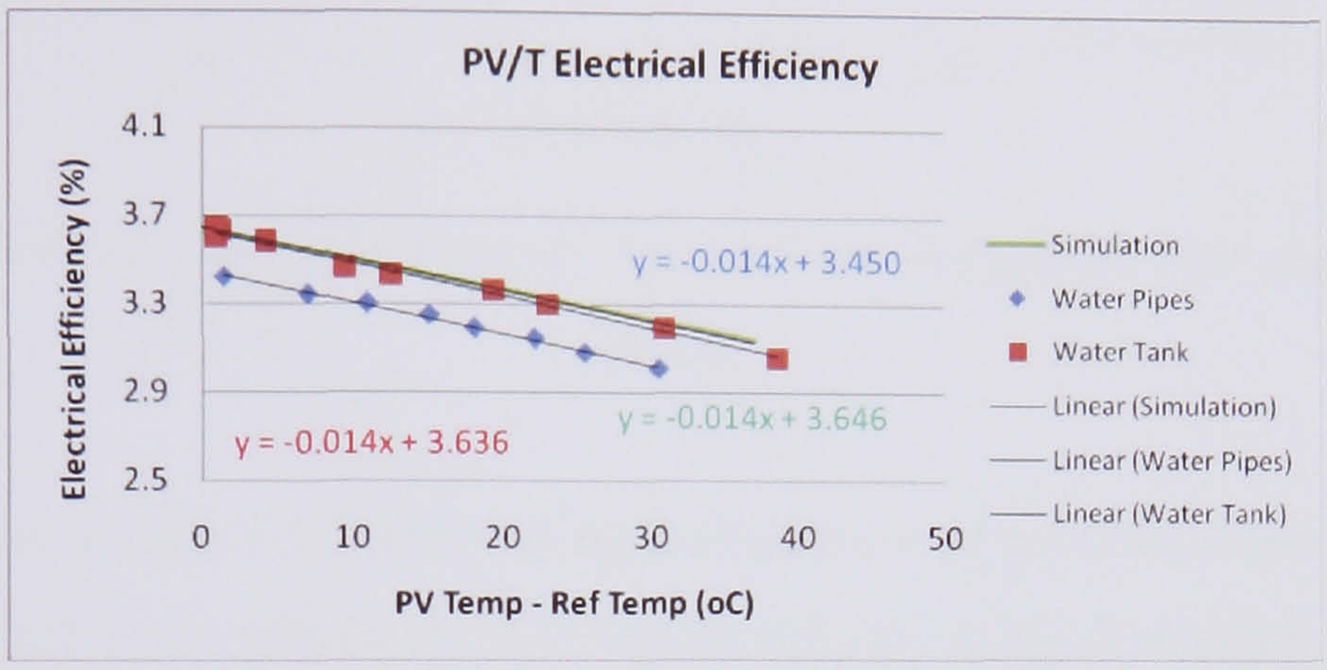

Figure 4.12 PV/T Electric Efficiency for the Tank, Serpentine pipe and Simulated model

As considering the thermal energy extraction and efficiency of the system it may be seen that the PV/T panel with the serpentine pipe works a little better than the panel with the tank. The cause of this, as can be seen from *Figure 4.13*, is the higher heat loss of the system using the tank as the heat exchanger device. The F_RU_L of the two systems was 7.683 W/m^2*K for the serpentine model and 14.31W/m^2*K for the tank. This difference could be influenced by the heat transfer contact between the PV laminate and the thermal absorber. The coefficient of $F_R(\tau\alpha)$ for the two models is 0.597 and 0.638 respectively. The difference of 0.04 is not significant and is caused by the irradiation level variation.

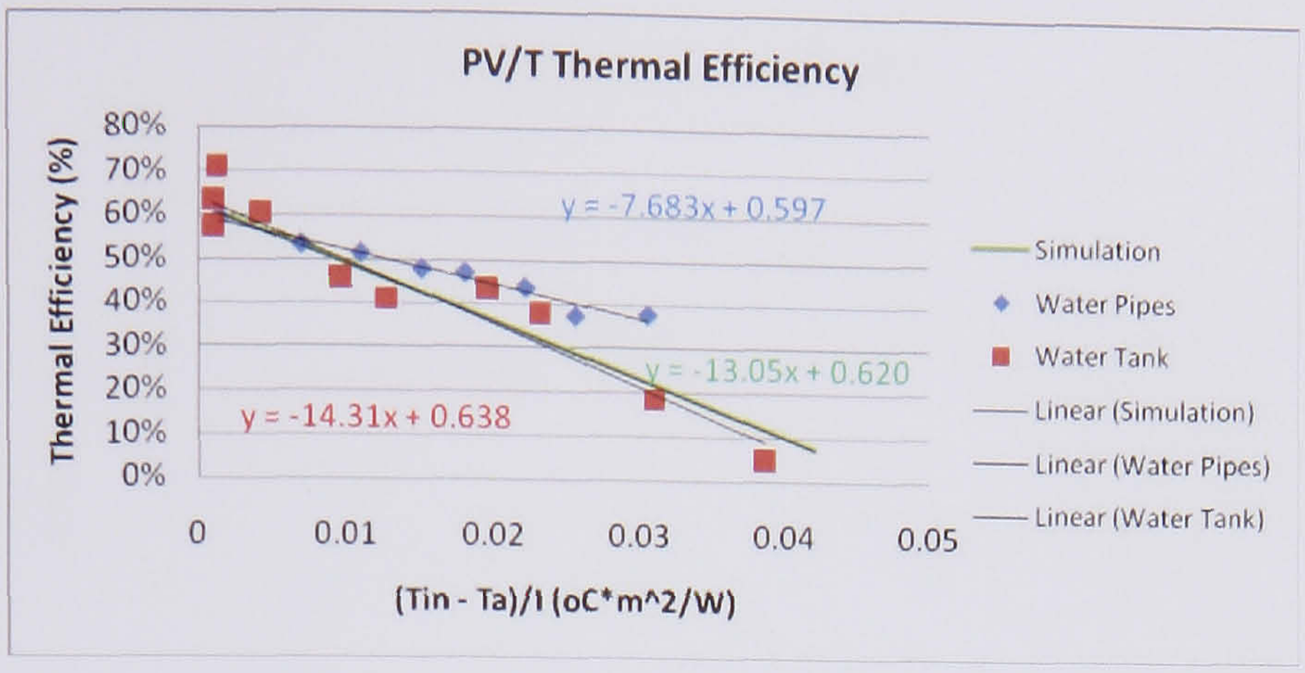

Figure 4.13 PV/T Thermal Efficiency for the Tank, Serpentine pipe and Simulated model

As mentioned in section 4.5 3 different methods were used to evaluate the models. The one explored here is the addition of the thermal and electrical efficiencies. As can be seen in *Figure 4.14* the two models agree well with the simulation and the small differences are caused by the heat loss coefficient. The same may also be observed in the primary energy saving efficiency as shown in *Figure 4.15*. The PV/T model with the serpentine tubes can work at higher temperature operating conditions with higher efficiencies cause of the lower heat loss coefficient in comparison with the system using the tank in the rear of the PV.

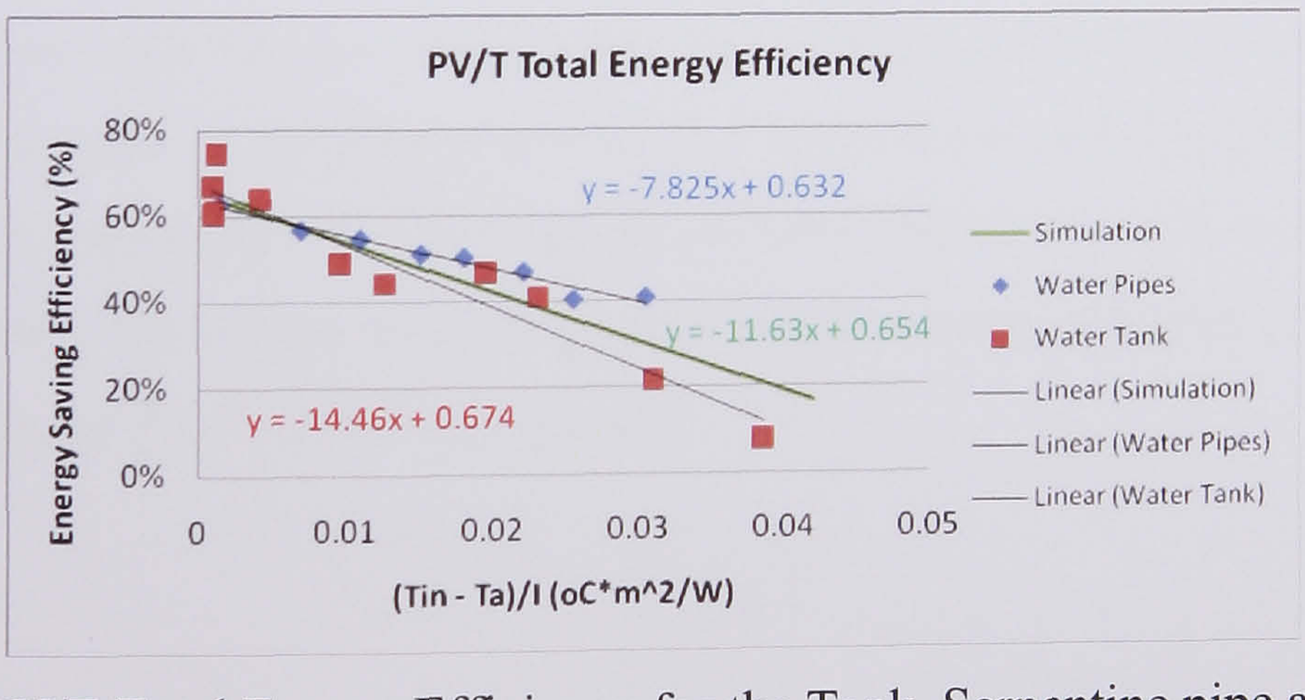

Figure 4.14 PV/T Total Energy Efficiency for the Tank, Serpentine pipe and Simulated model

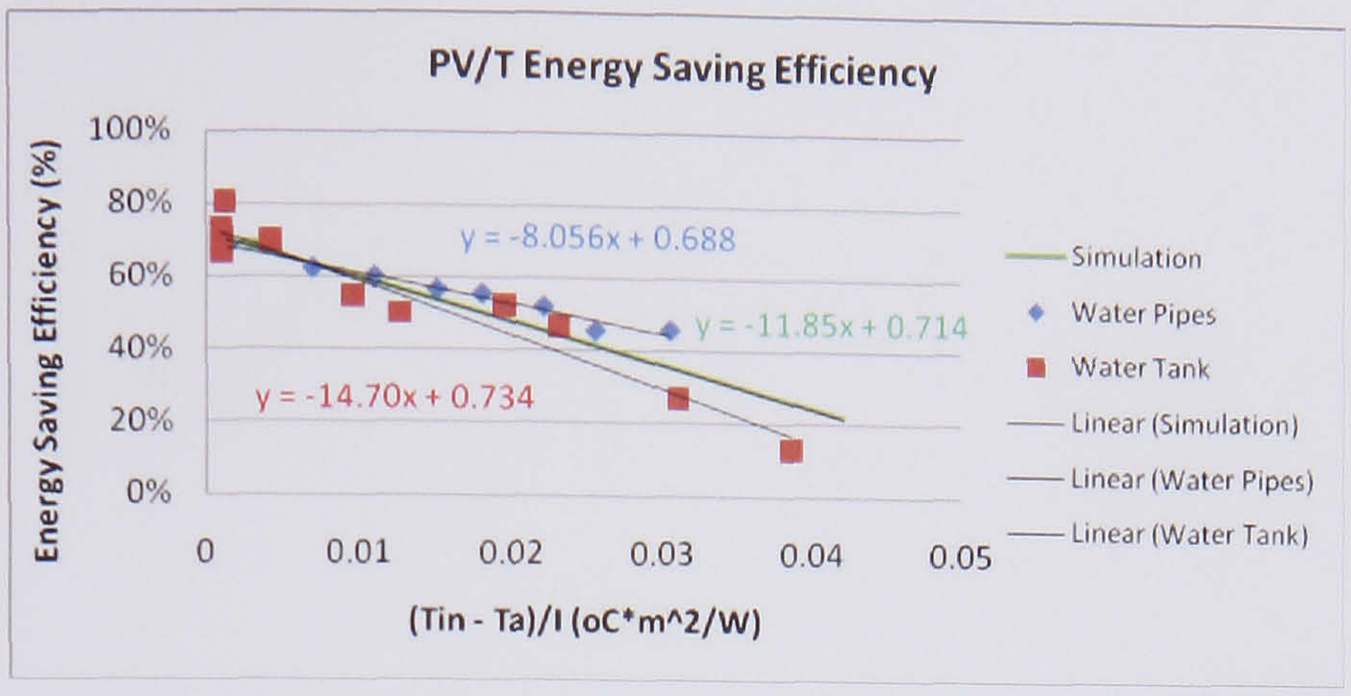

Figure 4.15 PV/T Energy Saving Efficiency for the Tank, Serpentine pipe and Simulated model

As explained in section 4.5 exergy was employed because the electricity and thermal energy were different in nature. By knowing that electrical energy is not affected by the ambient conditions and by using the equations to determine the thermal exergy efficiency of the systems, as seen in *Figure 4.16* the optimum operating conditions of the PV/T models are evaluated. From knowing that the electrical efficiency is around 3.5% and seeing the graph the models are more efficient when the inlet temperature of water is around 35 - 45 ^{o}C at 20 ^{o}C ambient and at 1000 W/m^2. As mentioned in section 2.5 cells efficiency is influenced on the thermal efficiency. According to the energy balance equation, when have lower PV cell efficiency then is being noticed a higher thermal efficiency and the vice versa. Here a higher thermal efficiency and thus also exergy efficiency that in the peak is around 21.5 % for water tank and 25% for serpentine tube. Again the PV/T model with the lower heat loss coefficient has better exergy efficiency and as seen from the graph it can work even at higher operating conditions than the PV/T model with the tank.

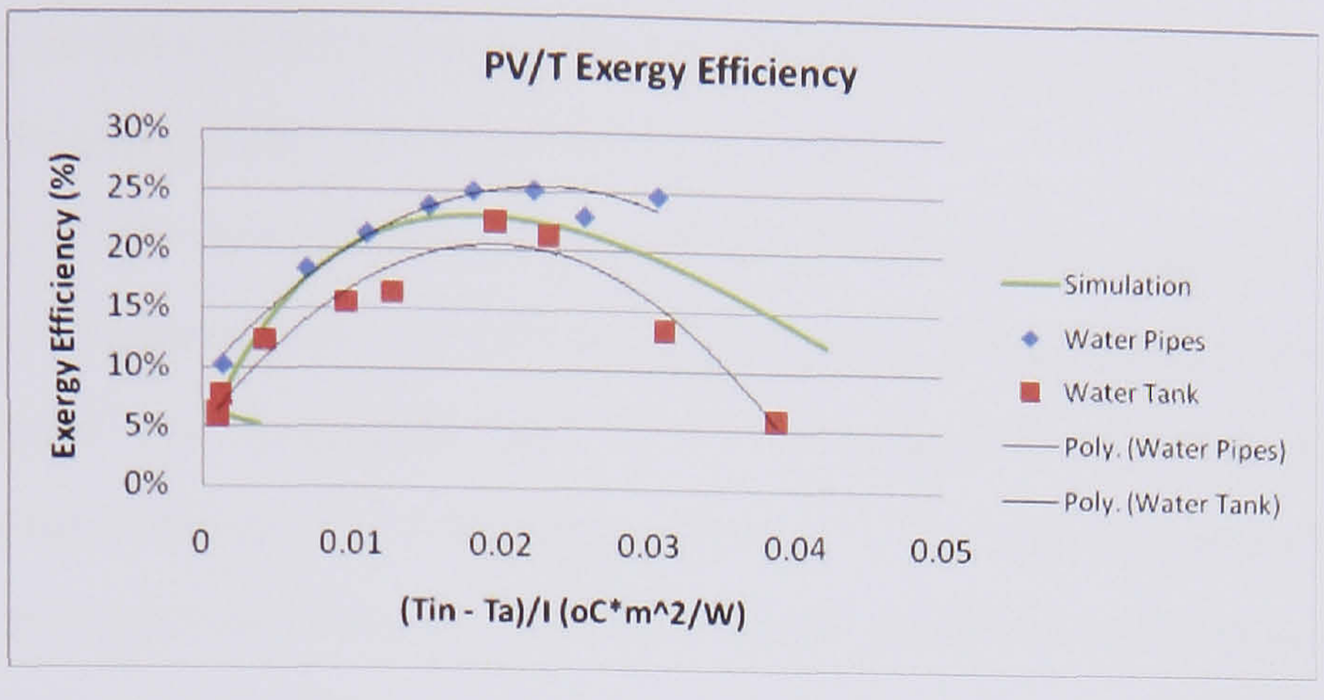

Figure 4.16 PV/T Exergy Efficiency for the Tank, Serpentine pipe and Simulated model

4.8 Conclusions

A test rig for two PV/T systems was constructed and experimental work was carried out in the laboratory. Thermal and electrical performance was studied to assess the efficiency of the system. The experimental results were compared with a simulated model by using TRNSYS.

The two PV/T modules tested were based on an existing PV panel incorporating a heat exchanger. The first was a serpentine copper pipe brazed to a copper sheet (W/D = 4.2) and placed in the rear of the PV with a thermal paste working to enhance heat transfer. The second incorporated a small rectangular tank (W/D = 1) with dimensions similar to the PV and total capacity of 4.3 litres.

To characterise the thermal and electrical performance of the panels three set of experiments were undertaken. The first explored heat transfer coefficient between the PV laminate and the copper plate acting as the absorber. The PV/T model with the serpentine pipe had better performance and thus the temperature of the PV was lower than the PV/T model with the tank.

The second set of experiments observed the performance of the panels with different flow rates. The results showed that as the flow rate increased the PV/T temperature decreased and in the same time the electrical and thermal efficiency was increased.

The third set of experiments investigated the performance of the system by increasing the inlet temperature of the water in the system. From these experiments the results were as expected. As the temperature of the water increased the systems' thermal and

electrical efficiencies reduced. Finally the total efficiency, the primary saving efficiency and exergy efficiency of the systems were determined.

Both systems provide satisfactory results with the PV/T model using the tank having higher total (63.2% for serpentine tube, 67.4% for tank) and primary energy saving effieciencies (68.8% for serpentine tube, 73.4% for tank) in respect with the serpentine tube while the collector works in the range of 20 – 35 ^{o}C. After this point the heat loss from the tank is bigger and thus the efficiency drops quicker than the serpentine model. As a conclusion it can be noticed that with an improvement in the contact between the PV laminate and the tank a better performance could be achieved. Also more insulation could reduce the heat losses. The flow condition and distribution inside the tank should also be taken into consideration as affects the heat transfer coefficient of the system. As far as consider the serpentine model a system having a W/D ratio less than 4 could also provide better results.

The most revealing results had to do with the exergy efficiency of the system. From these it was found that the optimum operating conditions of the two models for environmental conditions of 20 ^{o}C ambient temperature and 1000 w/m^2 irradiation are in the range of 35 – 45 ^{o}C of inlet water temperature. The model with the serpentine pipes can also work with higher inlet temperature but with lower exergy efficiency cause of the smaller heat loss coefficient.

The simulation model provided an understanding of how a real PV/T system would work in different conditions. Two parameters that were important when designing and estimating the performance of a system was the transmittance-absorptance product and the heat loss coefficient. The simulations results were close to both PV/T experimental models because the heat loss coefficient estimated was in the range of both predictions.

The analysis of energy yields shows that maximum energy yield is obtainable under the following conditions:

- The coefficient of absorptance for the absorber/PV cells should be as high as possible.

- The thermal contact between PV cells and the absorber is essential for a PV/T collector to improve the thermal yield. Special attention should be paid to assure that this thermal contact is as good as possible.
- The heat loss coefficient is a significant factor that affects the performance of the system. Lower heat loss means better thermal efficiency.
- Since the efficiency of PV cells decreases with increasing temperature on the panel, the temperature of the PV cells should be kept as low as possible, giving a low operating temperature. So an optimum point can be found with the exergy efficiency in order to get the maximum possible electrical but also thermal efficiency from the system.

CHAPTER 5: PHOTOVOLTACI/THERMAL SYSTEM AIR

5.1 Introduction

Photovoltaic (PV) cells suffer efficiency drop as their operating temperature increases especially under high insolation levels so cooling is beneficial. Air-cooling, either by forced or natural flow, presents an inexpensive and simple method of PV cooling and the solar preheated air could be utilized in built, industrial and agricultural sectors (*Figure 5.1*). However, systems with heat extraction by air circulation are limited in their thermal performance due to the low density, the small volumetric heat capacity and the small thermal conductivity of air and as a consequence measures for heat transfer augmentation are necessary.

This chapter presents the use of fins bonded to the back of a PV module and coupled to an air duct as a method of heat transfer augmentation in an air-cooled photovoltaic/thermal (PV/T) solar collector to improve its overall performance. The steady-state thermal and electrical efficiencies of the modified system are compared with those of simulation (using TRNSYS) and of a typical PV/T air system.

Temperature profiles of the outlet air, the PV rear surface and duct wall are presented confirming the contribution of the modifications in increasing system electrical and thermal outputs.

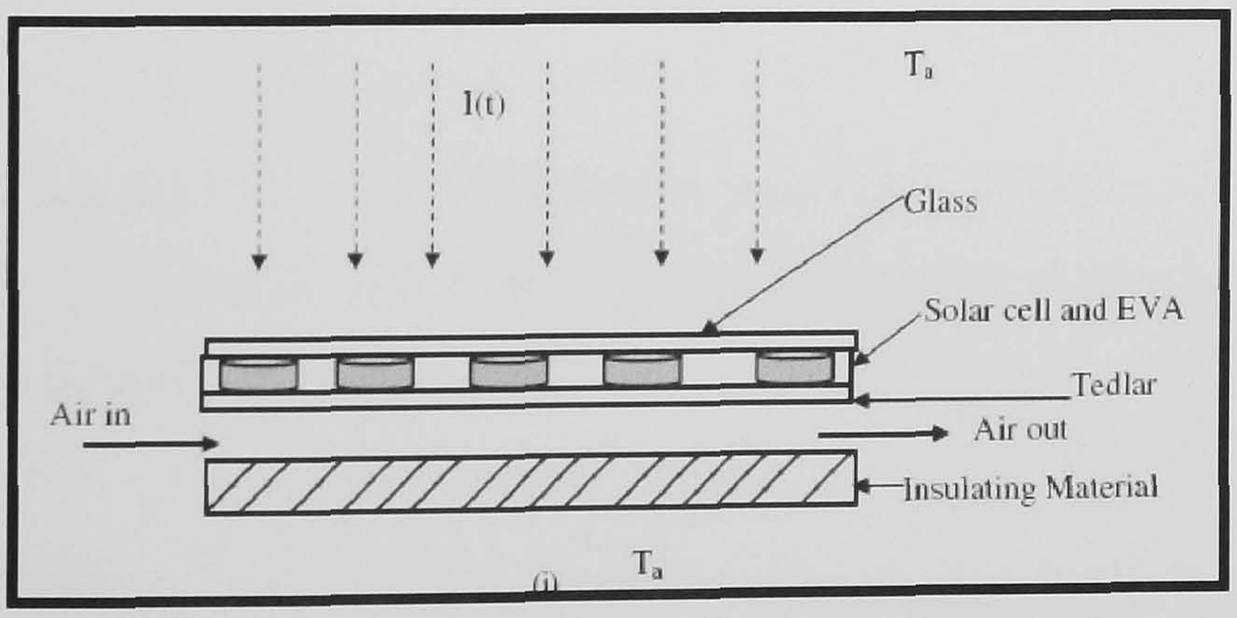

Figure 5.1 PV/T using Air as a fluid carrier (Tiwari, 2007)

5.2 Technical issues

The application of air as a heat transport medium has some advantages but also some disadvantages in comparison with water. To start with the advantages:

- No freezing and no boiling of the collector fluid.
- No damage if leakages occur.

The disadvantages are, however, rather severe:

- Low heat capacity and low heat conductivity, which result in a low heat transfer.
- Low density, which results in a high volume transfer.
- Heat losses through air leakage

5.2.1 Heat transfer from absorber to air

In air collectors, the air is always transported through a channel. However, the thermal performance of air collectors is not as high as the performance of liquid collectors. This is due to two effects.

- Air has a thermal conductivity that is 24 times lower than for water. Since $h = Nu \times k/D$ (Eq. 5.1) this reduces the heat transfer. This leads to the fact that for air collectors, the channel height has a large influence on the thermal efficiency. (Note that the channel height has no effect on the Reynolds number, since the decrease in flow velocity is compensated by the increase in channel width as can be seen from $Re = UD/\nu = \Phi L/\nu$ Eq. (5.2), in which Φ is the specific flow rate and L the collector length).
- Air has a much lower heat capacity. Therefore, the flow rate in an air collector is necessarily much larger than in a liquid collector. Due to the fact that (Zondag, 2005), $(\rho C_p)_{water}/(\rho C_p)_{air} = 4.2 \times 10^6/1.2 \times 10^3 = 3.5 \times 10^3$ (Eq. 5.3) a conventional fluid flow rate of 50 l/m^2/h for a liquid collector corresponds to an airflow of 175m^3/m^2/h, which is too high to be feasible in practice. Therefore, in practice a lower flow rate is used.

5.3 Thermal energy

The Hottel–Whillier–Bliss model (Duffie and Beckman, 1991) and modified by Florschuetz (1979) is used to study and compare the steady-state thermal efficiencies, n_{th} of the two PV/T air collector configurations. As mentioned in section 5.1 two models are going to be tested. One PV/T air model as shown in *Figure 5.2* and one with fins incorporated in the rear wall of the PV. For clearly separating the two systems in the

description of the chapter, the PV/T model with the duct behind the PV will be mentioned as REF system and the PV/T model with the fins in the rear of the PV will be mentioned as FIN system.

For the REF system, F' is calculated from the following modified equation from Duffie and Beckman (1991):

$$\overline{F'} = \left[1 + \frac{\overline{U}_L(h_c + h_r)}{h_c^2 + 2h_c h_r}\right]^{-1}$$

Eq. (5.4)

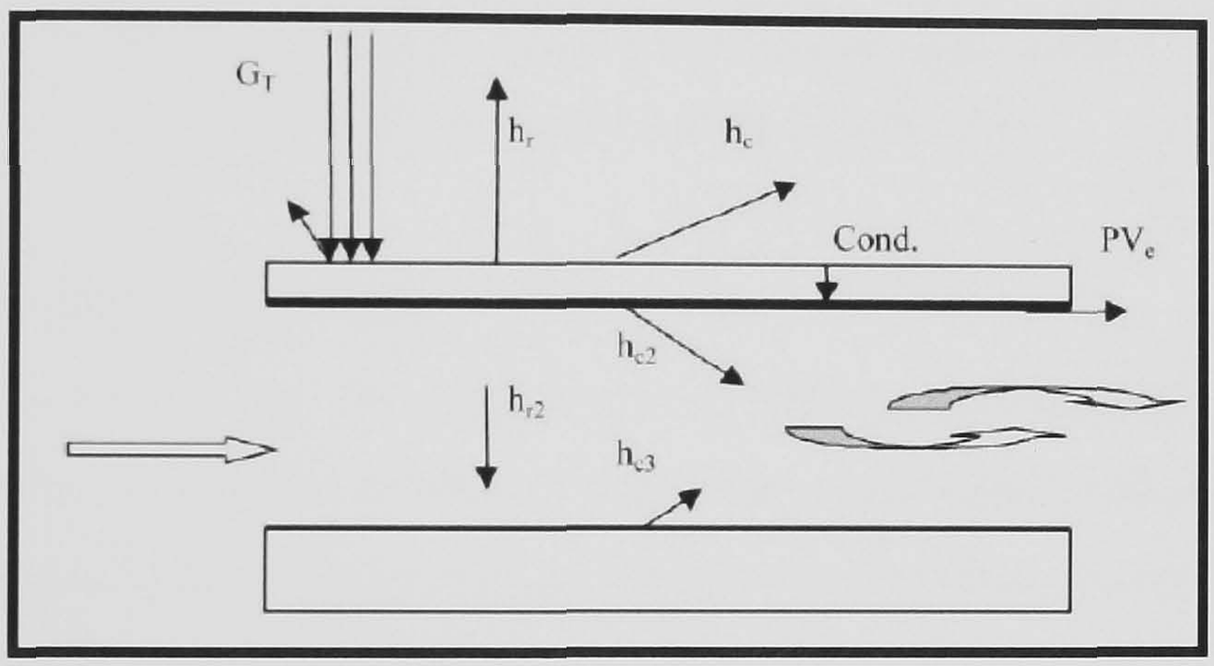

Figure 5.2 PV/T Air Heat Transfer

For the FIN system the following modified equation from Duffie and Beckman (1991) is used:

$$\overline{F'} = F_o\left[1 + \frac{2H\eta_f(1 - F_o)}{2HF_o + W}\right]$$

Eq. (5.5)

where F_o is equal to F' in Eq. (5.4), n_f is the fin efficiency factor (defined later), W is the inter-spacing of the fins. The relationship between F' and F_R is given by Florschuetz (1979) and can be seen in equation **(2.2.5)**.

5.3.1 FIN system

Figure 5.3 illustrates 3-dimensional diagram of a single rectangular fin representing the fins arrays used in the experimental rigs with important dimensions. The fin's thickness, t, is very small (0.5 mm) compared to its length L so that the effective convective

surface area of the fin(s) is $A_{fin} = 2LH$. The fin's height H is oriented along the z-coordinate, at right angles to the flow direction (x-axis).

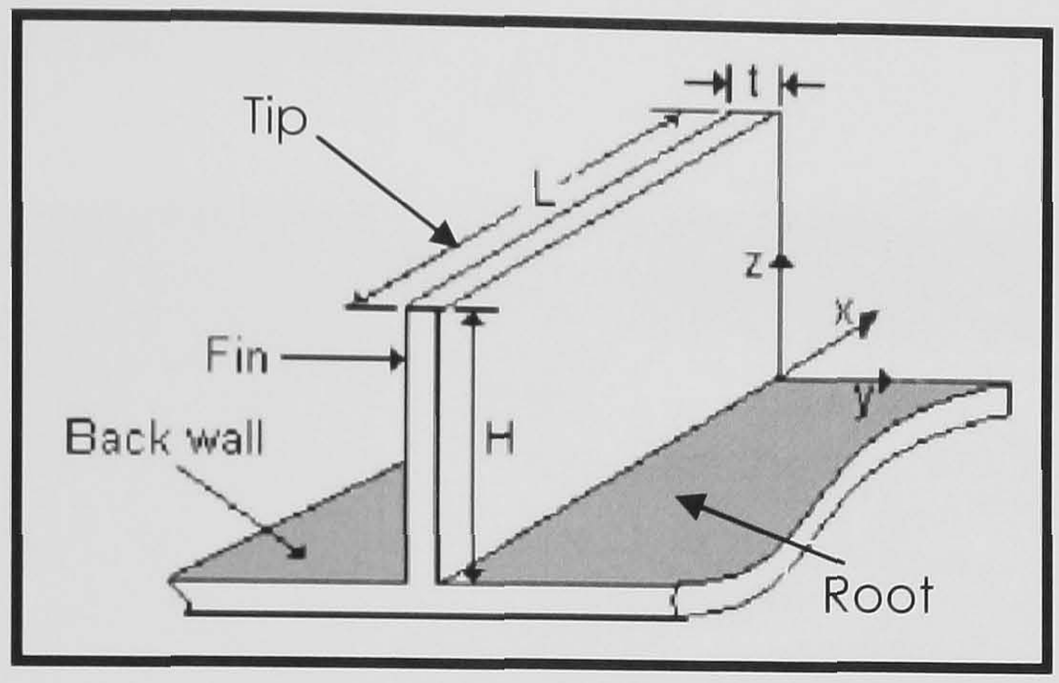

Figure 5.3 Schematic diagram of a Fin

5.3.1.1 Heat convection from fins

The fins have two boundaries, the root and the tip with the root temperature equal to T_w. The used fins are of rectangular profile with free tips (see *Figure 5.3*) and normally adiabatic tip analysis is used (Incropera and DeWitt, 1996). The maximum heat convected from the fins to the flowing air occurs when the fin's temperature is equal to the back wall temperature T_w and can be derived as (Incropera and DeWitt, 1996):

$$Q_{fin} = NA_f h_c \eta_f (T_w - T_f) \qquad \text{Eq. (5.6)}$$

where A_f is the fin surface area (=2HL) and the fin efficiency n_f is given by

$$\eta_f = \frac{\tanh mH}{mH} \qquad \text{Eq. (5.7)} \qquad \text{where } m = \sqrt{2h_c L/\kappa A_{cf}} \qquad \text{Eq. (5.8)}$$

with A_{cf} and k being the cross-sectional area of each fin and thermal conductivity of the fin material respectively. For tips fins, the parameter H in Eq. (5.8) is sometimes replaced by a parameter H_c called corrected fin height, where $H_c = (H + t/2)$ and t is the fin thickness. But if the fin is thin, its effect is negligible and may be ignored with little loss of accuracy (Incropera and DeWitt, 1996).

5.4 Experimental systems

Figure 5.4 illustrates cross-sectional view of the air channels for the REF system. The REF system represents the typical single-pass air channel attached behind the PV module and is used as a datum system.

Figure 5.4 PV/T Air Reference Model

The FIN system (*Figure 5.5*) consists of fins with rectangular profiles (Π) attached to the back wall of the air duct, for practical reasons and oriented parallel to the flow direction. Attaching them on the PV rear surface results in better PV cooling and increased heat production due to high PV temperature. In this case it requires incorporating the fins in the production phase of the PV module for good back thermal contact but makes it (PV) cumbersome, complex and heavy adding to the already high PV panel cost and transportation cost as well.

Figure 5.5 PV/T Air Model using fins in the back

Two identical prototype test models were constructed from a commercial pc-Si PV panel, of length 0.4 m, aperture area $A_a = 0.16\ m^2$. The air plenum at the rear of the panel was constructed from a thermal insulator board of thickness 5 cm on the backside and the edges with a thin aluminium sheet as inner lining.

The inlet vent is in the bottom of the PV as seen in *Figure 5.4* and forms a rectangular opening with length of 0.4 m and width 4 cm. The outlet vent is in the top of the PV as shown in *Figure 5.6*. A 5 cm diameter pipe is used to extract the air outside from the channel. The cross section of the circle were the anemometer is placed to measure the air velocity is $0.007854\ m^2$. The fan is placed on the top of the PV and extracts air from the pipe.

In order to improve PV module cooling, the channel surfaces, thin metallic sheet surface facing PV rear and the fins were painted black. The fins height and spacing distance was each equal to 3 cm.

Figure 5.6 Left: Fan used to suck air Right: PV/T Air Rig

For forced flow experiments, the air circulation was effected using a fan connected via a calibrated volumetric flow rate meter (m^3/ hr) to the output vents through a flexible air tube. Three set of experiments were tested one with different air inlet temperatures, the second with different flow rates and the third to evaluate the heat transfer contact with and without the fins. All tests were performed under steady-state conditions and efficiencies calculated with the same procedure as did in chapter 4.

For the natural flow, the inlet and outlet vents were left open to have free-flow air circulation and inlet air temperature was equal to the ambient temperature.

The airflow by natural convection in the channel depends on the weather conditions and is difficult to control it regarding stability and accurate measurements because of sporadic changes in weather conditions. The natural flow was experimentally tested by switching off the fan. Velocities of 0.5 m/s were recorded equal to a flow rate of 6.9 m^3/hr.

12 thermocouples were used to measure the essential temperatures and their locations in the REF and FIN systems. Type-K thermocouples were used for temperature measurements: PV module, rear copper wall, back ambient temperature, and the inlet and outlet air temperature. Thermocouples were also attached to the base of the fins in the FIN system in corresponding positions as that of the back wall.

To vary the air flow a controller was connected with the fan in order to achieve the desired flow rates. To vary the inlet air temperature a heater fan was placed in the back of the rig at a distance that does not affect the pressure between the inlet and outlet vent. In all tests the maximum power point was tracked in order to record the efficiency of the systems at steady state conditions.

5.5 Design procedure for cooling ducts to minimise efficiency loss due to temperature rise in PV arrays

A cooling duct may be fitted behind a PV array so that some of the solar energy absorbed by it and appearing as heat is transferred into the air in the duct and removed to the atmosphere by the resulting buoyant flow. The additional cooling lowers the operating temperature of the array and so increases the efficiency with which it converts solar energy to electricity.

Usually, the length L and width W of the duct are determined by the dimensions of the array, so that the principal design variable is the depth H of the duct. In a recent paper (Brinkworth and Sandberg, 2005a), it is reported that there is an optimum value of this quantity. This is taken here to be such that the temperature of the array at the top of the duct, where it is highest, has the lowest value that can be achieved in a given set of operating conditions.

The optimum is defined in terms of the hydraulic depth of the duct D, which for a given width is defined by

$$D = 2WH/(W + H)$$

Eq. (5.9)

Where W = 0.4 m and H = 0.03 m, so D = 0.0558 m

A design rule-of-thumb was given that the ratio L/D should be around 20. This is a robust rule, the value being nearly independent of other quantities, particularly the slope of the array to the horizontal, so that it will serve for most installations, whether on roofs or walls. In this case to reach the optimum level we needed a depth of only 1 cm. As this was difficult to construct, a depth equal to the height of the fin was used. The ratio of L/D was 7.16. As also Tonui (2006) reports that when the depth of the duct increases the temperature of the PV increases and the thermal efficiency decreases. This is valid for natural and forced flow. The cross sectional area of the free channel in the back of the PV is 0.012 m^2.

5.6 Experimental results

The parameters that are essential for characterization of a PVT/AIR collector intended for BIPV applications are the temperature of the PV module, T_{PV}, back wall, T_w and air outlet, T_{out}. T_{PV} gives a measure of the ventilation effected by the thermal unit attached to the PV module with respect to unventilated PV module. T_w is a measure of the shielding and cooling effect on the building as a result of PV module (or arrays) installation and airflow in the cavity, respectively. Finally, T_{out} determines the thermal efficiency and ventilation rates (in case of natural flow).

5.6.1 First set of experiments

Figure 5.7 and *5.8* shows the temperature in the front and back of the PV and the inlet and outlet air temperature. It may be seen in the first figure that the outlet temperature is low, implying that the heat transfer coefficient is not very high and this results in an elevated the PV temperature. The maximum PV temperature at the front and back is 60 and 50 °C and the air temperature difference is around 4.33 °C. In the second figure it may be seen that the fins have reduced the PV temperature and in the same time have increased the outlet air temperature. The fins reduced the front and back temperature to 52 and 48 °C respectively and the temperature difference between the inlet and outlet air

have increased to 9.34 °C. From the *Figure 5.8* it may be seen that the fin temperature is very close to the temperature in the back of the PV. This implies that there is very good conductivity between the base and the fin. The heat transfer coefficient of the REF case was h_{ca} = 30 W/m^2*K and for the FIN model is 150 W/m^2*K. From this it may be observed that with the fins we have an increase of 500 % in heat transfer.

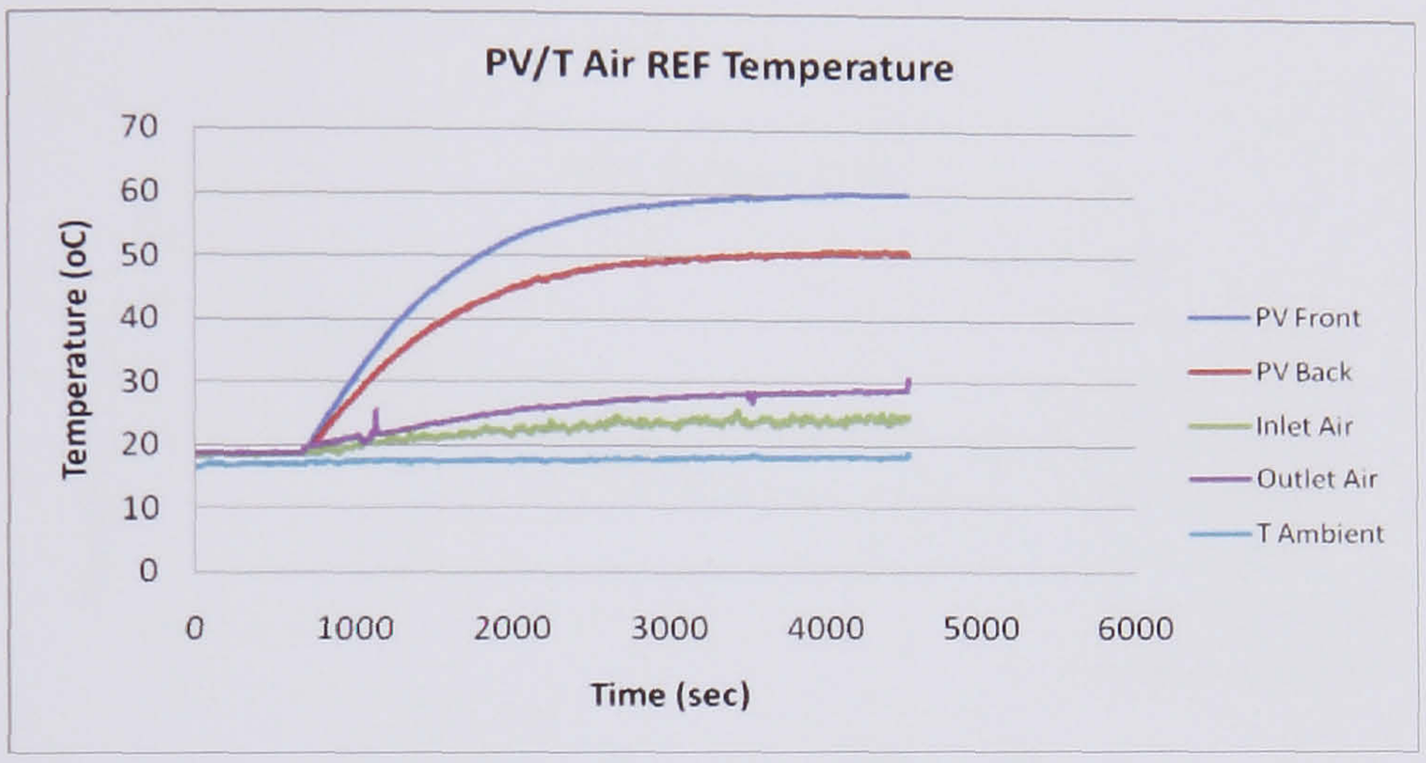

Figure 5.7 PV/T Air Reference Temperature at 0.9 m/s

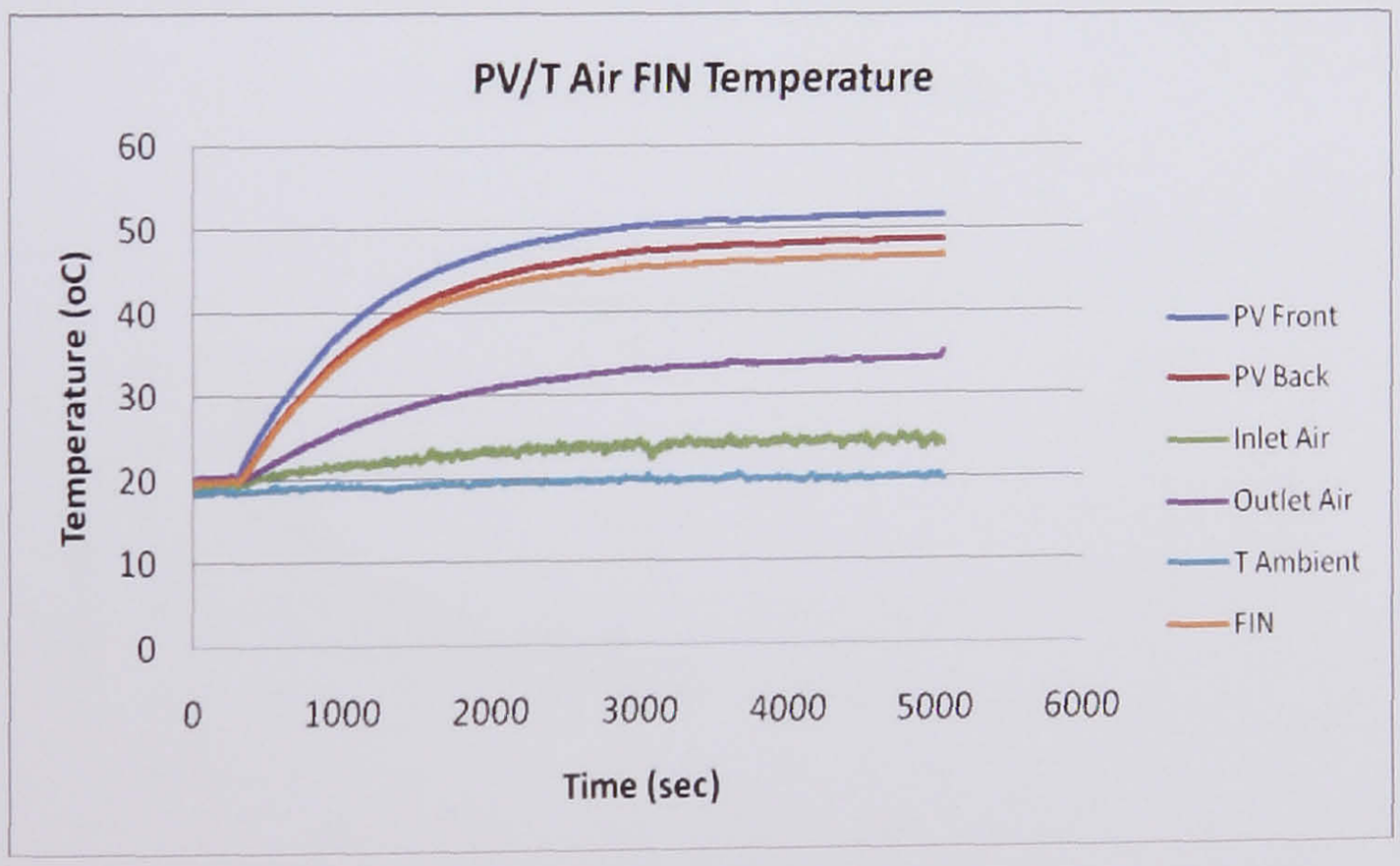

Figure 5.8 PV/T Air FIN Temperature model at 0.9 m/s

5.6.2 Second set of experiments

A set of experiments was taken with a range of flow rates from 5 – 117 m^3/hr and from these experiments it was possible to calculate the thermal and electrical efficiencies for each different flow rate and to observe the influence that flow rate has on the PV

temperature and on the outlet air temperature. Also the experimental values were compared with the simulations that were taken by the help of TRNSYS as also did in chapter 4. *Figure 5.9* and *5.10* show the influence flow rate has on PV temperature and the temperature difference between inlet and outlet. It may be seen that as the flow rate increases the PV and also the outlet air temperatures decreases. The simulation also shows that the values agree well with the models .

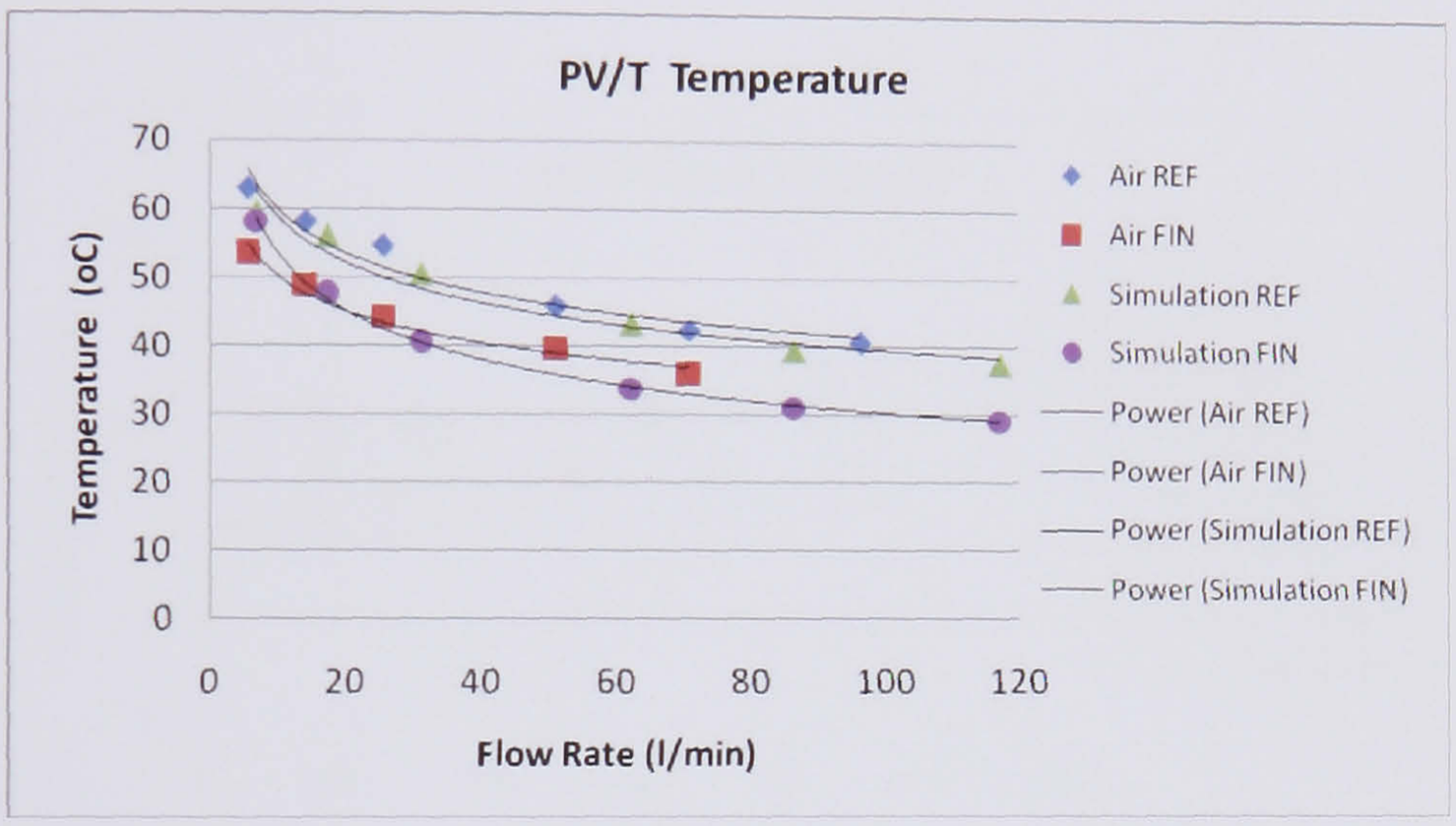

Figure 5.9 PV/T for REF and FIN models Temperature at different flow rates and compared with simulation

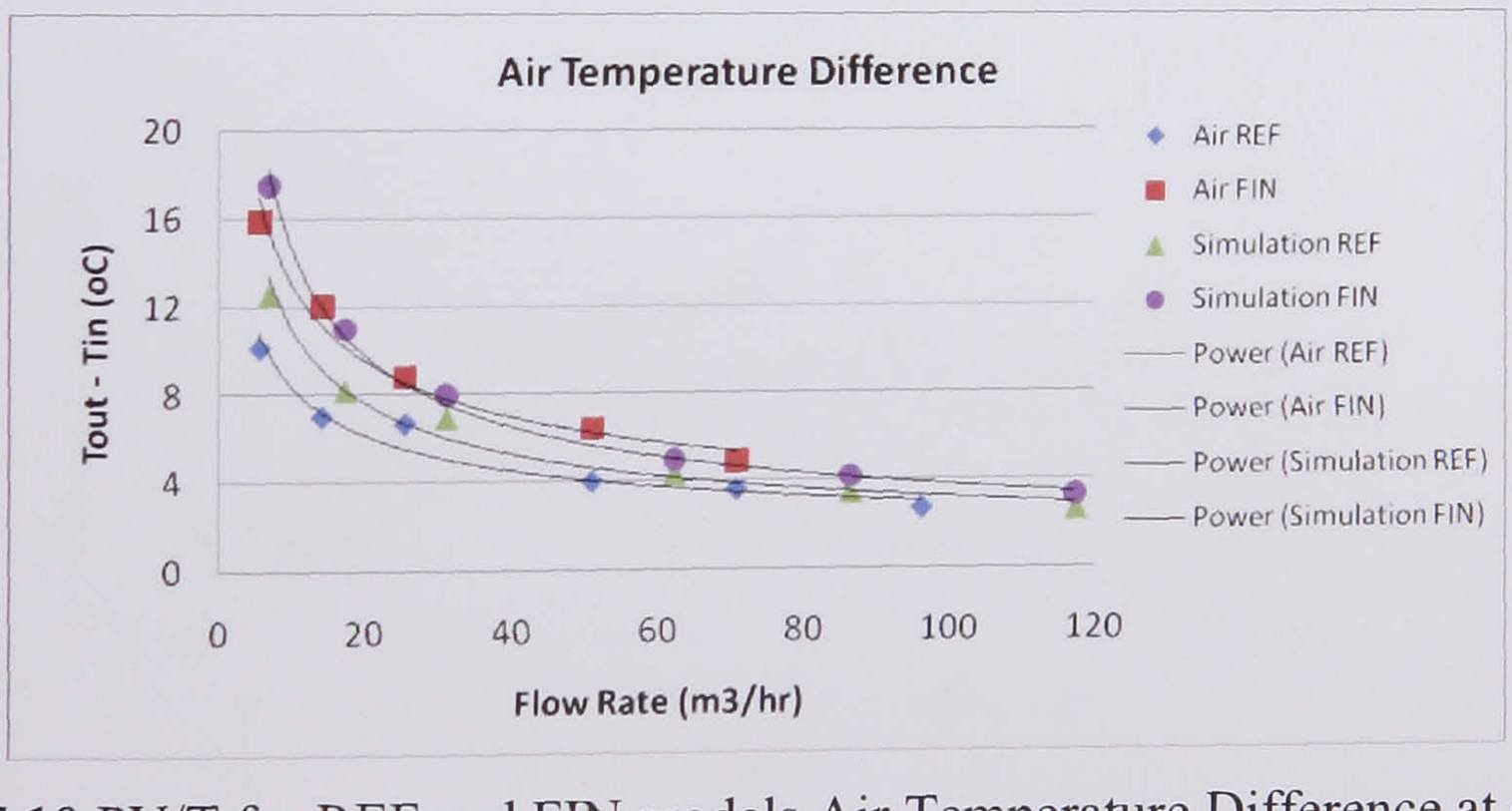

Figure 5.10 PV/T for REF and FIN models Air Temperature Difference at different flow rates and compared with simulation

Figure 5.11 compares the experimental and simulation values for REF and FIN cases. It may be observed that as the flow rate increases the electrical efficiency improves and

the FIN case give as higher efficiency values than the REF case. The increase of the heat transfer improves the system performance.

The same is being observed with the thermal efficiency of the system (*Figure 5.12*). The FIN model give as much higher thermal efficiency at the same flow rates with the REF case. As an example we see that at 25 m^3/hr for the experimental FIN thermal efficiency is 46.4% and the REF around 34.2%. This is an increase of 35% between the FIN and the REF model.

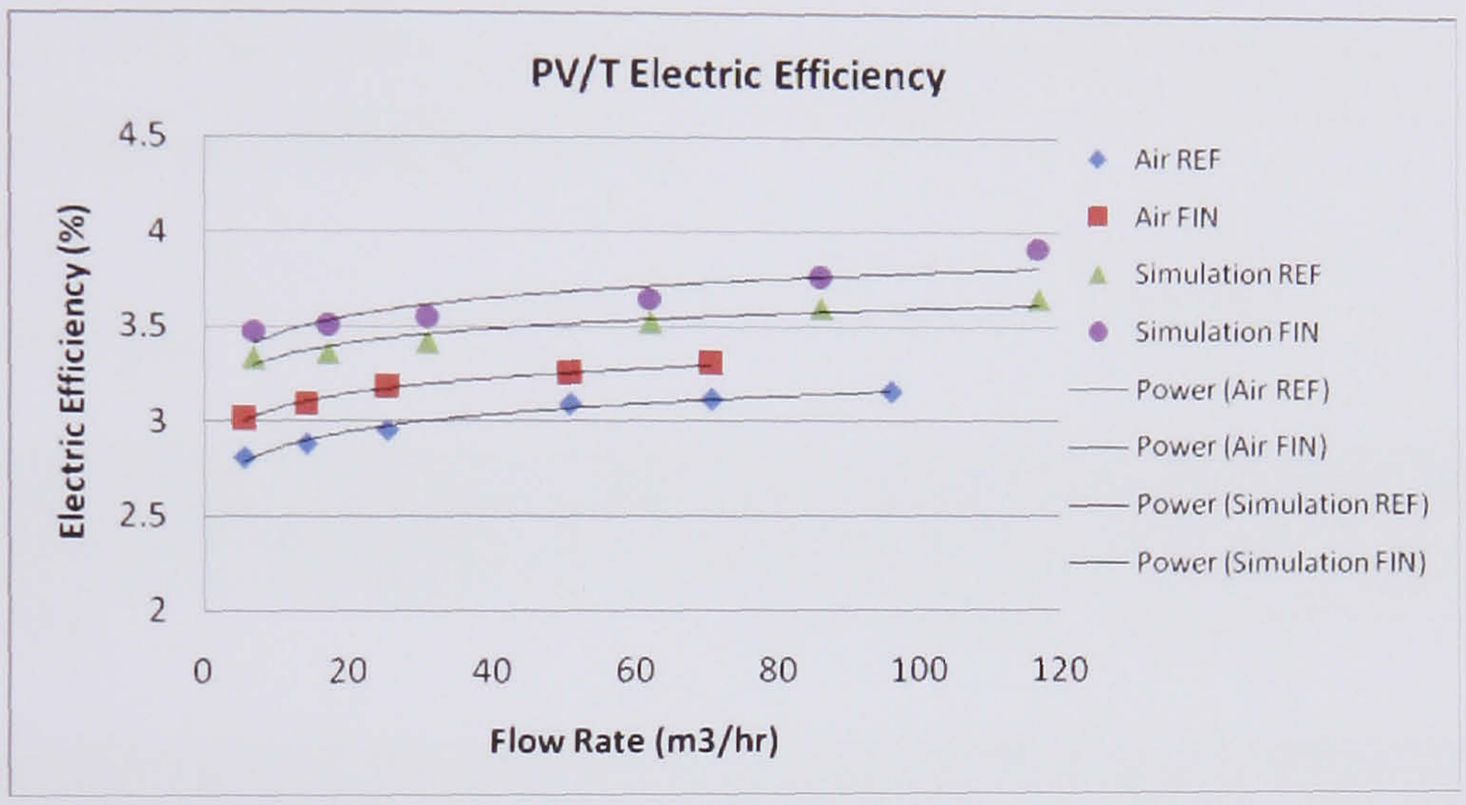

Figure 5.11 PV/T for REF and FIN models Electrical Efficiency at different flow rates and compared with simulation

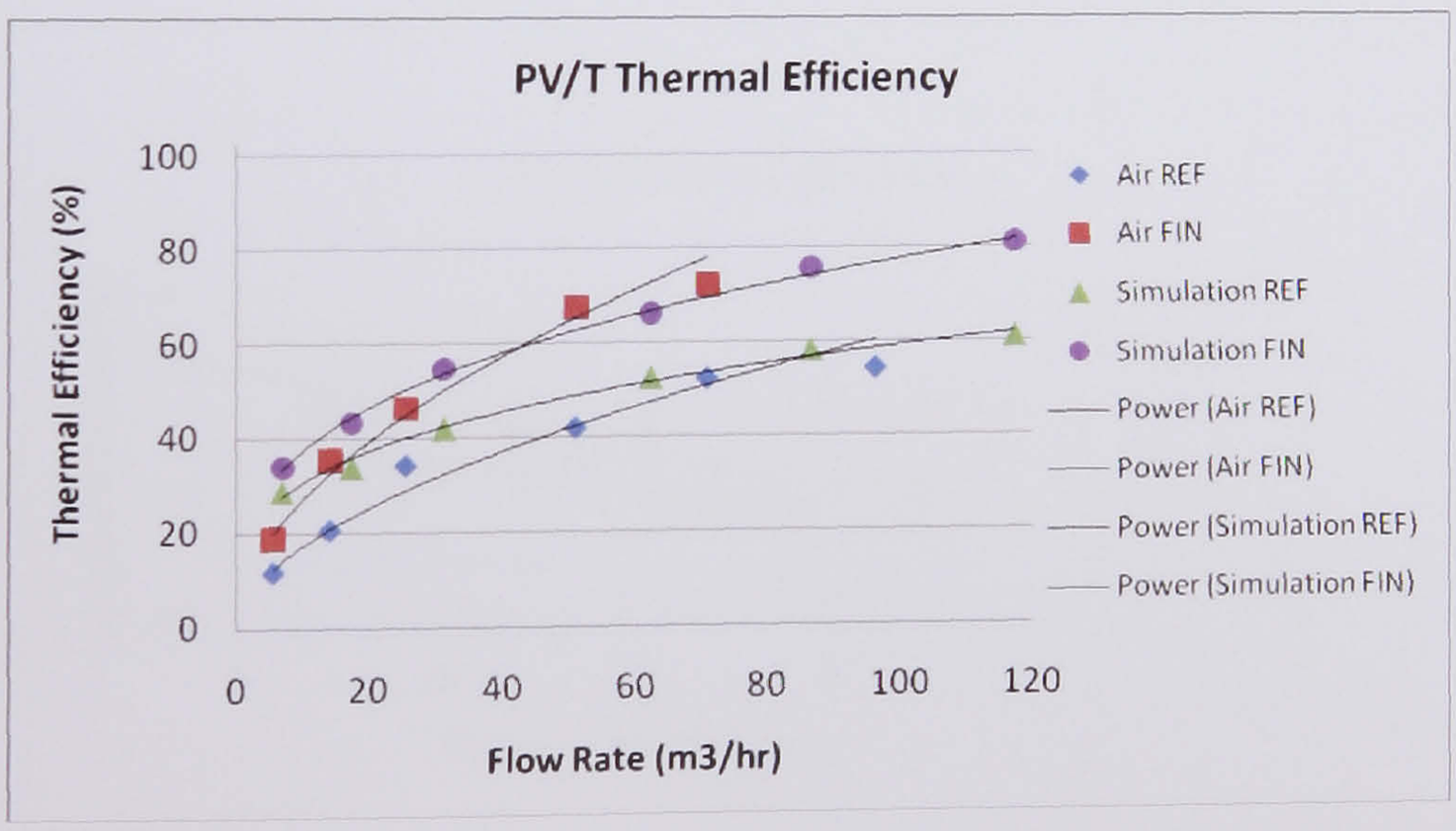

Figure 5.12 PV/T for REF and FIN models Thermal Efficiency at different flow rates and compared with simulation

5.6.3 Third set of experiments

The third set of experiments tests the systems with varying the inlet water temperature. The electrical efficiency can be presented in *Figure 5.13* as a function of the PV module temperature where the electrical efficiency is seen to drop with the rise in PV module temperature. The linear correlation between the electrical efficiency and the module temperature may be described by the linear curve and the linear equation describing it is given in *Table 5.1*.

Table 5.1 PV/T Air electrical efficiencies for experimental and simulated models

Linear equations describing the curves in Figure 5.13 **PV/T System Type**	**Equation**
PV/T Air REF	$n_{ele} = 3.006*(1 - 0.0013*(T_{pv} - 25))$
PV/T Air FIN	$n_{ele} = 3.193*(1 - 0.0025*(T_{pv} - 25))$
PV/T Air REF Simulation	$n_{ele} = 3.077*(1 - 0.0029*(T_{pv} - 25))$
PV/T Air FIN Simulation	$n_{ele} = 3.287*(1 - 0.0036*(T_{pv} - 25))$

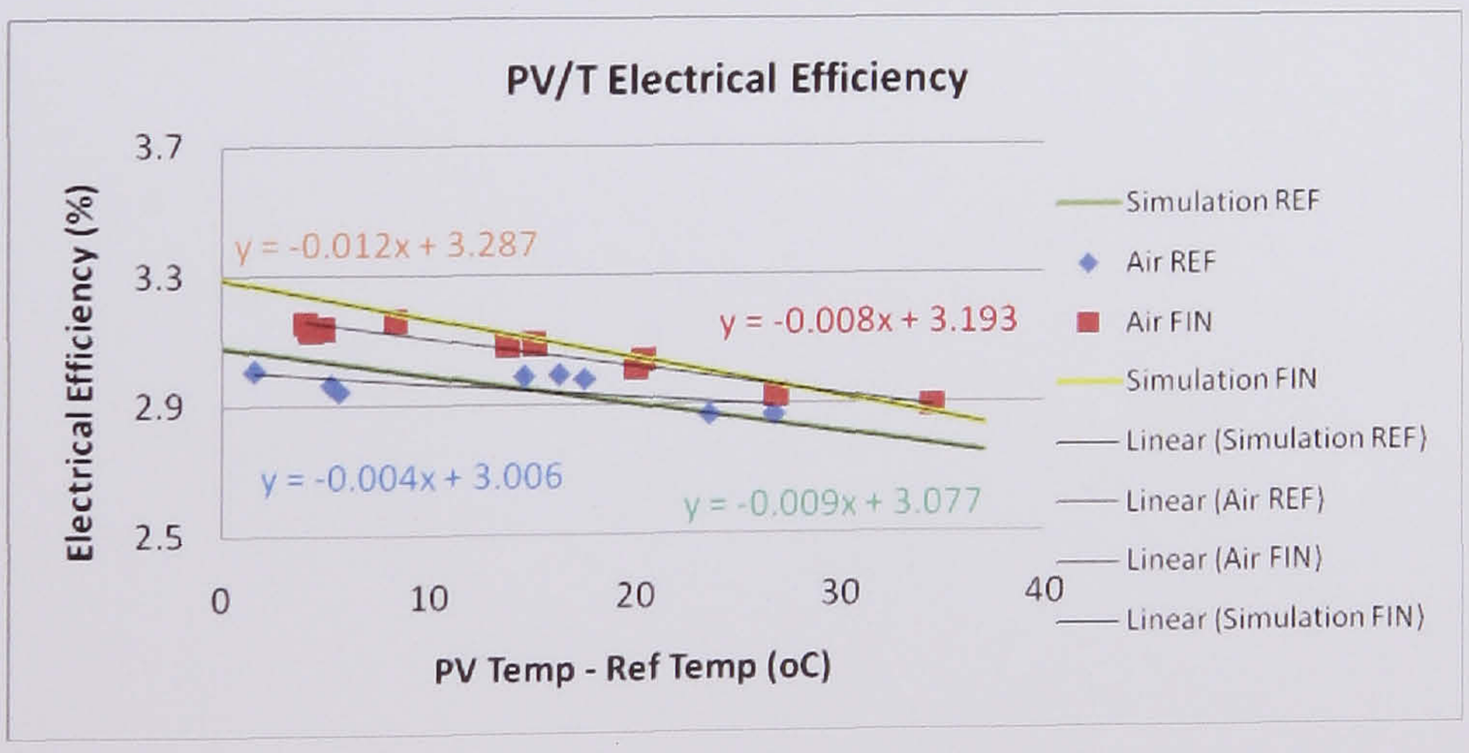

Figure 5.13 PV/T for REF and FIN models Electrical Efficiency as a function of Temperature Difference of PV and a Reference Temperature (25 °C) and compared with simulation

In *Figure 5.14*, the steady-state thermal efficiency n_{th}, obtained at different air inlet temperature, is plotted against $\Delta T/G$ (with $\Delta T = T_{in}-T_a$). The linear curves are summarized by the equations in *Table 5.2.* From the table 5.2, one notices that the maximum thermal efficiency that can be achieved by the REF and FIN system from these experiments are 30.4%, and 49.6%, respectively.

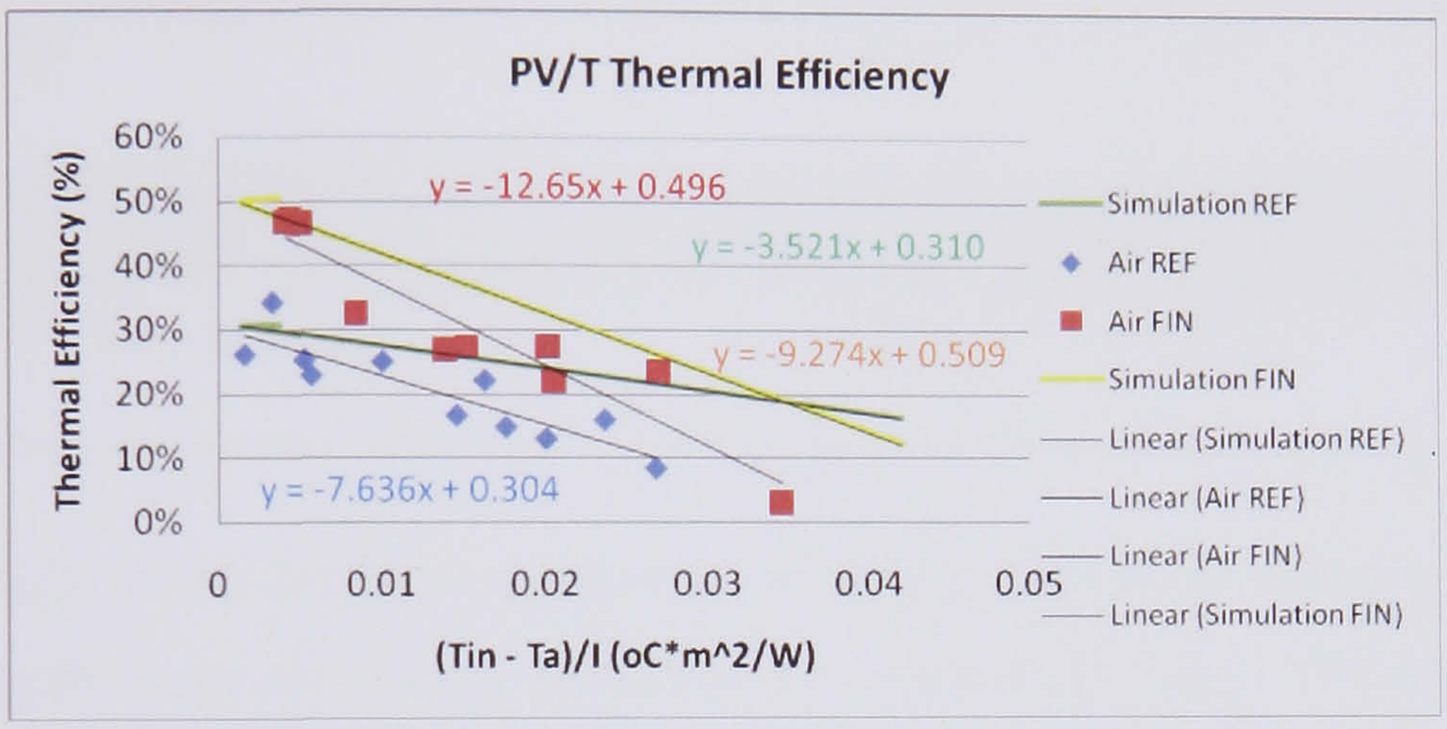

Figure 5.14 PV/T for REF and FIN models Thermal Efficiency as a function of $\Delta T/G$ and compared with simulation

Thus the results show that the FIN system has higher thermal efficiency that is around 63% higher than that of the REF system. The simulated with the experimental results show good agreement except the heat loss coefficient that was higher during the experiments.

Table 5.2 PV/T Air thermal efficiencies for experimental and simulated models

Linear equations describing the curves in Figure 5.14 PV/T System Type	**Equation**
PV/T Air REF	$n_{th} = 0.304 - 7.636*\Delta T/G$
PV/T Air FIN	$n_{th} = 0.496 - 12.65*\Delta T/G$
PV/T Air REF Simulation	$n_{th} = 0.310 - 3.52*\Delta T/G$
PV/T Air FIN Simulation	$n_{th} = 0.509 - 9.274*\Delta T/G$

From the results of the electrical and thermal efficiency, the energy saving efficiency, total energy efficiency and exergy efficiency were estimated. *Figure 5.15* shows the energy saving efficiency. At zero reduced temperature the efficiency of the REF and FIN system were 35.3% and 58% respectively from experiments and 39.2%, 59.7% from simulations. The experimental results are in good agreement with the simulations. By adding the electrical and thermal efficiency of the systems one obtains the total energy efficiency. *Figure 5.16* shows a similar trend in total energy efficiency performance for the FIN system in comparison with the REF. For zero reduced temperature there's the FIN system is around 58% more efficient than the REF system. The exergy efficiency is given in *Figure 5.17* and indicates the optimum working conditions for the unglazed PV/T Air system. For both systems it may be seen that the PV/T Air collector optimum working conditions is around 36 ^{o}C of inlet air temperature and the difference between the two systems at the optimum point is 4%.

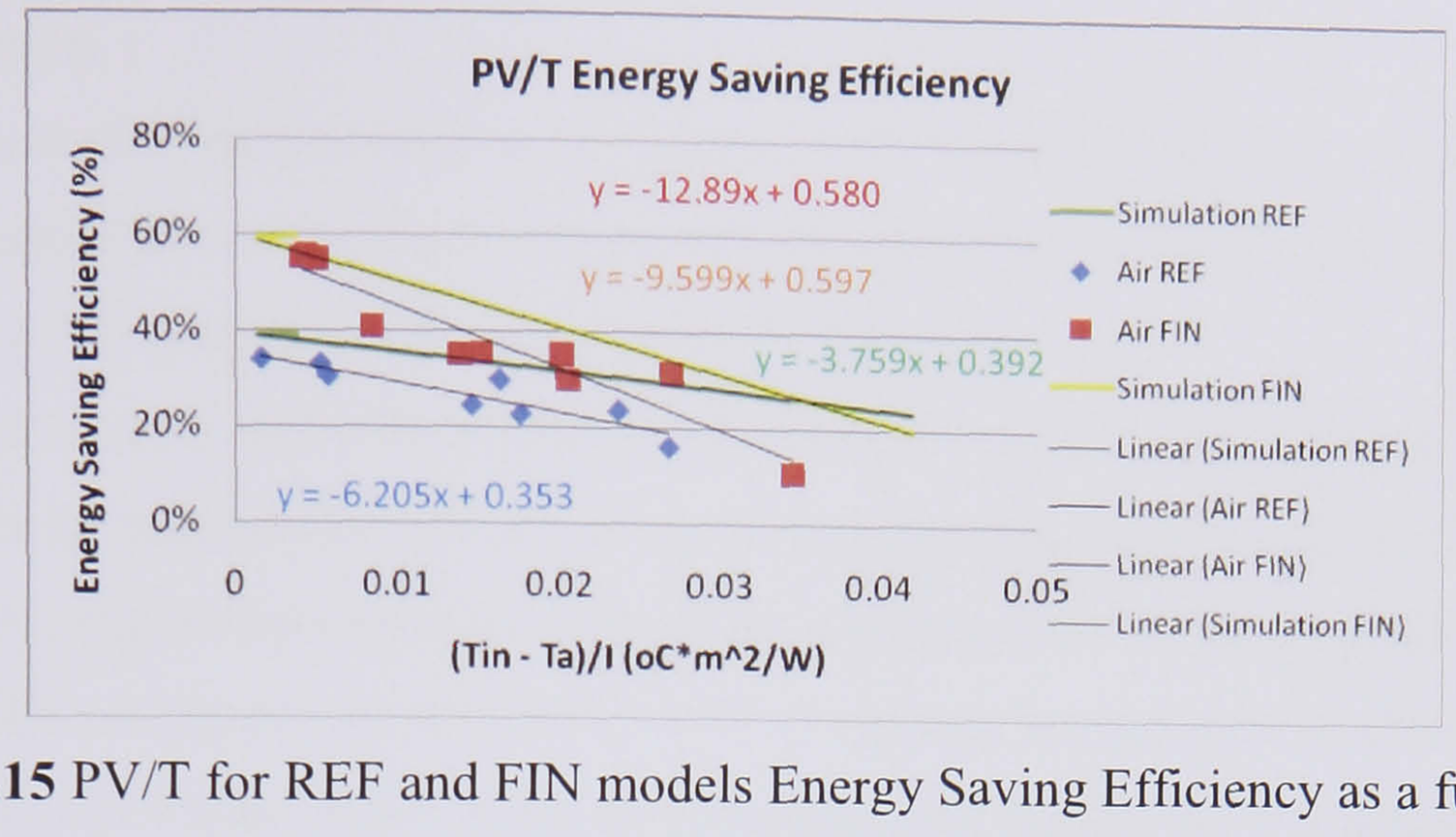

Figure 5.15 PV/T for REF and FIN models Energy Saving Efficiency as a function of ΔT/G and compared with simulation

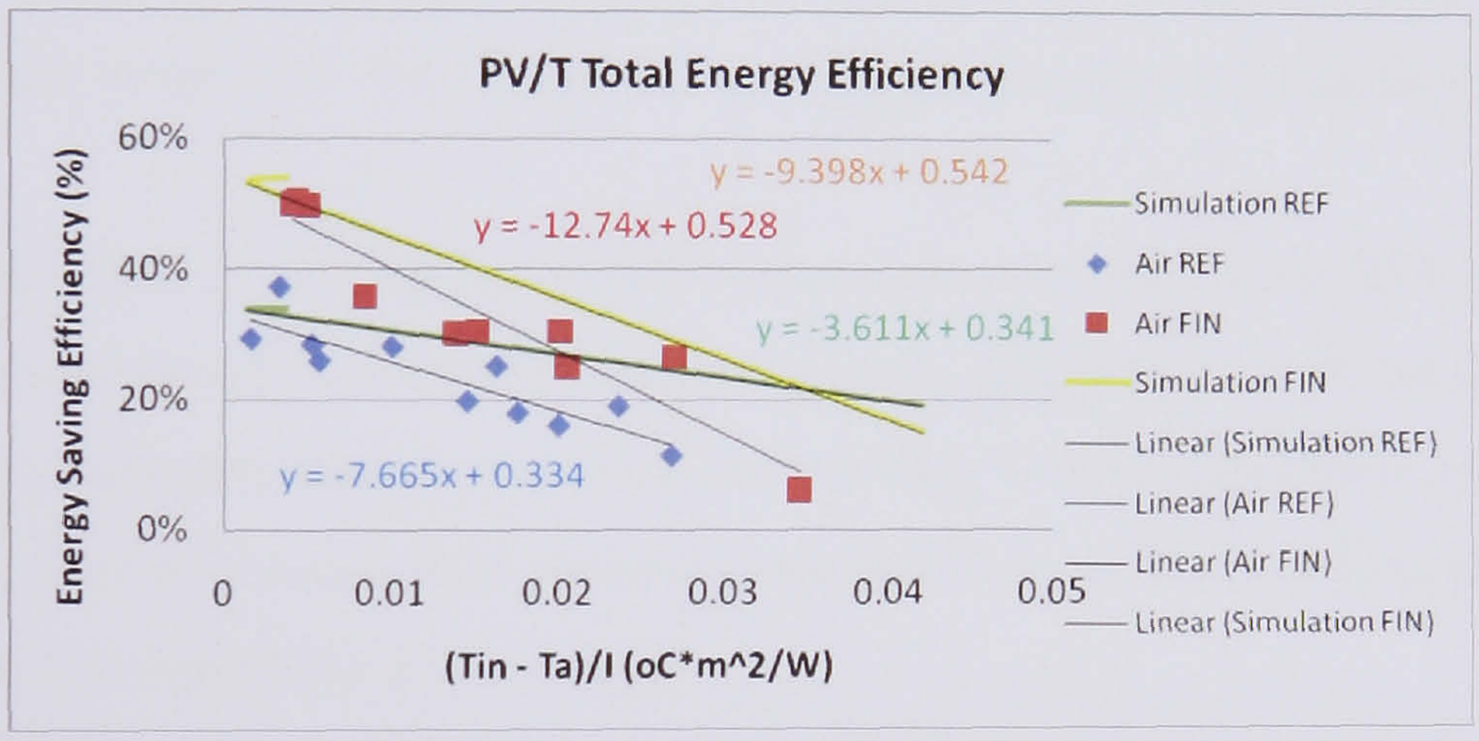

Figure 5.16 PV/T for REF and FIN models Total Energy Efficiency as a function of ΔT/G and compared with simulation

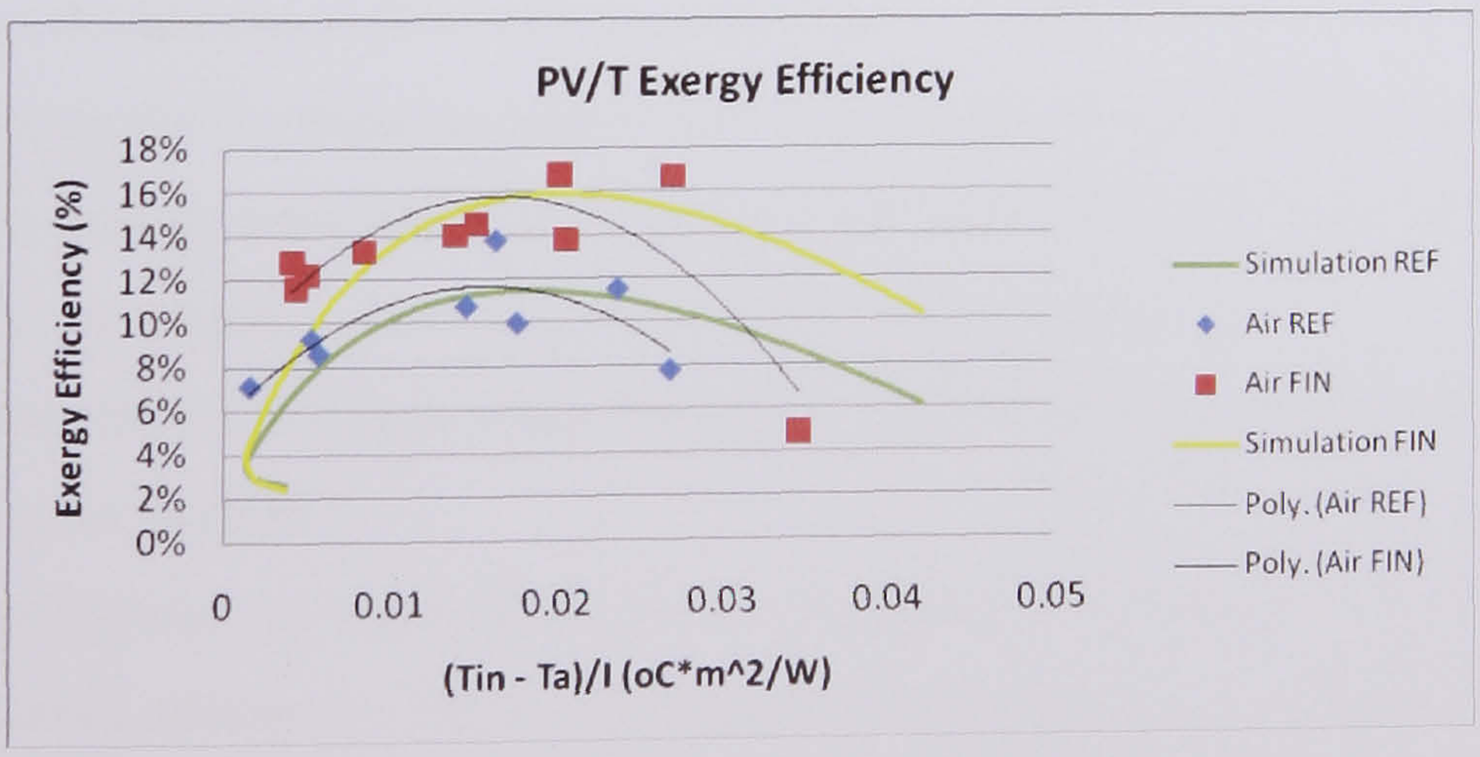

Figure 5.17 PV/T for REF and FIN models Exergy Efficiency as a function of ΔT/G and compared with simulation

5.7 Discussion

The electrical efficiency reduces with increasing PV module temperature and the suggested modification increases the thermal efficiency of the PVT/AIR collector by 35% for the FIN system, compared with the REF system.

In forced flow mode and airflow rate of 25 m^3/hr the corresponding air velocity is 0.9 m/sec while for natural flow of 5.65 m^3/hr the corresponding air velocity is 0.2 m/sec. The module temperature measured with no air circulation (i.e. under stagnation) for all the PVT/AIR configurations was about 90 °C at ambient temperature of about 20 °C and insolation level of 1000 W/m^2. With air circulation, the measured PV module temperatures ranged from 35 to 65 °C depending on the flow rate. Thus the air circulation by forced or natural flow in the air channel reduces the PV module temperature by at least 25 - 55 °C and thus contributes to improved electrical output power.

The addition of fins lowers the back wall temperature compared to the REF system for both natural and forced flows and could contribute to reducing the building overheating by reducing conduction heat gain through the building's wall or roof materials. For the FIN system, the fins enhance heat transfer from the PV to airflow resulting in a lower temperature than that of the REF system.

Closer inspection of the temperature profiles in the *Figure 5.9* shows that the fins reduce the back wall temperature by about 13 °C for both forced and natural flow.

The modified system gives higher outlet air temperature with respect to the REF system for both forced and natural flow with the FIN system. In the FIN system, heat is conducted along the fin from the base of the PV towards the tip and simultaneously the fin dissipates heat by convection to the flowing air and increases the rate of heat convection to the channel. Thus the FIN system is more effective in PV cooling and heat extraction than the REF system while the FIN is superior in reducing the back wall temperature than the REF.

The modified system can improve the energy saving in the buildings because of the increased overall efficiency. The heat produced can be channelled through a ducting system into the building interior for heating in winter. The suggested modification and

their mounting are practical in that they can easily be fabricated and attached in the building structure considering that the off-the-shelf modules are to be used.
The system, when operated in free flow mode, can provide thermal comfort with good user control at minimum capital cost and negligible operation and maintenance hence cost effective. The improved PVT/AIR system can be used also to heat air for several industrial or agricultural processes, such as drying of products, and could promote PV applications in these sectors.

5.8 Conclusions

The developed steady state model predicts and compares the thermal and electrical performance of PV/T collector with and without fins. The prediction results agreed with the results obtained from experiment carried out in the laboratory.
The possibility of generating electricity and heat energy from a commercial PV module adopted as a PVT/AIR solar collector with forced or natural airflow in the channel was demonstrated. Under natural flow, the temperature rise could reach up to about 10 to 15 ^{o}C for REF and FIN system and could induce sufficient airflow rate to effect adequate ventilation. For the forced convection with flow rate of 0.9 m/s (or 25 m^3/hr) the use of fins yields an efficiency of 46% in comparison with the REF system.

In connection with *Figure 5.10*, it is obvious that as the air temperature rise decreases with increasing mass flow rate, the collector thermal efficiency gets correspondingly higher and higher due to the decrease in the average temperatures of the absorber plate, thereby reducing the top losses. Increasing the flow rate will increase the heat transfer coefficient between the channel walls and the working fluid, resulting in a lower mean photovoltaic cells temperature. This will increase the electrical efficiencies of the collector. However the enhancement in the value of electrical efficiency is remarkably small compared with the increase in the value of mass flow rate. Nevertheless from *Figure 5.13*, *5.14* and *5.16* it may be shown that there is some contribution of the electrical efficiency to the total efficiency of the system. The combined efficiency varies from 11 to 72% at mass flow rate of 0.2 – 3.4 m/s (or 5.65 – 96 m^3/hr) and radiation intensity at 1000 W/m^2.

In general, results show that electricity production in a PV/T hybrid module decreases with increasing temperature of the air flow. This implies that the air temperature should be kept as low as possible. On the other hand, the system should deliver hot air for other purposes. A trade off between maximizing electricity production and producing hot air of useful temperatures is thus necessary. The simultaneous use of hybrid PV/T and fins has a potential to significantly increase in electrical production and reduce the cost of photovoltaic electricity.

It has been observed that the experimental results were slightly higher than as predicted in mathematical model. This characteristic may be due to the effect of IR radiation released by tungsten halogen lamps during the test.

The choice of the modification depends on the location of application which determines the optimization of the PVT/AIR collector required, whether for heating or cooling. In high latitude regions, heating in winter is more important than cooling in summer while the converse is true for low latitude and tropical regions. In such scenarios, use of FIN system is ideal for high latitude regions (more heating) where the high heat gain is exploited in winter. Therefore, the increased performance of the finned PVT/AIR system will contribute significantly towards wider application of PV systems and mitigation of energy supply of buildings and consequently lower CO_2 emission among other social benefits

CHAPTER 6: PHOTOVOLTAIC/THERMAL SYSTEM HEAT PIPE

6.1 Introduction

Usually, conventional solar collectors use pipes attached to the collecting plate and a heat transfer fluid, such as water, to transfer by natural or forced circulation the heat captured by the solar collector to a storage tank. Some of the shortcomings associated with conventional solar collectors include extra expense of the forced circulation system due to the pump and its extracted power, extra space required for the natural circulation system due to implicit position of the collector relative to the tank, the potential risk of cooling of stored hot water due to the reverse flow at night, freezing of the water on cold nights, pipe corrosion due to the use of water and the limited quantity of heat transferred by the heat transfer fluid.

Heat pipes offer a promising solution to these problems. The basic heat pipe is a closed container consisting of a small amount of vaporizable fluid (e.g., a refrigerant). The heat pipe employs an evaporating-condensing cycle, which accepts heat from an external source, uses this heat to evaporate the liquid (latent heat) and then releases latent heat by reverse transformation (condensation) at a heat sink region. This process is sustained by a return feed mechanism of the condensed fluid back to the heating zone. Heat pipes are very flexible systems with regard to effective thermal control. Their heat transfer coefficient in the evaporator and condenser zones can reach 10^3–10^5 W/m^{2}K, and their heat pipe thermal resistance to 0.01–0.03 K/W (Vasiliev, 2005).

Heat pipes designed to work under gravity with the condenser above the evaporator do not require external power or capillary action in order to return the heat transfer fluid to the evaporator (see *Figure 6.1*). This type of heat pipe is known as the gravity assisted heat pipe, closed two-phase thermosyphon or wickless gravity assisted heat pipe. Closed two-phase thermosyphon solar collectors consist of heat pipes (or thermosyphon tubes) filled with a refrigerant and used in closed loop water heating systems. Closed loop solar heating systems are suitable for domestic solar water heating, solar swimming pool heating or solar space heating systems. They are also suitable for areas with questionable water quality and all climatic conditions. Furthermore, they are the preferred option for extremely cold areas.

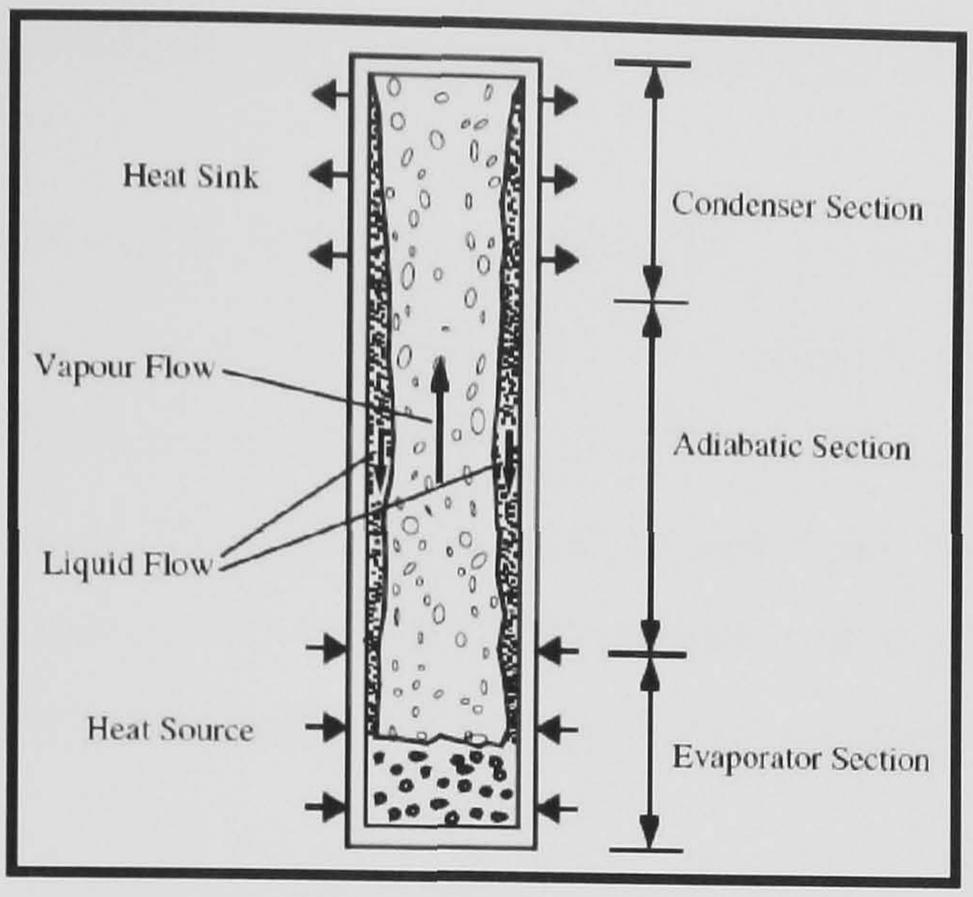

Figure 6.1 Schematic of a gravity assisted heat pipe (Srihajong, 2006)

In the present work the results of a theoretical and an experimental investigation of the energy behaviour of a new type of PV/T system employing heat pipes are presented. The system employs a gravity assisted loop heat pipe with the one model having a tank placed above the collector at such a height as to allow the natural return of the liquid phase to the lower part of the collector. The second model uses a series of manifolds coupled to the condenser side of the heat pipes.

The novelty of the system consists in the use of a new way to incorporate the heat pipe operation principle in a solar system and place that system in the back of a PV in order to reduce the panel temperature and improve the electrical efficiency of the system. In fact a loop heat pipe is introduced in both the collector and the tank or manifolds acting as a direct heat transfer device. One of the advantages of using heat pipes in the back of the PV are a) the thermal diode benefit when the collector temperature is less than storage water temperature; b) less area needed in the back of the PV to incorporate the heat pipes than the water coil layout; c) the reasonable resistance against corrosion by selecting a suitable working fluid to be compatible with the pipe wall material; d) the easy freeze protection; e) the lower pumping requirements. Because the PV/T system using heat pipes is not covering the same area as the PV/T system with the serpentine pipes in the back of the PV and because the thermal resistance of the heat pipes cause a reduction in the heat transfer it is obvious that the system with the serpentines work more effectively. But the advantages mentioned above can provide a useful new PV/T

approach that can be considered as an alternative technology used for different applications.

The research presented includes an analysis of the basic operation parameters of the system and specifically of the heat pipe, a study of the evaporation – condensation operation cycle, a quantitative investigation of the energy fluxes from the PV collector to the heat pipe and from the heat pipe to the tank or manifolds. The usefulness in evaluating the heat pipe parameters is to understand how a heat pipe works under specific conditions and how these parameters can help to design the PV/T heat pipe design.

6.2 Heat Pipe Capacity Limits

As mentioned in section 2.6, a heat pipe is a very efficient device in terms of the heat transfer. Capacity of heat pipe heat transfer is governed by several limits, namely capillary limit, sonic limit, boiling limit, entertainment limit, and viscous limit for a normal heat pipe working at the normal temperature. These limits determine the maximum heat transfer rate for an individual heat pipe under a given operating condition.

6.2.1 Capillary Limit

For a given capillary wick structure and working fluid combination, the pumping ability of the capillary structure to provide the circulation for a given working medium is limited. This limit is usually called the capillary or hydrodynamic limit (Faghri, 1995). The circulation of working fluid in the heat pipe can be achieved through the capillary pressure head on the condition that it is greater or equal to the sum of the pressure losses along the vapour-liquid path, which can be expressed as:

$$\Delta p_{cap,max} \geqslant \Delta p_g + \Delta p_{e,\delta} + \Delta p_{c,\delta} + \Delta p_l + \Delta p_v \qquad \text{Eq. (6.1)}$$

were Δp_v is the vapour pressure drop along the heat pipe and Δp_l is the pressure drop for the liquid due to the frictional drag at the liquid-vapour interfaces. $\Delta p_{e,\delta}$ and $\Delta p_{c,\delta}$ are the pressure drops due to the evaporation and condensation at the liquid-vapour interface, respectively, and usually can be neglected. Δp_g is the pressure drop in the liquid due to

the effect of the gravitational force in the direction of the heat pipe axis, and which can be expressed as

$$\Delta p_g = \rho_l g l_p \sin\Phi \qquad \text{Eq. (6.2)}$$

Using the Laplace-Young equation $\Delta p_{cap,max}$ for a normal wicked heat pipe is a function of the surface tension σ, the wetting angle θ, and the radius of curvature of the liquid-vapour interface in the evaporator, r_{ce}.

$$\Delta p_{cap,max} = (2\sigma / r_{ce}) \cos\theta \qquad \text{Eq. (6.3)}$$

For the wickless heat pipe, there is no capillary pressure along the pipe length, i.e

$$\Delta p_{cap,max} = 0$$

For constant heat addition and heat rejection, the liquid pressure drop, Δp_l may be found (Faghri, 1995):

$$\Delta p_l = -\left(\frac{\mu_l}{K A_l h_{fg} \rho_l}\right) l_{eff} q_e \qquad \text{Eq. (6.4)}$$

Where

$$K = r_{hl}^2 / 8 \qquad \text{Eq. (6.5)}$$

$$l_{eff} = 0.5 l_e + l_a + 0.5 l_c \qquad \text{Eq. (6.6)}$$

Determination of the vapour pressure drop, Δp_v, in the heat pipes is complicated because of the compressibility of vapour. Zhao (2003) gave the following expression for the vapour pressure drop:

$$\Delta p_v = \left(\frac{C(f_v Re_v)\mu_v}{2 r_{hv}^2 A_v \rho_v h_{fg}}\right) l_{eff} q_e \qquad \text{Eq. (6.7)}$$

The friction factor fv and the constant C can be determined once the local axial Reynolds number and Mach number are defined. These expressions are given below:

$$Re_v = \frac{2 r_{hv} q_e}{A_v \mu_v h_{fg}} \qquad \text{Eq. (6.8)}$$

$$M_v = \frac{q_e}{A_v \rho_v h_{fg} (R_v T_v)^{0.5}} \qquad \text{Eq. (6.9)}$$

For the different conditions, Kraus et al (1983) gave the expressions of f_v and C which are summarised in *Table 6.1*:

Table 6.1 Parameters against conditions for vapour pressure drop

Re	M	f	C
$Re_v \leqslant 2300$	$M_v \leqslant 0.2$	$(f_v Re_v) = 16$	$C = 1.00$
$Re_v \leqslant 2300$	$M_v > 0.2$	$(f_v Re_v) = 16$	$C = C_1 = \left(1 + \left(\frac{\gamma - 1}{2}\right) M_v^2\right)^{0.5}$
$Re_v > 2300$	$M_v \leqslant 0.2$	$(f_v Re_v) = 0.038$	$C = C_2 = \left(\frac{2\gamma_{hv} q_c}{A_v h_{fg} \mu_v}\right)^{0.75}$
$Re_v > 2300$	$M_v > 0.2$	$(f_v Re_v) = 0.038$	$C = C_1 C_2$

6.2.2 Sonic Limit

Sonic limit is reached under chocked working conditions where the vapour velocity may reach sonic or supersonic values during either start-up or steady state operation. With Mach number lower than 0.2, the vapour can be treated as incompressible. However when then vapour Mach number is high especially when the vapour flow approaches the sonic limitation, vapour compressibility must be taken into account. For M = 1 the maximum heat flow rate $q_{s,max}$ is:

$$q_{s,m} = A_v \rho_v h_{fg} (\gamma R_v T_v / (2(\gamma + 1)))^{1/2} \qquad \text{Eq. (6.10)}$$

6.2.3 Boiling Limit

Boiling limit happens when the radial heat flux or the heat pipe wall temperature becomes excessively high and boiling of the working fluid at the wall of heat pipe severely affects the circulation of the working fluid. Heat transfer from wicked surfaces is more complicated than that from plain surfaces due to the existence of capillary structure. Also the vapour formation may change with different types of wick structures and working fluids. For a wickless heat pipe with non-metallic working fluids, when the temperature difference across the wall is large, nucleate boiling takes place. When the

bubble population becomes so high that the interaction of the liquid and vapour stream causes a restriction of the liquid supply to the heating surface a continuous vapour film forms adjacent to the wall. The wall temperature increases rapidly and the critical heat flux is reached. Critical nucleate boiling limit for a cylindrical heat pipe can be expressed as (Zhao, 2003):

$$q_{b,m} = \frac{2\pi l_{eff} k_{eff} T_v}{h_{fg} \rho_v \ln(r_i/r_v)} \left(\frac{2\sigma}{r_n} - \Delta p_{c,m} \right) \qquad \text{Eq. (6.11)}$$

6.2.4 Entrainment Limit

The vapour and liquid in the heat pipe flow in opposite directions. When the vapour velocity is sufficiently high, the shear force exiting at the liquid-vapour interface may tear the liquid from the heat pipe wall and entrain it into the vapour flow stream. This reduces the return flow of condensate to the evaporator and limits the heat transfer capacity. In terms of the axial heat flow rate, the entrainment limit for the wicked heat pipe can be expressed as (Zhao, 2003):

$$q_{e,m} = A_v h_{fg} (\sigma \rho_v / (2 r_{h,w}))^{1/2} \qquad \text{Eq. (6.12)}$$

For the wickless heat pipe, Dpcap,max = 0. So the entrainment limit can be expresses as:

$$q_{e,m} = f_1(\phi) C_w^2 \frac{\pi d_i^{2.5}}{4} \frac{h_{fg} \sqrt{g \rho_v (\rho_l - \rho_v)}}{[1 + (\rho_v/\rho_l)^{0.25}]^2} \qquad \text{Eq. (6.13)}$$

where

$$C_w = 0.725$$

$$f_1(\phi) = \left(\frac{\phi}{180} + \sqrt{\sin 2\phi} \right)^{0.65}$$

6.2.5 Viscous Limit

When viscous forces dominate the vapour flow, the vapour pressure at the condenser end may reduce to zero. The heat transfer of heat pipe may be limited under this condition. A heat pipe operating at temperature below its normal operating range can encounter this limit.

$$q_{v,m} = \frac{r_v^2 h_{fg} \rho_v \rho_l A_v}{16 \mu_v l_{eff}} \qquad \text{Eq. (6.14)}$$

6.3 Simulation to calculate heat transfer limits

Considering the effect of gravity on the heat pipes, the maximum heat transfer capacity is governed by the mass of the liquid charge, which was expressed by Zhuang (1989) as:

$$G = (0.8l_c + 0.8l_e + l_a)\left(\frac{3\mu_l \rho_l \pi^2 d_i^2}{h_{fg} g}\right)^{1/3} q_c^{1/3} \qquad \text{Eq. (6.15)}$$

Therefore the heat transfer limit of a heat pipe will be

$q_c = \min\{q_{s,max}, q_{b,max}, q_{e,max}, q_{v,max}\}$

Based on the above expressions, a computer programme was developed by Zhao (2002) to calculate the heat transfer limits. The flow chart of the programm is shown in *Figure 6.2*, and the procedure is described below:

1) Input all the temperatures, including the working fluid, geometry of the heat pipe, operating temperature, and liquid filling level.
2) Calculate each limit and obtain the heat transfer limit of heat pipe.
3) Repeat step 1) – 2) when the conditions are changed.

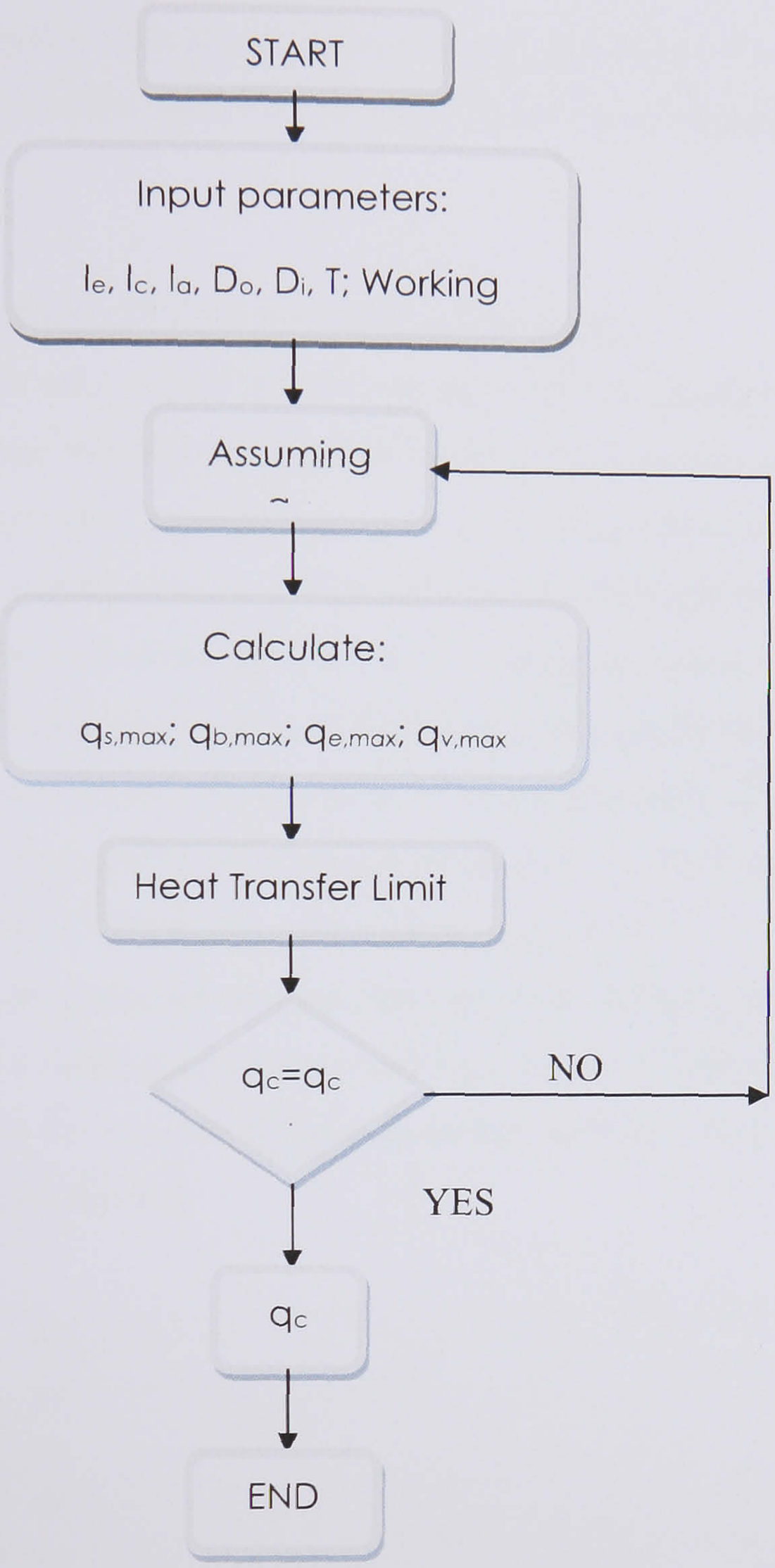

Figure 6.2 Flow chart of programming for heat transfer limitation of heat pipe

For a given heat pipe, the maximum heat transfer rate will be affected by the diameter, working temperature, fill level, inclination, wick conditions, and working fluid. As mentioned in the project objectives the heat pipes will be installed in the back of the PV and in vertical position. Therefore the adoption of a gravitational wickless heat pipe is appropriate. The subsequent analysis will be based on the example of a vertical wickless copper heat pipe of 10 mm diameter with the length of evaporation section of 260 mm,

the adiabatic section with 50 mm and condenser section of 130 mm. These dimensions were selected cause the same are going to be used also for testing the PV/T Heat pipe systems.

6.3.1 Working fluid effect on heat pipe performance

Working fluid is very important for a heat pipe and it is the prime consideration in the design of the pipe. Among the available working fluids mentioned in the literature review, water is widely used because of its good thermo-physical properties such as latent heat and surface tension, and the benefits of safety and environmental friendliness. However while water is suitable for the operating temperature higher than 30 °C it is impossible to evacuate the heat pipe further under the room temperature. Another fluid that can also be used is the N-pentane because of its lower boiling point of 36.2 °C (Riffat et al, 2002) and working temperature of -20 °C to 120 °C. Another new fluid is HFE7100 (C4F9OCH3) with boiling point of 60 °C.

After using the program that we described above the different working fluids were compared over a range of operating conditions. *Figure 6.3* shows the influence of the working fluid on the maximum heat transfer rate with the filling level at 1/3 of the evaporator length (90 mm).

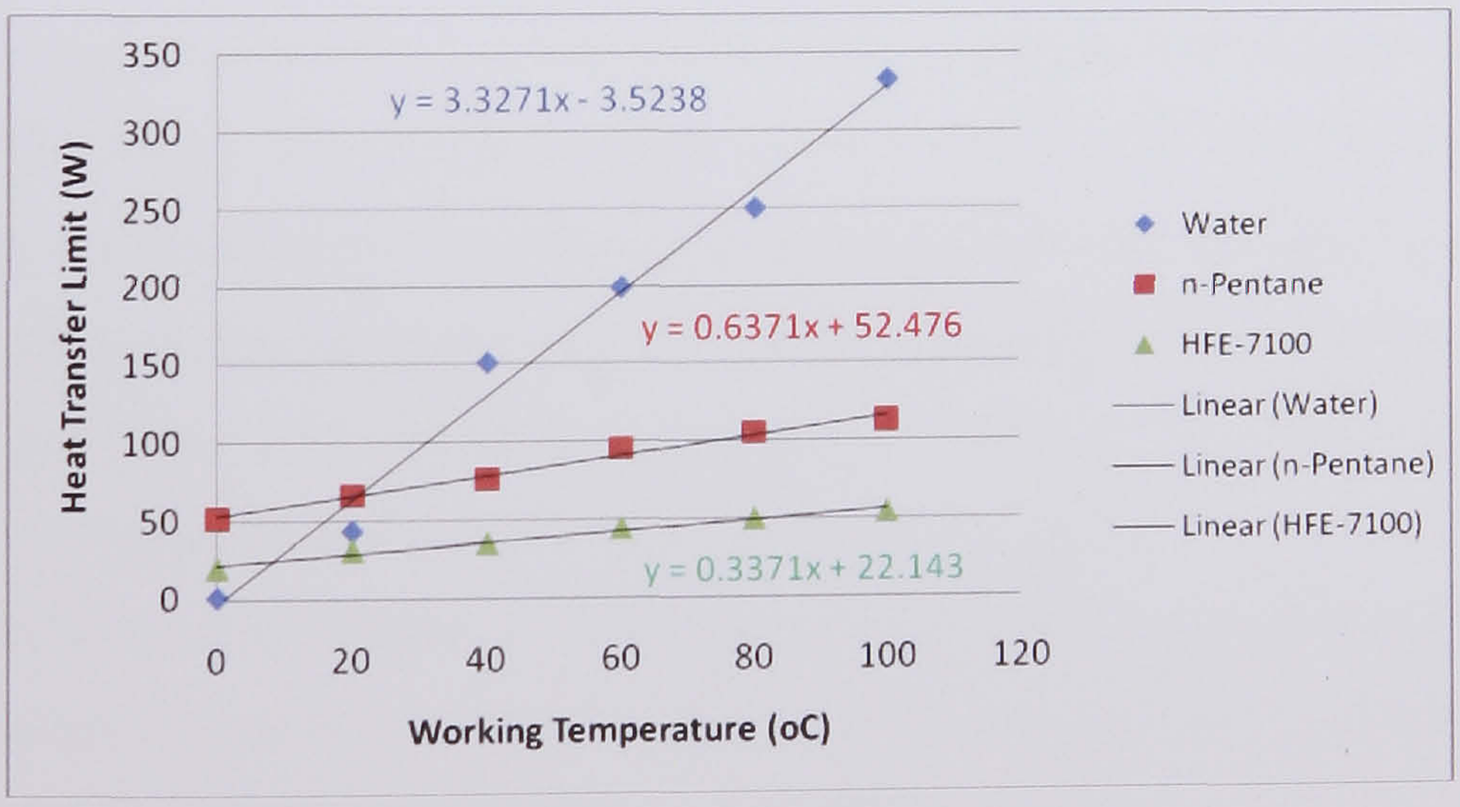

Figure 6.3 Heat transfer limit against working fluid

It may be seen that water works much better for the specific type of heat pipe from the other two fluids, especially from temperatures that start from 20 °C. Also water is better

than the other two fluids in terms of health and safety considerations. From the fluid properties we know that n-pentane is extremely flammable although its ODP = 0 (Ozone Depletion Potential) and GWP = 3 (Global Warming Potential). Similar values we can see with the HFE-7100 with ODP = 0 and GWP = 3.2. In addition, its chemical and thermal stability, non-flammability and low toxicity make it useful for many other industrial and specialty solvent applications. Of the three fluids therefore water was selected as it is safer and also cheaper to use than the other two.

A convenient means of quickly comparing working fluids is provided by the Merit number which is defined as:

$$M = \frac{\rho_L \sigma \lambda}{\mu_L} \qquad \text{Eq. (6.16)}$$

Where

M Merit number, W/m^2

ρ_L Liquid density, kg/m^3

σ Surface tension, n/m

λ Latent heat, J/kg

μ_L Liquid viscosity, Pa

The physical properties of the working fluids change radically with temperature [NIST (2003), NIST (1993)]. The dramatic change of the working fluid viscosity with temperature, especially as the temperature increase towards the boiling point, has a significant effect on the liquid transport factor (k). This leads to the increase of the liquid transport factor with temperature as shown in *Figure 6.4*, to a maximum point around the boiling point of the working fluid. *Figure 6.4* gives the Merit number at the boiling point for working fluids, covering temperatures ranges between – 73 °C and 227 °C. One obvious feature is the marked superiority of water with its high latent heat and surface tension compared with the other two fluids.

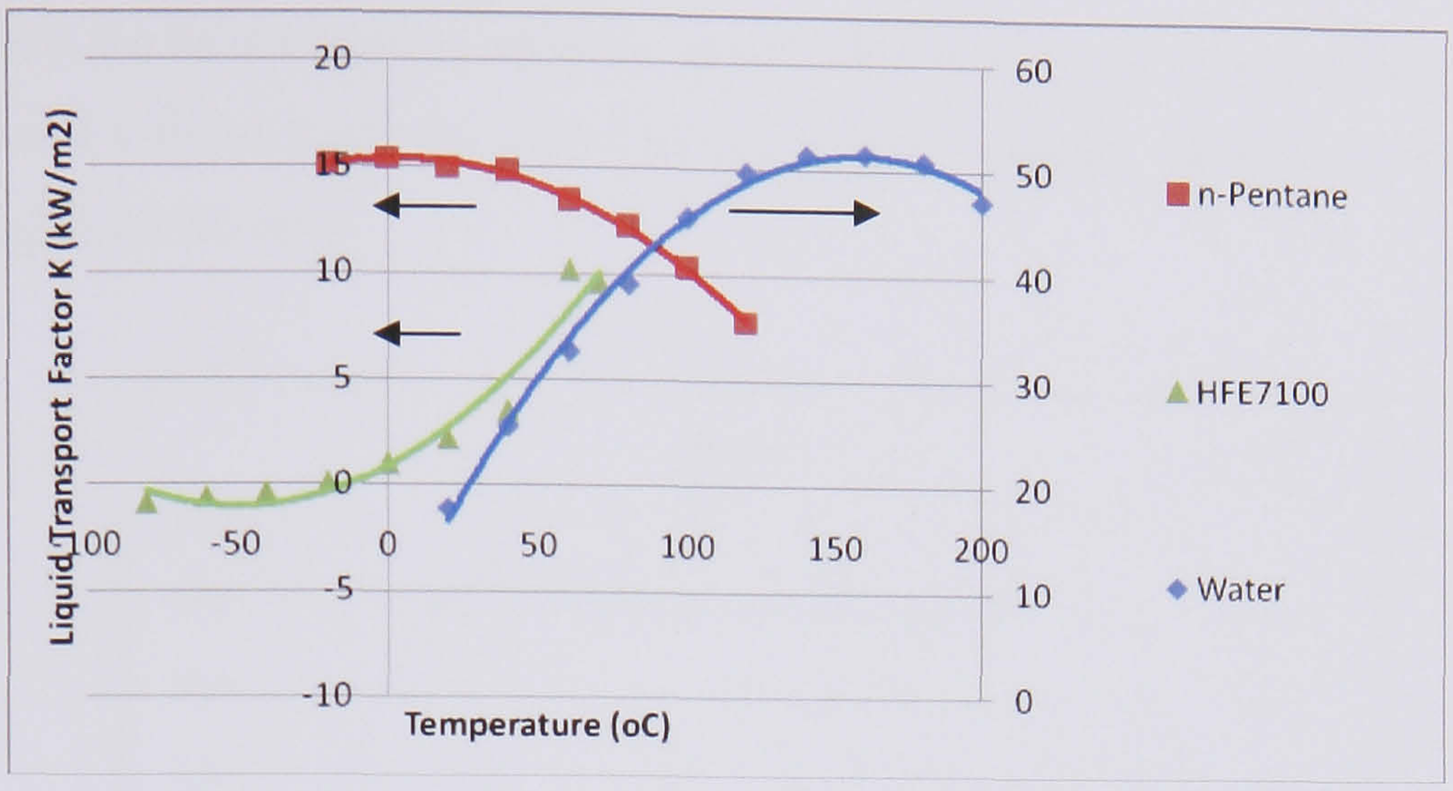

Figure 6.4 Liquid Transport Factor K of Water, n-Pentane and HFE-7100

6.3.2 Diameter effect on heat pipe performance

As mentioned in section 6.3 the heat transfer limit of a heat pipe is affected by various design factors. One such a factor is the diameter of the heat pipe. The calculations show in *Figure 6.5* that the heat transfer limit will increase greatly from around 36 W to 3000 W with increasing the inner diameter from 5 mm to 30 mm. i.e. as the diameter increases the heat transfer limit also increases.

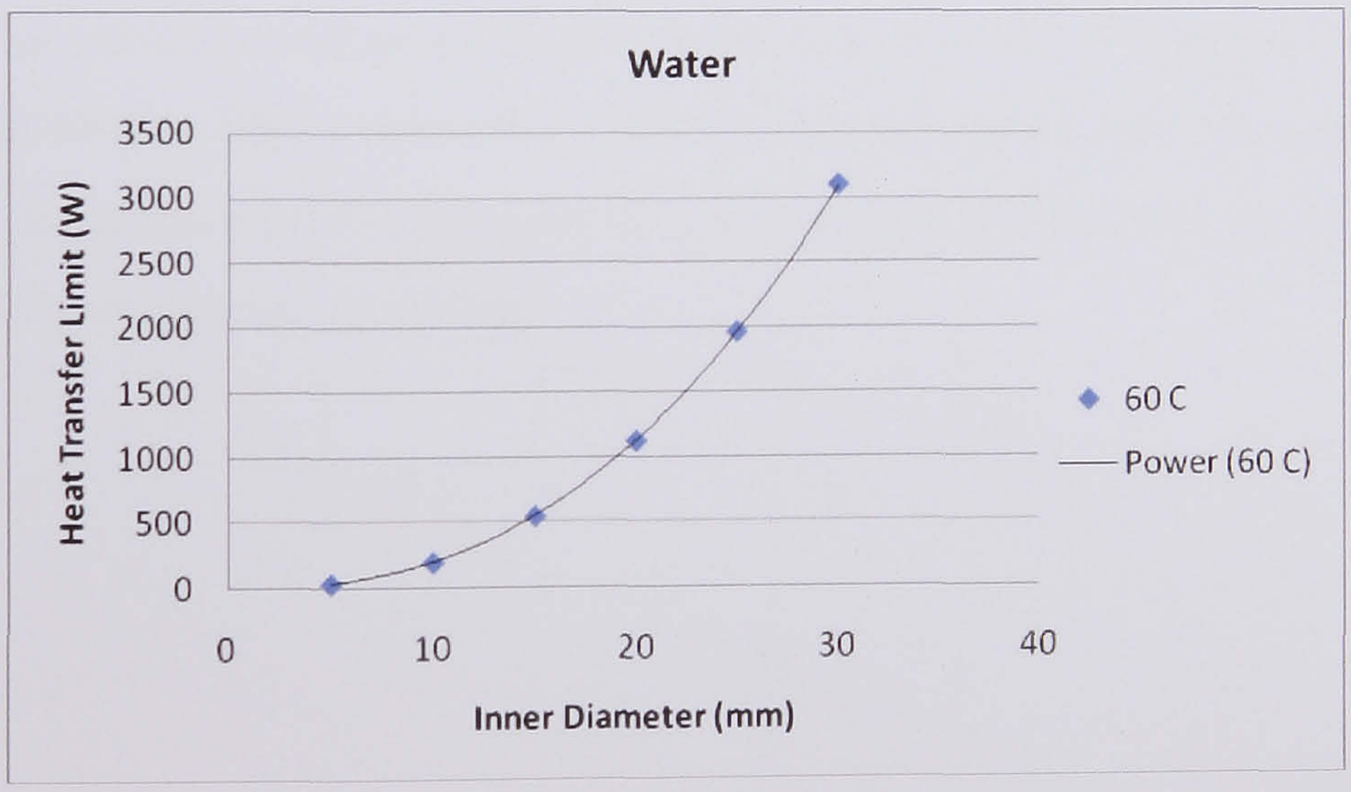

Figure 6.5 Heat transfer limit against the inner diameter for 60 ^{o}C operating temperature

6.3.3 Fill liquid level effect on heat pipe performance

The level of the liquid filling is also very important in the terms of the heat transport capacity in the heat pipe design. Calculation with water shows that the level of liquid

filling affects the heat transport capacity greatly only in the lower level. As can be seen from *Figure 6.6* above a certain level the heat transport capacity no longer varies with the working fluid fill ratio.

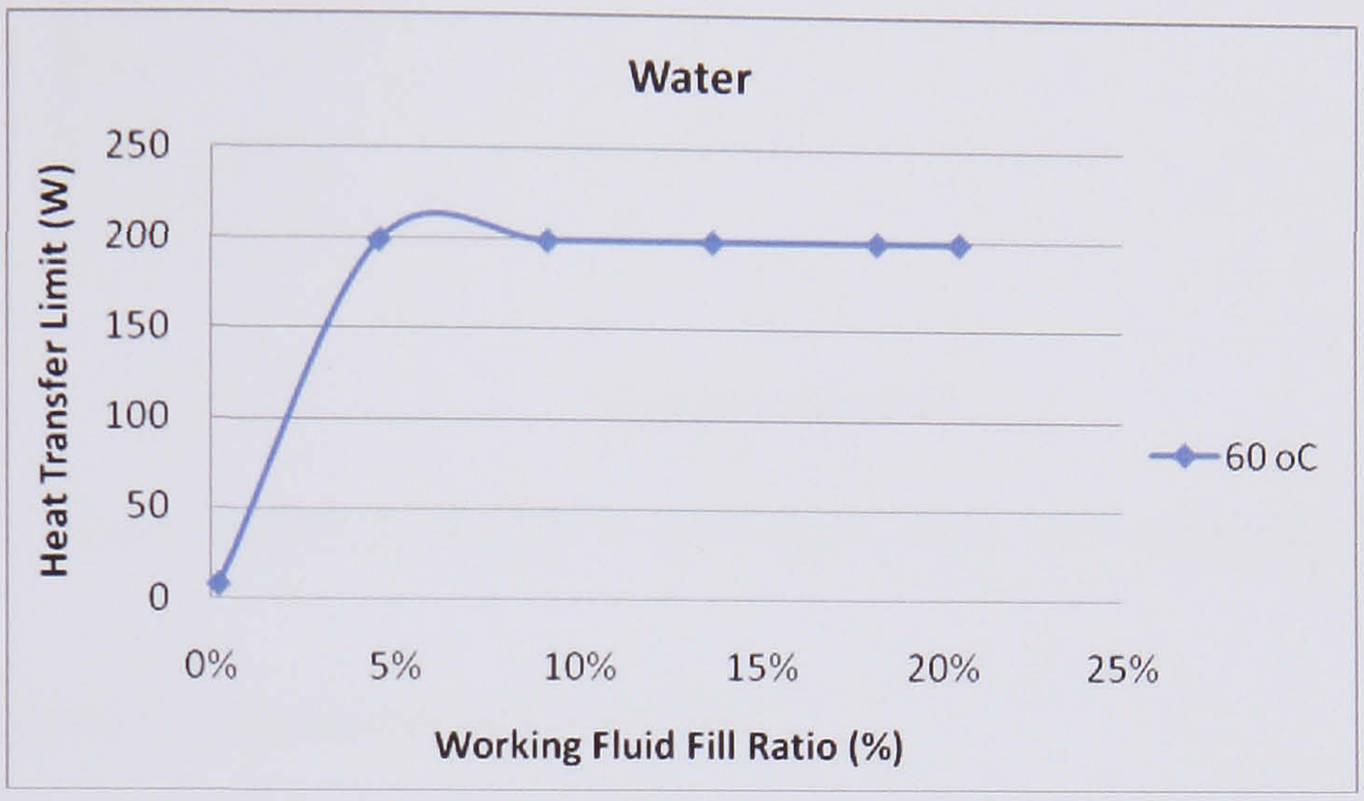

Figure 6.6 Heat transfer limit against working fluid fill ratio

6.3.4 Inclination angle effect on heat pipe performance

The position that a heat pipe is placed in, i.e. its inclination, especially for gravitational wickless heat pipes affects the performance of the system. From *Figure 6.7* it may be seen that at the vertical position the heat transfer limit is at 200 W and the highest value comes around 60 deg. Many researchers in their papers confirm that the maximum heat tansfer limit doens't come always in the vertical position (Terdtoon et. al., 1990, Negishi et. al., 1982, Payakaruk et. al., 2000).

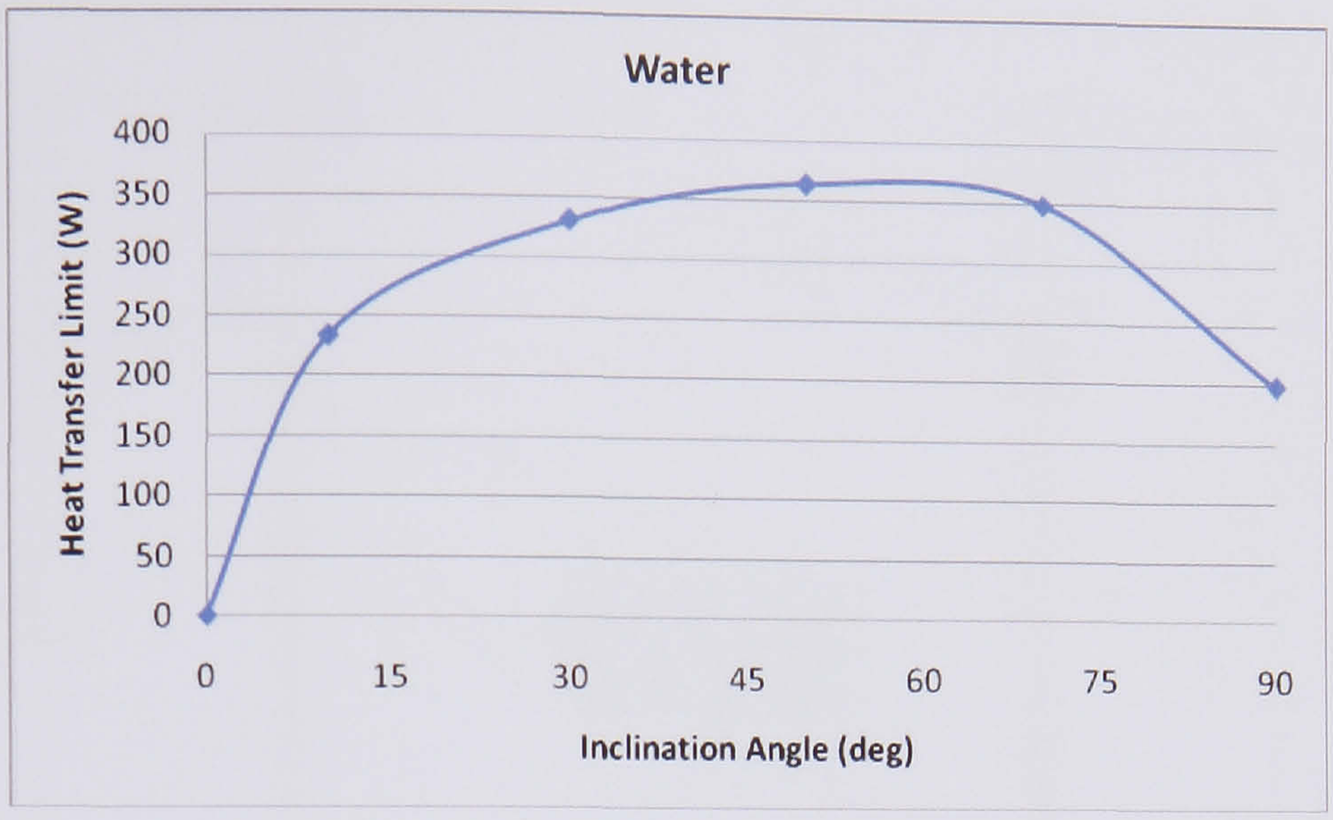

Figure 6.7 Heat transfer limit against inclination angle measured from horizontal

6.4 Experimental Performance of Heat Pipes

After evaluating the maximum heat transfer capacity of a heat pipe the next step was to check the real performance of the heat pipes that were going to be used for the PV/T experiments. As mentioned in section 6.1 two models were going to be incorporated in the back of the PV. One with the heat pipes condenser side inside a tank and the other inside a manifold as shown in *Figure 6.8*. Similar experiments were carried out in order to evaluate the heat transfer rate and thermal conductivity of the pipes. *Figure 6.9* shows the two rigs created for the experiments.

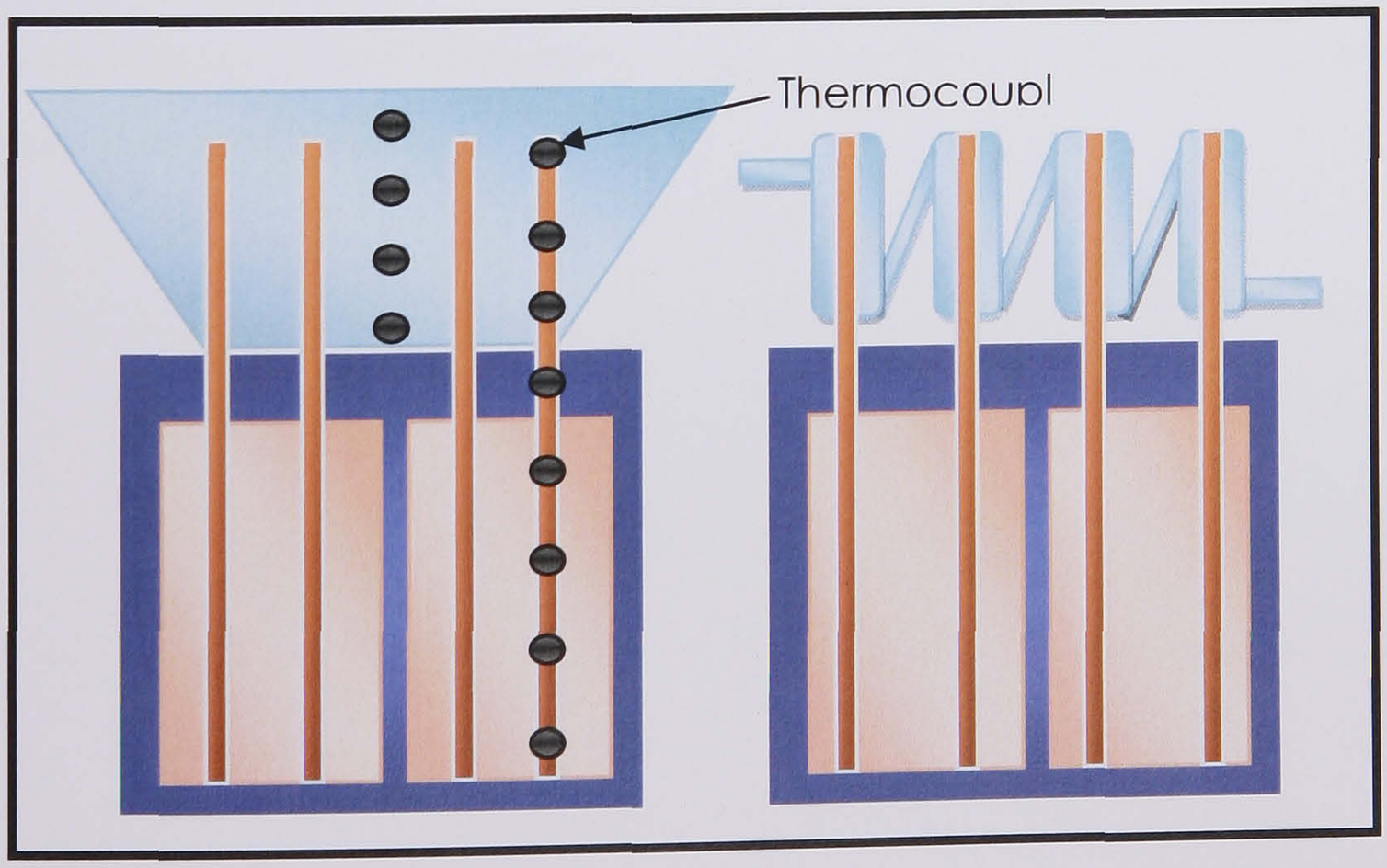

Figure 6.8 Schematic of PV/T heat pipe with tank and manifolds

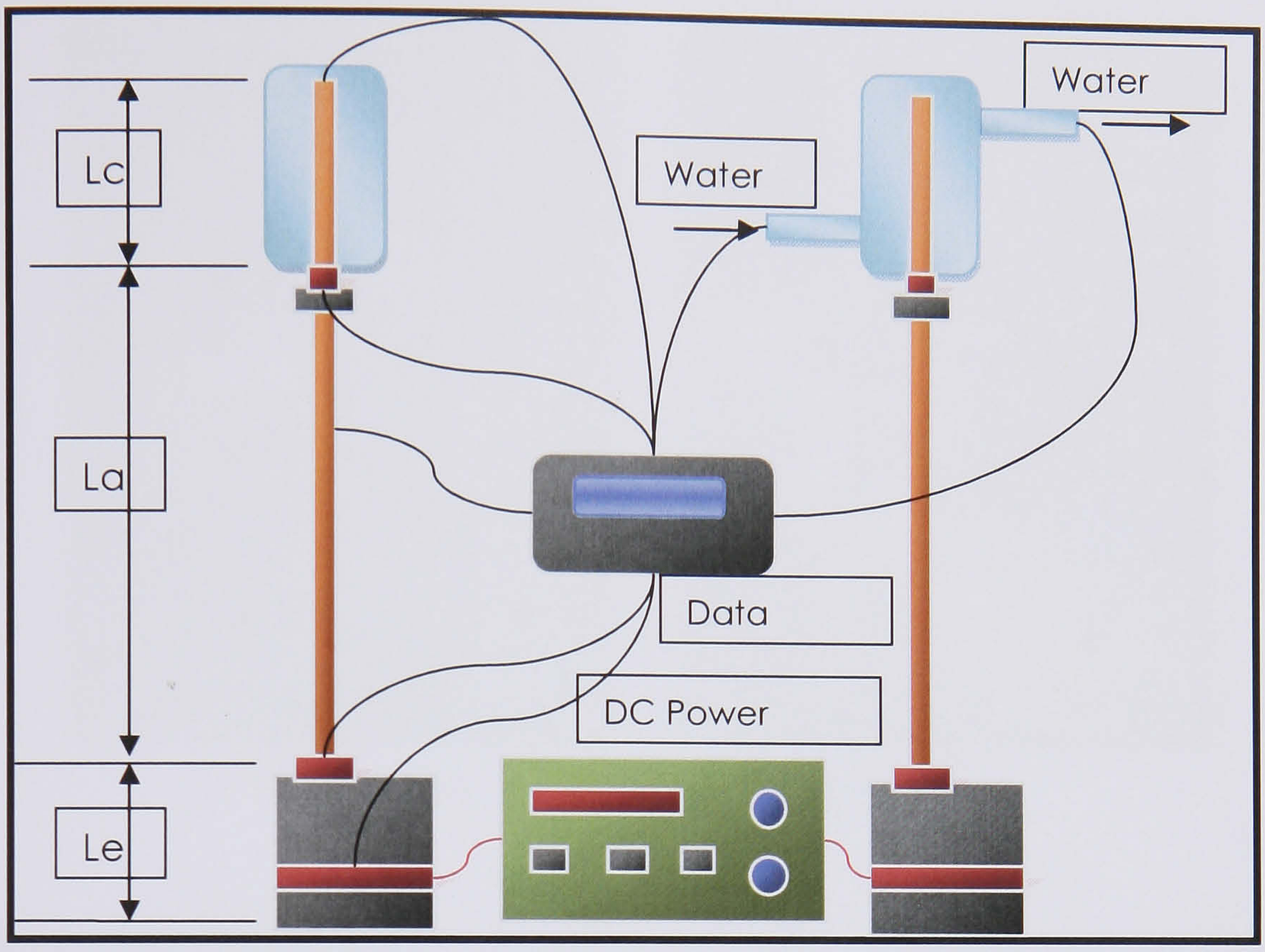

Figure 6.9 Heat Pipe Experimental Rigs, a) Heat pipe with Tank, b) Heat pipe with Manifold

6.4.1 Heat Pipe with a Tank

Figure 6.10 shows the experimental setup that consists of a heat pipe with a heating bath for the evaporator section and a cooling bath for the condenser section. Heat pipes were made of copper tubes with 10 mm diameter and evaporator and condenser length of 150 and 100 mm. The length of the adiabatic section was 190 mm. Water was selected as the heating and the cooling medium.

Figure 6.10 Heat Pipe Experiment with Tank

Since it is rather difficult to detect the inside temperature at the adiabatic section, the surface temperature of the adiabatic section was measured and used to determine the inside temperature on the basis of adiabatic process. Three temperature readings in the evaporator section were taken simultaneously; two readings at the adiabatic section and two readings at the condenser section were also taken, to observe the temperature distribution along whole length of the heat pipe.

The heat pipe evaporator received heat from a thermostat that was heating a bath, while the condenser was cooled by water through a cooling bath. To minimize heat losses to the environment, the heat pipe was insulated with a polyethylene sheet with thermal resistance of 0.74 m^2K/W.

In the *Figure 6.11* it may be seen that the experiment took 2.2 hours to complete. The bath temperature was 70 ^oC at the evaporator and in can see the temperature at the different sections of the heat pipe. The big bath that contained the evaporator section had 6 lt of water and heated the pipe and the condenser part was inside a small tank of 0.8 lt.

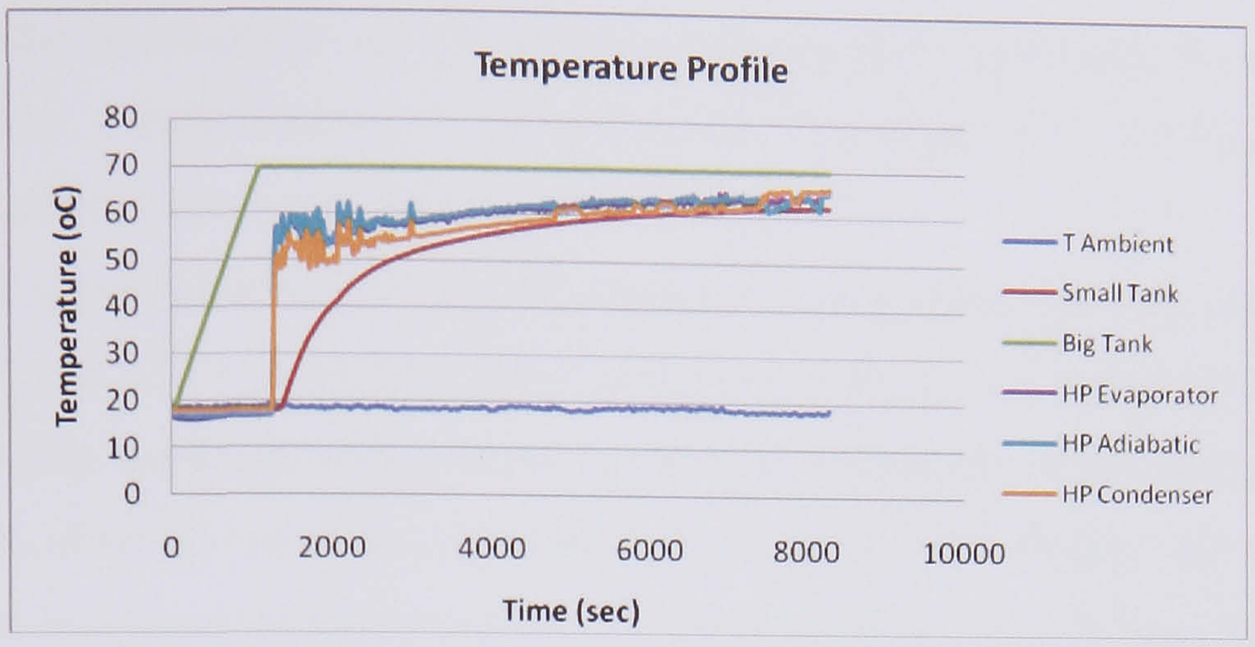

Figure 6.11 Temperature profile of Heat pipe experiment with Tank

Figure 6.12 shows the temperature difference between the evaporator section of the heat pipe and the condenser. As the time passes and the temperature in the small tank increases the temperature difference of the two parts reduces from 6 °C to 1 °C.

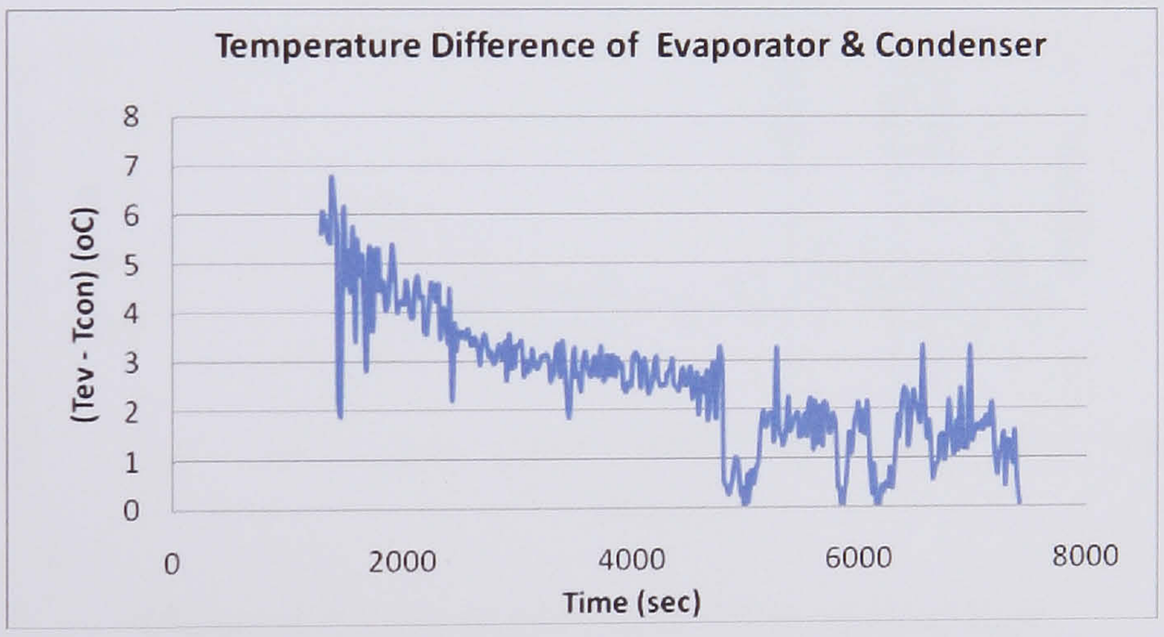

Figure 6.12 Temperature Difference of Evaporator and Condenser section

The effective thermal conductivity (K_{eff}) gives an indication of the additional heat flow rate resulting from the heat load. The K_{eff} for the heat pipe system is determined by the following equation:

$$K_{eff} = \frac{L \cdot \dot{Q}}{\Delta T \cdot A} \qquad \text{Eq. (6.17)}$$

where Q is the heat transfer rate, ΔT is the temperature difference between evaporator and condenser, L is the distance between the measuring points of T_{ev} and T_{con} and A is the cross-sectional area of the heat pipe (0.01382 m^2).

Figure 6.13 shows the effective thermal conductivity K_{eff} of the heat pipe system as a function of time. The results show that K_{eff} increases with increasing the heat load and with decreasing condenser temperature. The average measured thermal conductivity is 2411 W/mK about six times more than thermal conductivity of copper. According to Thermacore heat pipes thermal conductivity can range from 1 to 100 times that of copper (400 W/mK). The heat pipes that were used for the experiments manufactured from the technicians in the laboratory. A factor that the pipe could not achieve higher conductivity maybe cause of some air that remained inside the pipe. To mention that the big spites are not included in the calculation.

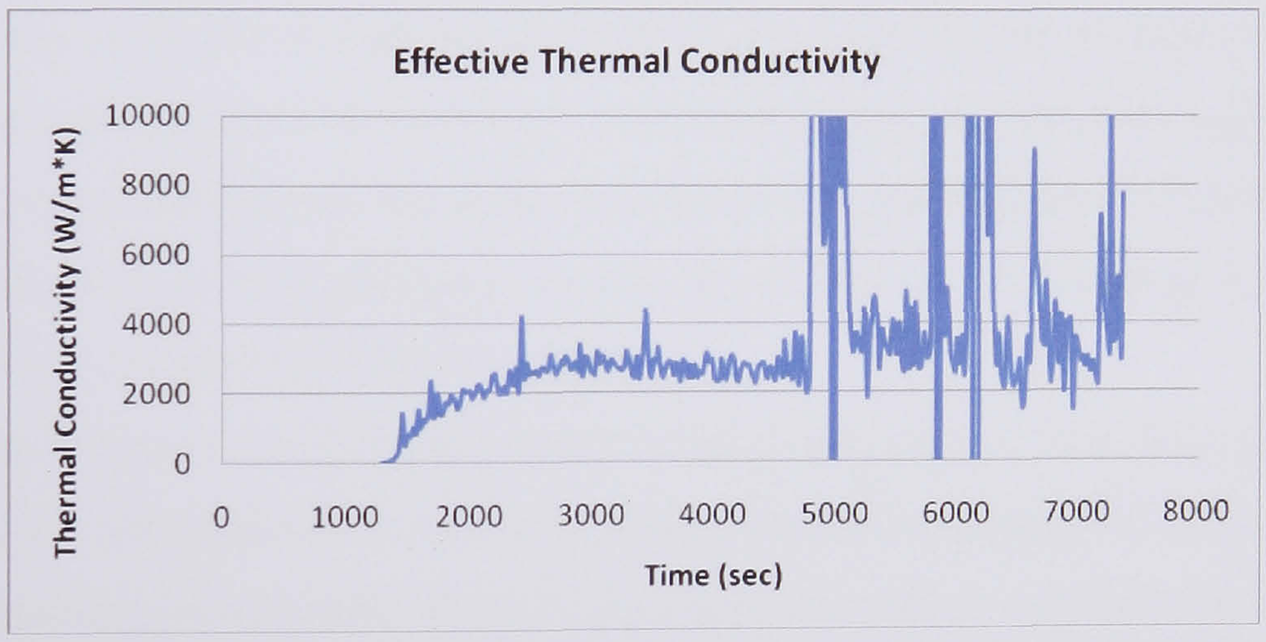

Figure 6.13 Thermal Conductivity of Heat Pipe

6.4.2 Heat Pipe with Manifold

The next experiment investigated a manifold supplying water at a constant flow rate. *Figure 6.14* shows the test rig. The heat transferred by the heat pipe was taken equal to the heat transferred from the condenser to the cooling water at steady state conditions. This was determined by measuring the temperature difference across the condenser and the volumetric flow rate of the cooling water and then, applying the following simple equation;

$$Q_w = \rho_w \cdot c_{p_w} \cdot \dot{V}_w \cdot \Delta T_w \qquad \text{Eq. (6.18)}$$

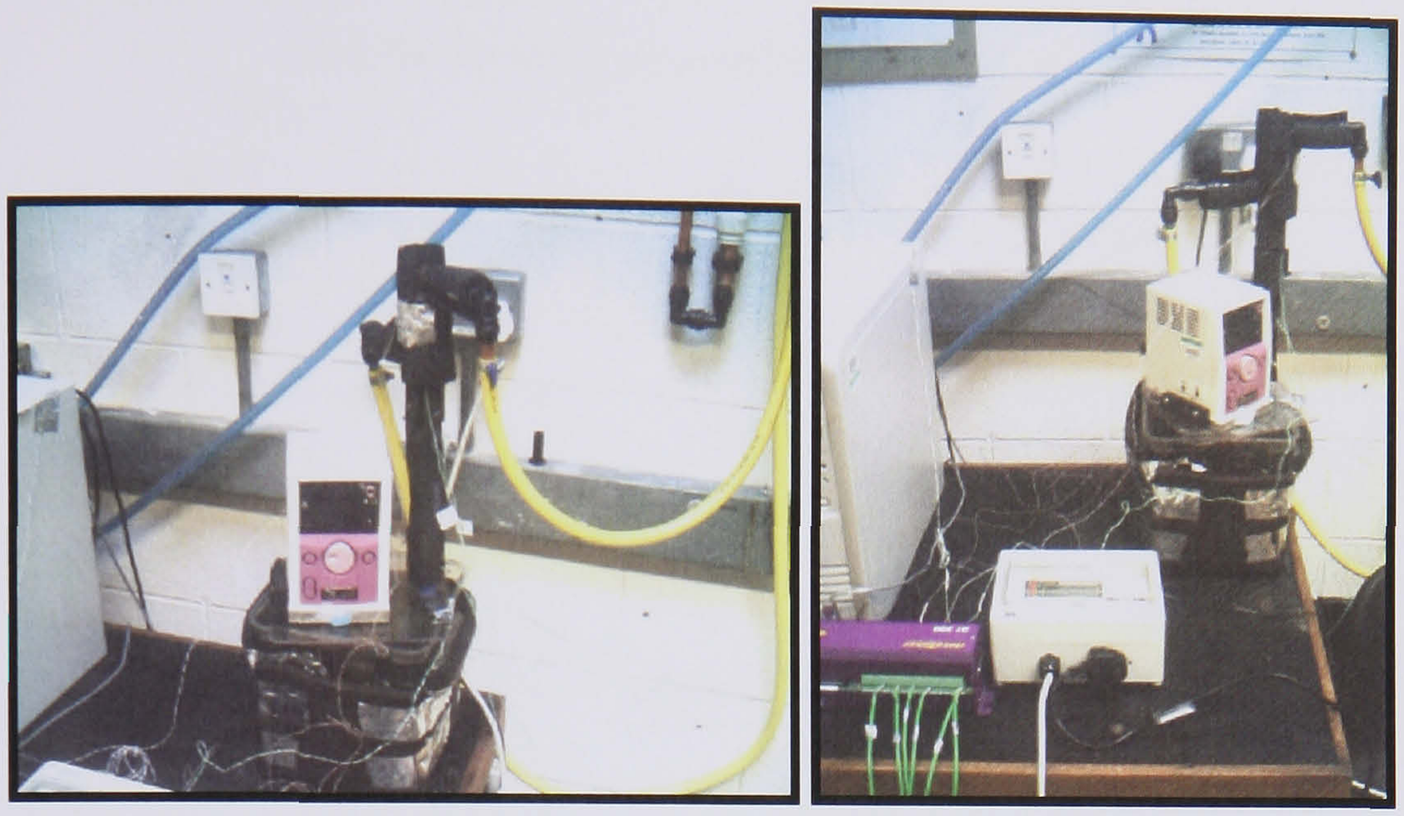

Figure 6.14 Heat Pipe with Manifold Test Rig

The heat pipe has the ability to transfer heat rapidly through its internal structure. This will result in a quick rise in wall temperature which could damage the heat pipe if the heat were not dispersed at the condenser. Therefore, before any heat was supplied to the evaporator, the condenser cooling water was allowed to run through the condenser jacket. The condenser flow rate and temperature was kept constant throughout the experiments by the use of a chillers' system.

Then, the power input was gradually raised to the desired power level. Enough time was allowed for the temperatures at various locations along the heat pipe to reach steady state before adding more power. At this stage, the power input, condenser water flow rate, temperatures at the various locations and heat pipe pressure were all recorded.

Figure 6.15 shows a graph of the temperature at the different sections of the pipe with different power input. It may be seen that the temperatures of the adiabatic and the condenser section are very close and this is probably caused by the high heat transfer rate and the insulation that covers the pipe.

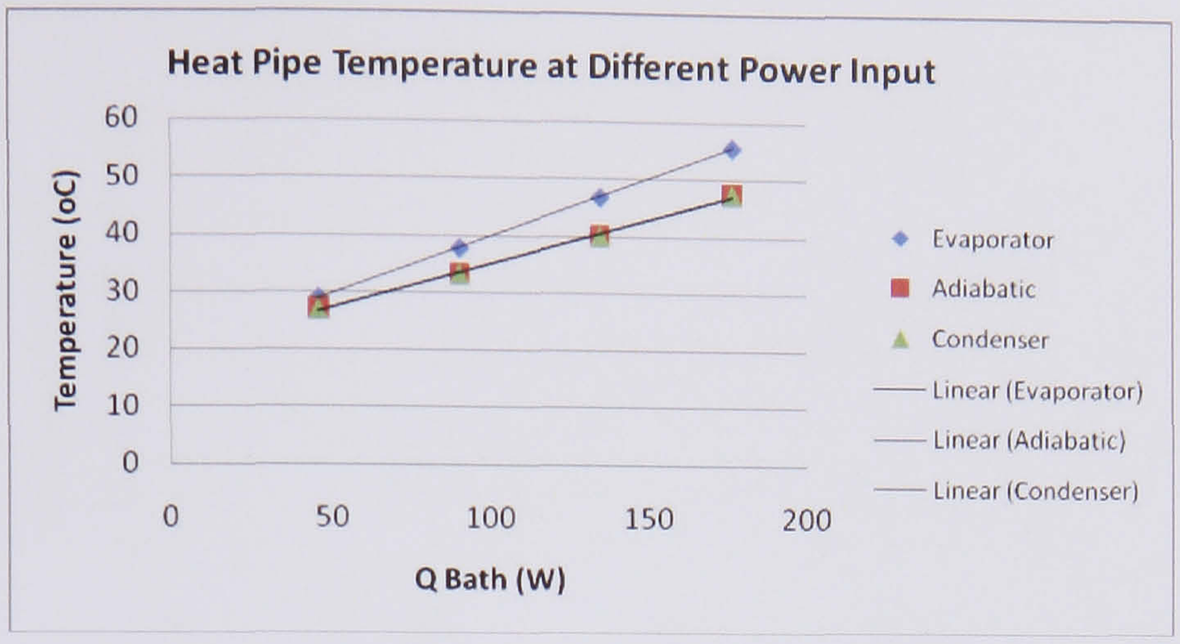

Figure 6.15 Heat Pipe Temperature at Different Power Input

After measuring the temperature difference between inlet and outlet and recording the steady flow rate it was possible to calculate how much of the energy delivered to the heat pipe was extracted at the manifold. *Figure 6.16* gives the power input versus the useful power delivered to the water. When the power delivered to the heat pipe is 46.07 W the power taken from the water is 37.23 W.

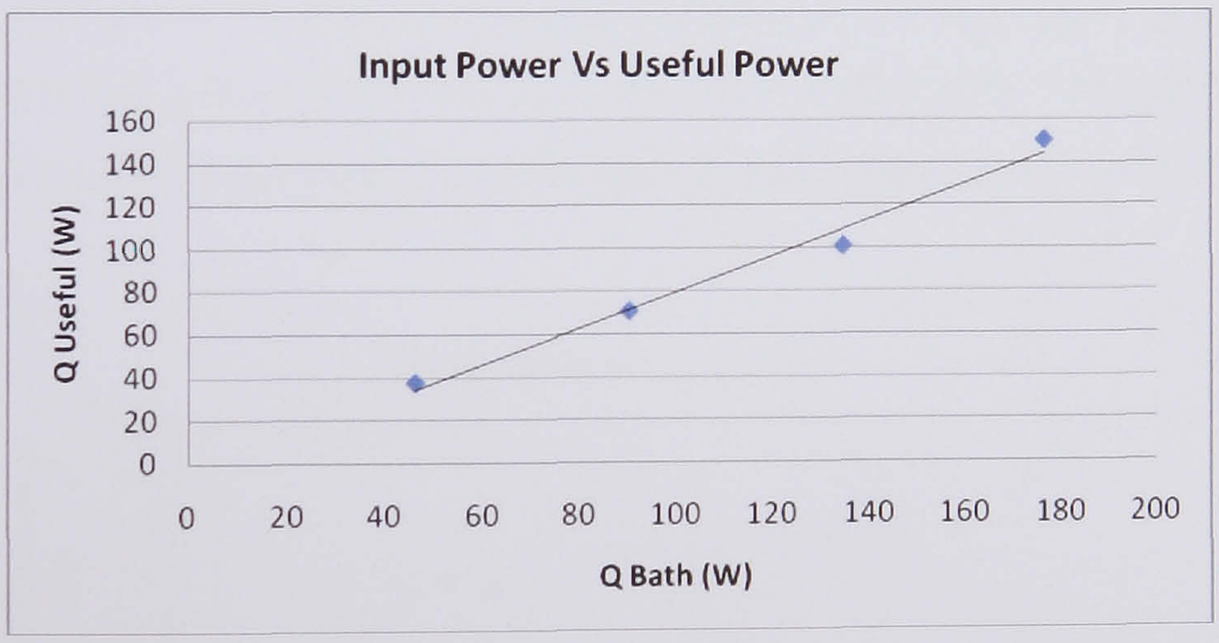

Figure 6.16 Input Power to Heat Pipe versus Useful Power

Figure 6.17 shows the variation of heat flux values versus evaporator temperature. Clearly, the heat pipe is greatly affected by the heat flux input. To calculate the heat flux the useful power was used divided by the area of the condenser section.

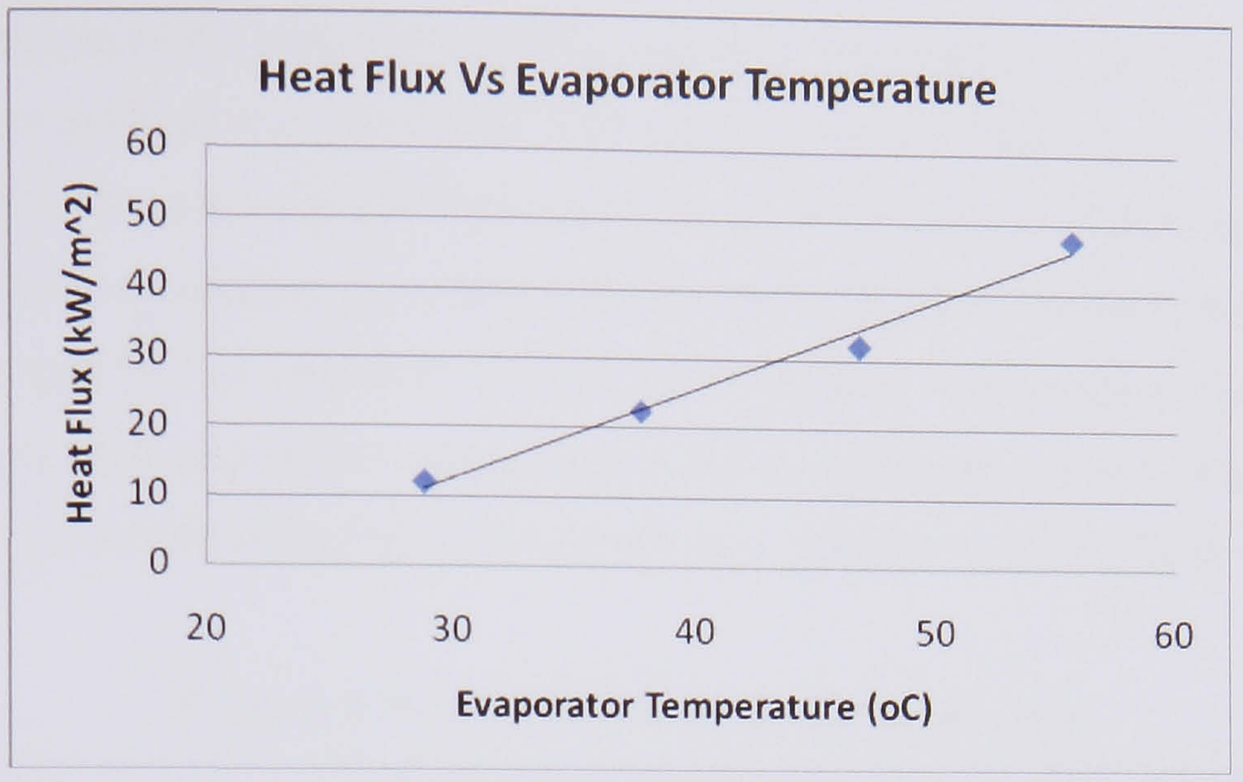

Figure 6.17 Heat Flux Vs Evaporator Temperature

At low heat flux inputs, less than 11.85 kW/m^2, the heat pipe had similar superheats, resulting in an average experimental heat transfer coefficient of approximately 4927 W/m^2*K. At heat fluxes of 47.67 kW/m^2 and more, the experimental heat transfer coefficient at this range of heat flux was approximately 6821 W/m^2*K as can be seen from *Figure 6.17* and *6.18*. The heat transfer coefficient is being calculated by dividing the heat transfer rate of heat pipe with the temperature difference of evaporator and condenser and this with the cross sectional area of the condenser side (0.0031416 m^2).

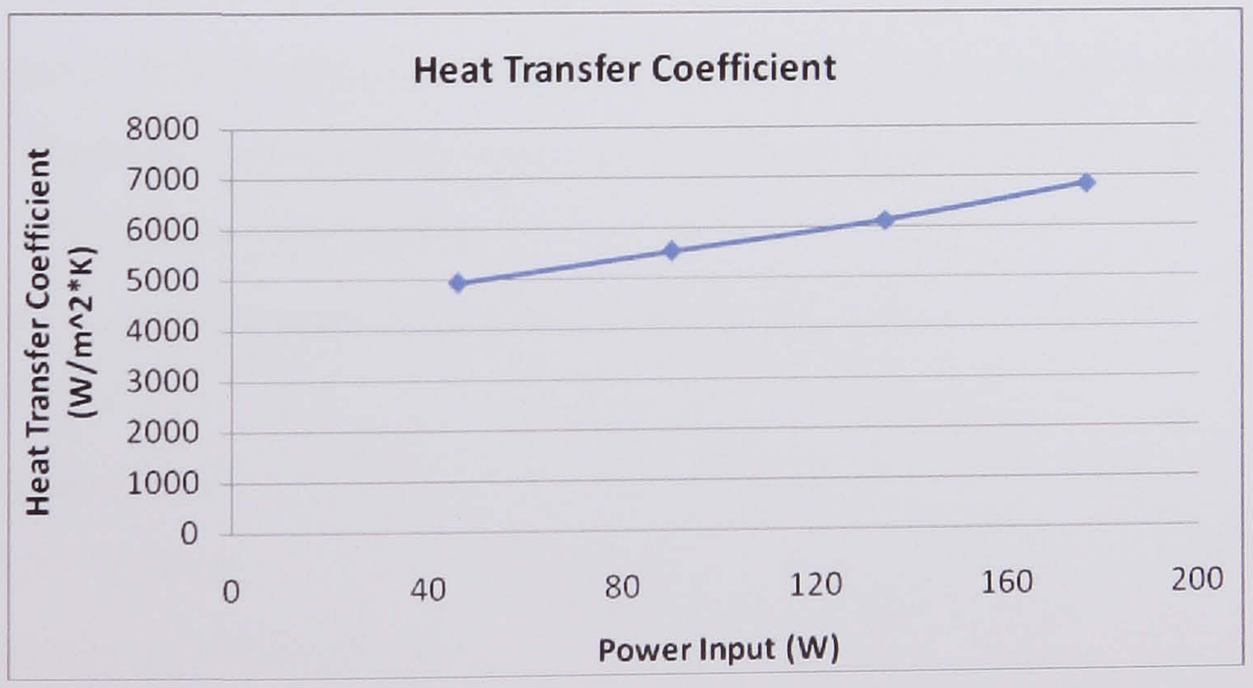

Figure 6.18 Heat Transfer Coefficient of Heat Pipe

The temperatures of the evaporator and the condenser at steady state were recorded and a temperature gradient was calculated. With the known power input the heat pipe performance at that load was measured in terms of conductivity as defined from (Eq. (6.17). The unit of conductivity is W/m*^{o}C or W/m*K. Thus for a heat pipe with a steady state heat load of 149.78 W, ΔT of 8.23 ^{o}C, distance between evaporator and condenser point of temperature measuremtn 0.315 m, and cross sectional area of condenser A of 0.0031416 m^2 the conductivity was 1584.94 W/m*K (*Table 6.2*).

Table 6.2 Thermal Conductivity of the heat pipe

Heat Input (W)	Temperature difference $\Delta T = Tev - Tcon$ (^{o}C)	Thermal Conductivity (W/m*K)
37.23	2.41	1548.94
70.31	5.82	1211.30
100.43	7.75	1299.33
149.78	8.23	1824.79

6.5 Design of the PV/T Heat pipe model

After evaluating the heat transfer capacity of a heat pipe in section 6.3 at the desired dimensions the maximum capacity was measured to be 200W, the next step was to design the 2 PV/T Heat pipe models.

Assuming the maximum solar radiation in a sunny day was:

$I_{max} = 1000$ W/m^2

and effective area was:

$A_{pv} = 0.4*0.4 = 0.16$ m^2

the total solar energy received was

$E_{max} = I_{max}*A_{pv} = 160$ W

If it is assumed that all this energy can be absorbed, then a heat pipe will be needed that the evaporation section will be the length of the PV. A pipe of 10 mm will be capable of

absorbing the heat. The dimensions of the different pipe sections are the same with the ones used in the previous simulations (Table 6.3).

Because the PV/T area is larger than the area of the hear pipe diameter two back plates were designed that was two slots in order to accommodate four pipes of the same length and size as shown in *Figure 6.19*. Because the cost of the copper was very high two copper plates with 5 mm thickness and area of 0.06 m^2 were manufactured and bonded to the PV with a thermal paste.

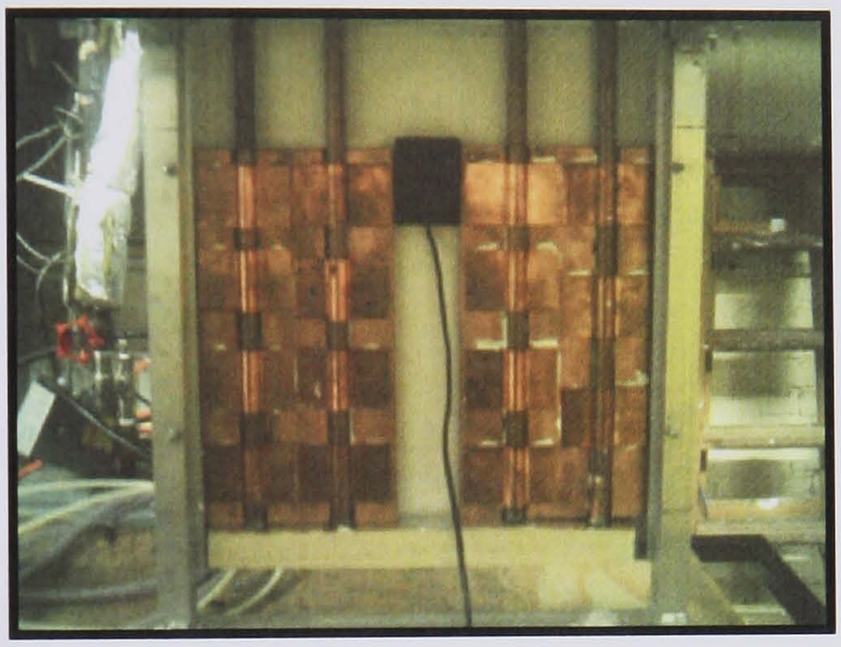

Figure 6.19 Back of PV with two copper plates incorporating four heat pipes

All the parameters relating to the heat pipe, used in this part of the research are listed in *Table 6.3*.

Table 6.3 Heat pipe dimensions

Working Fluid	Water
Outer Diameter (OD) (mm)	10
Thickness of heat pipe (mm)	0.5
Length of evaporation section (mm)	260
Length of adiabatic section (mm)	50
Length of condenser section (mm)	130
Liquid Filling Level (mm) – Filling Ratio (%)	90 – 20%

6.5.1 Sensitive parameters that affect the performance of a solar collector

The ability of an efficient solar collector to produce useful heat energy depends on many elements. Some of these elements are dimensional and rely on the design of the collector, while others are related to the operating conditions. Duffie (1991) introduced a famous equation (2.3.1) that may be used to assess the useful thermal energy (Q_{use}) produced by a flat plate solar collector considering most of the essential elements.

The heat removal factor is defined as the relationship between the actual useful energy of the collector to the useful energy gained at the fluid inlet temperature.

F_R = actual energy gained by the collector / energy gained when collector temperature equals to fluid inlet

Rearranging (2.3.1) the heat removal factor for most flat plate solar collectors, as stated by Beckman (1991), can be represented mathematically as:

$$F_R = m*c_p*(T_{f,out} - T_{f,in})/A_{col}*[Q_{solar} - U_L*(T_{f,in} - T_a)] \qquad \text{Eq. (6.20)}$$

Where m is the fluid mass flow rate (kg/sec)

C_p is the fluid specific heat capacity at constant pressure (kJ/kg*K)

$T_{f,in}$ is the inlet fluid temperature (K)

$T_{f,out}$ is the outlet fluid temperature (K)

6.5.1.1 Correlation of the heat removal factor and design parameters of a thermosyphonic wickless heat pipe solar collector

The principle of obtaining a relationship between the design parameters of a heat pipe solar collector and the heat removal factor was introduced by Kamminga (1986) and Tabassum (1988). The parameters that will be discussed in this analysis are; the evaporator and the condenser thermal resistances per unit area and the effect of the condenser size.

Due to the relatively small size of a heat pipes condenser, the thermal resistance is considered as the most crucial parameter in the design of heat pipe solar collectors. The condenser thermal resistance per unit area mainly depends on the structural design, the roughness of the surface, working fluid properties, pressure and temperature at the interface of the condenser inner surface (Zhao, 2003).

To simplify the analysis, the heat transfer process of the collector is divided into three parts at steady state. The first part refers to the heat gained by the collector panel (Q_{pl}). The second denotes the heat exchanged between the panel and the heat pipe, which could be taken as heat delivered by heat pipe evaporator (Q_e). The final part signifies the heat delivered to the heat pipe condenser (Q_c) and that could be presumed to be the useful heat gained by the collector. Assuming that these three heat transfer quantities are equal and the evaporator area is approximately equal to the collector area $A_e = A_{col}$ (this assumption is based on the idea that the heat pipe and the copper plate form an evaporator area equal with that of collector), the heat transfer quantities of the collector, the evaporator and the condenser could be respectively given by the following equations:

$$Q_{col} = A_{col}*[Q_{solar} - U_L*(T_p - T_a)] \quad \text{Eq. (6.21)}$$

$$Q_e = A_e*(T_{pl} - T_{hp})/R_e \quad \text{Eq. (6.22)}$$

$$Q_c = A_c*(T_{hp} - T_{c,in})/R_c \quad \text{Eq. (6.23)}$$

Where A_{col} is the collector area (m^2)

A_c is the condenser area (m^2)

A_e is the evaporator area ($=A_{col}$) (m^2)

T_{pl} is the collector panel temperature (^oC)

T_{hp} is the heat pipe temperature (^oC)

$T_{c,in}$ is the condenser inlet temperature (^oC)

R_e is the evaporator thermal resistance per unit area ($^oC*m^2/W$)

R_c is the condenser thermal resistance per unit ($^oC*m^2/W$)

Solving equations (6.21) and (6.22) results in obtaining Q_{evap} as:

$$Q_e = A_{col}/R_e*U_L+1\ [Q_{solar} - U_L*(T_{hp}-T_a)] \quad \text{Eq. (6.24)}$$

Similarly equations (6.22) and (6.23) can be solved to get Qc which is assumed equal to the useful heat gained by the collector Quse therefore:

$$Q_{use} = A_{col}/R_e*A_{col}*U_L+R_c*A_{col}*U_L+1\ [Q_{solar} - U_L*(T_{in} - T_a)] \quad \text{Eq. (6.25)}$$

The comparison of equations with the heat removal factor F_R we obtain the following formula:

$$F_R = 1/\ [R_e*U_L+R_c*U_L*(A_{col}/A_c)+1] \quad \text{Eq. (6.26)}$$

This formula could assist in determining the required thermal resistance of the condenser with respect to the evaporator thermal resistance, collector area, and overall heat transfer coefficient.

6.5.1.2 Evaporator and condenser thermal resistances

In most solar heat pipe applications, the design of the evaporator is a typical flat surface and does not include any complexity, and so its thermal resistance apparently depends on the properties of the surface. The heat removal factor F_R is dependent on the three ratios U_L/h_{ev}, U_L/h_{con} and A_{con}/A_{col} as shown in equation (6.26).

Normally, the evaporator design engages less attention in the design of solar heat pipe. However, to scrutinize its influence it is possible to use Kamminga's (1986) experimental measurements for Philips ETC-VTR 141 evacuated heat pipe solar

collector as guidance and assume a practical thermal resistance of 0.01 for the condenser and 1.932 for the overall heat loss coefficient. Considering these two factors the effect of the evaporator on the heat removal factor may be demonstrated as in *Figure 6.20*. This may possibly explain that the efficacy of the evaporator thermal resistance could have a major role merely when the condenser size is relatively large, and this is not a desirable situation. On the other hand, as the condenser size is reduced, it is possible to sense the weak reliance on the evaporator thermal resistance to alter the heat removal factor. *Figure 6.20* shows that when the condenser is not very efficient $U_L/h_{con}>0.01$, F_R is reduced but is relatively insensitive to variations of the ratio U_L/h_{ev}.

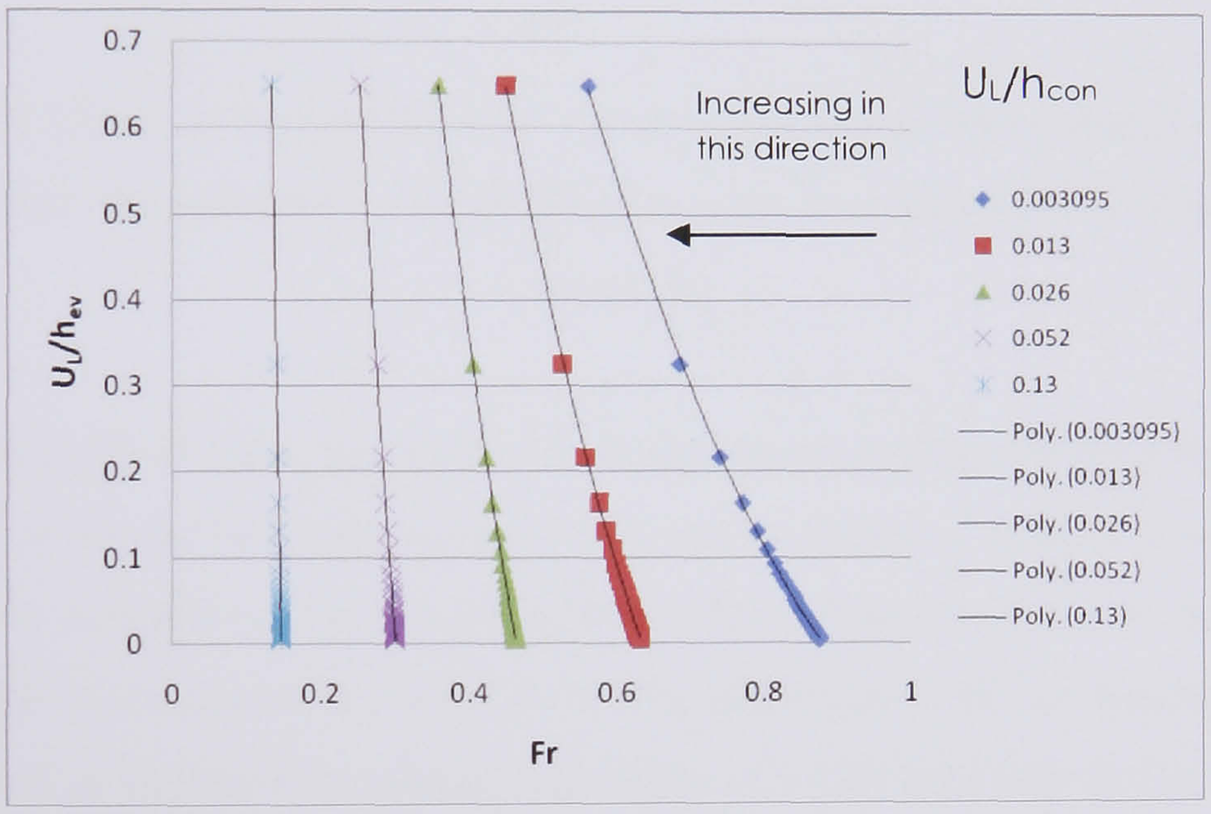

Figure 6.20 Effect on the heat removal factor of varying the ratio of the coefficient of heat loss from the collector to the coefficient of heat transfer across the evaporator

In contrast, the significance of the condenser thermal resistance may possibly be underlined in two ways. First, the relationship between the evaporator thermal resistance and the heat removal factor is re-evaluated for an inefficient condenser ($R_c = 0.1$) as shown in *Figure 6.21*. Under such conditions, reasonable heat removal factors can only be achieved with impractical evaporator thermal resistance and condenser size. At the same time, when the condenser area is increased relative to the collector area A_{con}/A_{col} then it may be observed that F_R increases as shown in *Figure 6.21*.

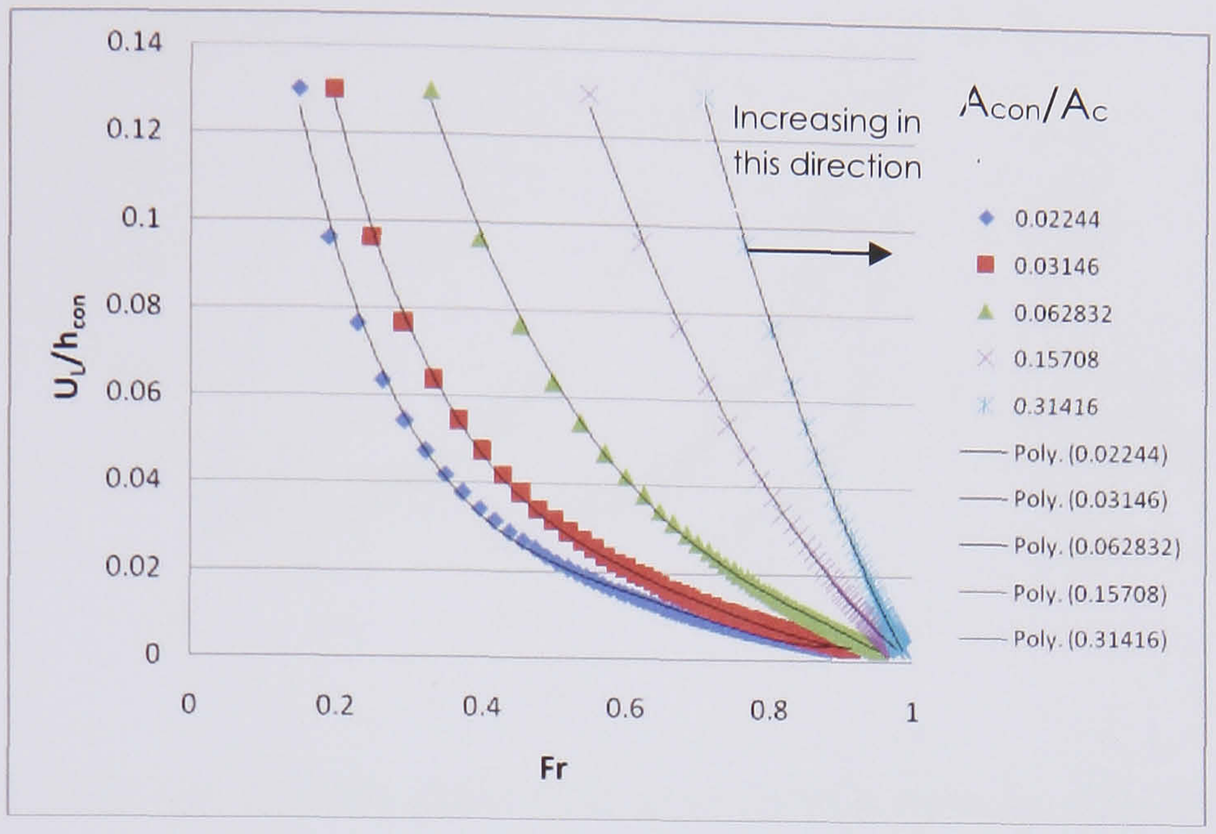

Figure 6.21 Effect on the heat removal factor of varying the ratio of the coefficient of heat loss from the collector to the coefficient of the heat transfer from condensate to manifold

From another point of view, the decisive role the condenser plays in determining the performance of a solar heat pipe collector's means of attaining acceptable heat removal factors may be realized by observing the direct effect of the condenser on the heat removal factor as illustrated in *Figure 6.22*. The effectiveness of the condenser thermal resistance may be explored by taking an example of a 0.06 area ratio in *Figure 6.22*, for which the reduction of the condenser thermal resistance from 0.04 to 0.003 produces a significant rise of about 0.3 in the heat removal factor. However if a relatively efficient condenser is used and after an increase in area ratio of beyond 0.04 no further contribution is being observed to the increase of F_R value as shown in *Figure 6.22*.

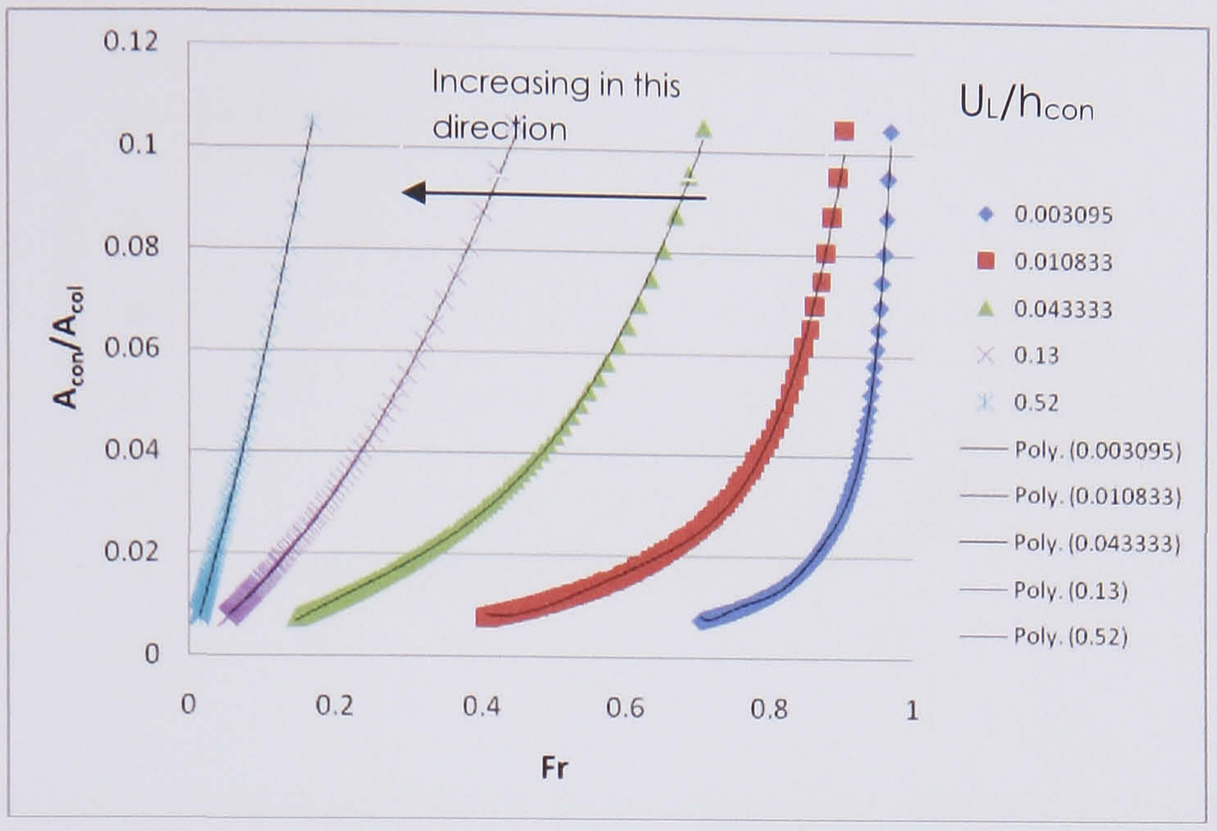

Figure 6.22 Effect on the heat removal factor of varying the ratio of the heat transfer area at the condenser to the area of collector plate

The desire of achieving high heat removal factors by employing efficient, low thermal resistance condensers is enhanced with the improvement of the overall heat loss coefficient as indicated in *Figure 6.23*. This could be accomplished by insulating the space around the performing heat pipe and so diminishing the convective heat losses. Such an effect may contribute an increase in the heat removal factor for an efficient condenser**.** Both the parameters U_L/h_{con} and A_{con}/A_{col} may be combined to form a ratio. The term U_L*A_{col} is the reciprocal of the thermal resistance to rate of heat loss to the atmosphere and $h_{con}*A_{con}$ is the reciprocal of the resistance to the transference of heat from the condensate to the fluid in the manifold. From *Figure 6.23* it may be seen that F_R has a maximum value when the ratio is above 20 and Fr is near 0.9 when the heat transfer of the evaporator increases.

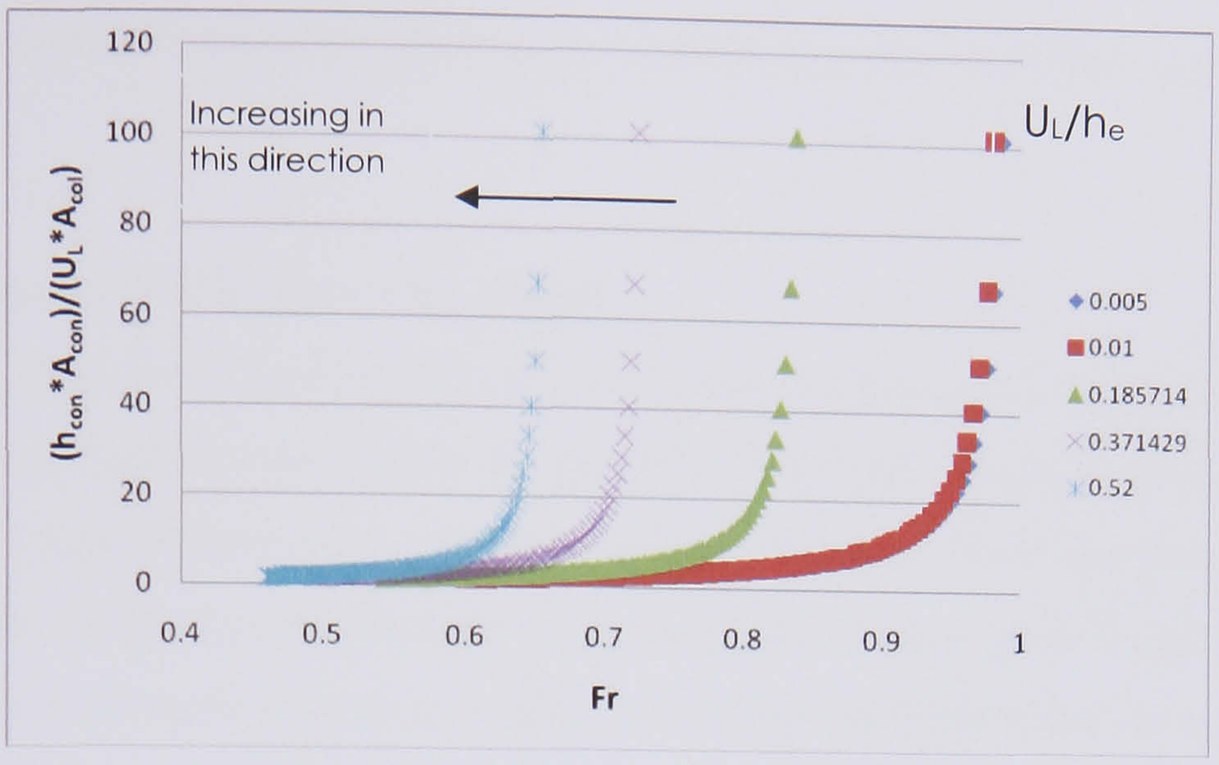

Figure 6.23 Effect on the heat removal factor varying the ratio of the resistance to heat loss from collector to the resistance to heat transfer from condensate to manifold

In the PV/T Heat pipe investigated here are the ratios of the equations are:

$A_{con}/A_{col} = 0.02683$

$U_L/h_{ev} = 0.005$

$U_L/h_{con} = 0.0025$

$F_R = 0.9106$

Where $A_{col} = 0.12\ m^2$ and $A_{con} = 3.22*10^{-3}\ m^2$

$U_L = 13\ W/m^2K$, $h_{ev} = 2600$ and $h_{con} = 5160$

The values of h_{ev} and h_{con} were calculated from equation (6.27) taken from Mathioulakis (2001) and equation (6.28) from Hussein (2006):

$$h_{ev} = 0.32 \frac{\rho_l^{0.65} k_l^{0.3} C_{pl}^{0.7} g^{0.2}}{\rho_v^{0.25} h_{fg}^{0.4} \mu_l^{0.1}} \left(\frac{p_{sat}}{p_a}\right)^{0.23} q_{ev}^{0.4} \qquad \text{Eq. (6.27)}$$

$$h_{co} = [0.997 - 0.334(\cos s)^{0.108}] \left[\frac{k_l^3 \rho_l^2 g \lambda}{\mu_l l_{co} (T_s - T_{co})}\right]^{0.25} \times [l_{co}/d_i]^{[0.254(\cos s)^{0.385}]} \quad W/m^2\,K \qquad \text{Eq. (6.28)}$$

The first step should be to choose a reasonable value of F_R which will define the limiting value of U_L/h_{ev}. Increasing the heat transfer area at the condenser has its practical limitations: for example a manifold has a greater propensity to lose heat if the dimensions are large. It will thus require better thermal insulation and thus incur a higher cost. The use of a larger condenser has inherent cost implications because special

internal and external structures and high thermal conductance materials may be required.

6.6 Experimental PV/T Heat Pipe Model

This section describes a new configuration that was developed to provide a compact PV/T Heat pipe system made with a group of four heat pipes placed in the back of the PV. The four pipes adhere their evaporator section with a flat plate absorber and with the condenser section inside a thermal reservoir or inside a manifold. Copper pipes charged with water were chosen according to the final application and the operational conditions.

6.6.1 Description of the PV/T Heat Pipe with Tank system

The system consists of a typical flat plate collector and a tank placed above the collector (*Figure 6.24*). Heat transfer from the collector to the tank is performed by the process of boiling in the evaporator, vapour flow, condensation in the condenser and condensate return. The evaporator of the heat pipe consists of two copper flat plates with slots that allow incorporating 4 heat pipes. Four heat pipes were used in order to absorb as much as possible heat from the whole area of the PV something that would be difficult with just using one heat pipe. The evaporator section of the pipes was soldered on the copper plate and a thermal paste also was used. The condenser section of the pipes that are placed inside the tank works as a heat exchanger. The basic characteristics of the system are summarised as follows:

- PV/T collector: dimensions 0.4X0.4 m and two copper flat plates with dimensions 0.3X0.2 m
- Tank: rectangular tank with water of 8.5 l.
- Heat pipe: 4 pipes of 10 mm diameter and 450 mm length. Evaporator length 0.26, adiabatic 0.05 m and condenser 0.14 m.

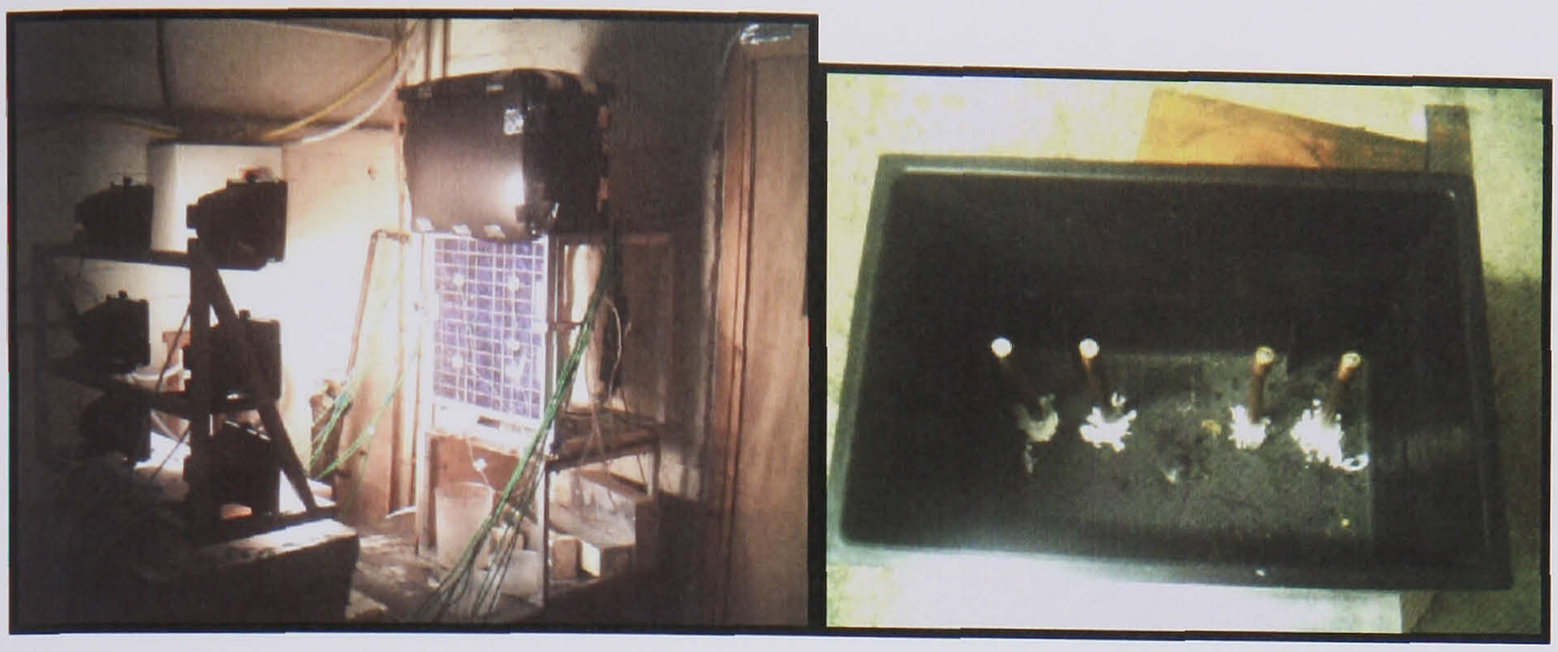

Figure 6.24 PV/T Heat Pipe with Tank

Physical quantities measured are: temperature in parts of the evaporator, the condenser and the tank as seen in *Figure 6.8*. Measurement series contain whole charge – discharge cycle starting either from a zero stored energy state with cold collector or from a state of high temperature in the tank. For temperature measurements 4 type K thermocouples were placed at equal spaced points inside and along the tank (see *Figure 6.8* black circles). The initial water temperature was near 18 ^{o}C and the duration of the experiment was 3 hr 40 min and the discharge and charge phase started 1 hr 40 min after the beginning of the experiment. An attempt was also made to improve the heat transfer enhancement by incorporating 10 fins to the condenser section of each of the 4 pipes as shown in *Figure 6.25*.

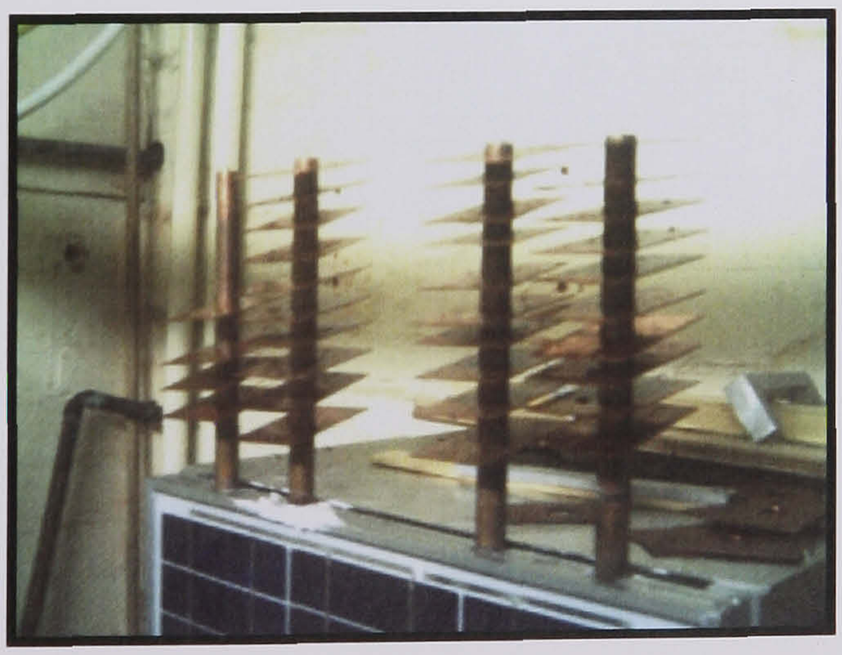

Figure 6.25 PV/T Heat Pipe with Tank using Fins

6.6.2 Description of the PV/T Heat Pipe with Manifold system

The system consisted of the same evaporator section as in 6.6.2 section and the condenser part of the pipe inside a manifold as shown in *Figure 6.26*. Heat transfer from the collector to the manifold is occured inside the manifold by the direct contact of the pipe with the water flowing around. The experiment started with initial temperature of 18 °C and flow rate of 0.3 l/min. The experiment worked in steady state conditions and the outlet heated water of 21.6 °C (see *Figure 6.31*) was dumped in a cooling fan heat exchanger as in *Figure 6.27*. The basic characteristics of the system are summarised as follows:

- PV/T collector: dimensions 0.4X0.4 m and two copper flat plates with dimensions 0.3X0.2 m
- Manifold: 4 cylindrical tubes of 30 mm OD diameter and 0.14 m length (see *Figure 6.8*)
- Heat pipe: 4 pipes of 10 mm diameter and 450 mm length. Evaporator length 0.26, adiabatic 0.05 m and condenser 0.14 m.

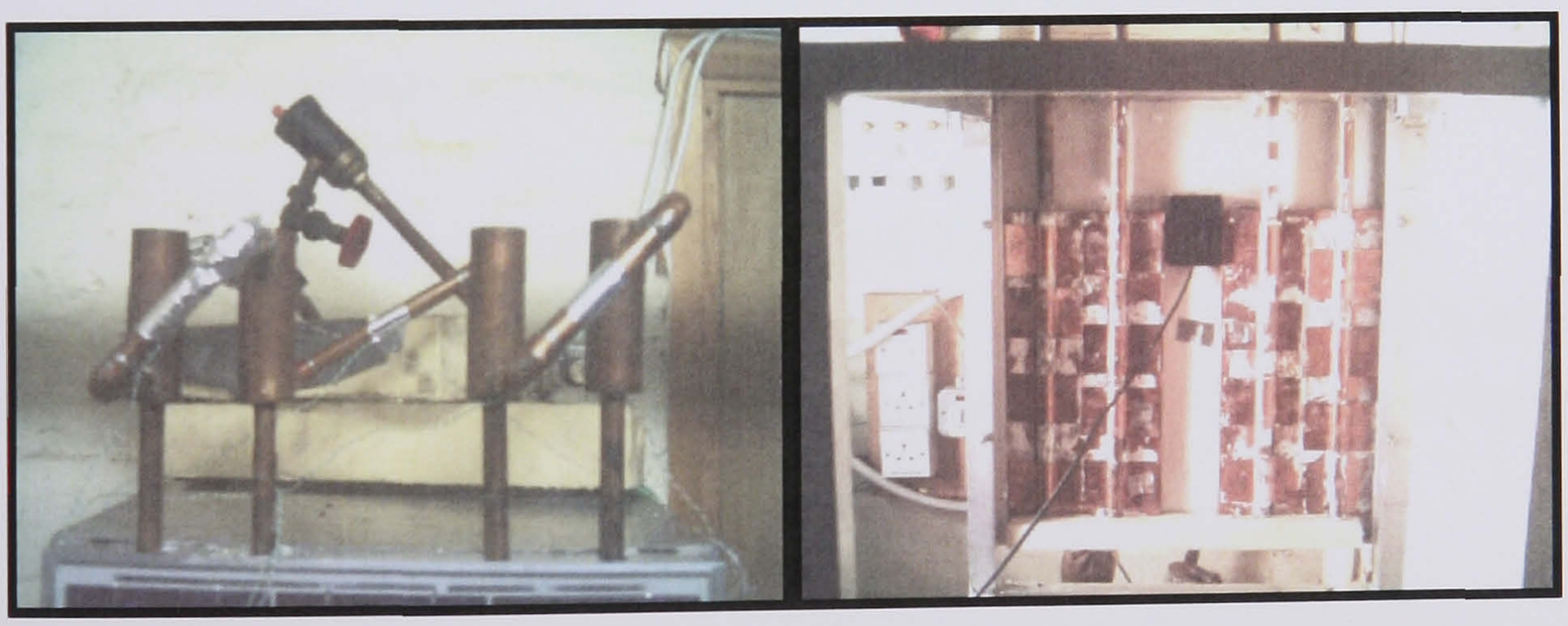

Figure 6.26a PV/Heat Pipe with Manifolds

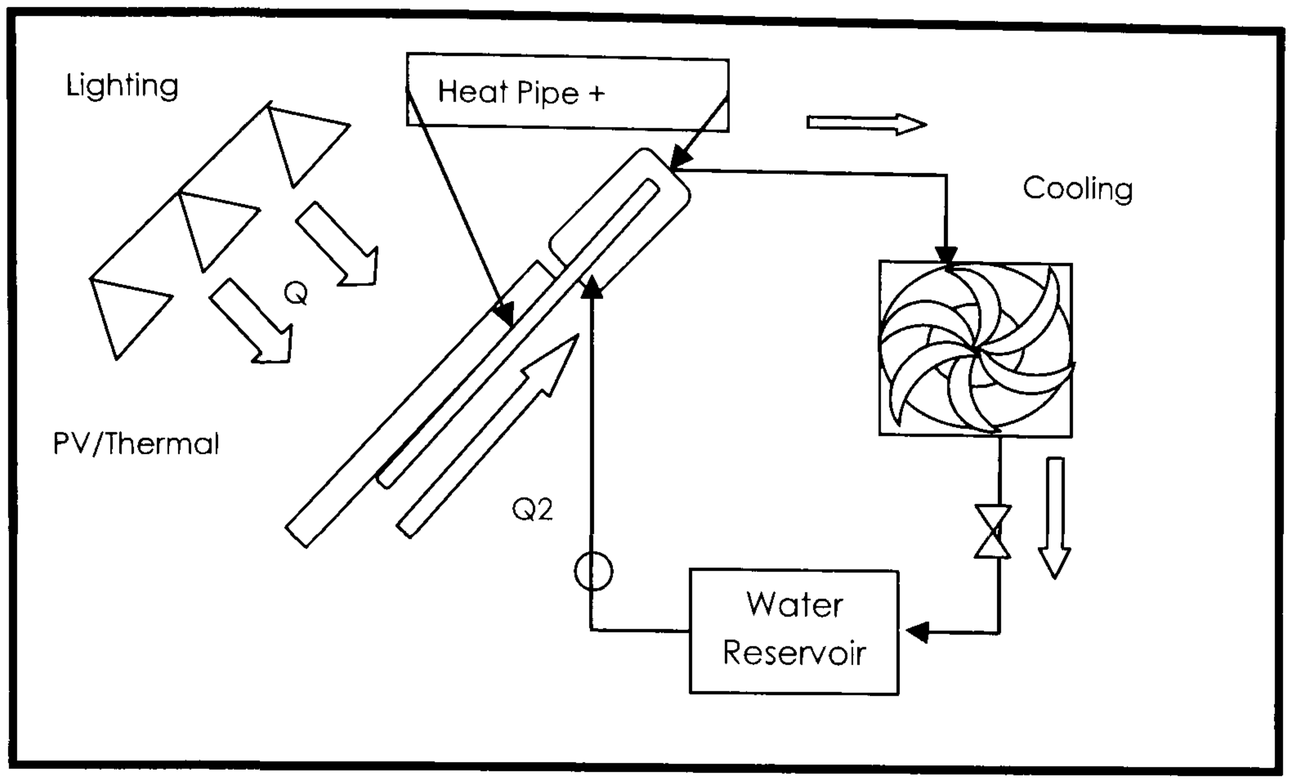

Figure 6.26b PV/T Heat pipe Schematic Rig

6.7 Experimental Results

Solar collectors could be experimentally tested by several methods. For many solar applications, some methods had been standardised by ASHRAE (Duffie, 1991). The testing principle of the various methods rationally divert from two fundamental procedures known as the instantaneous and calorimetric procedures (Hill, 1976). Both procedures could be implemented under transient steady state conditions.

6.7.1 Calorimetric method of testing used in the PV/T heat pipe with tank

The quantity of heat transferred to the water within the tank can be calculated by the water temperature variation, taking into account the water quantity and its specific heat:

$$Q_{\text{col}} = m_{\text{w}} C_{p,\text{w}} (T_{\text{w2}} \quad T_{\text{w1}})$$

where m_w is the mass of water within the storage tank, kg, $C_{p,w}$ is the specific heat associated with water, kJ/kg°C, and (T_{w2} - T_{w1}) is the temperature rise of water within the tank. T_{w1} is the temperature of the water within the tank at the beginning of the experiment while T_{w2} is the water temperature at the actual time.

The cumulative collection efficiency (n) can be expressed as a ratio of amount of heat stored in the tank to the total amount of solar energy incident on the collector for the same period of time, i.e.,

$$\eta = m_{\mathrm{w}} C_{p,\mathrm{w}} (T_{\mathrm{w2}} - T_{\mathrm{w1}}) / Q_{\mathrm{incident}}$$

It is noted that the cumulative efficiencies are calculated from the beginning of the experiment, and therefore these integrated efficiencies based upon the initial tank temperature are not instantaneous values. Actually this experiment works as a representative of a collector that is warming up without circulation of water. Thus the system works under unsteady state conditions and can not be compared with the system using the manifolds. So the efficiency will start to increase, reach a high point and later start to decrease with increase of water temperature.

The first set of experiments involves the evaluation of the electrical and thermal performance of the system with or without fins in the condenser section that is placed inside the water tank. From *Figure 6.27* and *6.28* show the electrical and thermal performance of the two systems. It is obvious that the use of the fins improves both the electrical and thermal efficiency. The improvement in the electrical efficiency is small in comparison with the thermal efficiency. Only 1.29 % increase for the electrical and 24.78% for the thermal efficiency.

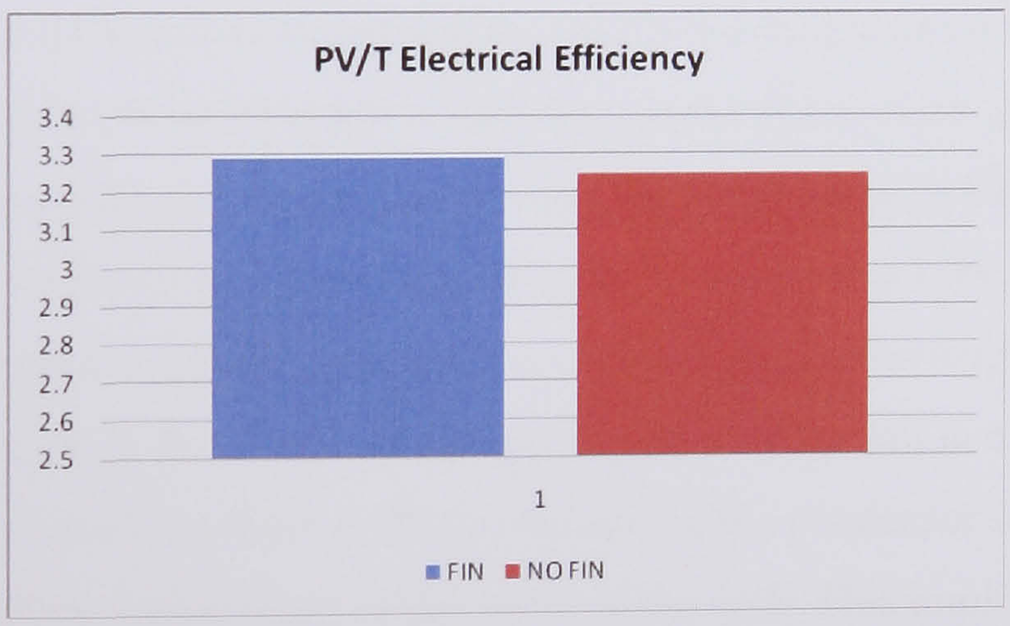

Figure 6.27 Comparison of electrical efficiency of PV/T Heat Pipe with and without Fins

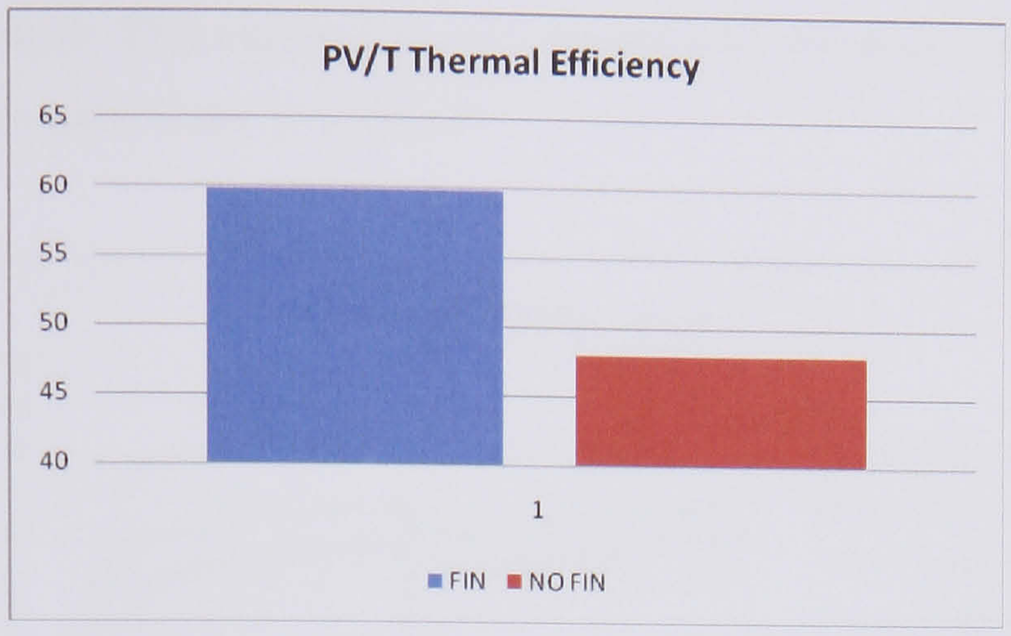

Figure 6.28 Comparison of thermal efficiency of PV/T Heat Pipe with or without Fins

The heat transfer mechanism from the collector to the tank is based on a continuous evaporation – condensation cycle of the working fluid. Water is evaporated in the evaporator which is coupled to the collector by absorbing heat. This heat is then transferred to the tank through the condenser. *Figure 6.29* gives the variation of the basic parameters of the system for irradiation of 1000 W/m^2.

As can be seen from *Figure 6.29* two discrete phases characterise the operation of the system during charging. In the first phase no heat transfer was observed, as evidenced by the temperature in the collector increasing rapidly but without heat transfer to the tank. This period lasts about 30 minutes until the second phase starts. Water in the lower part of the heat pipe is heated up gradually while the temperature in the condenser increases rapidly. In the second phase mass and heat transfer from the collector to the exchanger – condenser begins. The beginning of this phase is characterised by a sudden fall of the temperature in the evaporator (from *Figure 6.29* the fall in evaporation could not be seen) and adiabatic section, a steady increase of the condenser section and a gradual increase of the temperature of the water in the tank. This implies that the working fluid inside the heat pipes has started evaporating and transferring the heat to the condenser. It is actually the beginning of the activation of mass and heat transfer mechanism. In 1 hour and 40 minutes at an irradiation of 1000 W/m^2 the water temperature increased by 7 ^{o}C before change the water and put a new with a temperature of 18 ^{o}C. In the same period of time a similar increase of water temperature was

obtained as previously. This experiment was done in order to observe the performance of the system when have water withdrawal.

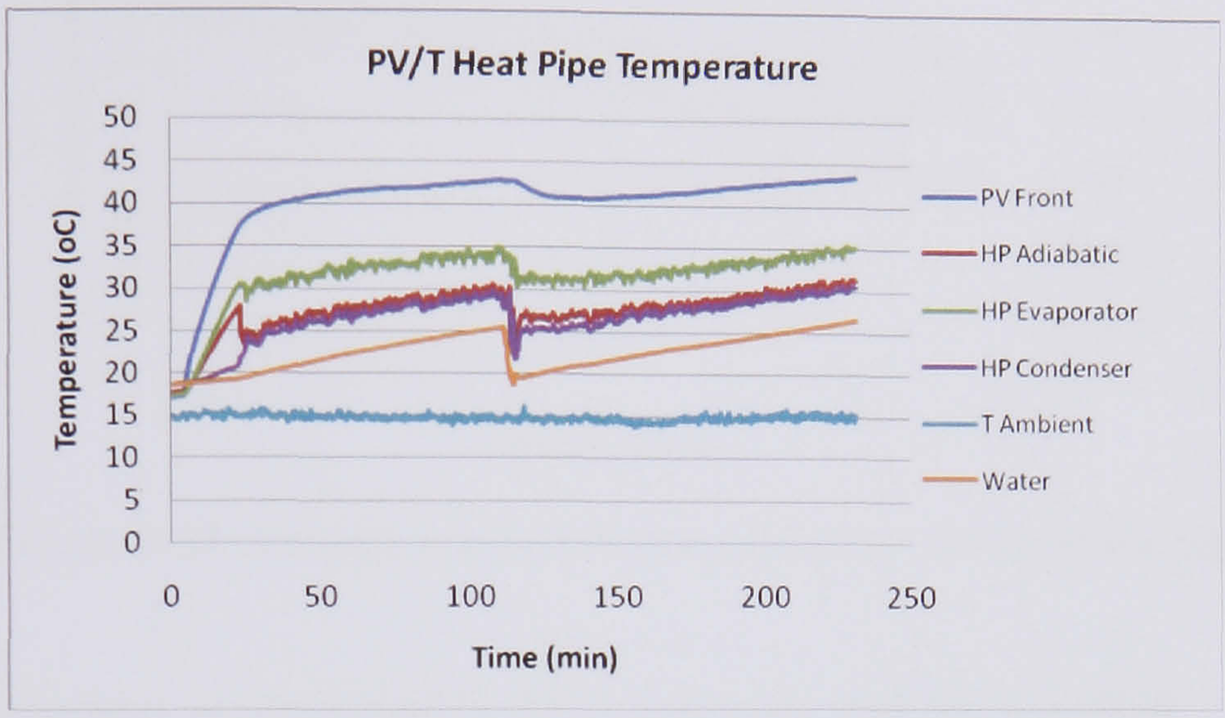

Figure 6.29 PV/Heat Pipe Temperature

Under real operating conditions the distribution of temperature inside the heat pipe during charging is not uniform. *Figure 6.30* shows a typical temperature distribution along the heat pipe for different periods during the experiment. The distance along the heat pipe is depicted along the horizontal axis following the route of the working fluid setting the starting point at the lowest part of the collector. In this figure can be seen that after the beginning of the charging phase the heat pipe remains isothermal along its length apart from the lower part of the condenser where the fluid is at a temperature lower than the condensation temperature.

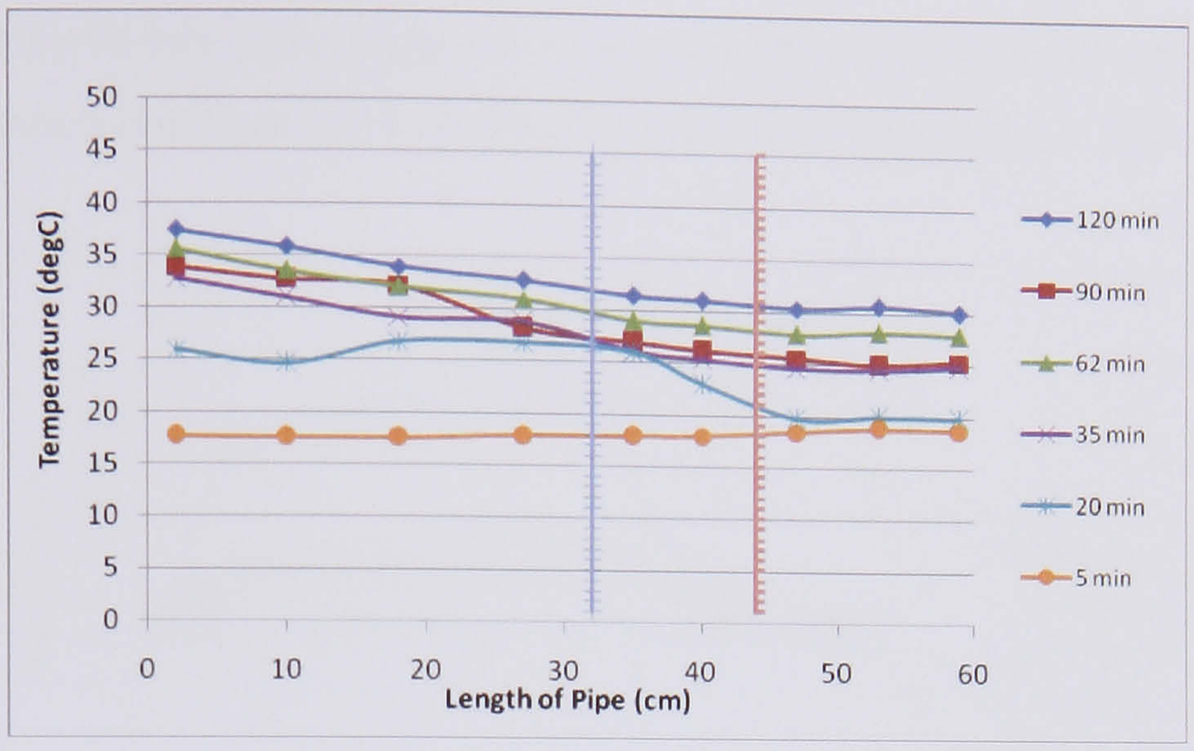

Figure 6.30 Temperature distributions along the length of the pipe

6.7.2 Instantaneous method used in PV/T heat pipe with the manifold

The method of testing that used for the test rig with manifolds measures the useful heat gained (Q_{use}) in terms of the fluid temperature difference between the inlet and outlet of the collector given by equation (2.3.1).

The efficiency of the collector may be determined by including the influential parameters that control the production of the useful energy. Thus the scope of measurements in addition to the parameters in the above equation may extend to include the incident solar radiation and ambient temperature. Therefore at steady state, the useful heat energy and the efficiency of the collector could be determined by the measurement of these parameters independently and the general formula that congregate then may be given by equations:

$n = Q_{use}/A_{col}*G = m*C_p*(T_{out} - T_{in})/A_{col}*G$ %

$n = F_R*[Q_{solar} - UL*(T_{in} - T_a)]$

The first set of experiments evaluating the thermal and electrical efficiencies for different flow rates. In *Figure 6.31* an example of the different flow rates can be seen that were used in order to determine the temperatures of the collector, the fluid inlet and outlet as also the temperature at the different sections of the heat pipe. As seen from the graph it takes 30 minutes before the heat pipe starts working and with a flow rate of 0.3 l/min an average PV temperature of 43 ^{o}C is achieved. The experiments worked under steady state conditions that reached after an hour and were repeated for 6 different flow

rates and as may be seen from *Figure 6.32* both the difference between outlet and inlet water temperature is affected as well the PV temperature from *Figure 6.33*.

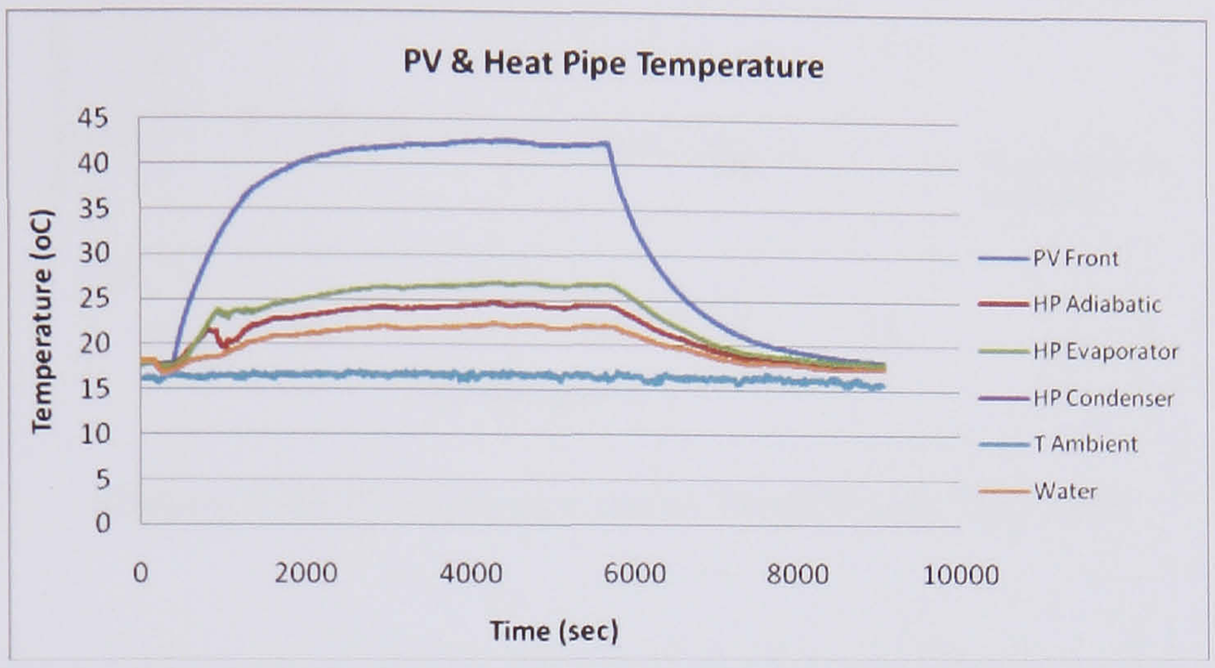

Figure 6.31 PV/T Heat Pipe Temperature with Manifold

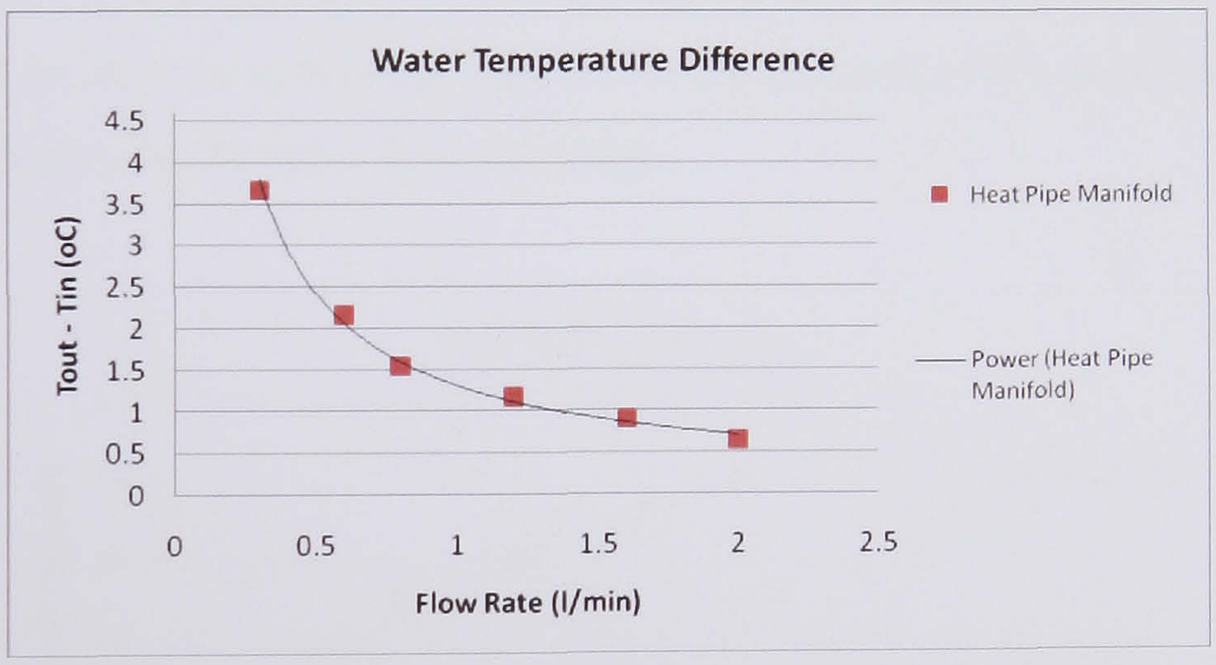

Figure 6.32 Water Temperature Difference for different flow rates

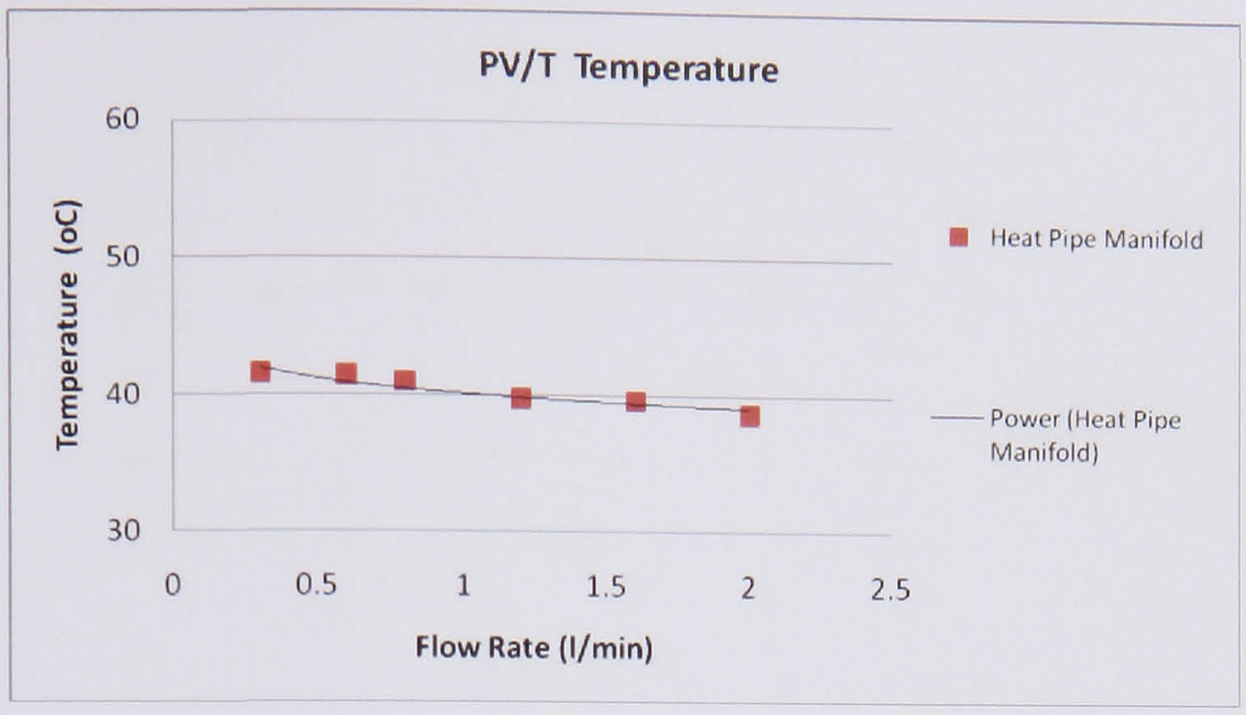

Figure 6.33 PV/T Temperature for different flow rates

From the same set of experiments the electrical and thermal efficiency were evaluated for the different flow rates. As may be sees from *Figure 6.34* and *6.35* as the flow rate increases both efficiencies increase. A 10% improvement in electrical efficiency is observed for an increase in flowrate from 0.3 to 2 l//min and a 10% improvement in thermal efficiency for the same flow rate range.

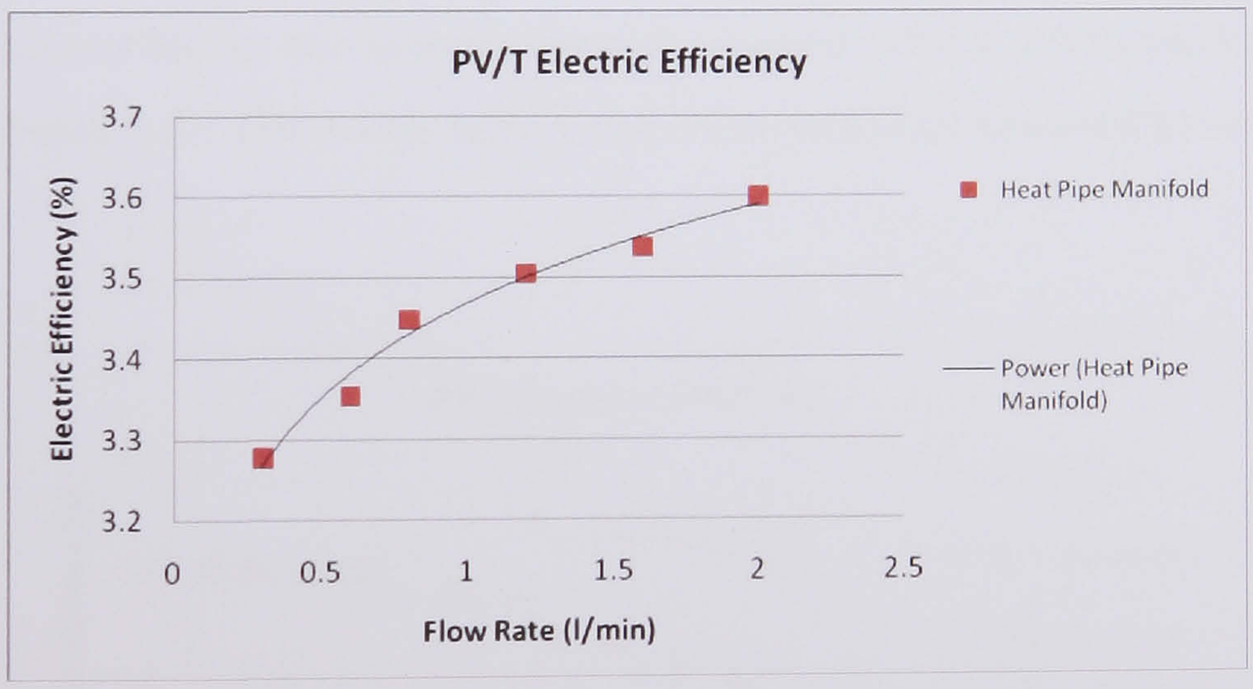

Figure 6.34 PV/T Heat Pipe Electrical Efficiency with Manifold

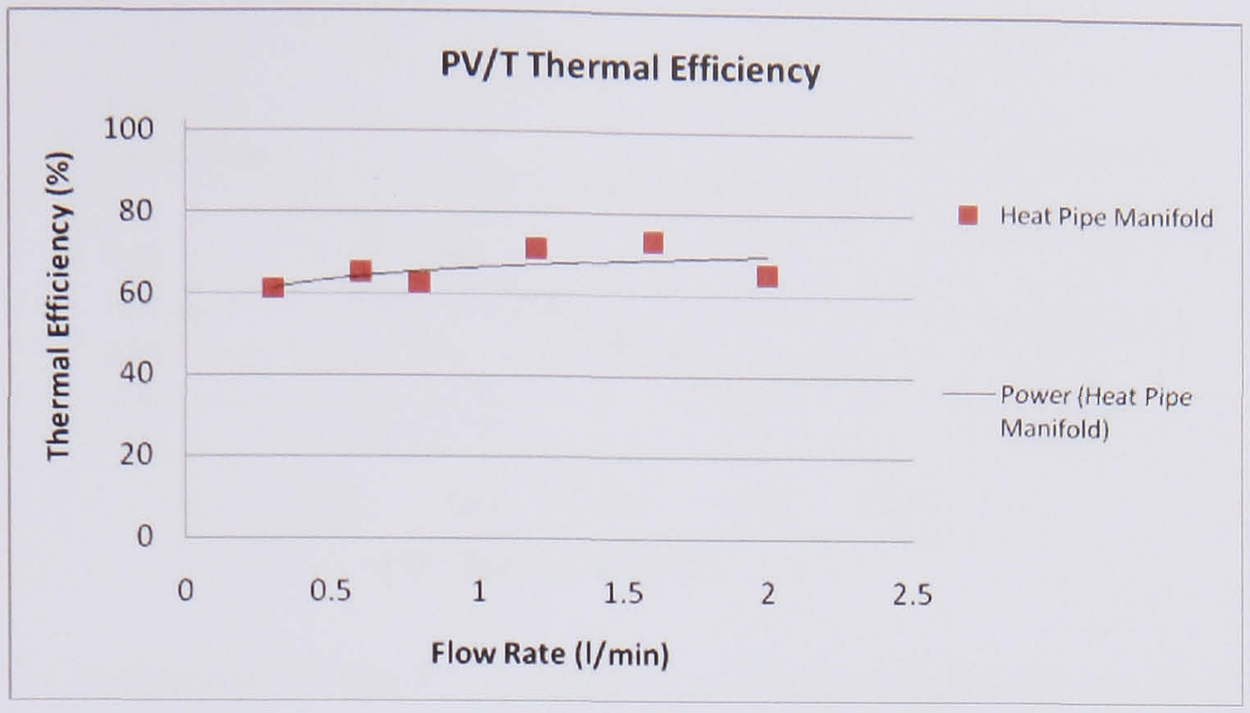

Figure 6.35 PV/T Heat Pipe Thermal Efficiency with Manifold

6.7.3 Comparing PV/T Heat Pipe system with Manifold and Tank

As mentioned the two systems are not working at the same conditions as the manifold works in steady state conditions and the tank system at unsteady state conditions. The manifold system tested 9 different experiments using different water temperatures at the manifold inlet. For the tank system 6 different experiments were completed by increasing the water tank temperature for each. From the results the electrical and thermal efficiency for the two systems were determined and the results can be seen in *Figures 6.36* and *6.37*. The x-axis in *Figure 6.36* is used to be valid with equation (2.4.6).

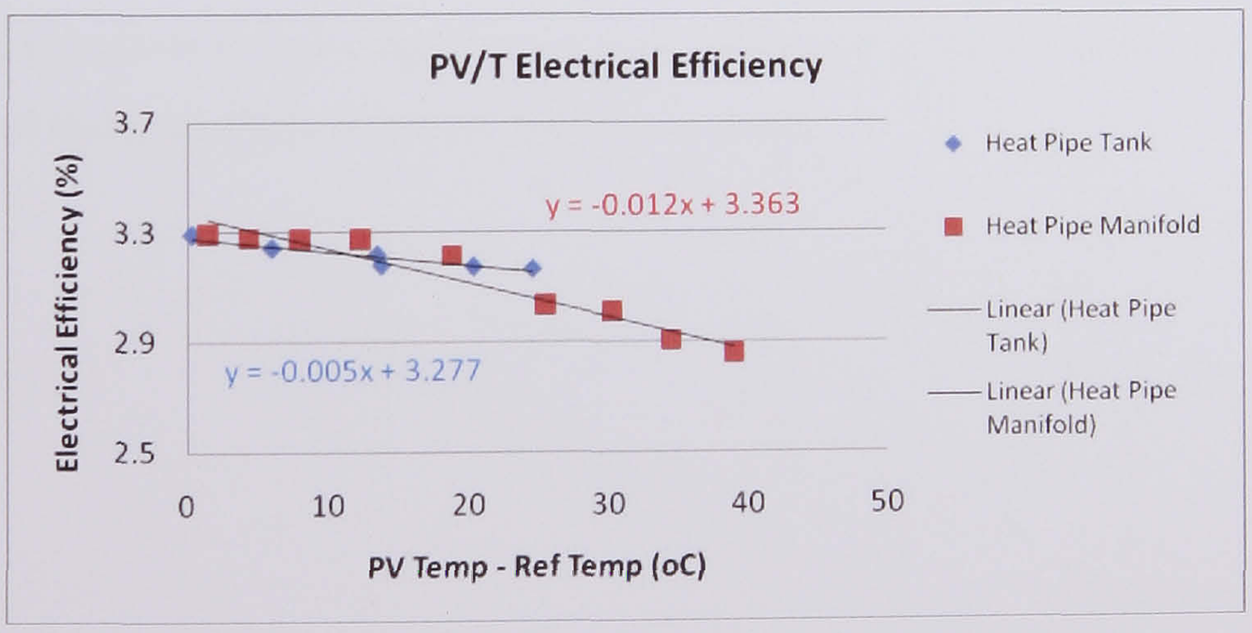

Figure 6.36 Comparison of the PV/T Heat Pipe Electrical Efficiency with Manifold and Tank

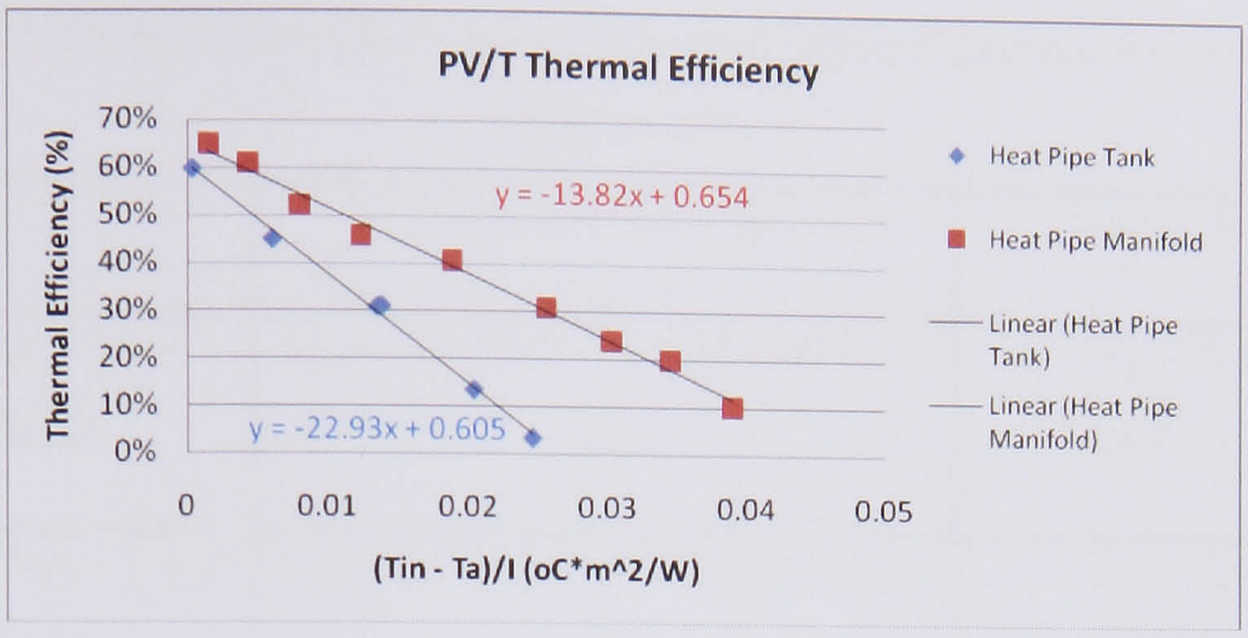

Figure 6.37 Comparison of the PV/T Heat Pipe Thermal Efficiency with Manifold and Tank

From the *Figure 6.36* both models have similar electrical efficiencies but the manifold has a higher electrical efficiency coefficient than the tank model. Considering the thermal efficiency it may be seen that the manifold has higher efficiency at zero reduced temperature than the tank model. The system with the manifold has an initial efficiency of 65.4% and the tank 60.5%, a percentage difference of 8%. Also the manifold system has a lower heat loss coefficient (U_L = 13.82 W/m^{2o}C) than the tank (U_L = 22.93 W/m^{2o}C). The manifold works more efficiently and the improvement in terms of heat loss coefficient in comparison with the tank is 40%. The tank's higher heat loss coefficient probably occurs because of the bottom part of the tank was partly insulated relative to the rest of the tank as the connection between the 4 pipes and the bottom of the tank did not allow the placing of insulation. *Table 6.4* gives the linear equations for electrical and thermal efficiencies for the two systems.

Table 6.4 PV/T Heat Pipe Electrical and Thermal Linear Equations for Manifold and Tank models

	Electrical Equations	Thermal Equations
PV/T Heat Pipe – Manifold	$n_{ele} = 3.363*(1 - 0.003568*(T_{pV} - 25))$	$n_{th} = 0.654 - 13.82*(\Delta T/G)$
PV/T Heat Pipe - Tank	$n_{ele} = 3.277*(1 - 0.001525*(T_{pv} - 25))$	$n_{th} = 0.605 - 22.93*(\Delta T/G)$

The two systems were further evaluated with the total energy efficiency, the energy saving efficiency and the exergy efficiency were evaluated as in previous chapters. *Figure 6.38, 6.39* and *6.40* show these parameters for the two models. As may be seen from the three graphs the system with the manifold works more efficiently than the tank system. In *Figure 6.38* the total sum of electrical and thermal efficiency is 68.8% and 63.8% for manifold and tank system respectively. The same trend may be observed in *Figure 6.39* were the energy saving efficiency is higher for the manifold model at 74.3% than the tank that is 69.1%. As observed from all graphs the system using the manifold as a heat exchanger performs better than the system with the tank. This can be seen most clear in *Figure 6.40* which shows the exergy efficiency of the two systems. This indicates that the manifold system works with 24% exergy efficiency when the inlet water working temperature is near to 40 ^{o}C at 20 ^{o}C ambient temperature and 1000 W/m^2 irradiation in comparison with the tank that achieves maximum exergy efficiency at 17% but the working temperature is in the region of only 33 ^{o}C on the same working conditions as previously. The data also indicate that the manifold system works effectively in a higher temperature range than the tank system.

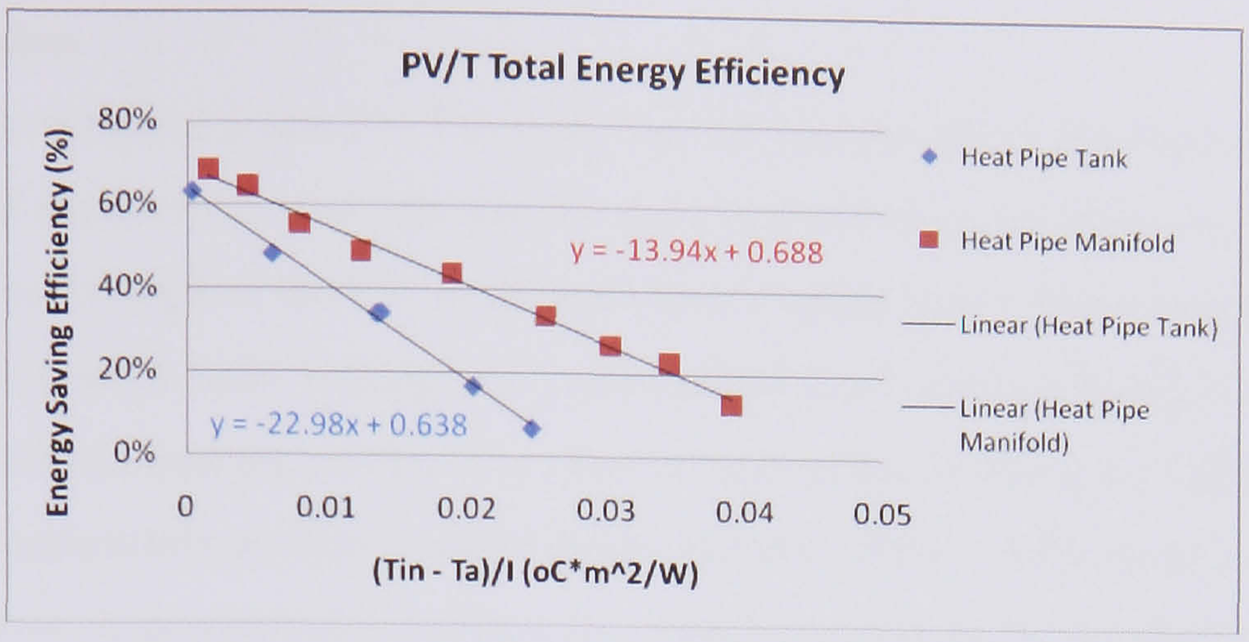

Figure 6.38 Comparison of the PV/T Heat Pipe Total Energy Efficiency with Manifold and Tank

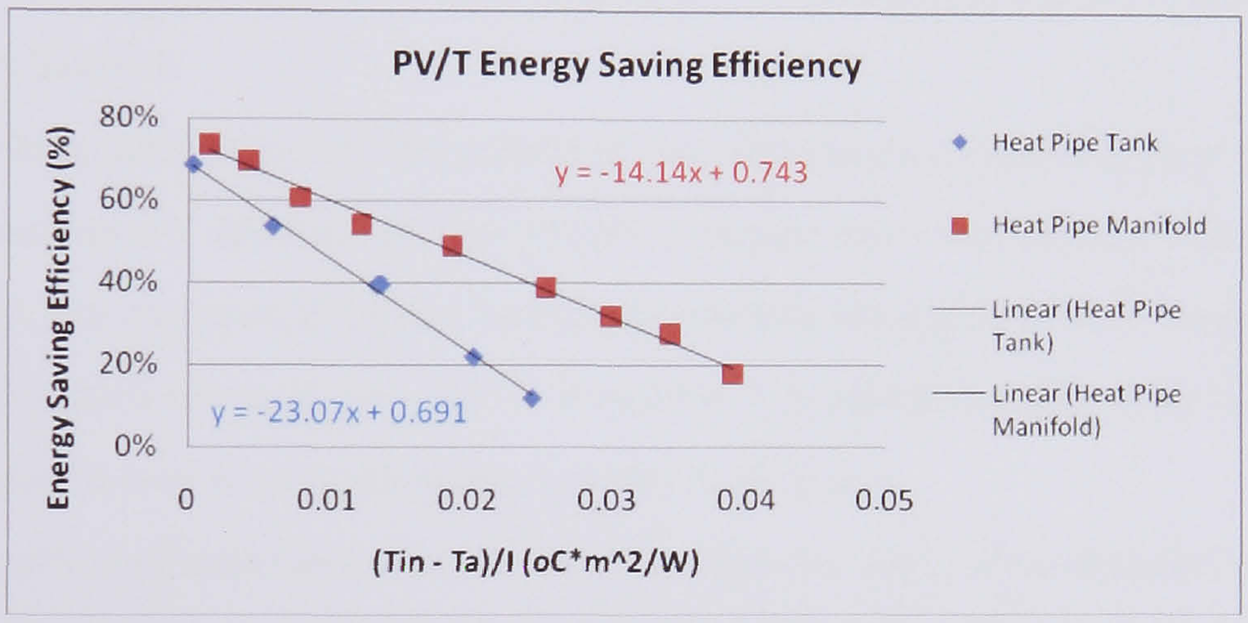

Figure 6.39 Comparison of the PV/T Heat Pipe Energy Saving Efficiency with Manifold and Tank

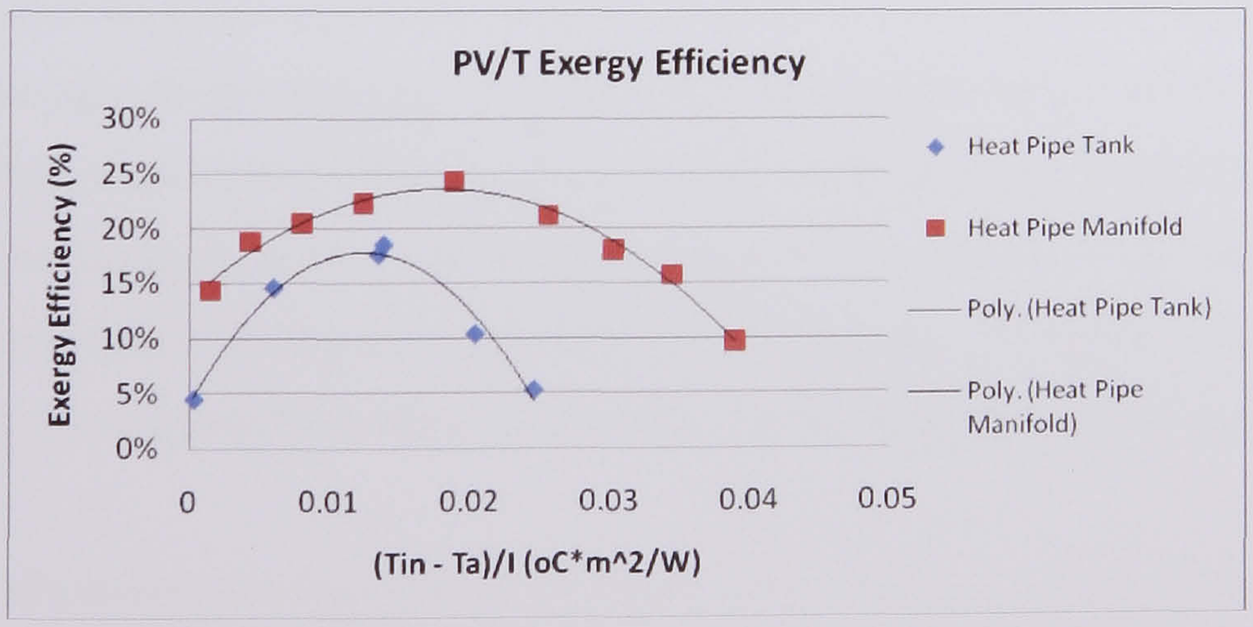

Figure 6.40 Comparison of the PV/T Heat Pipe Exergy Efficiency with Manifold and Tank

6.8 Conclusion

Chapter 6 investigated a new PV/T system that incorporates heat pipes that work with high thermal conductivity and heat transfer rates in place of water pipes or openings that transfer air in the back of the PV. Section 6.1 explored the heat transfer limits, such as capillary limit, sonic limit, boiling limit, entrainment limit and viscous limit for a normal cylindrical heat pipe and used a simulation to evaluate how a heat pipe is being affected by parameters such as working fluid, diameter of pipe, inclination angle and liquid fill level. A gravitational wickless heat pipe was selected for the simulation and experimental work on the PV/T Heat pipe system. This choice was based on the simple build of such a pipe and also cause the heat pipe would be assisted by gravity so a wick was not necessary. The effects of other parameters on the performance of heat pipe were discussed as follows:

- Working fluid was very important to the application of the heat pipe and its choice mainly depends on the operation temperature and the heat load that could carry. For the present case a low temperature working fluid was required with temperature range of 20 – 60 ^{o}C. From the simulation and from the Merit number it was found that water was the best choice.
- The effect of inner diameter of the heat pipe was also simulated and the results showed that the heat transfer limit increased greatly with increasing the diameter of the pipe. Also the heat transfer limit increased by increasing the operating temperature of the system.
- Another important parameter was the liquid filling level and the inclination angle of the pipe. In the first case the simulation showed that above certain fill level the heat transfer limit ceased to be increase and reached maximum. For the inclination angle it was seen that the maximum heat transfer limit was near 60 deg and that at 90 deg a value of 200 W was obtained. This phenomenon had been noticed and from other researchers. For this case the 90 deg was chosen.

Section 6.2 discussed two experiments that were performed to evaluate the performance of a heat pipe, which was used also on the PV/T model, as far as consider the heat transfer rate, thermal conductivity and heat flux. From the results it was found that the

heat pipes had a thermal conductivity of 2411 W/mK and that both the heat transfer coefficient and heat flux increase with the increase of evaporator temperature. By increasing the heat input in the pipe the heat transfer coeffiecient increased from 5000 to 7000 W/m^2K.

Using Kammingas correlation for heat removal factor it was noticed that the condenser area affects the performance of a system. From using the correlation of heat removal factor to our PV/T model it was estimated a F_R value of 0.91.

A rig was constructed and two PV/T models were tested. The condenser part of the heat pipes for the first model was inside a tank and fins were welded on the pipes in order to increase the heat transfer. The second model used a series of manifolds that water passed through them and extracting the heat from the condenser part of the heat pipes. The following observations can be done for the two PV/T systems:

- PV/T Heat pipe with tank

This model is a representative of a collector that is warming up without transfering that heat to a circulating fluid and works in unsteady state conditions. Thus the maximum instantaneous efficiency was recorded. The beginning phase of the heat pipe is characterised by an immobility period without heat transfer to the tank. The period before the pipe starts working is around 30 min. The results showed that the system with the fins in the condenser part of the heat pipe increased the thermal efficiency by 24.78%. It took 1 hour and 40 min to increase the temperature by 7 oC in a water tank filled with a volume capacity of 8.5 lt. By changing the initial water temperature in the tank it was noticed that this model has high heat losses (22.93 W/m^2K) and works in a small temperature range ($\Delta T/G$ = 0 -0.025, 20 – 45 ^oC). This application could be used as the thermosyphon for water heating. With a more efficient heat pipe a higher water temperature increase could be achieved in a shorter time. After the water temperature has reached an acceptable level (i.e. 40 – 55 ^oC) a discharge of the hot water and charge of new water with low temperature is being placed until the procedure starts again. Because the system also should take into consideration the PV performance the

temperature scale of such an application should be around 25 – 40 °C so can work as a pre-heating device.

- PV/T Heat pipe with manifolds

The same period of 30 min before the pipe starts transferring heat was observed in the model using the manifolds. The results showed that the PV/T temperature remains around 40 °C and noticed that by increasing the flow rate the electrical and thermal efficiency was improved. Testing the system with different inlet water temperatures it was noticed that the model with the manifolds works around 65.4% at zero reduced temperature and a heat loss coefficient of 13.82 W/m^{2}K. This application could be used by passing water from the manifold and heated up until the temperature of the water and collector's temperature reach a similar level and thus heat pipe stops transferring more heat and no further heat gain can be achieved. Special attention should be given to the PV performance thus a low temperature scale from 25 – 40 °C can be used for pre-heating purposes.

Using the total energy efficiency, primary energy saving efficiency and exergy efficiency it was noticed that both systems have the potential to be used as an alternative PV/T system. Adding the electrical and thermal efficiencies gave 68.8% and 63.8% for the system using the manifold and the tank respectively. Both systems have a high primary energy saving efficiency that reaches 74.3% and 69.1% respectively and can be compared with other PV/T systems. As far as consider the exergy efficiency as seen from Figure 6.40 the manifold performs better with the peak exergy being 24% at 40 °C inlet water temperature. The PV/T model with the tank cause of the high heat losses achieves a peak exergy at 17% but around 35 °C.

As a general conclusion can be noticed that heat transfer rate is favourable if low temperatures exist in the fluid that the heat is transfered. A temperature increase in the fluid causes an increase of temperature in the whole heat pipe, thus increasing the losses from the collector. Although heat transfer continues at higher temperatures, the increase of collector losses results in a decrease of the overall system efficiency. This means that

to maximise energy output it is worthwhile for the heat pipe to operate with large temperature differences between the collector and the fluid used.

By decreasing the volume capacity of water and using a better insulated tank system an improved performance could be obtained for the PV/T system using the tank. A better designed manifold could work better as a heat exchanger and a smaller adiabatic length of the heat pipe with further insulation will reduce the heat losses.

CHAPTER 7: PHOTOVOLTAIC/THERMAL SYSTEM PHASE CHANGE MATERIAL (PCM)

7.1 Introduction

Phase change materials (PCMs) absorb a large amount of energy as latent heat at constant phase transition temperature and are thus used for passive heat storage and temperature control. Many articles have been published by researchers who have used PCM in wallboards, in glazed facades or as a solar aided latent heat storage system. Incorporating a solid–liquid PCM with a phase change similar to the PV reference temperature of 25 ^{o}C for the thermal regulation of PV under cyclic time-dependent solar energy input is a novel approach to PV temperature control. Depending on ambient conditions, a PV/PCM system may enable the PV to operate near its reference temperature and thus with good solar to electrical conversion efficiency. Because the 25 ^{o}C of temperature is low grade heat a PCM could be used with a higher melting point and thus a compromise between electrical efficiency and temperature stored can be achieved. An additional potential benefit is that the energy stored in the PCM may be released to water or air with special designed heat exchangers.

This chapter presents an extensive unsteady state heat storage process and experimentally investigates the thermal behaviour of a phase change material, when used to moderate the temperature rise of PV in a PV/PCM system. A transient numerical model for predicting the thermal behaviour has been developed to optimise the PV/PCM system design. This chapter describes the experimental validation and application of the developed PV/PCM simulation model. From a review of the literature this appears to be the first time a TRNSYS model for a PV/PCM system has been built and validated using experimental data. Using the validated numerical model, behaviour is predicted for a range of PV/PCM systems and conditions. As described above the heat that was absorbed from the PCM could be used for heating water or air. So an experiment was set up incorporating water pipes inside the PCM container in order to extract that heat and improve the cyclic working conditions of the system.

Overall the benefits of a system using PCM are:

a) ability to cut the peak load and reduce the size of the system

b) stabilize PV cell temperature and thus improve electrical performance
c) larger heat storage capacity
d) improve heat storage discharge strategies

A drawback of using PCM is that when compared with a PV/T system using serpentines in the back it can't provide increased thermal efficiency.

7.2 PCM Thermo physical Properties

Knowledge of the main thermophysical properties of materials used for latent heat storage is essential for the design and study of the exchanger – accumulator and subsequent measures to optimize its performance. The main property is the enthalpy since the quantity of thermal that may be stored depends on the enthalpy variation around the phase change region.

Yingping reviewed methods such as differential scanning calorimetry (DSC) and differential thermal analysis (DTA) and pointed out their limitations for PCM property analysis. In the same work Yingping proposed a simple method to determine phase change temperature, undercooling, phase change enthalpy and the specific heat and conductivity of the solid and liquid phases with a study of temperature – time curves easily obtained in a simple experiment.

7.2.1 Description of the method

In the method presented by Yingping et al. a tested PCM sample and a heated sample with known thermal properties are subject to ambient air. Their temperature history upon cooling down from the same initial temperature to room temperature is recorded. A comparison of both curves, using a mathematical description of the heat transfer, allows the determination of the heat capacity, the enthalpy of the PCM from known specific heat of the reference material.

The experimental system built based on the criteria that Yingping designed is shown in *Figure 7.1* and consists of:

- Test tubes whose L/D ratio fulfils the condition Bi < 0.1; in this work the tubes used had a length (L) of 25 cm, diameter (D) 10 mm and glass thickness of 1 mm. The geometry of the tubes allows the heat transfer to be considered uni-

dimensional and each tube to be a lumped system in front of the ambient air. These two conditions are fulfilled when Bi < 0.1 (Biot number; $Bi = \alpha R/(2\lambda$, where R is the radius of the sample, λ is the thermal conductivity of the glass and α is the heat transfer coefficient between the tube and the environment.

- An insulated cooling chamber, with a temperature change during the experiment of less than 1 °C.
- A hot water bath, for heating the sample and the reference to an initial temperature
- Temperature sensors, type T thermocouples (accuracy 0.1 °C, thickness 0.127 mm), to measure the temperature of the PCM, water and ambient.
- Data acquisition equipment connected to a computer.

Two identical tubes, one containing the PCM to be tested and the other a reference substance whose specific heat is known i.e. distilled water, were heated up in the water bath to temperature above the melting point of the PCM material (*Figure 7.1*). Then the tubes were placed in a cooling chamber and the temperature T-history was recorded, until the temperature of the tubes reached ambient temperature. The whole experiment lasted about 2.2 hr.

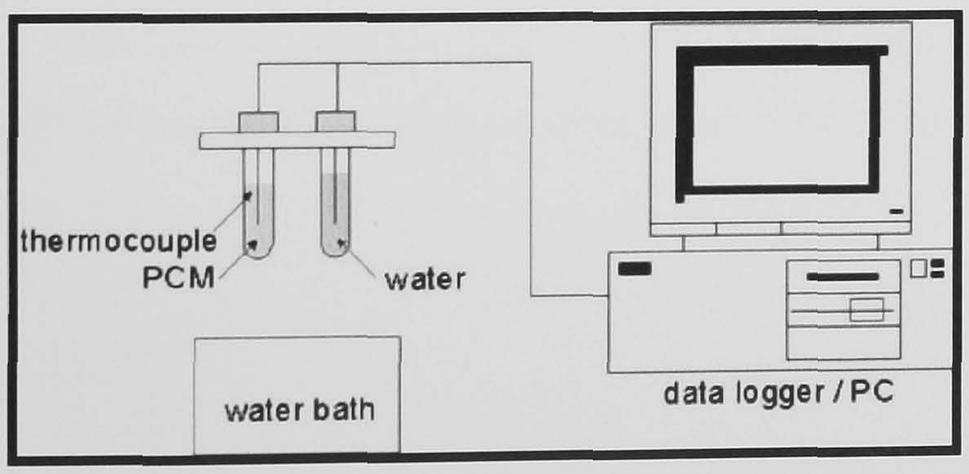

Figure 7.1 Schematic diagram of the experimental rig (Hong, 2004)

The outlined method allows the determination of the thermophysical properties most relevant for PCM research and development in a simple and economic way. Conventional calorimetric methods such as differential scanning calorimetry (DSC), differential thermal analyses (DTA) and adiabatic calorimetry are by comparison

complex and expensive. Although DTA and DSC methods are well developed, their shortcomings are obvious: the samples thus tested are very small (1 – 10 mg) so that the thermophysical properties of samples are usually different from those of bulk materials. DTA and DSC measurement rigs are complicated and expensive and they cannot measure heat of fusion, specific heats and thermal conductivities of several samples simultaneously. In addition, the phase change process of a PCM sample during measurement is hard to observe clearly when using conventional methods. The conventional methods are however superior in accuracy, but accuracy at this level may not be an absolute requirement.

Because the Yingping (1999) method had some incorrect assumptions, such as using a degree of supercooling as the end of latent heat period and neglecting sensible heat during phase change, which caused errors in determining the heat of fusion forced a modified method suggested by Hong (2004) was used. The modified method can be applied to several PCMs having different freezing patterns. In view of these facts, the present study used the improved T-history method of determining the melting point, degree of supercooling, heat of fusion, specific heat and thermal conductivity of several PCM samples. Using the method the thermophysical properties of A28 (alkane/aliphatie) and E44 (salt hydrate) both manufactured by EPS Ltd were measured. *Figure 7.2* and *7.3* give the T-history diagrams of A28 and E44 with water as the sample reference. It may be seen that the A28 is a PCM with no supercooling and melting point near 28 ^{o}C. This matches the data provided by same as EPS (Environmental Process Systems Ltd).

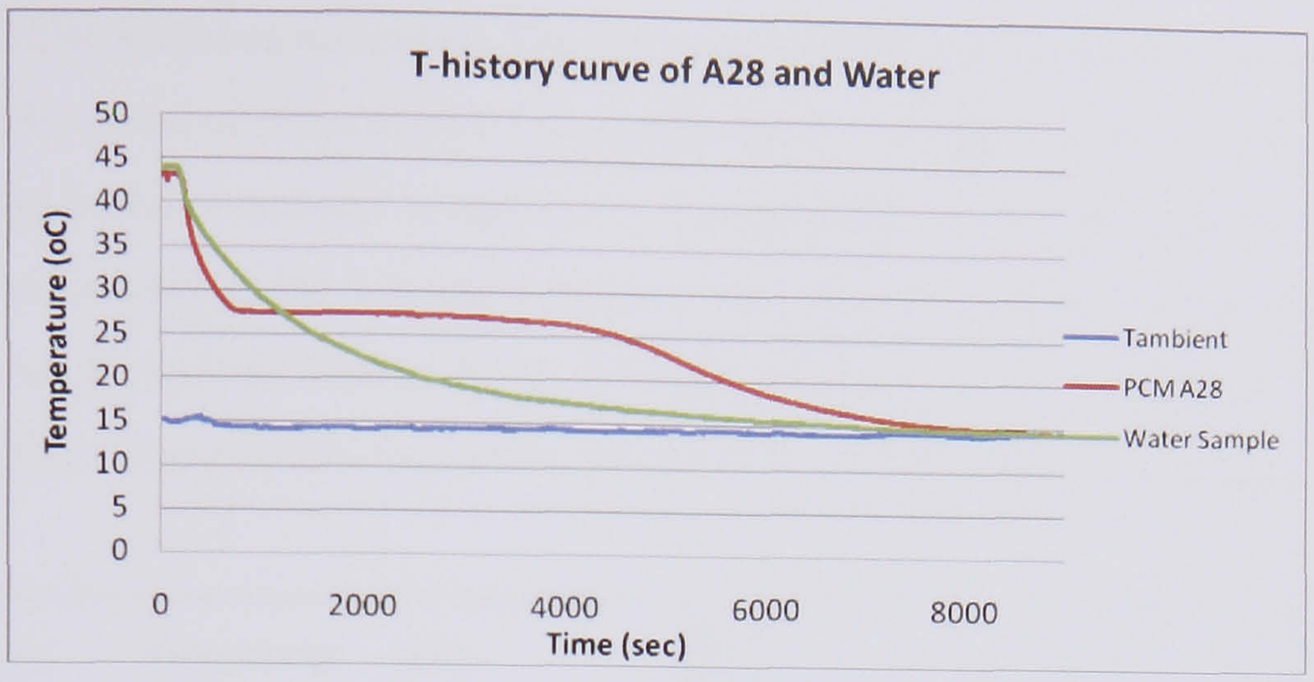

Figure 7.2 experimental results for A28 and Water Sample during cooling

Figure 7.3 the test data for E44 indicate the material has a supercooling characteristic. The supercooling temperature is around 40 °C and the phase change starts at 44 °C, a 4 °C range.

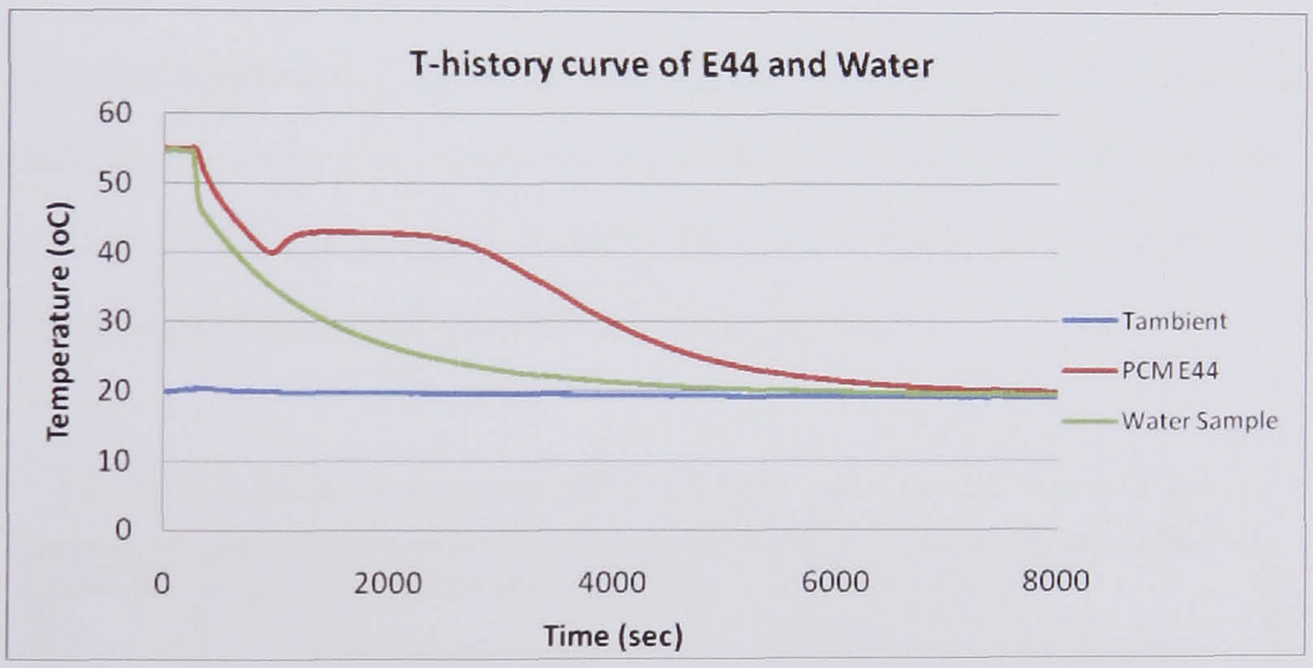

Figure 7.3 Experimental results for E44 and Water Sample during cooling

The procedure to calculate the data from the T – history curves involves the separation of the PCM curve in three areas as seen in *Figure 7.4*. The first area involves the liquid phase and starts from the initial temperature (T_o) of the PCM until the supercooling point (T_s). This area calculates the sensible heat during the liquid phase. The second area is the phase change area were the latent heat is being calculated from where the material starts to release its heat (T_m) until the point of inflection (b) that separates the boundary of phase change and solid state period, where the first derivative of T-history

curve for PCM becomes minimum. The last area calculates the sensible heat at the solid state from the point of inflection (T_i) to a point that can be taken as an arbitrary point (T_f) and that is above ambient temperature. The points of temperature that form the three areas are being used on the T-history curve of the reference material (water). Knowing the mass and the specific heat of PCM, tube and reference material and using the equations from Hong (2004) the values of specific heat and latent heat can be evaluated.

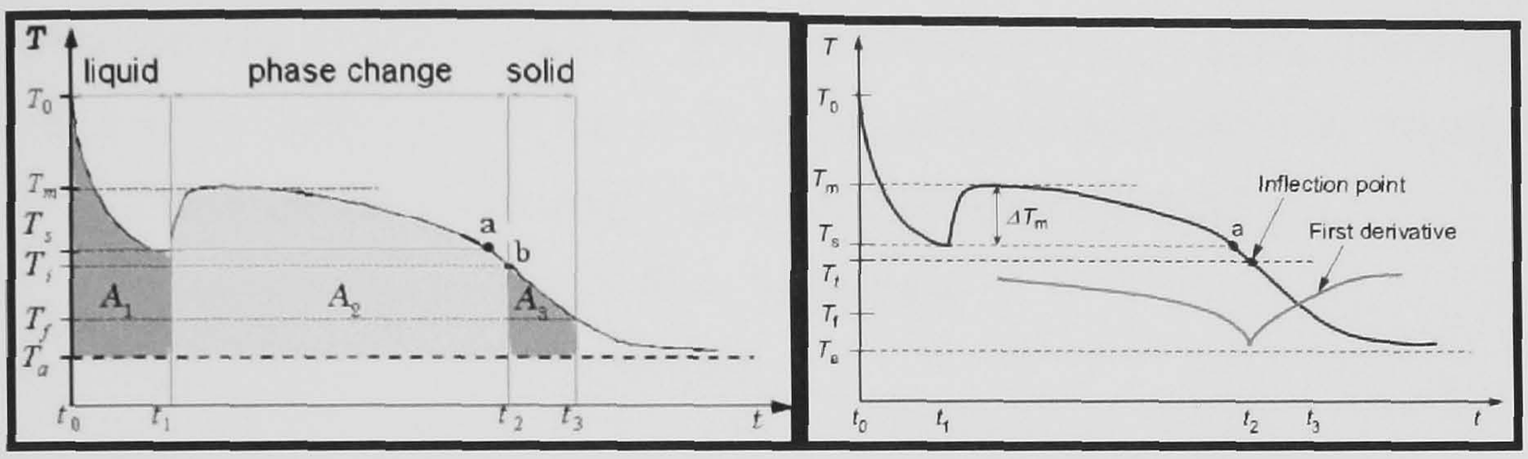

Figure 7.4 A typical T-history curve during cooling process with supercooling

The same is being applied for the PCM without the supercooling phenomenon with the difference that the boundary between the liquid and solid phase is the melting temperature (T_m). *Table 7.1* compares the values given from EPS Ltd and the values calculated use the mathematical formula of Hong (2004).

Table 7.1 PCM Properties of A28 and E44 given and calculated

PCM Type	Latent Heat from EPS (kJ/kg)	Latent Heat Calculated (kJ/kg)
A28	245	247.71
E44	105	112.93

The results agree well with those in the literature. This method is useful for rapid measurement of PCM candidates for use in engineering applications of latent thermal storage.

7.3 PV/PCM Thermal Model

A thorough understanding of the fundamental heat transfer processes involved is essential to predict accurately the thermal performance of combined PV/PCM systems and thus avoid costly system over-design.

In spite of the large number of research papers published on the applications of PCM over the last fifteen years, simulation of the behaviour of PCMs when used in real thermal applications with cyclic melting and solidification subject to realistic boundary conditions remains a challenging task. When modelling such a system the following can contribute to the complexity but haven't been taken under consideration for this model:

- nonlinear motion of the solid–liquid interface within the PCM,
- presence of buoyancy driven flows in the melt,
- volume expansion of the PCM, and
- density change in the PCM that ensues during melting/solidification.

7.3.1 Detailed Description of PV/PCM

A model was developed to evaluate the performance of a PV/PCM system. An energy flow analysis was developed based on *Figure 7.5*. The energy balance equations used to create a transient simulation program with the help of Thermal Energy Systems Specialists (TESS) owning the TRNSYS simulation software. The Type601 can be used to model both glazed and unglazed PV/PCMs. The unglazed PV/PCM does not include the transparent cover material shown in *Figure 7.5*.

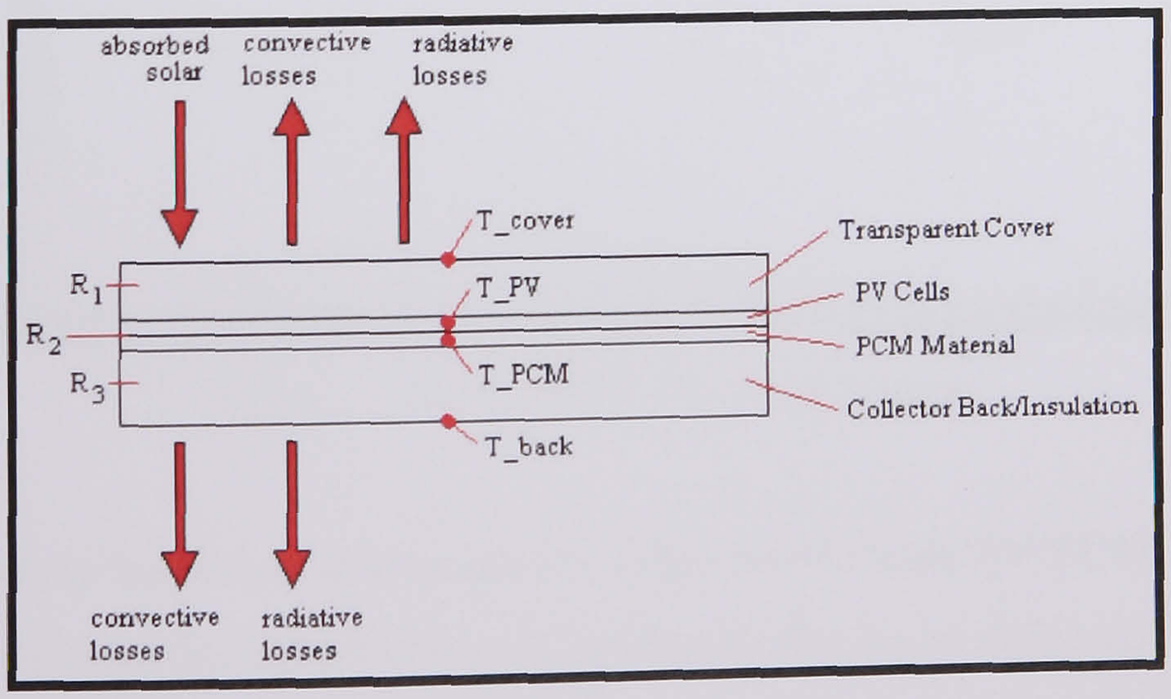

Figure 7.5 PV/PCM Array Configuration

Type 601 is designed to be able to model PV/PCM arrays that either have or do not have a transparent cover material protecting the PV material from ambient conditions. If a cover is specified, Type 601 requires that the user enter information about the cover material's refractive index, thickness and thermal conductivity. If a cover is included, Type 601 calculates incidence angle modifiers in order to determine the solar radiation absorbed by the PV cells themselves.

The individual IAM (incident angle modifier) values are provided to Type 601 by the standard TRNSYS "τα" routine (TRNSYS 16, Programmers Guide Manual section 8.4.4.18). This routine takes number of covers, radiation angle of incidence, and cover thickness –cover material index of refraction, absorber surface absorptance, and cover reflectance to diffuse radiation as arguments. It then returns an overall transmittance absorptance product for the cover system.

From the information indicated on *Figure 7.5* it is possible to evaluate the energy balance for every part of the glazed PV/PCM system.

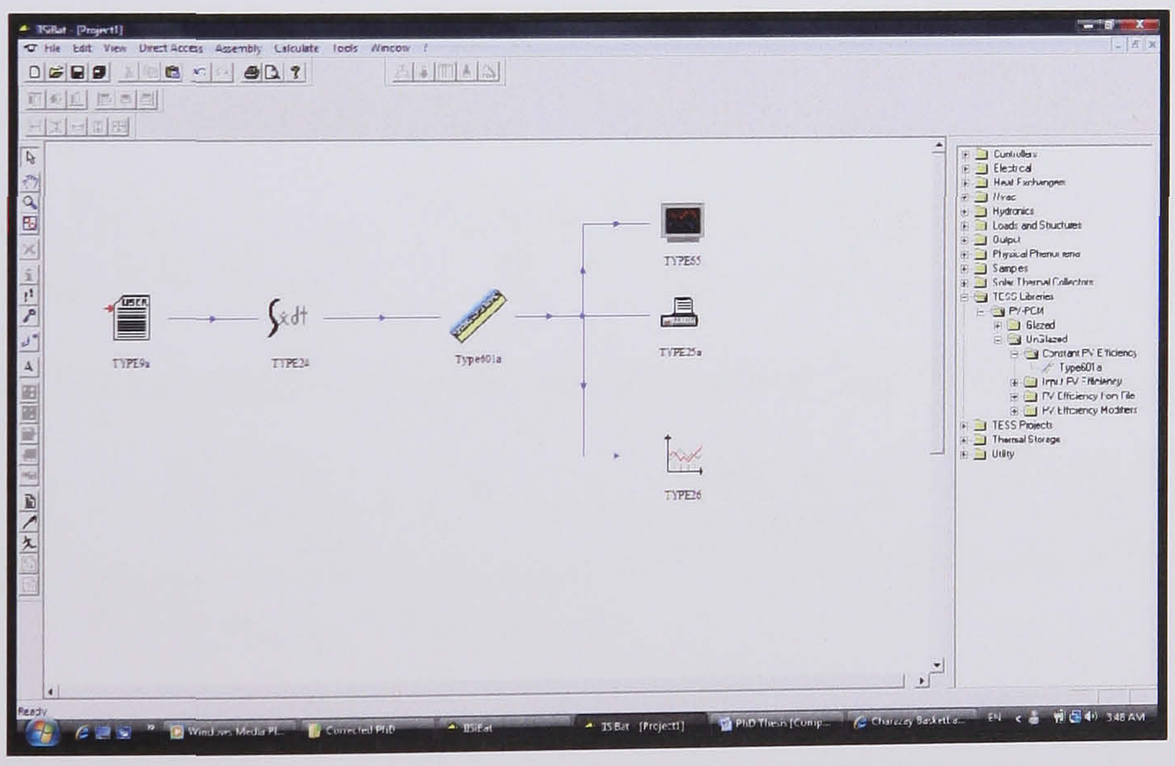

Figure 7.5a TRNSYS PV/PCM System

7.3.2 Completely Solidified or Completely Liquefied Glazed PV/PCM

This section includes the energy balance equations derived to evaluate the performance of the PV/PCM (the meaning of each indicator can be found in Appendix 1). The

PV/PCM system is being separated by four sections, the top surface transparent glazing, the PV cell, the PCM layer and the back insulation surface.

The energy balance on the top surface is given by (Eq. 7.1) for a PV/PCM array that includes a transparent glazing that protects the PV cells from ambient conditions.

$$\frac{T_{PV} - T_C}{R_1} = h_{conv,top}\left(T_C - T_{amb,top}\right) + h_{rad,top}\left(T_C - T_{rad,top}\right) \quad \text{(Eq. 7.1)}$$

The energy balance on the PV cells (the absorbing plate) is

$$S = \frac{\left(T_{PV} - T_C\right)}{R_1} + \frac{\left(T_{PV} - T_{PCM}\right)}{R_2} \quad \text{(Eq. 7.2)}$$

The energy balance on the PCM layer is

$$m\,C_p\,\frac{dT_{PCM}}{dt} = \frac{\left(T_{PV} - T_{PCM}\right)}{R_2} - \frac{\left(T_{PCM} - T_B\right)}{R_3} \quad \text{(Eq. 7.3)}$$

The energy balance on the back surface is

$$\frac{T_{PCM} - T_B}{R_3} = h_{conv,back}\left(T_B - T_{amb,back}\right) + h_{rad,back}\left(T_B - T_{rad,back}\right) \quad \text{(Eq. 7.4)}$$

In order to solve the system of equations, some simplification is necessary. (Eq. 7.1) can be solved for the cover temperature, T_C:

$$T_C = \frac{T_{PV}}{\left(1 + R_1\,h_{rad,top} + R_1\,h_{conv,top}\right)} + \frac{\left(R_1\,h_{rad,top}\,T_{rad,top} + R_1\,h_{conv,top}\,T_{amb,top}\right)}{\left(1 + R_1\,h_{rad,top} + R_1\,h_{conv,top}\right)} \quad \text{(Eq. 7.5)}$$

Similarly, (Eq. 7.2) can be solved for the temperature of the PV layer (T_{PV}) yielding

$$T_{PV} = \frac{R_1\,R_2\,S}{R_1 + R_2 - \dfrac{R_2}{\left(1 + R_1\,h_{rad,top} + R_1\,h_{conv,top}\right)}} + \frac{R_2\left(R_1\,h_{rad,top}\,T_{rad,top} + R_1\,h_{conv,top}\,T_{amb,top}\right)}{\left(R_1 + R_2\right)\left(1 + R_1\,h_{rad,top} + R_1\,h_{conv,top}\right) - R_2}$$

$$+ \left[\frac{R_1}{R_1 + R_2 - \dfrac{R_2}{\left(1 + R_1\,h_{rad,top} - R_1\,h_{conv,top}\right)}}\right] T_{PCM}$$

(Eq. 7.6)

Lastly, (Eq. 7.4) is solved for the insulation temperature, T_B

$$T_B = \frac{T_{PCM}}{R_3\left(h_{conv,back} + h_{rad,back}\right)+1} + \frac{h_{conv,back}\,T_B}{\left(h_{conv,back} + h_{rad,back} + \frac{1}{R_3}\right)} + \frac{h_{rad,back}\,T_{rad,back}}{\left(h_{conv,back} + h_{rad,back} + \frac{1}{R_3}\right)}$$

(Eq. 7.7)

Equations (Eq. 7.5) through (Eq. 7.7) are substituted into equation (Eq. 7.3) to generate a single differential equation that represents the energy balance on the entire PV/PCM system.

TRNSYS is equipped with a built-in utility subroutine that will analytically solve differential equations of the form

$$\frac{dT}{dt} = a\,T + b$$

(Eq. 7.8)

In which "a" and "b" can be assumed to be constant over a time step. The differential equation in this case will be written slightly differently as

$$m\,C_p\,\frac{dT_{PCM}}{dt} = a\,T_{PCM} + b$$

(Eq. 7.9)

Written in this form, the overall differential equation for the PV/PCM array is

$$a = \left(\frac{R_1}{R_2\left(R_1 + R_2 - \frac{R_2}{\left(1 + R_1\,h_{rad,top} + R_1\,h_{conv,top}\right)}\right)} - \frac{1}{R_2} - \frac{1}{R_3} + \frac{1}{R_3^2} \right)$$

$$b = \frac{R_1\,S}{R_1 + R_2 - \frac{R_2}{\left(1 + R_1\,h_{rad,top} + R_1\,h_{conv,top}\right)}} - \frac{\left(R_1\,h_{rad,top}\,T_{rad,top} + R_1\,h_{conv,top}\,T_{amb,top}\right)}{\left(R_1 + R_2\right)\left(1 - R_1\,h_{rad,top} + R_1\,h_{conv,top}\right) - R_2}$$

$$+ \frac{h_{conv,back}\,T_B}{R_3\left(h_{conv,back} + h_{rad,back}\right)+1} + \frac{h_{rad,back}\,T_{rad,back}}{R_3\left(h_{conv,back} + h_{rad,back}\right)+1}$$

a for (Eq. 7.10) and b for (Eq. 7.11)

It should be noted that the right hand side of equations (Eq. 7.10) and (Eq. 7.11) are divided by the (m C_p) product to obtain the pure "a" and "b" terms in (Eq. 7.8).

7.3.3 Two Phase Region between the Liquefaction and Solidification Temperatures

This section introduces the concept of energy required for a PCM material to melt or solidify. The equations were derived with the help of TESS that owns TRNSYS and connect the energy balance equation of (7.9) with the temperature of PCM needed to start liquefy or solidify.

The total energy required to fully melt or fully solidify the PCM material is

$$\dot{Q}_{solidification} = \dot{Q}_{liquefaction} = m\, h_{fg} \qquad \text{(Eq. 7.12)}$$

Adding this much energy to the fully solidified PCM material moves it from a quality of 0 (completely solid) to a quality of 1 (completely liquid). One can therefore write an expression for the change in PCM quality (X) associated with the addition or removal of a known quantity of energy.

$$X_{new} = X_{old} - \frac{\dot{Q}_{added}}{m\, h_{fg}} \qquad \text{(Eq. 7.13)}$$

Or, rearranging

$$(X_{old} - X_{new})\, m\, h_{fg} = \dot{Q}_{added} \qquad \text{(Eq. 7.14)}$$

The differential equation (Eq. 7.9) can also be rewritten as

$$m\, C_p \frac{dT_{PCM}}{dt} = \dot{Q}_{in} - \dot{Q}_{out} = a\, T_{PCM} - b \qquad \text{(Eq. 7.15)}$$

The energy added to the PCM layer in equation (Eq. 7.14) is the same as the net energy transfer (Q_{in} - Q_{out}) in equation (Eq. 7.15). One can therefore equate the two equations and solve for the change in PCM quality between the solidification and liquefaction temperatures. Based on the quality, the temperature of the two-phase PCM can be calculated as

$$T_{PCM} = (T_{liquefaction} - T_{solidification})\, X + T_{solidification} \qquad \text{(Eq. 7.16)}$$

Type 601 models a PCM material that has a constant specific heat below the complete solidification point and a constant specific heat (albeit perhaps a different specific heat) above the complete liquefaction point. Between the complete solidification and

liquefaction points, the temperature of the PCM material is allowed to vary linearly between the solidification and liquefaction temperatures. For many PCM materials, particularly pure PCM materials, the liquefaction and solidification temperatures are equal and the temperature of the material remains constant in the two phase region. The cooling curves for the solidification of two PCM materials (one with and one without equal solidification and liquefaction temperatures) are shown in *Figure 7.6*.

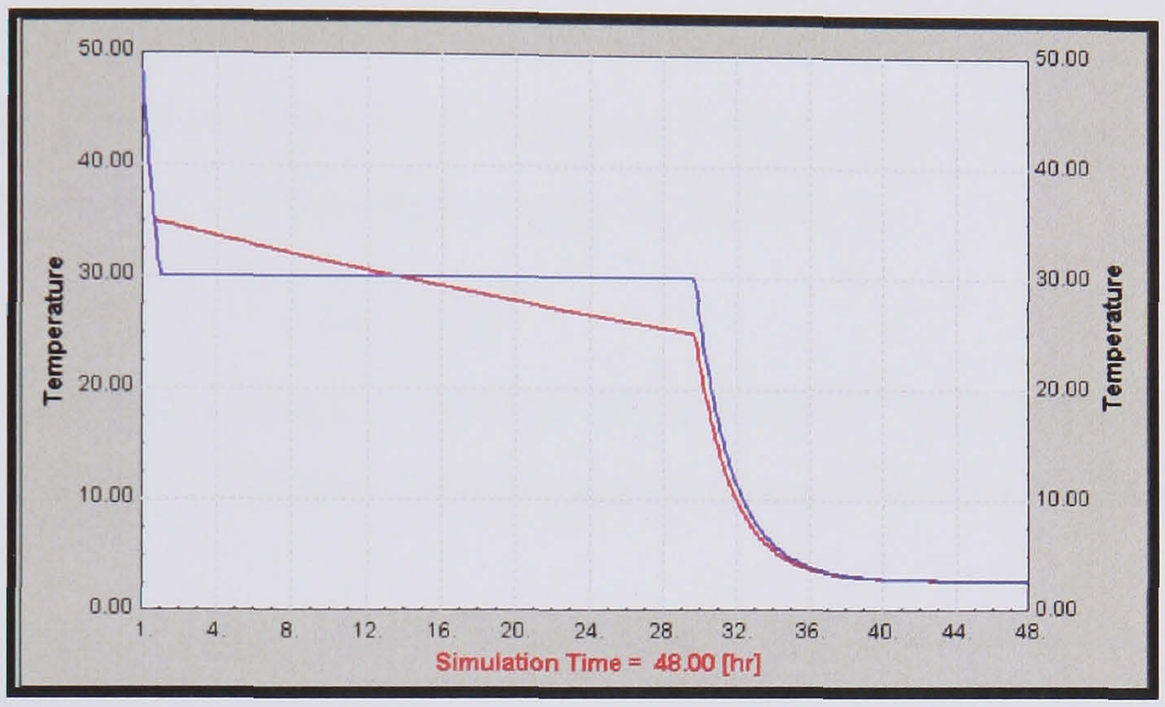

Figure 7.6 Cooling Curves for the Solidification of a Pure Material

The rationale behind including a PCM layer in a PV array is that PVs are more efficient at lower cell temperatures. For the cells in a standard PV array that heat up, the PCM layer in a PV/PCM array absorb the incident solar energy that is not being converted to electrical energy by the PV cells and melts thus keeping the PV cells cooler and more efficient. The drawback is that when the PCM has completely melted the PV temperature starts again to increase and the benefit from the PCM stops.

The PCM layer in Type 601 takes, as parameters, the PCM liquefaction and solidification temperatures, the latent heat of fusion for the material, its density and the thickness of the layer. The user also provides efficiency information for reference conditions as well as coefficients that describe how the overall efficiency changes with cell temperature and incident solar radiation.

The overall efficiency of the PV is calculated based on equation (Eq. 7.17).

$$\eta = \left(1 + \eta_{T,coef}\left(T_{PV} - T_{ref}\right)\right)\left(1 + \eta_{I,coef}\left(I_T - I_{T,ref}\right)\right)\eta_{ref} \qquad \text{(Eq. 7.17)}$$

7.4 TRNSYS 601 Model Simulation Results

The first simulation sought to explore various PCMs in order to see how long they will remain at a constant temperature during phase change. This first study used the duration index that measures which of the PCMs offers the longest of constant temperature at phase change. 4 PCM materials were studied E21, A28, E30 and E32 using the properties given by their manufacturer EPS Ltd. The results showed that E32 remains at the constant melting temperature longer than the other materials as can be seen from *Figure 7.7*.

•Duration Index [MJ/ (m^3°C)]: Comparison of how long a PCM will remain at a constant temperature during the phase change. Calculated as:

$$D.I. = h_f \rho / \Delta T \qquad \text{Eq. (7.18)}$$

Where h_f is Latent Heat (kJ/kg), ρ is density (kg/m^3) and ΔT is the temperature difference of Melting Temperature of the material and ambient temperature (°C).

To check the validity of the equation (7.18) with the new TRNSYS 601 model the same materials were used in the simulation, with the same ambient temperatures the same irradiance and convective losses as working conditions (Appendix 2 includes all the parameters needed in order to simulated a PV/PCM model). From *Figure 7.8* it may be observed that the same pattern of behaviour as that predicted by the duration index occurs. It may be seen that E32 takes longer to undergo complete melting in comparison with the other 3 materials. The duration that it takes for the materials to melt is 188 min for E32, 158 min for E30, 111 min for A28 and 88 min for A21.

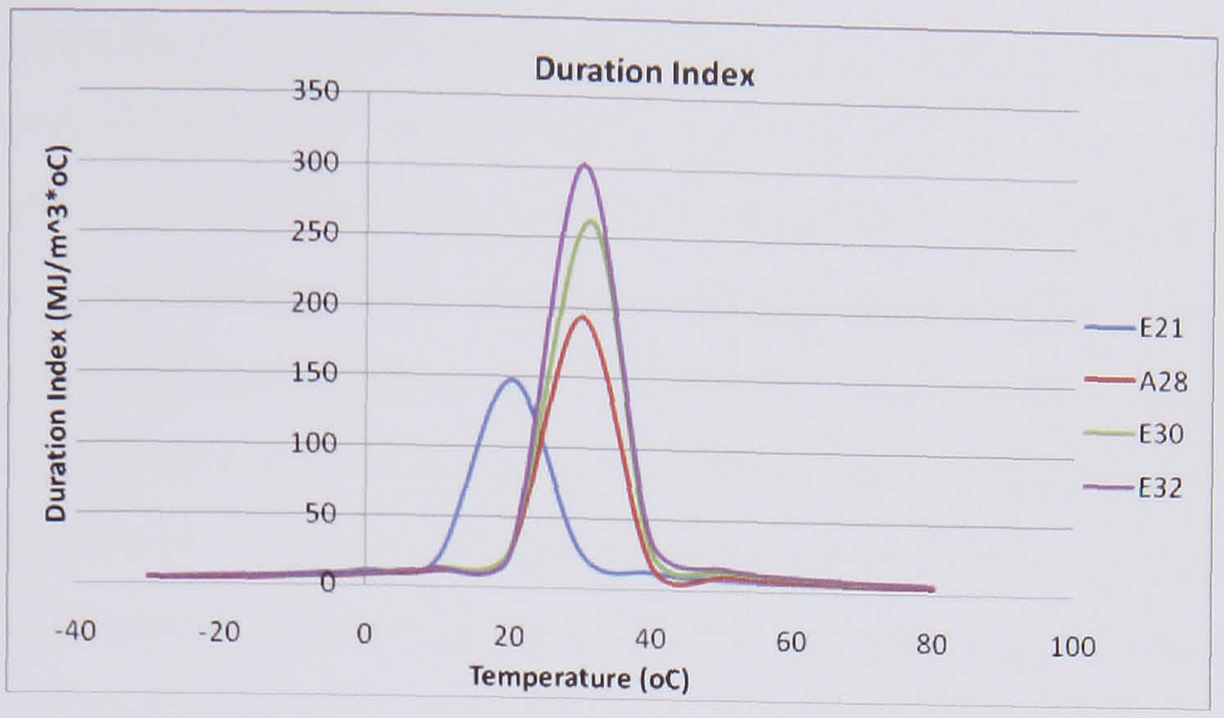

Figure 7.7 Duration Index for Phase Change Materials

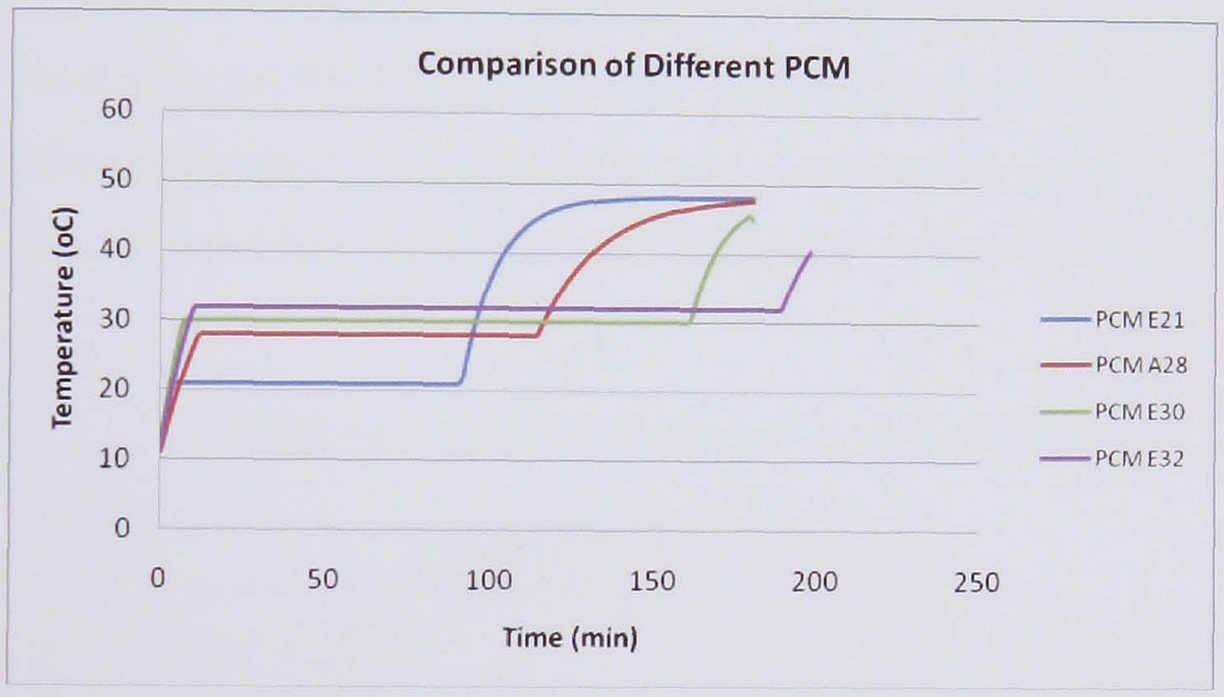

Figure 7.8 Comparisons of 4 Phase Change Materials

Because EPS Ltd were only able to supply A28 in order to do experiments only this material was simulated in the TRNSYS model. For that reason all the graphs below relate to A28 as a PCM.

7.4.1 Thermal conductivity influence on PV/PCM performance

An important factor that may affect the performance of the PV/PCM system is the conductivity between the PV frame with the PCM container and the PCM material. To determine if the thermal conductivity is a major design consideration before building this system a set of simulations was performed using the same working conditions and changing the conductivity betwen the PV and the PCM . *Figure 7.9* provides an

indication of how the PV and PCM respond to the changes in thermal conductivity at irradiation level of 1000 W/m^2 and ambient temperature at 20 °C. As may be observed when the thermal conductivity between the PV and the PCM is low (42.68 W/mK) then the PV temperature stabilizes at 60 °C quickly and after 64 min when the PCM has melted increases until again stabilizes at 72 °C. The PCM takes a long time to completely melt. With a high conductivity (500 W/mK) the PV temperature is held at a lower temperauture of 32 °C but maintains this temperature for only 36 min. These variations can be seen in the performance of the PV in *Figure 7.10* were the electrical efficiency is being directly affected by the thermal performance of the PCM. The higher conductivity provides higher electrical efficiency for a longer time than the simulation with low conductivity. It is therefore important to consider this aspect of the collector's design when designing the PV/PCM system. In *Figure 7.10* the electrical efficiency of the system having the highest conductivity seems to increase for a short period (inside the circle). This is caused by a mulfunction of the first time steps during the simulation.

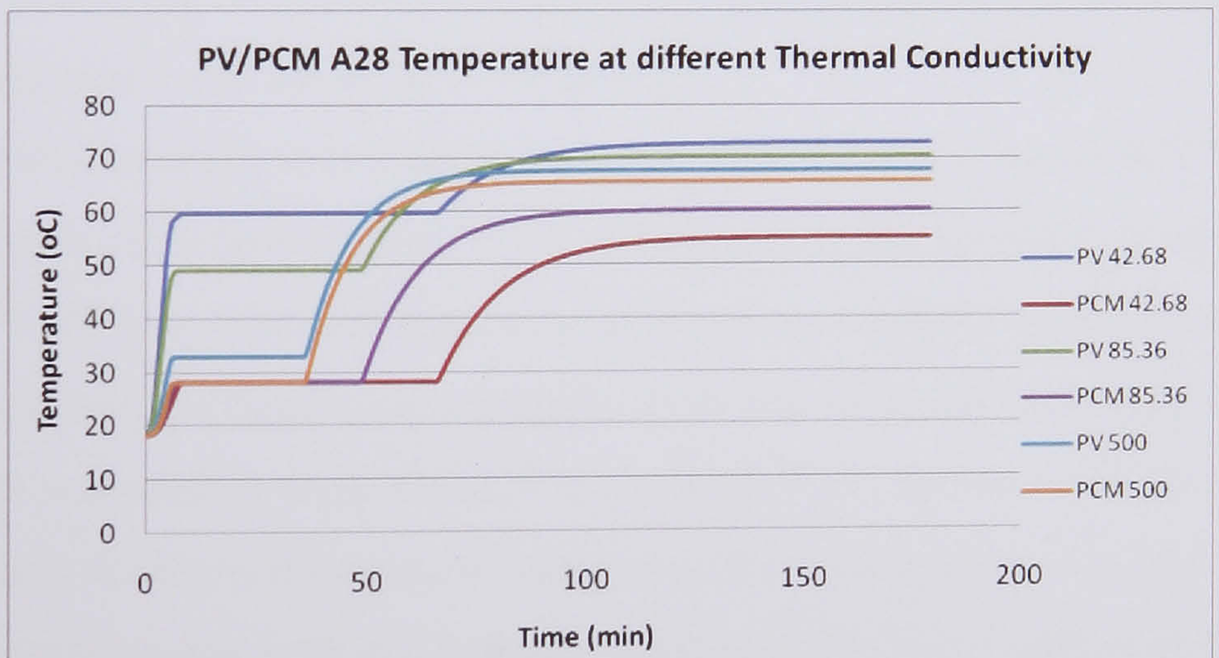

Figure 7.9 PV/PCM A28 Temperature performance at different thermal conductivities

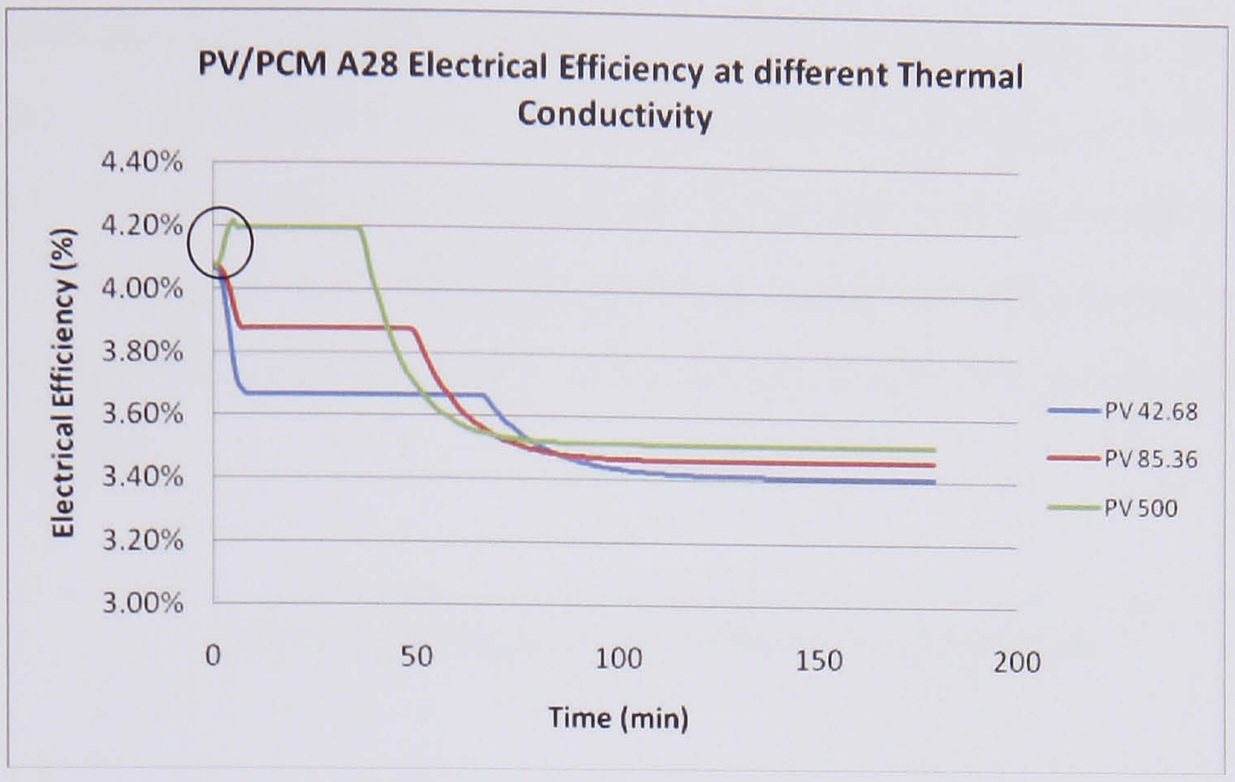

Figure 7.10 PV/PCM A28 Electrical Efficiency at different thermal conductivities

7.4.2 Parametric analysis

Purpose of the parametric study was to evaluate how the PV/PCM system responds in different working conditions. The parameters that were changed to assess the effect that have in the system are the material thickness (PCM quantity used in the back), the ambient temperature and the level of irradiation.

In the parametric analysis was assumed that the contact layer between the PV and the PCM is a copper plate (see *Figure 7.5*, R_2 resistance). In the simulations temperatures within the PV/PCM system and that of the ambient environment were all initially set to 20 ^{o}C, the heat transfer coefficients from the front and back surfaces of the PV/PCM system to the surrounding were set at 10 and 5 W/m^{2}K (to simulate natural ventilation conditions) and the top and bottom boundaries of the system were assumed to be adiabatic. Insolation was kept at a constant value of 1000 W/m/^{2} and a variable time step with a minimum value of 1 min was used for all simulations.

7.4.2.1 The performance PV/ PCM system with different PCM material thickness

First set of experiments tested the performance of the PV/PCM system incorporating different PCM depth (represented by varying the PCM depth). *Figure 7.11* presents predicted temperatures for PV/PCM with a PCM at depth of 30, 60 and 90 mm respectively. It can be seen that for the 30 mm thick PCM layer after 111 min the phase change is complete and the temperature of the PV starts increase significantly above the

35 °C. With a 60 mm layer the PV was kept at 35 °C for 224 min and for 90 mm for 338 min. This indicates that by increasing the material thickness we gain more time with the PV temperature near the reference temperature (25 °C) and thus have better electrical efficiency for longer time. A drawback is a heavier system and more expense. The same times are also observed when the system is discharging under cooling the process as seen in *Figure 7.12*.

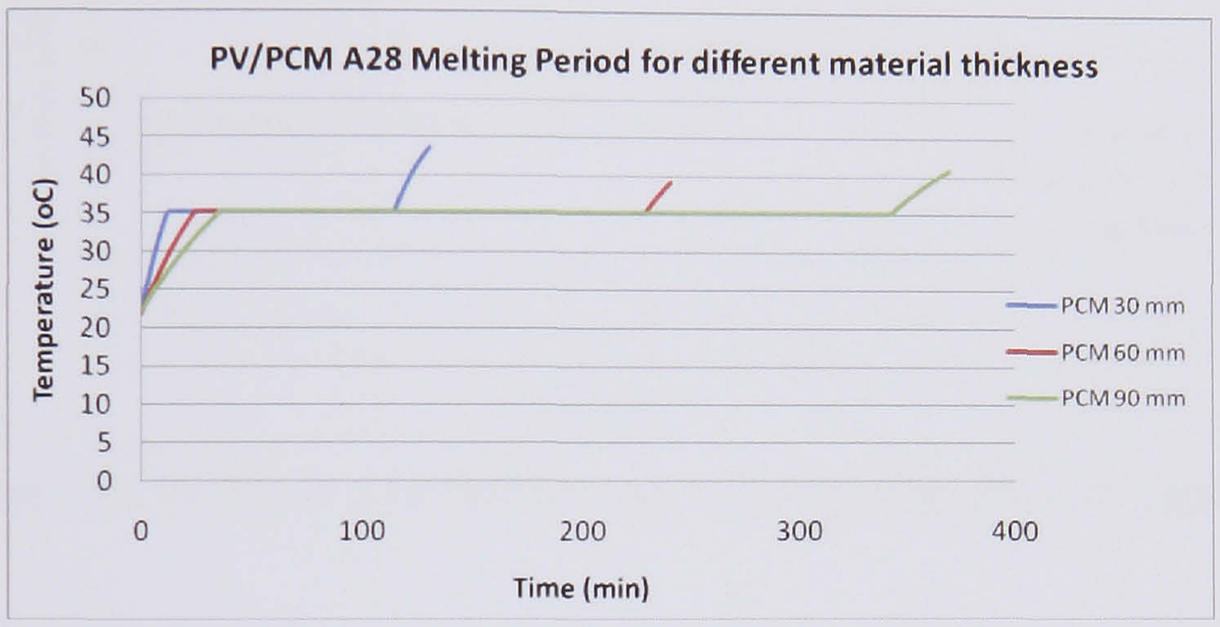

Figure 7.11 PV/PCM A28 Melting Period for different material thickness

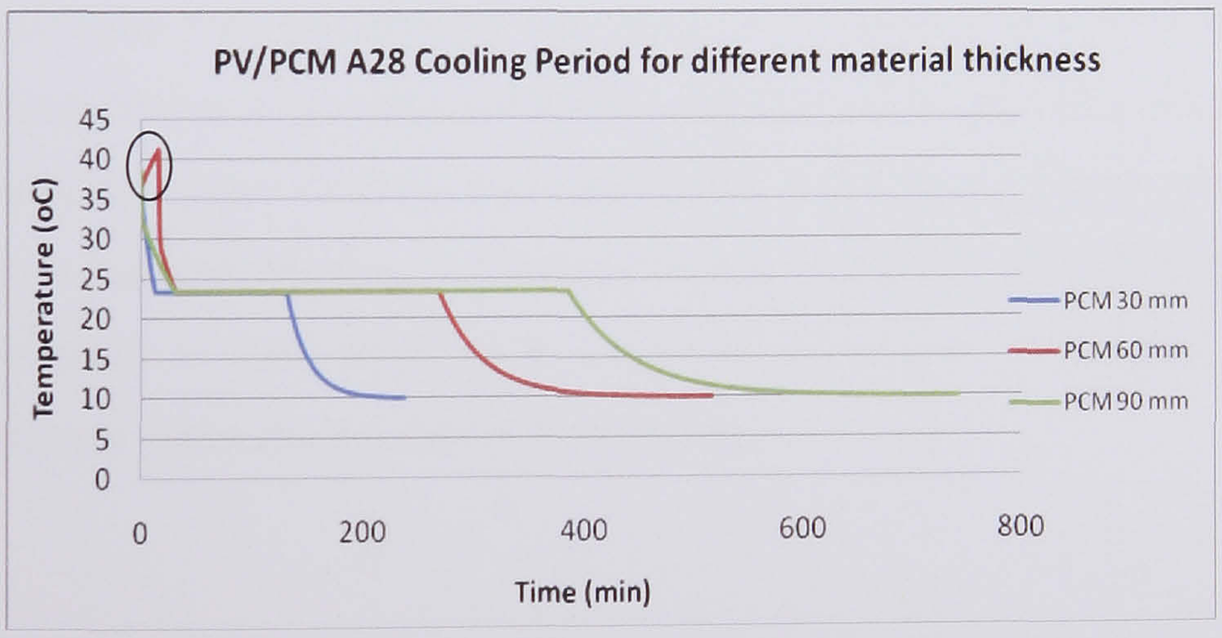

Figure 7.12 PV/PCM A28 Cooling Period for different material thickness

7.4.2.2 Thermal control achieved for different ambient temperatures and insolations

The effect of ambient temperature on the temperature of the front surface of PV/PCM system is shown in *Figure 7.13*. The ambient temperature was set to 10, 15 and 20 °C respectively. The PCM layer was at 30 mm. By increasing the ambient temperature the

temperature of the PV does not change significantly, however, as less heat is lost from the system because of the lower temperature difference between the system and ambient, the time required for the PCM melting is reduced. It takes 112 min when the ambient temperature is 10 °C, 90 min for 15 °C and 73 min for 20 °C.

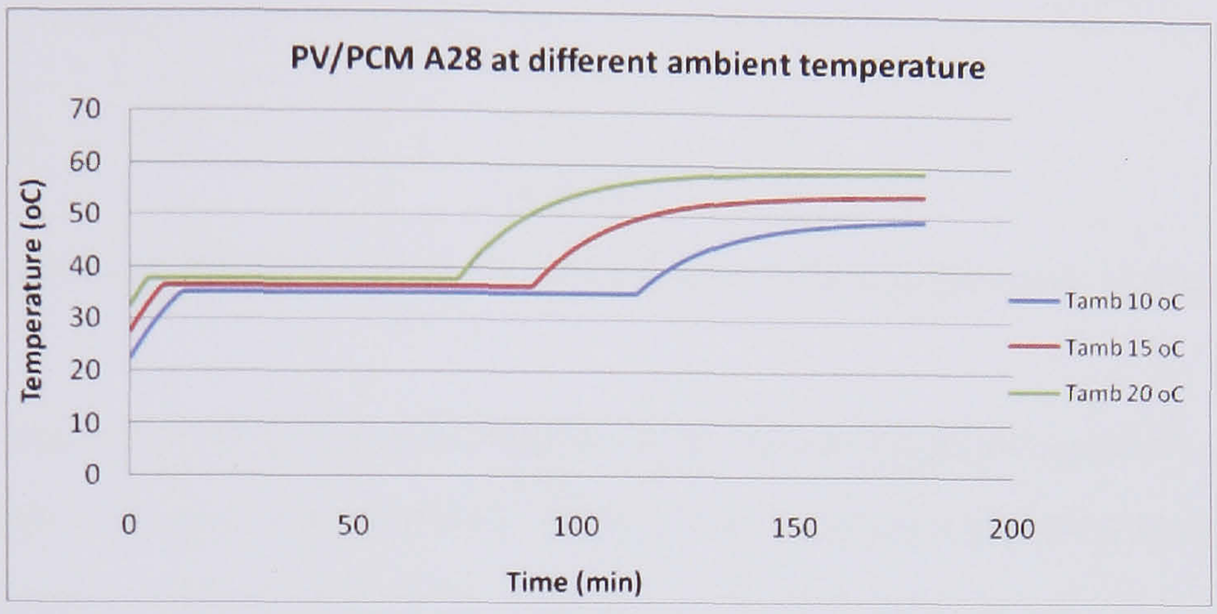

Figure 7.13 PV/PCM A28 Performance at different Ambient Temperature

In order to evaluate the effect of insolation on the thermal behaviour of the system, simulations with incident insolation intensities of 600, 800 and 1000 W/m^2 at 20 °C ambient temperature were undertaken. The predicted temperatures at the front surface of PV/PCM system for the three different levels of insolation are presented in *Figure 7.14*. With increasing insolation intensity the temperature at the front surface increases and the melt time is reduced. Melting is complete 48 min sooner for a PV/PCM system exposed continually to 1000 W/m^2 when compared to continual exposure to 800 W/m^2 and 72 min sooner when the insolation is 600 W/m^2.

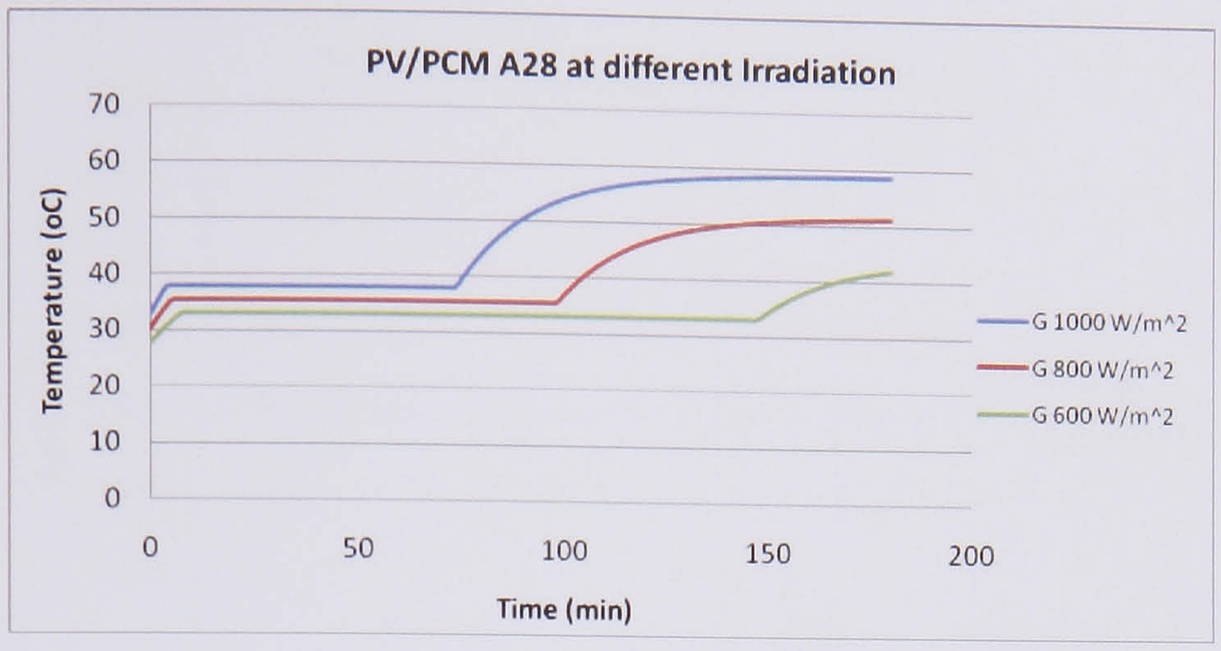

Figure 7.14 PV/PCM A28 Performance at different Incident Irradiation

To see how much a PV/PCM system improves the electrical performance a comparison was made with a system without PCM. *Figure 7.15* compares the temperature air cooled of PV temperature with the PV/PCM A28 at 30 mm thickness. It may be observed that the PV temperature without PCM reaches 62 ^{o}C and with PCM it is kept at 35 ^{o}C for 111 min. It is obvious that this big temperature difference will have an effect on the PV electrical efficiency as seen in *Figure 7.16*. For 111 min the electrical efficiency of the PV/PCM system is at 3.9% in comparison without PCM that is at 3.4% an improvement of 15%. The temperature of PV with the PCM does not converge with the system without PCM and reaches an equilibrium state at 50 ^{o}C.

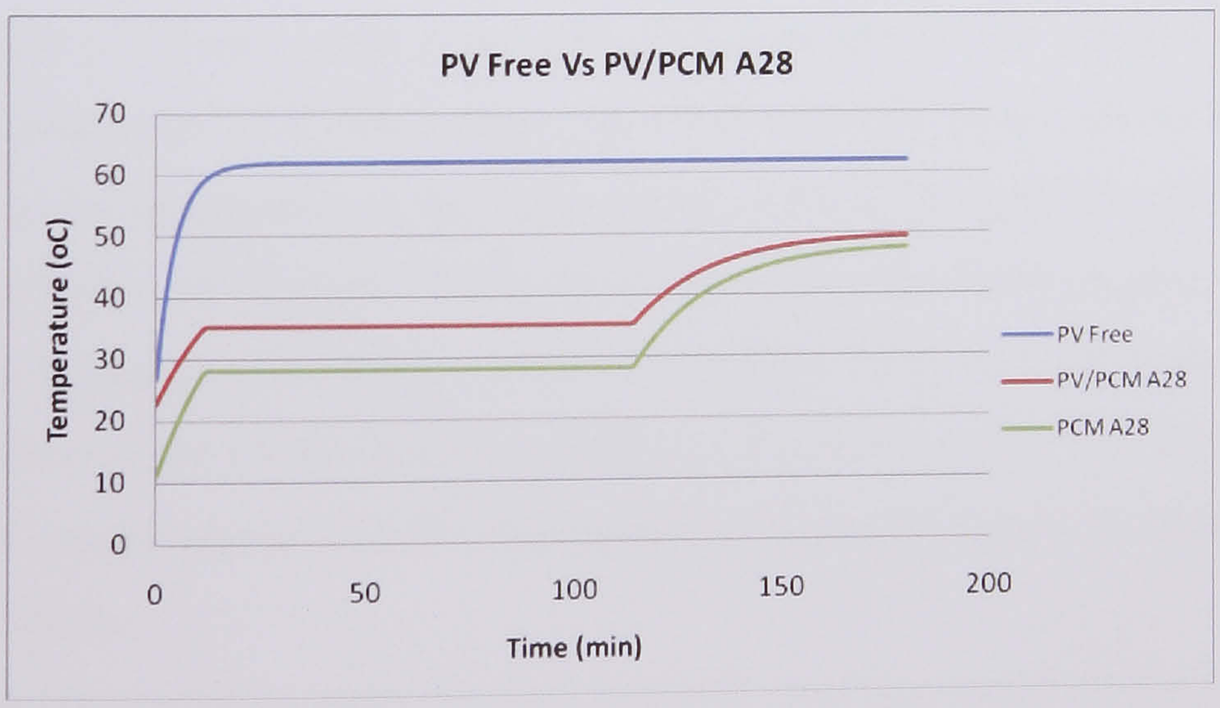

Figure 7.15 Comparing a PV free system with a PV/PCM A28 temperature

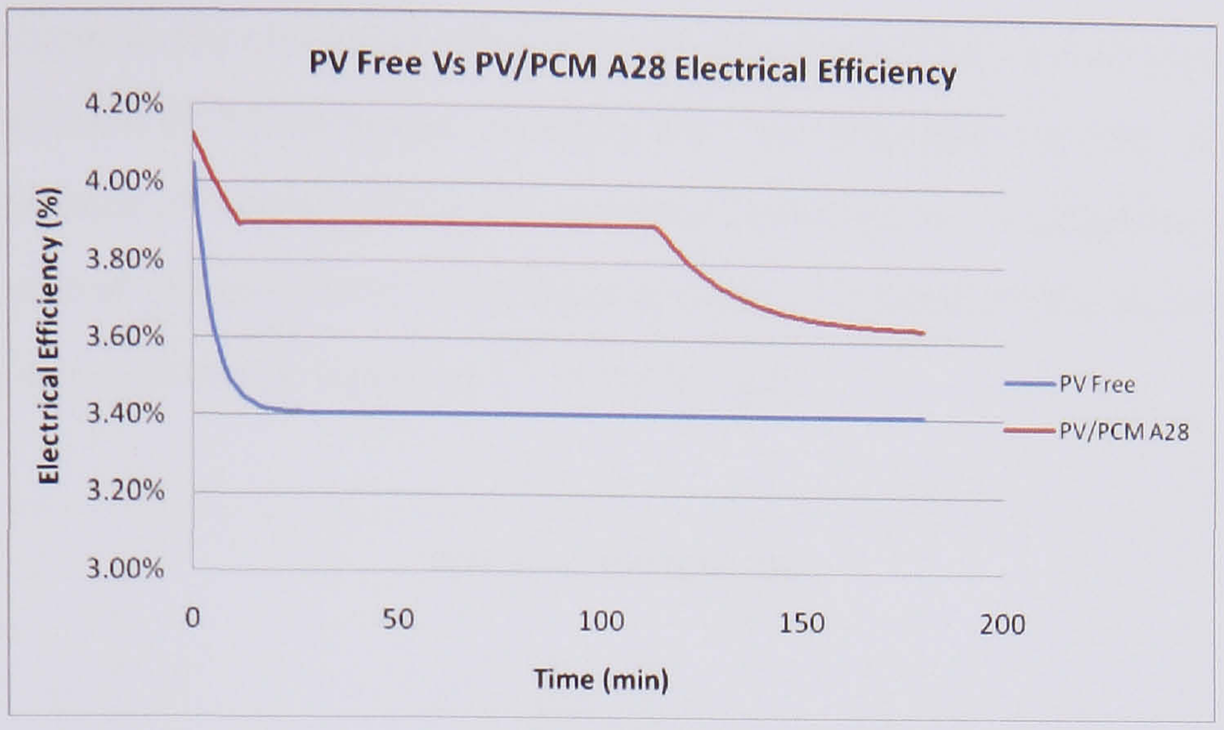

Figure 7.16 Comparing a PV free system with a PV/PCM A28 Electrical Efficiency

7.4.3 PV/PCM A28 system simulation for one day, under realistic ambient temperatures and insolation and 3 different PCM thicknesses

The thermal control performance of a PV/PCM system was predicted using realistic ambient temperature and insolation conditions for SE England for 3rd June. The initial system temperature was set to 14 ^{o}C at 00:00 h, the same as the ambient temperature. 3 different systems were simulated each with different PCM thickness in order to see how the whole system performs.

The predicted temperature of a PV is shown in *Figure 7.17* together with a system without PCM. It can be seen that the system with the PCM keeps the PV temperature well below that of the air cooled. Also as the PCM gets thicker the temperature of the PV remains near to the 25 ^{o}C for a longer period of time (see inside circle). During phase change, the temperature at the front surface of PV/PCM system with 30 mm PCM is maintained below 35 ^{o}C from 7:00 to 9:00 hr, and once the PCM became wholly liquid, the temperature of the PCM system rose rapidly. At 11:45 h the temperature at the front surface of the PV/PCM system reached a maximum of 54 ^{o}C. The system with 60 mm PCM depth can maintain PV temperatures below 35 ^{o}C until 10:45 hr and for 90 mm until 12:00 hr.

When no insolation was incident (during night), the temperature of the PV returned rapidly to ambient for the system without the PCM but for the other systems it remained at the melting temperature of the PCM until fully solidified (see inside circle).

The improvement in the electrical efficiency can be seen in *Figure 7.18* were it may be observed that as the PCM thickness increases then the efficiency remains steady and near their reference efficiency of the PV at normal ambient and irradiations conditions for a longer period of time (outside the lines is night). To simulate the electrical efficiency of the system the equation (7.17) was used.

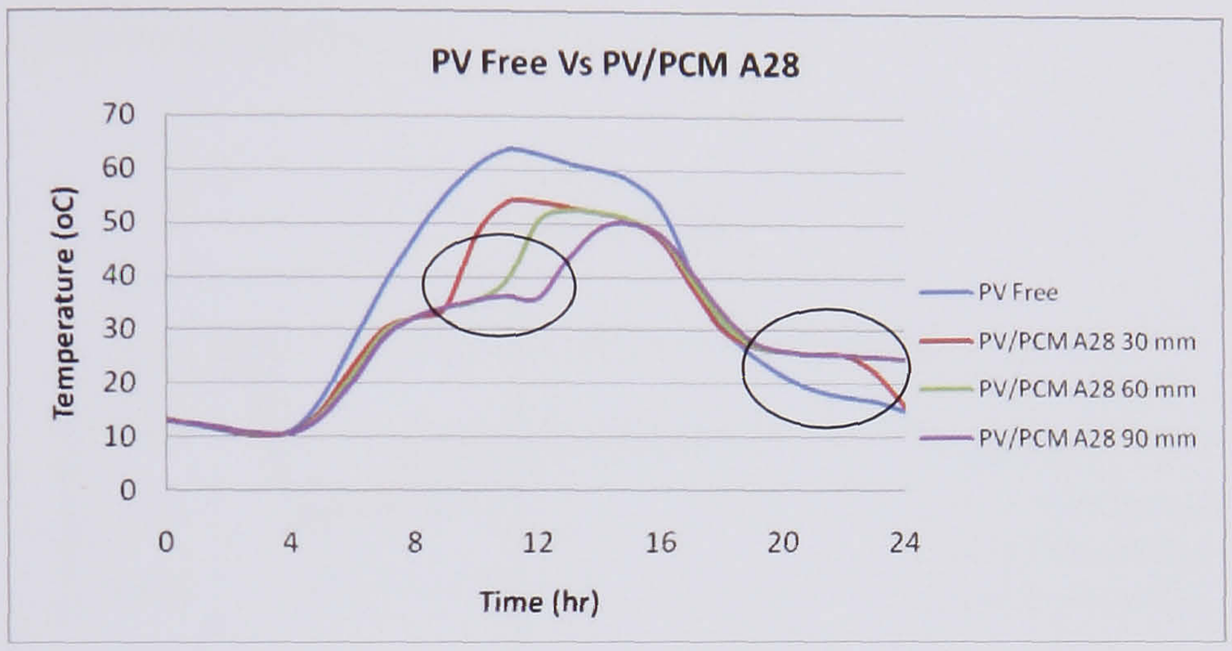

Figure 7.17 Comparison of a PV free system with a PV/PCM A28 Temperature for a typical summer day

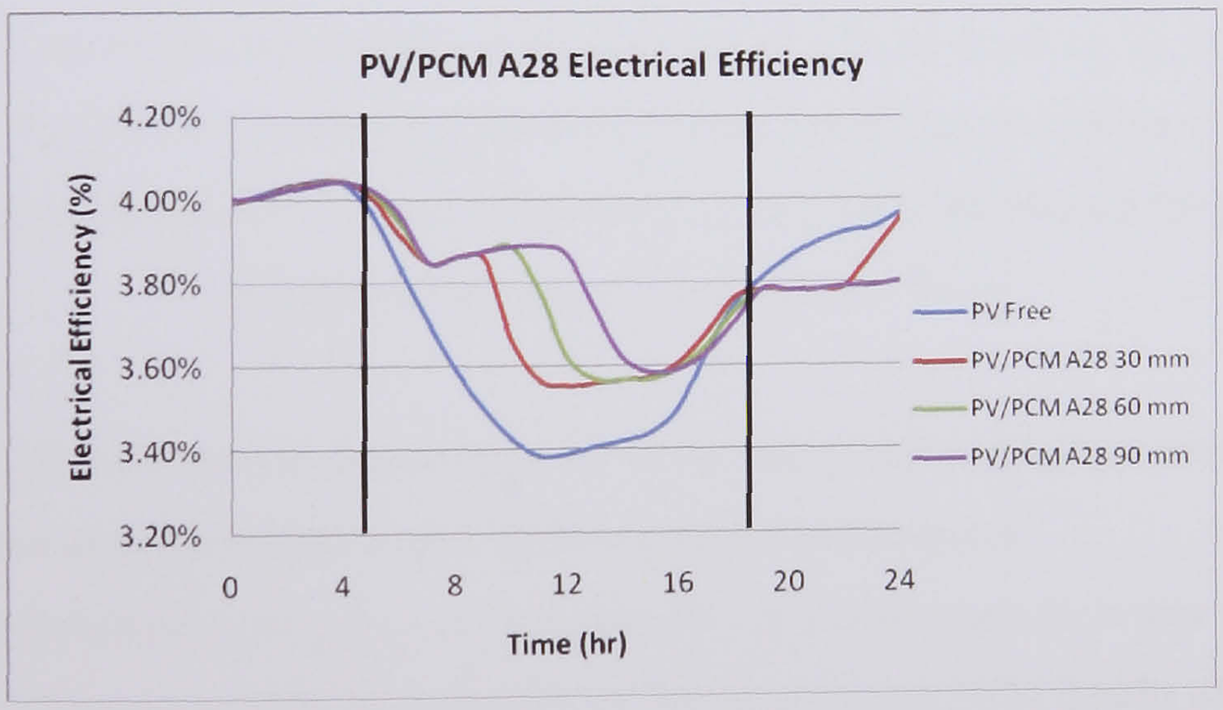

Figure 7.18 Comparison of a PV free system with a PV/PCM A28 Electrical Efficiency for a typical summer day

A plot of electrical efficiency against $(T_{pv} - T_{amb})/I$ enables a comparison of different PV/PCM systems to be made in terms of design conditions (i.e., insolation, ambient

temperature) rather than behaviour with time. The electrical conversion efficiency against $(T_{pv} - T_{amb})/I$ shown in *Figure 7.19* give a comparison for the systems with realistic test conditions (after the black line is consider night). The electrical conversion efficiency for the base case PV has the sharpest change in the narrowest range of $(T_{pv} - T_{amb})/I$ when compared with the system using PCM depths of 30, 60 and 90 mm. The electrical efficiency for the system with 30 mm PCM depth was above 3.6% even during the period of maximum insolation.

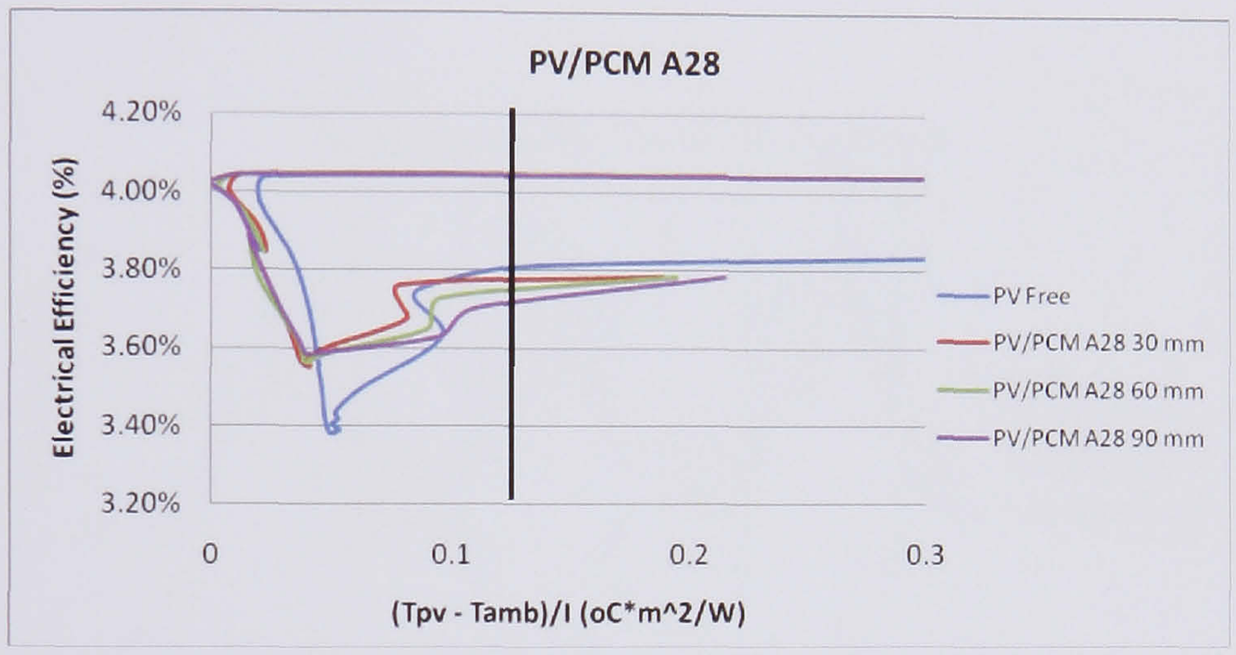

Figure 7.19 24 hr predicted electrical conversion efficiency on the front surface of the base case PV and at the front surfaces of system with a PCM depth of 30, 60 and 90 mm with $(T_{pv} - T_{amb})/I$ for a south–east orientation with insolation and ambient temperature for SE England on the 3rd of June. * T_{PV} and T_{amb} are the front surface temperature and ambient temperature, I is insolation W/m^2

7.4.4 PV/PCM A28 system simulation for three days, under realistic ambient temperatures and insolation and 3 different PCM thicknesses

A three day simulation using the weather data for typical summer days was undertaken to predict the heat accumulation in the PV/PCM system with PCM depths of 30, 60 and 90 mm and is presented in *Figure 7.20.* We first observe that as the PCM thickness gets larger, then the systems temperature remains lower than 40 ^{o}C for a longer time. The second is that for the 30, 60 mm and 90 mm depth of PCM a full transition to the molten state is achieved during night. This heat is being released during the night and depending from the application that the PV/PCM is needed this heat can be used for pre-

heating water, air or work as a building insulation. This will be discussed in section 7.5.2. If increase it further a problem will arise with absorbing heat during the day. As seen in the *Figure 7.20* at PCM thickness 90 mm, at the end of first day the PCM doesn't completely melts and thus in the next day the higher PV temperature gets higher than the previous day. The same is also observed in the end of the second day that again doesn't melts and forces the system to not perform at full capacity. To mention that inside lines with the same colour represent day and between two different colour lines is night.

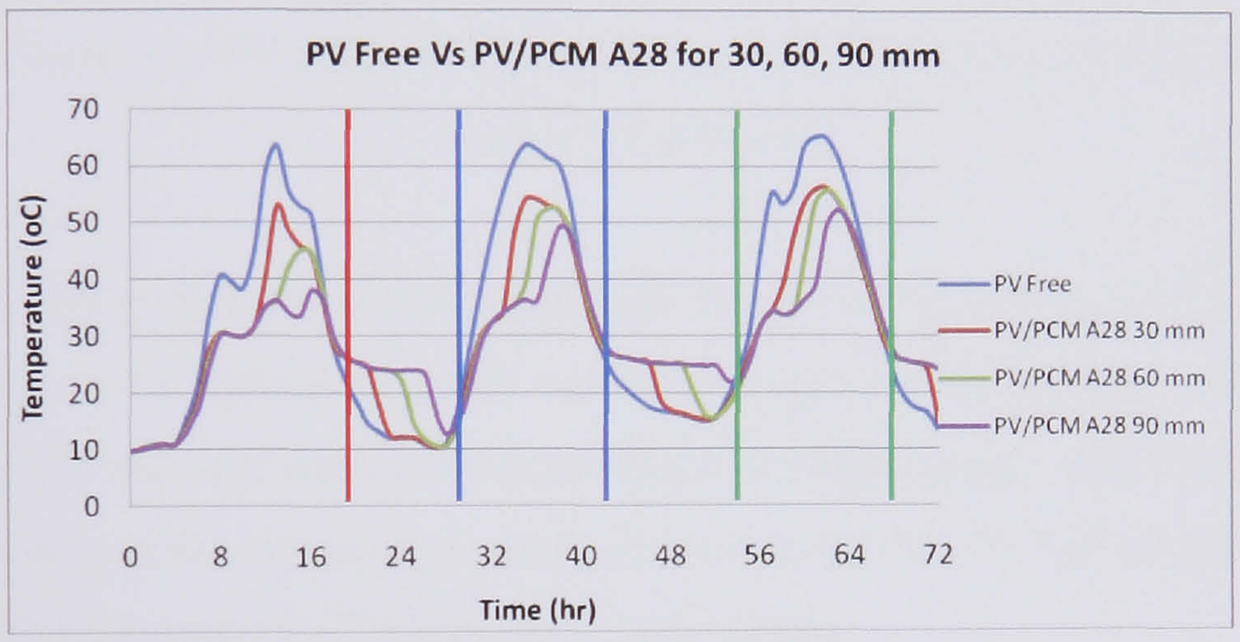

Figure 7.20 Average temperature evolutions for a three day simulation using weather data for the base case PV and at the front surface of PV/PCM system with PCM depths of 30, 60 and 90 mm

The predicted PV electrical conversion efficiencies for PV and system with PCM depths of 30, 60 and 90 mm are compared in *Figure 7.21*. For PV/PCM system with a PCM depth of 90 mm, PV electrical conversion efficiencies of over 3.8% were maintained over the longer period of the day.

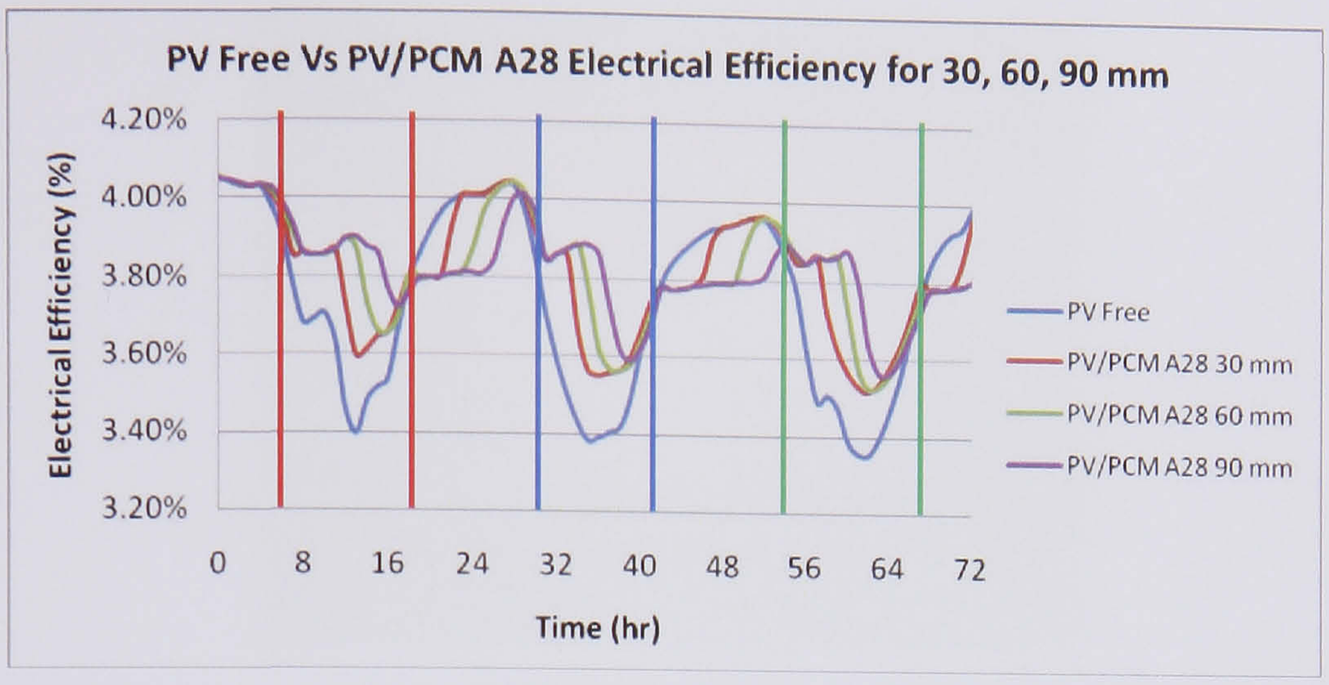

Figure 7.21 Electrical Efficiency evolutions for a three day simulation using weather data for the base case PV and at the front surface of PV/PCM system with PCM depths of 30, 60 and 90 mm

The study in this section revealed the potential that PV/PCM systems have in the performance of a PV system. Not only can use it to improve the electrical efficiency of the PV but PCM can also work as thermal energy storage system. Also the quantity of the material used in the system determines the period that the PV will remain cool enough by also the amount of energy that can be stored.

7.5 Experimental work

A series of experiments was undertaken to study the thermal behaviour of PV/PCM systems in order to validate the TRNSYS model.

Temperature measurements for a 0.4 m wide by 0.4 m high by 0.03 m thick PV/PCM system provided an experimental comparison with predictions for a natural convectively cooled system. The two experimental PV/PCM systems provided results which enabled detailed comparison of PV/PCM behaviour with prediction. Both PV/PCM systems had the same external dimensions. As shown in *Figure 7.22*, walls of the PCM container were fabricated from 2 mm thick copper plate. The dimensions of the container were 0.37 m wide by 0.37 m high by 0.03 m depth. The upper and lower horizontal faces and the vertical end faces of the PCM container were insulated with 0.027 m thick polystyrene insulation sheet with a thermal resistance of 1 m^2K/W.

Figure 7.22 PCM Copper Container

The thermophysical properties of the phase change materials applicable to experiments and simulations are shown in *Table 7.2*. The data sheet provided by the manufacturer EPS Ltd indicates the PCMs used in the experiments have stable performance throughout repeated phase change cycles. From the experimental observations there was no deterioration of the PCMs.

Table 7.2 EPS provided Thermo-Physical Properties of Phase Change Material (EPS Ltd)

PlusICE Type	Phase Change Temperature (^{o}C)	Density (kg/m^{3})	Latent Heat (kJ/kg)	Specific Heat (kJ/kg*K)	Thermal Conductivity (W/m*K)
A28	28	789	245	2.22	0.21
E30	30	1304	201	0.68	0.48

The temperatures on the convectively cooled PV and on the front surface of the PV/PCM system were measured by four K-type thermocouples. Two thermocouples were located within the PCM to measure temperature variation. The insolation intensity was 1000 W/m^{2} and the ambient temperature varied by less than 1 ^{o}C during the experiment.

7.5.1 PV/PCM A28 experiment

Figure 7.23 explores the importance of the thermal conductivity between the PV laminate and the copper container holding the PCM. As seen, the system with low conductivity has a PV temperature near 58 °C and the PCM melts after 111 min. After a thermal paste with thermal conductivity of 3 W/m*K was placed between the PV and the container the improved system temperature remained below 45 °C for 72 min. To mention that temperatures of *Figure 7.23* are the average recorded from each surface. This affects the performance of the PV electrical efficiency as seen in *Figure 7.24* and accordance with the $n_{pv} = n_o*(1 - \beta*(T_{pv} - T_{amb}))$ formula. The drawback is the increase of PV temperature after the PCM has completely melted (after 72 min) that result in reduced electrical efficiency. This increase of temperature is caused by the low thermal conductivity of the PCM material that works as an insulator that causes the quick increase of temperature after it has completely melted.

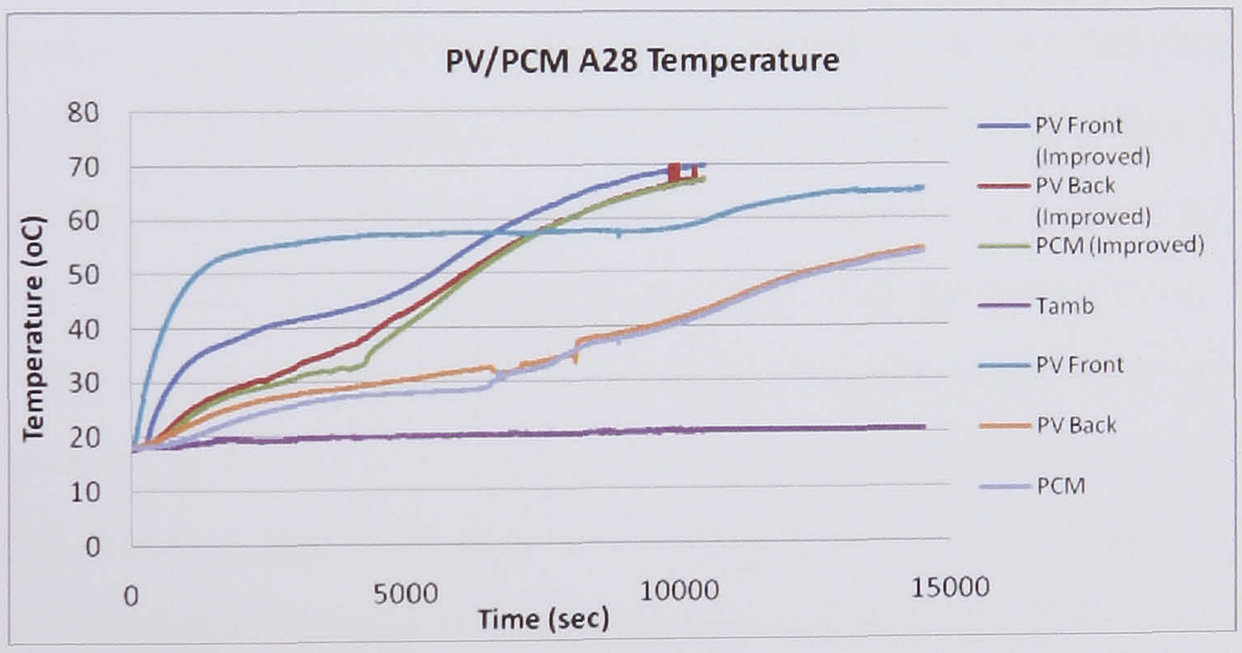

Figure 7.23 PV/PCM A28 Temperature with low and high thermal conductivity

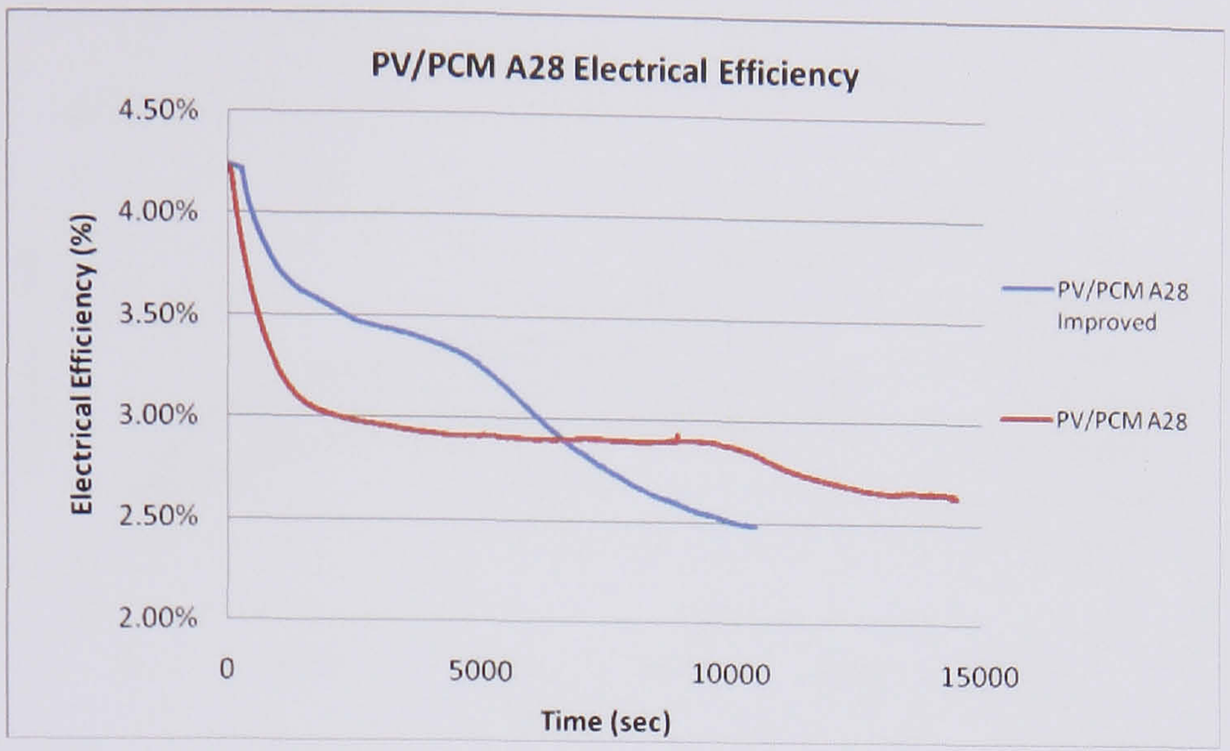

Figure 7.24 PV/PCM A28 Electrical Efficiency with low and high thermal conductivity

The next set of experiments used the same model and explored performance under different incident irradiation conditions. *Figure 7.25* shows how the system worked for insolation of 1000, 800 and 600 W/m^2. It may be observed that at 1000 W/m^2 the system temperature remains lower than 45 ^{o}C for 72 min, at 800 W/m^2 remains lower than 42 ^{o}C for 100 min and 600 W/m^2 remains lower than 40 ^{o}C for 127 min. When the three experiments finished the cooling down period was recorded to see how long it takes for system to cool. From *Figure 7.26* it may be seen that in all three conditions the time for solidifying is the same at around 82 min. In the experiments it may be observed that the melting point starts at 28 ^{o}C and finishes at 30 ^{o}C and is not as steady as the properties taken from the company say. The same can be seen in the cooling process. This may be caused of the variation of temperature inside the container affected by the location of the thermocouples or the PCM quality is being affected by segregation of material.

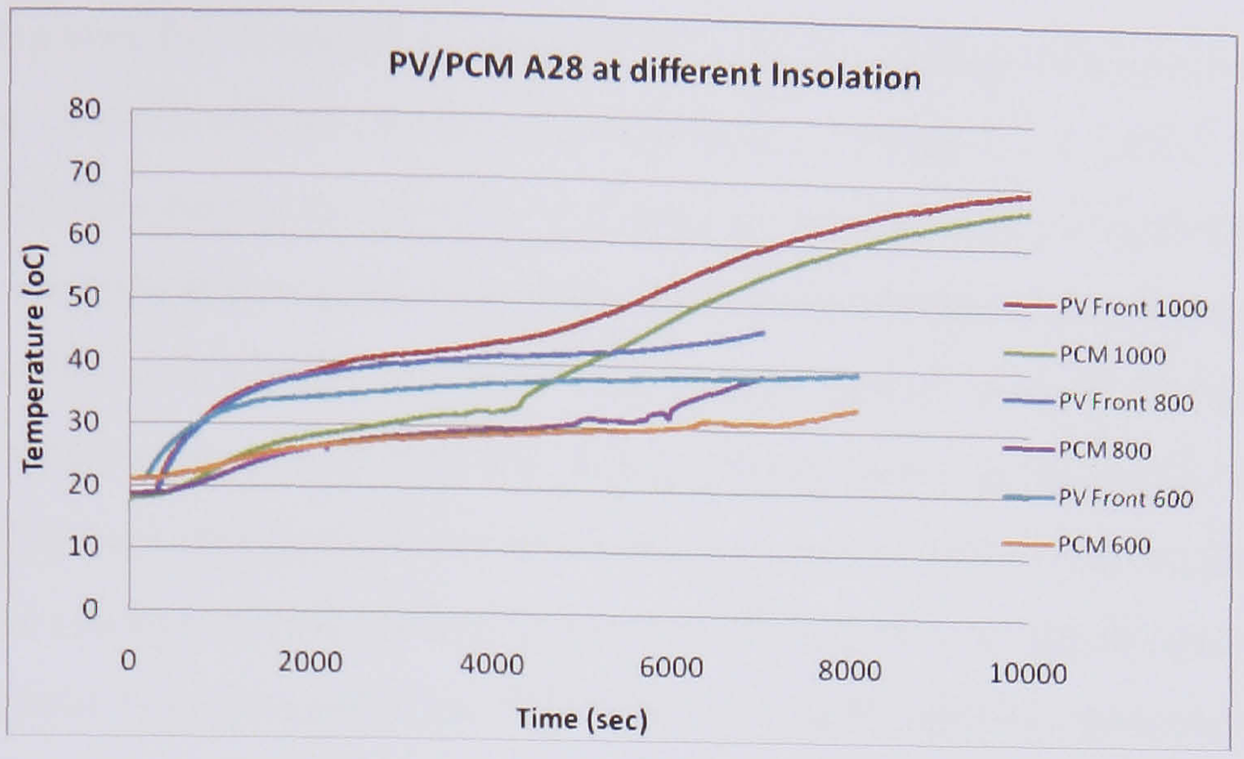

Figure 7.25 PV/PCM A28 for different incident irradiance conditions

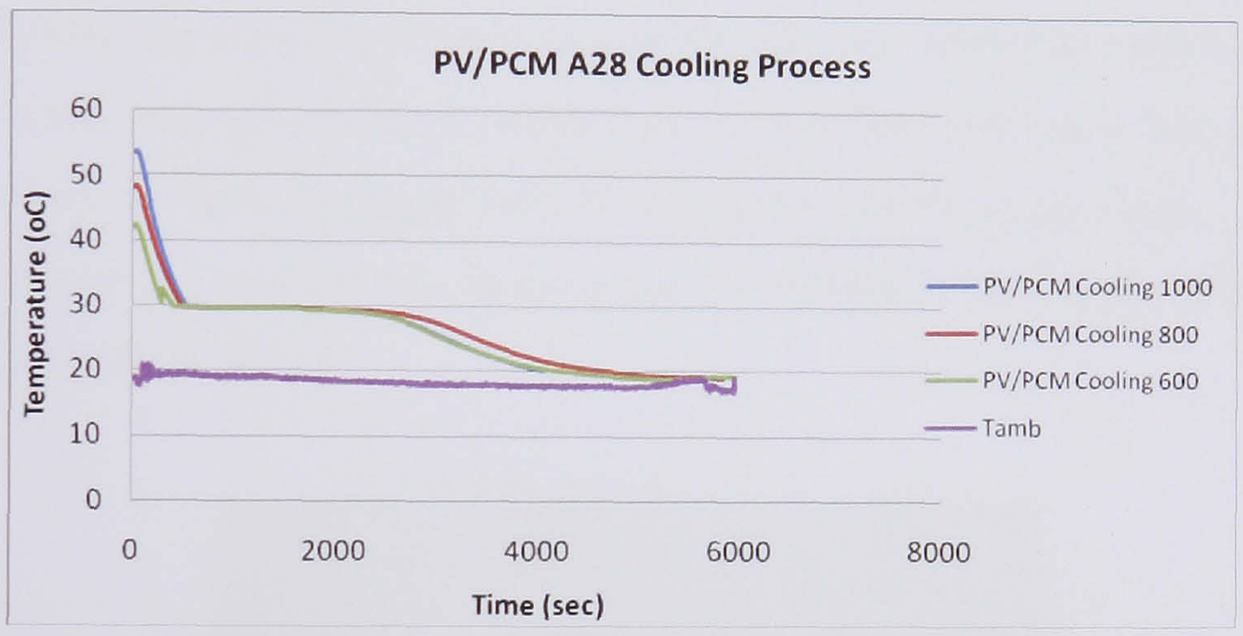

Figure 7.26 PV/PCM A28 Cooling Process

7.5.2 PV/PCM A28 with Water Pipes Experiments

From the previous experiments it was observed that the PCM can hold amounts of energy at specific temperatures for a long time and release it when addition of solar energy is ceases. The desired melting temperature of the PCM in order to keep the PV close at the reference temperature of 25 °C should be around the range above the ambient temperature and below 35 °C. So the thermal energy absorbed from sun can be released at this range of temperature. The range of 20 °C to 35 °C can be used for water pre-heating, for room air heating or for heating a pool. When real operating conditions were simulated for one and three days it was observed that it is possible to extract this amount of energy at the melting temperature of the PCM during the whole 24 hr period

of a day. However the temperature range of 20 to 35 °C is being considered as low grade heat thus the use of it will be limited. As mentioned in section 2.5.4.2 PV/T systems can be distinguished to panels and collectors. Panels are used to improve electrical efficiency and provide low grade heat and collectors to provide higher thermal energy and sacrifice electrical energy. A similar trend can be applied in the PV/PCM system. A PV/PCM system using a PCM with low melting temperature can be used to improve electrical efficiency and provide low grade heat or a system with PCM having a higher melting point can be selected for high grade heat. However to be able to use that heat and not overheat the system after the PCM has completely melted a heat exchanger should be incorporated in the system in order to extract that heat.

In order to remove heat effectively from the PCM the rig was modified to incorporate some pipes inside the copper container in order to have the ability to extract that heat and use it. In this way the PV temperature can be retain low level for a longer time and at the same time the thermal energy may be used for other purposes. *Figure 7.27* show the container with the pipes inside, as the pipes are welded in the copper side that has a contact with the PV laminate.

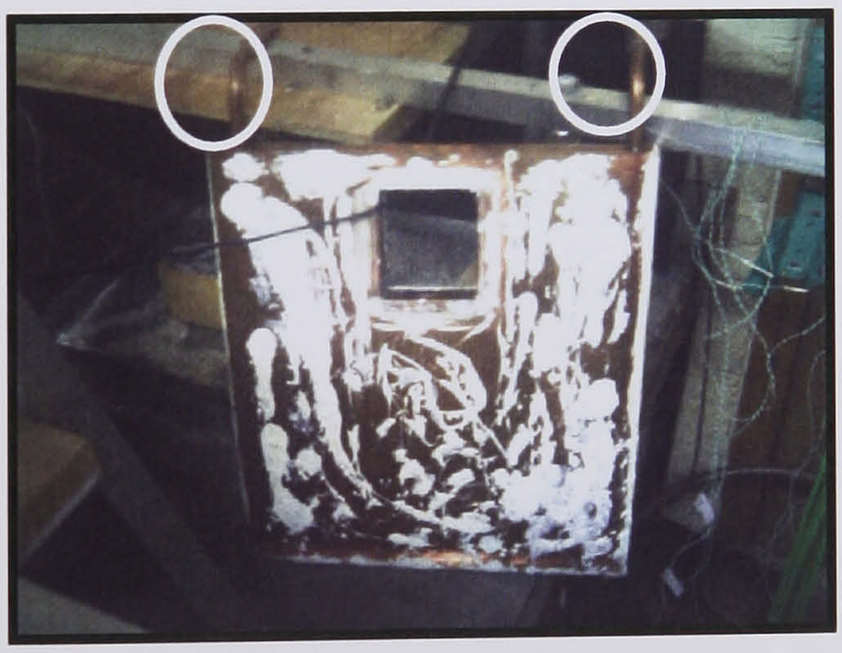

Figure 7.27a PV/PCM A28 Container with incorporating Pipes

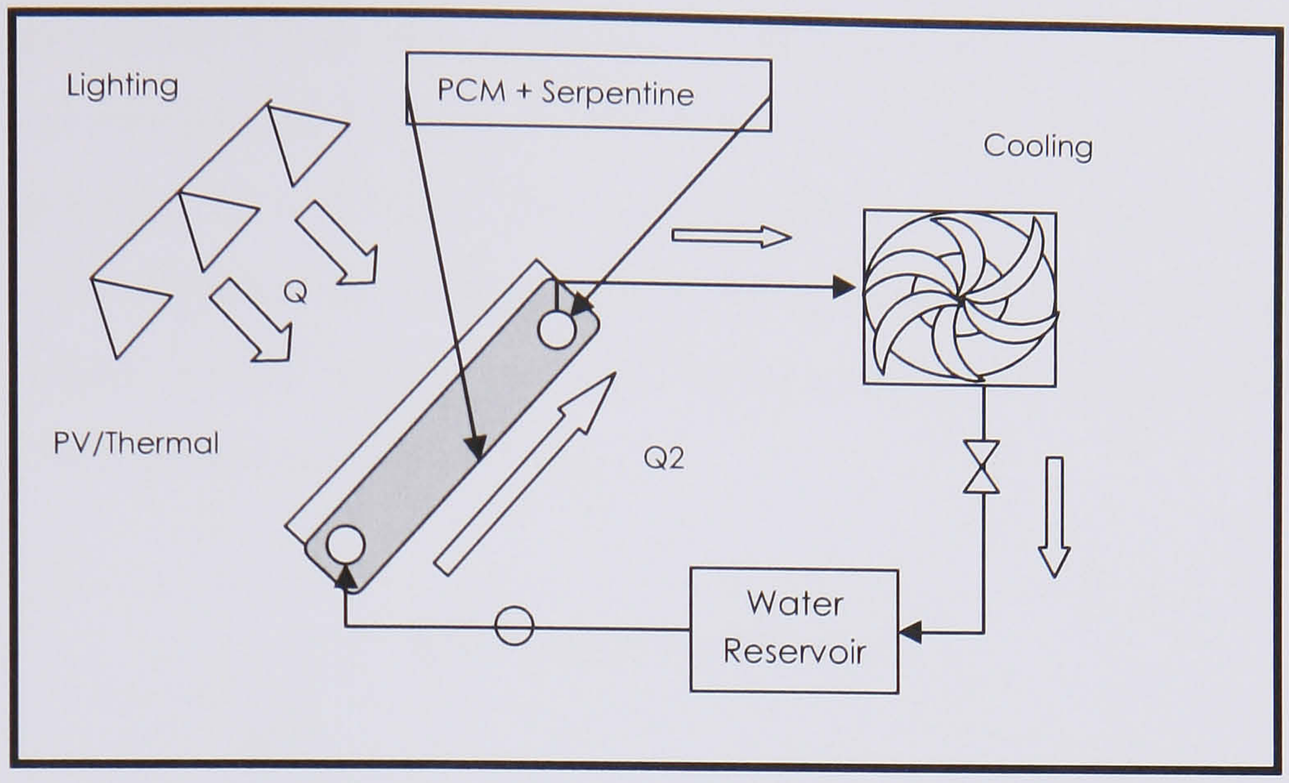

Figure 7.27b PV/PCM with serpentine pipes Schematic Rig

7.5.2.1 Varying the Flow Rate

The first set of experiments explored the effect of varying the flow rate of water. As seen in *Figure 7.28* the PV temperature is around 32 °C and the PCM near 26 to 27 °C. The flow rate used was 0.3 l/min and the experiment took 3 hr before the temperature stabilised. The inlet water temperature was 21 °C and the output 25 °C at 20 °C ambient temperature and an irradiance of 1000 W/m^2.

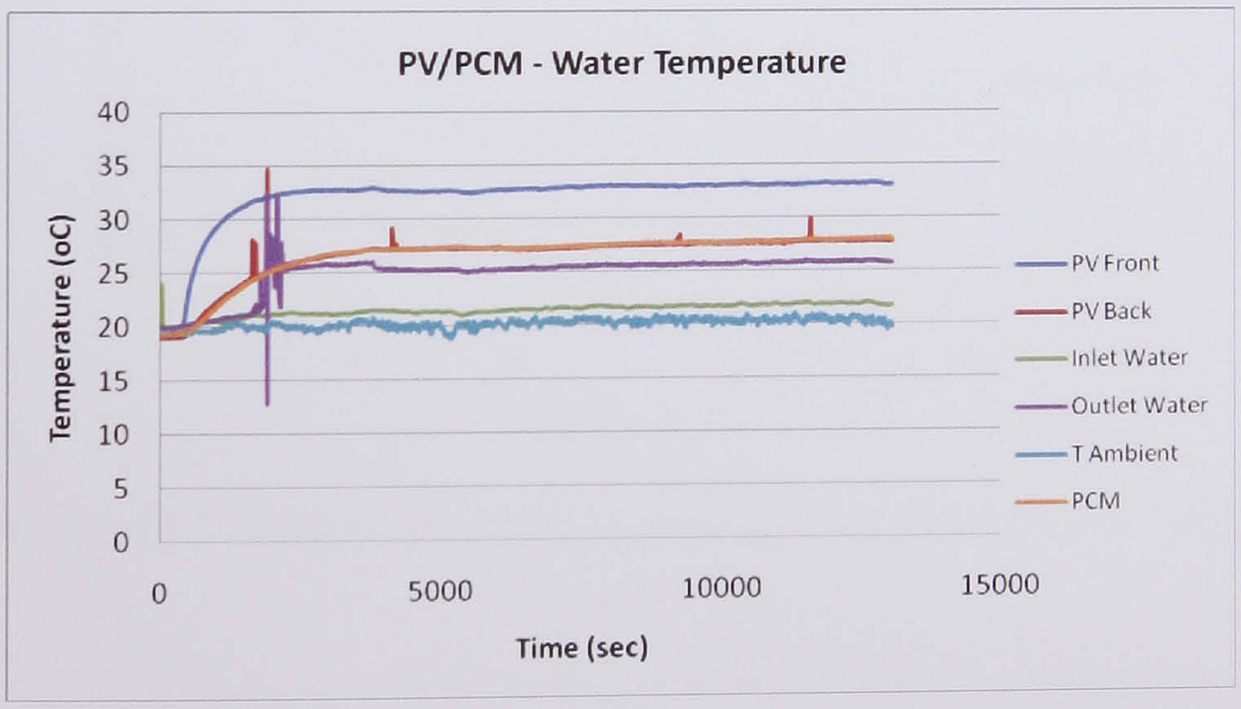

Figure 7.28 PV/PCM A28 – Water Temperature

The same experiment was undertaken with a change in the flow rate from 0.3 l/min to 0.8 l/min, 1.2 l/min and 2 l/min. *Figure 7.29* shows the temperature difference of outlet

and inlet water for the 4 flow rates and *Figure 7.30* gives the PV temperature at these flow rates. As may be seen from *Figure 7.29* where the experiments undertaken in chapter 4 are compared with results for the cooled PCM the PV temperature decreases as the flow rate increases. From Figure 7.30 it may be seen that the temperature of the PV/PCM – Water is about the same as of PV/Water system. The temperature difference beween the two systems is not significant.

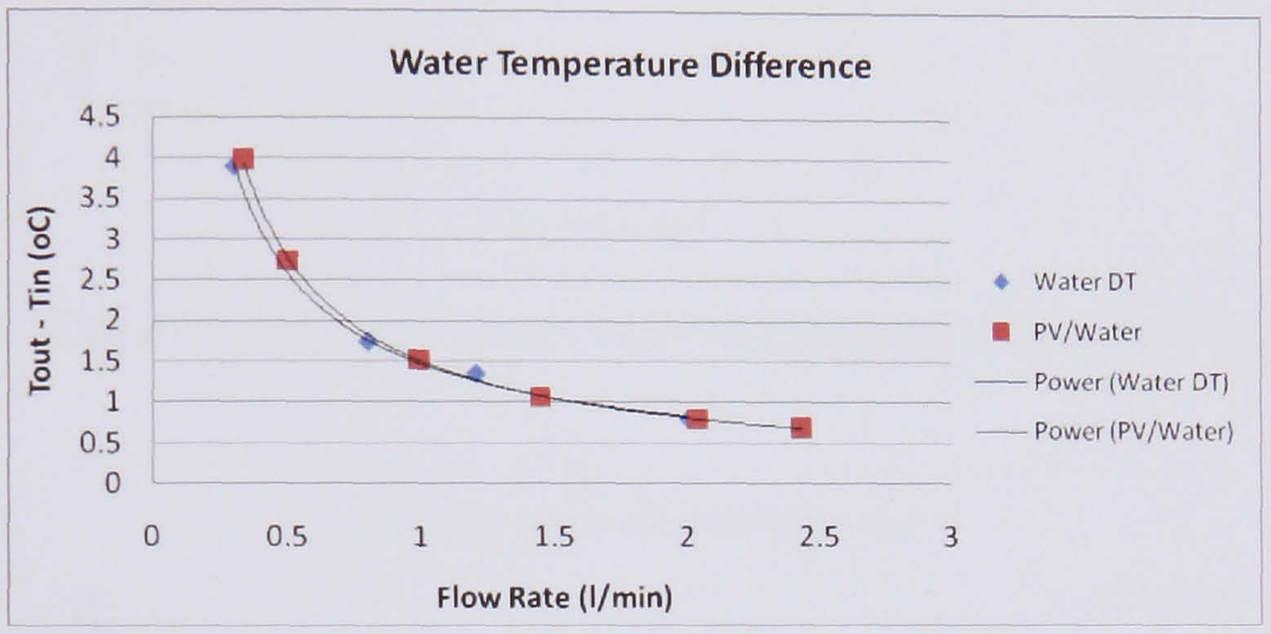

Figure 7.29 Water Temperature Difference at different Flow Rates

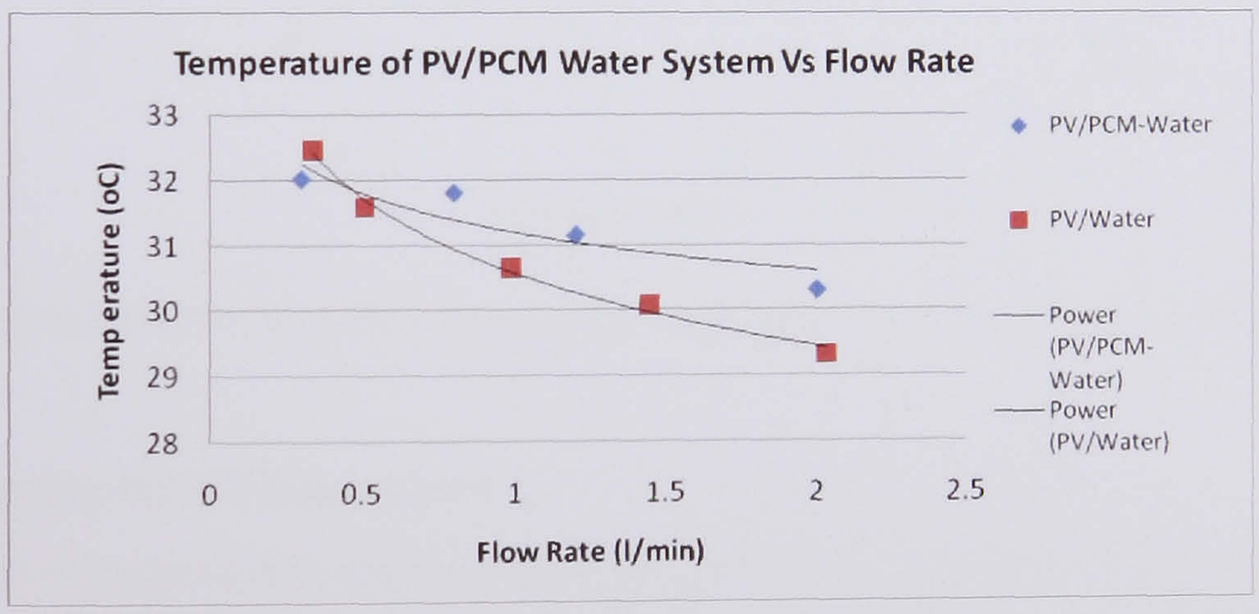

Figure 7.30 PV Temperature of the PV/PCM system for different Flow Rates

As the flow rate increases, the electrical and thermal efficiency of the system also increases. *Figure 7.31* shows the thermal efficiency of the system. At 0.3 l/min the thermal efficiency is 59% and reaches 84% at 2 l/min, an increase of 30%. In *Figure 7.32* were the electrical efficiency is shown the efficiency goes from 3.51% at 0.3 l/min to 3.69% at 2 l/min, an increase of 5%. A difference exists with the PV/Water model

because the area at the back of the PV has better contact and more uniform absorption that can transfer the heat to the pipes and to the PCM.

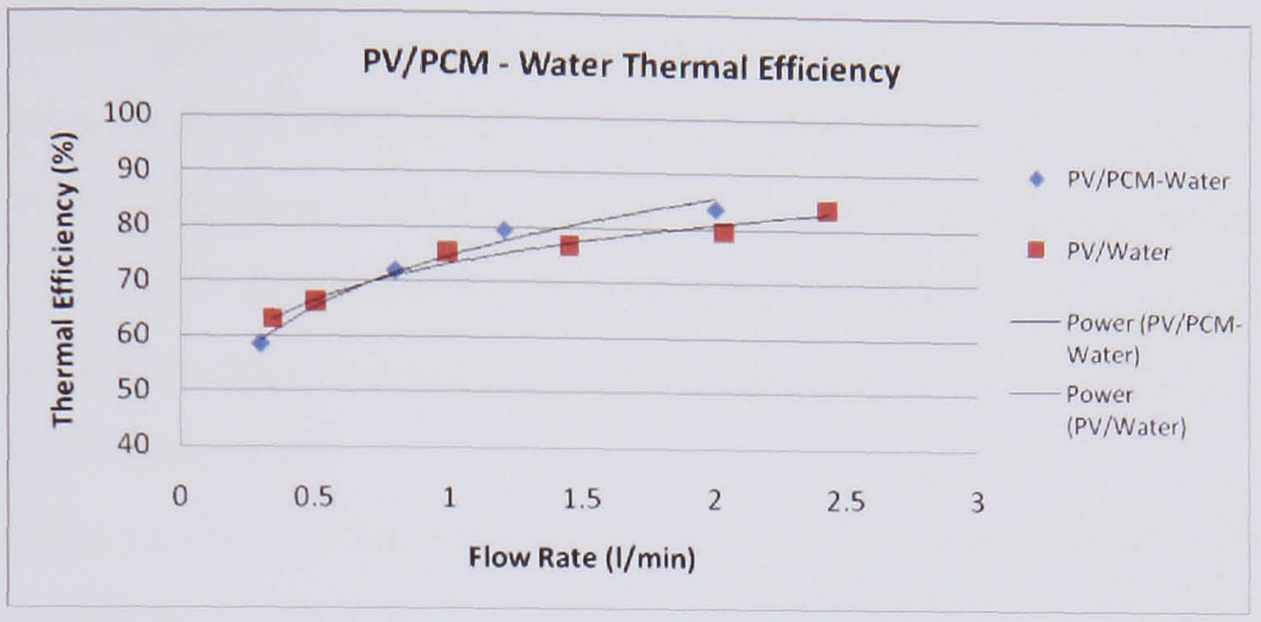

Figure 7.31 PV/PCM A28 – Water Thermal Efficiency at different Flow Rates

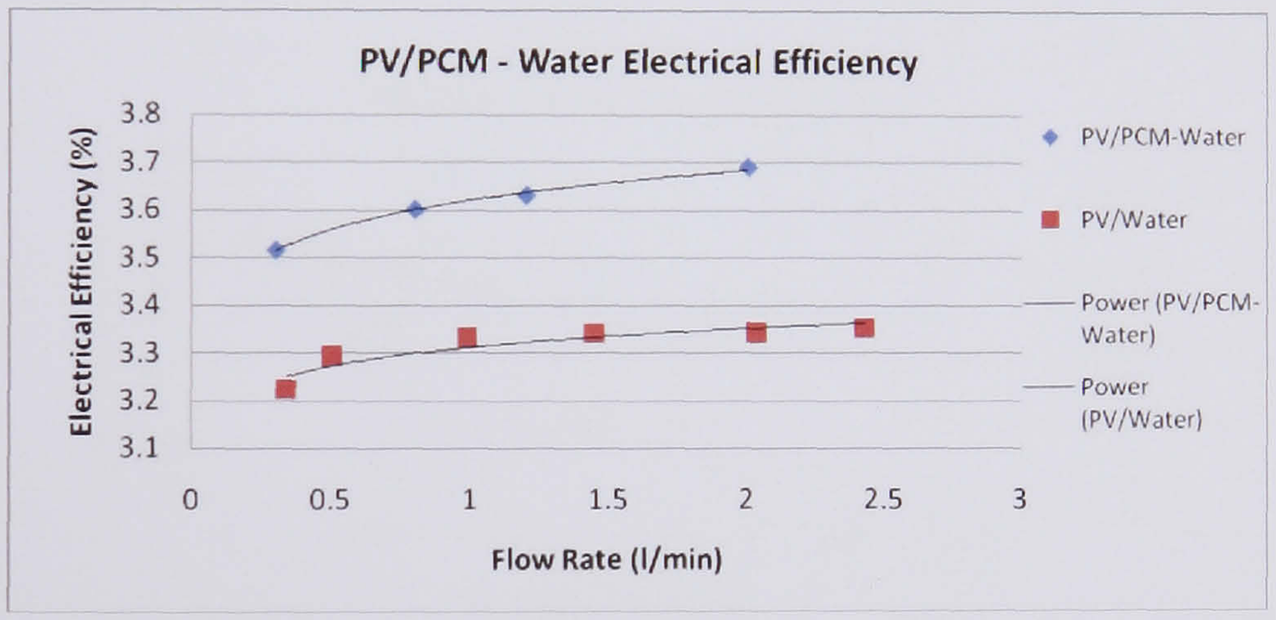

Figure 7.32 PV/PCM A28 – Water Electrical Efficiency at different Flow Rates

7.5.2.2 Varying Inlet Temperature

The next set of experiments explored the effect of varying the inlet temperature of the water over a range from 20 °C to 60 °C. As may be seen from *Figure 7.33* at zero reduced inlet temperature the efficiency for both is 59.8% but the PCM system shows significant improvement exhibiting a low thermal loss coefficient at 4.14 W/m^2K. A second point of interest relates to the points that are inside the circle. The point that is below the straight line gives a low thermal efficiency (32%). Occurs because the inlet and outlet temperature of the water are near the melting point of the PCM and thus the energy is not transferred to the fluid but remains in the material as latent heat. In the

circle above the line, the inlet and outlet temperature of the water and also the PCM temperature are above the range of melting temperature. This higher thermal efficiency (61% - 72%) is above the efficiency of zero reduced temperature meaning that this is the optimum point of operation. At this level the heat transport is via the latent and sensible energy stored in the PCM and the fluid passing absorbs the maximum of it. The obvious improvement in comparison with the system with simple water pipes passing in the back of the PV is that the PCM system managed to decrease the heat loss coefficient. For the PV/Water system this heat loss was 7.68 W/m^2K and for PV/PCM – Water is 4.14 W/m^2K, a reduction of 46%.

The same improvement may be observed in *Figure 7.34* for the electrical efficiency of the system. Inside the circle it may be seen that the PCM and the water system cool the PV and thus increase the effectiveness of the system.

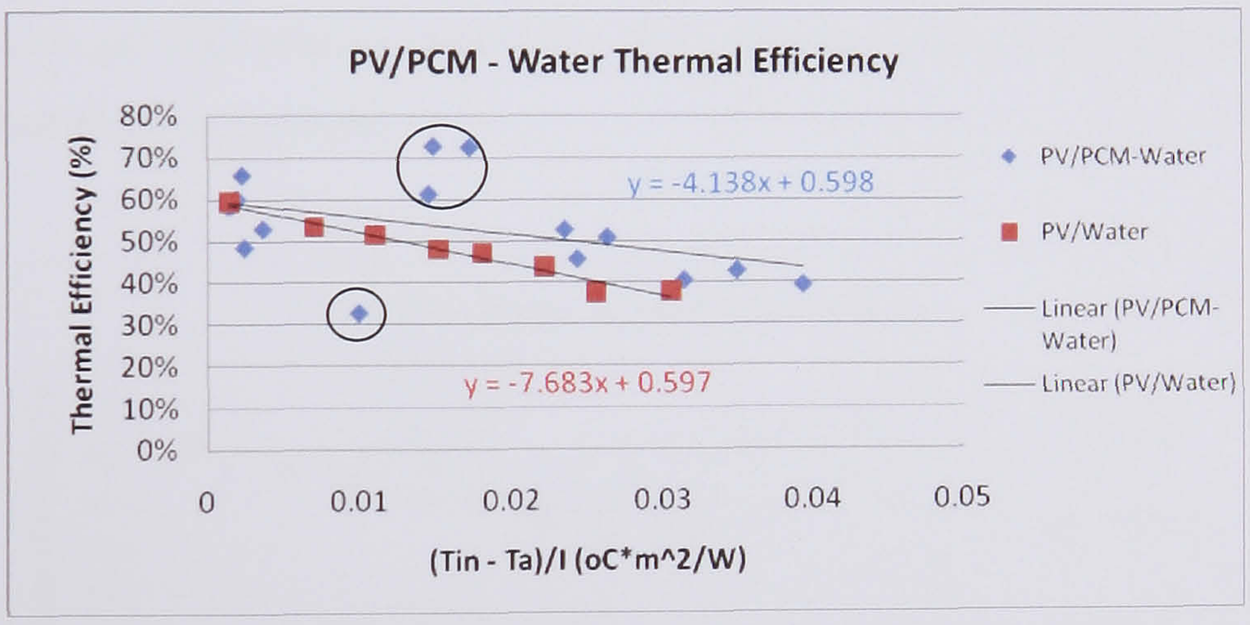

Figure 7.33 PV/PCM – Water Thermal Efficiency

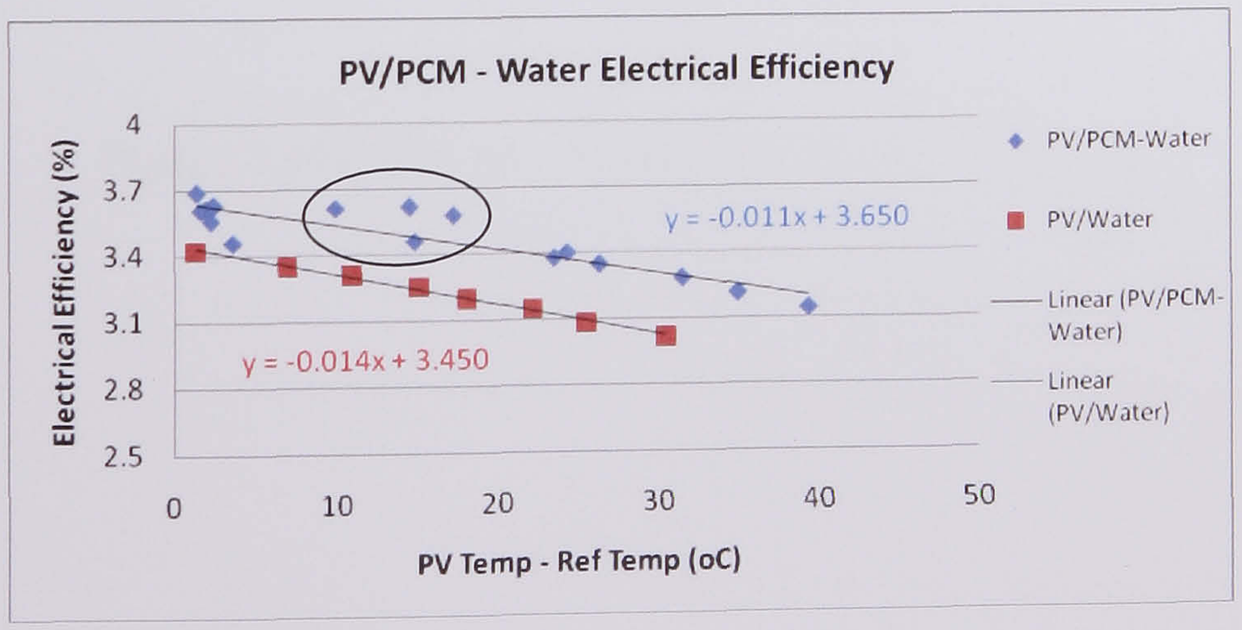

Figure 7.34 PV/PCM – Water Electrical Efficiency

By adding the thermal and electrical efficiency we get the total energy efficiency, as shown in *Figure 7.35*, the total efficiency is around 63.5%. As discussed in previous chapters the value of electric power and thermal energy differs due to the form of energy. Hence to correctly evaluate the energy saving of the system it is necessary to define the energy saving efficiency in terms of primary energy saving. As shown in *Figure 7.36* by diving the electrical efficiency by the electrical power generation (0.38) efficiency we get a total of 69.4%. For simplicity the efficiency of conventional heating systems has been assumed to be 100%. It has been found by Huang (1993) that the daily efficiency for most solar hot water heaters is around 0.50. This value can provide a criterion for checking the overall performance of a PV/Thermal system. It is expected that the primary-energy saving efficiency E_f for a PV/T system should exceed 0.50 in order to compete with a pure solar hot water system. From these two graphs the points inside the circle get efficiencies around 64 - 81% thus the water absorbs both sensible and latent heat from the system.

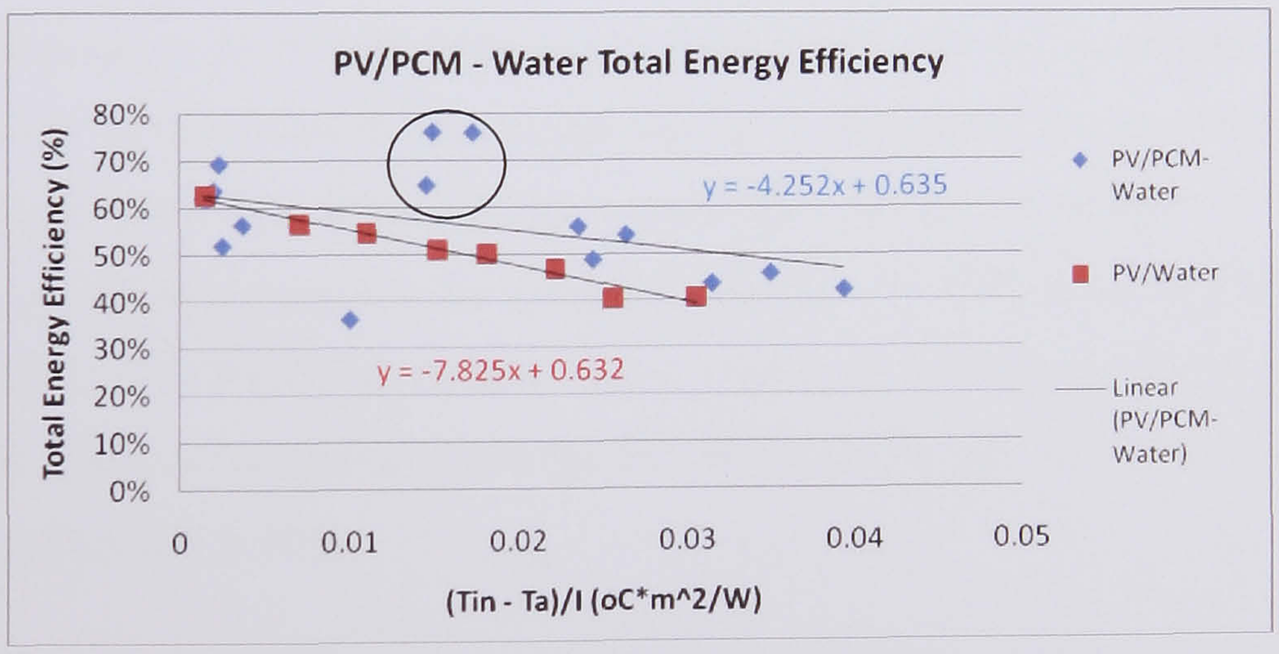

Figure 7.35 PV/PCM – Water Total Energy Efficiency

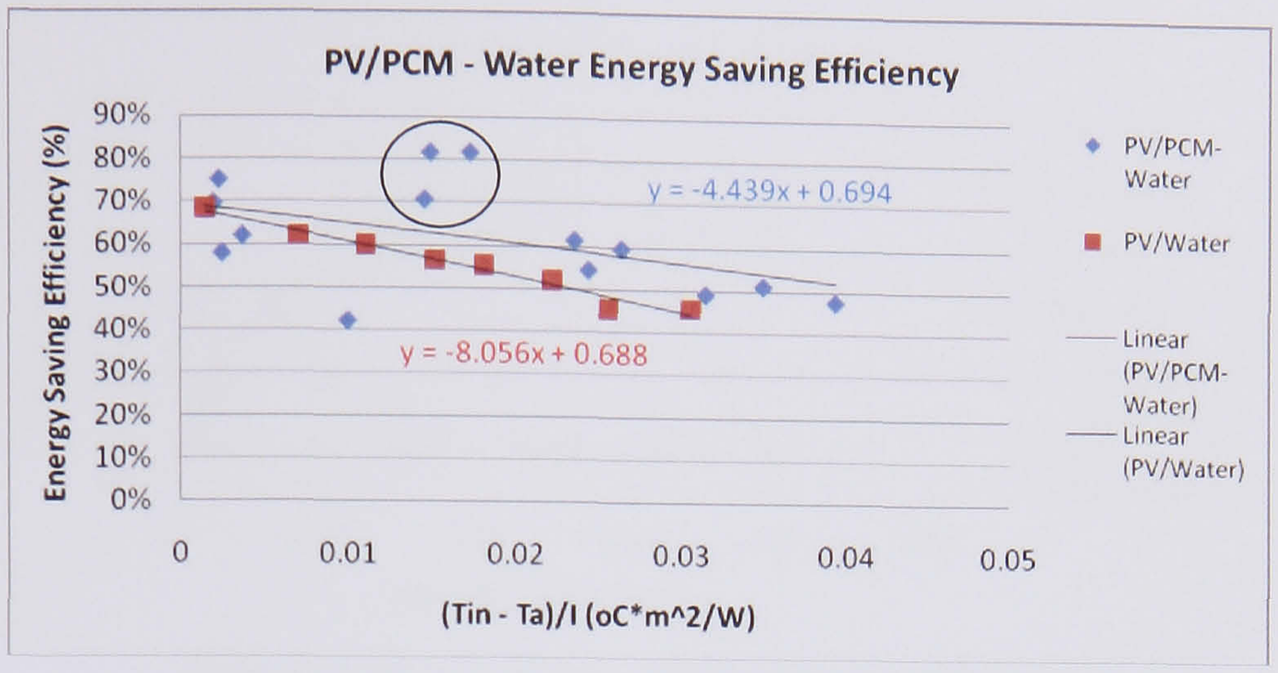

Figure 7.36 PV/PCM – Water Energy Saving Efficiency

PV/Thermal systems supply different forms of energy such as electrical and heat. Therefore to quantitatively evaluate the usefulness of the energy obtained it is necessary to adopt the concept ot exergy. The exergetic evaluation is a technique for evaluating the obtained energy by considering the temperature difference with the open air and paying attention to the work which can be taken out to the outside. As seen from *Figure 7.37* the optimum working conditions is when the heat medium at the system is 45 ^{o}C at ambient temperature 20 ^{o}C and irradiation at 1000 W/m^2. There the exergetic efficiency is around 34%. In the points that are inside the circle the system has absorbed the energy as sensible and latent heat causing PCM to melt. This energy is transfered to water and so the exergy efficiency reaches the optimum value of 34 - 36% when the heat medium is around 35 ^{o}C. The PV/PCM – Water model works more efficiently and in larger temperature range in comparison with the PV/Water model and the highest exergy efficiency difference is 10%.

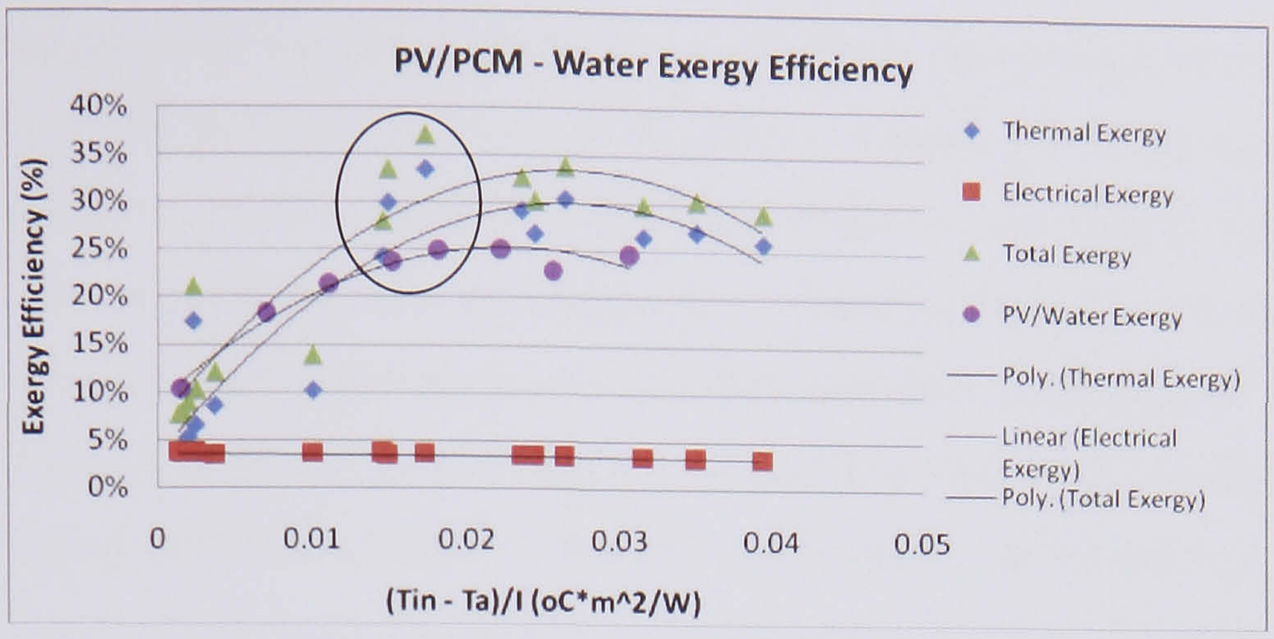

Figure 7.37 PV/PCM – Water Exergy Efficiency

7.6 Conclusion

From chapter 3 it was seen that as the temperature of the PV increases the electrical efficiency drops. Attempts to cool the PV in order to improve the electrical efficiency have been tested by passing air, water or incorporating heat pipes to the back of the PV. Another technology that can work as a heat absorber is a phase change material. This kind of material can absorb a large amount of energy as latent heat at a constant phase transition temperature. This chapter used PCM positioned in the back of the PV in order to absorb the heat by controlling the temperature in a region near the reference temperature (25 ^{o}C).

The first step of the study was to find out what kinds of materials exist that are near the characteristic temperature and to validate their thermophysical properties using a method developed by Yingping and improved by Hong.

A developed numerical PV/PCM model was created and validated successfully by comparison with experiments. With the help of TESS a simulation model was created from the energy balance equations in order to evaluate the performance of the system. This is to date the only numerical TRNSYS model for a system using PCM to moderate the temperature rise of PV that has been validated for identically sized geometries with realistic experimental conditions. The validated model provides a detailed insight into the thermal performance of a solid–liquid transition PCM when employed in a PV temperature control application.

From the simulations it was observed that the conductivity between the PV and the PCM container affects the performance of the system. Various PCM materials were simulated and it was possible to check which takes longer to melt. This provides an indication as to which PCM offer the longest phase transition period and so hold the PV close to its characteristic temperature and offer better electrical performance.

Also the difference in the ambient conditions, the incident irradiation and the thickness of the PCM positioned behind the PV affect the performance. As the ambient temperature or incident irradiation increases then the time for PCM to melt becomes shorter. As the volume of PCM increases the time for the PCM to fully melts increases.

Simulations were also performed under real operating conditions for one and three days for different thickness of PCM and it was discovered that as the thickness of the PCM increases, the PV is kept at lower temperature for a longer period of time during the day.

A series of experiments were performed with PCM A28 which has a melting of 28 ^{o}C exploring the impact of the conductivity between the PV laminate and PCM container and the behaviour of the system at different irradiations. The results from these experiments agreed well with simulation.

The stored energy at the phase transition temperature could be used in order to pre-heat water, air room or heating a pool. An adjustment was made to the existing model by incorporating water pipes inside the container in order to extract that heat. The model was tested with various flow rates and inlet temperature passing from the pipes. The outcome was that as the flow rate increases the electrical and thermal efficiency improves and the PV temperature reduces. Depending on the phase change temperature, the system works well enough when the inlet temperature is below or above the melting temperature. When the inlet is near the melting temperature we face a poor operation because much of the heat is being absorbed by the PCM as latent and sensible heat instead of being transferred to the fluid.

A last point is that to maintain the temperature on the front surface of the PV/PCM system at 25 ^{o}C, the characteristic temperature of the PV, the set transition temperature of the PCM should be higher than the ambient temperature and lower than 25 ^{o}C.

When real operating conditions were simulated for one and three days it was observed that it is possible to extract this amount of energy at the melting temperature of the PCM

during the whole 24 hr period of a day. However the temperature range of 20 to 35 °C is being considered as low grade heat thus the use of it will be limited. As mentioned in section 2.5.4.2 PV/T systems can be distinguished to panels and collectors. Panels are used to improve electrical efficiency and provide low grade heat and collectors to provide higher thermal energy and sacrifice electrical energy. A similar trend can be applied in the PV/PCM system. A PV/PCM system using a PCM with low melting temperature can be used to improve electrical efficiency and provide low grade heat or a system with PCM having a higher melting point can be selected for high grade heat. However to be able to use that heat and not overheat the system after the PCM has completely melted a heat exchanger should be incorporated in the system in order to extract that heat. This heat exchanger system may be a tank incorporating pipes that water could flow in order to extract the heat from the PCM. Thus when the PCM has completely melted the water will start flowing through the pipes in order to cool down the PCM and extract that heat. The advantage is twofold, first the PV is being kept as cool as possible for a longer time during the day and secondly the absorbed heat can be used fro preheating purposes. Another advantage of using PCM is the low thermal conductivity that can work as thermal insulator and thus reduce the heat losses.

CHAPTER 8: PHOTOVOLTAIC/THERMAL SYSTEM MICROENCAPSULATED PHASE CHANGE MATERIAL SLURRY (MCPCM)

8.1 Introduction

Energy storage in phase change materials allows very high energy densities to be achieved at well defined temperatures. Due to the low thermal conductivity of many phase change materials it is difficult to get high rates of heat transfer and rapid charging unless (Farid, 2004):

(i) high thermal conductivity materials are embedded in the phase change material, (for example fins),

(ii) the phase change materials are encapsulated in modules and a heat transfer fluid flows around them,

(iii) the phase change materials are microencapsulated and suspended in a carrier fluid to form a slurry. If the carrier fluid has higher thermal conductivity than the PCM or convection occurs in the microencapsulated PCM slurry an increased charging rate can be achieved.

Many thermal-energy systems have long sections of piping to convey heat-transfer fluids between the heat exchangers for source and sink. In such conventional systems, thermal energy is transferred by the sensible heat of a single-phase working fluid, being proportional to the source - sink temperature difference. Because the systems are often operated with small temperature differences, the single-phase fluid must be pumped at a high-volume flow rate. As a result, the system consumes a large amount of pumping power. The increase in the thermal capacity of heat-transfer fluid is an important problem and is of growing concern to engineers. The use of phase-change material PCM particles suspended in a single-phase working fluid would provide additional thermal capacity from the latent heat associated with the solid-liquid phase change (Yamagishi, 1999). These mixtures of PCMs and carrier fluids are called phase change slurries (PCSs).

Microencapsulated PCM slurries are advantageous because of latent heat effect associated with phase change process of material. The apparent specific heat capacity is

much higher than conventional sensible heat of a fluid without phase change, which may greatly enhance the heat transfer performance between the fluid and heat transfer surface. Furthermore, the agglomeration and deposition of particles in the fluid are avoided because the core material is always separated from the carried fluid by thin plastics shell (Wang, 2007).

When there are fine particles of non-encapsulated PCM the slightly sticky nature of the material often means the particles can stick together to form large lumps, clogging often occurs in a piping system, resulting in failure to circulate the slurry through the system (Winters, 1991).

The purpose of the present study was to investigate the feasibility of using slurry of microencapsulated phase change material MCPCM as a heat-transfer fluid. Besides the benefit of the additional thermal capacity, no special equipment for charging and discharging PCM particles is needed because the PCM is always separated from the suspending fluid. Therefore, this type of slurry can be treated as a conventional single-phase working fluid. Furthermore the fluid works as a storage, carrier and rejector of heat system advantage that can reduce size and cost of the system and stabilize the PVs cell temperature.

8.2 Microcapsules and slurry

Figure 8.1 is a photomicrograph of the two different MCPCM particles used in the present study. The two materials have a melting temperature of 26 ^{o}C and 33 ^{o}C and latent heat of 155 kJ/kg and 124 kJ/kg respectively.

The particle diameters given by the manufactures CIBA were in the range of 70 micron and 10-17 micron mean diameter for the 26 ^{o}C and 33 ^{o}C MCPCM respectively. The coating wall was made by an acrylic shell approximately 0.1 micron. Pure water was chosen as the suspending fluid for the MCPCM particles because it is easy to handle and does not react chemically with either the PCM or the coating material on the shell.

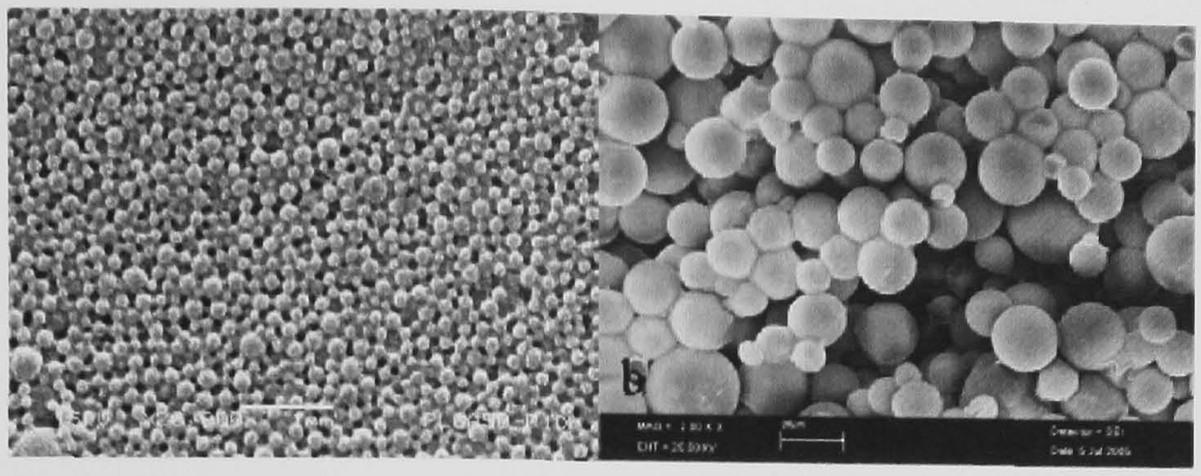

Figure 8.1 Microscopic Photo of Micro-PCM particles

The density, specific heat, thermal conductivity and latent heat of MCPCM slurry and its components are given in *Table 8.1*. These bulk physical properties are calculated from the combination of pure water, coating-wall material, and PCM using the equations given by Inaba et.al. (2004). The weight fractions of wall-coating material and PCM in the slurry were determined from manufactures from the feed weight used in the slurry during the manufacturing process. The particle volume fraction, Φ, in the slurry and the physical properties were estimated from these weight fractions. The weight ratios between the coating material and PCM were the same for all the slurry samples. When the particle volume fraction is 0.3, the volume fraction of the coating material in the slurry is approximately 0.07. The physical properties of a MCPCM particle were calculated under the assumption that all of the particles had the same diameter and the coated walls all had the same thickness. To prepare the slurry the weight ratio of PCM/coating was taken into account.

Table 8.1 Physical Properties of MCPCM Slurry (26 °C) and its Components (Approximation)

	Density (kg/m^3)	Specific Heat (kJ/kg*K)	Thermal Conductivity (W/m*K)	Latent Heat (kJ/kg)
PCM	780	2.2	0.34	155
Acrylic Shell	1490	1.67	0.42	-
Water (298 K)	997	4.18	0.61	-
MCPCM Particle	1000	1.75	0.31	124
MCPCM Slurry F = 10%	998	3.94	0.539	12.4
F = 20%	998	3.687	0.506	24.8
F= 30%	989	3.489	0.483	37.2
F = 40%	989	3.245	0.448	49.6

8.3 Slurry Performance

When the PCMs are properly selected and encapsulated, it is possible to achieve remarkable improvements in the heat storage and the transport capability of the fluid slurry (Wang, 2007). Equation 8.1 is the familiar relation describing the rate of heat storage within a material as its temperature increases.

$$Q = m*C_p*\Delta T \qquad \text{Eq. (8.1)}$$

The effective thermal capacity of a two component materials is therefore proportional to the ratio of the rate of heat transfer and its temperature change, as described by Eq. (8.2)

$$C_{pe,eff} = Q/m*\Delta T \qquad \text{Eq. (8.2)}$$

Expressing the heat transfer sum of the sensible and latent components, the effective heat capacity $C_{p,eff}$ becomes (Kasza and Chen, 1985):

$$C_{p,eff} = C_p + w_p \Delta H_m / \Delta T \qquad \text{Eq. (8.3)}$$

where w_p is the mass fraction of MPCM in the slurry; ΔH_m is the latent heat of the MPCM; ΔT is the difference between the slurry temperatures at the inlet and outlet of the test section. The latent heat of slurry increases with the mass faction, so too does the effective specific heat capacity of the slurry.

From equation (8.3) it can be seen that the latent heat capacity is comparably very large at a small temperature difference, but the contribution it makes to the weighted average heat capacity decreases as ΔT grows.

The amount of heat that can be stored by common heat transfer fluids, e.g. water or oils, depends on the usable temperature range that can be exploited. The efficiency of such heat transfer fluids is poor if an application allows only a small temperature difference. One solution to increase the efficiency of such applications is to use phase change materials. The energy that can be stored at the phase transition of some materials is very high. Paraffin is a PCM that can be pumped through pipes when it is micro-encapsulated and dispersed in a carrier fluid.

The capacity of such a PCS (phase change slurries) to store heat is computed with the following equation (Gschwander et al., 2004):

$$Q_{PCS} = x_{capsule} \Delta h_{capsule} + c_{p_{water}} \Delta T_{area\ of\ melting} \qquad \text{Eq. (8.4)}$$

where $\Delta T_{area\ of\ melting}$ is the melting range of the PCM

With a melting range around 4 K, the heat storage capacity can be calculated with Eq. (8.4) to be 44.4 kJ/kg for a 20% PCS with 26 °C melting temperature and 38.2 kJ/kg latent heat for 33 °C. Water without a PCM would absorb 16.8 kJ/kg over a 4 K temperature range or would have to be heated up or cooled down approximately 10.5 K and 9.1 K respectively to store or release the same quantity of heat.

The investigated PCS is advantageous for applications where only a small temperature difference can be used. With a high ΔT, water as a very cheap heat transfer fluid has clear advantages in comparison to PCS. Slurries promise advantages particularly in low-temperature applications, in comparison with water where only a small ΔT is usable.

The energy content of slurries h_{PCS} as a function of the temperature T and different fractions of capsules may be computed with the following formula (Gschwander et al., 2004).

$$h_{PCS}(\vartheta) = h_{capsule}(\vartheta)x_{capsule} + h_{water}(\vartheta)(1 - x_{capsule}) \qquad \text{Eq. (8.5)}$$

where h is the enthalpy per kilogram for the capsules or water and θ the temperature in °C. *Figure 8.2* and *8.3* shows the enthalpy – temperature diagram for the two MCPCM materials investigated in this chapter in comparison with water, at different MCPCM concentrations. This method is commonly known and used for simulations of PCMs (Lamberg, 2003).

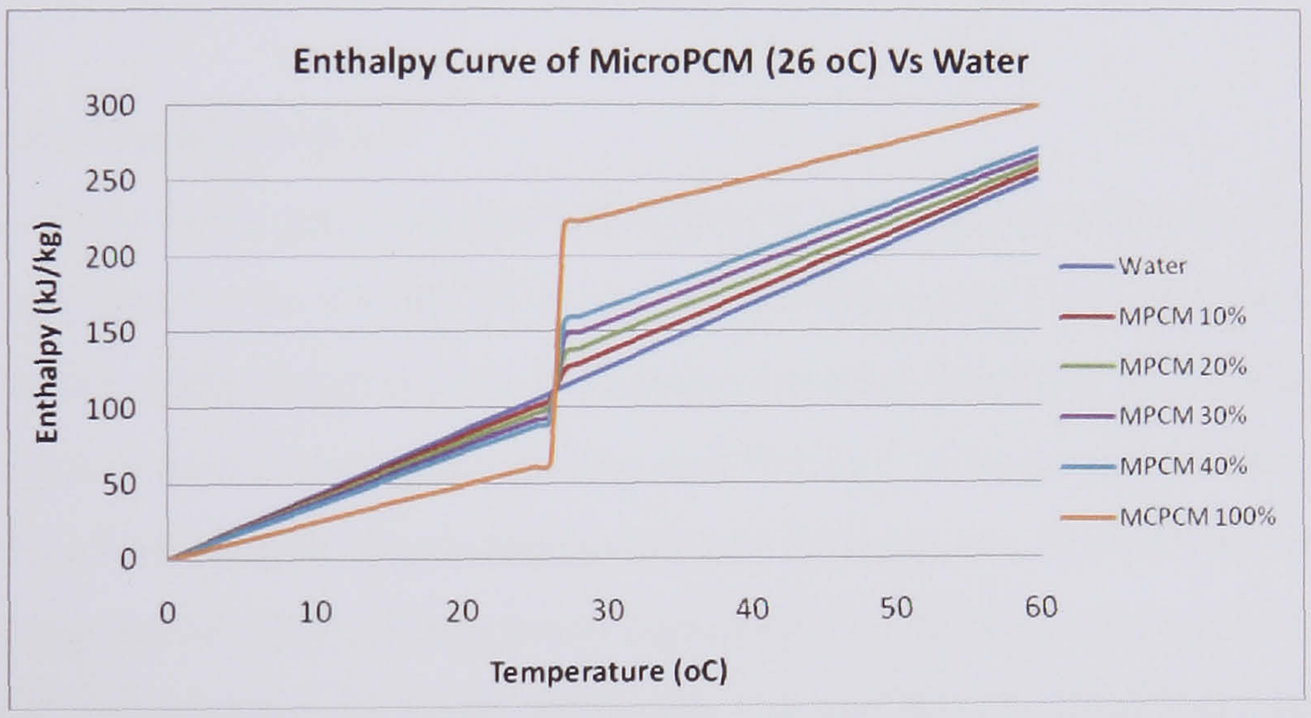

Figure 8.2 Enthalpy curves of PCS with different concentration of capsules and a melting range from 25 – 27 °C

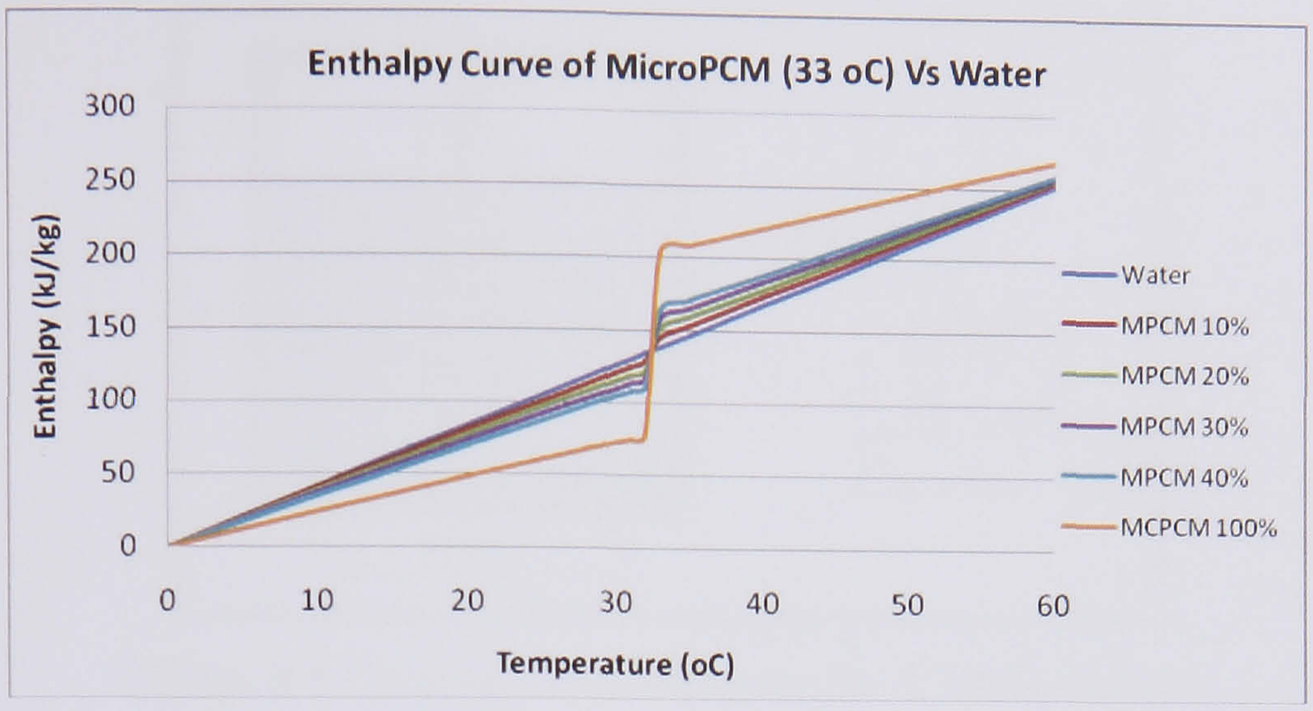

Figure 8.3 Enthalpy curves of PCS with different concentration of capsules and a melting range from 32 – 34 ^{o}C

8.3.1 Thermal Analysis (TA)

Thermal analysis technique is another measurement technique to determine the melting and freezing characteristics of MCPCM slurry The differential Thermal Analysis (TA) technique involves the determination of temperature-time diagrams, or the heating and cooling curves, recorded during the melting and freezing of the sample. It uses between 10gr – 10 kg of the sample, depending on the type of apparatus. With proper care, the rate of heating and cooling can be closely controlled and relatively accurate results can be gained. A literature survey of the techniques revealed that the most commonly employed experimental apparatus used is that of a simple test tube. Abhat (1978) constructed the same apparatus as in *Figure 8.4* to test samples under a variety of thermal cycling conditions.

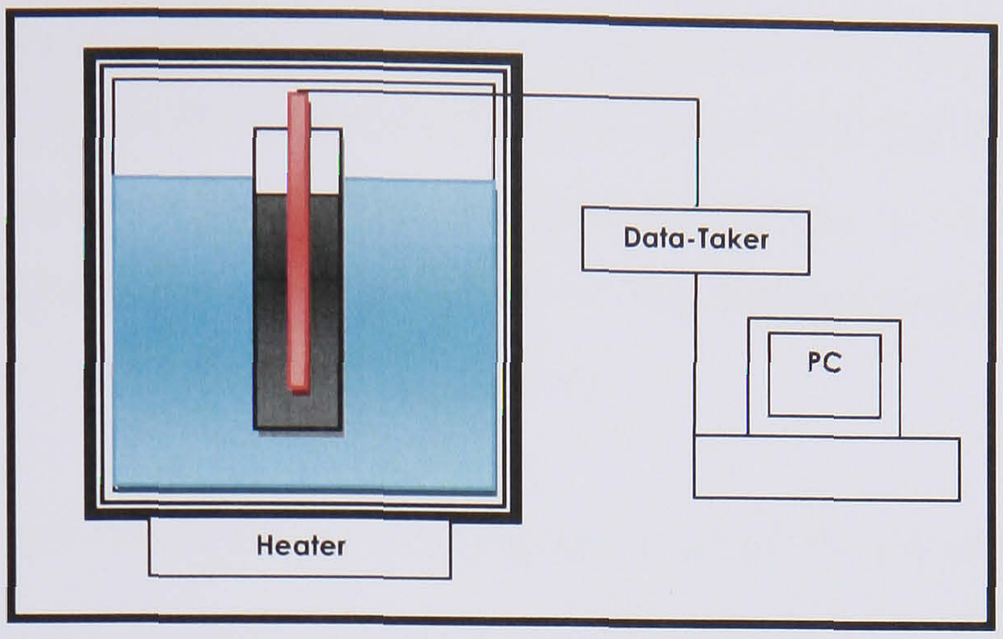

Figure 8.4 Glass test tube apparatus for TA measurement

8.3.2.1 Methodology

The MicroPCM slurries of 10%, 20%, 30% and 40% concentrations were evaluated using the TA technique. A cylindrical glass tube (10 mm diameter x 150mm) was used as a container for the microPCM slurries. The temperatures were measured using K-type thermocouples located at the centre of the tube. The glass tube filled with the slurry was initially submerged in a bath kept at 20 ^{o}C using an immersion thermostat. In order to heat the sample, the tube was transferred to another bath kept at 45 ^{o}C. Once the sample was fully heated, to complete the heating cycle and initiate the cooling phase, the sample was transferred back to the 20 ^{o}C bath.

It can be noted that a key factor to the experimental accuracy was the mixing or separation of the microPCM capsules. As a result, important experimental parameters other than the microPCM particle density and separation characteristics were the duration of test and quantity of sample. The longer the duration of experiment the more time the particles had to separate. Using a smaller quantity of sample (25 gr), the test took less time and could be done before stratification occurred. One drawback of using this smaller sample quantity was that the constant temperature region was less apparent.

8.3.2.2 TA Experimental Observations

Figures 8.5 and *8.6* show typical heating curves for the 26 ^{o}C and 33 ^{o}C samples respectively, obtained during TA measurements with 10%-40% microPCM slurries and for pure water. *Figures 8.7* and *8.8* show the cooling curves for the respective PSCs. As

seen in the figure the microPCM did not show the long and flat freezing/melting characteristics of a simple PCM cause of the low concentration and the mix with the water. However it could be observed that the slurries exhibited narrow freeze/melting ranges, which signified a phase change transition. The 10% concentrations did not show significant influence on the temperature variation.

Supercooling was not clearly shown from Figures. Compared with water, the slurries had more energy transport as they maintained a larger temperature difference in both the heating and cooling curves (as the rate of heat transfer depends on the temperature difference between the system and surroundings). The higher the concentration of microPCM, the greater the temperature difference between the PCS and the bath, and the greater rate of heat transfer.

In terms of energy storage, the microPCM slurry also provided a higher heat capacity compared with water but is not possible to evaluate it with this experimental method. This can be seen in *Figure 8.5* and *8.6* where the curves for the slurries lagged behind that of the water. This implies that they have a higher heat capacity, which took longer time to transfer all the heat. For example, compared with water, the 30% microPCM slurry took approximately one minute longer to reach 45 ^{o}C as its temperature reached the surrounding bath temperatures.

This seems very attractive since it has the unique advantage of maintaining a larger temperature difference in heat exchange components and hence could improve overall heat transfer.

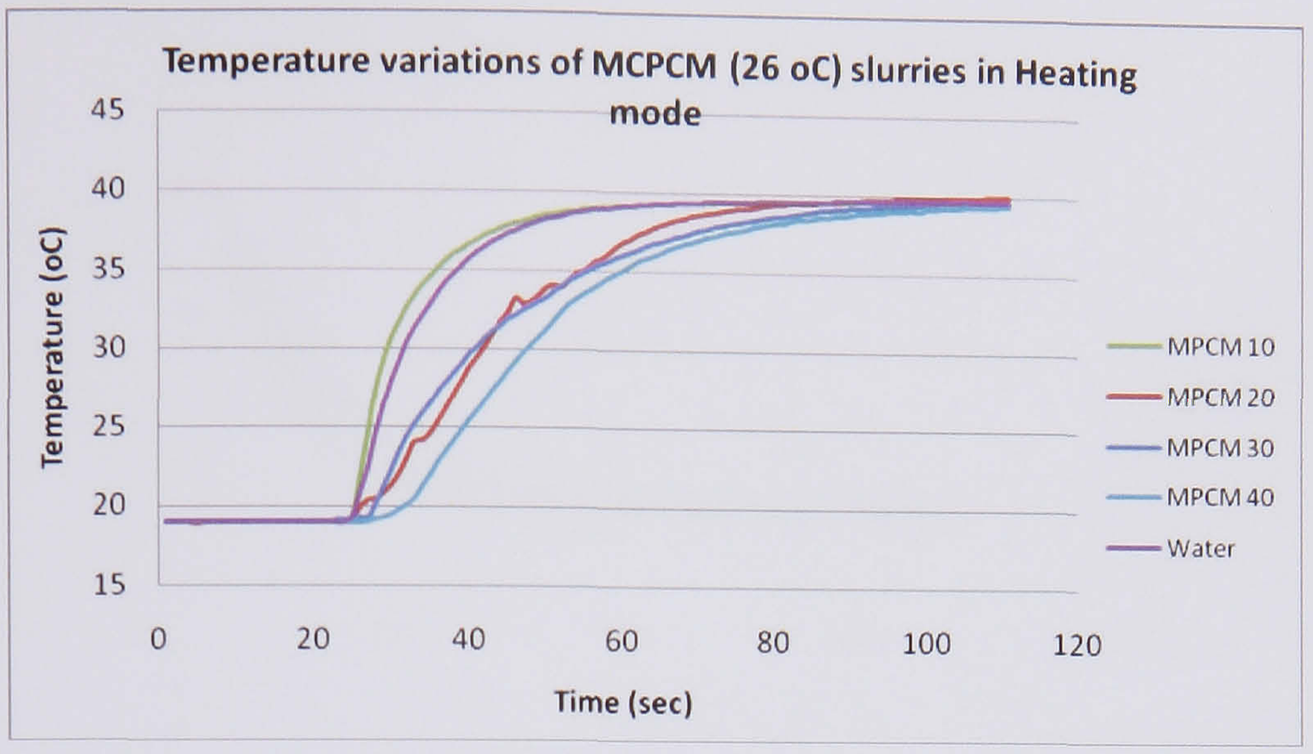

Figure 8.5 Temperature variations of MCPCM slurries (10% to 40%) in heating mode with PCM melting at 26 °C

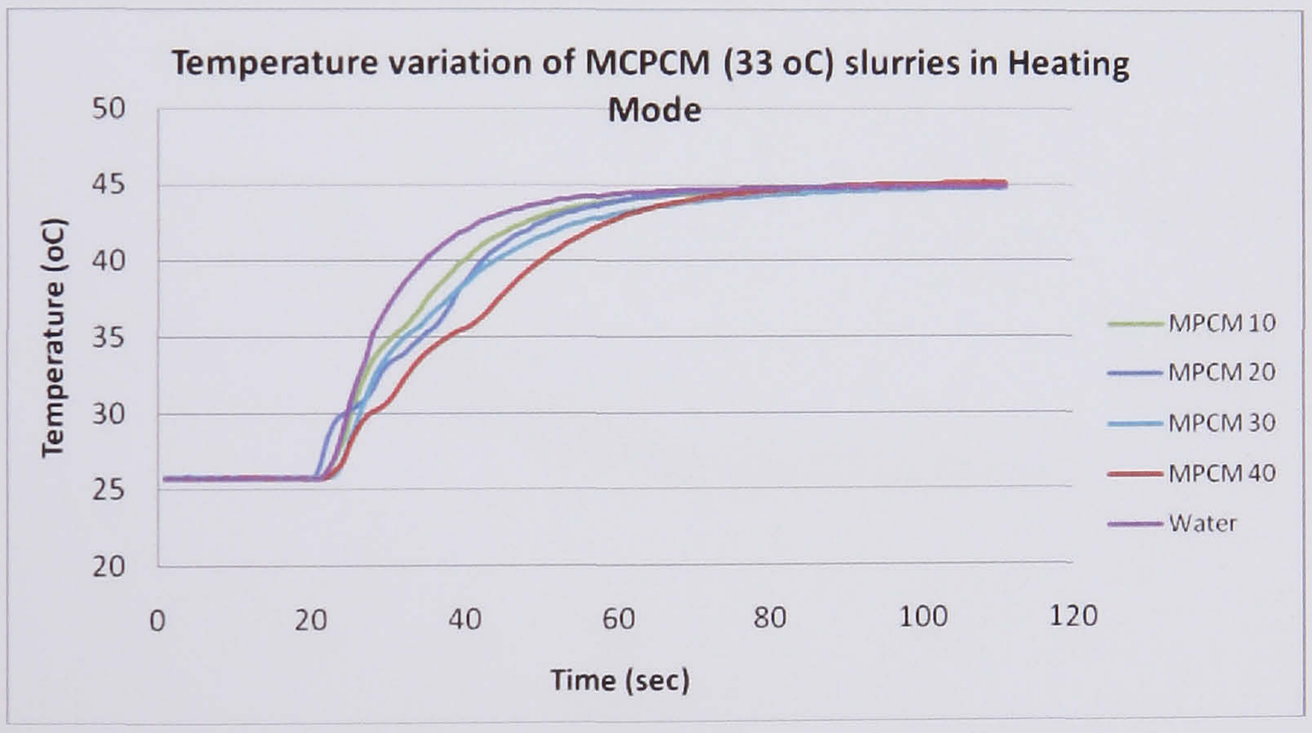

Figure 8.6 Temperature variations of MCPCM slurries (10% to 40%) in heating mode with PCM melting at 33 °C

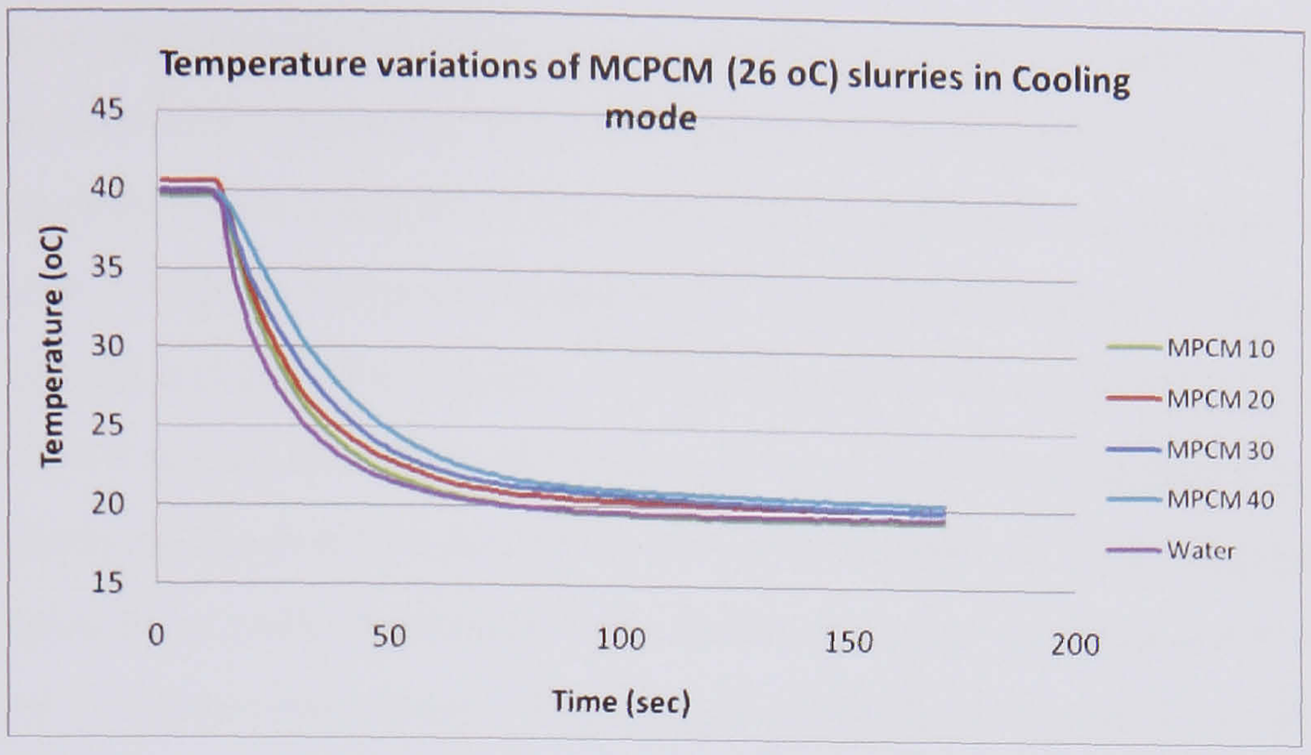

Figure 8.7 Temperature variations of MCPCM slurries (10% to 40%) in cooling mode with PCM melting at 26 °C

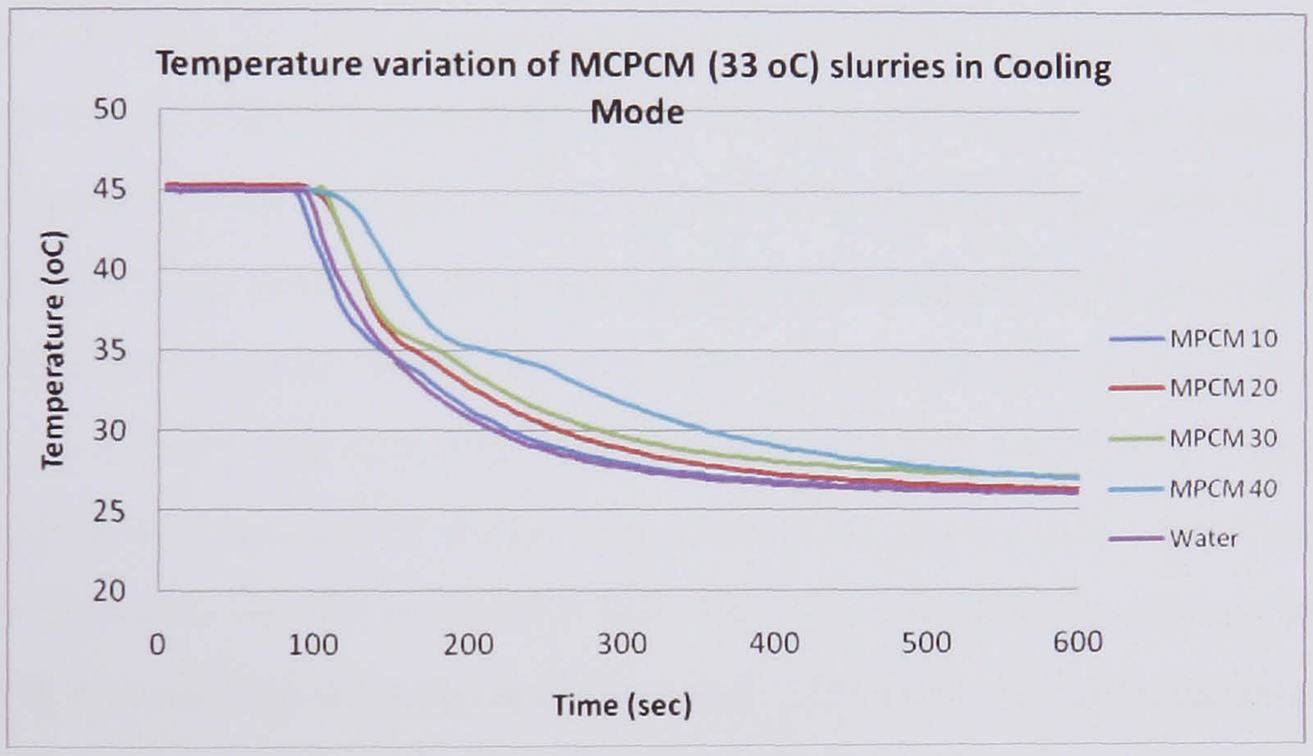

Figure 8.8 Temperature variations of MCPCM slurries (10% to 40%) in heating mode with PCM melting at 33 °C

8.4 MCPCM Slurry

In order to select a fluid as an energy transport medium, Goel (1994) notes that two main criteria have to be considered which are high thermal conductivity and high specific heat. However, a selection of the working fluid is governed by another important factor: its compatibility with PCM and the wall capsules. As a carrier fluid for the MCPCM, water can be used without any inconvenience. It is easy to handle, has low viscosity and no effect on the phase change material or the microcapsule wall.

Mixing the microencapsulated phase change particles and water is one of the most common operations for preparing the phase change slurry. The term mixing is applied to a process used to reduce a degree of non-uniformity or gradient of a property such as concentration, viscosity, temperature and so on. To promote a high rate of heat transfer, effective mixing is required to achieve a desired degree of homogeneity. Thus an electric stirrer was used to prepare the slurry. However, after the homogeneity of MCPCM slurry has been achieved and the stirrer was turned off, phase separation caused by gravity or centrifugal force between the suspended particles and water could be observed within several minutes. The capsules of PCM are lighter than water and generally float to the surface.

8.4.1 MCPCM Slurry in a Closed Loop System

Parameters affecting the heat storage performance of MCPCM slurry include bulk Stefan number, volumetric concentration etc. The bulk Stefan number is defined as the ratio of the sensible heat capacity of the suspension to its latent heat capacity. Charunyakorn (1991) notes that the bulk Stefan number significantly dominates the heat transfer performance of the MCPCM slurry. The Nusselt number can be considerably improved 1.5-2.5 times by reducing the bulk Stefan number, which corresponds to increasing the latent heat of the slurry. The effect of increasing the concentration is twofold: it decreases the Stefan number and raises the conductivity enhancement factor. Goel (1994) showed that the bulk Stefan number is the most dominant parameter. His results show that up to 50% reduction in the pipe wall temperature rise can be obtained by using the MCPCM suspension in place of a single-phase fluid. He concludes that for the best results, the bulk Stefan number should be maintained below (Ste<0.1). This can be achieved either by increasing the concentration of MCPCM or by reducing the duct radius. The concentration does play an indirect role in heat transfer through the bulk Stefan number.

Choi (1994) studied the effects of PCM-water slurry on the convective heat transfer coefficient in a turbulent flow and suggested that the effect of latent heat on the local heat transfer coefficients may also depend upon the slurry flow structure. In 1999, Yamagishi investigated the effect of turbulent and laminar slurry flows on local heat

transfer coefficients. His results interestingly show that when flows of the MCPCM slurries are at approximately the same mean flow velocity, higher particle fractions of 15% have a lower heat transfer augmentation than a 7% MCPCM slurry. This is because the flow of 7% slurry has higher Reynolds number than that of the 15% slurry. However if the particle volume fractions are the same for both laminar and turbulent flows, the heat transfer in the turbulent flow is more effective than in the laminar flow. The heat transfer augmentation associated with phase change depends upon not only the fraction of solid particles in the slurry but upon the degree of turbulence. The effects of duct-to-particle diameter ratio and degree of homogeneity of the suspension do not have a significant effect on the heat transfer characteristics of the phase change slurry (Goel, 1994).

Recently more papers have been published on theoretical or experimental approaches to clarify the merits of this medium. These studies focus mainly on heat capacitance and heat transfer coefficient. The major challenge in applying liquid-solid PCM to a convection heat transfer system is to achieve continuous circulation of the particles through the heat transfer flow loop. The current study employs a small scale rig with a closed loop circuit (*Figure 8.9b*), instead of a one way flow rig as used by many studies (*Figure 8.9a*), in order to circulate the suspension from the slurry reservoir through the test section and back to reservoir. The effects of repeated use of the slurry with liquid-solid phase change particles upon melting and solidifying can be investigated.

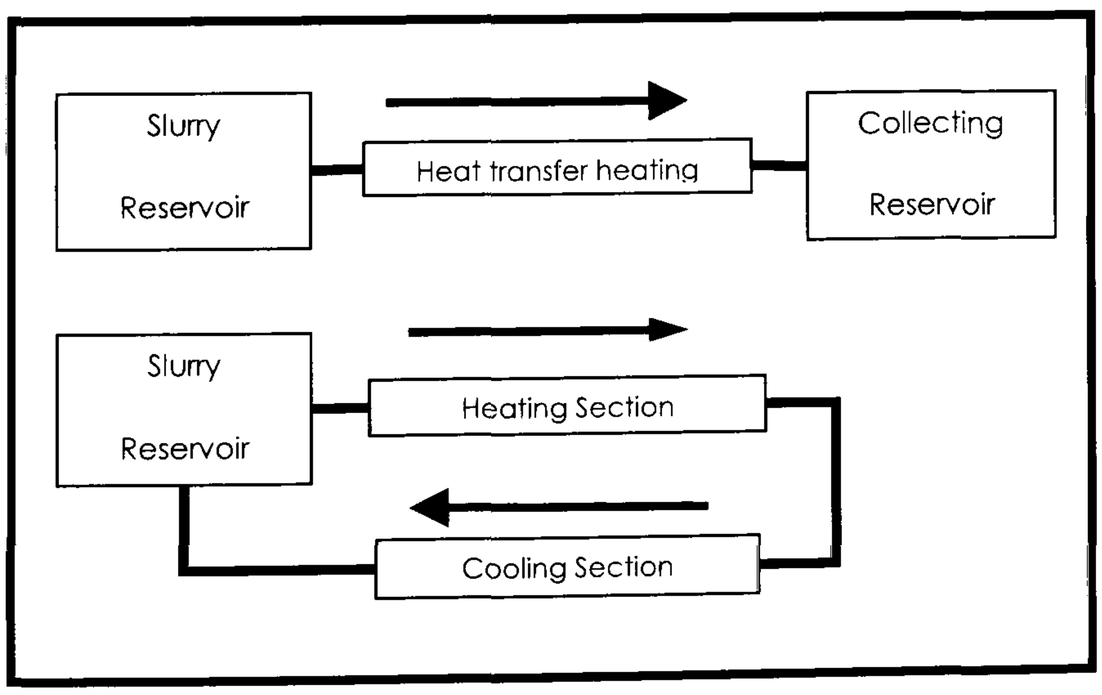

Figure 8.9 a) One way flow rig b) Closed loop rig

8.5 Description of the PV/MicroPCM Slurry System

The proposed experiment is based on incorporating MCPCM slurry within a PV system. The system works similar with chapter 4 but instead of water microPCM slurry is used. The PCM in microcapsules was selected to melt/freeze at temperatures near the characteristic temperature of the PV (25 °C). The system containing the MCPCM slurry is linked to a piping system that runs through a continuous loop. It was anticipated that a pump would be needed to circulate the fluid mixture to increase the extraction of heat from the panel into the thermal storage unit.

8.5.1 Experimental apparatus and method

Two microencapsulated PCM produced by CIBA with a melt temperature of 26 and 33 °C respectively has been analysed for use in a PV/MCPCM Slurry system.

This temperature range for the slurry was chosen as it matches closely with the working temperature of the PV/Water system taken from experiments in chapter 4. The microcapsules suspended in water with a 20% concentration and pumped around heating and cooling circuits using commercially available pumps.

*Figure 8.10, 8.11*and *8.12* illustrates the schematic diagram of the experimental apparatus and the view of the experimental rig. The rig consisted of two closed circuits, the primary and secondary circuit. The primary circuit consisted of a PV panel, a shell and tube copper heat exchanger unit that is incorporated in the back of the PV, a MCPCM slurry tank that the slurry passes for the electric mixer to keep the fluid mixed and homogeneous, a double diaphragm pump and a flow rate transmitter (turbine type). The secondary circuit comprised of a heat exchanger cooling fan, a pump and a variable flow meter. These two circuits were connected with a heat exchanger as can be seen in *Figure 8.11*.

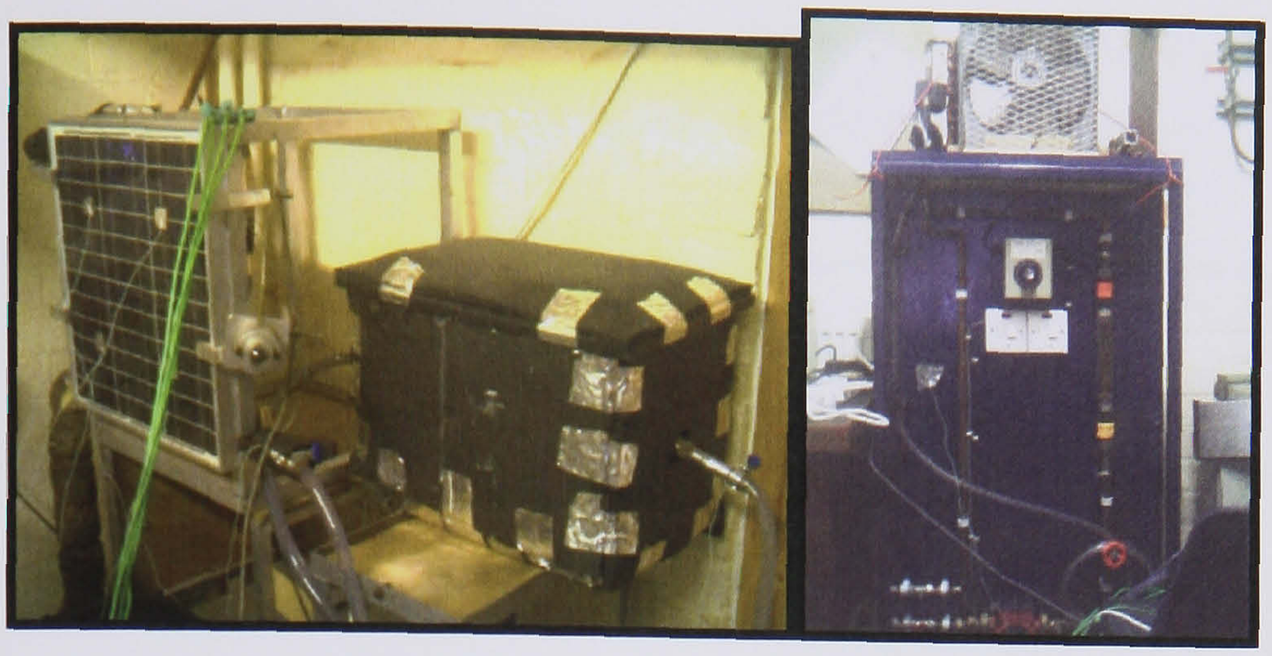

Figure 8.10 Left – Primary Circuit, Right – Secondary Circuit

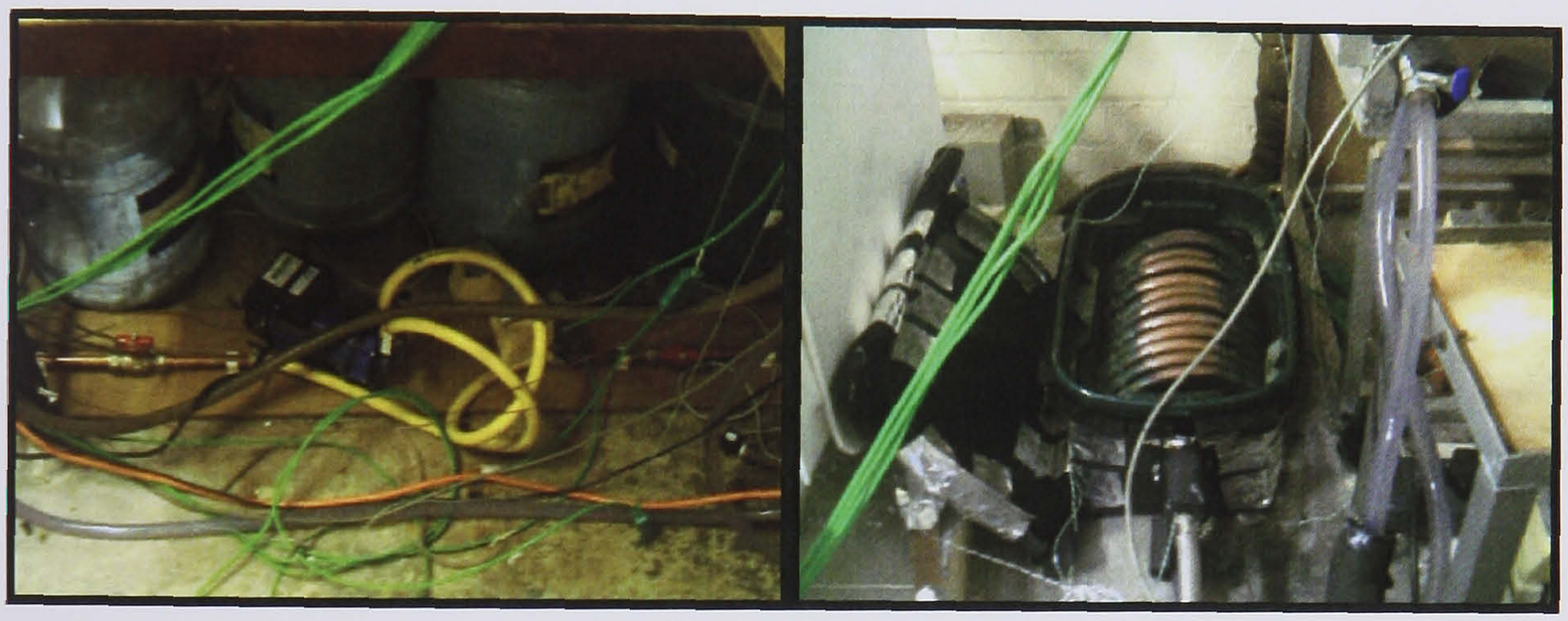

Figure 8.11 Left – Pump of Primary Circuit, Right – Heat Exchanger Unit connecting Primary and Secondary circuit

The temperatures of the working fluid at the inlet and outlet of the PV/MCPCM panel, heat exchanger and MCPCM tank were monitored using the K-type thermocouples attached to the outer wall of the pipes. The temperature of the water (or slurry) inside the tank was monitored using 6 thermocouples which were located at different positions in the tank. The heat exchanger, reservoir and pipes were insulated with a thermal resistance of 0.94 m^2K/W in order to minimise heat loss through the system. A DT500 data logger was connected to the thermocouples and a turbine flow meter to upload information into a PC. All thermocouples were scanned every 5 seconds.

The heat exchanger used in the present study was a shell and coil construction. The coil was 100mm diameter and 300mm length made from 12mm soft copper tubing. The water reservoir had a volume capacity of 15 litres. The slurry had a concentration of

20% due to its relatively high heat capacity and it was more reliable than a 30% or 40% concentration. *Figure 8.12* illustrates an operation cycle of the experiment.

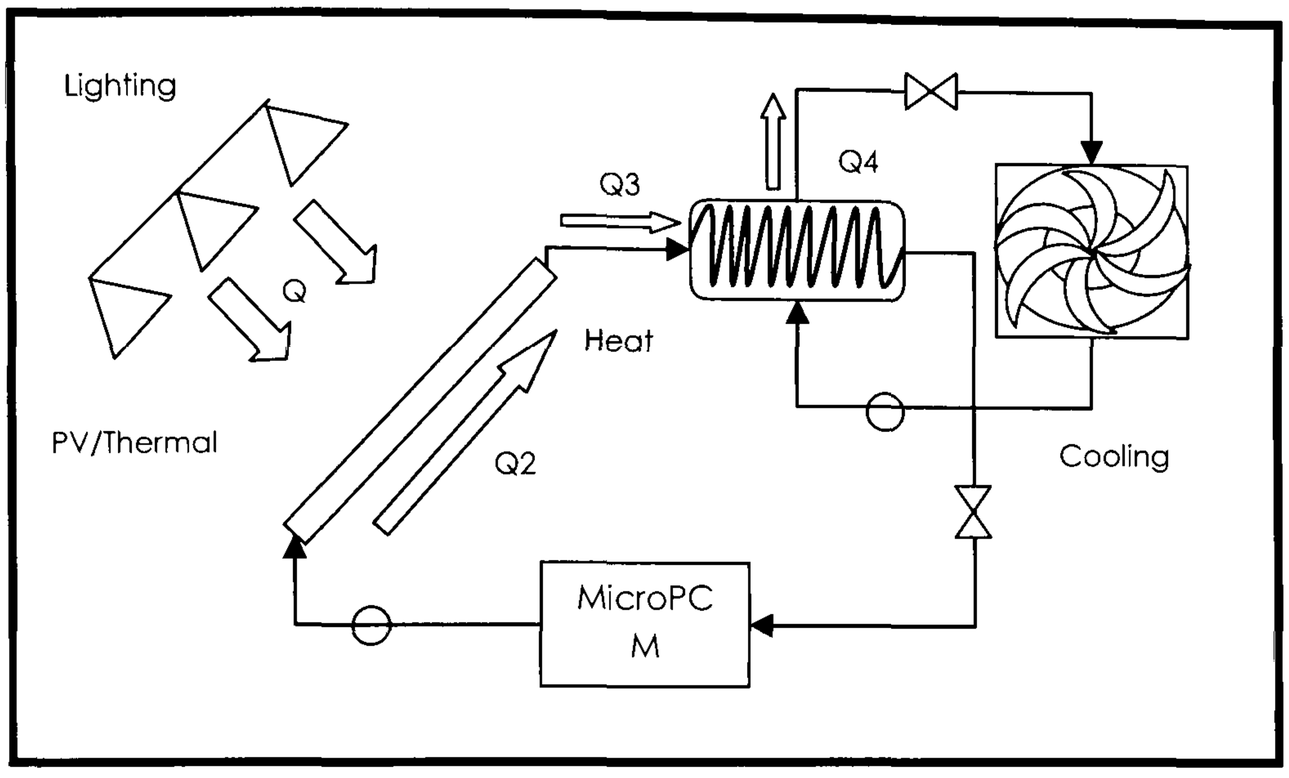

Figure 8.12 Operation cycle of the experiment

Initially the MCPCM was prepared and mixed in the reservoir before being fed into the system. Radiant flux generated from the lights heated the PV panel and that heat was absorbed by the panel. Heat was transferred into the working fluid passing through the pipe attached to the sheet and tube copper plate adhered in the back of the PV. As the temperature of the slurry rose to the phase change temperature the MCPCM particles would melt, which stored heat as latent heat of fusion. The working fluid was then circulated through the heat exchanger to reject heat into the secondary working fluid, which was water. Here, the MCPCM particles solidified. Then the slurry was circulated back into the MCPCM reservoir and again to the PV/MCPCM system and the process started again. Meanwhile the secondary working fluid entered the cooling fan heat exchanger and rejected heat.

As mentioned in the section 2.8.4.2 it is not possible to use the log-mean-temperature-difference (LMTD) method for the MCPCM slurry because neither the thermal capacity nor the local heat transfer coefficient is constant along the flow direction. Thus measurement of the amount of heat (Q_2) absorbed by the MCPCM slurry had to be determined from the amount of heat received by the secondary fluid ($Q_4 = m*cp*\Delta T$). It

was assumed that the heat loss of the system was small and could be neglected, thus $Q_2 = Q_3 = Q_4$

The test procedure for the PV/MCPCM rig was carried out in a number of steps which were:

1. The experiments were operated with the insolation of approximately 600 W/m^2, 800 W/m^2 and 1000 W/m^2 by adjusting the lighting system to obtain the required average irradiation.
2. Set the primary working fluid, MCPCM slurry, to the temperature of 23 °C or 30 °C, which was below the phase change temperature of the two MCPCM sample tested.
3. Circulate the primary working fluid to collect heat from the PV/MCPCM.
4. Adjust the flow rate of the primary working fluid to 0.3 l/min in order to record measureable values cause of the small area of the panel
5. Set the secondary working fluid, pure water, to the temperature of 20 °C.
6. Circulate the secondary working fluid to pick up heat from the primary working fluid in the heat exchanger.
7. Adjust the flow rate of the secondary working fluid to 0.3 l/min (see 4).
8. Running the system until an outlet temperature of the primary working fluid from the solar collector climbed above the PCM melting point.
9. Temperature profiles for each of the major components were taken from thermocouples located on the inlet and outlets to the heat exchanger and tank reservoir. A flow meter was used to record flow rates.

8.5.2 Calibration and verification

Initially, water was used as a primary working fluid to check heat losses of the system. *Table 8.2* illustrates measurement of irradiance (I) and calculation of the rate of heat transfer for Q_2, Q_3 and Q_4 from the PV collector rig using water as the primary working fluid. Heat loss through the system for the primary circuit between Q_2 and Q_3 was shown at around 5 W. Results show good agreement between the rate of heat input provided by the primary working fluid (Q_3) and the rate of heat transfer absorbed by the secondary working fluid (Q_4) with relatively low heat loss of 5 W. Hence it is

acceptable to determine the rate of heat transfer for the primary working fluid by the calculation of the rate of heat transfer from the secondary fluid ($Q_2 = Q_3 = Q_4$). The error for transferring heat from the primary to the secondary circuit is around 5.6% so the results would be underestimated during the experiments.

Table 8.2 Heat input and output of the PV/MCPCM collector system using water as the primary working fluid

Q_1 (W/m^2 or W)	Q_2 (W)	Q_3 (W)	Q_4 (W)
1000 or 163	**89**	**86**	**84**

Discrepancies arise on the one hand from the indirect determination of the latent heat, because the heat losses are calculated with water on the secondary side, as described. The heat losses with slurry have to be lower due to the lower temperatures during the melting process. *Figure 8.13* and *8.14* show PV temperature performance as well the inlet and outlet water temperature. It may be seen that at 1000 W/m^2 the PV front reaches 35 ^{o}C and the back 31 ^{o}C and water temperature difference is around 4 ^{o}C. At *Figure 8.14* we see the calibration that was undertaken in order to estimate the losses of transferring the heat from the primary circuit to the secondary. As can be seen the total power incident on the PV is around 163 W (I) and of that 89 W (Q_2) was extracted from the rear of the PV to water. The water outlet supplies the heat exchanger inlet with 86 W (Q_3) and the heat exchanger extracts 84 W, representing a total loss of around 5 W from the whole system.

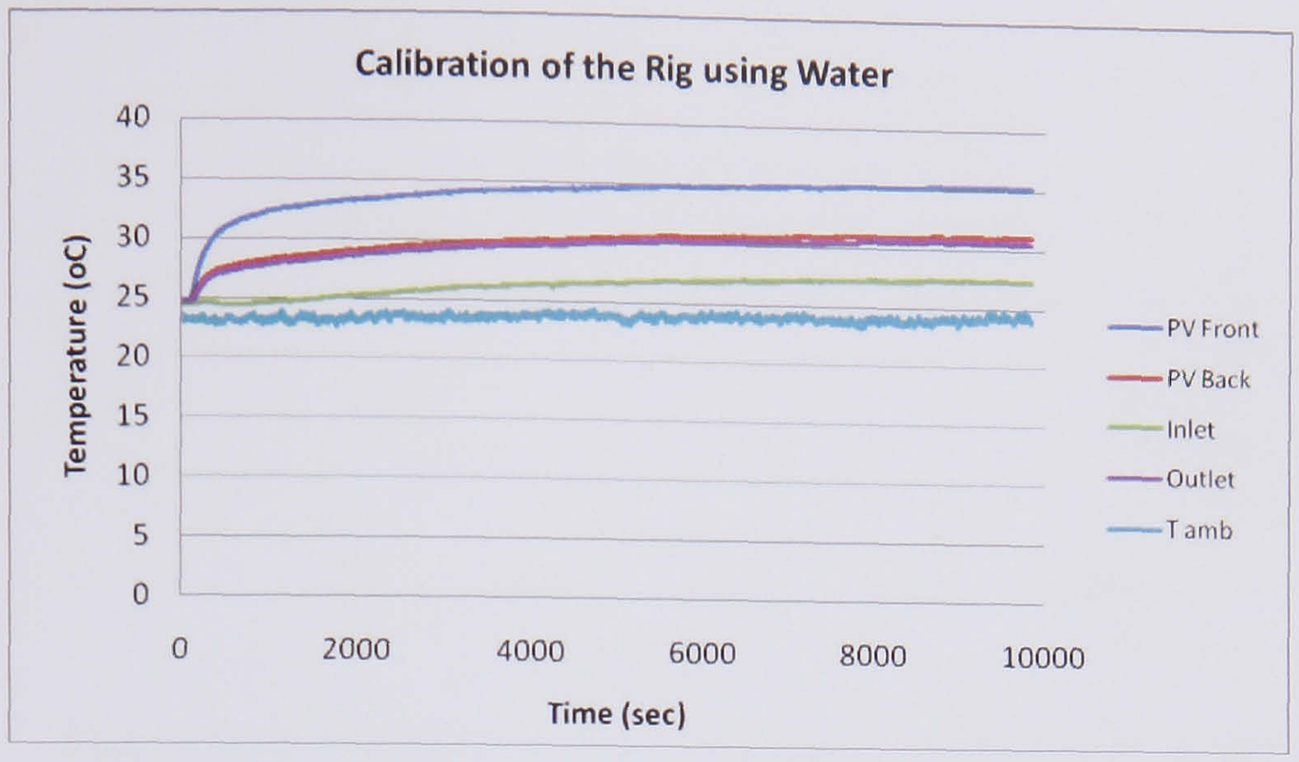

Figure 8.13 Calibration of the PV/Thermal system using Water

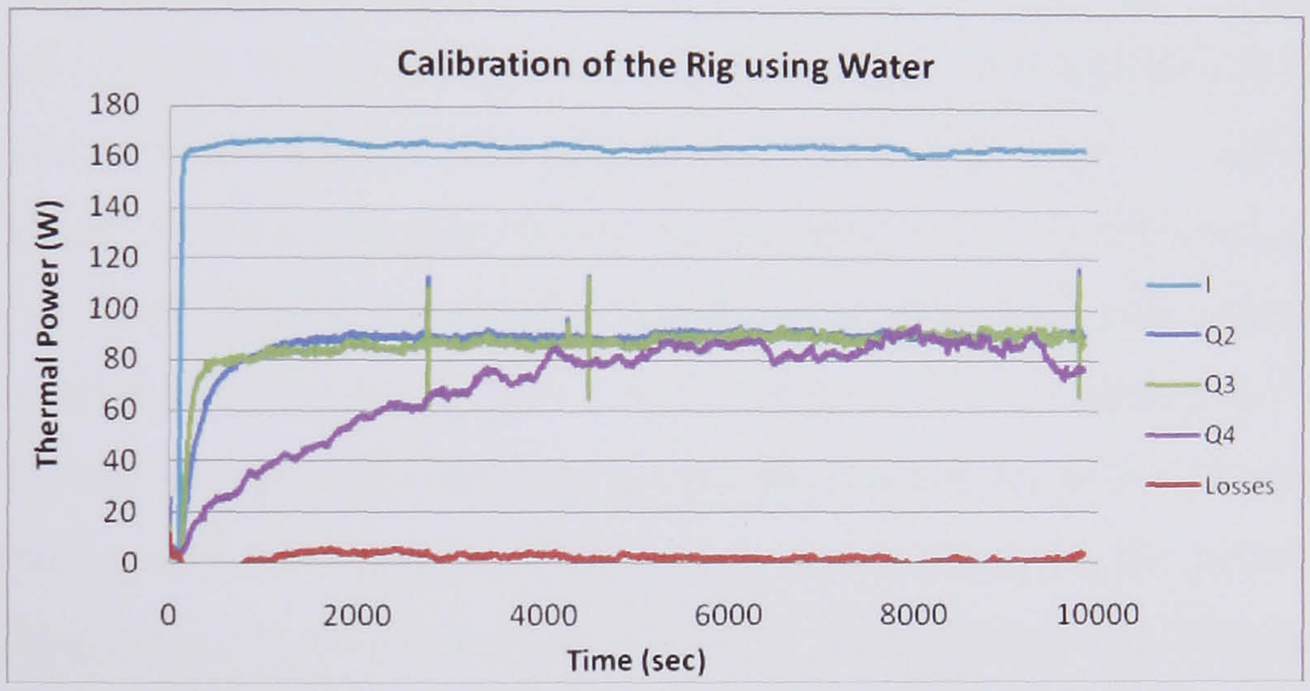

Figure 8.14 Thermal Power Calibration of the PV/Thermal system using Water

8.5.3 Performance of the PV/Thermal collector with the use of MCPCM slurry

After evaluating the loss of transferring the heat from the primary to the secondary circuit for water the experiment was repeated with the phase change slurry. As seen from *Figure 8.15* the PV temperature recorded on the front of the panel is 31 ^{o}C and 27 ^{o}C at the back, however this time the MCPCM temperature difference is 2.8 ^{o}C lower than with water which is caused by the latent heat absorbed near at the melting point of the PCM. To mention that the same set of experiments were performed for 33 ^{o}C MCPCM because the behaviour is similar with the 26 ^{o}C slurry.

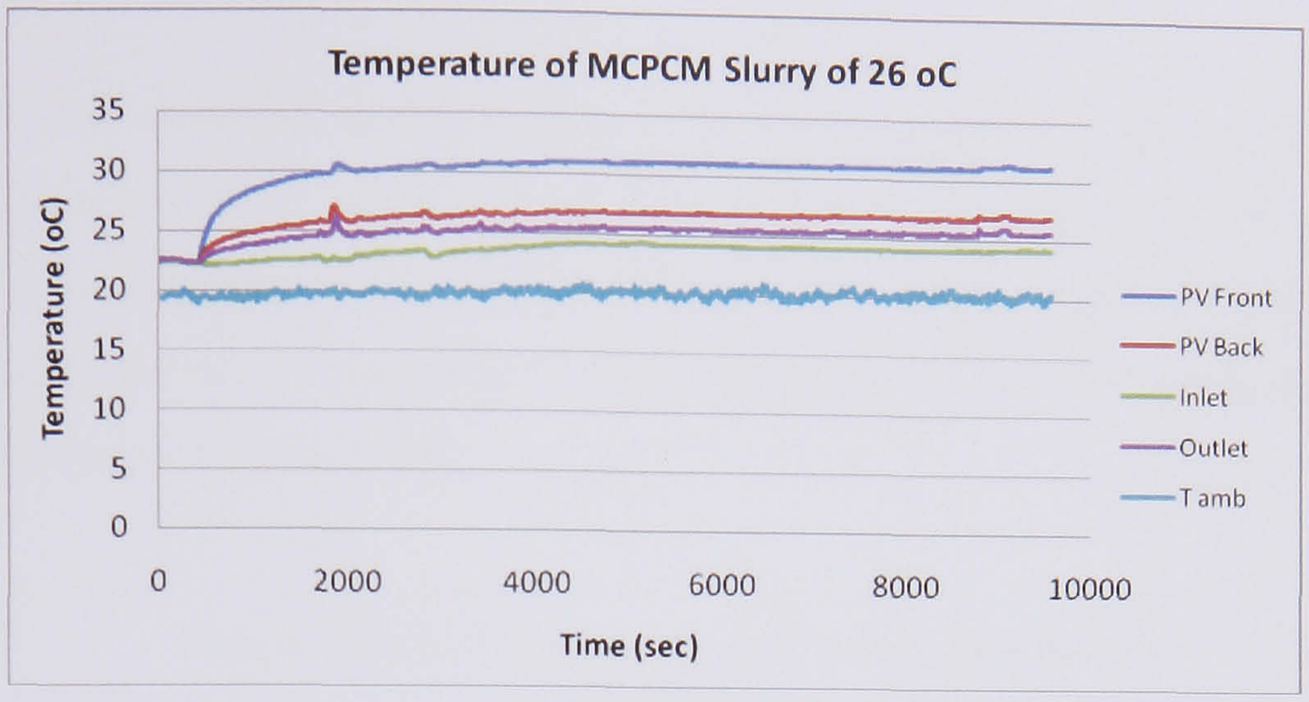

Figure 8.15 PV/MCPCM Slurry Melting Temperature at 26 °C

Figure 8.16 illustrates the temperature difference between the inlet and outlet of the PV/Thermal collector for the primary working fluid using water and 20% MCPCM slurry plotted against irradiance between 600 W/m^2 and 1000 W/m^2. At high irradiance the temperature difference for the working fluid measured between the inlet and outlet of the PV/Thermal collector were higher than those of at low irradiance, which resulted from the increased amount of heat flux. The use of phase change slurry was found to decrease the temperature difference between the inlet and outlet of the collector, because the slurry had greater thermal capacity than water. For example at 1000 W/m^2, the temperature difference between the inlet and outlet of the collector for 20% MCPCM slurry was around 2.8 °C comparing to 4 °C of the pure water.

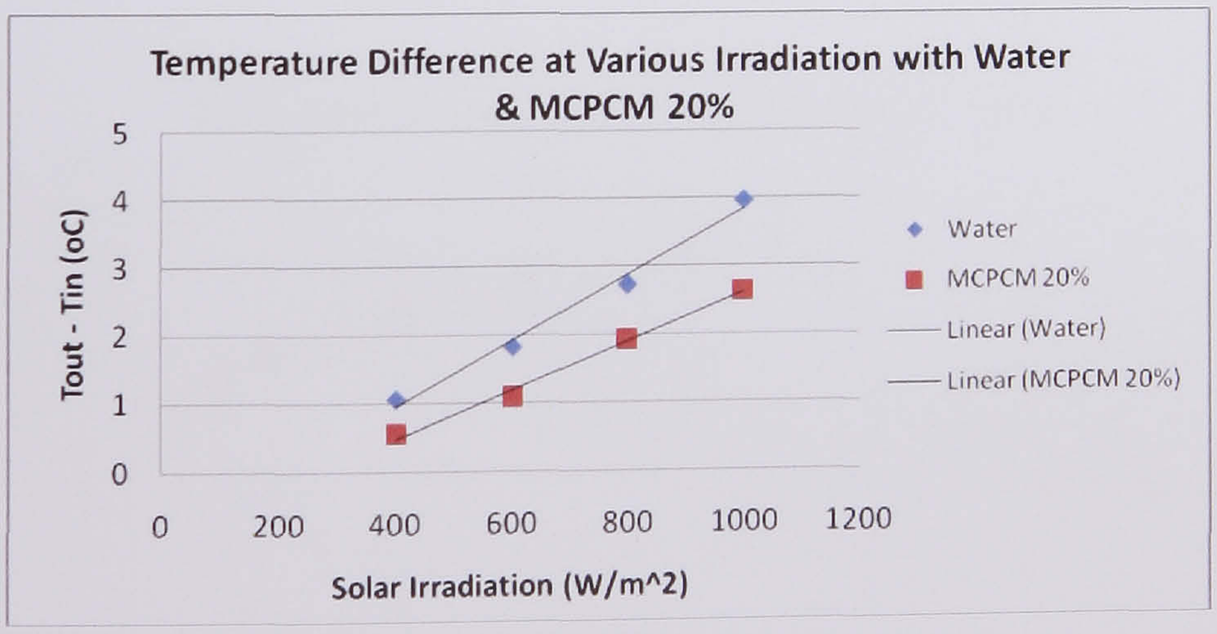

Figure 8.16 Temperature difference at various irradiation between water and MCPCM 20% (26 °C)

Figure 8.17 illustrates the maximum efficiency of the collector as a function of insolation from 600 W/m^2 to 1000 W/m^2. The intensity of irradiance was the main factor dominated the efficiency of the collector. The efficiency of the collector decreased as the insolation decreased. Overall the rate of heat transfer of the MCPCM slurry was higher than that of the pure water.

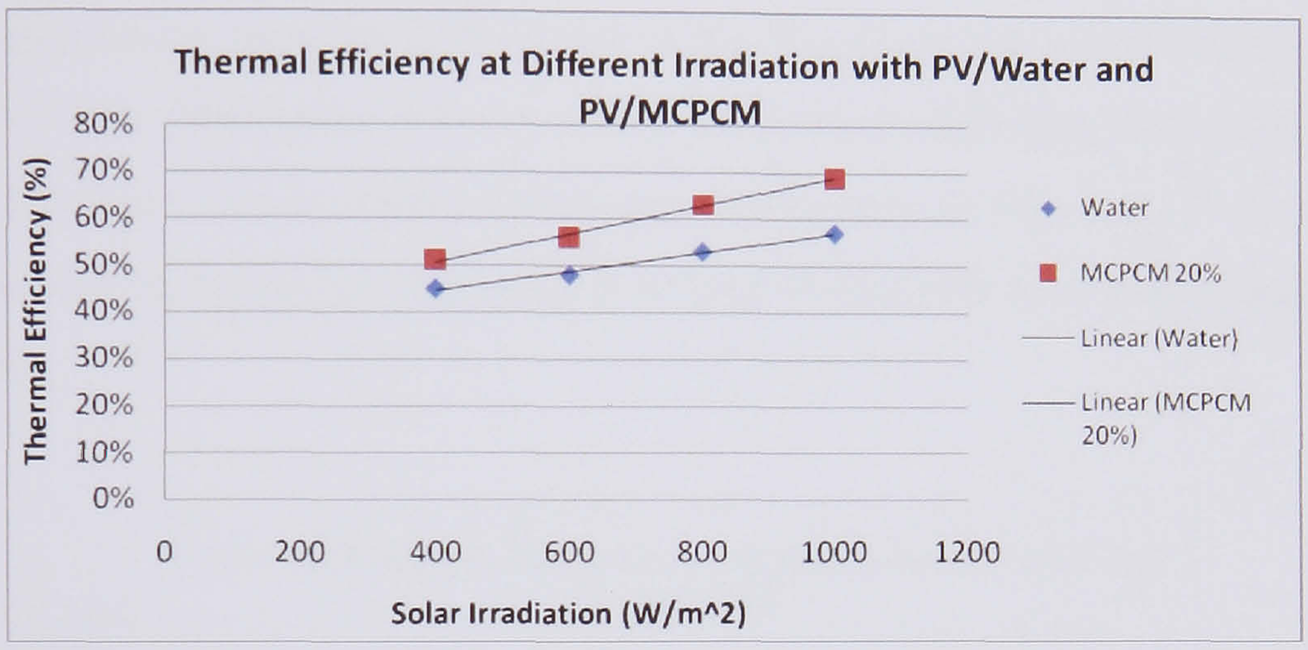

Figure 8.17a Thermal Efficiency of PV/MCPCM system in comparison with water at different irradiations

As Thaicham (2004) mentioned the phase change slurry has higher viscosity than water and so needs more pump power for the same flow rate. As seen in *Figure 8.18* the average increase of power need was 8% when using the MCPCM slurry.

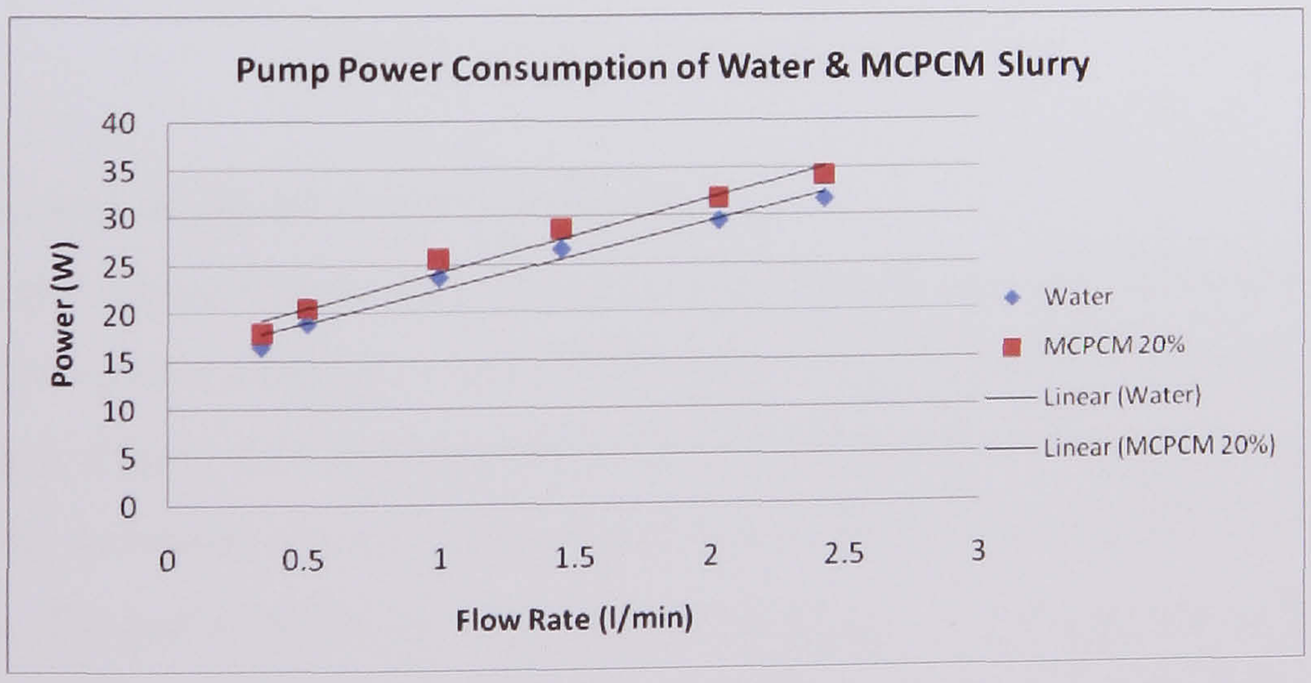

Figure 8.18 Pump Power Consumption of Water & MCPCM Slurry (20% - 26 °C)

To estimate in what degree the increase in pump power consumption affect the performance the additional power consumed was included to estimate the thermal efficiency of the system. The increase of 8% on power need means that the pump consumed 2 W more power than when using just water in the system. Because the 2 W is electrical power and is different in nature with thermal power as discussed in section 4.5.2 an efficiency factor of 0.38 is used to get the thermal power needed for a conventional plant to generate 2 W of electricity. The given amount of thermal power needed is 5.26 W. This value is being subtracted from the thermal power gained from the MCPCM slurry and the thermal efficiency can be seen in *Figure 8.13*. As can be seen the reduction in thermal efficiency is around 4% but still more than using water in the system.

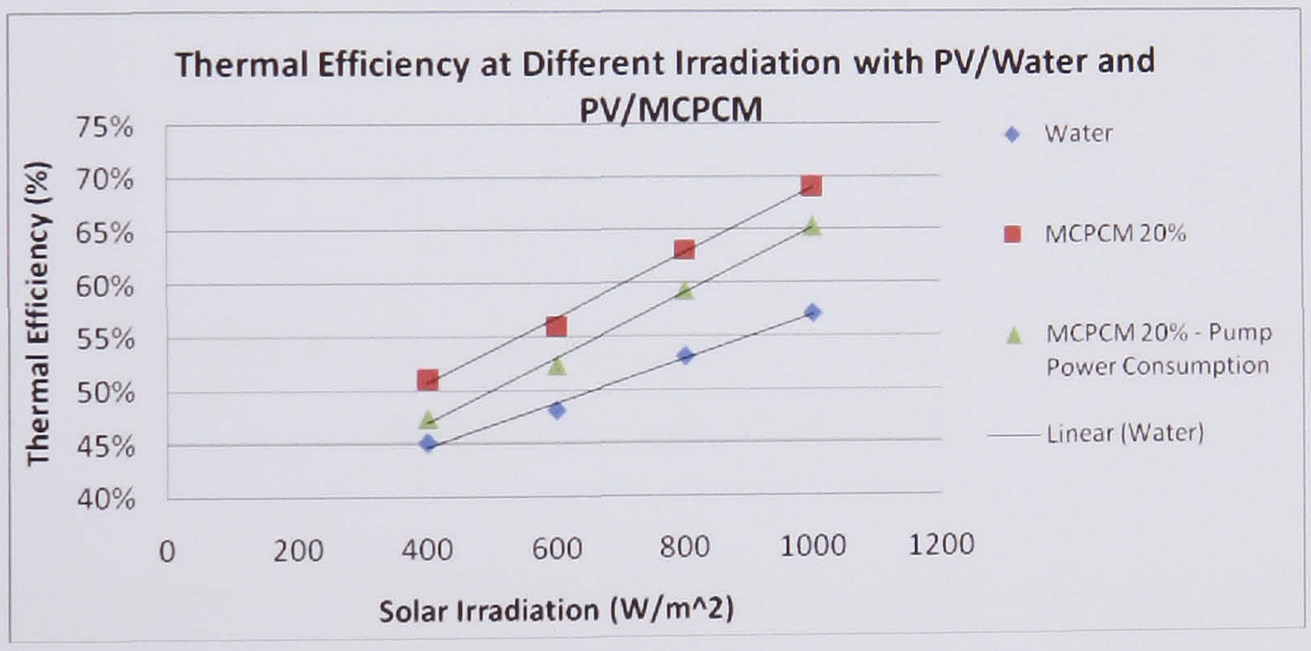

Figure 8.17b MCPCM Slurry Thermal Efficiency after subtracting the additional pump power consumption (20% - 26 °C)

8.5.4 Efficiency of the PV/MCPCM collector

The next sets of experiments were to find the thermal and electrical efficiencies of the PV/MCPCM system using 26 °C and 33 °C MCPCMs of different slurry inlet temperatures. *Figure 8.19* illustrates the efficiency of the PV/MCPCM collector plotted based on the secondary circuit against that for the water system at 1000 W/m^2 irradiation. The use of MCPCM slurry was found to improve the efficiency of the collector over the single phase working fluid. As discussed in section 2.8.3 the slurries

have higher heat capacity and observed near the melting point of the PCM. For example at 1000 W/m^2 the efficiency of the collector with MCPCM (26 °C slurry was shown at around 69% compared with 57% for pure water, an improvement of 21%. The same can be observed with the 33 °C slurry. Near the melting temperature the efficiency improvement is around 27% (69% for MCPCM and 54% for water). When the temperature range of inlet and outlet was out of the melting range of the PCM materials, then the thermal efficiency was very close to that of water (see blue circle in *Figure 8.19*).

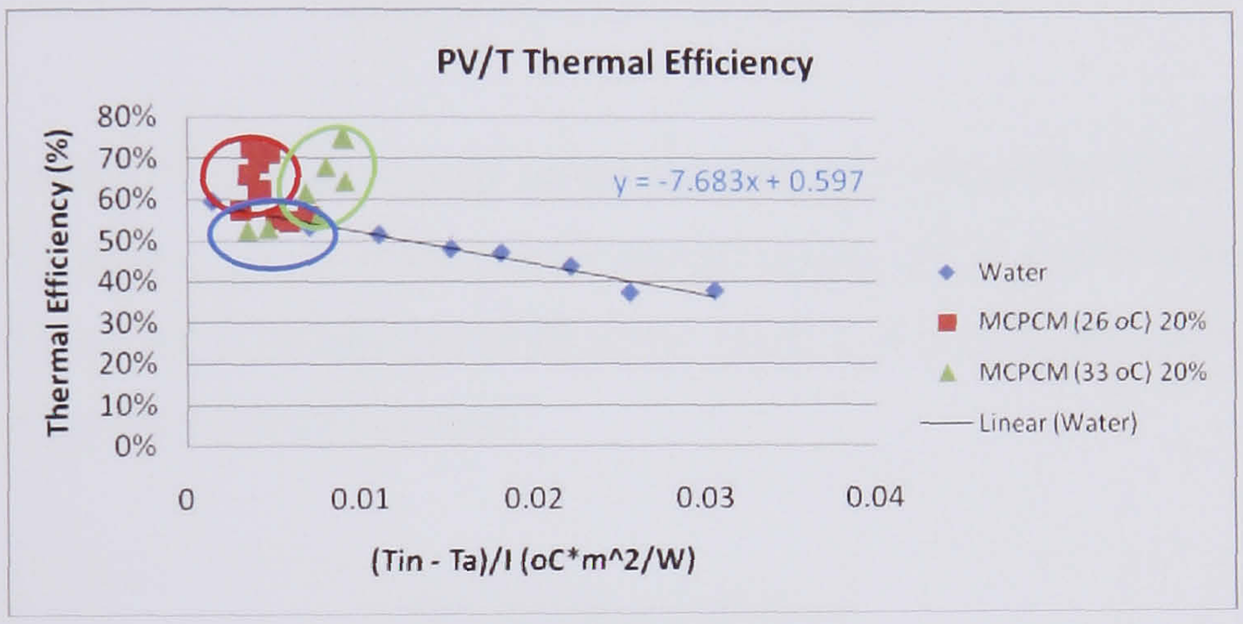

Figure 8.19 PV/MCPCM Thermal Efficiency in comparison with water and MCPCM slurry (26 oC and 33 oC PCM)

To maximise the benefit from the latent heat of fusion of this phase change slurry, it was decided that an average slurry inlet temperature of around the range of 22 °C to 24 °C and 29 °C to 31 °C respectively be maintained.

As far as the electrical efficiency is concerned it may be seen that there is no variation in comparison with water as seen in *Figure 8.20*.

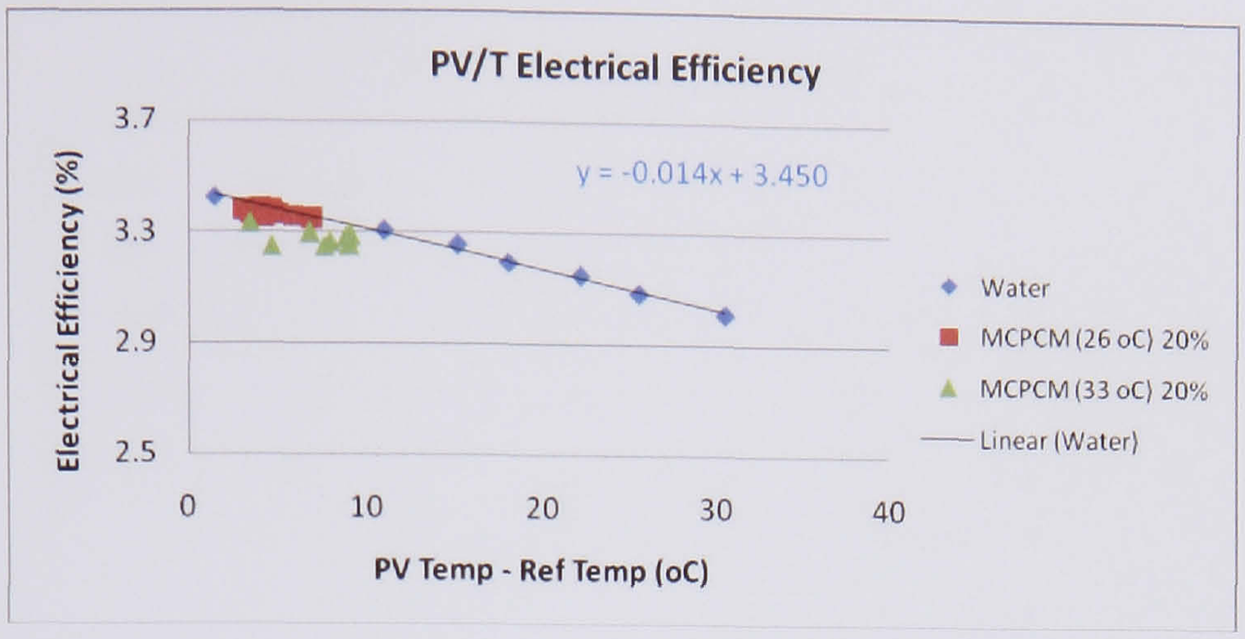

Figure 8.20 PV/MCPCM Electrical Efficiency in comparison with water and MCPCM slurry (26 °C and 33 °C PCM)

Figure 8.21 and *8.22* give as the total energy efficiency by adding the thermal and electrical efficiency of the systems and the energy saving efficiency. Both indexes give as higher efficiencies in comparison with water because of the increase in thermal efficiency of the PV/MCPCM system.

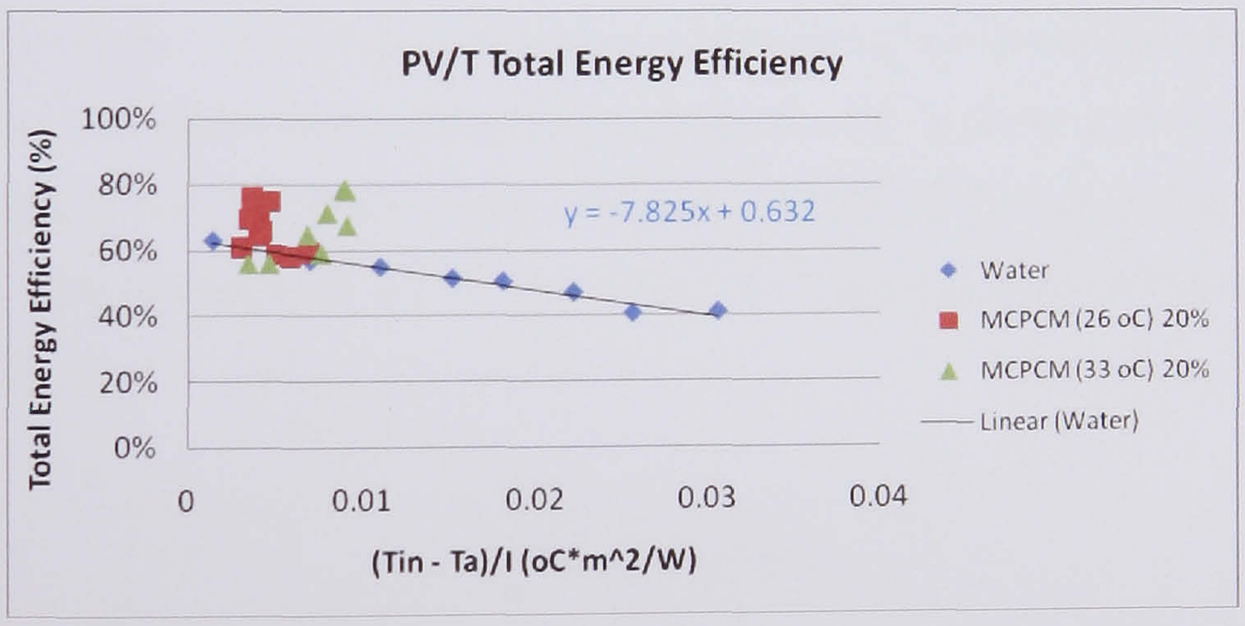

Figure 8.21 PV/MCPCM Total Energy Efficiency in comparison with water and MCPCM slurry (26 °C and 33 °C PCM)

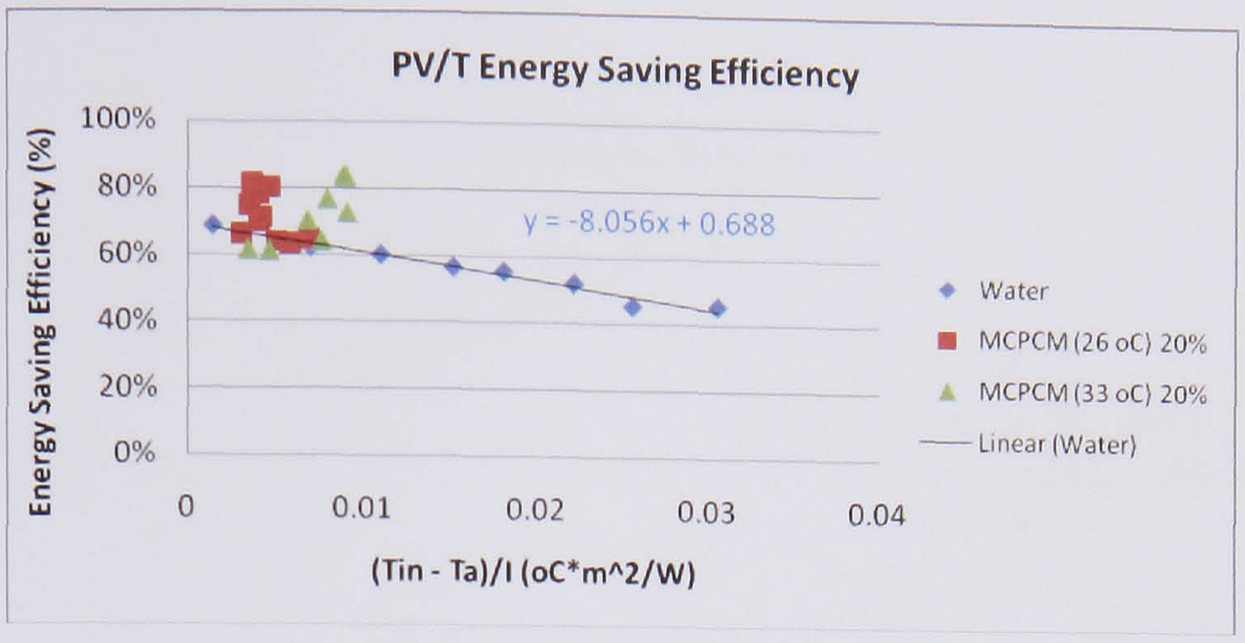

Figure 8.22 PV/MCPCM Energy Saving Efficiency in comparison with water and MCPCM slurry (26 oC and 33 oC PCM)

The improvement in the heat transfer of the PV/MCPCM system can be also seen by comparing the exergy analysis of PV/Water system. As seen in *Figure 8.23* and *Figure 8.24* the exergy efficiency of the MCPCM with melting temperature at 26 °C is 16% in comparison with 14% of water. The same with MCPCM with melting range at 33 °C with an exergy efficiency of 21.8% in comparison with 19% of water. In both materials a 15% improvement is observed. To mention that the comparison between the water and the MPCM system concerns the temperature range close to melting point and not the optimum point of water. It could be possible with a MCPCM having a melting temperature near the range of $\Delta T/G = 0.022$ (42 °C) to give as better efficiency (see *Figure 8.24*).

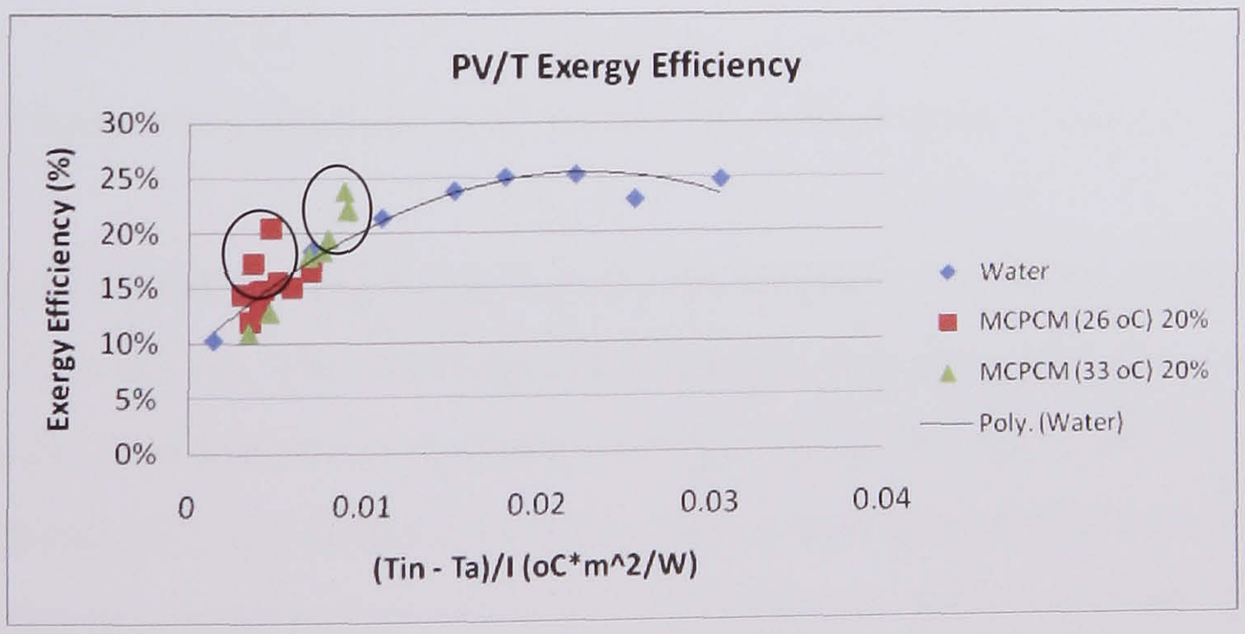

Figure 8.23 PV/MCPCM Exergy Efficiency in comparison with water and MCPCM slurry (26 °C and 33 °C PCM)

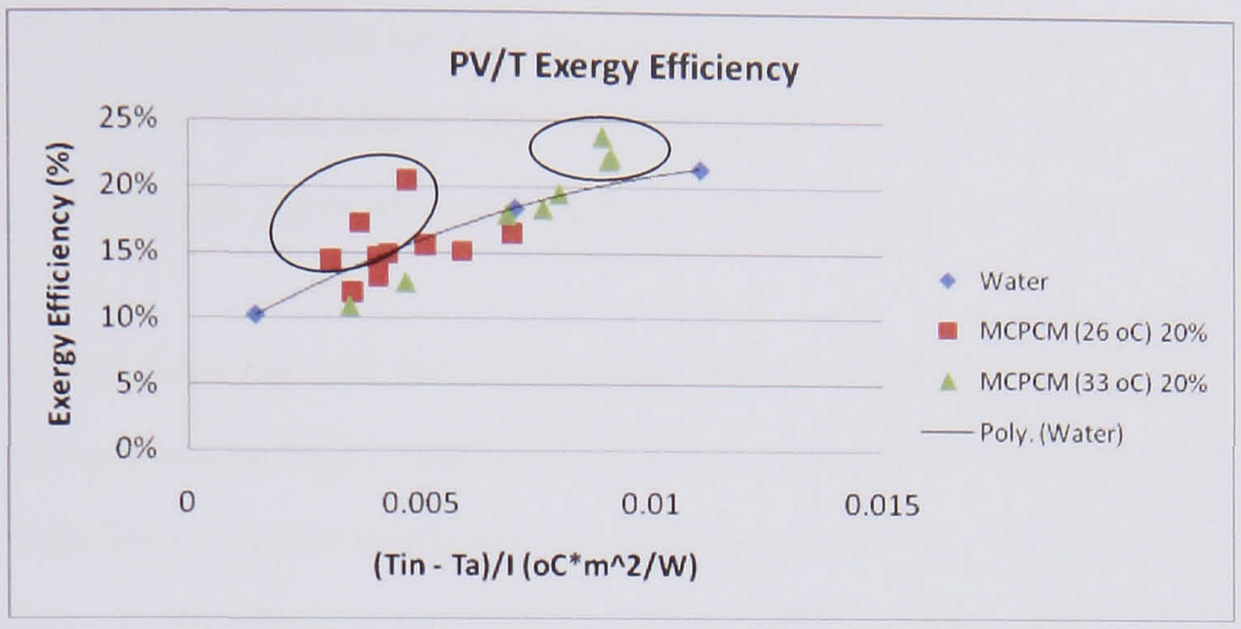

Figure 8.24 PV/PCM Exergy Efficiency in comparison with water and MCPCM (26 oC and 33 oC PCM) in ΔT/G range from 0.001 to 0.011 (21 °C to 35 °C)

8.6 Conclusion

When water was used as the heat transfer fluid in the PV/Thermal system a flow rate of 0.3 l/min was required to provide a water temperature difference of 4 °C. Fluid flow rate above this tended to flow through the panels without a measurable rise in temperature across the inlet and outlets of the PV panel. At this rate water was able to extract and remove energy gains and maintain PV temperature at 32 °C.

A 20% concentration PCM slurry was substituted for the water in the circuit. It was able to maintain a temperature difference around 2.8 °C with a flow rate of 0.3 l/min.

The specific heat of the slurry when the PCM material is solid or fully melted is near to that of water (4.18 kJ/kg*K). By running the circuit with an inlet temperature to the panels of around 23 °C and an outlet temperature of around 26 °C, an average specific heat for the slurry was calculated to be 9 kJ/kg*K, with at times a value of 11–12 kJ/kg*K.

When the fluid is near melting range then the heat capacity increases and improves the efficiency of the system. The calculated fluid specific heat capacity fell to near that of water when the flow and return temperature of the slurry was above 26 °C. A similar specific heat capacity was determined if the slurry return temperature was below 25 °C. A slurry return flow temperature below 26 °C would have led to very little, if any, of the PCM material in the microcapsules melting, with no latent energy absorption at phase

change. As a result the system was optimised so that the return flow temperature was around 25.5 °C. The slurry was cooled no lower than 23 °C to maximise solidification efficiency of the PCM in the slurry. On inspection there were no signs of deposition of the microcapsules in the pipes at bends or around the valves, and no degradation of the slurry.

The data obtained from the test facility has proven that a concentration of 20% microcapsules containing PCM can be used as the heat transfer fluid in a PV/Thermal application with the collector working mainly near the melting temperature of the MCPCM slurry. A drawback is the need for more pump power with using MCPCM slurry instead of water. Because at the same flow rate the MCPCM thermal efficiency improves around 21% a lower flow rate could be used and keep the thermal efficiency at the level of water. With this way a significant amount of energy could be saved. (i.e. 57% - 69% at 0.3 l/min, make it 57% - 57% at 0.2 l/min). Another important advantage of using PCM in a solar heating system is that the store/system temperature does not increase at the same rate as in a water store. The solar collectors can therefore operate at lower temperatures for an extended period of time, thus increasing the total amount of solar energy collected by the system. This system except the size reduction that can offer is suitable for cases that work with a narrowrer temperature range and for a system working around the phase transition temperature of the chosen PCM and for the specific application needed.

CHAPTER 9: PHOTOVOLTAIC/THERMAL SYSTEMS TECHNICAL, ECONOMIC AND ENVIRONMENTAL COMPARISON

9.1 Introduction

From previous chapters the performance of five different PV/Thermal systems was determined. As was mentioned in the literature review PV/Thermal systems with water and air have been evaluated by other investigations and the results from experiments carried out in this thesis agreed very well with the researchers' work. To evaluate if the three new PV/Thermal systems have the potential to be useful alternative technologies, for a hybrid PV and Thermal collector panel, a comparison was carried out. This comparison is based on the technical, economic and environmental aspects of the five systems. Thermal and electrical efficiency were compared in order to evaluate each of the PV/Thermal system.

After comparing their technical performance an economic comparison was carried out. For each of the five systems an attempt was made to estimate the cost of the different components required in order to build these hybrid systems. A simple payback method was used for different PV/Thermal surface areas (1, 10, 50, 100 and 140 m^2) and as a PV panel an assumption made that an amorphous silicon panel was used. The difference in comparison with the polycrystalline panel used in the experiments is the lower efficiency and degradation that amorphous panels face. To estimate the annual energy production a PV system using thin film panels and based in the Sustainable Research Building was monitored for two years and these values was used for the analysis.

From the PV/Thermal system's electrical and thermal performance it was possible to evaluate the quality of CO_2 emissions that can be saved. A Life Cycle Energy Analysis (LCEA) was also carried out for each system in order to evaluate how much energy is consumed in order to build the system and to estimate the energy payback period.

9.2 PV/Thermal Systems - Technical Comparison

When considering the design of a PV/Thermal collector, determination of the performance of the electrical and thermal output from the system allows the specific system to be evaluated. To mention that the comparison is not to indicate if the new

PV/T systems are better than PV/T with water and air but to assess if can be concerned as alternative technologies for use.

9.2.1 Total Energy Efficiency

The first law of thermodynamics tells us that work and heat are both forms of energy. Thus a simplistic first law approach is to consider them to be of equal value. A number of studies on PV/Thermal collectors have used a simple one-to-one energy approach to express the combined efficiency of the electrical and thermal output. (Sharan and Kandpal, 1992; Hegazy, 2000; Sopian et al., 1996, 1997; Abdalla and Wilson, 2001).

Figure 9.1 and *9.2* show the electrical and thermal efficiency of the PV/T systems. As can also be seen from *Table 9.1* the system integrating PCM to the rear of the PV module achieves higher electrical efficiency and the lowest heat loss coefficient and hence highest thermal efficiency of all the other systems as may be seen in *Table 9.1*. The hybrid systems incorporating heat pipes can be compared very well with the PV/Water system and have the potential to be competitive technology if heat loss coefficient issues are being resolved. PV/MCPCM system for very low grade temperature applications can provide thermal efficiencies that reach 70% and their electrical efficiency is equal with the one of PV/Water system. Last to mention PV/Air system that as discussed in section 5.2.1 cause of the lower thermal conductivity and heat capacity give the lowest thermal and electrical efficiencies. However for applications that need air heating achieves high efficiencies.

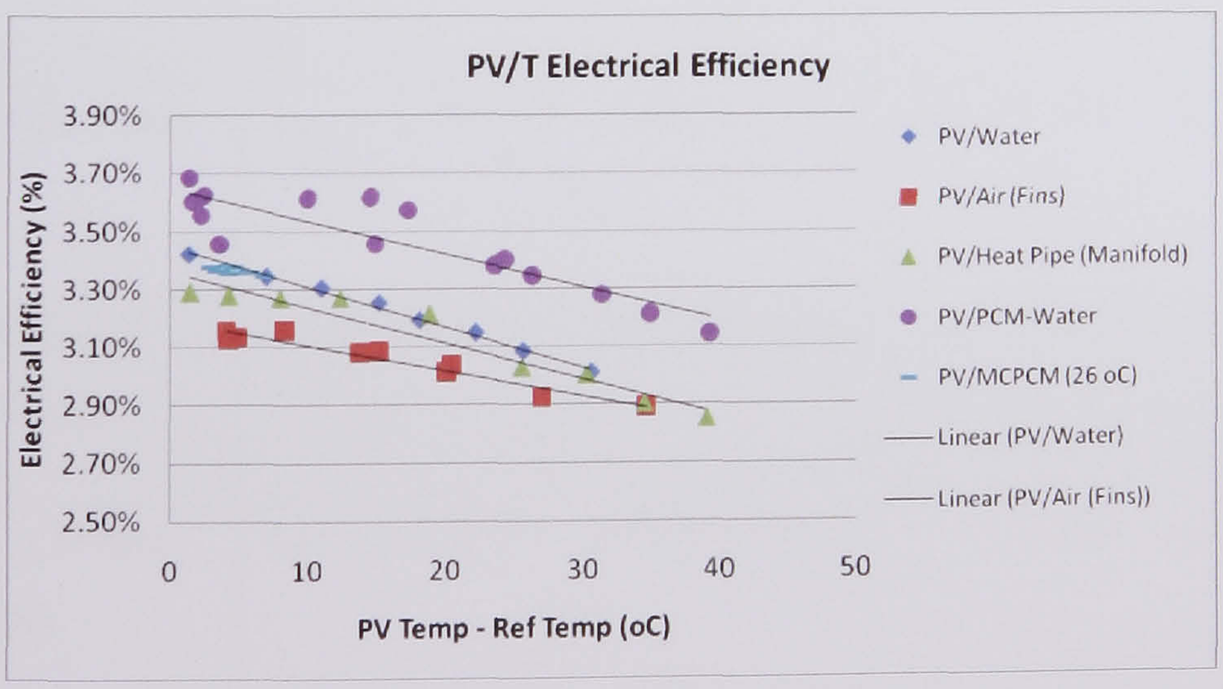

Figure 9.1 PV/Thermal Systems - Electrical Efficiency Comparison

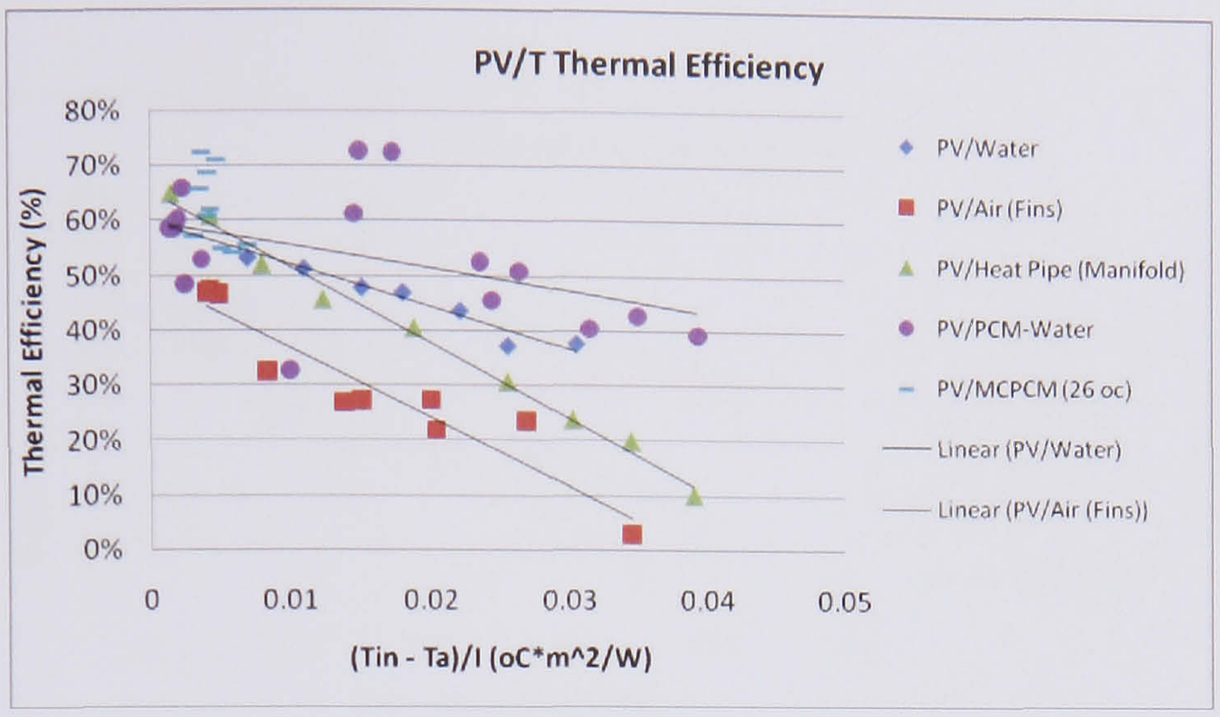

Figure 9.2 PV/Thermal Systems - Thermal Efficiency Comparison

Table 9.1 Electrical and Thermal Efficiency Equations of PV/T Systems

PV/Thermal Systems	PV/T Electrical Efficiency Equations	PV/T Thermal Efficiency Equations
PV	$n_{ele} = 3.5781*(1 - 0.00461*(T_{pv} - 25))$	-
PV Insulated	$n_{ele} = 3.4396*(1 - 0.00488*(T_{pv} - 25))$	-
PV/Water	$n_{ele} = 3.636*(1 - 0.00385*(T_{pv} - 25))$	$n_{th} = 0.597 - 7.683*(\Delta T/G)$
PV/Air (With Fins)	$n_{ele} = 3.193*(1 - 0.0025*(T_{pv} - 25))$	$n_{th} = 0.496 - 12.65*(\Delta T/G)$
PV/Heat Pipes (Manifold)	$n_{ele} = 3.363*(1 - 0.00356*(T_{pv} - 25))$	$n_{th} = 0.654 - 13.82*(\Delta T/G)$
PV/PCM – Water (A28)	$n_{ele} = 3.651*(1 - 0.00301*(T_{pv} - 25))$	$n_{th} = 0.598 - 4.138*(\Delta T/G)$
PV/MCPCM (26 °C)	$n_{ele} = 3.369$	$n_{th} = 0.69$

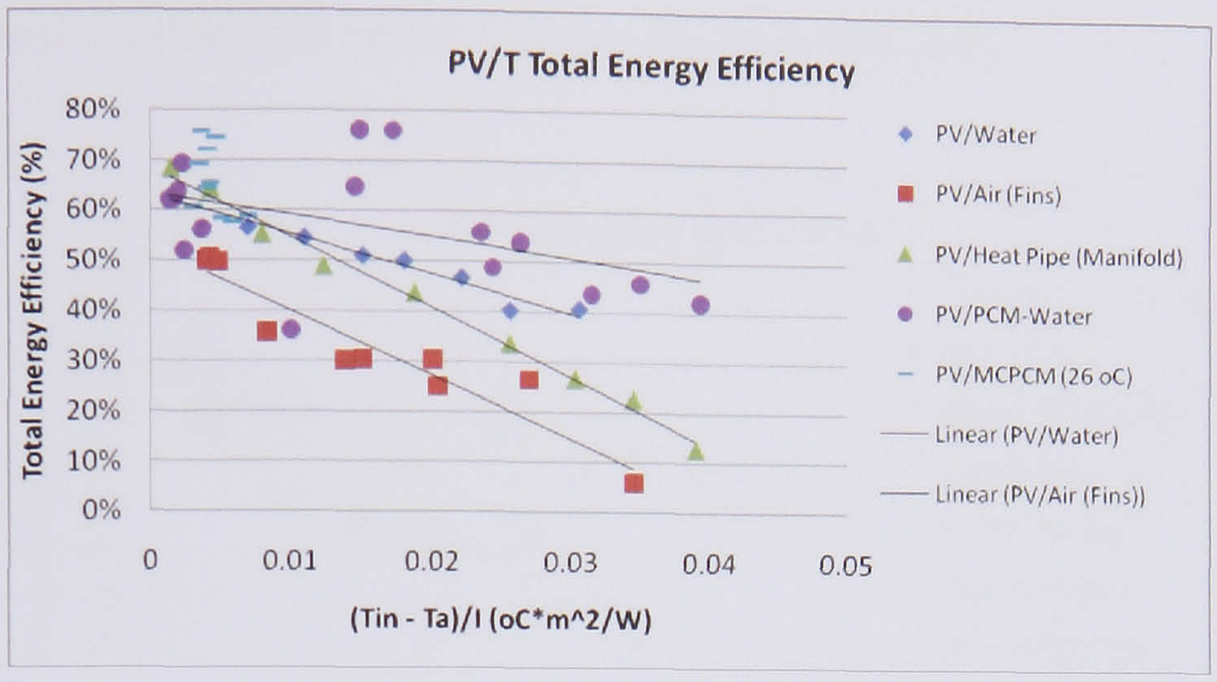

Figure 9.3 PV/Thermal Systems - Total Energy Efficiency

The same discussion can be provided from *Figure 9.3* that total energy efficiency of the systems is presented. A general conclusion that can be drawn is that thermal efficiency contributes around 94% to the total efficiency of the systems. However both the second law of thermodynamics and common sense tell us that electricity is not the same as heat, and not equally useful.

9.2.2 Primary Energy Saving Efficiency

To improve on the simple first law approach, one method that has been proposed is to use an energy efficiency ratio derived from conventional power plants to give a weighted overall efficiency measure (Huang et al., 2001). In this approach, a so called primary-energy saving efficiency is defined by equation (4.11) to give a favourable weighting to the electrical output. It has been found by Huang (1993) that the daily efficiency for most solar water heaters with cold-water start is around 50%. This value will provide a criterion for checking the overall performance of a PV/Thermal system. Therefore the systems should exceed this value in order to compete with a solar hot water system. *Figure 9.4* and *Table 9.2* give as the energy saving efficiency of PV/T systems. As may be seen all systems exceed the 50% thus could be competitive alternative choices for thermal heating. The same pattern is observed as in section 9.2.1. PV/PCM-Water system has the highest performance for the whole range of ($\Delta T/G$)

values and the lowest heat losses. PV/Water and PV/Heat pipe system follow with PV/Air perform less than the others but exceeding the 50% limit.

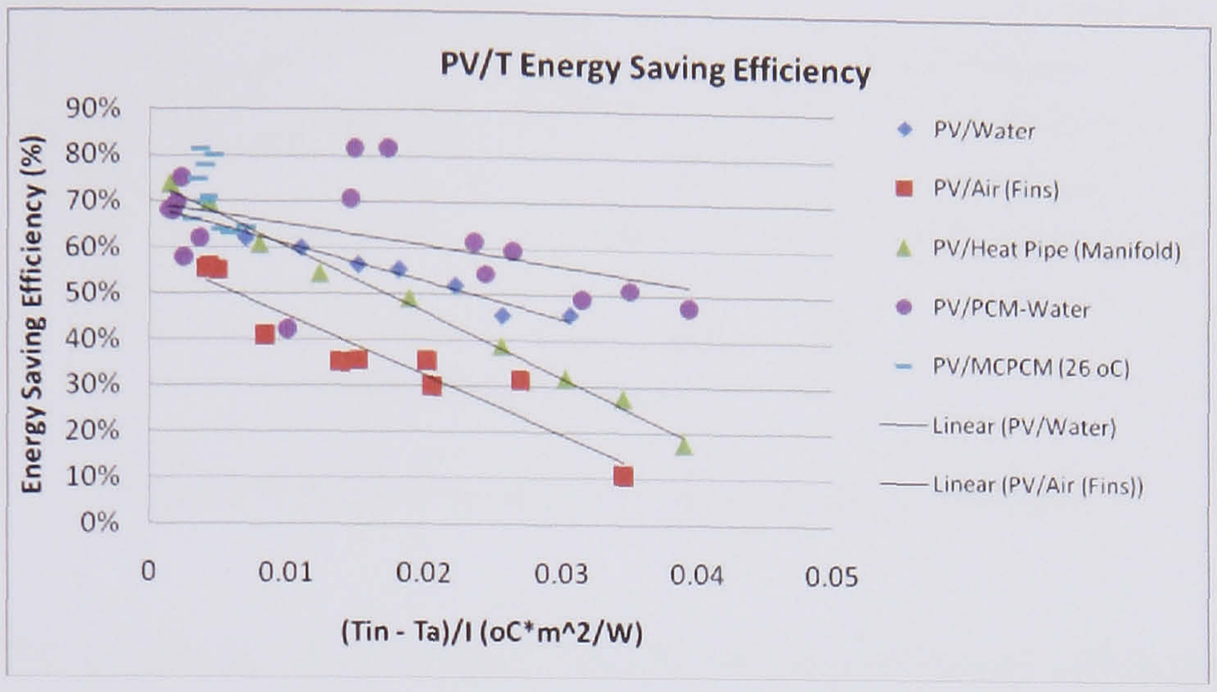

Figure 9.4 PV/Thermal Systems - Energy Saving Efficiency Comparison

9.2.3 Exergy Efficiency

The second law of thermodynamics addresses the fundamental limits that apply in the efficiency of conversion of heat to work. The predictions and formulations of the second law all follow from the simple observation that heat flows naturally from hot to cold objects but never the other way. The second law leads to a quantification of the relative value of different energy streams via exergy analysis. Exergy is defined as the maximum theoretical useful work obtainable from a system as it returns to equilibrium with the environment. Researchers in Japan have applied a similar idea to annual results from a flat plate PV/Thermal collector (Takashima et al., 1994; Fujisawa and Tani, 1997). *Figure 9.5* and *Table 9.2* give as the exergy efficiency of the PV/T systems. As can be seen the PV/PCM system has the highest exergy efficiency (34%) when inlet temperature is around 45 ^{o}C (or $\Delta T/G = 0.025$) and PV/Heat pipe is comparable with the PV/Water system with optimum exergy at 24% at T_{inlet} 40 ^{o}C. On the other hand PV/Air systems exergy reaches only 16% at around 38 ^{o}C as PV/MCPCM but the later is in the range of 0.005 ($\Delta T/G$) or temperature inlet around 25 ^{o}C.

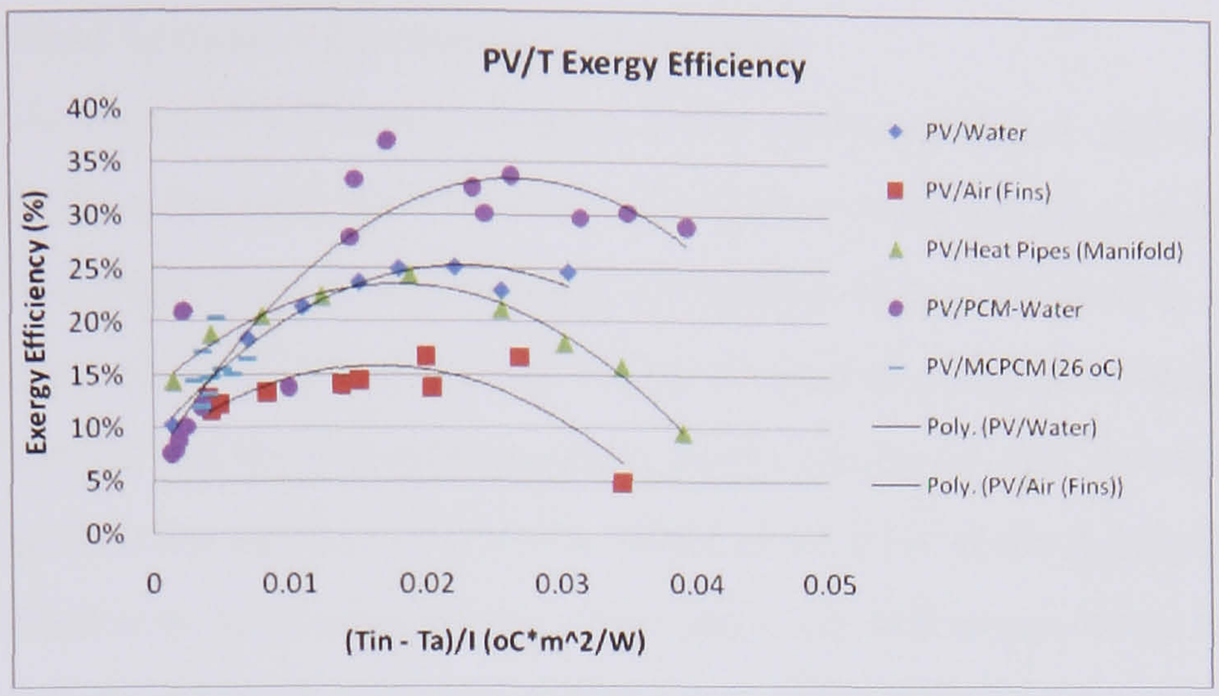

Figure 9.5 PV/Thermal Systems - Exergy Efficiency

Table 9.2 PV/T systems - total energy, energy saving and exergy efficiency equations

PV/Thermal Systems	PV/T Total Energy Efficiency Equations	PV/T Energy Saving Efficiency Equations	PV/T Exergy Peak Efficiency
PV/Water	$n_{tot} = 0.632 - 7.825*(\Delta T/G)$	$n_{pes} = 0.688 - 8.056*(\Delta T/G)$	$n_{exe} = 25\%$
PV/Air (With Fins)	$n_{tot} = 0.528 - 12.74*(\Delta T/G)$	$n_{pes} = 0.58 - 12.89*(\Delta T/G)$	$n_{exe} = 16\%$
PV/Heat Pipe (Manifold)	$n_{tot} = 0.688 - 13.94*(\Delta T/G)$	$n_{pes} = 0.743 - 14.14*(\Delta T/G)$	$n_{exe} = 24\%$
PV/PCM – Water (A28)	$n_{tot} = 0.635 - 4.25*(\Delta T/G)$	$n_{pes} = 0.694 - 4.44*(\Delta T/G)$	$n_{exe} = 34\%$
PV/MCPCM (26 °C)	$n_{tot} = 0.729$	$n_{pes} = 0.784$	$n_{exe} = 16\%$

9.3 PV/Thermal Systems - Economic Comparison

To evaluate the cost of PV/Thermal systems it was necessary first to choose a PV panel upon which to base the analysis. There are a number of different types of photovoltaic panels. The two main types available are (1) crystalline silicon PV and (2) amorphous silicon PV. Crystalline PV panels can be further divided into mono-crystalline and polycrystalline PV and the amorphous silicon panels can be divided into multi-junction and single junction amorphous silicon PV. While all of these technologies can be used to generate electricity from solar energy, there are some differences in the way that they are manufactured, and these differences affect their cost, as well as the way that they perform.

One of the main technical differences between crystalline and amorphous PV technologies is in their efficiency at converting solar energy into electricity. Crystalline PV panels now have efficiencies that range from 8 to 15%, while single junction a-Si modules often have efficiencies that range from 2 to 4%. The efficiency of a panel tells you how much electricity it can generate for a given area. This means that an a-Si 12 Watt panel will be larger in size than a crystalline panel with the same 12 Watt rating. A second difference between a-Si and crystalline PV has to do with their performance during the first few months after they are purchased. For a given amount of sunlight, the performance of crystalline PV panels is more or less constant from the time that they are bought. In contrast, most a-Si panels lose about 25% of their output during the first few months of use. After that, the performance stabilizes at a constant level. The final important difference between a-Si and crystalline PV panels is their price. The lower price of a-Si PV has convinced many to choose a-Si PV over the higher priced crystalline PV panels.

After considering the differences between these two panels a decision was made to use a product similar to one used on a building within the school of the Built Environment (the Sustainable Research Building [SRB]) on which monitoring could be performed. The product is Uni-Solar US-64 (United Solar Systems specification sheet). Each *UNI-SOLAR®* solar electric power module utilises proprietary Triple-Junction thin film silicon solar cells from United Solar Systems Corp. Each cell is composed of three semiconductor junctions stacked on top of each other. The bottom cell absorbs the red

light, the middle cell the green/yellow light and the top cell absorbs the blue light. This spectrum splitting capability is the key to higher efficiency, especially at lower irradiation levels and under diffuse light. The cells are produced in a roll-to-roll vacuum deposition process on a continuous roll of stainless steel sheet.

The modules are exceptionally durable. They are encapsulated in UV-stabilised polymers and framed with anodised aluminium. A lacquered Galvalume®-steel backing plate provides stiffness. The polymer encapsulation includes EVA and the fluoro-polymer TEFZEL®, a DuPont film. By-pass diodes are connected across each cell, allowing the modules to produce power even when partially shaded. Each module has either a weather resistant standard junction box, designed to accept 12.7 mm cable conduits or a Multi-Contact junction box (with a female connector and an MC-cable ending in a male connector) for easy plug-and-play series connection. These modules are appropriate for all applications from simple single module requirements to high voltage grid-connected applications. In *Figure 9.6* the general characteristics of the module may be seen.

	US-64
Rated Power (W)	64
Operating Voltage V_{MPP} (V)	16.5
Operating Current I_{MPP} (A)	3.88
Open Circuit Voltage V_{OC} (V)	23.8
Open Circuit Voltage V_{OC} @ -10°C and 1250 W/m² (V)[1]	27.1
Short Circuit Current I_{SC} (A)	4.80
Short Circuit Current I_{SC} @ 75°C and 1250 W/m² (A)	6.30
Series fuse rating (A)	8.0
Minimum blocking diode (A)	8.0
Weight (kgs)	9.17

Figure 9.6 Uni-Solar-64 Thin Film PV Characteristics (United Solar Systems specification sheet)

In order to estimate how much these PVs produce the 140 m^2 plant that exists in the SRB was monitored for a period of two years. *Figure 9.7* shows the global incident irradiation in the 5^o collector plane for the two years. Both of them give an annual availability of 888 kWh/m^2.

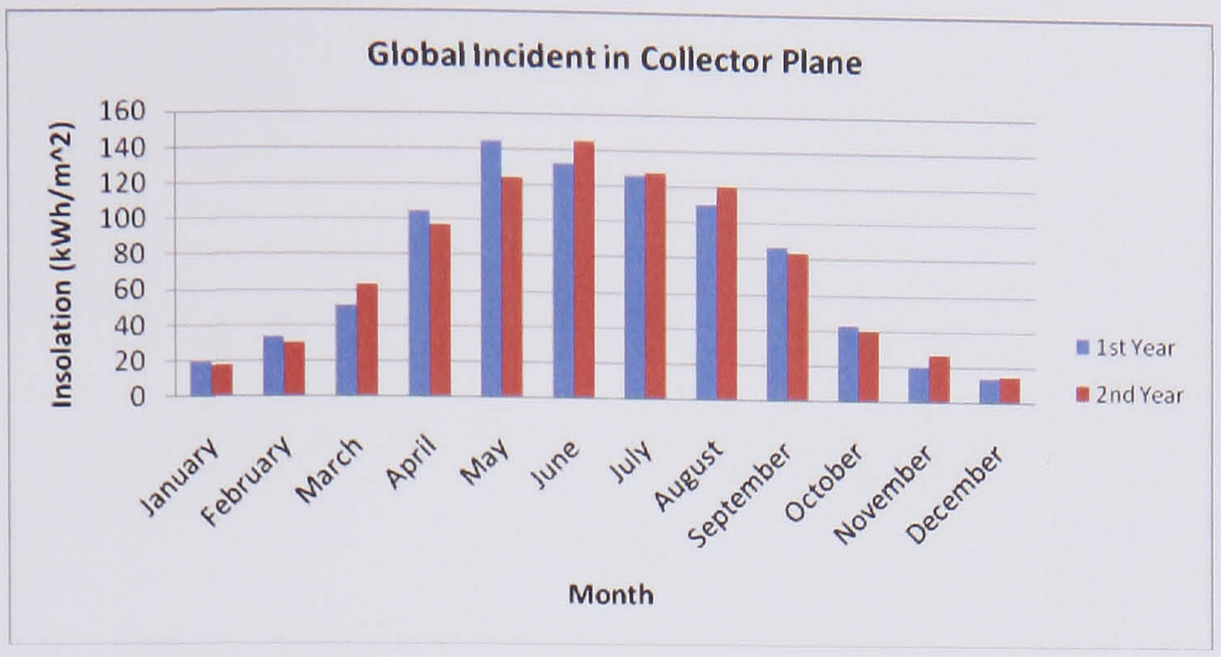

Figure 9.7 Global Incident Irradiation in Collector Plane

The annual energy produced was about 5408 kWh in the first and 4809 kWh in the second year respectively. The CO_2 emissions saved were 2558 kg of CO_2 the first and 2274 kg the second year. *Figure 9.8* and *9.9* give the monthly energy produced and CO_2 emissions saved.

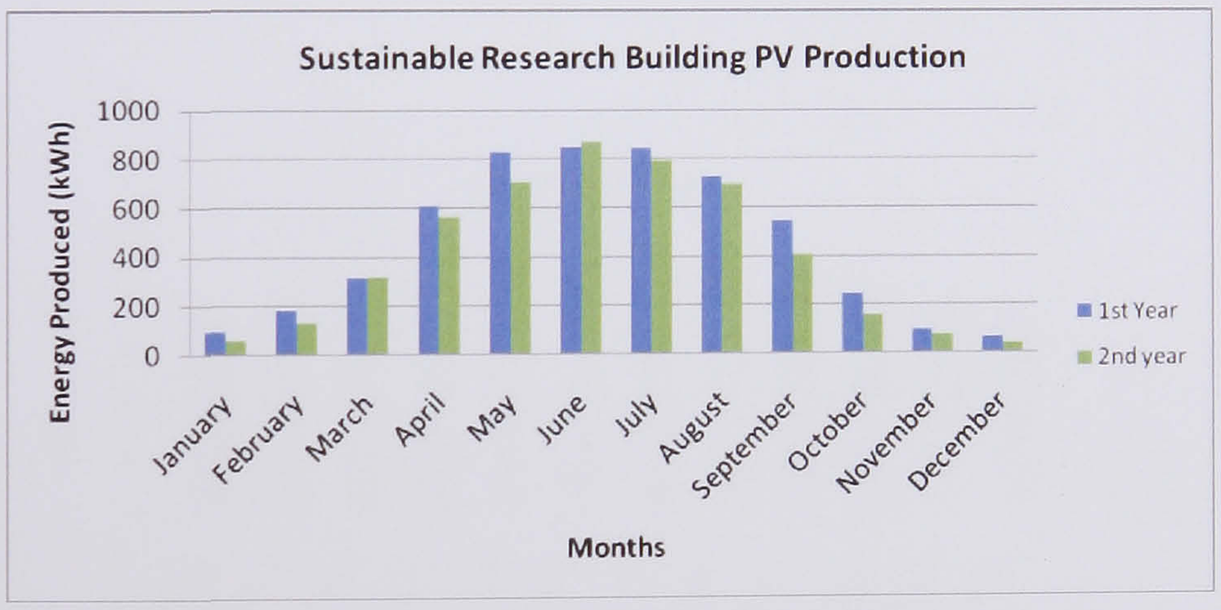

Figure 9.8 Sustainable Research Building PV Monthly Energy Production

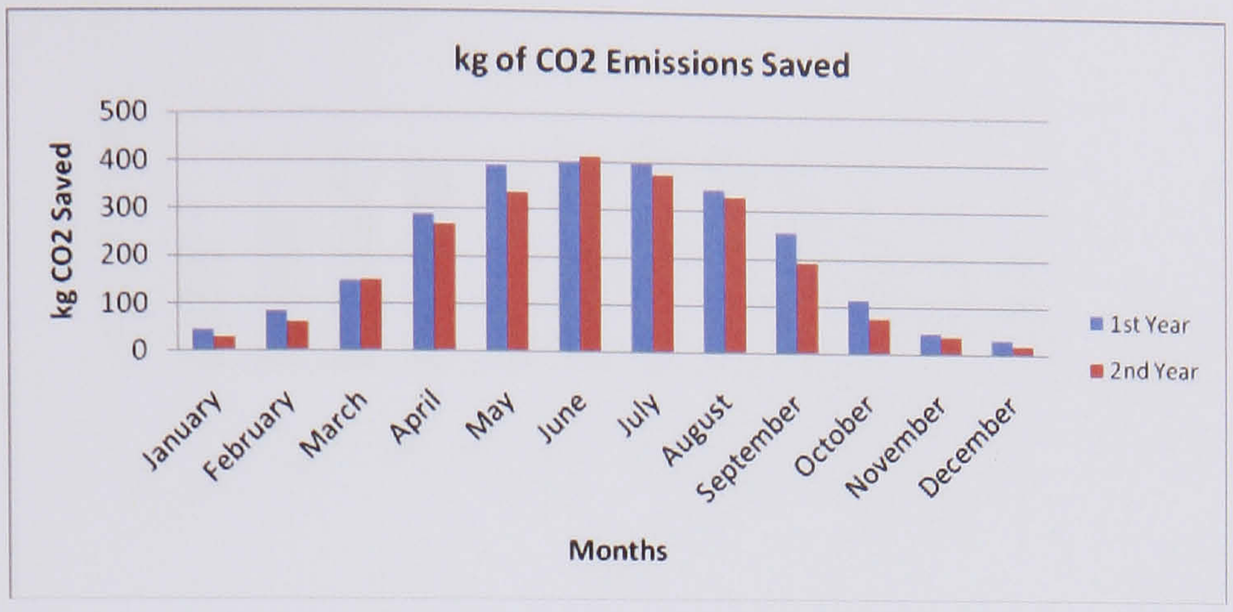

Figure 9.9 kg of CO2 emissions saved every month

In *Figure 9.10, 9.11* and *9.12* show the monthly values for inverter efficiency, performance ratio and the overall plant efficiency of the system. As seen the average inverter effieciency was near 85% and 83%, the performance ratio 64.2% and 52.7% and the average PV plant efficiency were 4.1% and 3.38% respectively for the two years. It may be seen that in the second year there was an 11% reduction in energy production.

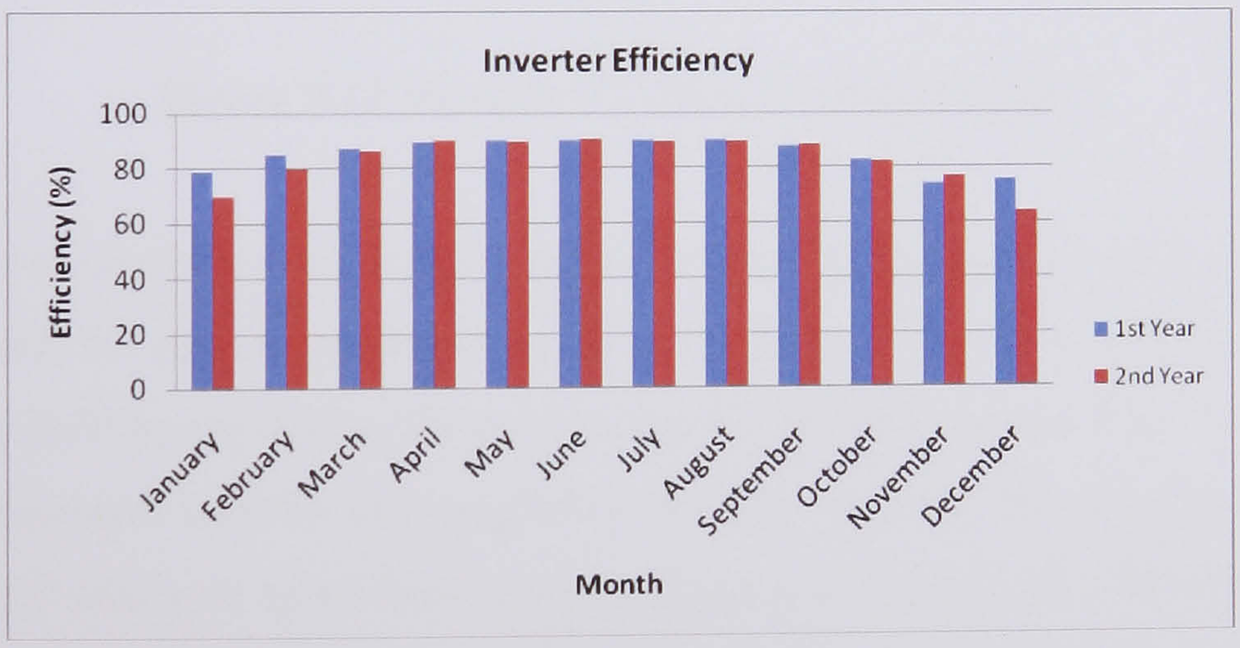

Figure 9.10 Monthly Inverter Efficiency

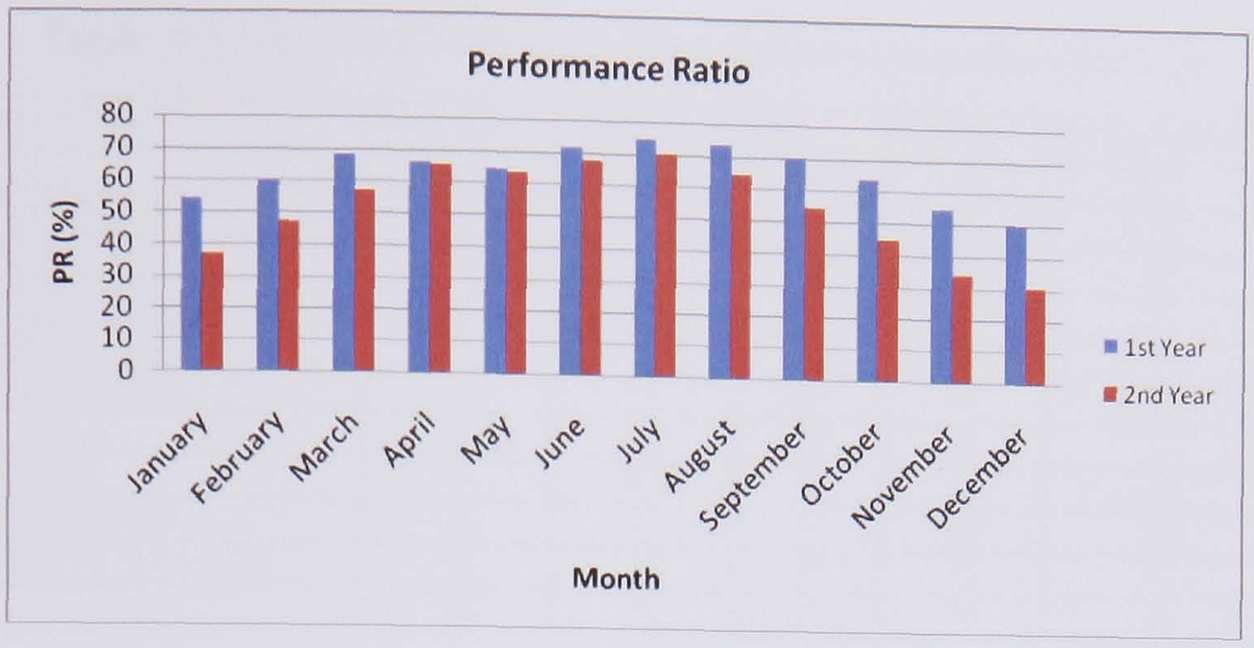

Figure 9.11 Monthly Performance Ratio

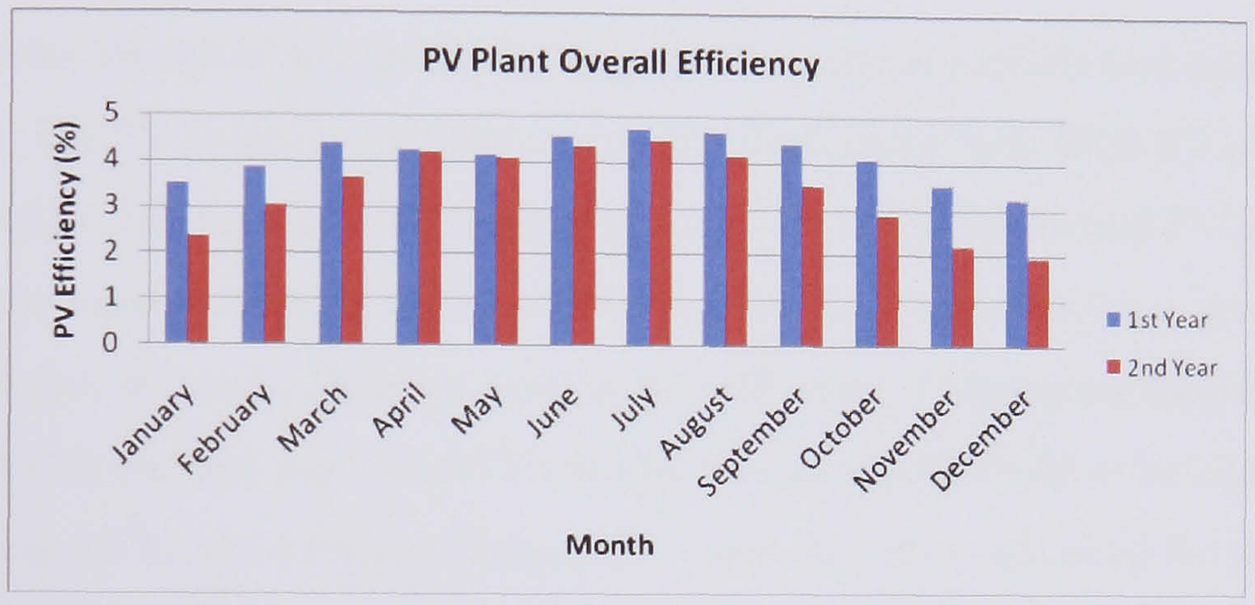

Figure 9.12 Monthly PV Plant Overall Efficiency

The monitored results will be used for the calculation of the payback time of PV/T systems. *Table 9.3* presents estimates of the cost of a PV/Thermal panel of 1 m^2. First this was obtained by estimating the cost for the thin film PV module for 1 m^2 and the various components used for the installation of SRB PV plant. The values are index linked to 2007 and were taken from manufacturers or published material (Bakker, 2005, Duckers, 2004, Bernal, 2006, Eiffert, 2003). For the PV/Thermal systems attempts were again made to estimate for a panel of 1 m^2 the components that would be used for the heat extraction from the panels. The prices are based on pro rata values based on larger arrays. From observing the *Table 9.3* it may be seen that PV/Thermal panels are 59%, 28%, 135%, 107% and 76% more expensive than the simple PV module.

Table 9.3 PV and PV/Thermal Panel Cost Estimation for 1 m^2

Product Investment in £/m^2	PV Simple	PV/Water	PV/Air	PV/PCM	PV/Heat Pipes	PV/MPCM
PV Panel	200	200	200	200	200	200
Solar Array Mounting Frame	30	30	30	30	30	30
Grid Connected Inverter	40	40	40	40	40	40
DC Disconect , Cables	25	25	25	25	25	25
AC Isolator , Cables	25	25	25	25	25	25
Installation and Commisioning	35	35	35	35	35	35
Pump or Fan	0	20	20	20	20	20
Water Storage & Pipes	0	100	0	100	100	100
PCM or MCPCM or Heat Pipes	0	0	0	250	150	50
Absorber Manufacturing Cost for PVT	0	40	30	60	60	50
Heat Exchanger	0	50	50	50	50	50
Total Net Capital Cost (£/m^2)	355	565	455	835	735	625

To estimate the electrical and thermal energy of the systems we followed different approaches. The PV system used the monitored values taken from SRB PV plant for 1 m^2. To calculate the electrical and thermal efficiencies of PV/Water and PV/Air the TRNSYS was used to simulate the two systems with the parameters taken from the experiments (i.e. thermal efficiency, heat loss coefficient). To estimate the performance for the PV/PCM the new built TRNSYS model was used with PCM to be E30 (melting temperature at 30 ^{o}C, see EPS Ltd Datasheet). From the values obtained for thermal energy a factor of 0.65 (thermal efficiency of 65% at zero reduced temperature for PV/PCM-Water) was applied in order to include the heat extraction achieved by water pipes passing from a PV/PCM-Water system. For PV/Heat pipe and PV/MCPCM systems the electrical energy from monitoring was used, and for thermal energy the irradiation values recorded from monitoring were multiplied by the thermal efficiency of the two systems in order to obtain the thermal energy. The results can be seen in *Table 9.4*. In particular, by collecting and using the thermal energy (usually lost) produced during PV modules operation it is possible to achieve two different goals: an increased amount of electrical yield (thanks to the lower operating temperature of modules) and an additional 'clean' energy flow to be used to replace traditional thermal energy sources.

From the derived thermal energy an assumption was made indicating that the yield of recovered heat that becomes a useful output for the user strictly depends on its final use; this may be calculated by means of the 'use coefficient' (Cu) that is the thermal energy

delivered to the user divided by the thermal energy recovered during PV/T system operation. If the final use is space heating, the coefficient Cu reaches the very low value of 0.2. As a matter of fact, in autumn and winter, when the user heat requirement is higher, the availability of the primary source (the sun) provides the lowest levels of the year. The exploitation of the recovered heat is obviously more interesting when it is used for domestic hot water (DHW) production, thanks to a more homogeneous demand distribution during the year. In this case, the calculated Cu rises to about 0.6.

Table 9.4 Monthly Electrical and Thermal Energy Produced for 1 m^2 of PV and PV/Thermal Panel

	PV Simple		PV/Water		PV/Air		PV/PCM		PV/Heat Pipe		PV/MCPCM	
Annual Saving (kWh)	Electrical	Thermal	Electrical	Thermal	Electrical	Thermal	Electrical	Thermal	Electrical	Thermal	Electrical	Thermal
January	0.687	0.000	0.767	0.000	0.774	0.000	0.879	6.743	0.781	0.000	0.781	0.000
February	1.309	0.000	1.375	9.911	1.394	4.971	1.585	9.194	1.413	12.736	1.413	10.614
March	2.264	0.000	2.135	17.431	2.175	8.738	2.381	14.065	2.216	22.423	2.216	18.686
April	4.366	0.000	4.509	39.286	4.627	19.682	4.898	41.518	4.744	50.586	4.744	42.155
May	5.918	0.000	5.921	58.507	6.095	29.307	6.448	57 825	6.269	75.328	6.269	62.774
June	6.068	0.000	5.266	50.502	5.386	25.313	5.702	39 759	5.508	65.015	5.508	54.179
July	6.021	0.000	5.427	44.953	5.608	22.497	5 661	85.041	5.790	58.020	5.790	48.350
August	5.200	0.000	4.779	44.822	4.883	22.468	5 132	35.923	4.987	57.712	4.987	48.093
September	3.880	0.000	3.646	32.320	3.735	16.195	3 892	39.180	3.823	41.638	3.823	34.698
October	1.754	0.000	1.640	10.670	1.663	5.351	1 805	9.535	1.687	13.729	1.687	11.441
November	0.696	0.000	0.843	0.000	0.850	0.000	0.940	4 624	0.858	0.000	0.858	0.000
December	0.471	0.000	0.566	0.000	0.570	0.000	0.651	2.938	0.574	0.000	0.574	0.000
Use Coefficient Cu				*0.6		*0.2		*0.6		*0.6		*0.6
Annual Total ES(kWh)	38.635	0.000	36.874	185.041	37.760	30.904	39.972	207.808	38.650	238.312	38.650	198.594

After evaluating the annual electrical and thermal energy produced the next step was to calculate the total annual saving, the payback time and the cost of the PV system per kWh energy produced. To extract the heat from the PV panel it is necessary to use a pump or a fan, and these two components require energy to work. To account for this it was necessary to estimate the energy produced in order for these components to work during a year. If consider that a system should stop working when the solar irradiation is less than 200 W/m^2 then an estimate from the solar irradiation recorded for the monitoring was used and obtained that the systems could work for 2922 hours a year was made. This irradiation level was used because below that point the thermal energy extracted is not significant and because the power needed for pump and fan covers the energy extracted. By multiplying the energy produced and the energy consumed with the current price of electricity (£0.08/kWh) it is possible to estimate the annual cost savings. As seen from *Table 9.5* the annual cost saving for PV/Thermal systems is higher than the simple PV.

During the period when the present study was undertaken the UK government offered financial support through mechanisms such as the DTI, a grant scheme for PV plants or thermal collectors (Latest UK solar grants, Heat my home). These schemes can cover 50% of the whole cost of the system. Taking advantage of such schemes could cut the cost to half i.e the £355 of PV to become only £177. By using this assumption and dividing the net capital cost estimated in Table 9.3 by the annual cost saving it is possible to provide a very approximate estimate of the time needed until the system is payed back. As seen from *Table 9.5* the payback time for a PV is 57 years and for the PV/Thermal systems is 46, 52, 51, 35 and 42 years. The cost savings takes into account also the costs produced by running the pump or fan.

Table 9.5 Payback period, annual CO_2 emission saving and cost of a PV system per kWh of energy produced

	PV Simple		PV/Water		PV/Air		PV/PCM		PV/Heat pipe		PV/MCPCM	
Annual Cost Saving (0.08 £/kWh)	3.091	0.000	2.950	14.803	3.021	2.472	3.198	16.625	3.092	19.065	3.092	15.887
Annual Running Time (hr)	0.000	0.000	0.000	2922.000	0.000	2922.000	0.000	2922.000	0.000	2922.000	0.000	2922.000
Pump, Fan Power (kW)	0.000	0.000	0.000	0.050	0.000	0.005	0.000	0.050	0.000	0.050	0.000	0.050
Total Power Required (kwh)	0.000	0.000	0.000	146.100	0.000	14.610	0.000	146.100	0.000	146.100	0.000	146.100
Running Cost (0.08 £/kWh)	0.000	0.000	0.000	11.688	0.000	1.169	0.000	11.688	0.000	11.688	0.000	11.688
Total Annual Cost Saving (£)	3.091		6.065		4.324		8.134		10.469		7.291	
Simple Payback Time (years)	57.428		46.577		52.609		51.325		35.104		42.858	
Total Emission of CO2 Saving (kg/year)	16.613	0.000	15.856	79.568	16.237	13.289	17.188	89.357	16.619	102.474	16.619	85.395
0.48 kg/kWh	16.613		95.424		29.526		106.545		119.094		102.015	
Cost of the PV System (£/kWh)	0.368		0.102		0.265		0.135		0.106		0.105	

The same calculations have been undertaken for different areas of PV panel in order to see how the payback is affected. As seen from *Figure 9.13* the payback period decreases as the area or units of PVs increases. It may be seen from the Figure that the PV/Heat Pipe give the lowest payback period. The points in the figure inside the circle are for the 1 m^2 of PV panel.

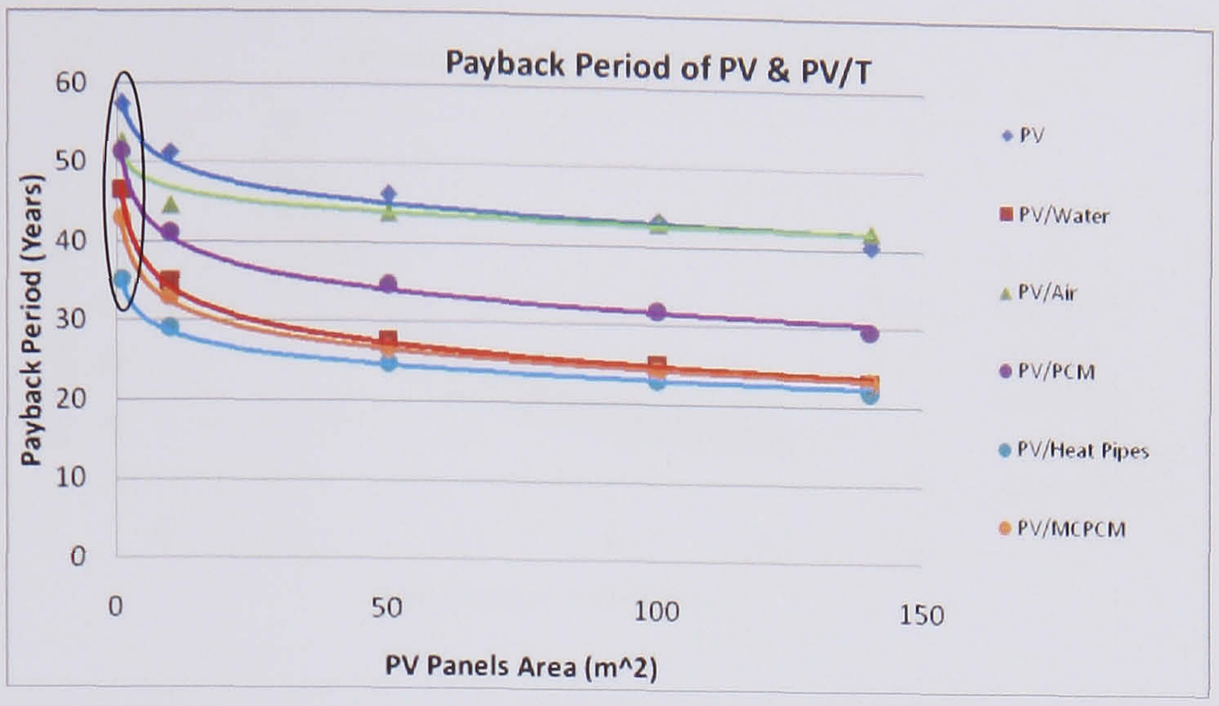

Figure 9.13 Payback Period for PV and PV/Thermal Systems for diffent panel area

Currently the price paid by the utilities for PV generated electricity entering the grid is just 8p/kWh. A simple calculation is taking 603.67 kWh of energy output per annum per kWp installed for an amorphous PV panel, and £2,800 per kWp unit installed cost (after receipt of the installation grant), it is apparent - given a return from energy produced for the grid of £48.3 (603.67 kWh x 8p) per annum per kWp installed - that it will (in financial terms), take 57 years to recover the initial installation costs. This is a long pay-back projection. Considering that most PV arrays carry a 20 year guarantee, and have a life expectancy of about 25 years, it is obvious that the economics for PV in the UK do not currently add up, and create an uninviting picture for investors and for the future of PV here.

If in the near future the cost of electricity is increased or the government decide to promote the clean renewable energy by increasing the price from energy coming from renewables then we could obtain lower payback periods. This can be seen from *Figure 9.14* were the payback periods for different prices of electricity are investigated. As may be observed as the cost of electricity increases, the payback reduces. As an example may be seen when the price reaches £0.4/kWh then PV and PV/Thermal systems could bring down the payback period near to 10 years. This price is very common to European countries like Germany and Greece that the clean electricity price is in the region of £0.34/kWh.

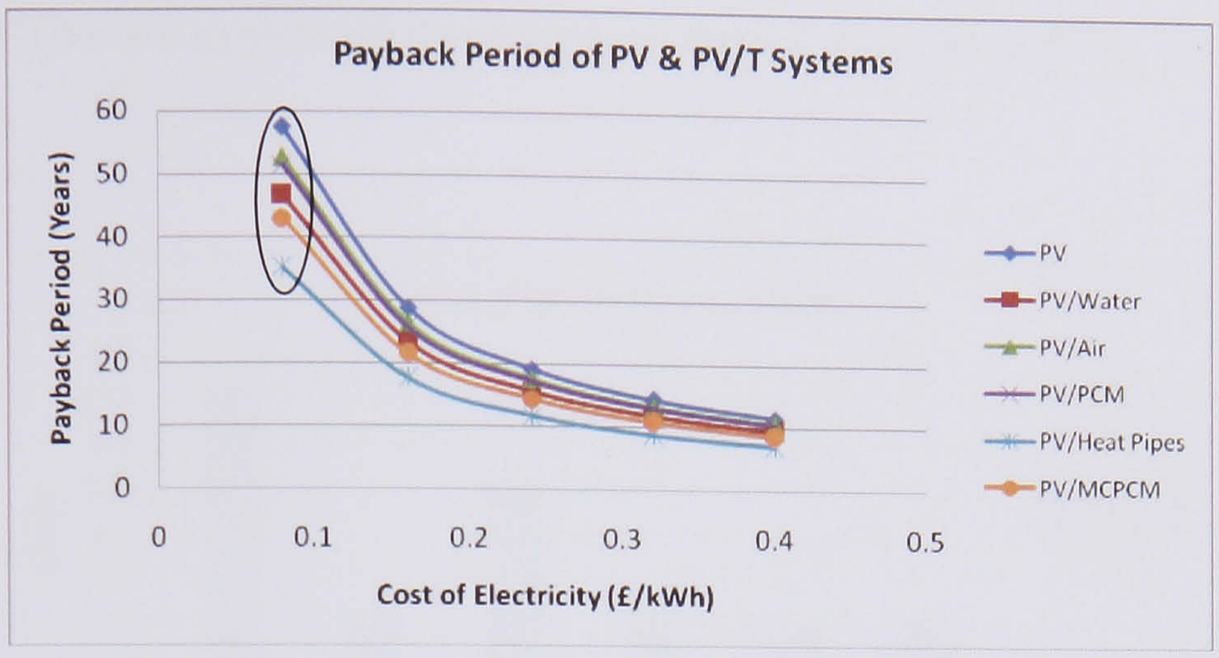

Figure 9.14 Payback period of PV and PV/Thermal Systems for different cost of electricity

The same can be observed with the grant schemes. As seen in *Figure 9.15*, when the contribution from government for the cost of the PV system increases, the payback time reduced. Figure range from 114 years with no grant contribution to 57 with a 50% grant.

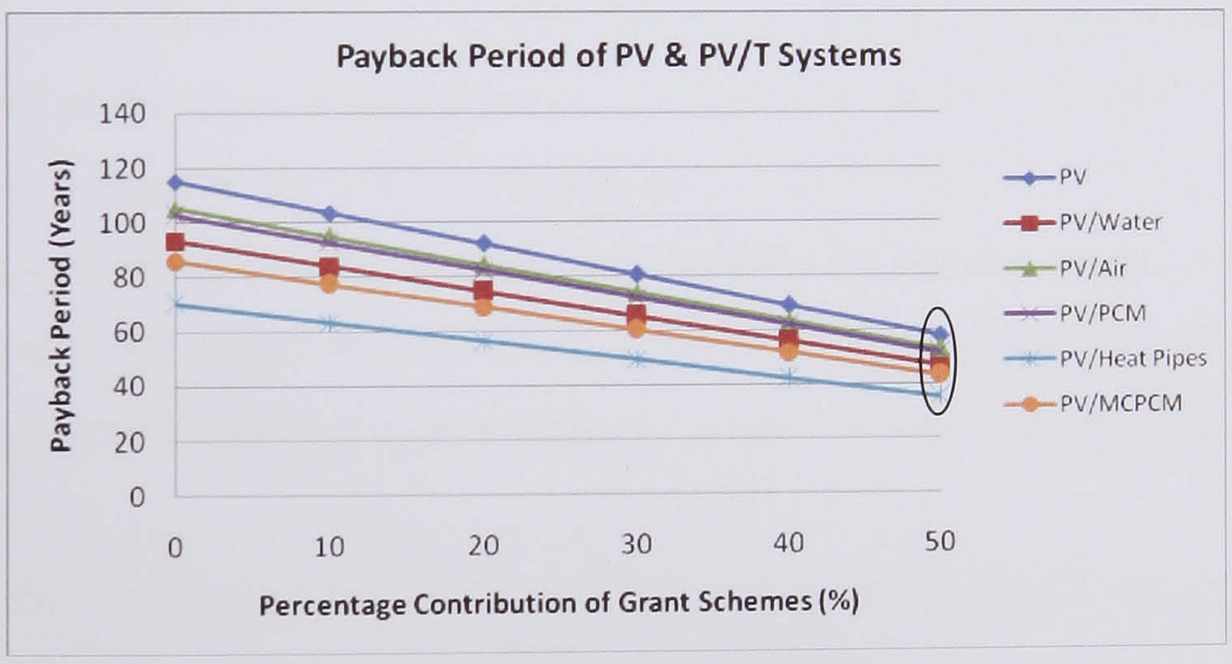

Figure 9.15 Payback period of PV and PV/Thermal Systems for different percentage contribution of grant schemes

An alternative way of comparing systems is to investigate the cost per kWh of energy produced from a PV or PV/Thermal system. This can be calculated by taking the net capital cost of each system and deviding it by the annual energy produced multiplied by an estimate of the years of operation (25 years). As seen from *Figure 9.16* the PV system has the higher (£0.368/kWh) cost per kWh of energy produced in comparison

with the PV/Thermal systems that reduce it by around 72%, 28%, 63%, 72% and 72% respectively.

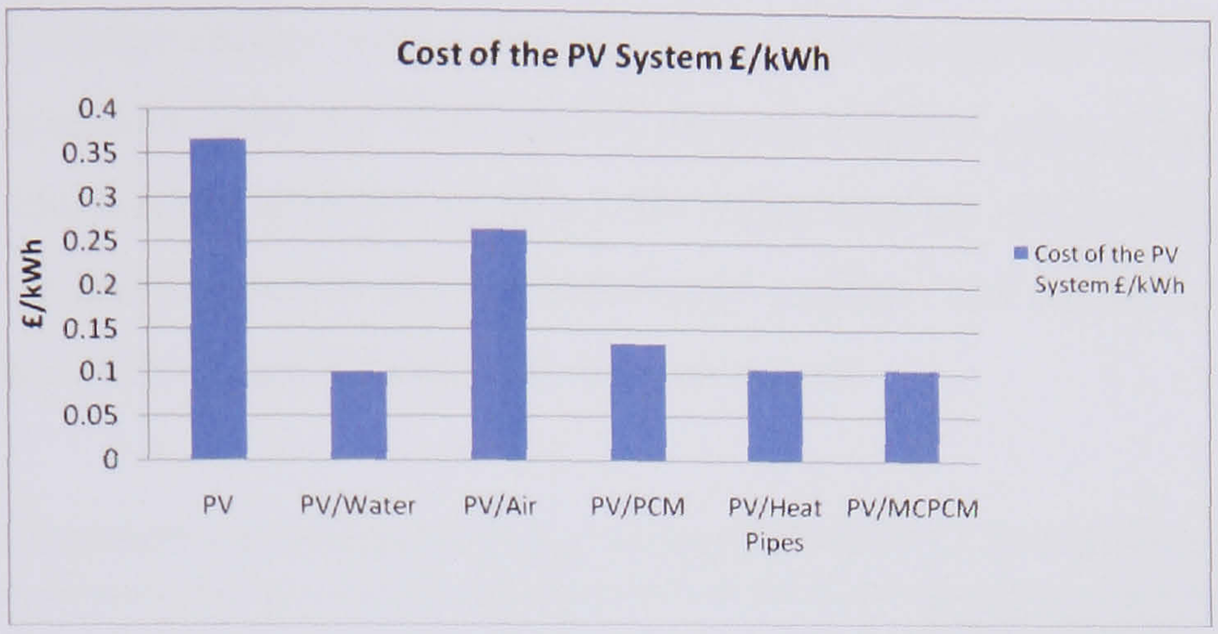

Figure 9.16 Cost of the PV and PV/Thermal systems per kWh energy produced

9.3.1 Comparison of a PV/T system with a side-by-side PV and Solar Thermal Collector system

To understand and evaluate the economic prosperity of a PV/T system a comparison with a side by side system was undertaken. In *Table 9.3b* the cost of a PV/T water system with a solar thermal collector system and a side by side PV + Solar thermal collector system was presented. It can be seen that the investment on the side-by-side system is about 39% higher than the PV/T system. The difference is caused by the additional collector frame and support, plus the higher installation cost in handling the larger system.

Table 9.3b Cost Estimation of a PV, a PV/T and a side by side PV + Solar Thermal Collector System for 1m^2

Product Investment in £/m^2	PV Simple	PV/T Water	Solar Thermal Collector	PV + Solar Thermal Collector
PV Panel	200	200	0	200
Solar Array Mounting Frame	30	30	30	60
Grid Connected Inverter	40	40	0	40
DC Disconect , Cables	25	25	0	25
AC Isolator , Cables	25	25	0	25
Installation and Commisioning	35	35	35	70
Pump or Fan	0	20	20	20
Water Storage & Pipes	0	100	100	100
PCM or MCPCM or Heat Pipes	0	0	0	0
Absorber Manufacturing Cost for PVT	0	40	200	200
Heat Exchanger	0	50	50	50
Total Net Capital Cost (£/m^2)	355	565	435	790

The same procedure was used as previously for estimation of thermal energy with the assumption that the solar thermal collector average daily efficiency is 50%. The overview of collector energy yield of the hybrid PV/T system and the side-by-side system can be seen in *Table 9.7*. With the two separate collector units of total surface area of 2 m^2, the combined energy yield is 7.3% higher than the PV/T system with 1 m^2 surface area. However in terms of combined energy yield per unit surface area the PV/T collector is then 86% higher than the side-by-side system.

Table 9.7 Overview of collectors energy yields: hybrid PV/T vs side-by-side system

	Side-by-side	PV/T
Surface Area (m^2)		
Solar Thermal Collector	1	1
PV Panel	1	1
Total	2	1
Energy Generation From Collector (kWh)		
Thermal Energy	213.56	192.75
Electrical Energy	34.77	38.63
Total Energy	248.33	231.38
Equivalent Energy Yield per unit surface area (kWh/m^2)	124.165	231.38

The payback period was evaluated for different panel areas, for different electricity cost and different grant schemes. As seen from *Figure 9.17* the PV/T system payback period of the cost of the investment was quicker than the side-by-side system. This difference is around 4 years more time to cover the investment for the side-by-side system. Figure 9.18 and 9.19 present the influence that an increase in electricity cost or an increase in grant scheme will have on the payback period of the systems. As can be seen by increasing both factors the payback period reduces and the PV/T system performs better than a side-by-side system.

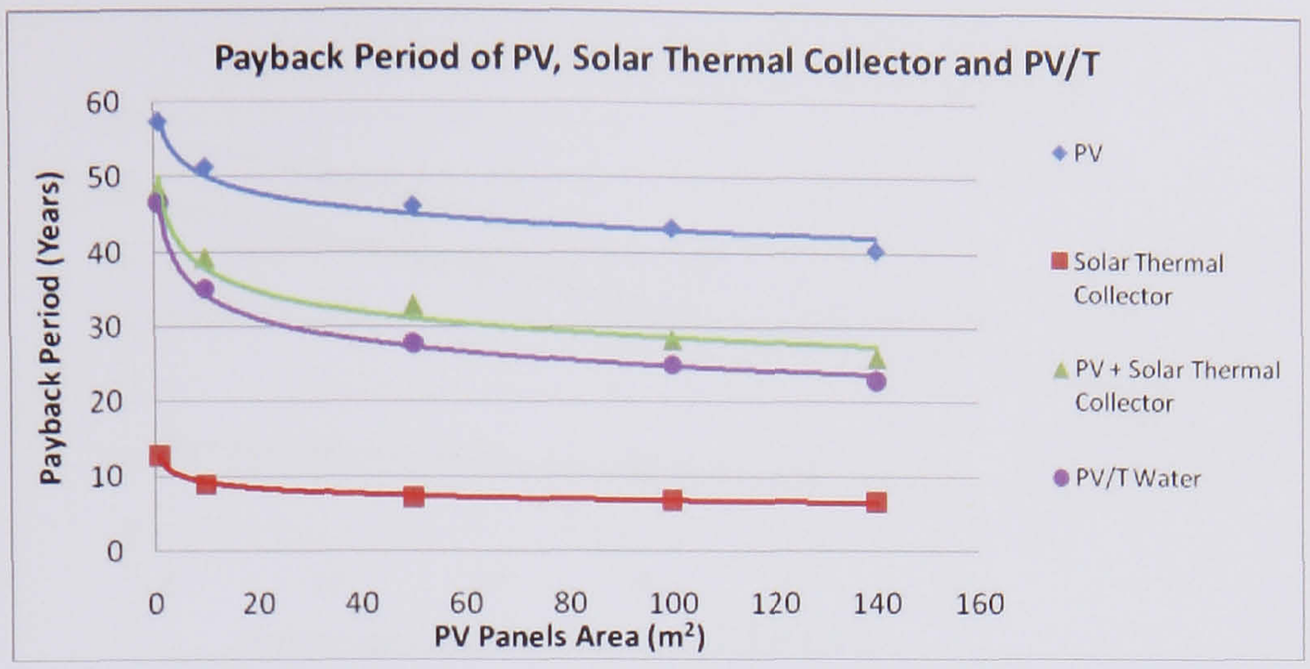

Figure 9.17 Payback Period for PV, Solar Thermal Collector and PV/Thermal System for diffent panel area

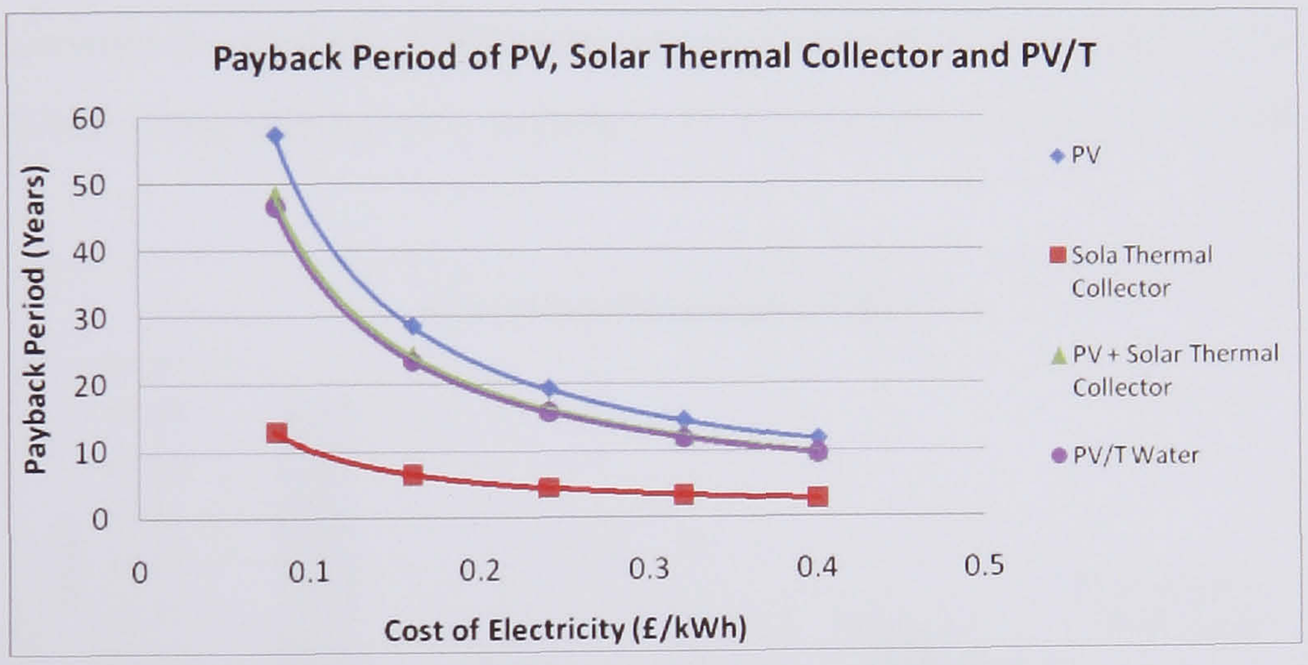

Figure 9.18 Payback period for PV, Solar Thermal Collector and PV/Thermal System for different cost of electricity

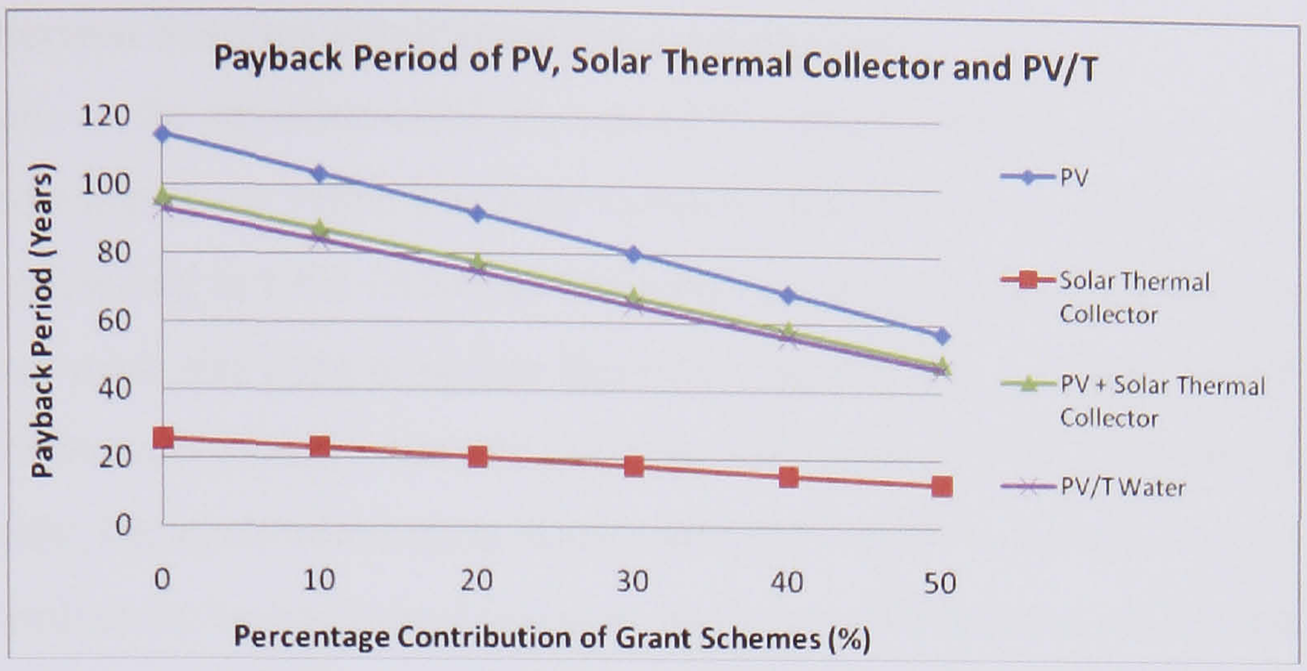

Figure 9.19 Payback period for PV, Solar Thermal Collector and PV/Thermal System for different percentage contribution of grant schemes

As far as consider the cost per kWh of energy produced the PV/T system value is £0.1018/kWh and the side-by-side system is £0.1273/kWh, a reduction of about 25%.

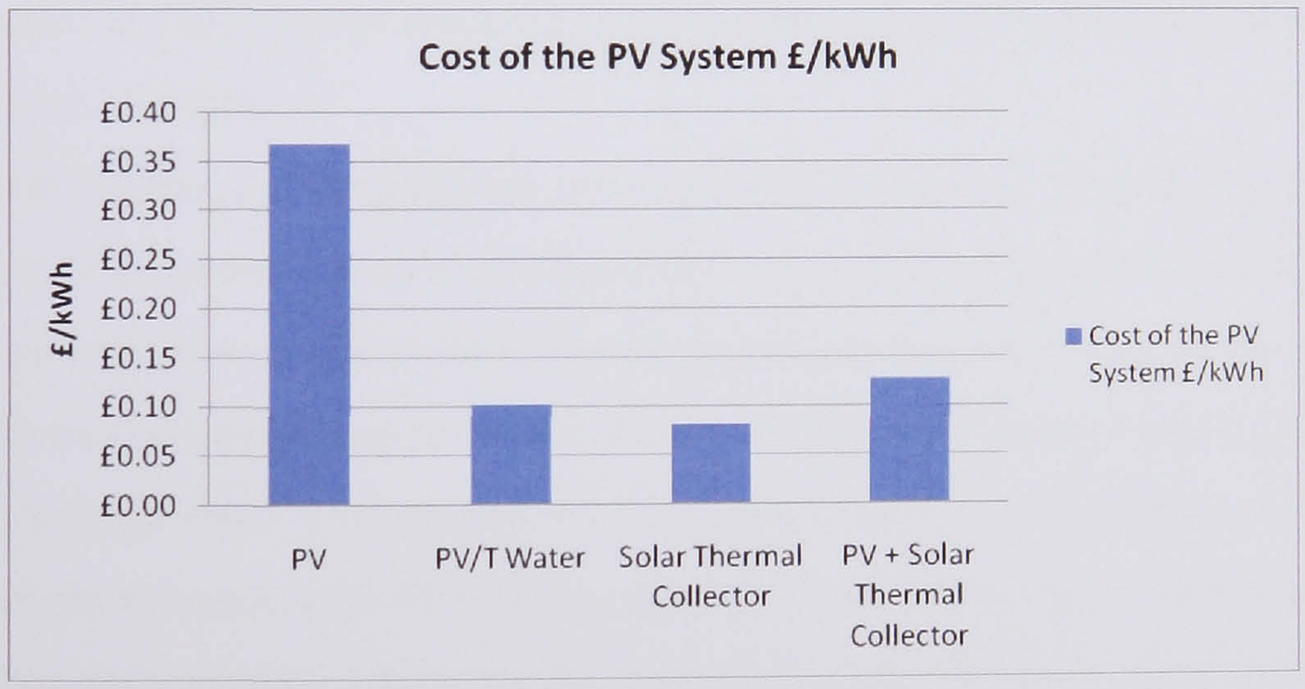

Figure 9.20 Cost of the PV, Solar Thermal Collector and PV/Thermal system per kWh energy produced

9.4 PV/Thermal Systems Environmental Comparison

Reliable data on the environmental impacts of PV module manufacture have been rather scarce for the last 10-15 years. The only extensive data collection based on production data were published in 1992 (Alsema) and were based on technology from the late 1980s. Later work was done to update these data but this was to a large extent based on secondary data sources and estimates (Alsema, 1998, 2000, 2006, Keoleian, 1997,). Consequently, life cycle assessment studies are often based on the old data set that does not really reflect the technological progress made over the past decade (Frankl, 1998, Krauter, 2004, Ardente, 2005).

The present study considered only one standard module type with 72 cells (1 m^2 module area), with glass/EVA/Tedlar lamination. The glass thickness was 3.6 mm and the modules were supported in an aluminium frame of mass 3.8 kg. Module efficiencies were assumed equal those of the commercially available module from Uni-Solar upon which the studies in this chapter are based (*Figure 9.6*). Module life time was assumed to be 30 years; the life time of electronic components of the PV systems (inverter) was assumed to be 15 years.

Environmental impacts during the use phase of a PV system are generally negligible; the replacement of electronic components (inverter) after 15 years is accounted for by including two inverters in the system. For all manufacturing processes we assumed the average electricity supply system for the Western- European continent (UCTE region), at medium voltage level. This system has an overall conversion efficiency of 31% and a greenhouse gas emission of 0.48 kg CO_2-eq/kWh. To do the analysis, values of energy intensity data were used to determine the embodied energy for each of the materials or components used. The values were taken from other researchers studies that analysed PVs or thermal solar collectors.

9.4.1 Energy Payback Time of PV systems

During the life of the PV system, no substances are emitted that might be harmful to the heath or environment. However, a great amount of energy is needed in their production. Furthermore at the end of their useful life, the installation must be disposed of and the residues dealt with. Life cycle energy analysis is a means of evaluation that consists of

analyzing all the energy flows associated with different production stages, in this case of the PV system connected to the grid. One of the parameters used by this method is the time needed to recuperate the invested energy or the Energy Pay-Back Time (EPBT)

$$\text{EPBT(years)} = \frac{E_{\text{invested}}}{E_{\text{PVa}}} \qquad \text{Eq. (9.1)}$$

The energy payback time is expressed in Eq. (9.1). $E_{invested}$ is the energy invested throughout the life of the PV system (extracting of raw material, fabrication of the modules and inverter, installation, operation, residual management) and E_{PVa} is the annual energy generated by the PV system. EPBT is expressed in years.

In PV systems the EPBT depends on numerous factors: cell technology, type of encapsulation, the module frame, the supporting structure, inverter, system efficiency, climate, site, inclination of the generator, etc. *Table 9.6* gives an indication of EPBT from work that has been done from other researchers.

Table 9.6 Estimates of energy payback times for various solar technologies

Technology	EPBT (yrs)	Reference
Crystalline Silicon	3.1 - 4	Alsema (2000)
Amorphous Silicon	2.5 - 4	Alsema (2000)
CdS/CdTe	1.1 - 1.7	Kato et al. (2001)
Flatcon (CPV)	0.7 - 1.3	Peharz and Dimroth (2005)

Table 1: Estimates of energy payback times for various solar technologies.

9.4.2 Factors Driving the Results of PV LCA

In summary, a set of parameters is responsible for the variability in the performance of different installations. Aside from the level of incident solar radiation, which depends on the latitude and the characteristics of the local air mass and reflects a natural characteristic of the site selected for the installation of the modules, other parameters are simple choices made by the user of the system, which are sometimes technology dependent, and other times are driven according to the purpose of the system. Some of these parameters are listed in *Table 9.7* and discussed in the next paragraphs. To value of this study is to present the different factors that can affect the LCA analysis. None of these are being included for this study.

Table 9.7 Factors affecting the EPBT of a system

Technology	System Configuration
Module technology	Array area
Module efficiency	Tilt angle and/or orientation
Tracking system	Mounting structure
Components' lifetime	Stand alone vs. grid connected
	Installation scale
	Other balance of system (BOS) components

9.4.2.1 Technological Options

Currently, PV module production centres on three types of technology: monocrystalline, polycrystalline, and thin film (amorphous) silicon. The manufacture of crystalline PV modules is more energy intensive than the manufacture of amorphous modules. The primary energy required for the fabrication of crystalline PV modules has been reported to be 2.9 to 3.8 times greater than the input for the same unit area of thin film modules. Primary energy requirements for manufacturing crystalline modules were found to range between 2,400 and 7,600 MJ/m^2 for poly-crystalline (mc-Si) modules and between 5,300 and 16,500 MJ/m^2 for mono-crystalline (sc-Si) modules, whereas the manufacturing energy requirement for thin film modules ranges from 710 to 1,980 MJ/m^2 (*Table 9.8*)

Table 9.8 Primary energy requirements for the production of PV modules (Alsema, 2000)

Primary energy requirements for the production of PV modules			
Multicrystalline Silicon (efficiency 13%: 130 W_p/m^2)		Amorphous Silicon Thin Film (efficiency 7%: 70 W_p/m^2)	
Without aluminium module frame	With aluminium module frame	Without aluminium module frame	With aluminium module frame
420 MJ_{prim}/m^2	460 MJ_{prim}/m^2	120 MJ_{prim}/m^2	160 MJ_{prim}/m^2
32 MJ_{prim}/W_p	35 MJ_{prim}/W_p	17 MJ_{prim}/W_p	23 MJ_{prim}/W_p

The primary energy input into the manufacturing phase affects the energy payback time of the modules, the higher the input primary energy the longer the payback time and vice versa.

The source of the energy mix is one of the factors that strongly influences the amount of emissions released (emissions released are also dependent in the type of materials used) during manufacture of the PV system's components. Most greenhouse gas emissions associated with PV systems (80 to 90%) are linked to electricity requirements for the fabrication of modules. Because the energy mix is critical in influencing its greenhouse gas emissions, the substitution of renewable electricity for fossil fuel based electricity in manufacturing the modules would be expected to reduce the emissions from the energy usage by significant amounts.

Of course, the energy conversion efficiency of the modules also affects the energy payback time of PV systems. The energy conversion efficiency measures the ratio between the electricity output of the panel and the incoming solar radiation perpendicular to the surface of the module, and is expressed as a percentage. The efficiency of a module is a function of the technology used; therefore, different brands, vintages, and types of modules have different efficiencies. The energy conversion efficiency of the PV modules often degrades over time. Improving both the energy conversion efficiency of the modules and their manufacturing efficiency, that is, reducing energy and material inputs, affects the life cycle cost (total cost of the electricity generated from the PV system) of the electricity produced by PV installations.

9.4.2.2 Incident Solar Radiation

Because the electricity output of a module depends on how much solar radiation reaches the surface of the module, the position of the module with respect to the sun is important. The electricity produced by the module depends on the orientation of the module's face and the angle with the horizontal plane. Modules may be mounted on a frame that tracks the position of the sun over time and increases the amount of incoming radiation. While some arrays move only along one axis based on a frame filled with refrigerant gas, other tracking systems move along three axes and are powered by a small electric motor. In this case some electricity generated by the system is consumed during its operation.

The choice of the tilt angle depends not only on the maximization of the energy output of the modules, which varies with the seasons of the year, but also on the economic and environmental cost of the structures to support the modules.

9.4.2.3 Balance of the System (BOS)

The Balance of the System (BOS) is the term used to refer to all the other components in the PV installation besides the modules. The BOS depends on the type of application and local conditions, and includes the structure to support the modules and the installation hardware. Batteries to store and deliver energy during load periods, as well as inverters might be necessary if the system is connected to a network that operates with alternate current (AC). Cables to interconnect modules and arrays to batteries and inverters are also part of the BOS. Batteries have emission impacts throughout their life cycle and potential disposal concerns at their end of life. The assessment of the energy, carbon, and other emissions associated with the BOS should also be part of a comprehensive LCA. *Table 9.9* shows energy inputs into some of the components used in the BOS from a previous investigation.

Table 9.9 Energy requirements for the production of PV components (Alsema, 2000)

Aluminum module frame	MJ/m^2	500
Array support – central plant	MJ/m^2	1800
Array support – rooftop	MJ/m^2	700
Inverter (3 kW)	MJ/W	1

Whenever energy to be recovered in the future is stored or converted, some losses occur; therefore, there are some efficiency losses associated with these practices that need to be included in the analysis. Accordingly, it is estimated that 10% of energy is lost in the system through BOS conversion efficiency losses, which accounts for inverter and storage losses. The inverter, a very important component of the balance of system (BOS), and converts the direct current (DC) generated by the PV modules into alternating current (AC) that can be used by the building.

9.4.2.4 Installation Type

The user's requirements of the installation can also influence the system's performance. While some PV systems are stand-alone systems that can only supply energy for small consumers, others are grid-connected. The scale of grid-connected systems is variable and affects the BOS of the system and its respective material requirements. According to Alsema (2000), different mounting options affect the amount of energy input into the systems; thus, the energy payback time for a rooftop system is typically 2.5 to 3 years, whereas the payback time for a ground mounted system is 4 years. The ground mounted PV system involves the installation of additional support structures to help generate the maximum possible electricity from the system. However, from the energy payback time estimates it is evident that the structures used to support the modules consume significant amounts of energy and also are responsible for GHG emissions. Indeed, concrete and steel used in the construction of the structures to support the modules are responsible for a considerable amount of energy input in some PV installations (1,100 MJ/m^2). The use of an existing structure, such as an existing building roof, to support the modules also reduces the environmental impacts of this electricity generation

alternative since the structure serves other functions in addition to supporting the modules. One advantage of using a special structure to support the modules is that they can be positioned in order to maximize the amount of effective solar radiation received; and therefore, the amount of electricity output of the modules.

Building-integrated PV (BIPV) are PV modules/laminates integrated in the building envelope such as PV shingles. While rooftop modules are placed on an existing structure through the use of simple frames to hold a set of modules, stand-alone systems demand manufacture and installation of special frames on the ground to support an array, which includes a set of modules.

The scale of grid-connected systems varies, and although a collection of small modules may match the energy produced in a larger installation, there are some advantages due to economies of scale in the construction of large-scale centralized systems. One advantage of a centralized system is that the materials used in the facility can be reused, recovered, and recycled more readily than if they were in dispersed installations.

9.4.2.5 Conversion Efficiency Trend

A comparison between crystalline and amorphous technologies shows that more efficient crystalline modules consume more energy during manufacturing than less efficient amorphous modules. However, the output of amorphous modules diminishes over time more dramatically than the efficiency of crystalline modules. The output of amorphous modules typically declines about 25% over the first few months of exposure to the sun due to the Staebler-Wronski effect, but then the efficiency tends to stabilize and minimal decay in the efficiency rates are observed after this point for the life-cycle of the PV. Another study by National Academy of Engineering reports that the power output of amorphous silicon modules decrease by 15-40% during the first few months of operation (due to Staebler-Wronski effect) after which the power output stabilizes itself.

9.4.2.6 Lifetime of the System

A LCA compares material and energy input and various emissions to the energy generated over a certain period, which usually equals to the lifetime of a major component of the system. In the case of PV systems, the crystalline modules have an

expected life time of 25 to 30 years and the UNI-SOLAR thin film modules have a life time warranty for 25 years. While some parameters are determined by the system designer, others are circumstantial, that is, they depend on local characteristics or natural conditions. The lifetime of the modules is an important parameter that affects both the electricity costs and the amount of reduced CO_2 emissions.

9.4.3Energy Return Factor

The energy payback time as an indicator of energy performance has an appeal because of its similarity with economic payback times. One advantage of the EPBT indicator is that it is additive, EPBT values for different system components may simply be added up to obtain the total system EPBT. A drawback of EPBT is that it does not account for the energy gain during the rest of the economic lifetime. An indicator that fulfills this requirement is the *energy return factor* (ERF) which expresses the total amount of energy saved per unit invested energy.

$$\text{Energy Return Factor (ERF)} = \frac{E_{\text{gen}} \times L}{E_{\text{input}}} = \frac{L}{EPBT} \qquad \text{Eq. (9.2)}$$

The formula Eq. (9.2) resembles the one for energy payback time with the addition of L the life time of the PV system. Obviously, modules with saved input over longer lifetimes will perform better using the ERF-indicator. A disadvantage of the ERF indicator is that it is not additive, i.e. ERF values of different system components cannot be added to obtain the ERF of the total system. With this definition an Energy Yield Factor of 3 would mean that the PV system produces three times the amount of energy which is consumed in its life cycle.

In this thesis data has been used from articles where the present understanding of the energy requirements of the present technologies in the PV industry (Alsema, 1998, 2000, 2002, 2005, Battisti, 2005, Fthenakis, 2004, Cellura, 2005, Frankl, 1998) is examined. The energy invested in the installation, maintenance operation and dismantling and recycling of the grid connected PV system has been considered as zero. This approximation, due to the lack of information about the subject, does not alter the results of the EPBT calculations, as the specific energy necessary in the fabrication

stage of the components is much greater than that invested in the other and so can be disregarded without influence the findings.

The main hypotheses of the LCA study are:

- PV module materials:
    1. pc-Si
    2. glazing (glass)
    3. aluminium frame
    4. other lamination materials (EVA, etc.)
- PV support structures: a horizontal flat roofs installation was assumed for which a support frame was required for the PV
    1. Aluminium
    2. galvanized iron (installation material)
- heat recovery unit materials:
    1. copper (sheet + pipes)
    2. PUR (insulation)
    3. aluminium (collector back cover)
    4. glazing (glass, only for glazed PVT systems)
    5. aluminium (additional collector frame, only for glazed PVT systems)
    6. heat exchanger (copper)
    7. PCM or MCPCM material

Table 9.10 a, b, c, d, e, f gives the components and the materials needed for the PV and PV/Thermal systems as also the energy requirements for 1 m^2 of panel.

Table 9.10a PV Components and Materials Energy Requirements

PV for 1 m^2			
Sub-Component and Material	Amount	Energy Requirement	Total
PV Solar Cells (MJ/m^2)	1	865	865
Glazed Covering (MJ/kg)	5	15	75
Lamination Material EVA-Tedlar (MJ/kg)	1	260	260
Aluminium Frame (MJ/m^2)	1	400	400
Inverters and Cabling (MJ/W)	64	2	128
Array Roof Support (MJ/m^2)	1	700	700
		SUM (MJ/m^2)	2428

Table 9.10b PV/T Water Components and Materials Energy Requirements

PV/Water for 1 m^2			
Sub-Component and Material	Amount	Energy Requirement	Total
Thermal Insulation (MJ/kg)	2	18.7	37.4
Collector Back Cover Aluminium ($MJ/m^{2)}$	3	400	1200
Sheet&Tube Copper in back of PV (MJ/kg)	6	100	600
		SUM (MJ/m^2)	1837.4

Table 9.10c PV/T Air Components and Materials Energy Requirements

PV/Air for 1 m^2			
Sub-Component and Material	Amount	Energy Requirement	Total
Thermal Insulation MJ/kg	2	18.7	37.4
Collector Back Cover Aluminium MJ/m^2	3	400	1200
Copper Plate in back of PV (MJ/kg)	4	100	400
		SUM (MJ/m^2)	1637.4

Table 9.10d PV/T PCM Components and Materials Energy Requirements

PV/PCM for 1 m^2			
Sub-Component and Material	Amount	Energy Requirement	Total
Thermal Insulation MJ/kg	2	18.7	37.4
Collector Back Cover Aluminium MJ/m^2	3	400	1200
Copper Plate in back of PV (MJ/kg)	4	100	400
Small Tank in back of PV (MJ/kg)	8	100	800
PCM Material (MJ/kg)	50	50	2500
		SUM (MJ/m^2)	4937.4

Table 9.10e PV/T MCPCM Components and Materials Energy Requirements

PV/MCPCM for 1 m^2			
Sub-Component and Material	Amount	Energy Requirement	Total
Thermal Insulation (MJ/kg)	2	18.7	37.4
Collector Back Cover Aluminium ($MJ/m^{2)}$	3	400	1200
Sheet&Tube Copper in back of PV (MJ/kg)	6	100	600
MCPCM Material (MJ/kg)	5	50	250
		SUM (MJ/m^2)	2087.4

Table 9.10f PV/T Heat Pipes Components and Materials Energy Requirements

PV/Heat Pipe for 1 m^2			
Sub-Component and Material	Amount	Energy Requirement	Total
Thermal Insulation (MJ/kg)	2	18.7	37.4
Collector Back Cover Aluminium ($MJ/m^{2)}$	3	400	1200
Sheet&Tube Copper in back of PV (MJ/kg)	6	100	600
Heat Pipes & Manifold (MJ/kg)	8	100	800
		SUM (MJ/m^2)	2637.4

Given that 95% of the energy used in the production of the silicon PV modules and the rest of the components come from electricity, the value of primary energy can be converted into electrical energy. Assuming an efficiency of the primary energy to electrical energy conversion of 35%, the equivalent of 1 kWh of electric energy is equal to 10.28 MJ_{prim}. After calculating the kWh of energy needed to produce 1 m^2 of panel the value divided was by the annual electrical energy and thermal energy production taken from *Table 9.4*. From this ratio it is possible to determine the EBPT. As seen in *Figure 9.17* the EBPT reduces in the PV/Thermal systems because of the additional thermal energy delivered by the hybrid systems.

To calculate the CO_2 payback the manufactory energy required and produced was assumed to have a greenhouse gas emission of 0.48 kg CO_2-eq/kWh. For the PV system the CO_2 payback is around 6 in comparison with the PV/Thermal systems which are near or below 1 (0.78, 1.74, 1.21, 0.73, 0.77).

As mentioned in section 9.4.3 to determine the Energy Return Factor the energy produced from the PV systems is multiplied by the life time of the system and divided

by the energy consumed in order to produce the system. From *Figure 9.17* it may be seen that the PV/Thermal systems give more times than the energy involved in their production. The ERF for the PV is just 4.9 times for PV/Water it is 16, for PV/Air is 5.3, for PV/PCM is 10.3, for PV/Heat Pipe is 16.8 and for PV/MCPCM is 16.2 respectively.

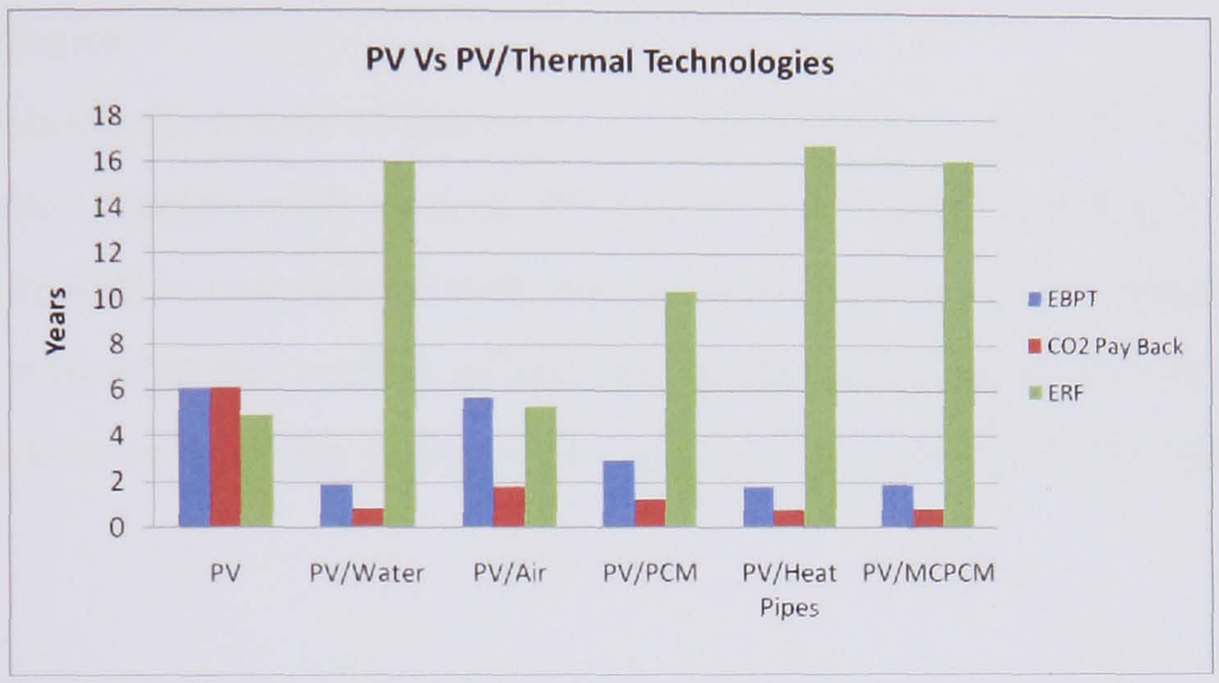

Figure 9.17 PV and PV/Thermal Technologies EBPT, CO_2 Payback and ERF

It may be seen that with increasing PV panel area there is also an increase of the CO_2 emissions saved. *Figure 9.18* shows for each PV/Thermal technology the amount of emissions saved by increasing the PV area.

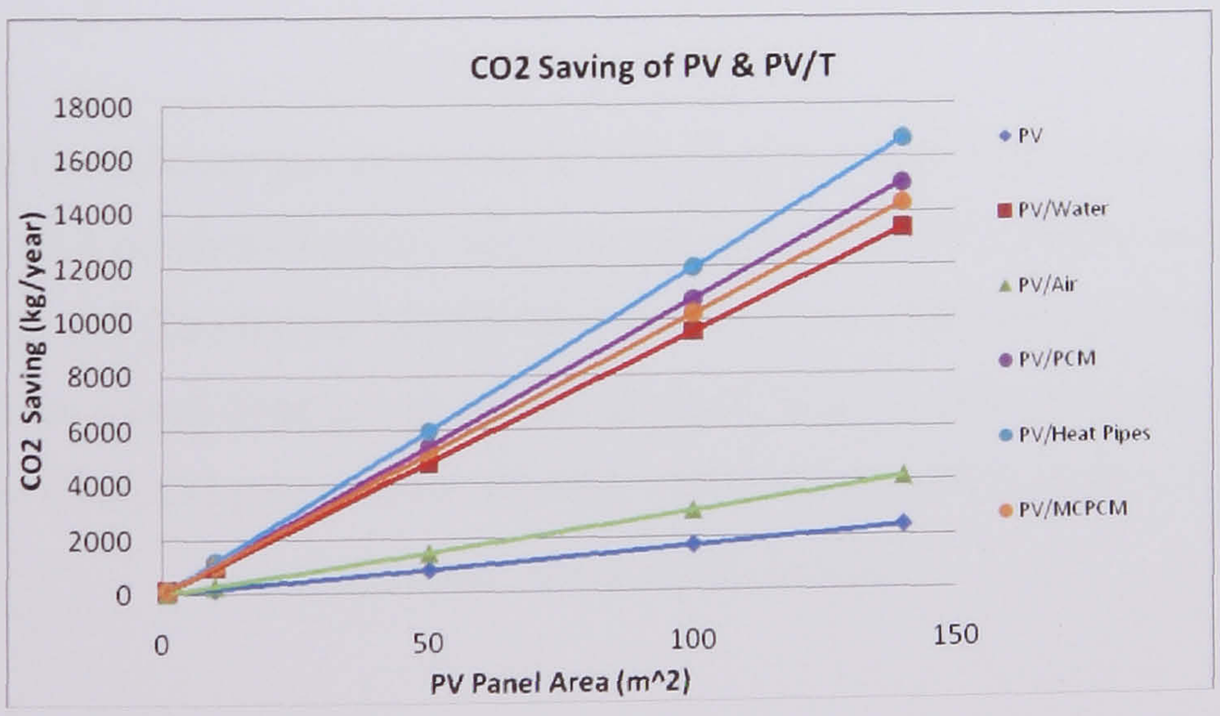

Figure 9.18 Emissions of CO2 saved per year with different PV panel area

Based on the LCA results' regarding greenhouse gas (GHG) emissions for module manufacturing it is possible to evaluate the life-cycle GHG emissions of our PV system, expressed in kg CO_2-eq per kWh in a similar way. For this evaluation the BOS data are used a 30 year system life time is assumed.

Dividing life cycle emissions made by the production of the systems by the useful electricity produced normalizes life cycle emissions and allows for comparison with other technologies.

Figure 9.19 shows the results of this exercise, and compares today's PV systems with a number of other energy supply options. PV with a GHG emission of 96 gr CO2- eq, performs quite well in comparison with fossil-fuel based technologies, but less so in comparison with wind and nuclear technology. At the same time the PV/Thermal technologies have reduced the emissions by around 70%, 7%, 52%, 71% and 69% respectively.

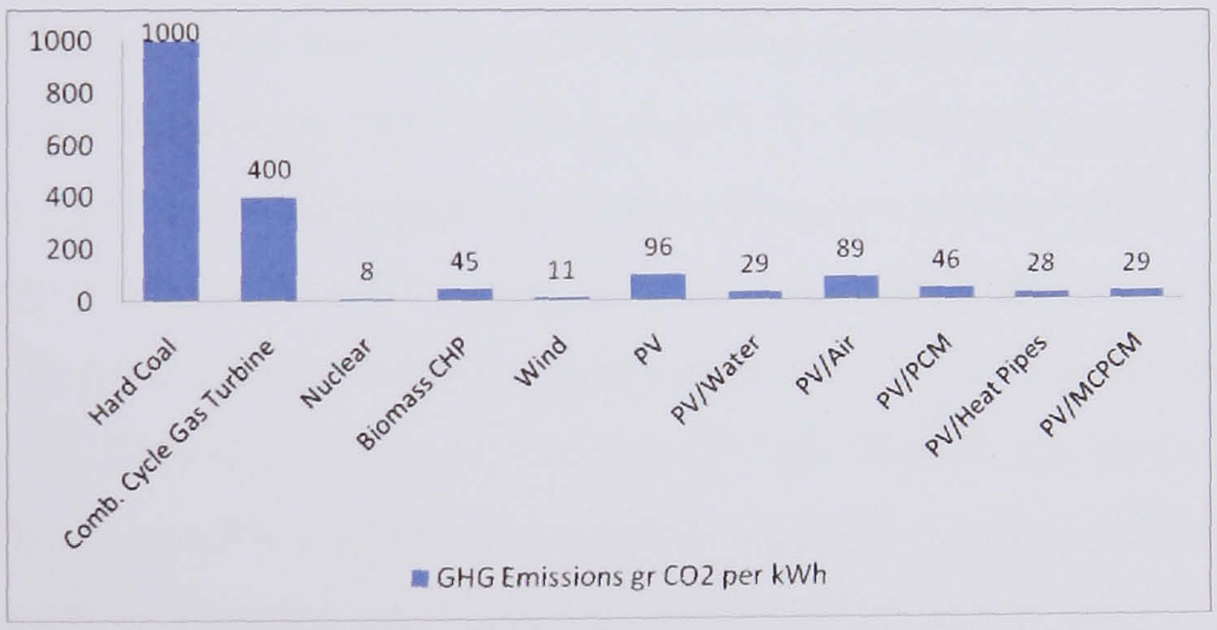

Figure 9.19 Greenhouse gas emissions of PV systems based on thin film technologies, compared with a number of other energy technologies. The PV systems are installed on a roof-top in UK (irradiation 888 kWh/m^2/yr) and have a 30 year life time. N.B. The emission from a coal-fired power plant (1000 gr/kWh) exceeds the Y-axis maximum (Sources: Coal, CC gas, nuclear, biomass and wind data derived from Ecoinvent database, www.ecoinvent.ch)

9.5 Conclusions

Three new PV/Thermal systems were compared with a PV system and two PV/T systems, the first used serpentine tubes, or a free channel for the system using water as a heat transfer medium and the second used an air passing from the rear of the PV with and without fins. This comparison was based on the technical, economic and environmental aspects of the five systems.

The technical comparison indicated that the new approaches of using heat pipes, phase change material and microPCM slurry have the potential to work as alternative PV/T systems. The system integrating PCM to the rear of the PV module performed better than all the other systems. Also the heat pipe system was performed equally with the PV/Water system. The PV/MCPCM system can work for applications that a small temperature difference is required and when the system works under a specific temperature range that includes the melting temperature of the PCM.

The PV/T systems cause of the additional energy that could generate had a better payback time than PV that was 57 years (PV/Thermal systems is 46 (PV/Water), 52 (PV/Air), 51 (PV/Heat pipe), 35 (PV/PCM) and 42 (PV/MCPCM) years). The cost of electricity as also the available grant can further reduce the payback times. The cost per kWh of energy produced for a PV system was the higher (£0.368/kWh) in comparison with the PV/Thermal systems that reduce it by around 72% (PV/Water), 28% (PV/Air), 63% (PV/PCM), 72% (PV/Heat pipe) and 72% (PV/MCPCM) respectively. A comparison between a PV/T system and a side-by-side PV and Solar Thermal Collector system was evaluated and the result indicated that the PV/T system achieved lower payback time by about 4 years and 25% lower cost of electrivity produced per kWh of energy produced. The most important benefit that a PV/T system can offer is the higher energy yield in the same surface area that reached about 86%.

The PV//T systems can reduce the CO_2 payback from 6 that is for PV to near or below 1 (0.78 PV/Water, 1.74 PV/Air, 1.21 PV/Heat pipe, 0.73 PV/PCM, 0.77 PV/MCPCM). The ability to generate more energy than a PV increases the Energy Return Factor from just 4.9 times for a PV to 16 for PV/Water, 5.3 for PV/Air, 10.3 for PV/PCM, 16.8 for PV/Heat pipe and 16.2 for PV/MCPCM respectively.

The Greenhouse Gas Emissions for a PV were 96 gr CO2- eq, a number that performs quite well in comparison with fossil-fuel based technologies, but less so in comparison with wind and nuclear technology. At the same time the PV/Thermal technologies have reduced the emissions by around 70% (PV/Water), 7% (PV/Air), 52% (PV/PCM), 71% (PV/Heat pipe) and 69% (PV/MCPCM) respectively.

CHAPTER 10: CONCLUSIONS AND FUTURE RECOMMENDATIONS

10.1 Conclusions

Most of the energy used in the World today comes from fossil fuels. The wealth of nations is linked with energy use which is the main factor driving the industrial and economic activity. Because of both rapid increase in population and economic development, the consumption of vast quantities of fossil fuels by mankind has increased dramatically. Today around 90% of UKs energy needs are met by fossil fuels and by 2010 will be a net importer of oil, gas and coal. There are two main problems to be concerned in the years to come. With the current use of fossil fuels the reserves will run out shortly. A few decades are the estimate for gas and oil and some centuries for coal. This need for high demand and low production of fossil fuels will increase the price of fuels and slow the current growth. The second problem is that by burning fossil fuels generation of harmful gasses fills the atmosphere. This impact on the environment by the CO_2 emissions causes the global warming. This effect could increase the earth's surface temperature 2-3 ^{o}C.

In the UK the domestic sector is responsible for consumption of the 30% of the total energy consumed. The majority of the consumption is for space and water heating applications. In the industrialized world this demand for low temperature heat is usually covered by consuming "high quality" resources such as fossil fuels, which are both limited in abundance and have a negative effect on the global environment. So in order to reduce the negative effects renewable energy could be used such as solar energy to provide the necessary low quality heat for building operation. At the Kyoto Summit, the UK has made a commitment to a 20% CO_2 reduction below 1990 level by the year 2010. This reduction will come mainly from employing renewable energy.

Most renewable energy sources are derived from solar radiation, including the direct use of solar energy for heating or electricity generation, and indirect forms such as energy from the wind, waves and running water, and from plants and animals. The use of renewable on a more significant scale than at present would at the very least replace a

further significant proportion of fossil and nuclear fuel use, thereby reducing the associated environmental impacts. Solar energy can be used in buildings to provide electricity or thermal energy for heating or cooling.

The conversion of solar energy to electrical and thermal energy has been practiced for many years. In order to convert the solar energy to electrical, photovoltaics are used. The widely used heat collection systems are flat-plate collectors for thermal applications. The markets for both solar thermal and PV are growing rapidly globally, but often the two technologies find themselves competing for sales in the residential sector. This competition arises because some families will choose to buy solar thermal collectors in order to heat their houses and others to supply them with green electricity. The limited space in the roofs and the cost of the technologies will prevent families to integrate both systems in their roof.

Hybrid energy systems combine the use of two or more alternative power sources and aim to increase the system's total efficiency. One relatively new type of PV panel is the hybrid PV panel. The photovoltaic/thermal (PV/T) system is a hybrid structure that has been examined quite thoroughly over the past years and makes use of the 70-95% of collected solar energy that is not converted into electricity by conventional solar cells. This heat extraction can be achieved by either air or a fluid coolant.

Based on the brief overview of the current status regarding the worlds and UKs energy consumption and the options for the future, and the potential of solar energy, this research investigates novel approaches for PV/T systems.

This PhD research focused entirely on the production of a hybrid PV/T fulfilling the main objectives that were to:

- improve performance of PV by reducing the temperature effect
- evaluate the PV/T system with water and air as a heat transfer medium and use the results as a benchmark
- investigate the heat pipe performance and develop a PV/T system that incorporates heat pipes

- evaluate the developed phase change material technology used as an absorber in back of the PV
- investigate and evaluate micro-encapsulated phase change materials for PV/T integration
- from the PV/T systems produce higher energy yield per surface area than a PV system
- use of an appropriate energy rating for electrical and thermal performance
- cost analysis of the systems and comparison with PV
- achieve improvements in greenhouse gas emissions savings in comparison with PVs

Some of the shortcomings associated with conventional solar collectors include:

a) extra expense of the forced circulation system due to the pump and its extracted power,
b) extra space required for the natural circulation system due to implicit position of the collector relative to the tank,
c) the potential risk of cooling of stored hot water due to the reverse flow at night,
d) freezing of the water on cold nights,
e) pipe corrosion due to the use of water
f) limited quantity of heat transferred by the heat transfer fluid.

The new approaches considered in this thesis present advantages than can overcome some of these problems. Some of these advantages and disadvantages are summarized below for each PV/T system separately:

<u>PV/T Heat Pipe:</u>

Advantages:

a) the thermal diode benefit when the collector temperature is less than storage water temperature;
b) less area needed in the back of the PV to incorporate the heat pipes than the water coil layout;

c) the reasonable resistance against corrosion by selecting a suitable working fluid to be compatible with the pipe wall material;
d) the easy freeze protection;
e) the lower pumping requirements;

Disadvantages:

a) the high thermal resistance of heat pipes cause a reduction in heat transfer in comparison with a PV/T water system with the serpentines in direct contact with the rear of the PV

PV/T PCM:

Advantages:

a) ability to cut the peak load and reduce the size of the system
b) stabilize PV cell temperature and thus improve electrical performance. The desired melting temperature of the PCM in order to keep the PV close at the reference temperature of 25 °C should be around the range above the ambient temperature and below 35 °C
c) the PCM can hold large amounts of energy at specific temperatures for a long time and release it when addition of solar energy is ceases
d) PCM's the low thermal conductivity can work as thermal insulator and thus reduce the heat losses
e) a PCM with low melting temperature can be used to improve electrical efficiency and provide low grade heat or a system with PCM having a higher melting point can be selected for high grade heat
f) improve heat storage discharge strategies: to be able to use that heat and not overheat the system after the PCM has completely melted a heat exchanger should be incorporated in the system in order to extract that heat. The advantage is twofold, first the PV is being kept as cool as possible for a longer time during the day and secondly the absorbed heat can be used for preheating purposes.

Disadvantages:

a) it can't provide increased thermal efficiency when compared with a PV/T system using serpentines in direct contact with the rear of the PV
b) a PV/T system having PCM in the back increase the weight of the system

PV/T MCPCM:

Advantages:

a) the use of phase-change material PCM particles suspended in a single-phase working fluid would provide additional thermal capacity from the latent heat associated with the solid-liquid phase change
b) no special equipment for charging and discharging PCM particles is needed because the PCM is always separated from the suspending fluid. Therefore, this type of slurry can be treated as a conventional single-phase working fluid.
c) furthermore the fluid works as a storage, carrier and rejector of heat system, advantage that can reduce size and cost of the system
d) stabilize the PVs cell temperature
e) another important advantage of using PCM in a solar heating system is that the store/system temperature does not increase at the same rate as in a water store. The solar collectors can therefore operate at lower temperatures for an extended period of time, thus increasing the total amount of solar energy collected by the system.

Disadvantages:

a) need for more pump power with using MCPCM slurry instead of water
b) is suitable for cases that work with a narrower temperature range and for a system working around the phase transition temperature of the chosen PCM

The research started from a review of solar thermal collectors and photovoltaics performance and applications. From the review the designs of flat-plate, and evacuated tube thermal collectors were presented. It was concluded that the solar components affect the performance of the system such as glazing and absorber plate. These two

components affect the parameters of solar absorption and heat loss from the system. This was followed by thermal and thermodynamic analysis of the collectors and a description of the methods used to evaluate their performance. From the review of PV technology different cell technologies were evaluated and concluded that the energy conversion efficiency is affected by the temperature of the PV cells.

After describing the two solar technologies and presenting the factors that affect their performance the new hybrid PV/T system was reviewed and the current status was reported. The review was concentrated on flat plate PV/T systems using water and air as a heat transfer medium. From the report it was concluded that the conduct between the absorber and the cell is an important parameter that affects the performance of the system. PV cells and thermal absorber plate should be well adhered together in order to decrease cell temperature and achieve high heat transfer to the passing fluid. Also it was discussed the option of a PV/T system having an extra cover that could reduce the heat loss coefficient and give better thermal efficiency but sacrifice the electrical efficiency. This thesis concentrated on PV/T systems without an extra cover and from Figure 2.30 the loss mechanisms parameters that affect the performance of the system can be seen. The parameters affecting PV/T performance was the absorption and reflection factor of PV surface, the mass flow rate, the absorber plate parameters (i.e. tube spacing, tube diameter, fin thickness), the absorber to fluid thermal conductance and the different PV cell technology used. From the review also investigated that three performance indicators should be used to assess the PV/T system performance. These were total energy efficiency, primary energy saving efficiency and exergy efficiency that could help to compare the different PV/T systems among them.

An extended literature review was undertaken to introduce the new technologies that could be used in the PV/T system. The first technology reviewed the basic principles of heat pipes. Different types of heat pipes were investigated according with their structure, shape and working fluid used. It was concluded that these devices are capable of transporting a large quantity of heat and this can vary in accordance with the shape, size and working fluid used. Also reported applications were heat pipes were used in solar

collectors. In these thesis solar collectors using a wickless gravity assisted heat pipe was reviewed and showed that these systems can provide additional advantages over conventional solar collectors. Some of these advantages were lower pumping requirements and freeze protection. Two heat exchanger types and different working fluids were assessed and the conclusion is that both parameters affect the performance of the system. Both heat exchanger types with the condenser section of the heat pipe inside a tank or inside a manifold gave satisfactory results. Best performance was obtained when using a working fluid with high latent heat, high liquid thermal conductivity, and low viscosity.

Next review looked at the current state of research in phase change materials, with the main focus being on the assessment of the thermal properties of various PCMs, methods of heat transfer enhancement and design configurations of heat storage facilities to be used as a part of solar passive and active space heating systems. One advantage of using PCM was the relatively large amount of latent heat associated with the phase transition that gives a higher energy storage density compared to the traditional sensible heat storage systems, and therefore allows a reduction of volume and mass. Another advantage is the isothermal behaviour during melting/freezing which reduces the temperature range of operation. Phase change materials were classified as organic and inorganic materials mentioning their advantages and disadvantages. The use of nucleating and thickening agents was recommended to reduce supercooling and phase segregation. Also commercially PCM were presented with melting temperatures ranging from 22 – 31 ^{o}C. For the PV/T system these materials could be candidates to be used to bring the PV temperature near the reference temperature (25 ^{o}C) of the PV in order to improve its performance. One major problem for latent heat storage systems is that most of the PCM have low thermal conductivity. Thus techniques were reported like fins that could improve the rate of heat transfer as also focused on the performance of PCM on rectangular enclosures. Review showed that PCM could be used in buildings either incorporated in the walls, roof or floor, either used in solar collectors. Solar collectors incorporating PCM in their structure or inside a storage unit were presented and results showed improved heat transfer rate and improvement is heat loss coefficient.

Another interesting technology reviewed was to use phase change material inside small containers in order to improve the heat transfer coefficient of the system. Many conventional thermal energy systems often operate with the use of a single phase working fluid is likely to require high volumetric flow rate. PCMs can be encapsulated in small micro-spheres and suspended in a working fluid to form slurry. This improves the thermal characteristics of a heat transfer fluid through use of the latent heat of fusion. It was concluded that by increasing the heat transfer coefficient by introducing the use of a suspended particles of PCM in the carrier fluid would permit the use of smaller flow rate. Applications that the MCPCM could be used were in textiles or inside building structure. Two new applications reviewed, one was using MCPCM slurry in a ceiling in order to provide cooling to the building and the other a solar collector/storage system that could retain heat at high temperatures for a longer time than water.

From literature review the different technologies potential were evaluated and provided an understanding of the operating conditions. Before investigate the PV/T systems using the new approaches it was necessary to investigate the performance of the PV with or without insulation in order to evaluate how the temperature affect the performance of a polycrystalline PV. A set of experiments were undertaken to evaluate how the temperature affects the current, the voltage, the power and the electrical efficiency of the PV. From the results it was concluded that the uninsulated PV performed better than insulated. At 1000 W/m^2 the electrical performance was 3.88% for insulated and 4.02% for uninsulated system. After validating that the temperature affects negatively the performance of the PV two experiments were performed using water and air to cool down the PV.

These two experiments used the same PV and followed the PV/T guidelines mentioned in the literature review for systems working with water and air in the rear of the PV. The purpose of these experiments was to use their results as a benchmark tool to the new approaches in order to perform a comparison and assess the potential that these new systems can have.

The PV/T model using water investigated two heat extraction devices, the first being a serpentine tube adhered in a copper sheet and the second a rectangular tank creating a flow channel in the back of the PV. The heat transfer coefficient with the serpentine tube was higher (129.21 W/m^2K) than with the rectangular tank (73.87 W/m^2K) in the rear of the PV cause of the better contact between PV laminate and copper sheet. By varying the flow rate in experiments it was noticed that both systems achieve better thermal and electrical performance. In the same time the PV temperature reduces as the difference between water outlet and inlet. Between the two systems the PV incorporating the rectangular tank had a better thermal performance than the serpentine pipe cause water passing in the rear of the PV covers the full area of the panel in comparison with the serpentine pipes. Despite the better thermal efficiency of the tank system (63.8% to 59.7% of serpentine pipe) the heat loss coefficient in higher operating temperatures is higher (14.31 W/m^2K to 7.68 W/m^2K of serpentine). This is may be cause of the higher capacity of water passing the channel below the PV and thus causing higher heat losses. From exergy analysis it was possible to identify the optimum working conditions of the two systems. It was found that both systems work better when the inlet temperature is in the range of 35 – 45 ^oC with peak efficiencies 21.5% for the water tank and 25% for the serpentine tube. With the experiments also a similar model was simulated using TRNSYS in order to identify which factors affect the performance of the system and how useful this simulation can be for predicting PV/T system performance. From the results it was concluded that it the simulated model was closer to the model with the serpentine tubes and the two factors that affect the performance of the system are the heat loss coefficient and the transmittance-absorptance product.

The PV/T system using air investigated two experimental models. The first model used a free channel having a duct depth of 3 cm and air passing from it, and the second incorporated fins bonded to the back of the PV in order to achieve heat transfer augmentation and improve its overall performance of the system. The heat transfer coefficient for the system with the fins was 500% better than the system without fins. This resulted in lower PV temperature and higher temperature difference between air outlet and inlet. Different flow rates were tested and observed that the increase of flow

rate improves the electrical and thermal performance. Fins increase the thermal performance by 35% at 25 m^3/hr flow rate in comparison with the system having no fins. When the inlet air temperature was varied it was observed that the system with the fins at zero reduced temperature has a thermal efficiency of 49.6% in comparison with no fins that achieves an efficiency of 30.4%. The exergy efficiency shows that both systems works best when the inlet temperature is around 36 °C and PV/T model with the fins achives 16% exergy efficiency 4% more than the system without fins. Both models were simulated using TRNSYS and their performance was in good agreement with the experimental results.

These two models worked as a benchmark to the new PV/T models that use heat pipes, phase change material and microencapsulated phase change material slurry to cool down the same PV.

Before investigate the performance of the PV/T model using heat pipes first a simulation was performed in order to identify the performance of a heat pipe by changing parameters such as the working fluid, diameter of heat pipe, liquid fill level and inclination angle. It was observed that water performs better at operating temperatures ranging from 20 °C and above. By increasing the diameter of the heat pipe the heat transfer capacity increases and above a certain level the heat transport capacity no longer varies with the level of liquid filling. The inclination angle affects the heat transfer capacity of the heat pipe by reaching its maximum around 60 deg. Also two experiments were performed in order to evaluate the heat transfer coefficient and thermal conductivity of the pipe that was created in our labs. It was observed that the thermal conductivity is 6 times (2411 W/mK) higher than the conductivity of copper and the heat transfer coefficient increased from 5000 – 7000 W/m^2K when the power input to the heat pipe was increased. The heat pipe constructed and used was underperforming in comparison with pipes that achieve thermal conductivities from 100 to 200 that of copper. The principle of obtaining a relationship between the design parameters of a heat pipe solar collector and the heat removal factor was introduced by Kamminga (1986). The parameters that affect the performance of a heat pipe solar collector was; the evaporator and the condenser thermal resistances per unit area and the effect of the

condenser size. After investigating the performance of a heat pipe and estimating the heat removal factor of our model (FR = 0.9106) from Kammingas model the next step was to observe the performance of the two PV/T models using heat pipes in the rear of the PV. The main difference between the two systems was in the condenser section. The first model used a manifold for water passing from each condenser and in the second model the condenser section of the heat pipes was inside a tank. The model with the condensers inside the tank was adhered with fins in order to increase the heat transfer area of the condenser section. The result with fins showed an increase of 1.29 % for the electrical and 24.78% for the thermal efficiency. When comparing the two different PV/T models it was observed that the system with the manifold (65.4%) had higher thermal efficiency than the system with the tank (60.5%). Also the system with the tank had higher heat losses cause of the bad insulation in the bottom of the tank and the larger capacity of water resulting in bigger losses. The exergy efficiency confirmed this observation. For PV/T model with the manifold the system could work in higher operating range (30 – 50 ^{o}C) with peak exergy efficiency at 24% than the model with the tank (25 – 35 ^{o}C, 17%) .

Incorporating a solid–liquid PCM with a phase change similar to the PV reference temperature of 25 ^{o}C for the thermal regulation of PV under cyclic time-dependent solar energy input was the next novel approach. Four PCMs (E21, A28, E30, and E32) were selected having a melting temperature near the reference temperature of 25 ^{o}C. From using the duration index indicator and comparing with the transient numerical model developed it was observed that E32 takes longer to undergo complete melting. From the TRNSYS model developed it was possible to evaluate the parameters that affect a PV/T system using PCM in the rear. One such a parameter is the thermal conductivity between the PCM container and the PV rear surface. At higher conductivity the PV keeps the temperature at lower level than with systems with bad conductivity. Another parameter that affected the performance of the system was the thickness of the PCM that by increasing it kept the PV temperature near the reference temperature (25 ^{o}C) longer time and thus had better electrical efficiency for longer time. By increasing the ambient temperature the temperature of the PV does not change significantly, however, as less

heat is lost from the system because of the lower temperature difference between the system and ambient, the time required for the PCM melting is reduced. Also with increasing insolation intensity the temperature at the PV surface increased and the melt time reduced. A simulation was carried out for one and three days and it was observed that by having more PCM in the rear of the PV a lower temperature is maintained for longer time and more energy is absorbed ready to be used during the night. The experiments undertaken with A28 as PCM validated the simulated results. From the experiments and simulations it was observed that the PCM can hold amounts of energy at specific temperatures for a long time and release it when addition of solar energy is ceases. Depending from the PCM melting temperature used a PV/PCM system using a PCM with low melting temperature can be used to improve electrical efficiency and provide low grade heat or a system with PCM having a higher melting point can be selected for high grade heat. To be able to use that heat and not overheat the system after the PCM has completely melted a heat exchanger incorporated in the system was used in order to extract that heat. Comparing the PV/T model with serpentine tubes and with the model incorporating pipes inside the PCM tank it was concluded that the model with the PCM had better electrical efficiency but similar thermal efficiency at different flow rates. When varying the inlet water temperature the thermal efficiency at zero reduced temperature was the same (59.8% - 59.7%) but the model with the PCM had lower heat loss coefficient (7.68 W/m^2K to 4.13 W/m^2K) because the material was working as an insulator. However it was noticed that when the inlet temperature of the water was near melting point the efficiency of the system dropped to 32% cause much of the heat was retained by the PCM as a latent heat. When the inlet water temperature exceeded the melting point of PCM it was observed that the efficiency increased and reached around 70%. This indicated that the system except from the lower heat loss, the water absorbed latent and sensible heat. This phenomenon can be observed from exergy efficiency when comparing with the PV/T model using serpentine tubes in the rear. The results showed that the exergy efficiency without the PCM was 24% - 25% instead of 30% - 34% with the PCM.

Due to the low thermal conductivity of many phase change materials it is difficult to get high rates of heat transfer therefore the phase change materials can be microencapsulated and suspended in a carrier fluid to form slurry. The use of phase-change material PCM particles suspended in a single-phase working fluid would provide additional thermal capacity from the latent heat associated with the solid-liquid phase change. The technique of thermal analysis investigated the performance of two phase change slurries with different melt temperatures (26 ^{o}C and 33 ^{o}C) and concentrations (10%, 20%, 30% and 40%). Results showed that the temperature difference between the fluid and bath for the MCPCM slurries were higher than that of pure water in both heating and cooling mode. Furthermore the slurry with high concentrations had the bigger temperature differences comparing to those of the small concentrations. This was because most of the energy was used during the transition of phase with no change in temperature. Thus the suspension of MCPCM particles in a carrier fluid was found to increase the heat transportation of the working fluid. The PCM in microcapsules was selected to melt/freeze at temperatures near the characteristic temperature of the PV (25 ^{o}C). To evaluate the performance of a PV/T model a rig was constructed consisted of two closed circuits, the primary and secondary circuit. The primary circuit consisted of a PV panel, a shell and tube copper heat exchanger unit that is incorporated in the back of the PV, a MCPCM slurry tank that the slurry passes for the electric mixer to keep the fluid mixed and homogeneous, a double diaphragm pump and a flow rate transmitter (turbine type). The secondary circuit comprised of a heat exchanger cooling fan, a pump and a variable flow meter. These two circuits were connected with a a shell and coil heat exchanger cause it was not possible to use the log-mean-temperature-difference (LMTD) method for the MCPCM slurry because neither the thermal capacity nor the local heat transfer coefficient is constant along the flow direction. The error for transferring heat from the primary to the secondary circuit was around 5.6%.
For 1000 W/m^2, the temperature difference between the inlet and outlet of the collector for 20% MCPCM slurry was around 2.8 ^{o}C comparing to 4 ^{o}C of the pure water. Overall the rate of heat transfer of the MCPCM slurry was higher than that of the pure water because the apparent specific heat capacity is much higher than conventional sensible heat of a fluid without phase change, which greatly enhanced the heat transfer

performance between the fluid and heat transfer surface. Near the melting temperature the efficiency improvement was around 21% (69% for MCPCM and 57% for water). When the temperature range of inlet and outlet was out of the melting range of the PCM materials, then the thermal efficiency was very close to that of water. A drawback was the need for more pump power with using MCPCM slurry instead of water.

To evaluate if the three new PV/Thermal systems have the potential to be useful alternative technologies, for a hybrid PV and Thermal collector panel, a comparison was carried out. This comparison was based on the technical, economic and environmental aspects of the five systems.

The system integrating PCM to the rear of the PV module achieved higher electrical efficiency and the lowest heat loss coefficient and hence highest thermal efficiency of all the other systems. The hybrid systems incorporating heat pipes can be compared very well with the PV/Water system and have the potential to be competitive technology if heat loss coefficient issues are being resolved. PV/MCPCM system for very low grade temperature applications can provide thermal efficiencies that reach 70% and their electrical efficiency is equal with the one of PV/Water system. Last to mention PV/Air system cause of the lower thermal conductivity and heat capacity give the lowest thermal and electrical efficiencies.

When the green electricity price increases the payback period for a PV can reach the 11.48 years and for the PV/Thermal systems is 9.31 (PV/Water), 10.52 (PV/Air), 7.02 (PV/Heat pipe), 10.26 (PV/PCM) and 8.57 (PV/MCPCM) years. As also observed as the grant scheme increases, the payback reduces. An alternative way of comparing systems is to investigate the cost per kWh of energy produced from a PV or PV/Thermal system. The PV system has the higher (£0.368/kWh) cost per kWh of energy produced in comparison with the PV/Thermal systems that reduce it by around 72% (PV/Water), 28% (PV/Air), 63% (PV/Heat pipe), 72% (PV/PCM) and 72% (PV/MCPCM) respectively. When comparing a PV/T system with a side-by-side PV and Solar Thermal Collector system the first system achieves lower payback time and also for the same surface area a higher energy yield.

For the PV system the CO_2 payback is around 6 in comparison with the PV/Thermal systems which are near or below 1 (0.78, 1.74, 1.21, 0.73, 0.77). The Energy Return Factor for the PV is just 4.9 times for PV/Water it is 16, for PV/Air is 5.3, for PV/PCM is 10.3, for PV/Heat Pipe is 16.8 and for PV/MCPCM is 16.2 respectively.
It was observed that PV with a GHG (Greenhouse Gas Emissions) emission of 96 gr CO2- eq, performs quite well in comparison with fossil-fuel based technologies, but less so in comparison with wind and nuclear technology. At the same time the PV/Thermal technologies have reduced the emissions by around 70% (PV/Water), 7% (PV/Air), 52% (PV/Heat pipe), 71% (PV/PCM) and 69% (PV/MCPCM) respectively.

10.2 Recommendations for Future Work

Further research can be carried out in the following areas:

For PV/Heat pipe system

i. perform experiments with a flat heat pipe or a closed loop heat pipe that will cover the whole area in the back of the PV and achieve higher thermal conductivities
ii. perform experiments with different number of heat pipes. An optimum number of heat pipes incorporated in the back of the PV could be found
iii. design different manifold configurations and achieve an optimum design
iv. use different working fluids in the heat pipe and evaluate with different conditions which can work most effectively
v. improve the systems design and develop a transient numerical model or use a CFD software to simulate the PV/Heat pipe performance
vi. take into consideration of cost issues in designing a PV/T Heat pipe model

For PV/PCM system

i. depending from the application needed perform experiments with different PCM melting temperatures. PCM with high melting temperatures can work for higher heat grade than PCM with lower melting temperatures
ii. perform experiments to see how much energy can extract when irradiation has finished

iii. improve designs by increasing heat transfer rate by incorporation of fins

iv. take into consideration of cost issues in designing a PV/T PCM model

For PV/MCPCM system

i. perform experiments with different MCPCM melt temperature depending from the application needed. See PV/PCM i.

ii. perform experiments for all $\Delta T/G$ range to observe the performance of the collector

iii. a better heat exchanger system can be designed to enhance the microPCM heat transfer coefficient

iv. investigate how much the pump power consumption can decreased. As a MCPCM slurry can give higher heat transfer rate in comparison with water at the same flow rate we could reduce the flow rate and achieve the same heat transfer rate as a water system can achieve when works at higher flow rate

v. a theoretical model can determine the local bulk mean temperature of MCPCM flowing through a heat exchanger

vi. take into consideration of cost issues in designing a PV/T MCPCM model

References

A

Abhat. A. (1983), "*Low Temperature Latent Heat Thermal Storage: Heat Storage Materials*". Solar Energy Vol.30.No.4.pp 313-332

Adams W.G. and R.E. Day (1887), "*The action of light on selenium in Royal Society*", London

Affolter P. (1997), "*New generation of hybrid solar PV/T collectors—feasibility study*" (phase 1). Report DIS 56360/16868

Affolter P, Haller A, Ruoss D, Toggweiler P. (2000), "*A new generation of hybrid solar collectors—Absorption and high temperature behaviour evaluation of amorphous modules*". 16th EPSEC Glasgow

Agarwal RK, Garg HP. (1994), "*Study of a photovoltaic-thermal system—thermisyphonic solar water heater combined with solar cells*". Energy Conversion Management; 35(7):605–20.

Akbarzadeh A., T. Wadowski, (1996), "*Heat pipe-based cooling systems for photovoltaic cells under concentrated solar radiation*", Appl. Therm. Eng. 16 (1) (1996) 81–87.

Akyurt M., (1984), "*Development of heat pipes for solar water heaters*", Solar Energy 32 (1984) 625–631.

Alisetti E.L., S.K. Roy (1999), "*Forced convection heat transfer to phase change material slurry in circular ducts*", Journal of Thermophysics Heat Transfer 14 (1) 115–1180.

Erik A. Alsema, Mariska J. de Wild-Scholten, "*Environmental Impacts of Crystalline Silicon Photovoltaic Module Production*", Copernicus Institute of Sustainable Development and Innovation, 13th CIRP INTERNATIONAL CONFERENCE ON LIFE CYCLE ENGINEERING

Erik Alsema, "*Energy requirements of thin film solar cell modules: a review*", Renewable and Sustainable Energy Reviews, 2 (1998) 387-415

E.A. Alsema*, E. Nieuwlaar, "*Energy viability of photovoltaic systems*", Energy Policy 28 (2000) 999}1010

Erik A. Alsema and Mariska J. de Wild-Scholten, "*ENVIRONMENTAL IMPACTS OF CRYSTALLINE SILICON PHOTOVOLTAIC MODULE PRODUCTION*", Mater. Res. Soc. Symp. Proc. Vol. 895 © 2006 Materials Research Society 0895-G03-05.1

E.A. Alsema, M.J. de Wild-Scholten, V.M. Fthenakis, "*ENVIRONMENTAL IMPACTS OF PV ELECTRICITY GENERATION - A CRITICAL COMPARISON OF ENERGY SUPPLY OPTIONS*", Presented at the 21st European Photovoltaic Solar Energy Conference, Dresden,Germany, 4-8 September 2006

E.A.Alsema, P.Frankl, K.Kato, "*Energy payback time of photovoltaic energy systems: present status and prospects*", 2nd world conference on photovoltaic solar energy conversion, Vienna 6-10 july 1998

Ardente Fulvio, Giorgio Beccali, Maurizio Cellura,Valerio Lo Brano, "*Life cycle assessment of a solar thermal collector: sensitivity analysis, energy and environmental balances*", Renewable Energy 30 (2005) 109–130

Fulvio Ardente, Giorgio Beccali, Maurizio Cellura*, Valerio Lo Brano, "*Life cycle assessment of a solar thermal collector*", Renewable Energy 30 (2005) 1031–1054

ASHRAE Standard 93, (1986), "*Methods of testing to determine the thermal performance of solar collectors*", ANSI/ASHRAE 93- 1986; 1986.

ASTM, (1998), "*Standard test methods for electrical performance of non-concentrator terrestrial photovoltaic modules ad arrays using reference cells*", standard E1036. West Conshohocken, PA: American Society for Testing and Materials; 1998.

Augood P.C., M. Newborough, D.J. Highgate (2001), "*Thermal behaviour of phase-change slurries incorporating hydrated hydrophilic polymeric particles*", Experimental Thermal and Fluid Science 25 457–468.

B

Bakker M, Zondag HA, Elswijk MJ, Strootman KJ, Jong MJM. (2005), "*Performance and costs of a roof-sized PV/ thermal array combined with a ground coupled heat pump*". Solar Energy; 78:331–9.

Riccardo Battisti, Annalisa Corrado, "*Evaluation of technical improvements of photovoltaic systems through life cycle assessment methodology*", Energy 30 (2005) 952–967

Bazzo E., M. Nogoseke, (2003) "*Capillary pumping systems for solar heating application*", Applied Thermal Engineering 23 (2003) 1153–1165

Bergene T., O.M. Lovvik, (1995), "*Model calculations on a flat plate solar heat collector with integrated solar cells*", Solar Energy 55 (6) 453–462.

Bernal J.A, Rodolfo D.L, "*Economical and environmental analysis of grid connected photovoltaic systems in Spain*", Renewable Energy 31 (2006) 1107–1128

Biswas DR (1977). "*Thermal energy storage using sodium sulphate decahydrate and water*". Solar Energy; 19:99–100.

Bloem H, De-Grijs JC, De-Vaan RLC., (1982) "*An evacuated tubular solar collector incorporating a heat pipe*". Phillips Technical Rev 1982; 40:181±91.

Boukhanouf R., A. Haddad, M.T. North, C. Buffone, "*Experimental investigation of a flat plate heat pipe performance using IR thermal imaging camera*", Applied Thermal Engineering 26 (2006) 2148–2156

BP (2007), "*Statistical Review Charting Tool*", [Electronic Version], Retrieved October 2006, http://www.investis.com/bp_acc_ia/stat_review_06/htdocs/index.html

Brown R.C, J.D. Rasberry, S.P. Overmann (1998), "*Microencapsulated phase-change materials as heat transfer media in gas-fluidized beds*", Powder Technol. 98 (3) 217–222.

C

Cabeza L.F., J. Illa, J. Roca, F. Badia, H. Mehling, S. Hiebler, F. Ziegler (2001), "*Immersion corrosion tests on metal-salt hydrate pairs used for latent heat storage in the 32 to 36 oC temperature range*", Mater. Corros. 52 140–146.

Cabeza L.F., H. Mehling, S. Hiebler (2001), "*Immersion corrosion tests on metal-salt hydrate pairs used for latent heat storage in the 48 to 58 oC temperature range*", Mater. Corros., in press.

Chapin D.M., Fuller C.S., Pearson P.L., 1954, "*A New Silicon p-n Junction Photocell for Converting Solar Radiation into Electrical Power*", Journal of Applied Physics, 1954, 25, p 676

Chalmers, B. (1964), "*Principles of Solidification*". John Wiley & Sons, Inc. New York.

Charalambous PG, Maidment G, Kalogirou SA, Yiakoumetti K. (2007), "*Photovoltaic thermal (PV/T) collectors: a review*". Applied Thermal Engineering; 27:275–86.

Charunyakorn P., S. Sengupta, S.K. Roy (1991), "*Forced convection heat transfer in microencapsulated phase change material slurries: flow in circular ducts*", Int. J. Heat Mass Transfer 34 (3) 819–833.

Chen, K., and M. M. Chen (1987), "*Analytical and Experimental Investigation of the Forced Convective Heat Transfer of Phase-Change Slurry Flows*", *Proc. Int. Symp. Multiphase Flows _II.*, Ziejiang Univ. Press, China, p. 496

Chris Laughton, "*The special nature of the UK solar market*", Retrieved 12 November 2007, http://www.greenenergy.org.uk/sta/solarenergy/documents/UKSolarMarket.pdf

Choi E., Y. Cho, H.G. Lorsch (1993), "*Forced convection heat transfer with phase-change-material slurries: turbulent flow in a circular tube*", Int. J. Heat Mass Transfer 37 (2) (1993) 207–215.

Chow TT, He W, Ji J. (2006), "*Hybrid photovoltaic-thermosyphon water heating system for residential application*". Sol Energy; 80(3):298–306.

Chow T.T., W. He a, J. Ji b, A.L.S. Chan, (2006), "*Performance evaluation of photovoltaic–thermosyphon system for subtropical climate application*", Solar Energy xxx (2006)

Chow T.T., (2003), "*Performance analysis of photovoltaic-thermal collector by explicit dynamic model*", Solar Energy 75 143–152

Chow TT, Hand JW, Strachan PA. (2003), "*Building-integrated photovoltaic and thermal applications in a subtropical hotel building*". Applied Thermal Engineering; 23:2035–49.

Chun W., Y.H. Kang, H.Y. Kwak, Y.S. Lee, (1999), "*An experimental study of the utilization of heat pipes for solar water heaters*", Applied Thermal Energy 19 (1999) 807–817.

Climator, 2004. Available from /www.climator.comS.

Clearly, C., S. Day, R. Lindsay, C. Murry, R. Gupta, B. Larkin, H. Thompson, M. Wiggin, and J. S. O' C. Young (1990), ''*Hydraulic Characteristics of Ice Slurry and Chilled Water Flows*,'' *IEA District Heating: Advanced Energy Transmission Fluid-Final Report of Research*, Novem BV, Sittard, Netherlands

Colvin, D. P., and J. C. Mulligan (1986), "*Spacecraft Heat Rejection Methods: Active and Passive Heat Transfer for Electronic Systems*," Phase I, Final Rep., AFWAL-TR-86-3074

Colvin, D. P., J. C. Mulligan, and Y. G. Bryant (1992), "*Enhanced Heat Transport in Environmental Systems Using Microencapsulated Phase Change Materials*," *Proc. Int. Conf. Environmental Systems*, Seattle, WA, p. 717

Coventry J.S, K. Lovegrove, (2003), "*Development of an approach to compare the 'value' of electrical and thermal output from a domestic PV/thermal system*", Solar Energy 75 (1) 63–72.

Cox CH, Raghuraman P. (1985), "*Design considerations for flat-plate photovoltaic/thermal collectors*". Sol Energy; 35(3):227–41.

Cristopia Energy Systems, 2004. Available from /http://www.cristopia.comS.

D

Del Cueto JA, (2002), "*Comparison of energy production and performance from flat-plate photovoltaic module technologies deployed at fixed tilt*". In Proceeding of the 29th IEEE PV specialists conference, New Orleans, USA; 20–24 May 2002.

De Vries H.F.W., W. Kamminga, J.C. Francken, (1980) "Fluid circulation control in conventional and heat pipe planar solar collectors", Solar Energy 24 (1980) 209–213.

De Vries DW. (1998), "*Design of a photovoltaic/thermal combi-panel*". PhD report, EUT

Paul Denholm, Gerald Kulcinski, "*Net energy balance and greenhouse gas emissions from renewable energy storage systems*", ECW report number 223-1, 2003

Dincer I., M.A. Rosen, (2002), "*Thermal energy storage, Systems and Applications*", John Wiley & Sons, Chichester (England).

R. Donek, T. Heck, S. Hirschberg, "*Greenhouse gas emissions from energy systems: comparison and overview*" PSI Annual Report 2003 Annex IV, Switzerland http://gabe.web.psi.ch/pdfs/Annex_IV_Dones_et_al_2003.pdf

DTI (2006a), *"Energy Consumption in the UK"*, [Electronic Version], Retrieved October 2006, http://www.dti.gov.uk/files/file11250.pdf

DTI (2006b), *"The Energy Challenge"*, [Electronic Version], Retrieved October 2006, http://www.dti.gov.uk/files/file31890.pdf

Duffie JA, Beckman WA, 1991, "*Solar engineering of thermal processes*". New York: Wiley; 1991.

Dunn P.D., D.A. Reay, (1994), "*Heat Pipes*", fourth ed., Pergamon Press Ltd., New York, 1994.

E

Eames I.W., K.T. Adref (2002), "*Freezing and melting of water in spherical enclosures of the type used in thermal (ice) storage systems*", Appl. Thermal Eng. 22 733–745.

Eames P.C., P.W. Griffiths (2006), "*Thermal behaviour of integrated solar collector/storage unit with 65 _C phase change material*",Energy Conversion and Management 47 3611–3618

E.R.G. Eckert, R.J. Goldstein, W.E. Ibele, S.V. Patankar, T.W. Simon, P.J. Strykowski, K.K. Tamma, T.H. Kuehn, A. Bar-Cohen, J.V.R. Heberlein, D.L. Hofeldt, J.H. Davidson, J. Bischof, F. Kulacki (1997), "*Heat transfer—a review of 1994 literature*", Int. J. Heat Trasfer 40 3729–3804.

Egolf P.W., (2001), "*Proceedings of the Fourth Workshop on Ice Slurries of the International Institute of Refrigeration*", Grand Cube, Osaka, November 12-13

Egollf P.W., Derrick Ata-Caesar1, Andrej Kitanovski, Osmann Sari, Jonas Brulhart, Samuel Perrin, "*Thermal Energy Transport and Storage with Multi-Functional Fluids: The Effective Thermal Conductivity*"

EIA (2000), *"International Energy Outlook"*, [Electronic Version], Retrieved June 2003, http://tonto.eia.doe.gov/FTPROOT/forecasting/04842000.pdf

Eiffert ImaginIt LLC, "*Guidelines for the Economic Evaluation of Building-Integrated Photovoltaic Power Systems*" , International Energy Agency PVPS Task 7: Photovoltaic Power Systems in the Built Environment, January 2003 • NREL/TP-550-31977

EPS Ltd., (2004). Environment Processing System Limited. Available from: /http://www.epsltd.co.ukS.

Esen M., H. Esen, (2005), "*Experimental investigation of a two-phase closed thermosyphon solar water heater*", Solar Energy 79 (2005) 459–468.

Esen M., T. Yuksel, (2000), "*Performance of thermosyphon flat plate solar collector with heat pipes*", Firat University Journal of Science and Engineering 12 (2000) 201–207.

Evans DL, (1981), "*Simplified method for predicting photovoltaic array output*". Solar Energy 1981; 27(6):555–60.

F

Fahgri, A., (1995). "*Heat Pipe Science and Technology*". Taylor & Francis, Washington.

Fan Y.F., X.X. Zhang, X.C. Wang, J. Li, Q.B. Zhu (2004), "*Super-cooling prevention of microencapsulated phase change material*", Thermochimica Acta 413 1–6

Feldman K.T., D.D. Kenney, M.W. Edenburn, (1981) "*A passive heat pipe cooled photovoltaic receiver*", Conference record, 15th IEEE PVSC, 1981, pp. 165–172.

Field H., Solar Cell Spectral Response Measurement Errors Related to Spectral Band Width and Chopped Light Waveform, *Presented at the 26th IEEE Photovoltaic Specialists Conference, September 29*B *October 3, 1997, Anaheim, California*

Florschuet L.W., (1979), "*Extension of the Hottel–Whillier model to the analysis of combined photovoltaic/thermal flat plate collectors*", Solar Energy 22 (4) 361–366.

Florida Solar Energy Centre (2007), "*Solar Electricity Basics*", Retrieved 2007, http://www.fsec.ucf.edu/en/consumer/solar_electricity/basics/how_pv_cells_work.htm

Fouda AE, Despault GJG, Taylor JB, Capes CE. (1984). "*Solar storage system using salt hydrate latent heat and direct heat exchanger*". *Solar Energy* 32:57}65.

P. Frankl, A. Masini,1 M. Gamberale and D. Toccaceli, "*Simplified Life-cycle Analysis of PV Systems in Buildings: Present Situation and Future Trends*", PROGRESS IN PHOTOVOLTAICS: RESEARCH AND APPLICATIONS Prog. Photovolt. Res. Appl. 6, 137±146 (1998)

Frisby Company (2007), www.frisby.com.

Vasilis Fthenakis1, and Erik Alsema, "*Photovoltaics Energy Payback Times, Greenhouse Gas Emissions and External Costs: 2004–early 2005 Stat*us", PROGRESS IN PHOTOVOLTAICS: RESEARCH AND APPLICATIONS Prog. Photovolt: Res. Appl. 2006; 14:275–280

Fujisawa T., T. Tani, (1997), "*Annual exergy evaluation on photovoltaic– thermal hybrid collector*", Solar Energy Materials and Solar Cells 47 (1–4) 135–148.

Furbo S, Jivan Shah L. (2003), "*Thermal advantages for solar heating systems with a glass cover with antireflection surfaces*". Sol Energy; 74:513–23.

Furbo S, Jivan Shah L, Overvad Jensen L, Larsen E, Olsson G. (2004), "*Advantages by utilizing antireflection treated glass covers for PV modules*". In: ISES Eurosun, Freiburg

G

Ghaddar N., Y. Nasr, (1998), "*Experimental study of a refrigerant charged solar collector*", International Journal of Energy Research 22 (1998) 625–638.

Garg H.P, R.S. Adhikari, (1997), "*Conventional hybrid photovoltaic/thermal (PV/T) air heating collectors: steady-state simulation*", Renewable Energy 11 (3) 363–385.

Gibbs B.M., S.M. Hasnain (1995), "*DSC study of technical grade phase change heat storage materials for solar heating applications*", Proceedings of the 1995 ASME/JSME/JSEJ International Solar Energy. Conference. Part 2, 1995.

Global Change Temperature, Retrieved 12 November 2007, http://drake.marin.k12.ca.us/stuwork/rockwater/PLANKTON/Taking%20a%20stand.html

Goel M., S.K. Roy, S. Sengupta (1994), "*Laminar forced convection heat transfer in microencapsulated phase change material suspensions*", Int. J. Heat Mass Transfer 37 (4) 593–604.

Griffiths P.W., P.C. Eames (2006), "*Performance of chilled ceiling panels using phase change material slurries as the heat transport medium*" Applied Thermal Engineering

Gschwander S., P. Schossig, H.-M. Henning (2004), "*Micro-encapsulated paraffin in phase-change slurries*", Solar Energy Materials & Solar Cells

H

Hart, R., and F. Thornton (1982), ''*Microencapsulation of Phase Change Materials*,'' Final Rep., DOE Contract No. 82, 80, Ohio

Hasnain, S.M, (1998). "*Review on Sustainable Thermal Energy Storage Technologies, Part 1: Heat Storage Materials and Techniques*". Energy Conversion & Management, 39, pp.1127-38.

Hayakashi B, Muzusaki K, Satoh T, Hatanaka T. (1989), "*Research and development of photovoltaic/thermal hybrid solar power generation system*". In: ISES Solar World Congress, Kobe

Hegazy AA. (2000), "*Comparative study of the performances of four photovoltaic/thermal solar air collectors*". Energy Conversion Management; 41:861–81.

Heine D. (1981), "*The chemical compatibility of construction materials with latent heat storage materials*", Proceedings of the International Conference on Energy Storage, Brighton, UK.

Hendrie SD. (1982), "*Photovoltaic/thermal collector development program*"—final report. Report, MIT

Ho C.J., J.F. Lin, S.Y. Chiu (2004), "*Heat transfer of solid–liquid phase change material suspensions in circular pipes: effects of wall conduction*", Numer. Heat Transfer: Part A 45 171–190.

Holman, J. P. (1981), *Heat Transfer*, 5th ed., McGraw-Hill, New York, p. 174

Hu X., Y. Zhang (2002), "*Novel insight and numerical analysis of convective heat transfer enhancement with microencapsulated phase change material slurries: laminar flow in a circular tube with constant heat flux*", Int. J. Heat Mass Transfer 45 3163–3172.

Huang BJ, Lin TH, Hung WC, Sun FS. (1999), "*Solar photo-voltaic/thermal co-generation collector*". In: ISES Solar World Congress, Jerusalem

Huang B.J., T. H. Lin, W. C. Hung and F. S. Sun, (2001), "*Performance Evaluation of Solar Photovoltaic/Thermal Systems*", Solar Energy Vol. 70, No. 5, pp. 443–448

Huang M.J, P.C. Eames a, B. Norton (2004), "*Thermal regulation of building-integrated photovoltaics using phase change materials*", International Journal of Heat and Mass Transfer 47 2715–2733

Huang M.J, P.C. Eames, B. Norton (2000), "*The application of computational fluid dynamics to predict the performance of phase change materials for control of photovoltaic cell temperature in buildings*", in: Proceedings of VI World Renewable Energy Congress, July, Brighton, UK, pp. 2123–2126.

Huang M.J, P.C. Eamesa, B. Norton (2006), "*Comparison of a small-scale 3D PCM thermal control model with a validated 2D PCM thermal control model*", Solar Energy Materials & Solar Cells

Huang M.J ,P.C. Eames a, B. Norton (2005), "*Phase change materials for limiting temperature rise in building integrated photovoltaics*", Solar Energy

Hussein, H.M.S., (2002). "*Transient investigation of a two phase closed thermosyphon flat plate solar water heater*". Energy Conversion and Management 43, 2479–2492.

Hussein, H.M.S., Mohamad, M.A., El-Asfouri, A.S., (1999a). "*Transient investigation of a thermosyphon flat-plate solar collector*". Applied Thermal Engineering 19, 789–800.

Hussein, H.M.S., Mohamad, M.A., El-Asfouri, A.S., (1999b). "*Optimization of a wickless heat pipe flat plate solar collector*". Energy Conversion and Management 40, 1949–1961.

Hussein, H.M.S., Mohamad, M.A., El-Asfouri, A.S., (2001). "*Theoretical analysis of laminar-film condensation heat transfer inside inclined wickless heat pipes flat-plate solar collector*". Renewable Energy 23, 525–535.

I

International Statistics (2002), http://www.iea-pvps.org), "*International Energy Agency Photovoltaic Power Systems Programme*".

IEA (2005b), *"World Energy Outlook"*, [Electronic Version], Retrieved October 2006, http://www.iea.org//textbase/nppdf/free/2005/weo2005.pdf

IEA (2005a), *"National Survey Report of PV Power Applications in UK"*, [Electronic Version], Retrieved October 2006

http://www.iea-pvpsuk.org.uk/resources/documents/iea-pvps_nsr2005uk.pdf

IEA – PVPS T7 – 4 Report (2002), "*Potential for Building Integrated Photovoltaic*", Retrieved October 2006,

http://iea-pvps.org/products/download/rep7_04.pdf

IEA-PVPS, "*Compared assessment of selected environmental indicators of photovoltaic electricity in OECD cities*", website www.iea-pvps.org.

Inaba H. (2000), Int. J. Therm. Sci. 39, 991-1003

Inaba H., Myoung-Jun Kim, Akihiko Horibe, "Melting Heat Transfer Characteristics of Microencapsulated Phase Change Material Slurries With Plural Microcapsules Having Different Diameters", Vol. 126, AUGUST 2004 Copyright © 2004 by ASME Transactions of the ASME

International Association of Electrical Inspectors, PV Characteristic I-V curve, Retrieved 2007, http://www.iaei.org/subscriber/magazine/04_d/wiles_figure2.gif

Ismail, K.A.R., Abogderah,M.M., (1998), "*Performance of a heat pipe solar collector*". Journal of Solar Energy Engineering 120, 51–59.

Ismail, K.A.R., Abogderah, M.M., (1992). "*Residential solar collector with heat pipes*". In: Proceedings 8th International Heat Pipe Conference, Beijing, China.

Ito S, Matsubayashi T, Miura N. (2004), "*Studies of a heat pump using dual heat sources of solar heat and ambient air*". In: Eurosun, Freiburg

J

Jahns E, (1999), "*Microencapsulated phase change materials*", Proceedings of the 4th IEA ECES IEA Annex 10 Workshop, Benediktbeuern (Germany).

Joshi AS, Tiwari A, (2006), "*Energy and exergy efficiencies of a hybrid photovoltaic–thermal (PV/T) air collector*". Renewable Energy, doi:10.1016/j.renene.2006.11.013

Joudi KA, Abd-Al Hussain TA, Abdul-Majeed PM., (1991) "Improved heat transport of heat pipes with an internal wall separating liquid vapour streams". Energy Conversion and Management; 31(2):141-8

Joudi, K.A., Al-Tabbakh, A.A., (1999) "*Computer simulation of a two phase thermosyphon solar domestic hot water heating system*". Energy Conversion and Management 40, 775–793.

K

Kalogirou S. (2004), "*Solar thermal collectors and applications*", Progress in energy and Combustion science, Volume 30, p 231-294

Kalogirou S.A., (2001), "*Use of TRNSYS for modelling and simulation of a hybrid PV–thermal solar system for Cyprus*", Renewable Energy 23 (2) 247–260.

Kaminaga F, Hashimoto H, Feroz C, Goto K, Masumura K., (1997) "*Heat transfer characteristics of evaporation and condensation in a two-phase closed thermosyphon*". In: Preprints of 10th International Heat Pipe Conference. Session H-1-6 Sep. 21-25, Stuttgart, Germany. 1997.

Kammen D.M., Retrieved (2007),"*Stand alone photovoltaic system design and principles*", http://ist-socrates.berkeley.edu/~kammen/er120/ER120-L5_PV_Design_edited.pdf

Kasza K.E., M.M. Chen (1984-85), "*Improvement of the performance of solar energy or waste heat utilization systems by using phase-change slurry as an enhancement heat-transfer storage fluid*", J. Solar Energy Eng. 107 229–236.

Keoleian Gregory and Geoffrey McD. Lewis, "*Application of Life-cycle Energy Analysis to Photovoltaic Module Design*", PROGRESS IN PHOTOVOLTAICS: RESEARCH AND APPLICATIONS, VOL. 5, 287±300 (1997)

Komp R. (2002), "*Practical photovoltaics—electricity from solar cells*", 3rd ed. revised. Ann Arbor: Aatec Publications;

Krauter (2004), "*Increased electrical yield via water flow over the front of photovoltaic panels*", Solar energy materials & solar cells, 82 (2004) 131-137

Krauter SCW. (2004), "*Development of an integrated solar home system*". Solar Energy Materials & Solar Cells; 82:119–30.

S. Krauter, R. Ruther, "*Considerations for the calculation of greenhouse gas reduction by photovoltaic solar energy*", Renewable Energy 29 (2004) 345–355

Kreider JF, (1982), *"The* solar heating design process". New York: McGraw-Hill;

[Klein SA, (1975), "*Calculation of flat plate collector loss coefficients*": Solar Energy 1975; 17:79–80.

Kreith F, Kreider JF (1978). "*Principles of solar engineering*". New York: McGraw-Hill;

L

Lambarski TJ. (1984), "*Electrical design guidelines for photovoltaic/thermal systems*". In: 17th IEEE, Kissimmee

Lane G.A. (1983), "*Solar Heat Storage: Latent Heat Material*", vol. I, Background and Scientific Principles, CRC Press, Florida.

Lane G.A. (1986), "*Solar Heat Storage: Latent Heat Material*", vol. II, Technology, CRC Press, Florida.

Lee C.H., H.K. Choi (1998), "*Crystalline Morphology in High-Density Polyethylene/Paraffin Blend for Thermal Energy Storage*", Polym. Composites 19 (6) 704–708.

Leenders F, Schaap AB, Ree BCG, van der Helden, WGJ van. (2000), "*Technology review on PV/Thermal concepts*". In: 16th EPSEC, Glasgow

Leenders F, van der Ree BCG, Soerensen H. (2001), "*PV/T road map—from R&D to market introduction*". Northsun Leiden

Legierski Jarosław, Bogusław Wiecek Gilbert de Mey, (2005) "*Measurements and simulations of transient characteristics of heat pipes*", Microelectronics Reliability

Li H., A. Akbarzadeh, P. Johnson, "*The thermal characteristics of a closed two-phase thermosyphon at low temperature difference*", Heat Recovery Systems & CHP 11 (6) (1991) 533–540.

Lin Q, Furbo S, 1998, "*Solar heating systems with evacuated tubular solar collector*". Proceedings of the Eurosun'98 Conference on CD-ROM, Portoroz, Slovenia; 1998

Littwin DA, Willis DB., (1985), "T*he use of heat pipes to conserve energy in petroleum refineries. Energy Progress*", pp:198-202.

Loferski JJ, Case C, Doodlesack G, Roessler B, Dobbins R, Russell T et al. (1982), "*Design and construction of a hybrid Photovoltaic (3 kWp)-thermal solar energy system for a residential/commercial building*". In: 16th IEEE, San Diego

M

McMahon, W. A., Jr., W. W. Harlowe, Jr., and D. J. Mangold (1982), ''Feasibility Study of Utilizing Phase Change Coolant for Protective Garment,'' Final Rep., Contract

No. DAAK 60-81-C-0098, U.S. Army Natick Research and Development Command, MA

Mathioulakis E., V. Belessiotis, "*A new heat pipe type solar domestic hot water system*", Solar Energy 72 (2002) 13–20.

Matter and Energy Laws, Retrieved 12 November 2007, http://bioweb.wku.edu/courses/Biol280/280mat.HTML

P.J Meier, G.L Kulcinski, "*Life cycle energy requirements and greenhouse gas emissions for building integrated photovoltaic systems*", April 2002 University of Wisconsin, Energy Center of Wisconsin, www.ecw.org

Morikama Y., H. Suzuki, F. Okagawa, K. Kanki (1985), "*A development of building elements using PCM*", Proceedings of the International Symposium on Thermal Application of Solar Energy, Hakone (Kanagawa, Japan).

Moshfegh B, Sandberg M, (1998), "*Flow and heat transfer in the air gap behind photovoltaic panels*". Renewable Sustainable Energy Review 1998; 2:287–301.

Morita Y., T. Fujisawa, T. Tani, (2000), "*Moment performance of photovoltaic/ thermal hybrid panel (numerical analysis and exergetic evaluation)*", Electrical Engineering in Japan 133 (2) (2000) 81–87. Translated from Denki Gakkai Ronbunshi, Vol. 119-D, No. 1, January 1999, pp. 81.87

Mulligan, J. C., D. P. Colvin, and Y. G. Bryant (1994), ''*Use of Two-Component Fluids of Microencapsulated Phase-Change Materials for Heat Transfer in Spacecraft Thermal Systems*,'' AIAA Paper No. 94, 2004

Myers DR, Emery K, Gueymard C, (2002), "*Revising and validating spectral irradiance reference standards for photovoltaic performance*". In: ASES/ASME solar 2002 conference proceeding, Reno, Nevada; 15–20 June 2002.

N

Nagano K, Mochida T, Shimakura K, Murashita M. (2001), "*Performance of hybrid wallboards united with PV cells*". In: ISES Solar World Congress, Adelaide

Naumann R., H.H. Emons (1989), "*Results of thermal analysis for investigation of salt hydrates as latent heat-storage materials*", J. Thermal Analysis 35 1009–1031.

Naveed AT, Kang EC, Lee EJ. (2006), "*Effect of unglazed transpired collector on the performance of a polycrystalline silicon photovoltaic module*". Journal Solar Energy Engineering ;128:349–53.

Negishi K., Sawada T., (1983), "*Heat Transfer Performance of an Inclined Two-Phase Closed Thermosyphon*", Int. J, Heat Mass Transfer, Vol 26, No 8, pp 1207-1213

Nguyen-Chi H, Abhat A., (1979) "*Performance evaluation of gravity assisted copper-water heat pipes with liquid*". AIAA Journal 1979; 17(9):1003±11.

Nguyen-Chi, M. Groll, Th. Dang-Van, (1979), "*Experimental investigation of closed two-phase thermosyphons*". AIAA 14th Thermophysics Conference, Orlando, Florida, June 4–6, 1979, pp. 239–246.

Nishikawa M, Sone T, Ito S. (1993), "*A heat pump using solar hybrid panels as the evaporator*". In: ISES Solar World Congress, Budapest

Nolay P., (1987), "*Developpement dune methode generale danalyse des systemes photovoltaiques*". MS Thesis, Ecole des Mines, Sophia-Antipolis, France; 1987.

O

Oliveti, G., Arcuri, N., (1996). "*Solar radiation utilisability method in heat pipe panels*". Solar Energy 57, 345–360.

Orel ZC, Gunde MK, Hutchins MG, 2002, "*Spectrally selective solar absorbers in different non-black colours*". Proceedings of WREC VII, Cologne on CD-ROM;

Ortabasi U., F. Fehlner, (1979) "*Cusp mirrors-heat-pipe evacuated tubular solar thermal collector*", Solar Energy 24 (1979) 477–489.

P

Padmanabhan P.V, M.V. Murthy (1986), "*Outward phase change in a cylindrical annulus with axial fins on the inner tu*be", International Journal of Heat and Mass Transfer 29 (12) 1855–1868.

Park R., Y. Lee, (1992) "*Two-phase closed thermosyphons with two fluid mixture*", in: Proceedings of 8th International Heat Pipe Conference, Beijing, China, vol. 2, 1992, pp. 220–225.

Payakaruk, T., Terdtoon, P., Ritthidech, S., (2000). "*Correlations to predict heat transfer characteristics of an inclined closed two-phase thermosyphon at normal operating conditions*". Applied Thermal Engineering 20, 781–790.

PCM thermal solutions (USA), 2004. Available from /www.pcm-solutions.comS.

Platz R, Fischer D, Zufferey MA, Anna Selvan JA, Haller A, Shah A. (1997), "*Hybrid collectors using thin-film technology*". In: 26th PVSC Anaheim, CA

Pluta Z., W. Pomierny, (1995), "*The theoretical and experimental investigation of the phase-change solar thermosyphon*", Renewable Energy 6 (1995) 317–321.

Porisini F.C (1988), "*Salt hydrates used for latent heat storage: corrosion of metals and reliability of thermal performance*", Solar Energy 41 193–197.

Prakash J. (1994), "*Transient analysis of a photovoltaic-thermal solar collector for co-generation of electricity and hot air/water*". Energy Conversion Management ;35(11):967–72.

Q

R

Raghuraman P. (1981), "*Analytical predictions of liquid and air photovoltaic/thermal, flat-plate collector performance*". Journal Solar Energy Engineering;103:291–8.

Radziemska E, Klugmann E, (1999), "*Effect of temperature on conversion efficiency of solar module*". Proceedings of the XXIII IMAPS Conference, Kołobrzeg, Poland; 1999. p. 97.

Radziemska E., (2002), "*The effect of temperature on the power drop in crystalline silicon solar cells*". Renewable Energy 2002; 28:1.

Radziemska E, Klugmann E, (1999), "Thermally affected parameters of the current–voltage characteristics of silicon photocell". Energy Convers Mgmt 2002; 43:1999.

Rittidech S., S. Wannapakne, (2007) "*Experimental study of the performance of a solar collector by closed-end oscillating heat pipe (CEOHP)*", Applied Thermal Engineering 27 (2007) 1978–1985

Roger Kubarych (2005), "*How oil shocks affect markets: consider the five most recent scenarios*". International Economy, The. Summer 2005. FindArticles.com. Retrieved 12 Nov. 2007. http://findarticles.com/p/articles/mi_m2633/is_3_19/ai_n15787119

Ross, R.G. (1980) "*Flat-Plate Photovoltaic Array Design Optimization*", Conference Record, 14th IEEE Photovoltaic Specialists Conference, San Diego, pp. 1126-1132.

Roy, S. K., and S. Sengupta (1991), ‘‘*An Evaluation of Phase Change Microcapsules for Use in Enhanced Heat Transfer Fluids*,’’ *Int. Commun. Heat Mass Transfer*, 18, 495.

Rubitherm GmbH, 2004. Available from: /http://www.rubitherm.deS.

Russell R.F., (1982), "*Uniform temperature heat pipe and method of using the same,*" Patent US4320246, 1982, USA

Ryu HW, Woo SW, Shin BC, Kim SD (1992). "*Prevention of sub cooling and stabilization of inorganic salt hydrates as latent heat storage materials*". Solar Energy Mater Solar Sells; 27:161–72.

S

Salem A. Said and Bilal A. Akash, (1999), "*Experimental Performance of a Heat Pipe*", Int. Comm. Heat Mass Transfer, Wol. 26, No. 5, pp. 679-684

Salyer I.O., A.K. Sircar, R.P. Chartoff (1986), "*Analysis of crystalline paraffinic hydrocarbons for thermal energy storage by differential scanning calorimetry; Part 1, Pure hydrocarbons*", 15th North American Thermal Analysis Society Conference, Cincinnati, OH.

Sandnes B, Rekstad J, 2002, "*A photovoltaic/thermal (PV/T) collector with a polymer absorber plate, experimental study and analytical model*". Solar Energy 2002; 72(1):63–73.

Sandnes B. (2003), "*Exergy Efficient Production, Storage and Distribution of Solar Energy*", Ph.D Thesis

Sayigh A.A.M, (1991), "*Photovoltaic and Solar Radiation in Generating Electricity from the Sun*", F.C Treble, and Editor: BPCC Wheatons Ltd: Exeter 1991

Schossig P., H.-M. Henninga, S. Gschwandera (2005), T. Haussmann, "*Micro-encapsulated phase-change materials integrated into construction materials*", Solar Energy Materials & Solar Cells

Schweiger H, 1997, "*Optimisation of solar thermal absorber elements with transparent insulation*". Thesis, Universitat Politecnica de Catalunya, Terrassa, Barcelona, Spain

Shalaby M.A., F.F. Araid, G.I. Sultan, M.M. Awad, (2000) "*Heat transfer performance of a two-phase closed thermosyphons*", in: Proceedings of 6th International Heat Pipe Symposium, Chiang Mia, 2000, pp. 269–278.

Sharma SD (1999). "*Thermal energy storage systems using phase change material for temperature applications*". Ph.D Thesis.

SHIA (2006), *"Solar Heating and Cooling Programme"*, Annual Report, [Electronic Version], Retrieved October 2006, http://www.iea-shc.org/publications/annualreports/2006_SHC_Annual_Report.pdf

Shiraishi M., Y. Kim, M. Murakami, P. Terdtoon, (1996) "*A correlation for the critical heat transfer rate in an inclined two-phase closed thermosyphon*", in: Proceedings of 5th International Heat Pipe Symposium, Melbourne, 1996.

Spanos, L. Duckers, "*Expected cost benefits of building-integrated PVs in UK, through a quantitative economic analysis of PVs in connection with buildings, focused on UK and Greece*", Renewable Energy 29 (2004) 1289–1303

Srihajong N., S. Ruamrungsri, P. Terdtoon , P. Kamonpet , T. Ohyama, "Heat pipe as a cooling mechanism in an aeroponic system", Applied Thermal Engineering 26 (2006) 267–276

Shon, C. W.,and M. M. Chen (1984), ''*Heat Transfer Enhancement in Laminar Slurry Pipe Flows with Power Law Thermal Conducti*vities,'' *J. Heat Transfer*, 106, 539

Sohn C.W., M.M. Chen (1981), "*Micro convective thermal conductivity in disperse two-phase mixture as observed in a low velocity Couette flow experiment*", J. Heat Transfer 103 47–50.

E. Streicher, W. Heidemann, H. Müller-Steinhagen, "*Energy Payback Time – A Key Number for the Assessment of Thermal Solar Systems*", Proceedings of EuroSun2004, 20 - 23 June 2004, Freiburg, Germany

Smith DR, Biringer KL, Pritchard DA. (1978), "*Combined photovoltaic thermal collector testing*". In: 13th IEEE, Washington.

Solar Irradiation Spectrum vs silicon cell spectrum, Retrieved 2007, http://www.vicphysics.org/documents/events/stav2005/spectrum.JPG

Soltau H, 1992, "*Testing the thermal performance of uncovered solar collectors*". Solar Energy 1992; v 49(4): p 263–72.

Sopian K.S., H.T. Yigit, H.T. Liu, S. Kakac, T.N. Veziroglu, (1996), "*Performance analysis of photovoltaic/thermal air heaters*", Energy Conversion and Management 37 (11) 1657–1670.

Sopian K, Liu HY, Kakac S. (1997), "*Research and development of hybrid photovoltaic thermal solar air heaters*". International Journal Global Energy Issues; 9(4–6):382–92.

Sopian K.S., H.T. Liu, S. Kakac, T.N. Veziroglu, (2000), "*Performance of a double pass photovoltaic thermal solar collector suitable for solar drying systems*", Energy Conversion and Management 41 (4) 353–365.

Southface (2007), "*How Solar thermal collector systems work*", Retrieved 2007, http://www.southface.org/solar/solar-roadmap/solar_how-to/solar-how_solar_works.htm

Spate F, Hafner B, Schwarzer K., 1999, "*A system for solar process heat for decentralised applications in developing countries*". Proceedings of ISES Solar World Congress, Jerusalem, Israel on CD-ROM

Speyer R.F., (1994), "*Thermal Analysis of Materials*", Marcel Dekker, New York.

Sudhakar SV, Sharon M. (1994), "*Fabrication and performance evaluation of a photovoltaic/thermal hybrid system*". SESI J; 4(1):1–7.

T

TEAP Energy Products, 2004. Available from /http://www.teappcm.comS.

Terdtoon P., N. Waowaew, P. Tantakom, (1999), "*Internal flow patterns of an inclined, closed two-phase thermosyphon at critical state: case study 1, effect of aspect ratio*", Experimental Heat Transfer 347–358.

Terdtoon P., Shiraishi M., Murakami M., (1990), "*Effect of Inclination Angle on Heat transfer Characteristics of Closed Two-Phase Thermosyphon*", Annual symposium of the Institute of Space and Aeronautical Science of Japan

Terdtoon P., S. Ritthidej, M. Shiraishi, (1996) "*Effect of aspect ratio and Bond number on heat transfer characteristics of an inclined two-phase closed thermosyphon at normal operating condition*", in: Proceedings of 5th International Heat Pipe Symposium, Melbourne, 1996.

Tiwari Arvind, M.S. Sodha, (2007), "*Parametric study of various configurations of hybrid PV/thermal air collector: Experimental validation of theoretical model*", Solar Energy Materials & Solar Cells 91 17–28

Tiwari Arvind, M.S. Sodha, (2006), "*Performance evaluation of hybrid PV/thermal water/air heating system: A parametric study*", Renewable Energy 31 2460–2474

Tiwari Arvind, M.S. Sodha, Avinash Chandra, J.C. Joshi, (2006), "*Performance* evaluation of photovoltaic thermal solar air collector for composite climate of India", Solar Energy Materials & Solar Cells 90 175–189

Tonui J.K, Y. Tripanagnostopoulos, (2006), "*Air-cooled PV/T solar collectors with low cost performance improvements*", Solar Energy xxx (2006)

Tonui J.K, Y. Tripanagnostopoulos, (2007), "*Improved PV/T solar collectors with heat extraction by forced or natural air circulation*", Renewable Energy 32 623–637

Tripanagnostopoulos Y, Souliotis M, Nousia, (2000), "*Thermal Solar collectors with coloured absorbers*". Solar Energy 2000; 68: 343–56.

Tripanagnostopoulos Y, Nousia Th, Souliotis M, Yianoulis P. (2002), "Hybrid photovoltaic/thermal solar systems". Solar Energy; 72(3):217–34.

Tripanagnostopoulos Y, Nousia Th, Souliotis M. (2000), "*Low cost improvement to building integrated air cooled hybrid PV-thermal systems*". In: 16th EPSEC, Glasgow, 2000.

Tripanagnostopoulos Y, Nousia Th, Souliotis M. (2001), "*Test results of air cooled modified PV modules*". In: 17th EPSEC, Munich, 2001.

Tripanagnostopoulos Y, Tzavellas D, Zoulia I, Chortatou M. (2001), "*Hybrid PV/T systems with dual heat extraction operation*". In: 17th EPSEC, Munich, 2001.

Tripanagnostopoulos Y, Bazilian M, Zoulia I, Battisti R. (2002), "*Hybrid PV/T system with improved air heat extraction modification*". In: PV in Europe, Rome, 2002.

Tripanagnostopoulos Y, Souliotis M, Battisti R. Corrado A. (2006), "Performance, cost and life-cycle assessment study of hybrid PVT/air solar systems2. PIP; 14:65–76.

U

US Department - Energy Efficiency and Renewable Energy, Retrieved 2007, http://www1.eere.energy.gov/solar/sh_basics_collectors.html

V

Van der Ree, BCG. (1996), "*Testing a prototype PV/Thermal collector*". Report TNO 95-BBI-R1666, 1996.

Velraj R., R.V. Seeniraj, B. Hafner, C. Faber, K. Schwarzer (1999), "*Heat transfer enhancement in a latent heat storage system*", Solar Energy 65 171–180.

Vineet Veer Tyagi, D. Buddhi (2005); "*PCM thermal storage in buildings: A state of art*", Renewable and Sustainable Energy Reviews

W

Werner Weiss, Irene Bergmann and Gerhard Faninger, 2003, Solar Heating Worldwide, "Markets and contribution to the energy supply", Institute for Sustainable Technologies

Wikipedia (2007), "*Oil and natural gas prices*", Retrieved 12 November 2007, http://en.wikipedia.org/wiki/Oil_price_increases_of_2004-2006#Causes http://en.wikipedia.org/wiki/Natural_gas_prices#Trends_in_natural_gas_prices

Wim G. J. van Helden1*,y, Ronald J. Ch. van Zolingen2 and Herbert A. Zondag, (2004), "*PV Thermal Systems: PV Panels Supplying Renewable Electricity and Heat*", Progress. Photovoltaic: Resources. Applied. 2004; 12:415–426 (DOI: 10.1002/pip.559)

Winston R, O'Gallagher J, Muschaweck J, Mahoney A, Dudley V (1999). "*Comparison of predicted and measured performance of an integrated compound parabolic concentrator (ICPC)*". Proceedings of ISES Solar World Congress on CDROM, Jerusalem, Israel; 1999

Winters, P. J. (1991), ''*Phase Two Laboratory Testing of Direct Freeze Ice Slurry District Cooling*,''Final Rep., DOE Contract No. DE-FG01- 88CE26559

World Watch Institute (2006), *"Renewable: Global Status Report"*, [Electronic Version], Retrieved October 2006, http://www.ren21.net/globalstatusreport/download/RE_GSR_2006_Update.pdf

X

Y

Yamagishi Y., H. Takeuchi, A.T. Pyatenko (1999), "*Characteristics of microencapsulated PCM slurry as a heat-transfer fluid*", AIChE J. 45 (4) 696–707.

Yanadori M, Masuda T. (1989). "*Heat transfer study on a heat storage container with a phase change materials: Part 2*". *Solar Energy* 42:27}34.

Yinping Z., J. Yi, J. Yi (1999), "*A simple method, the T-history method, of determining the heat of fusion, specific heat and thermal conductivity of phase-change materials*", Measurement Sci. Technol. 10 201–205.

Yasushi Y., T. Hiromi, T.P. Alexander, K. Naoyuki (1999), "*Characteristics of microencapsulated PCM slurry as a heat-transfer fluid*", AIChE J. 45 (4) 696–707.

Younger PR, Kreisman WS, Nowlan MJ, Solomon JS, Strong SJ. (1981), "*Combination photovolaic/thermal solar collectors for residential applications*". In: 15th IEEE, Orlando, 1981.

Z

Zalba B., Marín J.M., Cabeza L.F. and Mehling H. (2003), "*Review on thermal energy storage with phase change: materials, heat transfer analysis and applications*". Applied Thermal Engineering 23, 251 – 283.

Zhang Y.W., A. Faghri (1995), "*Analysis of forced convection heat transfer in micro capsulated phase change material suspensions*", J. Thermophysics Heat Transfer 9 (4) 727–732.

Zondag, HA, Bakker M, Helden WGJ, editors. (2005), "*PVT Roadmap—a European guide for the development and market introduction of PV-Thermal technology*". Report EU-Project PV-Catapult /www.pvtforum.orgS, 2005.

Zondag HA, De Vries DW, Van Steenhoven AA, Van Helden WGJ, Van Zolingen RJC. (1999), "*Thermal and electrical yield of a combi-panel*". In: ISES Solar World Congress, Jerusalem, 1999.

Zondag HA, De Vries DW, Van Helden WGJ, Van Zolingen RJC, Van Steenhoven AA. (2003), "*The yield of different combined PV-thermal collector designs*". Solar Energy; 74:253–69.

Zondag HA, Jong MJM, Van Helden WGJ. (2001), "*Development and applications for PV thermal*". In: 17th EPSEC 2001, Munich, 2001.

Zondag HA, Van Helden WGJ. (2003), "*PV-Thermal domestic systems*". In: Third WCPEC, Osaka, 2003.

Zondag HA, (2005), " *Flat plate PV-Thermal collectors and systems: A review*", Renewable and sustainable energy reviews, (2007), doi:10.1016/j.rser.2005.12.012

Zondag HA, Eisenmann W, Borg NJCM vd. (2005), "*PVT performance measurement guidelines—guidelines for performance measurements of liquid-cooled non-concentrating PVT collectors using c-Si cells*". Report D8-6 PV-Catapult (see /www.pvtforum.orgS), 2005.

Appendix 1

Nomenclature

η	[0..1]	The overall efficiency of the photovoltaic array.
$\eta_{T\ coef}$	[0..1]	A coefficient that describes the change in photovoltaic array efficiency as a function of cell temperature
$\eta_{I\ coef}$	[0..1]	A coefficient that describes the change in photovoltaic array efficiency as a function of incident solar radiation.
T_{PV}	[°C]	The PV cell temperature
I_T	[kJ/hr.m^2]	The total amount of solar radiation incident on the PV collector surface.
T_{ref}	[°C]	Cell temperature at the conditions under which the reference PV efficiency was measured.
$I_{T\ ref}$	[kJ/hr.m^2]	The total amount of solar radiation incident on the PV collector surface at the conditions under which the reference PV efficiency was measured.
η_{ref}	[0..1]	The overall efficiency of the photovoltaic array under reference conditions.
IAM	[0..1]	The combined incidence angle modifier for the PV cover material.
IAM_{beam}	[0..1]	The incidence angle modifier for the PV cover for beam radiation.
$IAM_{diffuse}$	[0..1]	The incidence angle modifier for the PV cover for diffuse radiation.
IAM_{ground}	[0..1]	The incidence angle modifier for the PV cover for ground reflected radiation.
I_{beam}	[kJ/hr.m^2]	The beam radiation incident on the PV surface.
$I_{diffuse}$	[kJ/hr.m^2]	The diffuse radiation incident on the PV surface.
I_{ground}	[kJ/hr.m^2]	The ground reflected radiation incident on the PV surface.
$\theta_{diffuse\ effective}$	[degrees]	The effective incidence angle of diffuse solar radiation on the PV surface.
β	[degrees]	The slope of the PV surface.
$\theta_{ground\ effective}$	[degrees]	The effective incidence angle of ground reflected solar radiation on the PV surface.
$\dot{P}_{pv}$	[kJ/hr.m^2]	The power generated by the PV
$(\tau\alpha)_n$	[0..1]	The transmittance absorptance product of the PV cover for solar radiation at a normal angle of incidence.
A	[m^2]	The PV surface area.
$h_{com\ top}$	[kJ/hr.m^2.K]	The convective heat transfer coefficient for the top surface of the PV.
$h_{rad\ top}$	[kJ/hr.m^2.K]	The radiative heat transfer coefficient for the top surface of the PV.

$h_{com\ back}$	[kJ/hr.m^2.K]	The convective heat transfer coefficient for the back surface of the PV.
$h_{rad\ back}$	[kJ/hr.m^2.K]	The radiative heat transfer coefficient for the back surface of the PV.
$T_{amb\ top}$	[°C]	The temperature to which the PV convectively loses energy off its top surface.
$T_{amb\ back}$	[°C]	The temperature to which the PV convectively loses energy off its back surface.
$T_{rad\ top}$	[°C]	The temperature to which the PV radiatively loses energy off its top surface.
$T_{rad\ back}$	[°C]	The temperature to which the PV radiatively loses energy off its back surface.
R_1, R_2, R_3	[hr.m^2.K/kJ]	The thermal resistance of the cover material, PV cell backing, and back insulation materials respectively.
X	[0..1]	PCM material quality (0: completely liquid, 1: completely solid)
m	[kg]	Mass of the PCM layer
h_{fg}	[kJ/kg]	The energy of solidification or energy of liquefaction of the PCM material, per unit mass.

Appendix 2

PARAMETER / INPUT / OUTPUT LIST

PARAMETERS

Parameter Number	Name	Unit	Typical Value	Comment
1	PV efficiency mode	-	1	The mode defining how the PV efficiency should be calculated by the model: 1 = Constant PV efficiency 2 = Linear modifiers for off-rated cell temperature and incident radiation 3 = Efficiency provided as an INPUT to the model 4 = User-provided data file of PV efficiency as a function of cell temperature and incident radiation
2	Cover mode	-	1	This parameter indicates whether the PV system has a transparent cover: 0 = No cover, 1 = Covered
3	Area	m^2	1.0	The area of the PV array: consistent with the provided efficiency parameters and inputs
4	Resistance of PV cell backing material	$h.m^2.K/kJ$	0.0	The resistance to heat transfer for the material separating the PV cells and the PCM layer.
5	Resistance of back insulation material	$h.m^2.K/kJ$	3.0	The resistance to heat transfer for the back of the collector.
6	Top emissivity	0..1	0.9	The emissivity of the outer surface for long-wave radiation exchange with the sky.
7	Back emissivity	0..1	0.9	The emissivity of the collector back surface for long-wave radiation exchange with the zone.
8	Absorptance	0..1	0.9	The absorptance of the PV surface for solar radiation.
9	PCM layer thickness	m	0.03	The thickness of the PCM layer
10	PCM layer density	kg/m^3	1000.0	The density of the PCM layer material.
11	Solid phase specific heat	kJ/kg.K	2.50	The specific heat of the PCM layer material in its completely solidified state.
12	Liquid phase specific heat	kJ/kg.K	2.50	The specific heat of the PCM layer material in its completely liquefied state.
13	Energy of solidification	kJ/kg	1000.0	The energy per unit mass required to transform the PCM from 100% solid to 100% liquid.
14	Initial PCM temperature	C	20.0	The temperature of the PCM layer at the beginning of the simulation.
15	Solidification temperature	C	20.0	The temperature below which the PCM is completely solidified.
16	Liquefaction temperature	C	40.0	The temperature above which the PCM is completely liquefied.
PV Efficiency Mode 2 (PV efficiency modifiers) and Cover Mode 0 (uncovered PV)				
17	Reference PV efficiency	0..1	0.12	The efficiency of the PV cells in converting incident radiation to electricity at the provided reference conditions.
18	Reference temperature	C	25.0	The reference temperature at which the efficiency of the PV cell is provided.
19	Reference radiation	$kJ/hr.m^2$	3600.0	The reference total incident solar radiation at which the efficiency of the PV cell is provided.
20	Efficiency modifier - temperature	1/C	-0.005	The multiplier to correct the rated PV cell efficiency as a function of cell temperature. Efficiency = Nominal Efficiency * Xt*Xr where Xt = 1 + this parameter*(Tpv-Treference)
21	Efficiency modifier - radiation	$hr-m^2/kJ$	0.000025	The multiplier to correct the rated PV cell efficiency as a function of incident solar radiation. Efficiency = Nominal Efficiency * Xt*Xr where Xr = 1 + this parameter*(Incident solar-Incident solar at reference condition)

INPUTS				
Input Number	**Name**	**Unit**	**Typical Value**	**Comment**
1	Ambient temperature	C	20.0	The temperature of the environment for calculating losses from the collector surfaces (top and back).
2	Sky temperature	C	20.0	The temperature of the sky for calculating long-wave radiation losses from the collector surface.
3	Zone temperature	C	20.0	The temperature of the air located behind the back surface of the collector.
4	Back radiant temperature	C	20.0	The temperature of the surfaces located behind the collector. This temperature will be used for radiative loss calculations from the back surface of the collector.
5	Top heat loss coefficient	kJ/hr-m²-K	64.0	The convective heat transfer coefficient from the cover surface to the ambient air. A commonly used correlation is hconv=3.6*(5.7+3.8* windspeed in m/s)
6	Back heat loss coefficient	kJ/hr-m²-K	11.0	The convective heat transfer coefficient from the back surface of the collector to the zone air.
7	Incident solar radiation	kJ/hr-m²	0.0	The rate at which incident solar radiation (beam + diffuse) strikes the sloped collector surface.

OUTPUTS			
Output Number	**Name**	**Unit**	**Comment**
1	PV efficiency	-	The efficiency of the PV cells in converting incident solar radiation to electrical energy: expressed as a fraction.
2	PV power	kJ/hr	The rate at which the photovoltaic cells are producing electrical power.
3	Mean PV temperature	C	The temperature of the PV cells.
4	Cover temperature	C	The temperature of the PV/PCM array cover
5	PCM temperature	C	The temperature of PCM layer
6	Back surface temperature	C	The temperature of the back surface of the collector (zone air / collector back interface).
7	Absorbed solar radiation	kJ/hr	The net rate at which solar radiation is absorbed by the collector. This value does not include the radiation that was absorbed by the PV cells and converted to electrical energy.
8	Collector top losses - convective	kJ/hr	The rate at which energy is lost to the environment through convection from the top surface of the collector.
9	Collector top losses - radiative	kJ/hr	The rate at which energy is lost to the environment through radiation losses from the top surface of the collector.
10	Collector back losses - convective	kJ/hr	The rate at which energy is convected from the back of the collector to the zone air.
11	Collector back losses - radiative	kJ/hr	The net rate at which energy is radiated from the back of the collector to the zone surfaces.
12	PCM net energy transfer rate	kJ/hr	The rate at which heat is transferred into the PCM material at the current time step.
13	PCM quality	0..1	The quality of the PCM material at the end of the time step. 0 = fully solid, 1 = fully liquid, -0.1 = subcooled solid, 1.1 = superheated liquid. 0 to 1 = partially solid / partially liquid (2-phase)
14	Elapsed time – subcooled	hr	The elapsed time that the PCM material has been below a quality of 0.0
15	Elapsed time – two phase	hr	The elapsed time that the PCM material has been in a two-phase condition.
16	Elapsed time – superheated	hr	The elapsed time that the PCM material has been above a quality of 1.0